CENTER FOR COMPUTER RESEARCH IN MUSIC AND ACOUSTICS
MAY 2001

DEPARTMENT OF MUSIC
REPORT NO. STAN-M-108

# WAVE AND SCATTERING METHODS FOR THE NUMERICAL INTEGRATION OF PARTIAL DIFFERENTIAL EQUATIONS

STEFAN DAMIAN BILBAO

CCRMA
DEPARTMENT OF MUSIC
STANFORD UNIVERSITY
STANFORD, CALIFORNIA 94305-8180

# WAVE AND SCATTERING METHODS FOR THE NUMERICAL INTEGRATION OF PARTIAL DIFFERENTIAL EQUATIONS

A DISSERTATION
SUBMITTED TO THE DEPARTMENT OF ELECTRICAL ENGINEERING
AND THE COMMITTEE ON GRADUATE STUDIES
OF STANFORD UNIVERSITY
IN PARTIAL FULFILLMENT OF THE REQUIREMENTS
FOR THE DEGREE OF
DOCTOR OF PHILOSOPHY

Stefan Damian Bilbao
May 2001

© Copyright 2001 by Stefan Damian Bilbao
All Rights Reserved

I certify that I have read this dissertation and that in my opinion it is fully adequate, in scope and quality, as a dissertation for the degree of Doctor of Philosophy.

Julius O. Smith III
(Principal Adviser)

I certify that I have read this dissertation and that in my opinion it is fully adequate, in scope and quality, as a dissertation for the degree of Doctor of Philosophy.

Ivan R. Linscott

I certify that I have read this dissertation and that in my opinion it is fully adequate, in scope and quality, as a dissertation for the degree of Doctor of Philosophy.

Perry R. Cook

I certify that I have read this dissertation and that in my opinion it is fully adequate, in scope and quality, as a dissertation for the degree of Doctor of Philosophy.

Robert M. Gray

Approved for the University Committee on Graduate Studies:

# Abstract

Digital filtering structures have recently been applied toward the numerical simulation of distributed physical systems. In particular, they have been used to numerically integrate systems of partial differential equations (PDEs), which are time-dependent, and of hyperbolic type (implying wave-like solutions, with a finite propagation velocity). Two such methods, the *multidimensional wave digital filtering* and *digital waveguide network* approaches both rely heavily on the classical theory of electrical networks, and make use of *wave variables*, which are reflected and transmitted throughout a grid of *scattering junctions* as a means of simulating the behavior of a given model system. These methods possess many good numerical properties which are carried over from digital filter design; in particular, they are numerically robust in the sense that stability may be maintained even in finite arithmetic. As such, these methods are potentially useful candidates for implementation in special purpose hardware.

In this thesis, the subtext is that such scattering-based methods can and should be treated as finite difference schemes, for purposes of analysis and comparison with standard differencing forms. In many cases, these methods can be shown to be equivalent to well-known differencing approaches—we pay close attention to the relationship between digital waveguide networks and *finite difference time domain* (FDTD) methods. For this reason, it is probably most useful to think of scattering forms as alternative realizations of these schemes with good numerical properties, in direct analogy with ladder, lattice and orthogonal digital filter realizations of direct form filters. We make use of this correspondence in order to import (from the finite difference setting) two techniques for approaching problems with irregular boundaries, namely coordinate changes, and a means of designing interfaces between grids of different densities and/or geometries. We also make use of the finite difference formulation in order to examine initial and boundary conditions, parasitic modes, and take an extended look at the numerical properties of all the commonly encountered forms of the waveguide network in two and three spatial dimensions.

Another question is of the relationship between wave digital and waveguide network schemes. Although they are quite similar from the standpoint of the programmer, in that the main operation, scattering, is the same in either case, conceptually they are very different. A multidimensional wave digital network is derived from a compact circuit representation of model system of PDEs.

The numerical routine is itself a discrete time and space image of the original network. Waveguide meshes, however, are usually formulated as collection of lumped scattering junctions which span the problem domain, connected by bidirectional delay lines. Lacking a multidimensional representation, then, it is not straightforward to design a mesh which numerically solves a given problem. A useful result is that waveguide meshes can be obtained directly from a system by almost exactly the same means as a wave digital network. This unification of the two methods opens the door to a larger class of methods which are of neither type, and yet which consist of the same numerically robust basic building blocks.

On the applied side, special attention is paid to problems in beam, plate and shell dynamics; though these systems are in general much more complex than the transmission line and parallel-plate problems which have been discussed extensively in the literature, they can be dealt with using both wave digital filters and waveguide networks, though several new techniques must be introduced. Several simulations are presented.

# Preface

This thesis is, if anything, long; there have been a few reasons for this. At the beginning stages of research, the focus was on the digital synthesis of musical sound through the use of physical modeling techniques. Since all physical models of vibration in acoustic instruments can be framed in terms of coupled sets of partial differential equations, the problem, then, is one of the numerical integration of these equations, subject to initial and boundary conditions and external excitations. There are, of course, many ways of designing such simulation algorithms. We began by looking at digital waveguide networks, which have been used successfully for this purpose for some time, but soon turned to multidimensional wave digital filtering methods, which are based on some similar ideas, yet within a powerful framework for attacking a much more general (and not necessarily musical) class of problems. Wave digital filters, even for filtering applications, are hardly as well-known here in the U.S. as they are in Europe, so it would not have been particularly helpful to anyone (or wise) to present a few results with only passing nods to the literature. Some rather extensive background information was thus compiled, in the form of a summary of most of the work that has gone on in this field to date (to this author's knowledge)[†]. Because of their fundamental similarities to these wave digital filtering simulation methods, waveguide networks were always slated for a (presumed cursory) second look; upon this reexamination, however, they seemed deserving of an in-depth parallel development all their own, requiring yet more background material.

Traditional approaches to numerical integration usually involve the direct discretization of a given set of equations by a variety of techniques, such as finite difference, finite element and spectral or collocation methods. The methods we will discuss, however, have their roots elsewhere, in electrical network theory, digital filtering and scattering theory. The most general goal of this author has been to provide a unified treatment of wave digital filtering and digital waveguide network simulation techniques, and also to answer, or at least pose some questions about how they fit into the larger picture of numerical integration methods as a whole. As might be expected, this thesis suffers in certain respects (notation among them) from the mismatch between the points of view of the electrical engineer and the specialist in numerical methods. Needless to say, there is much insight to be gained in the attempt to resolve some of the many outstanding distinctions.

---

[†] It is worth stating, for the record, that the single best reference on this subject is Gunnar Nitsche's doctoral dissertation [131]; I have referred to and borrowed from it quite a bit, and in fact, several topics in this thesis have appeared there, in a somewhat more compact form. Unfortunately, it is only available in German, and this was another reason for attempting a comprehensive review in English.

Looking back, one of the few regrets of this author has been the erosion of the emphasis on musical sound synthesis applications. Although we will spend a good deal of time later on looking at ways of extending these techniques to simulate the vibration of stiff systems such as beams, plates, and shells, which are the sound-producing mechanisms (resonators) in many musical instruments, we have not done the hard work of optimizing the algorithms for the audio frequency range—the computer program one writes in order to listen to a struck xylophone bar will assuredly be very different from one designed to check the modal frequencies of an I beam under stress. We have tried to lay down the basic principles, however, and nothing would be more rewarding than listening to a real-time waveguide or wave digital chime based on a cylindrical shell model.

# Acknowledgements

Stanford Electrical Engineering advising is notoriously overbooked. I thus feel very lucky to have had two advisers with whom I had frequent contact. My principal adviser, Professor Julius Smith, allowed me complete freedom in my choice of topic for this project, and through the CCRMA affiliates program, provided welcome financial support from the outset. Julius is a master of the trade, and I learned a lot by watching him at work. I thank my associate adviser, Ivan Linscott, of STAR Lab, for arranging funding during the latter part of my program, and for the numerous coffee breaks during which all sorts of wayward subjects, technical or not, were fair game. Both were always very cheerful, brimming with ideas, helpful in getting me motivated, and fair-minded. I also thank Professor Robert Gray of ISL, who served on my reading committee, and Professor Simon Wong of CIS, my orals chair. Finally, I thank the third member of my orals and reading committee, Professor Perry Cook of Princeton, who made a long trip out to the West Coast for my defense only to be greeted by foul October weather.

Professor Alfred Fettweis was very obliging and helped me to get my initial footing in this field, as was Gunnar Nitsche, who, during the course of a five-hour dinner (on him) in an empty Chinese restaurant in Hildesheim, Germany, took the trouble to explain his dissertation to me in English, page by page. This thesis is an outgrowth of their work, more than anyone else's, and I am greatly indebted to them. I also thank Dirk Dahlhaus, of the Swiss Federal Institute of Technology and Xiaomin Wang, formerly of the University of Notre Dame, for setting me straight on a few technical matters at the heart of wave digital filtering. Thanks also to the several members of the Stanford Mechanical Engineering department who took the time to talk with me: Professors Charles Steele and Thomas Hughes were especially helpful, as was Kian-Meng Lim. I'd also like to thank Jim Donohoe at Ames Research, as well as the members of the Radioscience Group at STAR lab. Thanks also to professor Eli Turkel of Tel Aviv University for getting me untangled with regard to some specifics of perfectly matched layers.

Thanks to the CCRMA DSP group members of my generation, all of whom I consulted frequently, namely Tim Stilson, Bill Putnam, Scott Levine, Gary Scavone and especially Scott Van Duyne (who got me interested in this topic at the outset), Tony Verma and Dave Berners, one of the few people I know who understands how things work. Thanks also to the many other friends I've made at CCRMA over the past few years, including Bob Sturm, Fabien Gouyon, Tamara Smyth, Hendrik Purwins, Patty Huang, Peer Landa, Stefania Serafina and Sile O'Modhrain. CCRMA is an exceptionally smoothly run lab, with a nearly invisible bureaucracy, and for this I thank Julius, Chris Chafe, John Chowning, Max Mathews, Heidi Kugler, Gary Scavone, and Vibeke Cleaver. A special thanks to our system administrator Fernando Lopez-Lezcano for not only keeping the network afloat, but for taking the time to get my own computer working (and I thank Dave Berners in this regard as well). Thanks also to Jay Kadis for allowing me to inhabit the CCRMA studios at a below-market rate. I wish them all well.

During my time as a student intern at IRCAM in Paris, Miller Puckette (now at UCSD) and David Zicarelli (now at Cycling'74) were instrumental in helping me get my bearings in computer music. I also send my best wishes to the late, great Professor Ivan Tcherepnin at Harvard.

Thanks to the many friends I made at Stanford over the last few years. I look forward to joining my fellow EE parolees Tony Verma and Rob Batchko on the outside.

My biggest thanks go to my family. I'd like to take the opportunity to dedicate this thesis to my sister, Maya. Catch her TV show "Structures" weeknights on Rogers Cable 10, in Toronto.

# Contents

**Preface** vii

**Acknowledgements** ix

**1 Introduction** **1**

- 1.1 An Overview of Scattering Methods . . . 3
  - 1.1.1 Case Study: The Kelly-Lochbaum Digital Speech Synthesis Model . . . 3
  - 1.1.2 Digital Waveguide Networks . . . 12
  - 1.1.3 A General Approach: Multidimensional Circuit Representations and Wave Digital Filters . . . 18
- 1.2 Questions . . . 25
- 1.3 Summary and Results . . . 26

**2 Wave Digital Filters** **33**

- 2.1 Introductory Remarks . . . 33
- 2.2 Classical Network Theory . . . 35
  - 2.2.1 N-ports . . . 35
  - 2.2.2 Power and Passivity . . . 36
  - 2.2.3 Kirchoff's Laws . . . 38
  - 2.2.4 Circuit Elements . . . 39
- 2.3 Wave Digital Elements and Connections . . . 41
  - 2.3.1 The Bilinear Transform . . . 41
  - 2.3.2 Wave Variables . . . 43
  - 2.3.3 Pseudopower and Pseudopassivity . . . 45
  - 2.3.4 Wave Digital Elements . . . 46
  - 2.3.5 Adaptors . . . 51
  - 2.3.6 Signal and Coefficient Quantization . . . 54
  - 2.3.7 Vector Wave Variables . . . 56

3 **Multidimensional Wave Digital Filters** **61**
3.1 Introductory Remarks . . . . . 61
3.2 Symmetric Hyperbolic Systems . . . . . 63
3.3 Coordinate Changes and Grid Generation . . . . . 67
3.3.1 Structure of Coordinate Changes . . . . . 68
3.3.2 Coordinate Changes in (1+1)D . . . . . 69
3.3.3 Coordinate Changes in Higher Dimensions . . . . . 70
3.4 MD-passivity . . . . . 73
3.5 MD Circuit Elements . . . . . 77
3.5.1 The MD Inductor . . . . . 77
3.5.2 Other MD Elements . . . . . 80
3.5.3 Discretization in the Spectral Domain . . . . . 81
3.5.4 Other Spectral Mappings . . . . . 83
3.6 The (1+1)D Advection Equation . . . . . 85
3.6.1 A Multidimensional Kirchoff Circuit . . . . . 85
3.6.2 Stability . . . . . 87
3.6.3 An Upwind Form . . . . . 88
3.7 The (1+1)D Transmission Line . . . . . 89
3.7.1 MDKC for the (1+1)D Transmission Line Equations . . . . . 90
3.7.2 Digression: Derivation of an Inductive Lattice Two-port . . . . . 92
3.7.3 A MDWD Network for the (1+1)D Transmission Line . . . . . 94
3.7.4 Energetic Interpretation . . . . . 95
3.7.5 Simplified Networks . . . . . 96
3.8 The (2+1)D Parallel-plate System . . . . . 98
3.8.1 MDKC and MDWD Network . . . . . 99
3.9 Finite Difference Interpretation . . . . . 101
3.9.1 MDWD Networks as Multi-step Schemes . . . . . 101
3.9.2 Numerical Phase Velocity and Parasitic Modes . . . . . 105
3.10 Initial Conditions . . . . . 109
3.11 Boundary Conditions . . . . . 112
3.12 Balanced Forms . . . . . 115
3.13 Higher-order Accuracy . . . . . 119

4 **Digital Waveguide Networks** **127**
4.1 Introductory Remarks . . . . . 127
4.1.1 FDTD and TLM . . . . . 129
4.2 Digital Waveguides . . . . . 130
4.2.1 The Bidirectional Delay Line . . . . . 130

4.2.2 Impedance . . . . . . . . . . . . . . . . . . . . . . . . . . . . . . . 131
4.2.3 Wave Equation Interpretation . . . . . . . . . . . . . . . . . . . . . 132
4.2.4 Note on the Different Definitions of Wave Quantities . . . . . . . . . . . . . 132
4.2.5 Scattering Junctions . . . . . . . . . . . . . . . . . . . . . . . . . . 134
4.2.6 Vector Waveguides and Scattering Junctions . . . . . . . . . . . . . . . 136
4.2.7 Music and Audio Applications of Digital Waveguides . . . . . . . . . . . . . 139
4.2.8 Transitional Note . . . . . . . . . . . . . . . . . . . . . . . . . . . 141
4.3 The (1+1)D Transmission Line . . . . . . . . . . . . . . . . . . . . . . . . 141
4.3.1 First-order System and the Wave Equation . . . . . . . . . . . . . . . . 142
4.3.2 Centered Difference Schemes and Grid Decimation . . . . . . . . . . . . . . 142
4.3.3 A (1+1)D Waveguide Network . . . . . . . . . . . . . . . . . . . . . . 145
4.3.4 Waveguide Network and the Wave Equation . . . . . . . . . . . . . . . . 147
4.3.5 An Interleaved Waveguide Network . . . . . . . . . . . . . . . . . . . . 148
4.3.6 Varying Coefficients . . . . . . . . . . . . . . . . . . . . . . . . . . 151
4.3.7 Incorporating Losses and Sources . . . . . . . . . . . . . . . . . . . . 157
4.3.8 Numerical Phase Velocity and Dispersion . . . . . . . . . . . . . . . . . 160
4.3.9 Boundary Conditions . . . . . . . . . . . . . . . . . . . . . . . . . . 161
4.4 The (2+1)D Parallel-plate System . . . . . . . . . . . . . . . . . . . . . . 163
4.4.1 Defining Equations and Centered Differences . . . . . . . . . . . . . . . 164
4.4.2 The Waveguide Mesh . . . . . . . . . . . . . . . . . . . . . . . . . . 166
4.4.3 Reduced Computational Complexity and Memory Requirements in the Standard Form of the Waveguide Mesh . . . . . . . . . . . . . . . . . . . . . 174
4.4.4 Boundary Conditions . . . . . . . . . . . . . . . . . . . . . . . . . . 176
4.5 Initial Conditions . . . . . . . . . . . . . . . . . . . . . . . . . . . . . . 180
4.6 Alternative Grids in (2+1)D . . . . . . . . . . . . . . . . . . . . . . . . . 183
4.6.1 Hexagonal and Triangular Grids . . . . . . . . . . . . . . . . . . . . . 183
4.6.2 The Waveguide Mesh in Radial Coordinates . . . . . . . . . . . . . . . . 186
4.7 The (3+1)D Wave Equation and Waveguide Meshes . . . . . . . . . . . . . . 193
4.8 The Waveguide Mesh in General Curvilinear Coordinates . . . . . . . . . . . . 196
4.9 Interfaces Between Grids . . . . . . . . . . . . . . . . . . . . . . . . . . 201
4.9.1 Doubled Grid Density Across an Interface . . . . . . . . . . . . . . . . . 202
4.9.2 Progressive Grid Density Doubling . . . . . . . . . . . . . . . . . . . . 208
4.9.3 Grid Density Quadrupling . . . . . . . . . . . . . . . . . . . . . . . . 211
4.9.4 Connecting Rectilinear and Radial Grids . . . . . . . . . . . . . . . . . . 214
4.9.5 Grid Density Doubling in (3+1)D . . . . . . . . . . . . . . . . . . . . 217
4.9.6 Note . . . . . . . . . . . . . . . . . . . . . . . . . . . . . . . . . . 219
4.10 Incorporating the DWN into the MDWD Framework . . . . . . . . . . . . . . . 219

4.10.1 Multidimensional Unit Elements . . . . . . . . . . . . . . . . . . . . . . . . . . 221
4.10.2 Hybrid Form of the Multidimensional Unit Element . . . . . . . . . . . . . . . 223
4.10.3 Alternative MDKC for the (1+1)D Transmission Line . . . . . . . . . . . . . 224
4.10.4 Alternative MDKC for (2+1)D Parallel-plate System . . . . . . . . . . . . . . 227
4.10.5 Higher-order Accuracy Revisited . . . . . . . . . . . . . . . . . . . . . . . . 229
4.10.6 Maxwell's Equations . . . . . . . . . . . . . . . . . . . . . . . . . . . . . . 232

**5 Applications in Vibrational Mechanics 239**

5.1 Transverse Motion of the Ideal Beam . . . . . . . . . . . . . . . . . . . . . . . . 240
5.1.1 Finite Differences . . . . . . . . . . . . . . . . . . . . . . . . . . . . . . . . 241
5.1.2 Waveguide Network for the Euler-Bernoulli System . . . . . . . . . . . . . . . 242
5.1.3 Boundary Conditions in the Waveguide Network . . . . . . . . . . . . . . . . 247
5.2 Timoshenko's Beam Equations . . . . . . . . . . . . . . . . . . . . . . . . . . . 249
5.2.1 MDKC and MDWDF for Timoshenko's System . . . . . . . . . . . . . . . . . 252
5.2.2 Waveguide Network for Timoshenko's System . . . . . . . . . . . . . . . . . 254
5.2.3 Other Waveguide Networks for Timoshenko's System . . . . . . . . . . . . . . 256
5.2.4 Boundary Conditions in the DWN . . . . . . . . . . . . . . . . . . . . . . . . 260
5.2.5 Simulation: Timoshenko's System for Beams of Uniform and Varying Cross-sectional Areas . . . . . . . . . . . . . . . . . . . . . . . . . . . . . . . . 261
5.2.6 Improved MDKC for Timoshenko's System Via Balancing . . . . . . . . . . . 263
5.3 Longitudinal and Torsional Waves in Rods . . . . . . . . . . . . . . . . . . . . . 265
5.4 Plates . . . . . . . . . . . . . . . . . . . . . . . . . . . . . . . . . . . . . . . . 265
5.4.1 MDKCs and Scattering Networks for Mindlin's System . . . . . . . . . . . . . 269
5.4.2 Boundary Termination of the Mindlin Plate . . . . . . . . . . . . . . . . . . . 273
5.4.3 Simulation: Mindlin's System, for Plates of Uniform and Varying Thickness . 278
5.5 Cylindrical Shells . . . . . . . . . . . . . . . . . . . . . . . . . . . . . . . . . . 280
5.5.1 The Membrane Shell . . . . . . . . . . . . . . . . . . . . . . . . . . . . . . . 280
5.5.2 The Naghdi-Cooper System II Formulation . . . . . . . . . . . . . . . . . . . 282
5.6 Elastic Solids . . . . . . . . . . . . . . . . . . . . . . . . . . . . . . . . . . . . 285
5.6.1 Scattering Networks for the Navier System . . . . . . . . . . . . . . . . . . . 287
5.6.2 Boundary Conditions . . . . . . . . . . . . . . . . . . . . . . . . . . . . . . . 288

**6 Conclusions and Future Directions 293**

6.1 Answers . . . . . . . . . . . . . . . . . . . . . . . . . . . . . . . . . . . . . . . 293
6.2 Future Directions . . . . . . . . . . . . . . . . . . . . . . . . . . . . . . . . . . 299
6.2.1 Passivity vs. Stability . . . . . . . . . . . . . . . . . . . . . . . . . . . . . . 300
6.2.2 Higher-order Accuracy . . . . . . . . . . . . . . . . . . . . . . . . . . . . . . 300
6.2.3 MDKC Modeling of Boundaries . . . . . . . . . . . . . . . . . . . . . . . . . 301

6.2.4 Multi-grid Methods Using MDKCs . . . . . . . . . . . . . . . . . . . . . . . 304
6.2.5 Spectral Mappings and Network Transformations . . . . . . . . . . . . . . . 305
6.2.6 Finite Arithmetic Testing . . . . . . . . . . . . . . . . . . . . . . . . 306
6.2.7 Time-varying Systems . . . . . . . . . . . . . . . . . . . . . . . . . 306

**Afterword** **311**

**A Finite Difference Schemes for the Wave Equation** **313**

A.1 Von Neumann Analysis of Difference Schemes . . . . . . . . . . . . . . . . . . . 313
A.1.1 One-step Schemes . . . . . . . . . . . . . . . . . . . . . . . . . . 314
A.1.2 Multi-step Schemes . . . . . . . . . . . . . . . . . . . . . . . . . . 315
A.1.3 Vector Schemes . . . . . . . . . . . . . . . . . . . . . . . . . . . 318
A.1.4 Numerical Phase Velocity . . . . . . . . . . . . . . . . . . . . . . . 319
A.2 Finite Difference Schemes for the (2+1)D Wave Equation . . . . . . . . . . . . . 319
A.2.1 The Rectilinear Scheme . . . . . . . . . . . . . . . . . . . . . . . . 320
A.2.2 The Interpolated Rectilinear Scheme . . . . . . . . . . . . . . . . . . 322
A.2.3 The Triangular Scheme . . . . . . . . . . . . . . . . . . . . . . . . 326
A.2.4 The Hexagonal Scheme . . . . . . . . . . . . . . . . . . . . . . . . 328
A.2.5 A Fourth-order Scheme . . . . . . . . . . . . . . . . . . . . . . . . 332
A.3 Finite Difference Schemes for the (3+1)D Wave Equation . . . . . . . . . . . . . 335
A.3.1 The Cubic Rectilinear Scheme . . . . . . . . . . . . . . . . . . . . . 336
A.3.2 The Octahedral Scheme . . . . . . . . . . . . . . . . . . . . . . . . 338
A.3.3 The (3+1)D Interpolated Rectilinear Scheme . . . . . . . . . . . . . . . 340
A.3.4 The Tetrahedral Scheme . . . . . . . . . . . . . . . . . . . . . . . . 344

**B Applications in Fluid Dynamics** **347**

B.1 Nonlinear Circuit Elements . . . . . . . . . . . . . . . . . . . . . . . . . 347
B.2 Burger's Equation . . . . . . . . . . . . . . . . . . . . . . . . . . . . . 349
B.3 The Gas Dynamics Equations . . . . . . . . . . . . . . . . . . . . . . . . 351
B.3.1 MDKC and MDWDF for the Gas Dynamics Equations . . . . . . . . . . . . 353
B.3.2 An Alternate MDKC and Scattering Network . . . . . . . . . . . . . . . . 355
B.3.3 Entropy Variables . . . . . . . . . . . . . . . . . . . . . . . . . . 357

**Bibliography** **361**

# List of Figures

1.1 *Concatenated acoustic tube model of the vocal tract.* . . . . 4

1.2 *An acoustic tube and a representation of the traveling wave solution.* . . . . 6

1.3 *Junction between two acoustic tubes.* . . . . 6

1.4 *Signal flow graph for an $N$ tube vocal tract model.* . . . . 9

1.5 *All-pole lattice filter.* . . . . 11

1.6 *A portion of a general network of one-dimensional acoustic tubes and its digital realization using of paired bidirectional delay lines and scattering junctions.* . . . . 13

1.7 *Junction of $M$ acoustic tubes.* . . . . 14

1.8 *Regular mesh of acoustic tubes, and the associated DWN.* . . . . 16

1.9 *Wave digital discretization of a one-port circuit element.* . . . . 20

1.10 *Wave digital discretization of a parallel connection of two one-ports.* . . . . 20

1.11 *Wave digital discretization of an LC harmonic oscillator.* . . . . 22

1.12 *Multidimensional wave digital discretization of a distributed one-port circuit element.* 24

1.13 *Steps in the construction of a multidimensional wave digital filtering simulation routine.* 24

1.14 *Steps in the construction of multidimensional wave digital filtering and digital waveguide network simulation routines, viewed as part of a generalized family of passive numerical methods.* . . . . 29

2.1 *N-port.* . . . . 35

2.2 *Kirchoff connections of $M$ ports.* . . . . 38

2.3 *One-port elements.* . . . . 39

2.4 *Other one-ports.* . . . . 40

2.5 *Two-ports.* . . . . 41

2.6 *Spectral mapping corresponding to the trapezoid rule.* . . . . 42

2.7 *Wave digital one-ports.* . . . . 47

2.8 *Other wave digital one-ports.* . . . . 48

2.9 *Resistive voltage source.* . . . . 48

2.10 *Wave digital two-ports.* . . . . 49

2.11 *The unit element and its continuous-time counterparts.* . . . . . . . . . . . . . . . . . . 50
2.12 *Three-port adaptors.* . . . . . . . . . . . . . . . . . . . . . . . . . . . . . . . . . . 52
2.13 *Signal truncation at a three-port adaptor.* . . . . . . . . . . . . . . . . . . . . . . . . 55
2.14 *Three-port vector adaptors.* . . . . . . . . . . . . . . . . . . . . . . . . . . . . . . 57
2.15 *Coupled inductance and capacitance.* . . . . . . . . . . . . . . . . . . . . . . . . . . 58
2.16 *Wave digital coupled inductances and capacitances.* . . . . . . . . . . . . . . . . . . . 59

3.1 *Sampling grids.* . . . . . . . . . . . . . . . . . . . . . . . . . . . . . . . . . . . . 70
3.2 *(2+1)D sampling grids.* . . . . . . . . . . . . . . . . . . . . . . . . . . . . . . . . 71
3.3 *k-dimensional domain G.* . . . . . . . . . . . . . . . . . . . . . . . . . . . . . . . . 74
3.4 *Inductor and its wave digital one-port.* . . . . . . . . . . . . . . . . . . . . . . . . . 77
3.5 *MDWD one-ports.* . . . . . . . . . . . . . . . . . . . . . . . . . . . . . . . . . . . 81
3.6 *MDKC and MDWD network for the (1+1)D advection equation.* . . . . . . . . . . . . 86
3.7 *Signal flow graph for Figure 3.6(b).* . . . . . . . . . . . . . . . . . . . . . . . . . . 86
3.8 *Simplified signal flow graph for Figure 3.6(b), for* $v_0 = |\alpha|$, $\alpha < 0$. . . . . . . . . . . . 87
3.9 *An upwind-differencing form for the advection equation.* . . . . . . . . . . . . . . . . 88
3.10 *Signal flow graph for Figure 3.9(b), for* $\alpha > 0$. . . . . . . . . . . . . . . . . . . . . 89
3.11 *MDKCs for the (1+1)D transmission line system.* . . . . . . . . . . . . . . . . . . . . 91
3.12 *Equivalent two-ports.* . . . . . . . . . . . . . . . . . . . . . . . . . . . . . . . . . . 92
3.13 *Signal flow diagram for the MDWD lattice or Jaumann two-port.* . . . . . . . . . . . . 94
3.14 *MD-passive forms for the (1+1)D transmission line equations.* . . . . . . . . . . . . . . 94
3.15 *Simplified MDWD network for the (1+1)D transmission line equations.* . . . . . . . . 96
3.16 *Signal flow graph for the MDWD network of Figure 3.15(b).* . . . . . . . . . . . . . . . 97
3.17 *MDKC for the (2+1)D parallel-plate system in rectangular coordinates.* . . . . . . . . . 99
3.18 *MDWD network for the (2+1)D parallel-plate system, in rectangular coordinates.* . . . 100
3.19 *Simplified MDWD network for the (2+1)D transmission line equations, in the lossless, source-free and constant parameter case.* . . . . . . . . . . . . . . . . . . . . . . . . . . 101
3.20 *Computational stencils of the equivalent multi-step schemes of MDWD networks for the (1+1)D transmission line equations.* . . . . . . . . . . . . . . . . . . . . . . . . . . 105
3.21 *Steady-state MDWD network for the lossless, source-free constant-coefficient (1+1)D transmission-line equations.* . . . . . . . . . . . . . . . . . . . . . . . . . . . . . . . 106
3.22 *MDWD network for the source-free (1+1)D transmission line equations.* . . . . . . . . 110
3.23 *Balanced MDKC for the (1+1)D transmission line equations.* . . . . . . . . . . . . . . 117
3.24 *Unit shifts in the coordinates defined by* (3.90). . . . . . . . . . . . . . . . . . . . . . 120
3.25 *MDKC for the lossless source-free transmission line equations, according to the decomposition given by* (3.92). . . . . . . . . . . . . . . . . . . . . . . . . . . . . . . . . 122
3.26 *Unit shifts in the coordinates defined by* (3.98). . . . . . . . . . . . . . . . . . . . . . 124

4.1 *Bidirectional delay line.* . . . . . . . . . . 130
4.2 *Oriented bidirectional delay line.* . . . . . . . . . . 133
4.3 *Graphical representations of scattering 4-port junctions.* . . . . . . . . . . 136
4.4 *Waveguide splitter.* . . . . . . . . . . 138
4.5 *Typical digital waveguide configuration for musical sound synthesis.* . . . . . . . . . . 139
4.6 *Other waveguide network configurations.* . . . . . . . . . . 141
4.7 *Interleaved sampling grid for the (1+1)D transmission line.* . . . . . . . . . . 144
4.8 *(1+1)D waveguide network.* . . . . . . . . . . 145
4.9 *Simplified (1+1)D waveguide network.* . . . . . . . . . . 147
4.10 *Bidirectional delay line.* . . . . . . . . . . 149
4.11 *Split equivalent to the bidirectional delay line.* . . . . . . . . . . 149
4.12 *(1+1)D interleaved waveguide network.* . . . . . . . . . . 149
4.13 *Wave quantities in the interleaved network of Figure 4.12.* . . . . . . . . . . 150
4.14 *Waveguide network for the (1+1)D transmission line equations with spatially-varying coefficients.* . . . . . . . . . . 151
4.15 *Waveguide network for system* (4.43). . . . . . . . . . . 159
4.16 *Numerical dispersion curves for various values of* $\lambda$. . . . . . . . . . . 161
4.17 *Boundary terminations of the waveguide network.* . . . . . . . . . . 162
4.18 *Interleaved computational grid for the (2+1)D parallel-plate system.* . . . . . . . . . . 166
4.19 *(2+1)D waveguide mesh and a representative scattering junction.* . . . . . . . . . . 167
4.20 *(2+1)D interleaved waveguide mesh.* . . . . . . . . . . 169
4.21 *(2+1)D waveguide mesh for the varying-coefficient system* (4.58), *with losses and sources.* . . . . . . . . . . 172
4.22 *Grid decomposition for the standard waveguide mesh.* . . . . . . . . . . 175
4.23 *Grid terminations at a southern boundary.* . . . . . . . . . . 176
4.24 *(2+1)D waveguide mesh terminations at a southern boundary, for the grid arrangement of Figure 4.23(a).* . . . . . . . . . . 179
4.25 *(2+1)D waveguide mesh terminations at a southern boundary, for the grid of Figure 4.23(b).* . . . . . . . . . . 180
4.26 *Alternative sampling grids.* . . . . . . . . . . 183
4.27 *Scattering junctions on hexagonal and triangular grids.* . . . . . . . . . . 184
4.28 *Interleaved grid in radial coordinates.* . . . . . . . . . . 188
4.29 *Waveguide mesh for the (2+1)D parallel-plate system, in radial coordinates.* . . . . . . . . . . 189
4.30 *Representative scattering junctions for the waveguide mesh for the (2+1)D parallel-plate system, in radial coordinates.* . . . . . . . . . . 190
4.31 *Central scattering junction for the waveguide mesh in radial coordinates.* . . . . . . . . . . 191
4.32 *Simulation of a circular parallel-plate system using a radial waveguide mesh.* . . . . . . . . . . 194

4.33 *Regular grids in (3+1)D.* . . . . . 195
4.34 *(2+1)D DWN for the parallel-plate system in general non-orthogonal curvilinear coordinates.* . . . . . 199
4.35 *Interface between mesh and mesh with doubled grid density* . . . . . 202
4.36 *Irregular interface between meshes of differing densities.* . . . . . 205
4.37 *Simulation of a parallel-plate system, with an inductive feature surrounded by a region of doubled grid density.* . . . . . 208
4.38 *Progressive grid density doubling.* . . . . . 209
4.39 *Grid density quadrupling across an interface.* . . . . . 211
4.40 *Numerical reflection at mesh interfaces.* . . . . . 213
4.41 *Interface between radial and rectilinear meshes.* . . . . . 214
4.42 *Simulation of wave propagation in a U-shaped tube.* . . . . . 217
4.43 *Grid density doubling across an interface in (3+1)D.* . . . . . 218
4.44 *Signal flow diagrams of the DWN and MDWD networks for the (1+1)D lossless source-free transmission line.* . . . . . 220
4.45 *Multidimensional unit element.* . . . . . 222
4.46 *Series/parallel connection of N two-ports.* . . . . . 224
4.47 *MDKCs for the lossless source-free (1+1)D transmission line equations.* . . . . . 225
4.48 *MD network equivalent to type III DWN for the lossless source-free (1+1)D transmission line equations under an alternative spectral mapping.* . . . . . 227
4.49 *Alternative MDKC for the (2+1)D parallel-plate system in rectangular coordinates.* . . 228
4.50 *MD network equivalent to type III DWN for the lossless source-free (2+1)D parallel-plate system under an alternative spectral mapping.* . . . . . 229
4.51 *Modified MDKC for the lossless, source-free (1+1)D transmission line system.* . . . . 230
4.52 *Multidimensional DWN suitable for a qth-order spatially accurate solution to the (1+1)D transmission line equations.* . . . . . 232
4.53 *MDKC and MDWD network for Maxwell's equations.* . . . . . 236
4.54 *Modified MDKC and multidimensional DWN for Maxwell's equations.* . . . . . 237
4.55 *Computational grid for FDTD applied to Maxwell's equations.* . . . . . 238

5.1 *(1+1)D DWN for the Euler-Bernoulli system.* . . . . . 243
5.2 *Scattering junctions of Figure 5.1, with incoming and outgoing voltage waves indicated.*244
5.3 *An equivalent form for duplicate bidirectional delay lines running between a parallel and a series junction.* . . . . . 244
5.4 *Boundary terminations for the Euler-Bernoulli system.* . . . . . 250
5.5 *MDKC for Timoshenko's system.* . . . . . 253
5.6 *MDWD network for Timoshenko's system.* . . . . . 253
5.7 *Transformed MDKC for Timoshenko's system.* . . . . . 254

5.8 *Waveguide network for Timoshenko's system, in a multidimensional form.* . . . . . . 255
5.9 *DWN for Timoshenko's system.* . . . . . . . . . . . . . . . . . . . . . . . . . . . . 255
5.10 *An alternate DWN for Timoshenko's system.* . . . . . . . . . . . . . . . . . . . . . 257
5.11 *Another alternate DWN for Timoshenko's system.* . . . . . . . . . . . . . . . . . . 258
5.12 *Left end boundary terminations for the DWN for Timoshenko's system.* . . . . . . . 261
5.13 *Simulation: evolution of the transverse velocity distribution along a Timoshenko beam of uniform thickness, with free ends.* . . . . . . . . . . . . . . . . . . . . . . . . . 262
5.14 *Simulation: evolution of the transverse velocity distribution along a Timoshenko beam of linearly-varying thickness, with clamped ends.* . . . . . . . . . . . . . . . . . . . 262
5.15 *Balanced MDKC for Timoshenko's system.* . . . . . . . . . . . . . . . . . . . . . . 264
5.16 *MDKC and MDWD network for Mindlin's system.* . . . . . . . . . . . . . . . . . . . 270
5.17 *Modified MDKC and multidimensional DWN for Mindlin's system.* . . . . . . . . . . 271
5.18 *Computational grid for the DWN for Mindlin's system.* . . . . . . . . . . . . . . . . 273
5.19 *Southern computational grid boundary at $y = 0$ for the DWN for Mindlin's system.* . 274
5.20 *Various lossless southern boundary terminations for the DWN for Mindlin's system.* 276
5.21 *DWN simulation of Mindlin's system, for a steel plate of uniform thickness, with free edges.* . . . . . . . . . . . . . . . . . . . . . . . . . . . . . . . . . . . . . . . . 279
5.22 *DWN simulation of Mindlin's system, for a steel plate of varying thickness, with clamped edges.* . . . . . . . . . . . . . . . . . . . . . . . . . . . . . . . . . . . . . 279
5.23 *MDKC for the cylindrical membrane shell system.* . . . . . . . . . . . . . . . . . . 282
5.24 *Computational grid for the DWN for Naghdi and Cooper's system II.* . . . . . . . . . 284
5.25 *MDKC and MDWD network for the Navier system.* . . . . . . . . . . . . . . . . . . 289
5.26 *Modified MDKC and multidimensional DWN for the Navier system.* . . . . . . . . . 290
5.27 *Computational grid for the DWN for Navier's system.* . . . . . . . . . . . . . . . . 291

6.1 *Network decomposition of passive symmetric hyperbolic systems.* . . . . . . . . . . . . 294
6.2 *The generalized family of passive numerical methods.* . . . . . . . . . . . . . . . . . 298
6.3 *A region with one spatial boundary.* . . . . . . . . . . . . . . . . . . . . . . . . . . 303
6.4 *MDKC for the time-varying (1+1)D transmission line system.* . . . . . . . . . . . . 309

A.1 *Computational grid and numerical dispersion for the rectilinear scheme.* . . . . . . . 321
A.2 *Computational grid and numerical dispersion for the interpolated rectilinear scheme.* 323
A.3 *Stability bounds for the interpolated rectilinear scheme.* . . . . . . . . . . . . . . . . 325
A.4 *Computational grid and numerical dispersion for the triangular scheme.* . . . . . . . 328
A.5 *Computational grid and numerical dispersion for the hexagonal scheme.* . . . . . . . 331
A.6 *Stability bound for the fourth-order scheme.* . . . . . . . . . . . . . . . . . . . . . . 334
A.7 *Computational grid and numerical dispersion for the fourth-order scheme.* . . . . . . 335
A.8 *Computational grid and numerical dispersion for the cubic rectilinear scheme.* . . . . 337

A.9 *Computational grid and numerical dispersion for the octahedral scheme.* . . . . . . . . 339
A.10 *Stability and passivity bounds for the (3+1)D interpolated rectilinear scheme.* . . . . . 341
A.11 *Computational grid and numerical dispersion for the (3+1)D interpolated rectilinear scheme.* . . . . . . . . . . . . . . . . . . . . . . . . . . . . . . . . . . . . . . . . . 343
A.12 *Computational grid and numerical dispersion for the tetrahedral scheme.* . . . . . . . . 346

B.1 *MDKC and MDWD network for the (1+1)D inviscid Burger's equation.* . . . . . . . . 350
B.2 *MDKC and MDWD network for the (1+1)D gas dynamics system.* . . . . . . . . . . . 354
B.3 *Alternative networks for the (1+1)D gas dynamics system.* . . . . . . . . . . . . . . . . 356

# Chapter 1

# Introduction

The subject of this thesis is the numerical simulation of physical systems. In particular, we look at systems which are dynamic and distributed. By *dynamic*, we mean that the system's state evolves as time progresses, and by *distributed*, that the system is defined over some region in space, called the *problem domain*. The systems of interest here, always described mathematically by sets of partial differential equations (PDEs) complemented by initial and boundary conditions and possibly external excitations, span a large range of physical scenarios, including electromagnetics, acoustics, transmission lines, the vibration of elastic systems such as strings, membranes, beams, plates and shells, and even nonlinear fluid dynamics.

The simulation techniques that we will discuss are based on analogies between the systems mentioned above and electrical networks, and make use of *scattering* principles. The time-evolution of the state of a system is modeled as the movement of energy as it is reflected, transmitted and propagated throughout an electrical network; the energy is carried by *waves*. The chief benefit of a network formulation is that there is direct access to a measure of the system energy, which can be used to bound the size of the solution of the system as it evolves over time. Because many physical systems, in the absence of external excitations, are inherently *passive* (i.e., they do not produce energy on their own), a network model for a system of PDEs is useful in that this passivity is reflected in an obvious way; a simple positivity condition on all the circuit element values is all that is required. When such a network model is transferred to a discrete setting in an appropriate way (where it will eventually be implemented as a computer program, operating as a recursion over a numerical grid), this passivity condition becomes a sufficient and trivially verifiable condition for the *numerical stability* of the resulting simulation. It is interesting that these numerical methods have their roots in *digital filter design* techniques, which were, in turn, based on discrete physical models of mechanical or electrical circuit elements and the connections between them. In a sense, then, simulation is a more "natural" use for these structures than filtering. Many important ideas regarding the good behavior of these methods in finite machine arithmetic, however, were first introduced in the filtering context—these also result from passivity in the network model.

We will be primarily concerned with two such methods. The first is based on *wave digital filtering*, a filter design technique which was initially intended as a means of translating a lumped analog electrical filtering network into discrete time, while preserving its topology and energetic properties (passivity in particular). Because the voltages and currents in a closed analog electrical network will evolve according to a set of *ordinary differential equations* (ODEs), these digital filter networks can also be viewed as numerical integration methods. The extension of wave digital filters to multiple dimensions, in which case they are referred to as *multidimensional wave digital filters* (MDWDFs), is direct and makes use of a distributed network formulation of a given system as a means of arriving at a simulation routine. Here there is a compact (though quite abstract) multidimensional circuit representation of the model system of PDEs, just as a lumped network is a representation of a system of ODEs. Despite the sometimes abstruse formalism underlying the construction of MDWDFs for simulation (invoking various coordinate changes, spectral mappings, and the use of non-physical "circuit elements" which are distributed, and may have a directional character), these numerical methods always involve the scattering of digital signals over a numerical grid of nodes which fills the problem domain, and are straightforward to program.

The second method, though very similar to the first from the standpoint of the programmer, in that the basic signal processing operation is the scattering of wave variables, is of a seemingly different origin. Here, the network is composed of a large number of connected elements, which are essentially transmission lines, or *waveguides*, so as to fill the problem domain. Wave propagation along a given waveguide is modeled, in discrete time, by a pair of digital delay lines which transport wave signals in opposite directions. A *digital waveguide network* (DWN), then, is usually thought of as a large network of *lumped* elements; there is traditionally not a multidimensional representation, as there is for MDWDFs. We will spend some time looking at the relationship between DWNs and the MDWD networks mentioned above.

These network approaches are relative newcomers in the field of numerical simulation. There are, of course, many other, older ways of designing a simulation method; the most well-established and straightforward tack makes use of *finite difference approximations* to the model system of PDEs. Partial derivatives are replaced by differences between quantities on a numerical grid, and a recursion (or difference scheme) results. These methods are simpler to program, but the wave/scattering interpretation is lost, and the verification of numerical stability can be very involved, especially in the presence of boundary conditions. Because the electrical network models mentioned above also operate, ultimately, as recursions on grids, it is reasonable to ask how scattering methods fit into the finite difference picture. The eventual identification of scattering methods with standard finite difference methods may come as something of a disappointment to anyone who feels that these methods are completely novel. It is best, however, to think of these methods as a different way of organizing calculation, which leads to more robust numerical behavior. As might be expected, an analogous situation exists in filter design between direct form and ladder/lattice/orthogonal structures.

The most general goal of this thesis is to provide a unified picture of how these scattering methods are related to each other and to finite differences. It is possible to rephrase this goal as an attempt to answer a basic set of questions; we will pose these questions in §1.2. Before we get to that stage, however, it is useful to outline the basics of these methods in a little more detail.

## 1.1 An Overview of Scattering Methods

In all of the next chapter and in large parts of the following two, we will be forced to make a long detour in order to fully lay out the details of how scattering-based numerical simulation methods are designed. In this section, we take a brief and informal look at many of the relevant ideas, while putting aside the full development until later. The reader who has some familiarity with wave digital filters and digital waveguide networks may safely skip this section.

### 1.1.1 Case Study: The Kelly-Lochbaum Digital Speech Synthesis Model

As we mentioned above, all the numerical methods to be discussed in this thesis have their origin in digital filter design, even though they are intended, ultimately, for use in simulation, and not filtering. Though these two goals may seem to be at cross purposes, there is a very early instance of an engineering problem which straddles both worlds.

Kelly and Lochbaum [104] developed a digital speech synthesis model by treating the vocal tract as a slowly time-varying circular one-dimensional acoustic tube of variable cross-sectional area, excited at one end (periodically by the glottis, or by turbulent noise), and radiating a speech waveform at the other—see Figure 1.1(a). At any given time $t$, the shape of the tube as a function of the spatial coordinate $x$ determines the system resonances, or formants [145], which serve as important perceptual cues for the listener in distinguishing among various voiced and unvoiced vocal sounds. The problem, then, is to develop a numerical method, suitable for computer implementation, which somehow simulates the time-evolution of the acoustic "state" of the vocal tract, i.e., the *pressure* and *velocity* distributions in the interior. We follow the standard exposition of the Kelly–Lochbaum model here, as per [30, 145].

#### Concatenated Acoustic Tube Model of the Vocal Tract

The first step towards a digital model is in representing the tube as a series of $N$ concatenated tubes of constant cross-sectional areas, as in Figure 1.1(b) (where $N$=8). The tubes are assumed to be of equal length $\Delta$; if $L$ is the total length of the vocal tract, we have $N\Delta = L$. In the limit as $\Delta$ becomes small, the shape of the approximation of the series of tubes will converge to that of continuous vocal tract shown in Figure 1.1(a).

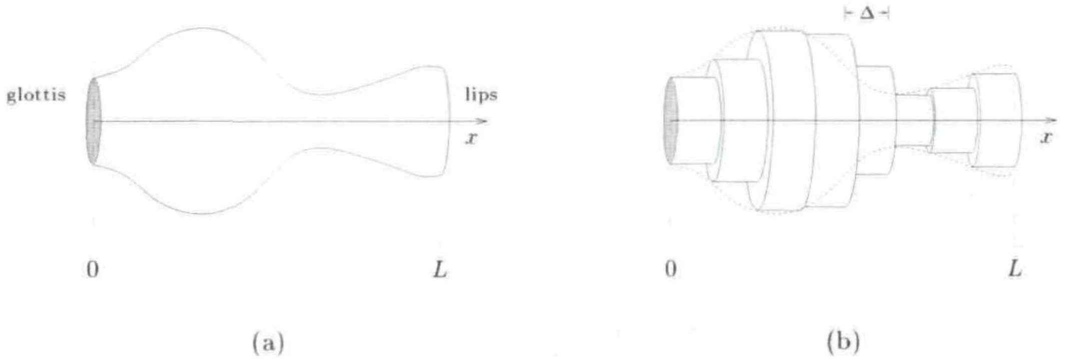

Figure 1.1: (a) *The vocal tract, modeled as a single one-dimensional acoustic tube of varying cross-sectional area and* (b) *an eight tube model suitable for discretization.*

### Wave Propagation in a Tube of Constant Cross-Sectional Area

The concatenated tube model is useful because the acoustic behavior of a single tube of constant cross-sectional area $A$ is quite simple to describe, in terms of a volume velocity $u(x,t)$, and a pressure deviation $p(x,t)$ from the mean tube pressure. Provided wavelengths are long in comparison with the tube radius, and that pressures do not become too large (both these requirements are easily satisfied in the speech context), the time-evolution of the acoustic state of any single tube, such as that shown in Figure 1.2(a), will be described completely by

$$
\begin{aligned}
\frac{\rho}{A}\frac{\partial u}{\partial t} + \frac{\partial p}{\partial x} &= 0 && \text{(1.1a)}\\
\frac{A}{\rho\gamma^2}\frac{\partial p}{\partial t} + \frac{\partial u}{\partial x} &= 0 && \text{(1.1b)}
\end{aligned}
$$

subject, of course, to initial conditions, and the effect of the boundary terminations on adjacent tubes. Given that the cross-sectional tube area $A$, the air density $\rho$ and the sound-speed $\gamma$ are constant, the general solution to (1.1) can be written as

$$
\begin{aligned}
p(x,t) &= p^l(t+x/\gamma) + p^r(t-x/\gamma) && \text{(1.2a)}\\
u(x,t) &= \underbrace{Yp^l(t+x/\gamma)}_{u^l} \; \underbrace{-Yp^r(t-x/\gamma)}_{u^r} && \text{(1.2b)}
\end{aligned}
$$

Here the physical pressure $p$ has been decomposed into a sum of a *leftward-traveling wave* $p^l$ and a *rightward-traveling wave* $p^r$; both are arbitrary functions of one variable. The volume velocity $u$, which is dual to $p$ in the system (1.1), can be similarly expressed as a sum of leftward- and rightward-traveling velocity waves $u^l$ and $u^r$. But these velocity waves are simply the pressure waves, scaled by the tube *admittance*, defined by

$$Y \triangleq \frac{A}{\rho\gamma}$$

In addition, the rightward-traveling wave component of the velocity is sign-inverted with respect to the corresponding pressure wave.

System (1.1) can be simplified to a single second-order PDE in pressure alone,

$$\frac{\partial^2 p}{\partial t^2} = \gamma^2 \frac{\partial^2 p}{\partial x^2} \tag{1.3}$$

from which the traveling pressure wave solution is more easily extracted. The volume velocity satisfies an identical equation.

Consider one of the tube segments of length $\Delta$ from Figure 1.1(b). It should be clear that we can represent the pressure traveling-wave solution to (1.1) by using two delay lines, each of duration $\Delta/\gamma$; see Figure 1.2. We can obtain the physical pressure at either ends of the tube by summing the leftward- and rightward-traveling components, as per (1.2a). (The physical volume velocity can be obtained, from (1.2b), by taking the difference of $p^l$ and $p^r$, and scaling the result by $Y$.) The discrete-time implementation of this single isolated acoustic tube is immediate. Taking

$$T \triangleq \frac{\Delta}{\gamma} \tag{1.4}$$

as the *unit delay*, or *sampling period* for our discrete-time system, we can see that there is no loss in generality in treating the paired shifts as *digital* delay lines, accepting and shifting discrete-time pressure wave signals, at intervals of $T$ seconds. The discrete-time model of the acoustic tube will still calculate an exact solution to system (1.1), at times which are integer multiples of $T$. (This solution can be considered to be exact at *all* time instants as long as all signals in the network are assumed to be *bandlimited* to half of the sampling rate, $F_s = 1/T$.)

Also note that because the traveling pressure and volume velocity waves are simply related to one another by a scaling, then in a computer implementation, it is only necessary to propagate one of the two types of wave in a given discrete tube section—we will assume, then, that pressure waves are our signal variables.

### Junctions Between Two Uniform Acoustic Tubes

Consider now a *junction* between two of the uniform acoustic tubes in the concatenated tube model shown in Figure 1.1(b). The wave speeds in all the tubes are assumed to be constant, and equal to $\gamma$, so that the discrete-time representation of any single tube will have the form of the pair of digital delay lines shown in Figure 1.2(b). At the junction between the $i$th and $(i+1)$th tubes (of cross-sectional areas $A_i = A(i\Delta)$ and $A_{i+1} = A((i+1)\Delta)$ respectively), for $i = 1, \ldots, N-1$, we will then

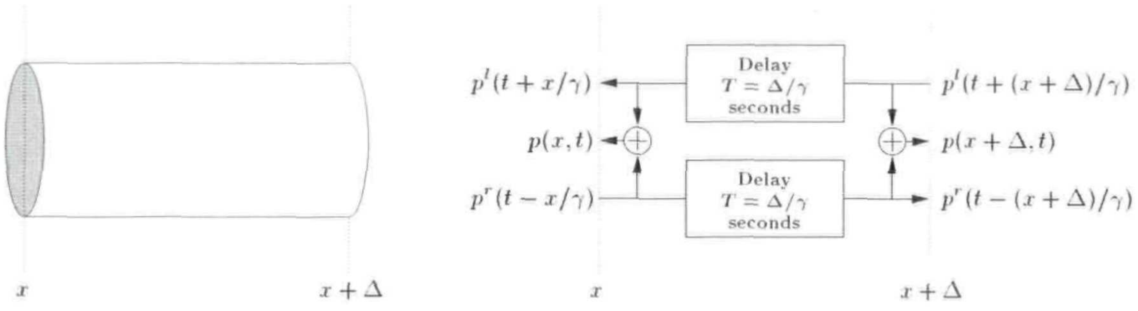

$x$
$x+\Delta$
Delay $T=\Delta/\gamma$ seconds
Delay $T=\Delta/\gamma$ seconds
$p^l(t+x/\gamma)$
$p(x,t)$
$p^r(t-x/\gamma)$
$p^l(t+(x+\Delta)/\gamma)$
$p(x+\Delta,t)$
$p^r(t-(x+\Delta)/\gamma)$
$x$
$x+\Delta$

(a) (b)

Figure 1.2: (a) *An acoustic tube and* (b) *a representation of the traveling wave solution: traveling pressure waves can be added together at either end of the tube to give the physical pressure, as per* (1.2a).

have a pressure and a velocity on either side; we will write these pressure/velocity pairs as $(p_i, u_i)$, and $(p_{i+1}, u_{i+1})$ respectively—see Figure 1.3(a). Continuity arguments (or conservation laws) dictate that these quantities should remain unchanged as we pass through the boundary between the two tubes, and thus

$$p_i = p_{i+1} \qquad\qquad u_i = u_{i+1} \tag{1.5}$$

Note that we have dropped the arguments $t$ and $x$, since the relationships of (1.5) hold instantaneously, and only at the tube boundaries.

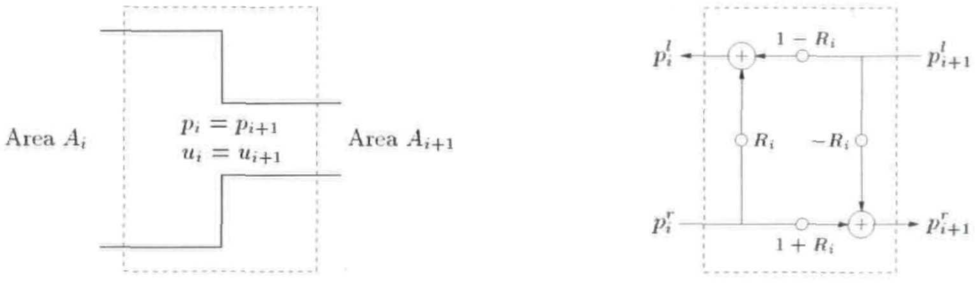

Area $A_i$
$p_i = p_{i+1}$
$u_i = u_{i+1}$
Area $A_{i+1}$
$p_i^l$
$1-R_i$
$p_{i+1}^l$
$R_i$
$-R_i$
$p_i^r$
$1+R_i$
$p_{i+1}^r$

(a) (b)

Figure 1.3: (a) *The junction between the ith and* $(i+1)$*th acoustic tubes in the Kelly-Lochbaum vocal tract model, and* (b) *the resulting scattering junction for pressure waves.*

As per (1.2a) and (1.2b), the pressures and velocities can be split into leftward- and rightward-traveling waves as

$$p_i = p_i^l + p_i^r \qquad\qquad u_i = Y_i\left(p_i^l - p_i^r\right) \tag{1.6a}$$

$$p_{i+1} = p_{i+1}^l + p_{i+1}^r \qquad\qquad u_{i+1} = Y_{i+1}\left(p_{i+1}^l - p_{i+1}^r\right) \tag{1.6b}$$

where $Y_i$, the admittance of the $i$th tube, is defined by

$$Y_i \triangleq \frac{A_i}{\rho\gamma} \tag{1.7}$$

It is then possible, using (1.6) to rewrite (1.5) purely in terms of the wave variables, as

$$p_i^l = \mathcal{R}_i p_i^r + (1-\mathcal{R}_i)p_{i+1}^l \tag{1.8a}$$

$$p_{i+1}^r = (1+\mathcal{R}_i)p_i^r - \mathcal{R}_i p_{i+1}^l \tag{1.8b}$$

where $\mathcal{R}_i$ is defined by

$$\mathcal{R}_i \triangleq \frac{Y_i - Y_{i+1}}{Y_i + Y_{i+1}}$$

Here we have written a formula for calculating the pressure waves $p_i^l$ and $p_{i+1}^r$ *leaving* the junction in terms of the waves $p_i^r$ and $p_{i+1}^l$ *entering* the junction—see Figure 1.3(b) for the resulting signal-flow diagram. In particular, (1.8) can be viewed as a *scattering* operation; *incident* waves on either side of an interface are *reflected* and *transmitted* according to the mismatch in the admittances between the two tubes. The mismatch is characterized by the *reflection parameter* $\mathcal{R}_i$ which is bounded in magnitude by 1, *as long as the admittances of the two tubes are positive.* (If $Y_i = Y_{i+1}$, for instance, then $\mathcal{R}_i = 0$, and there is no reflection at the interface.) As we mentioned before, the calculations (1.8) should be viewed as occurring pointwise at the junction interface itself, which does not occupy physical space.

Suppose that we define a set of *power-normalized* wave variables by

$$\underline{p}_i^l = \sqrt{Y_i}p_i^l \qquad\qquad \underline{p}_i^r = \sqrt{Y_i}p_i^r \tag{1.9}$$

Then the scattering operation (1.8) can be written, in matrix form, as

$$\begin{bmatrix}\underline{p}_i^l\\ \underline{p}_{i+1}^r\end{bmatrix} = \begin{bmatrix}\mathcal{R}_i & \sqrt{1-\mathcal{R}_i^2}\\ \sqrt{1-\mathcal{R}_i^2} & -\mathcal{R}_i\end{bmatrix}\begin{bmatrix}\underline{p}_i^r\\ \underline{p}_{i+1}^l\end{bmatrix} \tag{1.10}$$

Because the $\mathcal{R}_i$ are bounded in magnitude by 1, it is easy to see that scattering, in this case, corresponds to an orthogonal matrix transformation applied to the input wave variables.

### Power Conservation at Scattering Junctions

At the junction between the $i$th and $(i+1)$th tubes, the continuity relations (1.5), when multiplied together, imply that

$$p_i u_i = p_{i+1} u_{i+1}$$

This is simply a statement of *conservation of power* at the interface. Using the definitions of traveling wave variables from (1.6), we then have that

$$\left(p_i^l + p_i^r\right) Y_i \left(p_i^l - p_i^r\right) = \left(p_{i+1}^l + p_{i+1}^r\right) Y_{i+1} \left(p_{i+1}^l - p_{i+1}^r\right)$$

or, rearranging terms,

$$Y_i \left(p_i^l\right)^2 + Y_{i+1} \left(p_{i+1}^r\right)^2 = Y_i \left(p_i^r\right)^2 + Y_{i+1} \left(p_{i+1}^l\right)^2$$

In other words, the sum of the squares of the *incident waves*, weighted by their respective tube admittances, is equal to the same weighted square sum of the *reflected* waves. Assuming that the $Y_i$ are positive, then, a weighted $L_2$ measure of the signal variables (pressure waves) is preserved through the scattering operation. This reflects the inherent *losslessness* of the tube interface.

In terms of the power-normalized variables defined by (1.9), and scattered according to (1.10), we will have (due to the orthogonality of the scattering matrix),

$$\left(\underline{p}_i^l\right)^2 + \left(\underline{p}_{i+1}^r\right)^2 = \left(\underline{p}_i^r\right)^2 + \left(\underline{p}_{i+1}^l\right)^2$$

Thus the $L_2$ norms of the incident and reflected vectors of power-normalized wave variables are the same.

### Discrete-time Vocal Tract Model

Now that we have discussed both the digital delay line representation of wave propagation within a single acoustic tube, as well as the scattering that occurs at any junction between adjacent tubes, we are now ready to present the full discrete-time model of the vocal tract. For an $N$ tube model of the vocal tract, then, we will have the digital signal flow graph shown in Figure 1.4. Here, the scattering junctions are indicated by rectangles, marked by $\mathbf{S}_i$ (representing a matrix transformation of the form of (1.8) or (1.10), which is parametrized by $\mathcal{R}_i$, which itself depends on the adjoining tube admittances $Y_i$ and $Y_{i+1}$).

The structure is driven at the left end, by an input waveform (typically an impulse train, for voiced speech or by white noise for unvoiced speech, or a combination of the two), and an output speech waveform is emitted at the right end. The grey boxes, representing boundary conditions at

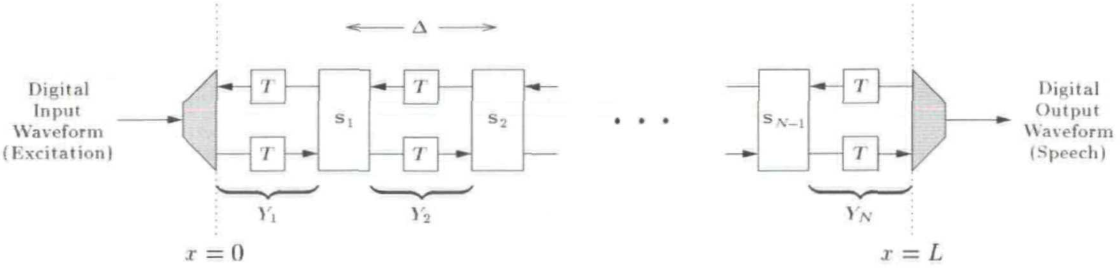

Figure 1.4: *Signal flow graph for an N tube vocal tract model.*

the glottis and lips, we leave unspecified—such terminations can be modeled in a variety of ways [145].

Leaving aside a discussion of these boundaries, we can see that a single cycle in the recursive structure shown in Figure 1.4 (one pass through the main loop of the computer program that it implies) will involve two distinct steps:

- Wave variables incident on the junctions are *scattered.*
- The output waves are *shifted* to the inputs of the junctions immediately to the left and right.

We have already seen that the scattering operation preserves a weighted $L_2$ norm of the signal variables; it should be obvious that the shifting operation also does so, trivially (indeed, in the computer program, shifting amounts to no more than a permutation of the set of pressure signals stored in memory). Thus we have a simple positive definite measure of the state of the tube in terms of signal values stored in the delay registers which remains constant as time progresses (again, excepting the effect of the boundary conditions). What is more, this *numerical stability* property of this structure is very easy to verify; we need only check that all the reflection coefficients $\mathcal{R}_i$ are bounded by 1 in magnitude, or equivalently, that all the admittances are positive. The excitation at the left boundary will, of course, introduce energy into the system, but we can at least be sure that signal energy is not being produced in the problem interior. The energy drain at the radiating (right) boundary is similarly localized.

Several other features are worthy of comment. First, we have treated the vocal tract here as a *static* or *time-invariant* linear (LTI) system. As we mentioned before, however, the configuration of the vocal tract must necessarily change during any utterance—these variations are assumed to be slow with respect to the frequency content of the excitation. The slow variation in the acoustic tube profile will cause shifts in the system resonances (formants), and these shifts will be perceived, by the listener, as phoneme transitions. In our discussion of scattering and energy conservation in the Kelly-Lochbaum model, we have not taken the time variation of the tube cross-sectional areas (and thus the reflection coefficients) into account. It should be clear, though, that if we are using the power-normalized signal variables defined by (1.9), then scattering defined by (1.10) at any junction remains an orthogonal (and thus norm preserving) operation, even if the $\mathcal{R}_i$ are functions of time[†] [166]. Second, it is also simple to extend the model to include the nasal pathways (necessary for the production of certain vocal sounds, and also modeled as acoustic tubes [30]), without compromising overall losslessness. Third, we note that the stability of this model can be maintained even if the reflection coefficients $\mathcal{R}_i$ are quantized [166]—this will necessarily occur in any finite word-length machine implementation. As long as the quantized coefficients remain bounded by 1, then we still have a perfectly lossless system. Signal quantization can also be performed so as to maintain overall stability, though the system will become more generally *passive* and not strictly lossless. Fourth, although the acoustic tube of varying cross-sectional area is often considered to be analogous to a lossless electrical transmission line of spatially-varying inductance and capacitance, it is better thought of as a special case of the latter. For the acoustic tube, the local admittance varies directly with the cross-sectional area, but the wave speed $\gamma$ remains constant; this is important, because for a given tube length of $\Delta$, the time delay is dependent on the wave speed, from (1.4). For a transmission line, both the admittance and the wave speed may vary from point to point along its length. We cannot then approximate the full transmission line by concatenated uniform transmission line segments in the same way as for the acoustic tube without losing synchronization of the resulting discrete-time structure (i.e., delay durations in the segments are not all the same). We will show how to solve this problem in Chapter 4.

### Relationship to Digital Filters

Discrete-time structures such as that shown in Figure 1.4 are also used in digital filtering applications [134, 139], in which case, the notion of a *spatial location* associated with a particular junction or delay element is often lost. For example, consider the digital filter structure shown in Figure 1.5(a). With $x(n)$ as a real discrete-time input sequence indexed by integer $n$, and $y(n)$ as the output sequence, this structure is called an *all-pole lattice filter* [134], when any of the types of section shown in Figure1.5(b), (c) or (d) is used. $T$ is the sample period, or unit delay, and the structure is parameterized by the constants $k_i$, $i = 1, \ldots, N$. It is possible to show that $x(n)$ and $y(n)$ are related by the familiar all-pole difference equation

$$y(n) = x(n) + \sum_{i=1}^{N} a_i y(n-i) \tag{1.11}$$

---

[†] It should be said, however, that a time-varying acoustic tube is not, strictly speaking, a lossless system—energy is pumped into the system by the variations themselves. While the lossless time-varying concatenated acoustic tube model may be a useful signal processing construct, it can not be said to correspond to the numerical solution of a commonly-known system of PDEs. We will revisit the full time-varying system more rigorously in §6.2.7.

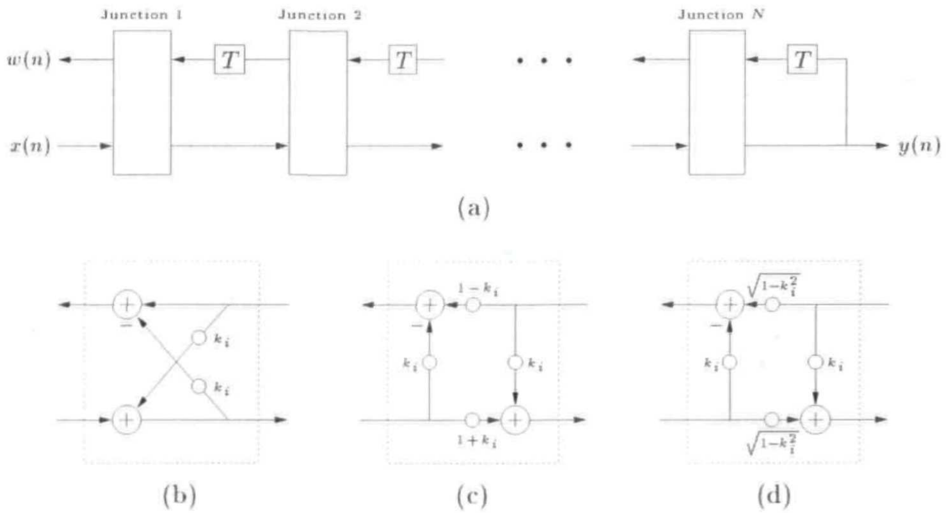

Figure 1.5: (a) *An all-pole lattice filter, and* (b) *a standard lattice junction,* (c) *a Kelly-Lochbaum junction and* (d) *a normalized lattice junction.*

where the direct-form filter coefficients $a_i$, $i = 1, \ldots, N$ can be derived from the $k_i$ through simple recursive procedures [134]. While the direct-form filter implementation implied by (1.11) requires fewer arithmetic operations than the lattice forms in Figure 1.5, the lattice implementation may be preferable because (a) stability is guaranteed by the simple condition $|k_i| < 1$, for all $i$, (determining stability by direct examination of the $a_i$ is difficult, though it can of course be performed by finding the equivalent set of $k_i$ parameters) and (b), pole locations are much less sensitive to coefficient quantization when applied to the $k_i$ rather than the $a_i$. We also mention that the same structure also doubles as a useful *all-pass* filter design [134], when $x(n)$ is taken as the input and $w(n)$ as the output. It is also possible to extend this filter design in order to implement any general stable pole-zero filter by summing readout taps from the leftward signal path into the output [139].

The structure of Figure 1.5(a) is quite similar to the Kelly-Lochbaum discrete-time acoustic tube model, but there are two minor differences. First, the Kelly-Lochbaum structure contains delay elements in both the leftward and rightward signal paths, reflecting the traveling-wave nature of the solution to the physical acoustic tube problem. In the lattice filter structure, however, the delays all occur in the upper (leftward) signal path. It is possible to transform the Kelly-Lochbaum structure into the lattice form by signal flow-graph manipulations involving pushing delays through the junctions, combining them, and then downsampling by a factor of two—this can be done provided the acoustic tube model is terminated by a zero or infinite impedance at the right end [166]. (We remark that this downsampling operation can also be applied to digital waveguide meshes in higher dimensions, in which case we will refer to it as *grid decimation*; we will examine grid decimation for a variety of mesh forms in Appendix A.) Second, the Kelly-Lochbaum and normalized junctions in our treatment of the acoustic tube model differ slightly from the signal flow graphs shown in Figure 1.5(c) and (d). This difference is due to our choice of pressure waves instead of velocity waves as our signal set. While these quantities are dual in the one-dimensional acoustic tube, this symmetry is lost when we move to acoustics problems in higher dimensions, and it is more natural to work with pressure variables[†].

The same lattice structure is also arrived at in the analysis context when *linear predictive coding* (LPC) techniques are applied to a speech waveform [124]. The assumption underlying LPC is that speech can be treated as a source signal (such as a glottal waveform), filtered by the vocal tract, and the goal is to design an all-pole filter of the form of (1.11) which models the system resonances (or formant structure). Though this filter is obtained through purely autoregressive (i.e., non-physical) analysis of a given measured speech signal, the reflection coefficients $k_i$ (also known as *partial correlation* or PARCOR coefficients) are calculated as a byproduct of the main calculation of the direct form filter coefficients $a_i$. The $k_i$ are identical to the $\mathcal{R}_i$ in the acoustic tube model, except for a sign inversion. This is not to say that the filter arrived at through LPC immediately implies a particular vocal-tract shape; it is best thought of as the solution to a filter-design or system identification problem, devoid of any physical interpretation [145]. We note, though, that transmission-line models such as the concatenated acoustic tube model have long been used for such system identification purposes in the *inverse scattering* context, in which case they are sometimes referred to as "layer-peeling" or "layer-adjoining" methods [22, 23, 213]. Provided certain assumptions are made about the glottal waveform and the effects of radiation on the measured speech waveform, it is possible to make some inferences about the vocal tract shape [30].

### 1.1.2 Digital Waveguide Networks

The principal components of the Kelly-Lochbaum speech synthesis model, paired delay lines which transport wave signals in opposite directions, and the scattering junctions to which they are connected, are the basic building blocks of *digital waveguide networks* (DWNs) [166]. Keeping within the acoustic tube framework, it should be clear that *any* interconnected network of uniform acoustic tubes can be immediately transferred to discrete time by modeling each tube as a pair of digital delay lines (or *digital waveguide*) with an admittance depending on its cross-sectional area[††]. At a junction where several tubes meet, these waves are scattered. See Figure 1.6 for a representation of a portion of a network of acoustic tubes, and its DWN equivalent.

The scattering operation performed on wave variables must be generalized to the case of the

---

[†] Another reason for our choice of pressure waves is that when we transfer digital waveguide networks to the electrical framework in Chapter 4, then pressure waves become *voltage waves*, which are also the signal variables in the wave digital filtering literature.

[††] In order for the network to be synchronic, or realizable as a recursive computer program, all the delay durations must be integer multiples of a common unit delay (the sampling period). Because the physical length of a digital waveguide is directly proportional to the delay (by a factor of $\gamma$, the wave speed), a synchronic DWN always corresponds to a network of acoustic tubes whose lengths are appropriately quantized.

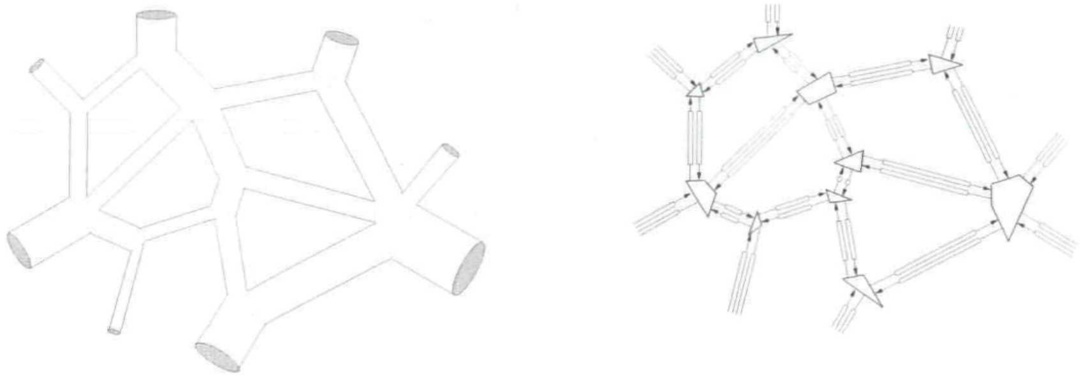

(a) (b)

Figure 1.6: (a) *A portion of a general network of one-dimensional acoustic tubes and* (b) *its discrete-time realization using paired bidirectional delay lines and scattering junctions.*

junction of $M$ tubes, as shown in Figure 1.7. Though we will cover this operation in more detail in Chapter 4, and in the wave digital context in Chapter 2, we note that as for the case of the junction between two tubes, the scattering equations result from continuity requirements on the pressures and volume velocities at the junction. That is, if the pressures in the $M$ tubes at the junction are $p_j$, and the velocities are $u_j$, $j = 1, \ldots, M$ (we now fix the sign of $u_j$ to be positive if velocities are in the direction of the junction), then the relations are

$$p_1 = p_2 = \ldots = p_M \triangleq p_J \tag{1.12a}$$

$$u_1 + u_2 + \ldots + u_M = 0 \tag{1.12b}$$

In other words, the pressures in all the tubes are assumed to be identical and equal to some *junction pressure* $p_J$ at the junction, and the flows must sum to zero, by conservation of mass. These are the acoustic analogues of Kirchoff's Laws for a *parallel* connection of $M$ electrical circuit elements, where pressures are interpreted as voltages, and velocities as currents[†].

The pressures and velocities can be split into *incident* and *reflected* waves $p_j^+$ and $p_j^-$ as per (1.2a) and (1.2b), by

$$p_j = p_j^+ + p_j^- \qquad\qquad u_j = Y_j\left(p_j^+ - p_j^-\right)$$

where $Y_j$ is the admittance of the $j$th tube. The scattering relation, which can then be derived from

---

[†] In the electrical setting, there is of course a dual set of laws describing a *series* connection, but there is no simple acoustic analogue for such a connection.

(1.12), is

$$p_k^- = -p_k^+ + \frac{2}{\sum_{j=1}^M Y_j}\sum_{j=1}^M Y_j p_j^+ \qquad k = 1, \ldots, M \tag{1.13}$$

and can be represented graphically as per Figure 1.7(b).

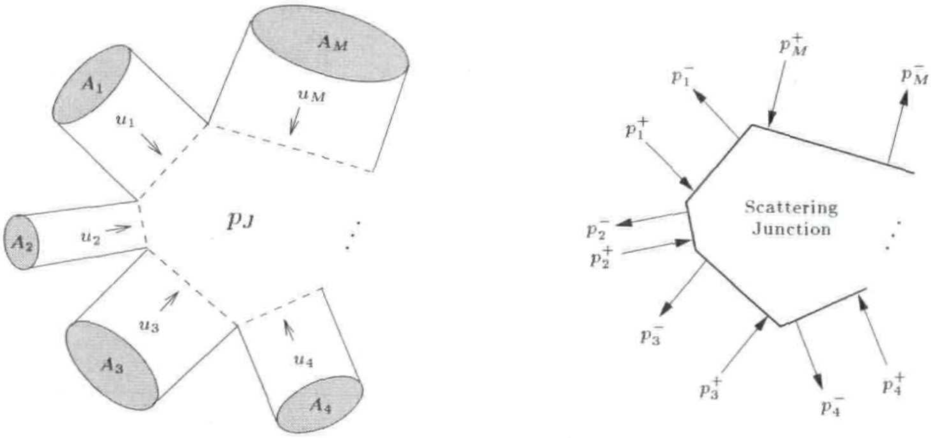

(a) (b)

Figure 1.7: (a) *A junction of $M$ acoustic tubes, indicating the pressures $p_j$ and volume velocities $u_j$ in the $j$th tube, $j = 1, \ldots, M$ at the junction and* (b) *a scattering junction relating outgoing pressure waves $p_j^-$ to incoming waves $p_j^+$, $j = 1, \ldots, M$.*

It is worth examining this key operation in a little more detail. First note that the scattering operation can be broken into two steps, as follows. First, calculate the junction pressure $p_J$, by

$$p_J = \sum_{j=1}^M \alpha_j p_j^+ \qquad \text{where} \qquad \alpha_j \triangleq \frac{2Y_j}{\sum_{j=1}^M Y_j} \qquad \text{for} \quad j = 1, \ldots, M \tag{1.14}$$

Then, calculate the outgoing waves from the incoming waves by

$$p_k^- = -p_k^+ + p_J \qquad\qquad k = 1, \ldots, M$$

Although (1.13) produces $M$ output waves from $M$ input waves, and can thus be written as an $M \times M$ matrix multiply, the number of operations is $O(M)$ ($M$ multiplies and $2M-1$ adds). Also note that the physical junction pressure is calculated, from (1.14), as a natural by-product of the scattering operation; because in a numerical integration setting, this physical variable is always what we are ultimately after, we may immediately suspect some link with standard differencing methods, which operate exclusively using such physical "grid variables". In Chapter 4, we examine the relationship between finite difference methods and DWNs in some detail.

It is simple to show that the scattering operation also ensures that

$$\sum_{j=1}^{M} Y_j (p_j^+)^2 = \sum_{j=1}^{M} Y_j (p_j^-)^2 \tag{1.15}$$

which is, again, merely a restatement of the *conservation of power* at a scattering junction. Notice that if *all the admittances are positive*, then a weighted $L_2$ norm of the wave variables is preserved through the scattering operation. (If power-normalized variables are employed, then scattering is again equivalent to an $M \times M$ orthogonal matrix transformation.) The network as a whole will behave losslessly through the scattering and shifting operations which constitute a single step in the global recursion that such a network implies.

### Waveguide Meshes and the Wave Equation

The DWN shown in Figure 1.6(b) is *unstructured*; though the individual acoustic tubes are assumed to have lengths proportional to the delays in the resulting digital waveguides, they do not fall in any regular arrangement. In fact, although we have drawn what appears to be a network spanning two-dimensional space, we have not associated any physical coordinates with the various tube endpoints; it should be clear that losslessness of the digital structure is unaffected by the network topology. At each step in the computer implementation of the DWN, signals are scattered, then shifted—the notion of "where the signals are" is unimportant in this abstract setting.

Consider now a regular arrangement, or *mesh* [198] of acoustic tubes, as in Figure 1.8(a). The tubes are all of length $\Delta$ and admittance $Y$, and intersections of four tubes occur at grid points in a Cartesian coordinate system. The resulting DWN is shown in Figure 1.8(b); any scattering junction is linked to its four neighbors to the north, south, east and west by bidirectional delay lines of delay $T = \Delta/\gamma$. We have indicated the scattering operation by the letter **S**. Because the admittances of all the tubes are identical, this scattering operation at any junction, from (1.13), has a particularly simple form:

$$\begin{bmatrix} p_N^- \\ p_S^- \\ p_E^- \\ p_W^- \end{bmatrix} = \underbrace{\frac{1}{2}\begin{bmatrix} -1 & 1 & 1 & 1 \\ 1 & -1 & 1 & 1 \\ 1 & 1 & -1 & 1 \\ 1 & 1 & 1 & -1 \end{bmatrix}}_{\mathbf{S}} \begin{bmatrix} p_N^+ \\ p_S^+ \\ p_E^+ \\ p_W^+ \end{bmatrix} \tag{1.16}$$

where $p_j^+$ and $p_j^-$ are the incident and reflected pressure waves from direction $j$, $j = N, E, S, W$. Because the tube admittances are all identical, the scattering matrix **S** is orthogonal here, even if we are not using power-normalized waves.

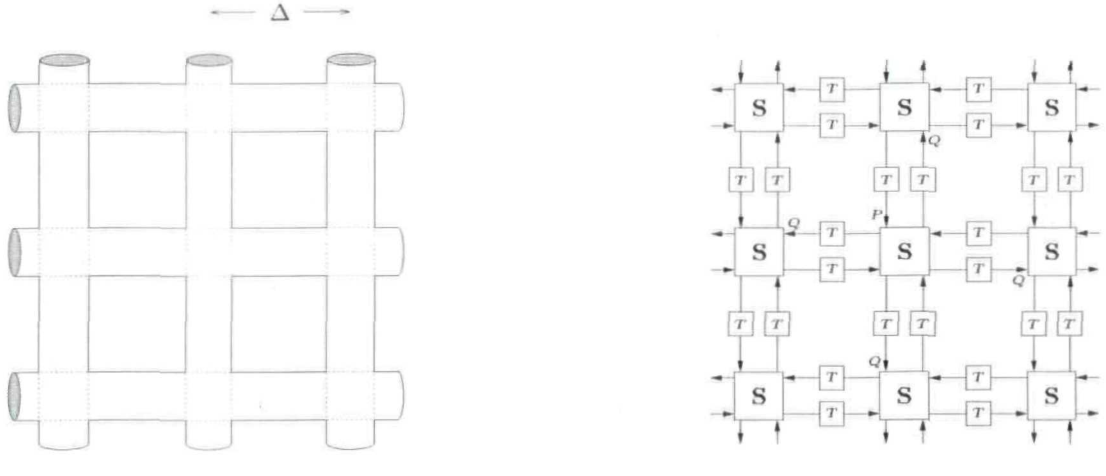

(a) (b)

Figure 1.8: (a) *A regular mesh of acoustic tubes of equal admittances and* (b) *the associated digital waveguide network.*

Referring to Figure 1.8(b), suppose we initialize this structure with a single incident pressure wave $p_N^+ = 1$ at location $P$, the north port of some junction. After scattering, the energy of the incident wave has been distributed among four reflected waves; from (1.16), we will have $p_S^- = p_E^- = p_W^- = 1/2$ and $p_N^- = -1/2$. After a delay of $T$ seconds, these reflected waves are then shifted to the inputs of the four neighboring junctions, at points labeled $Q$. This process is then repeated, and over many time steps, signals will have propagated far from the original excitation at point $P$. At any time step, however, it should be clear that the sum of the squares of the signals in all the delay registers will be 1.

It is possible to view this propagation of signal energy (in a very rough sense) as a discrete time and space version of *Huygens' Principle* [35], an early description of diffraction phenomena: the advance of a wave-front can be analyzed by considering each point on the wave-front to be the generator of a secondary source of waves. A mesh of acoustic tubes, however, is far from a physical medium supporting multidimensional wave propagation, and a basic question which then arises is: is this network of one-dimensional acoustic tubes approximating the behavior of a two-dimensional acoustic medium?

### DWNs and Numerical Integration

To answer this question, let us consider the two-dimensional waveguide mesh at a junction with coordinates $x = i\Delta$ and $y = j\Delta$, for integer $i$ and $j$. The discrete-time junction pressure $p_{J,i,j}(n)$ at time $t = nT$, for integer $n$ (recall that our digital waveguide network operates with a sampling period of $T$), can be written in terms of the four incident wave variables at the same location, from

(1.14), as

$$p_{J,i,j}(n) = \frac{1}{2}\left(p^{+}_{N,i,j}(n) + p^{+}_{E,i,j}(n) + p^{+}_{S,i,j}(n) + p^{+}_{W,i,j}(n)\right)$$

By tracing the propagation of the wave variables through the network backwards in time through two time steps, it is in fact possible to write a recursion in terms of the junction pressures alone,

$$p_{J,i,j}(n) + p_{J,i,j}(n-2) = \frac{1}{2}\Big(p_{J,i-1,j}(n-1) + p_{J,i+1,j}(n-1) + p_{J,i,j-1}(n-1) + p_{J,i,j+1}(n-1)\Big) \tag{1.17}$$

Assume, for the moment, that these discrete time and space junction pressure signals are in fact samples of a continuous function $p(x, y, t)$ of $x$, $y$ and $t$. Expanding the terms in the recursion above in Taylor series about the location with coordinates $x = i\Delta$ and $y = j\Delta$, at time $t = (n-1)T$ gives

$$T^2 \left.\frac{\partial^2 p}{\partial t^2}\right|_{x,y,t-T} + O(T^4) = \frac{\Delta^2}{2}\left.\left(\frac{\partial^2 p}{\partial x^2} + \frac{\partial^2 p}{\partial y^2}\right)\right|_{x,y,t-T} + O(\Delta^4)$$

Recalling that $\Delta = \gamma T$, where $\gamma$ is the speed of wave propagation in the one-dimensional tubes, and discarding higher-order terms in $T$ and $\Delta$ (they are assumed to be small), we get

$$\frac{\partial^2 p}{\partial t^2} = \tilde{\gamma}^2\left(\frac{\partial^2 p}{\partial x^2} + \frac{\partial^2 p}{\partial y^2}\right) \tag{1.18}$$

This is simply the *two-dimensional wave equation*, with the wave speed $\tilde{\gamma}$ defined by

$$\tilde{\gamma} = \gamma/\sqrt{2} \tag{1.19}$$

This equation describes wave propagation in a lossless two-dimensional acoustic medium, and the DWN of Figure 1.8(b) can thus be considered to be a *numerical integrator* of this equation, assuming the wave speeds in the tubes are set according to (1.19); the discrete Huygens' principle interpretation of the behavior of the mesh is justified, at least in the limit as $T$ and $\Delta$ become small[†]. The recursion (1.17) in the junction pressures, however, can be seen as a simple *finite difference scheme* which could have been derived directly from (1.18) by replacing the partial derivatives by differences between values of a *grid function* $p_{i,j}(n)$ on a numerical grid. Because the DWN operates using wave variables, we can see that the DWN is simply a different organization of the same calculation; in particular, it has been put into a form for which all operations (scattering, and shifting) rigidly enforce conservation of energy, in a discrete sense.

We can also reconsider the Kelly-Lochbaum model in this light; forgetting, for the moment, about the approximation of the tube by a series of concatenated *uniform* tubes, it is possible to write the equations of motion for the gas in the tube directly [145] as

---

[†] What we have done, in the jargon of numerical integration methods, is to show the *consistency* [176] of the waveguide mesh with the two-dimensional wave equation.

$$\begin{aligned}\frac{\rho}{A(x)}\frac{\partial u}{\partial t}+\frac{\partial p}{\partial x} &= 0 && (1.20a)\\ \frac{A(x)}{\rho\gamma^2}\frac{\partial p}{\partial t}+\frac{\partial u}{\partial x} &= 0 && (1.20b)\end{aligned}$$

subject to initial conditions and boundary conditions at the glottis and lips. This system is identical in form to (1.1) for a uniform tube, except for the variation in $x$ of the cross-sectional area. It can be condensed to a single second-order equation in the pressure alone,

$$\frac{\partial^2 p}{\partial t^2}=\frac{\gamma^2}{A(x)}\frac{\partial}{\partial x}\left(A(x)\frac{\partial p}{\partial x}\right) \tag{1.21}$$

which is sometimes called ***Webster's horn equation*** [15, 30, 66]. Due to the variation in the cross-sectional area, it is not equivalent to the one-dimensional wave equation (1.3), and does not possess a simple solution in terms of traveling waves (which is why we needed a concatenated uniform tube model in the first place). Returning now to the DWN of Figure 1.4, it can be shown that the junction pressures $p_{J,i}(n)$ (at spatial locations $x = i\Delta$ and at time $t = nT$ for $i$ and $n$ integer) satisfy a recursion of the form

$$p_{J,i}(n)+p_{J,i}(n-2)=\frac{2}{Y_i+Y_{i+1}}\Big(Y_ip_{i-1}(n-1)+Y_{i+1}p_{i+1}(n-1)\Big) \tag{1.22}$$

where $Y_i$ is the admittance of the $i$th acoustic tube, running from $x = (i-1)\Delta$ to $x = i\Delta$. With the $Y_i$ set according to (1.7), it is again possible to show that (1.22) is a finite difference scheme for (1.21), with $\Delta = \gamma T$.

### 1.1.3 A General Approach: Multidimensional Circuit Representations and Wave Digital Filters

For the Kelly-Lochbaum vocal tract model, it is straightforward to arrive at a numerical scattering formulation of the problem; the approximation of a smoothly-varying tube by a series of concatenated tubes is intuitively satisfying, and leads immediately to a wave variable numerical solution to Webster's equation. The identification of the mesh of one-dimensional tubes of Figure 1.8(a) as a numerical solver for the two-dimensional wave equation is more difficult, because it is by no means clear that such a mesh behaves like a two-dimensional acoustic medium (say). Although as we have seen, it is possible to prove (through a finite difference treatment) that the tube network is indeed solving the right equation, we have not shown a way of ***deducing*** such a structure from the original defining PDE system. If one wants to develop a DWN for a more complex system (such as a stiff vibrating plate of variable density and thickness, for example), then guesswork and attempts at invoking Huygens' principle will be of limited use.

The scattering operation we introduced in §1.1.1 and §1.1.2 is at the heart of all the numerical methods we will discuss in this thesis, whether they are based on digital waveguide networks or wave digital filters, which we will shortly introduce. A given system of PDEs is numerically solved by filling the problem domain with scattering nodes, or junctions, such as that shown in Figure 1.7(b), which calculate reflected waves from incident waves according to (1.13) (or its series dual form). The topology of the network of interconnected junctions will be dependent on the particulars of the system we wish to solve. As we have seen, these scattering junctions act as power-conserving signal processing blocks, and in a DWN, they are linked by discrete-time acoustic tubes, or transmission lines, which are also power-conserving, and serve to transport energy from one part of the network to another. The key concept here is the ***losslessness*** of the network components, which is dependent on the ***positivity*** of the various circuit element values (admittances); as we have seen, this positivity condition ensures that some squared norm of the signals in the discrete-time network will remain constant as time progresses. In other words, the simulation routine that such a network implies is guaranteed stable by enforcing this condition.

Wave digital filters (WDFs) are also based on the idea of preserving losslessness (and more generally ***passivity***) in a discrete-time simulation of a physical system, though the approach is somewhat different from what we have just seen. As they were originally intended to transfer analog electrical filter (RLC) networks to discrete time, it is best to begin by looking briefly at lumped circuit elements. A *one-port element*, such as that shown at left in Figure 1.9 is characterized by a voltage $v$, and a current $i$, both of which are functions of time $t$. In the time domain, the one-port generally relates $v(t)$ and $i(t)$ through some combination of differential or integral operators. If the one-port (or more generally, $N$-port) is linear and time-invariant, then there is a simple description of its behavior in the frequency domain, but we will wait until Chapter 2 before entering into the details. An analog filter is simply an interconnected network of such elements; it is operated by applying a voltage at one pair of free terminals, and then reading the filtered output at another pair. In particular, if the network is made up of passive elements such as resistors, capacitors, inductors etc., then it must behave as a stable filter.

Fettweis [46] developed a procedure for mimicking the energetic behavior of an analog filtering network in discrete time. The input and filtered output become digital signals, and the filtering network becomes a recursion, to be realized as a computer program. Most importantly, the digital network has the same topology as the analog network, and can be thought of as its discrete-time "image." One-ports (or more generally $N$-ports) are first characterized in terms of ***wave variables***,

$$\begin{aligned} a &= v + iR \\ b &= v - iR \end{aligned}$$

where $R$ is some arbitrary positive constant, assigned to the particular one-port, called a *port*

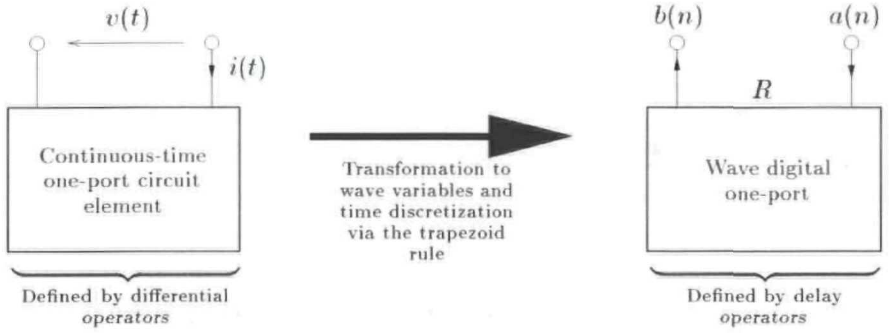
$v(t)$
$i(t)$
Continuous-time one-port circuit element
Transformation to wave variables and time discretization via the trapezoid rule
$b(n)$
$a(n)$
$R$
Wave digital one-port
Defined by differential operators
Defined by delay operators

Figure 1.9: *Wave digital discretization of a one-port circuit element.*

*resistance.* The continuous-time element, described by differential operators, is then replaced by a discrete-time element operating on digital signals, and composed of algebraic operations and delay operators or shifts. The signal $a(n)$ is called the *input wave*, and $b(n)$ is the *output wave*; both are discrete-time sequences indexed by integer $n$. If the discretization procedure is carried out in an appropriate way (to be more precise, differentiation is approximated by the trapezoid rule of numerical integration), then the resulting *wave digital one-port* has energetic properties very similar to the continuous element from which it is derived. In particular, if the analog element is passive (lossless), then the wave digital element can be considered to passive (lossless) in a similar sense. In fact, if a wave digital circuit element is composed of delay operators (hence requiring memory), then a weighted sum of the squares of the signal values stored in the element's delay registers is the direct counterpart to the physical energy stored in the electric and magnetic fields surrounding the corresponding analog element. The passivity property is contingent on the *positivity* of the port resistance; given this constraint, it can often be chosen such that there is no *delay-free path* from the input $a(n)$ to the output $b(n)$. We will see the importance of making the correct choice of $R$ shortly in an example.

Consider a parallel connection of two one-port circuit elements, as shown in Figure 1.10(a). The

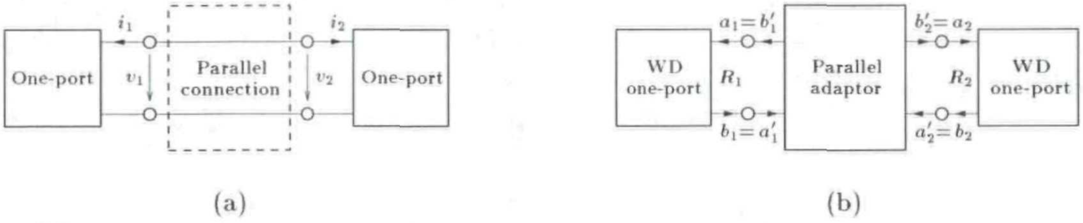
$i_1$
$i_2$
One-port
$v_1$
Parallel connection
$v_2$
One-port
$a_1 = b_1'$
$b_2' = a_2$
WD one-port
$R_1$
Parallel adaptor
$R_2$
WD one-port
$b_1 = a_1'$
$a_2' = b_2$

(a) (b)

Figure 1.10: (a) *Parallel connection of two continuous-time one-ports and* (b) *its wave digital counterpart.*

one-ports are defined by some relationship between their respective voltages and currents, which we will write as $v_1$, $i_1$ and $v_2$, $i_2$. For such a parallel connection, *Kirchoff's Laws* dictate that

$$v_1 = v_2 \qquad\qquad i_1 + i_2 = 0 \tag{1.23}$$

(We could equally well treat this as a series connection, by reversing the directions of the arrows which define $v_2$ and $i_2$ in Figure 1.10(a).) We can now define two sets of wave variables at the two one-ports by

$$\begin{aligned} a_1 &= v_1 + i_1R_1 & \qquad a_2 = v_2 + i_2R_2 \\ b_1 &= v_1 - i_1R_1 & \qquad b_2 = v_2 - i_2R_2 \end{aligned}$$

In the scattering formulation, the Kirchoff connection is treated as a *separate two-port element*, with inputs $a_1'$ and $a_2'$ and outputs $b_1'$ and $b_2'$. These are simply the outputs and inputs, respectively, of the one-ports, as shown in Figure 1.10(b).

Kirchoff's Laws for the parallel connection can then be rewritten in terms of the wave variables as

$$b_1' = \mathcal{R}a_1' + (1-\mathcal{R})a_1' \tag{1.24a}$$

$$b_2' = (1+\mathcal{R})a_1' - \mathcal{R}a_2' \tag{1.24b}$$

where the reflection coefficient $\mathcal{R}$ is defined by

$$\mathcal{R} \triangleq \frac{R_2 - R_1}{R_2 + R_1}$$

Equations (1.24) define a wave digital two-port *parallel adaptor*. They are identical in form to the equations defining a parallel junction of two acoustic tubes, from (1.8)—this is to be expected, since Kirchoff's Laws (1.23) are equivalent to the pointwise continuity equations (1.5) at an acoustic junction. Thus all comments we made about scattering junctions in §1.1.1 hold for the wave digital adaptor as well; in particular, if we define power-normalized waves, then the scattering operation again is equivalent to an orthogonal (i.e., $L_2$ norm-preserving) transformation, as long as the port resistances $R_1$ and $R_2$ are chosen positive (implying, again, that $|\mathcal{R}| < 1$).

### WDFs and the Numerical Integration of ODEs

In the closed network of Figure 1.10, we have left the two one-ports unspecified. Suppose we connect an inductor, of constant inductance $L > 0$ at the left-hand port, and a capacitor of constant capacitance $C > 0$ at the right-hand port, as shown in Figure 1.11(a). Then the voltage-current relations are defined by

$$v_1 = L\frac{di_1}{dt} \qquad\qquad i_2 = C\frac{dv_2}{dt}$$

When these relations are closed by Kirchoff's parallel connection rules (1.23), it is possible to write a single second-order ODE describing the time-evolution of the circuit state,

$$\frac{d^2w}{dt^2} = -\frac{1}{LC}w$$

where $w(t)$ stands for any of the voltages or currents in the network. This network thus behaves as a harmonic oscillator, of frequency $1/\sqrt{LC}$; the voltages and currents, assumed real, evolve according to

$$w(t) = A\cos(t/\sqrt{LC}) + B\sin(t/\sqrt{LC})$$

for some arbitrary constants $A$ and $B$ determined by the initial voltages and currents in the network. The network is also lossless; if we define the total stored energy of this network $E(t)$ by

$$E(t) \triangleq \underbrace{\frac{1}{2}Li_1^2}_{\substack{\text{Energy stored in magnetic field}\\ \text{surrounding inductor}}} + \underbrace{\frac{1}{2}Cv_2^2}_{\substack{\text{Energy stored in electric field}\\ \text{surrounding capacitor}}} \tag{1.25}$$

then

$$\frac{dE}{dt} = Li_1\frac{di_1}{dt} + Cv_2\frac{dv_2}{dt} = i_1v_1 + i_2v_2 = 0 \qquad \Longrightarrow \qquad E(t) = \text{constant}$$

In other words, energy is traded back and forth between the two circuit elements, but is not dissipated.

Though we have not explicitly derived the forms of the wave digital inductor and capacitor, this

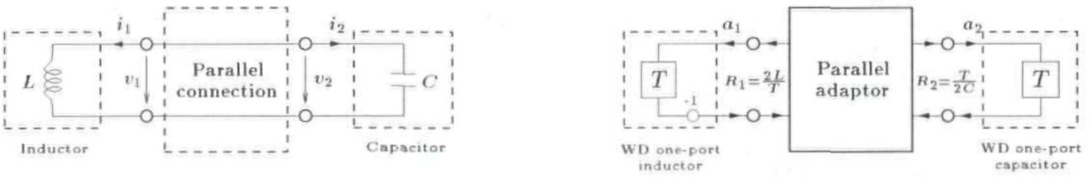

(a) (b)

Figure 1.11: *The LC harmonic oscillator*—(a) *a parallel connection of an inductor, of inductance $L$ and a capacitor of capacitance $C$, and* (b) *the corresponding wave digital network.*

is a good opportunity to see what these elements look like—the wave digital network corresponding to the LC harmonic oscillator circuit is shown in Figure 1.11(b). (The reader may glance ahead to §2.3.4 for a glimpse of how these forms are arrived at.) We have a parallel adaptor, which is a digital signal processing block defined by equations (1.24), terminated on delay elements (one of which incorporates a sign inversion). Special choices of the port resistances $R_1$ and $R_2$ (marked in the figure) were chosen in order to obtain these simple signal-flow graphs. This diagram implies a recursion, which, like the digital waveguide network methods consists of a scattering step, and a delay step (possibly with sign inversion). Because it makes use of only two delay operators, it should be obvious that this simple network must behave as a *two-pole resonator*—the discrete-time counterpart to the continuous-time harmonic oscillator. The wave digital network thus behaves as a *numerical integrator*.

We can define the total discrete-time stored energy of this network by

$$E_{WD}(n) = \frac{1}{R_1}(a_1(n))^2 + \frac{1}{R_2}(a_2(n))^2$$

which is simply a weighted sum of the squares of the signal values stored in the delay registers at time step $n$. Clearly, this quantity remains unchanged after undergoing delays and the scattering operation, i.e., we have

$$E_{WD}(n) = \text{constant}$$

It is simple to identify this quantity with the energy (1.25) of the continuous-time LC network. Although this example is very simple, the same ideas can be applied to large networks, and the result is always an explicitly recursible structure for which passivity can be simply guaranteed.

### Multidimensional WDFs as PDE Simulators

Wave digital filter networks are derived from lumped analog circuits, and we have seen that they can be interpreted as numerical ODE integrators. Most importantly, we saw that a given analog circuit immediately implies a corresponding WDF structure; if the original circuit is lossless, then the WDF network, which is its discrete-time image, will be lossless as well. It is easy to extend the maintenance of losslessness to the more general case of *passivity* (i.e., we allow our networks to dissipate energy, as well as recirculate it).

Fettweis and Nitsche [62] found a way of directly extending this simulation technique to distributed systems. First, it is necessary to generalize the definition of a circuit element to multiple dimensions, in which case it is called an *MD circuit element*; an MD one-port is shown at left in Figure 1.12. The one-port is still defined in terms of a voltage $v$ and current $i$ across its terminals, but these quantities are now more generally functions of an $n$-dimensional spatial coordinate $\mathbf{x}$ as well as time $t$. In particular, $v$ and $i$ will be in general related by partial differential operators. Though the representation is the same as in the lumped case, this circuit element is itself a *distributed* object, occupying physical space. Such a distributed circuit element is merely a generalization of a lumped one-port circuit element; it should not be conceived of as a physical entity. The rules of classical network theory, however (and in particular Kirchoff's connection rules), can still be applied in order to form combinations of such objects.

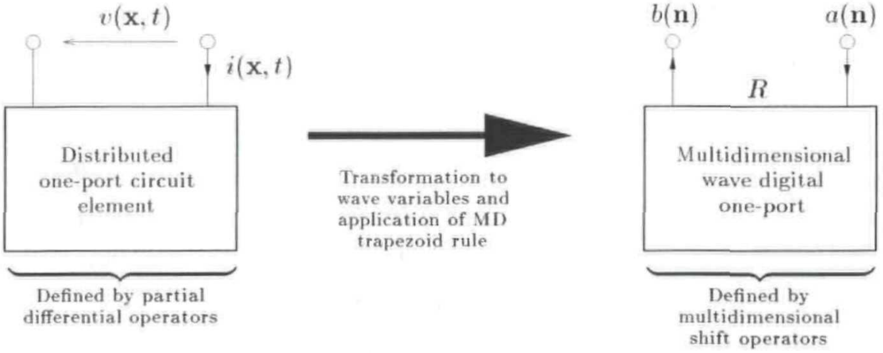
$v(\mathbf{x},t)$
$i(\mathbf{x},t)$
Distributed one-port circuit element
Transformation to wave variables and application of MD trapezoid rule
$b(\mathbf{n})$
$a(\mathbf{n})$
$R$
Multidimensional wave digital one-port
Defined by partial differential operators
Defined by multidimensional shift operators

Figure 1.12: *Multidimensional wave digital discretization of a distributed one-port circuit element.*

It is also possible to extend the notions of passivity and losslessness to multiple dimensions, and to introduce wave variables, which, like the voltages and currents, will also be distributed quantities. Finally, it is also possible to discretize these elements in such a way that this passivity is retained in the discrete time and space domain (through the use of the trapezoid rule in multiple dimensions). the result is the multidimensional wave digital (MDWD) element shown at right in Figure 1.12. Just as for the lumped case, where differential operators are mapped to *delays*, here partial differential operators are mapped to *shifts* in the discrete multidimensional problem space. We again have an input wave $a$ and an output wave $b$, which take on values at a discrete set of locations; these are to be interpreted as *grid functions* over a set of points, indexed by an integer-valued vector $\mathbf{n}$.

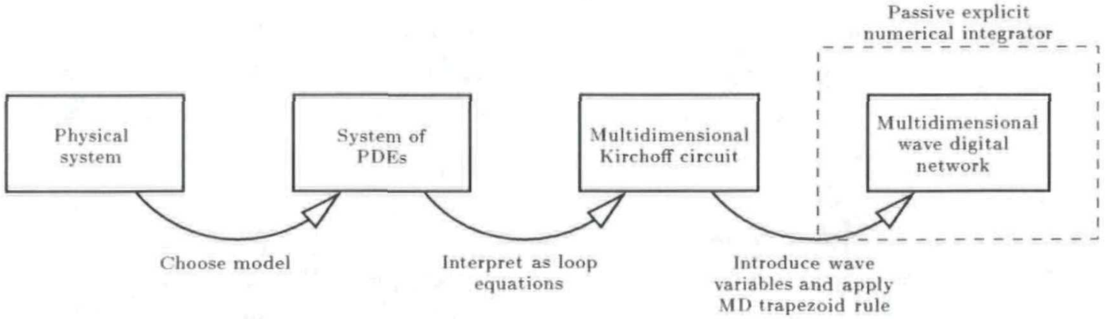
Passive explicit numerical integrator
Physical system
System of PDEs
Multidimensional Kirchoff circuit
Multidimensional wave digital network
Choose model
Interpret as loop equations
Introduce wave variables and apply MD trapezoid rule

Figure 1.13: *Steps in the construction of a multidimensional wave digital filtering simulation routine.*

Though we will discuss the MDWD discretization procedure in much more detail in Chapter 3, we outline the basic steps in Figure 1.13. Beginning from a given passive physical system, we first model it with a suitable system of PDEs. It may be possible, then, to interpret the individual equations as *loop equations* in a closed multidimensional Kirchoff circuit (MDKC) made up of elements of the form shown at left in Figure 1.12. Typically, the *currents* flowing through the "wires" in such a network will be the dependent, or state variables describing the physical system; all the partial differential operators are then consolidated in the various elements. For a first-order system of PDEs, it will usually be true that the number of equations is equal to the number of loops in the circuit. It is important, at this stage, to ensure that such a network representation is composed of multidimensional circuit elements which are individually passive—this can generally be determined by a cursory examination of the circuit element values (such as inductances, capacitances, etc., which may be functions of several variables). Once the work of manipulating the system into a suitable circuit form is complete, the discretization step is immediate, and a multidimensional wave digital network results; if the MDKC is made up of passive elements, then the discrete network will be as well. It can then be interpreted as a *stable explicit numerical integration scheme* for the original defining system of PDEs. The basic operations will be, just as for DWNs, the *scattering* and *shifting* of wave variables through a numerical grid of nodes. The resulting structures, however, differ markedly from DWNs in many ways, though they can still be viewed as finite difference schemes.

We note that each of the various steps (i.e., the arrows in Figure 1.13) involves a good deal of choice (and experience) on the part of the algorithm designer. For a given system, there is almost always a variety of PDE systems which could serve as adequate models; not all are suitable for circuit-based discretization. It is also true that for a given system of PDEs, there is not a unique network representation (though they should all be related by equivalence transformations from classical network theory). Finally, though Fettweis et al. make use of the MD trapezoid rule as a means of arriving at a passive discrete network, this is by no means the only way of proceeding—many integration rules possess the desired passivity-preserving properties. We will explore the consequences of these choices extensively throughout the rest of this thesis.

## 1.2 Questions

Before launching into a full technical summary and listing results in the next section, it is worthwhile to take a step back and view the underlying motivations for writing this thesis. The general goal of this project can be expressed as an attempt to answer, or at least address several general questions about wave digital filter and digital waveguide network numerical simulation algorithms:

- *To what types of systems can wave digital and digital waveguide network simulation approaches be applied?*
- *What features do these two methods share, and what distinguishes them?*
- *What are their relative advantages?*

- *Can they be unified in a formal way?*
- *What extensions and improvements can be made to the existing forms of these methods?*

These were the guiding questions that the author had in mind throughout this project; all the results have some bearing on their answers. The impatient reader can flip to §6.1 for these answers—some clear-cut, some much less so.

## 1.3 Summary and Results

The typical thesis paradigm consists of a single isolated problem statement, followed by a development culminating in a main result. Because this thesis is intended not only as an exposition of results but as a review of and introduction to scattering methods, it would have been somewhat unnatural and probably detrimental to arrange the material in this way. We have thus attempted to interleave review, problems and results in a more natural order. Because of this, it might be a little difficult for the reader to tell what the principal new results were. We here provide a chapter-by-chapter summary, with results appearing in the sections indicated by bold-faced numbers.

### Chapter 2: Wave Digital Filters

Chapter 2 is intended as a review of lumped wave digital filters, minus any discussion of filtering applications, since we will only be looking at simulation applications in the remainder of the thesis. Because these concepts are used extensively throughout the sequel, the reader is advised to begin here, even though discussion of numerical methods for PDE solving does not begin in earnest until the next chapter. We follow the standard development (as in, say, Fettweis's comprehensive review paper [46] which is the chief reference for this chapter) and begin with a brief introduction to the theory of electrical $N$-port devices [12], and, in particular, the key concept of ***passivity***, which later plays a pivotal role as the stability criterion for multidimensional simulation networks. We then review the basics of the lumped wave digital discretization procedure, involving the use of a passivity-preserving continuous-to-discrete spectral bilinear transformation (the trapezoid rule in the time domain) and the transformation to wave variables. The wave digital counterparts of the standard circuit elements (capacitors, inductors, resistors, transformers, etc.) are then introduced, as are adaptors, which are simply the wave variable counterparts to Kirchoff's series and parallel connection rules. The chapter is concluded with a brief description of finite word-length arithmetic properties of WDFs, and a look at some specialized vector elements that will later come in handy (and are in fact necessary) for the simulation of some elastic dynamic systems. It is important to keep in mind that though we only discuss lumped elements and networks in Chapter 2, the basic set of construction rules (essentially classical electrical network theory) remains unchanged when we move to a multidimensional setting in the next chapter.

### Chapter 3: Multidimensional Wave Digital Filters

Chapter 3 begins with a review of some of the basics of symmetric hyperbolic systems of partial differential equations, and then proceeds to the generalization of electrical network passivity into multiple dimensions, where it has been called *MD-passivity* [48, 85]; this can be done in a straightforward way through the application of coordinate transformations [62, 122]. Next, we introduce *multidimensional circuit elements* [45], which are similar to their lumped counterparts, except that they are distributed objects and may have particular directions associated with them. The transformation to wave variables and discretization proceeds as in the lumped case, but now the trapezoid rule must be interpreted in a directional sense, as must be the associated MD *spectral bilinear transformations.* We then proceed through some treatments of typical model problems, namely the *advection equation* [176], the *transmission line system* [107], and its extension to two spatial dimensions, in which case it is called the *parallel-plate system* [60, 61]. We write down *multidimensional Kirchoff circuit* representations (MDKCs) and show the discrete time and space counterparts (MDWDFs) for all these systems. We then spend some time in **§3.9.1** examining MDWD structures as finite difference schemes and make some comments about modal behavior, paying particular attention in **§3.9.2** to *parasitic modes.* In **§3.10** we present a new treatment of the initialization of MDWD methods, and then give a brief overview of methods for setting boundary conditions. *Balanced forms* are introduced in **§3.12** as a means of increasing the computational efficiency of MDWD methods; to date they have been notoriously sub-optimal in that the maximum allowable time step can be a great deal smaller than that of conventional finite difference methods (such as, for example, the *finite-difference time domain* (FDTD) method [184, 214] and, by extension, DWNs). Finally, in **§3.13** we turn to a means of incorporating higher-order spatially accurate [176] methods into a circuit framework; this is surprising, because it had long been assumed that MDWD methods, traditionally based on the use of the trapezoid rule could be no better than second-order accurate [130]. We circumvent this problem by applying an alternative integration rule, which is also passivity-preserving (and which will also serve as a "back-door" into the realm of digital waveguide networks).

### Chapter 4: Digital Waveguide Networks

Chapter 4, which is concerned with digital waveguide networks, is rather large, and can be conveniently divided into three principal parts.

The first part of the chapter, from §4.1 to §4.5, deals with the relationship between digital waveguide networks and finite difference methods of the FDTD variety; we showed a very simple example of such a correspondence in §1.1.2. We reintroduce digital waveguide networks, now in the electrical context, so as to make easier the eventual comparison with the wave digital networks of Chapters 2 and 3—the acoustic tubes in the Kelly-Lochbaum model of §1.1.1 and the waveguide mesh of §1.1.2 are thus replaced by transmission line sections, and pressures and velocities become voltages and currents. After a brief review of the fundamentals, we reexamine the transmission line and parallel-plate test problems in **§4.3** and **§4.4**. Here, DWN structures that numerically integrate these systems are built "the hard way" (i.e., by association with finite difference methods and FDTD, without the benefit of a multidimensional representation), and we uncover several distinct families of such networks, in **§4.3.6** and **§4.4.2**, with different passivity properties. We also examine the initialization of these networks in **§4.5**, and the implementation of boundary conditions in **§4.3.9** and **§4.4.4**.

The next part of Chapter 4, from §4.6 to §4.9 is of a more applied nature—here we discuss several variations on the DWN form, specifically for the transmission line and parallel-plate problems. First, we take a cursory look at some other recently proposed two- and three-dimensional DWN structures in **§4.6** and §4.7, extending them to the variable-coefficient case where necessary. (The spectral analysis of these DWNs is postponed until Appendix A.) We then introduce some generalized DWNs which may be useful in "real-world" problems, in particular those involving irregular boundary configurations and sharp variations in material parameters. We look at DWNs in the important special case of polar coordinates in **§4.6.2**, and then extend the same technique to general curvilinear coordinate systems in **§4.8**. Another means of tackling such irregularities, with an eye towards computational efficiency considerations, involves the use of multigrid DWNs; a "fine" DWN can be used over any part of the problem domain where greater detail is required, and may be interfaced to a "coarse" DWN operating over the remainder of the domain. The interface between such DWNs can be designed so as to maintain perfect losslessness, while introducing minimal numerical reflection. We look at several types of such layers, in two and three spatial dimensions, as well as a way of interfacing grids in different coordinate systems, in **§4.9**. Several simulations are presented, in **§4.6.2**, **§4.9.1**, and **§4.9.4**.

Up until this point in Chapter 4, we treat digital waveguide networks as large collections of scattering junctions connected by paired delay lines, just like the Kelly–Lochbaum model of §1.1.1 and the mesh of §1.1.2. While this is a useful vantage point, especially when it comes to constructing irregular networks such as those discussed in **§4.9**, and for finding proper passive boundary terminations, it is somewhat lacking in that it does not allow the algorithm designer any guidance in the construction of these methods for more complex systems. Indeed, when faced with a many-variable system (such as, for example, the thirteen-variable system of PDEs which models vibration in a stiff cylindrical shell, to be discussed in §5.5.2), it becomes difficult to proceed as was done for the comparatively simple transmission line test problems in **§4.3** and **§4.4**. A MDWD-based method does not fall prey to these design difficulties because it follows directly from a multidimensional circuit representation of a given defining system of PDEs; in other words, a passive numerical method can be automatically generated from the model system, regardless of its complexity. It is true, however, that this circuit representation is highly non-unique—we have all of classical network theory at our disposal in order to manipulate it. What is more, while WDF discretization is based on the use of the trapezoid rule (or bilinear transform), in multiple dimensions, the family of passive integration rules is much more general. The most important result in this thesis is presented in **§4.10**; we use the flexibilities mentioned above in order to show that a DWN also can be viewed as the discrete image of an MDKC. As such, it can be directly incorporated into the same family as the WDF-based methods; the relationship is shown in Figure 1.14. The range of physical systems to which the DWN can be applied as a simulation method is thus considerably enlarged to include any system that has been dealt with using MDWDFs. MDWDFs and DWNs are now on an equal footing, (and we will emphasize the fraternal relationship between the two methods repeatedly in Chapter 5). We develop alternative network representations suitable for DWN discretization for the transmission line and parallel-plate systems in **§4.10.3** and **§4.10.4**, then continue our previously postponed treatment of higher-order spatially accurate DWNs in **§4.10.5**, and finally conclude with a DWN for Maxwell's Equations in **§4.10.6**. The DWN for this last system, in that it is equivalent to Yee's original FDTD formulation completes the circle of ideas begun in the first part of the chapter.

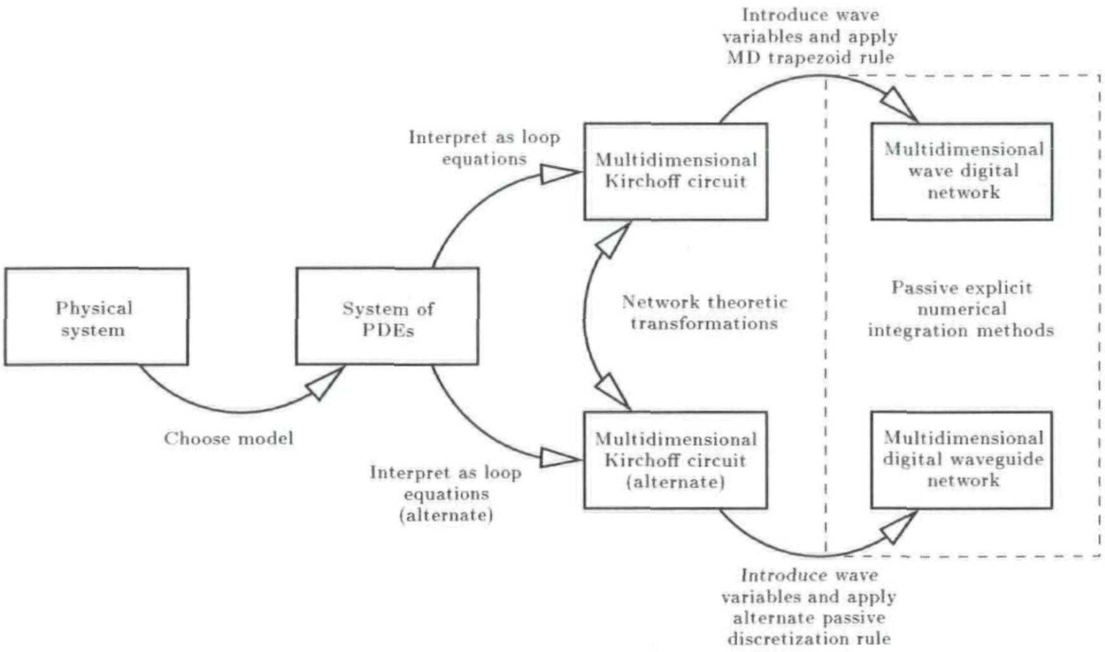
Introduce wave variables and apply MD trapezoid rule
Interpret as loop equations
Multidimensional Kirchoff circuit
Multidimensional wave digital network
Physical system
System of PDEs
Network theoretic transformations
Passive explicit numerical integration methods
Choose model
Interpret as loop equations (alternate)
Multidimensional Kirchoff circuit (alternate)
Multidimensional digital waveguide network
Introduce wave variables and apply alternate passive discretization rule

Figure 1.14: *Steps in the construction of multidimensional wave digital filtering and digital waveguide network simulation routines, viewed as part of a generalized family of passive numerical methods.*

### Chapter 5: Applications in Vibrational Mechanics

In Chapters 3 and 4, scattering structures are developed to numerically integrate certain simple systems of PDEs, in particular the transmission line equations and the parallel-plate system. In this chapter, we show how the same ideas can be applied to another set of systems, namely those describing the mechanical vibrations of elastic solid media under various conditions. These systems can become quite complex, compared with the simple transmission-line test problems, but as we will see, circuit representations can be developed as before, though several new techniques must be introduced. We look at such systems in order of increasing dimensionality, loosely following the organisation of the text by Graff [77]. Liberal use is made of the unifying result of **§4.10** in order to develop wave digital and digital waveguide simulation networks in a parallel fashion for these systems. We first examine the simplest stiff distributed system, the classical, or ideal Euler-Bernoulli beam in **§5.1**, mainly in order to indicate the difficulties inherent in designing scattering methods for systems which are not symmetric hyperbolic (though we show that it is indeed possible). We then turn to the modern (and much more suitable, in the scattering context) Timoshenko beam theory, which was first treated by Nitsche in [131], and present a variety of distinct scattering methods in **§5.2**, while indicating the relevant differences, especially with respect to stability. We also apply the system balancing approach (introduced in **§3.12**) to the Timoshenko beam in **§5.2.6** in order to show that it is possible to drastically reduce the computational requirements in certain cases, and take an extended look at boundary conditions in **§5.2.4**. Then follows a look at stiff plate theory, and in particular the two-dimensional analogue of the Timoshenko beam, called the Mindlin plate, in **§5.4**. Here, due to the couplings between the variables, we are forced to make use of vector scattering elements, which were introduced in §2.3.7 for this very purpose. Boundary conditions for waveguide networks for the Mindlin plate are dealt with in detail in **§5.4.2**. We next spend some time examining network representations for two cylindrical shell models, first the membrane shell in **§5.5.1**, and then the more modern model of Naghdi and Cooper in **§5.5.2**. Finally, for completeness sake, we revisit in §5.6 Nitsche's MDKC for the full three-dimensional elastic solid dynamic system [131]; as for all the systems in this chapter, we show the alternative network form suitable for DWN discretization in **§5.6.1**. In keeping with the more applied flavor of this chapter, we also present simulation results for Timoshenko's beam system and the Mindlin plate in **§5.2.5** and **§5.4.3**, respectively, under both uniform and spatially-varying material parameter conditions.

### Chapter 6: Conclusions and Future Directions

In Chapter 6 we address the general questions of the last section, and then make some suggestions for future research; in particular, we mention some partial results that could not be easily fit into the main chapter development, namely the application of circuit methods to time-varying systems in **§6.2.7** (and an application to time-varying vocal tract modeling is indicated), and a possible foundation for a theory of the boundary termination of passive distributed networks in **§6.2.3**.

### Appendix A: Finite Difference Schemes for the Wave Equation

Appendix A serves a dual purpose. First, it is intended as a review of the basics of the spectral or *Von Neumann* analysis of finite difference schemes; this analysis is quite powerful and revealing if the underlying physical model problem is linear and shift-invariant. We pay close attention to the ***numerical stability*** conditions that can be arrived at through a straightforward application of these spectral methods. For this review portion of the appendix, we depend primarily on the excellent text by Strikwerda [176]. (For the reader with no prior exposure to the analysis of finite difference methods, §A.1 could well serve as point of departure, before jumping directly into network and scattering theory in Chapter 2.) We then systematically revisit all of the large variety of forms of DWN for the two- and three-dimensional wave equation, applying this spectral analysis to the equivalent difference schemes. The comparison of the Von Neumann numerical stability conditions with the passivity conditions on the associated mesh structures yields somewhat surprising results, for the so-called triangular (**§A.2.3**) and interpolated meshes (**§A.2.2**, **§A.3.3**) structures; indeed, the conditions do not coincide in these cases, leaving us with some fundamental and puzzling questions about the nature of this discrepancy. In addition, we also introduce some techniques for rigorously analyzing certain vector-type schemes (the hexagonal scheme, in **§A.2.4** and the tetrahedral scheme, in **§A.3.4**), and look at a theoretical means of obtaining optimally direction-independent numerical dispersion properties for certain schemes for which we have free parameters at our disposal (the interpolated schemes in **§A.2.2** and **§A.3.3**). Throughout the appendix we pay particular attention to evaluating the relative memory requirements and computational efficiency of the various schemes, and provide numerical dispersion error plots for all the schemes.

### Appendix B: Applications in Fluid Dynamics

In Appendix B, we summarize some of the interesting new developments in applying wave digital filtering methods to strongly nonlinear problems in fluid dynamics. Though there are no significant new results in this appendix, we take the opportunity to elucidate some connections to current trends in the analysis of such systems involving so-called *skew self-adjoint* forms; in doing so, we highlight certain unforeseen shortcomings of Fettweis's MDKC and MDWD network representations of these systems, and indicate a possible way of avoiding these difficulties in **§B.3.3** by making use of *entropy variables*. In keeping with the overall goal of unifying wave digital and digital waveguide network approaches to numerical integration, we also show in **§B.3.2** how the methods of **§4.10** can be applied to the one-dimensional gas dynamics system in order to yield a DWN-like structure.

# Chapter 2

# Wave Digital Filters

## 2.1 Introductory Remarks

The entry point, for any study of numerical methods based on wave and scattering ideas, must necessarily be a review of *wave digital filters* (WDFs) [41, 46]. This filter design technique, proposed by Alfred Fettweis in the early 1970s, was an attempt at translating analog filters into the digital realm with a pointed emphasis on preserving as much of the underlying physics as possible. In particular, a digital filter structure arrived at through Fettweis's procedure has the same precise network topology and energetic properties as the lumped analog electrical circuit (called the *reference circuit*) from which it is derived.

The theory is straightforward; analog circuit components ($N$-port devices or elements), usually defined by a voltage-current relation, are first given an equivalent characterization in terms of *wave variables*. While this is merely a change of variables, it has the advantage of allowing an alternate description of the dynamic behavior of the network: energy incident on a circuit element (incident from the rest of the network to which it is connected through a *port*) may be reflected back from the element through the same port, or transmitted through to another part of the network through a different port. The incident, reflected and transmitted energies are carried by *waves*[†]. The reflectances and transmittances themselves are determined by arbitrary positive constants called *port resistances* which are assigned to individual wave ports. An important result of using wave variables is that the entire network may then be parametrized by these reflection and transmission coefficients which are, at least for passive networks, bounded independently of the numerical circuit element values themselves (inductances, capacitances and resistances etc.), which may vary over a wide range.

The true advantage of using wave variables becomes much more tangible when we seek to obtain, from a given analog filter design, a digital filter structure. This is usually done in the WDF context at steady state via a particular type of *bilinear transformation* or *spectral mapping* [41] from continuous to discrete frequency variables. Unless wave variables are employed, the resulting filter structure will usually not be recursively computable, and hence not directly implementable as a computer program. In addition, because the reflectances and transmittances of the network (which become the *filter multiplier values*) are bounded in a simple way, a host of desirable filter properties result which are especially valuable in a fixed-point computer implementation: complete elimination of certain types of limit cycles or parasitic oscillations and very low sensitivity of the filter response to coefficient truncation are the most frequently mentioned [46]. A further advantage stems from the fact that because the network topology of the reference circuit has been inherited by the digital filter structure, we have convenient access to a simple energy measure for the discrete dynamical system; this energy, which is a direct analogue of the energy stored in the electrical and magnetic fields surrounding the reference circuit, may be used as a discrete-time Lyapunov function [37, 42] in order to provide further rules for dealing with the inevitable truncation of the filter state in a fixed-point implementation.

---

[†] Though it is perhaps difficult to conceive of wave motion in a lumped system (i.e., one with negligible spatial extent) such as an analog electrical network, it should be mentioned that so-called wave variables may be interpreted as traveling waves in a network whose components are connected by transmission lines of vanishing length [161].

Many of the underlying ideas, however, had existed for some time before they coalesced into Fettweis's digital filter design technique. In fact, it is perhaps best to describe wave digital filtering not as an unprecedented invention, but as the successful synthesis of two principal preexistent ideas. The crucial wave variable and scattering concepts were borrowed from microwave filter design [11, 12], and digital structures based on the reflection and transmission of waves had appeared previously, especially in "layer-peeling" and "layer-adjoining" methods for solving inverse problems that arise in geophysics [22, 23, 213], and in models of the human vocal tract used in the analysis and synthesis of speech [104, 145], as we saw in §1.1.1. Many other digital filter structures make use of similar ideas, and have similar useful properties—among these are digital ladder and lattice forms [79], normalized filters [80] and orthogonal filters. This last type of structure has been formally unified with WDFs in [192]. The other cornerstone of wave digital filtering, the concept of a continuous-to-discrete spectral mapping which is, in some-sense, energy preserving, was not new to circuit discretization approaches. It appeared in the 1960s in the numerical analysis community which was concerned with the stability of the discretization of sets of ordinary differential equations (ODEs); indeed, wave digital filtering can be thought of as an *A-stable* [32, 65, 75] numerical method which discretizes the defining differential equations of an analog electrical network.

Wave digital filtering has, since its inception, developed in many directions, and has become a large subfield of the vast expanse of digital filter design. Because this thesis is devoted to the use of wave digital filters for simulation purposes, and not for filtering, this introductory chapter is intended merely to motivate material in the sequel, and to provide enough basic information for the reader to understand the WDF symbology (which is, unfortunately, somewhat idiosyncratic and takes a bit of getting used to). Indeed, many filtering issues do not arise at all in a simulation setting, at least from the point of view of traditional numerical analysis[†]. The single best WDF review paper is certainly [46], which is filled with practical filter design information and references. We briefly mention that some of the recent lines of development have been in the areas of multi-rate systems and filter banks [54, 117, 186], cochlear modelling [76], vocal tract modelling [177], the modelling of nonlinear circuit components [39] such as transistors [36], switching elements [151] as well as applications to nonlinear transmission lines [40, 126]. The concept of a generalized adaptor (see §2.3.5) with memory, as another means of approaching nonlinear circuit elements has been explored in [154]. Another important direction has been the generalization of WDFs to the multidimensional case [62], and we will discuss this in detail in the next chapter.

## 2.2 Classical Network Theory

### 2.2.1 N-ports

Classical network theory [12] is partly concerned with the properties of connections of *N-port* devices. In the abstract, an $N$-port is a mathematical entity whose internal behavior is only accessible through its *$N$ ports.* With the $j$th port is associated a *current* $i_j$, a *voltage* $v_j$, and two *terminals* (see Figure 2.1). The two terminals of any port must always be connected to the terminals of another port. A *network* is simply a collection of $N$-ports connected such that no port is left free[††].

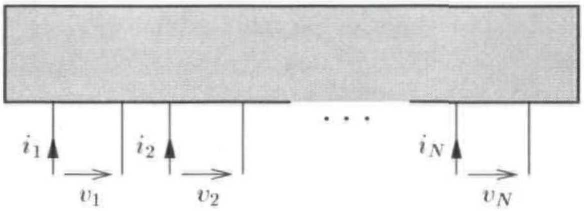

Figure 2.1: *N-port.*

For lumped networks, the voltages, currents and possibly element values in the networks are allowed to be real-valued functions of a sole real parameter $t$ which is usually interpreted as physical time. Multidimensional networks [208] are more general in the sense that the voltages, currents and port resistances may be functions of one or many other parameters, which may represent spatial dimensions. In this introductory chapter, we will be concerned only with lumped networks, but it should be kept in mind that Chapter 3 and parts of Chapters 4 and 5 are devoted chiefly to a particular class of multidimensional network which can represent the behavior of a distributed physical system.

---

[†] A good example of such a concern presents itself when we look into spectral analysis of difference schemes in Appendix A. Simulation people are usually interested in the convergence of approximate numerical schemes, in the limit as a grid spacing or time step becomes small; digital filtering people would think of this as matching a digital frequency response to that of the analog response (of the physical system) near the spatial or temporal DC frequency; for musical sound synthesis, however, these grid spacings or time steps are generally fixed (by the ***sampling rate***), so it might be worthwhile to look at a measure of the spectral fit over the entire spectrum.

[††] More generally, network theory treats so-called *t-terminal* or *multi-pole networks* [206], for which terminals are not necessarily associated in pairs.

If an $N$-port is *linear* and *time-invariant* (LTI), then the port quantities may exhibit a purely exponential time-dependence at a single complex frequency $s$. For such an *exponential state* [12], it is also useful to define, for any port with voltage $v(t)$ and current $i(t)$, the complex amplitudes $\hat{v}$ and $\hat{i}$. We can then write

$$v(t) = \hat{v}e^{st} \qquad\qquad i(t) = \hat{i}e^{st}$$

Under certain conditions [12], a LTI network will possess an $N \times N$ *impedance matrix*† $\mathbf{Z}$, so that the steady-state voltages and currents are related by

$$\hat{\mathbf{v}} = \mathbf{Z}\hat{\mathbf{i}} \tag{2.1}$$

where $\hat{\mathbf{v}}$ and $\hat{\mathbf{i}}$ are the column $N$-vectors containing the amplitudes $\hat{v}_1, \ldots, \hat{v}_N$ and $\hat{i}_1, \ldots, \hat{i}_N$ respectively. In general, if the $N$-port contains elements which behave as differential or integral operators, then we will have $\mathbf{Z} = \mathbf{Z}(s)$. The *admittance* of such an $N$-port is defined as

$$\mathbf{Y} = \mathbf{Z}^{-1}$$

at frequencies $s$ for which $\mathbf{Z}$ is invertible, and as infinity otherwise.

In most cases of interest, the entries of $\mathbf{Z}(s)$ will be rational functions of $s$. An $N$-port so defined is called *real* if the coefficients of these rational functions are real numbers. In this case, there is no loss in generality [12] in considering the port voltages and currents to be real-valued functions of $t$, in which case we may write, for an exponential state,

$$v(t) = \mathrm{Re}\left(\hat{v}e^{st}\right) \qquad\qquad i(t) = \mathrm{Re}\left(\hat{i}e^{st}\right)$$

Now $v(t)$ and $i(t)$ are referred to as the real instantaneous port voltage and current respectively.

### 2.2.2 Power and Passivity

The total instantaneous power absorbed by a real $N$-port is defined by

$$w_{inst}(t) = \sum_{j=1}^{N} v_j(t)i_j(t) \tag{2.2}$$

---

† A linear and time-invariant $N$-port need not have an impedance; the ideal transformer, for example, does not. In such cases, a more general "hybrid" matrix [12], from which all relevant properties may be deduced, can be defined. We will make special use of hybrid forms in §4.10.

where $v_j(t)$ and $i_j(t)$ are the real instantaneous voltage and current at port $j$. In general, for an $N$-port which contains stored energy $E(t)$, which dissipates energy at rate $w_d(t)$, and which contains sources which provide energy at rate $w_s(t)$, then the energy balance

$$\int_{t_1}^{t_2} (w_{inst} + w_s - w_d)\, dt = E(t_2) - E(t_1) \tag{2.3}$$

must hold over any interval $[t_1, t_2]$. Such an $N$-port is called *passive* if we have

$$\int_{t_1}^{t_2} w_{inst} dt \geq E(t_2) - E(t_1) \tag{2.4}$$

over any time interval; the increase in stored energy must be less than the energy delivered through the ports. The $N$-port is called *lossless* if (2.4) holds with equality over any interval.

For a linear time-invariant $N$-port, in an exponential state of complex frequency $s$, we can define the *total complex power* absorbed to be the inner product

$$w = \hat{\mathbf{i}}^* \hat{\mathbf{v}}$$

and the *average* or *active power* as

$$\bar{w} = \mathrm{Re}(\hat{\mathbf{i}}^* \hat{\mathbf{v}})$$

where $^*$ denotes transpose conjugation. For an $N$-port defined by an impedance relationship, we may immediately write, in terms of the voltage and current amplitudes,

$$\bar{w} = \mathrm{Re}\left(\hat{\mathbf{i}}^* \hat{\mathbf{v}}\right) = \frac{1}{2}\left(\hat{\mathbf{i}}^* \hat{\mathbf{v}} + \hat{\mathbf{v}}^* \hat{\mathbf{i}}\right) = \frac{1}{2}\left(\hat{\mathbf{i}}^* \mathbf{Z} \hat{\mathbf{i}} + \hat{\mathbf{i}}^* \mathbf{Z}^* \hat{\mathbf{i}}\right) = \frac{1}{2}\left(\hat{\mathbf{i}}^* \left(\mathbf{Z} + \mathbf{Z}^*\right) \hat{\mathbf{i}}\right)$$

For such a real LTI $N$-port, *passivity* may be defined in the following way. If the total active power absorbed by an $N$-port is always greater than or equal to zero for frequencies $s$ such that $\mathrm{Re}(s) \geq 0$, then it is called *passive*. This implies that

$$\mathbf{Z} + \mathbf{Z}^* \geq \mathbf{0} \qquad \text{for} \qquad \mathrm{Re}(s) \geq 0 \tag{2.5}$$

A matrix $\mathbf{Z}$ with such a property is called a *positive* matrix. In the present case of a real $N$-port, $\mathbf{Z}$ is called *positive real* (though in general, positivity is all that is required for passivity). If the average power absorbed is identically zero for $\mathrm{Re}(s) = 0$, or, in terms of impedances, if

$$\mathbf{Z} + \mathbf{Z}^* = \mathbf{0} \qquad \text{for} \qquad \mathrm{Re}(s) = 0$$

then the $N$-port is called *lossless*.

### 2.2.3 Kirchoff's Laws

Connections between individual ports can be made through an appeal to *Kirchoff's Laws*, which specify two important connection rules. *Kirchoff's Voltage Law* (KVL) states that for a series connection, as pictured in Figure 2.2(a), the currents will be equal in all ports to be connected, and that the sum of the voltages at all ports is zero, or, in other words, if we have a series connection of $M$ ports,

$$\begin{aligned} i_1 = i_2 = \ldots = i_M \\ v_1 + v_2 + \ldots + v_M = 0 \end{aligned}$$

*Kirchoff's Current Law* (KCL) specifies the dual relationship among the voltages and currents in the case of a parallel connection of $M$ ports, as per Figure 2.2(b), as

$$\begin{aligned} v_1 = v_2 = \ldots = v_M \\ i_1 + i_2 + \ldots + i_M = 0 \end{aligned}$$

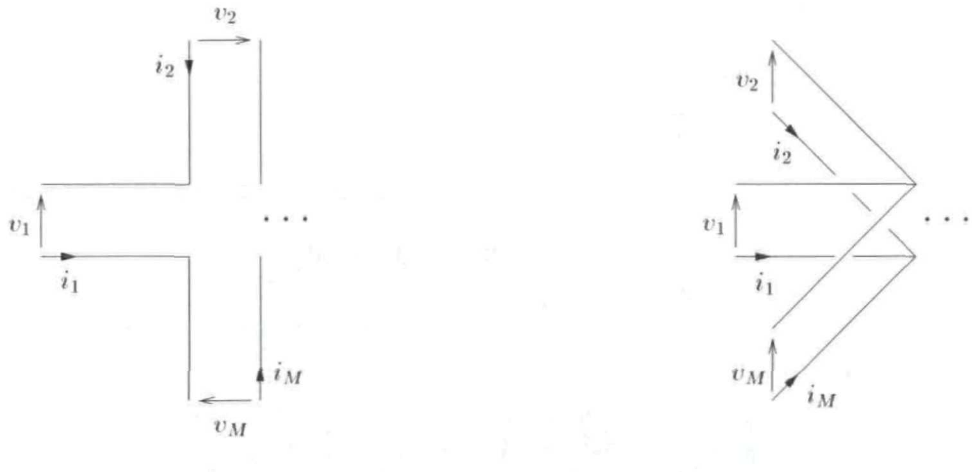

(a) (b)

Figure 2.2: *Kirchoff connections of $M$ ports, in* (a) *series and* (b) *parallel.*

Both sets of constraints hold instantaneously and can be thought of as $M$-ports in their own right. In addition, both types of $M$-port are passive, and in fact lossless. For example, in the case of a series connection of $M$ ports where the currents at every port are the same and equal to $i$, we have, from (2.2), that

$$w_{inst} = \sum_{j=1}^{M} i_j v_j = i \sum_{j=1}^{M} v_j = 0$$

Losslessness of the parallel connection can be similarly demonstrated. It is possible to show, through the use of *Tellegen's Theorem* [136] that a network made up of Kirchoff connections of passive $N$-ports will behave passively as a whole.

### 2.2.4 Circuit Elements

The most commonly encountered linear *one-ports* are the *inductor* of inductance $L$, the *resistor* of resistance $R_0$ and *capacitor* of capacitance $C$; their schematic representations are shown in Figure 2.3.

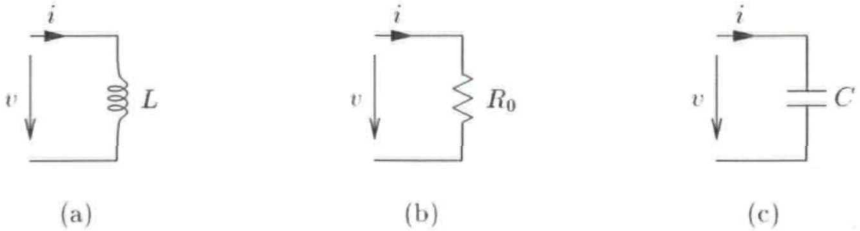

Figure 2.3: *One-port elements—* (a) *an inductor of inductance* $L$, (b) *a resistor of resistance* $R_0$ *and* (c) *a capacitor of capacitance* $C$.

The equations relating voltage and current in the three one-ports, as well as their associated impedances are as follows:

$$\text{Inductor}: \qquad v = L\frac{di}{dt} \qquad Z = Ls \tag{2.6}$$

$$\text{Resistor}: \qquad v = R_0 i \qquad Z = R_0 \tag{2.7}$$

$$\text{Capacitor}: \qquad i = C\frac{dv}{dt} \qquad Z = \frac{1}{Cs} \tag{2.8}$$

Each of these circuit elements is passive as long as its element value ($L$, $C$ or $R_0$) is positive[†]; the inductor and capacitor are easily shown to be lossless as well. The inductor and capacitor are examples of *reactive* circuits elements—all power instantaneously absorbed by either one will be stored and eventually be returned to the network to which it is connected. The resistor is passive, but not lossless.

In addition to the one-ports mentioned above, we can also define the *short-circuit*, *open-circuit*,

---

[†] More generally, we allow these values to be zero as well. In these cases, the inductor and resistor are interpreted as short-circuits, and the capacitor as an open-circuit.

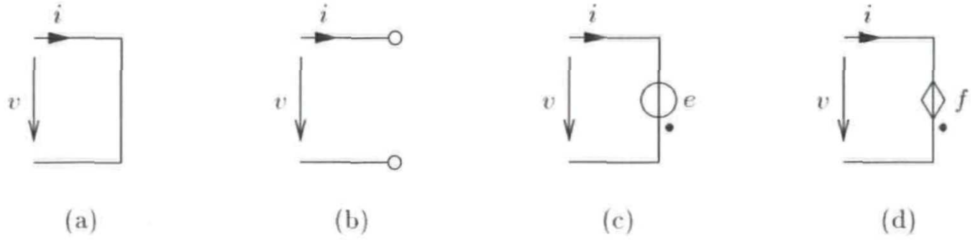

Figure 2.4: *Other one-ports*— (a) *short-circuit*, (b) *open-circuit*, (c) *voltage source and* (d) *current source. Dots adjacent to the sources indicate polarity.*

*current source* and *voltage source* (see Figure 2.4) by

$$\begin{aligned}
&\text{Short-circuit}: && v = 0\\
&\text{Open-circuit}: && i = 0\\
&\text{Voltage source}: && v = e(t)\\
&\text{Current source}: && i = f(t)
\end{aligned}$$

The impedances of the short- and open-circuit one-ports are zero and infinity, respectively. Both are lossless.

The *two-ports* which will occur most frequently in this thesis are the *transformer* and *gyrator*, both shown in Figure 2.5. Each of these two-ports has two voltage/current pairs, one for each port. The transformer has associated with it one free parameter $n$, called the *turns ratio*, and the gyrator is defined with respect to a parameter $R_G > 0$, as well as a direction, represented graphically by an arrow. The relation among the port variables in each case is given by

$$\text{Transformer}: \qquad v_2 = nv_1 \qquad i_1 = -ni_2 \tag{2.9}$$

$$\text{Gyrator}: \qquad v_1 = -R_G i_2 \qquad v_2 = R_G i_1 \tag{2.10}$$

It is easily checked that both the transformer and gyrator are lossless two-ports. The gyrator is the first example we have seen so far of a *non-reciprocal* element—that is, its impedance matrix is not Hermitian; while we will not make nearly as much use of it here as the other elements, it will find a place in certain parts of this work, especially in dealing with physical systems which have a certain type of asymmetric coupling (see Chapter 5), in optimizing certain wave digital structures for simulation (see §3.12), and will play a pivotal role in linking digital waveguide networks to wave digital networks (see §4.10).

There are other $N$-ports of interest in network theory, many of which have been applied successfully in wave digital filter designs, such as circulators as well as time-varying [178] and non-linear elements [36, 39, 64, 151], which have been used to study the propagation of nonlinear waves in

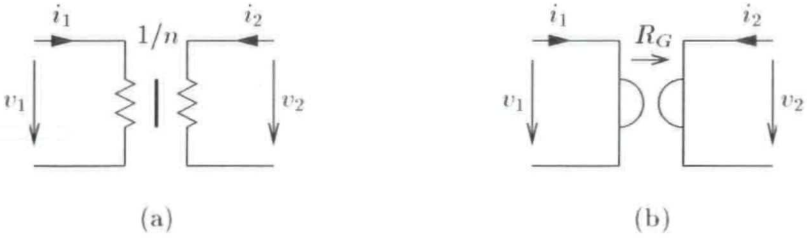

Figure 2.5: *Two-ports— (a) a transformer, of turns ratio $n$ and (b) a gyrator, of gyration coefficient $R_G$.*

lumped circuits [126]. For numerical integration purposes, however, the above set of elements proves to be an amply sufficient set of basic tools. An exception will be the non-linear distributed elements which appear in the circuit-based approach to fluid-dynamical problems; we mention these elements briefly in Appendix B.

## 2.3 Wave Digital Elements and Connections

### 2.3.1 The Bilinear Transform

Wave digital filters result from the mapping of a lumped analog electrical network (usually made up of the elements mentioned in the previous section connected using Kirchoff's Laws, and which is intended for use as a filter) into the discrete-time domain. In the linear time-invariant case, this translation is carried out using a particular type of spectral mapping between the analog frequency variable $s$ and a new discrete frequency variable $\psi$ which will be a rational function of $z^{-1} = e^{-sT}$ which is interpreted as a unit delay, of duration $T$; the mapping affects only reactive $N$-ports, i.e., those whose behavior is frequency-dependent, such as the inductor and capacitor. *Memoryless* elements, such as the transformer, gyrator and resistor (as well as the parallel or series connection, interpreted as an $N$-port) are frequency-independent, and will be unaffected by such a transformation.

The frequency mapping proposed by Fettweis[†] in [41] is a particular type of bilinear transform, given by

$$s \rightarrow \psi \triangleq \frac{2}{T}\frac{1-e^{-sT}}{1+e^{-sT}} = \frac{2}{T}\frac{1-z^{-1}}{1+z^{-1}} \tag{2.11}$$

---

[†] Fettweis in fact proposes the mapping $s \rightarrow (1-z^{-1})/(1+z^{-1})$, which is similar to (2.11) except for the factor of $2/T$. Although this factor is of little importance in filtering applications, it is necessary here for the interpretation of such mapping as an integration rule. This should become clear in Chapter 3.

We can then write

$$\mathrm{Re}(\psi) = \frac{2}{T}\frac{1-e^{-2\mathrm{Re}(s)T}}{|1+e^{-sT}|^2} = \frac{2}{T}\frac{1-|z|^{-2}}{|1+z^{-1}|^2}$$

so clearly

$$\begin{array}{ccccc}
\mathrm{Re}(s) > 0 & \Longleftrightarrow & \mathrm{Re}(\psi) > 0 & \Longleftrightarrow & |z| > 1 \\
\mathrm{Re}(s) < 0 & \Longleftrightarrow & \mathrm{Re}(\psi) < 0 & \Longleftrightarrow & |z| < 1 \\
\mathrm{Re}(s) = 0 & \Longleftrightarrow & \mathrm{Re}(\psi) = 0 & \Longleftrightarrow & |z| = 1
\end{array}$$

This implies that stable, causal transfer functions in $s$ will be mapped to stable causal transfer functions in the discrete variable $z^{-1}$, and moreover that positive real functions will be mapped to functions which are *positive real in the outer disk* [162]. Such functions are often called *pseudopassive* [42], and have an energetic interpretation similar to that of their counterparts in the analog domain. (Indeed, Fettweis views pseudopassivity as simply passivity using a warped frequency variable $\psi$ [46].)

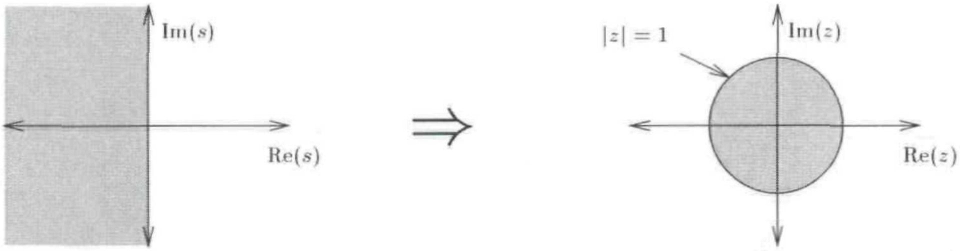

Figure 2.6: *Spectral mapping corresponding to the trapezoid rule.*

In particular, for a harmonic state—that is, for real frequencies $\omega$ such that $s = j\omega$ and $z = e^{j\omega T}$, we have that

$$\omega \rightarrow \frac{2}{T}\tan\left(\frac{\omega T}{2}\right) \tag{2.12}$$

so that the entire analog frequency spectrum is mapped to the discrete frequency spectrum exactly once. In particular, we have that the analog DC frequency $s = 0$ is mapped to discrete DC $z = 1$, and that analog infinite frequency is mapped to the Nyquist frequency. It should be clear that there will be significant warping of the spectrum away from either extreme.

It is also worthwhile examining the mapping (2.11) on the unit circle in the low-frequency limit, in which case we can expand the right side of the mapping about $\omega = 0$, to get

$$\frac{2}{T}\tan\left(\frac{\omega T}{2}\right) = \omega - \frac{T^2}{12}\omega^3 + \ldots$$

The mapping (2.12) can be rewritten as

$$\omega \rightarrow \omega + O(\omega^3 T^2)$$

The frequency mapping thus becomes more accurate near $\omega = 0$ in the limit as $T \rightarrow 0$. The order of this approximation (namely to $T^2$) will play an important role in numerical integration methods, because it defines the accuracy of a numerical scheme [65, 131, 176].

It is important to mention that the time-domain interpretation of the bilinear mapping (2.11) is called the ***trapezoid rule*** for numerical integration. That is, treating $z^{-1}$ as the unit delay, the right-hand side of (2.11) serves as an approximation to the derivative in a discrete-time setting. For example, in the case of the inductor, application of the mapping yields the following difference equation relating the voltage and current:

$$v(n) + v(n-1) = \frac{2L}{T}\Big(i(n) - i(n-1)\Big) \tag{2.13}$$

It should be understood here that $v(n)$ and $i(n)$ in (2.13) now represent discrete approximations to the voltage and current of (2.7) at time $t = nT$, for integer $n$[†]. Generalizations of the WDF approach to cases in which the $N$-port of interest is time-varying or non-linear are based on this time-domain formulation, because in these cases, we no longer have a well-defined notion of frequency.

For the rest of this section, so as to avoid unnecessary extra notation, we will assume that we have discrete time voltages and currents. Thus $v$ and $i$ now refer to sequences $v(n)$ and $i(n)$, for $n$ integer, and the steady state quantities $\hat{v}$ and $\hat{i}$ are complex amplitudes of a sequence at the discrete frequency $z$.

### 2.3.2 Wave Variables

At this point, one may assume that we have finished; indeed, we can derive a discrete-time equivalent to any LTI $N$-port (graphically represented by a signal flow diagram involving shifts and arithmetic operations), and such elements can be connected using Kirchoff's Laws, which remain unchanged by the mapping (2.11). In particular, a network consisting of a collection of connected passive $N$-ports will possess a discrete equivalent of the passivity property, which has been called ***pseudopassivity***

---

[†] Since the two systems are assumed to be the same, modulo a spectral warping, we will not use a special notation to distinguish a discrete variable from a continuous one; the type of variable should be clear from context, and in cases where confusion may arise, we will always explicitly note the argument. In Chapter 4, however, we will use capital letters to distinguish discrete from continuous variables; this notational switch is unfortunate, but is a compromise necessary in order to remain coherent with the different literatures.

[42]. The problem, however, is that a simple application of the bilinear transform to a given $N$-port usually leaves us with port variables which are not related to each other in a strictly causal way. For example, the difference equation (2.13) that results in the case of the inductor relates $v(n)$ to $i(n)$ at every time step $n$ so that if we try to connect such a discrete-time one-port to another which has the same property (using Kirchoff's Laws, which are memoryless), we necessarily end up with non-realizable *delay-free loops* [46] in our resulting signal flow diagram. In other words, we will not be able to explicitly update all the port variables in our algorithm using only past values stored in the delay registers.

The problem of these delay-free loops was solved by Fettweis [41] with the introduction of *wave variables*, a concept with a long history borrowed from microwave electronics [11, 12]. For a port with voltage $v$ and current $i$, *voltage waves* are defined by

$$a = v + iR \qquad \text{Input voltage wave} \qquad (2.14a)$$
$$b = v - iR \qquad \text{Output voltage wave} \qquad (2.14b)$$

$a$ and $b$ are referred to as *wave variables*, and in particular, $a$ is called an ***input wave*** and $b$ an ***output wave***; the significance of these names will become clear in the examples of §2.3.4. This definition holds instantaneously, and will also be true for continuous $v$ and $i$, though we will almost never have occasion to refer to analog wave variables in this thesis. The parameter $R > 0$ is a free parameter known as the *port resistance*—its choice is governed by the character of the element itself. We also can define the *port conductance* $G$ by

$$G = \frac{1}{R} \qquad (2.15)$$

at a port with port resistance $R$.

It is also possible to define *power-normalized* waves [46] $\underline{a}$ and $\underline{b}$ at any port with port resistance $R$ by

$$\underline{a} = \frac{v + iR}{2\sqrt{R}} \qquad \text{Input power wave} \qquad (2.16a)$$
$$\underline{b} = \frac{v - iR}{2\sqrt{R}} \qquad \text{Output power wave} \qquad (2.16b)$$

The two types of waves are simply related to each other by

$$a = 2\sqrt{R}\underline{a} \qquad (2.17a)$$
$$b = 2\sqrt{R}\underline{b} \qquad (2.17b)$$

but power-normalized quantities have certain advantages in cases for which a port resistance is time-varying or signal dependent (indeed, in these cases, power-normalized waves *must* be employed if passivity in the digital simulation is to be maintained). In general, however, in view of (2.17), it should be assumed that we are using voltage waves unless otherwise indicated.

The steady state quantities $\hat{a}$ and $\hat{b}$ are defined in a manner identical to (2.14), where we replace $v$ and $i$ by $\hat{v}$ and $\hat{i}$.

### 2.3.3 Pseudopower and Pseudopassivity

Fettweis [42] defines the *instantaneous pseudopower* absorbed by a port with port resistance $R$ (real) at time step $n$ in terms of the discrete input and output wave quantities as

$$w_{inst}(n) = \frac{1}{R}\left(a^2(n) - b^2(n)\right) = 4\left(\underline{a}^2(n) - \underline{b}^2(n)\right) \tag{2.18}$$

which, when the transformation (2.14) is inverted, gives

$$w_{inst}(n) = 4v(n)i(n)$$

This discrete power definition coincides with the standard definition of power in classical network theory from (2.2), aside from the factor of 4, which is of no consequence if definition (2.18) is applied consistently throughout a wave digital network.

For a real LTI $N$-port, in an exponential state of complex frequency $z$, the steady-state average pseudopower may be written in terms of the $N \times 1$ vectors $\underline{\hat{\mathbf{a}}}$ and $\underline{\hat{\mathbf{b}}}$ which contain the power-normalized complex amplitudes $\underline{\hat{a}}_j$ and $\underline{\hat{b}}_j$, for $j = 1, \ldots, N$ as

$$\bar{w} \;=\; 4\left(\underline{\hat{\mathbf{a}}}^*\underline{\hat{\mathbf{a}}} - \underline{\hat{\mathbf{b}}}^*\underline{\hat{\mathbf{b}}}\right)$$

The steady-state reflectance $\underline{\mathbf{S}}(z^{-1})$ is defined by

$$\underline{\hat{\mathbf{b}}} = \underline{\mathbf{S}}\,\underline{\hat{\mathbf{a}}}$$

and gives

$$\bar{w} = 4\left(\underline{\hat{\mathbf{a}}}^*(\mathbf{I}_N - \underline{\mathbf{S}}^*\underline{\mathbf{S}})\underline{\hat{\mathbf{a}}}\right)$$

where $\mathbf{I}_N$ is the $N \times N$ identity matrix. For *pseudopassivity* [42], we require, then (recalling that the bilinear transform (2.11) maps the right half $s$-plane to the exterior of the unit circle in the $z$ plane) that

$$\underline{\mathbf{S}}^*(z^{-1})\underline{\mathbf{S}}(z^{-1}) \leq \mathbf{I}_N \qquad \text{for} \qquad |z| \geq 1 \tag{2.19}$$

$\underline{\mathbf{S}}(z^{-1})$ is sometimes called a *bounded real* matrix. If (2.19) holds with equality for $|z| = 1$, then it is called *lossless bounded real* (LBR) [193]. In general, to bounded real matrix reflectances there correspond positive real matrix impedances, and vice versa. In terms of voltage wave quantities, we have for a wave digital $N$-port, that

$$\hat{\mathbf{a}} = 2\mathbf{R}^{\frac{1}{2}}\underline{\hat{\mathbf{a}}} \qquad \hat{\mathbf{b}} = 2\mathbf{R}^{\frac{1}{2}}\underline{\hat{\mathbf{b}}}$$

where $\mathbf{R}^{\frac{1}{2}}$ is the diagonal square root of the matrix containing the $N$ port resistances $R_1, \dots, R_N$ on its diagonal. We then have

$$\mathbf{S} = \mathbf{R}^{\frac{1}{2}}\underline{\mathbf{S}}\mathbf{R}^{-\frac{1}{2}}$$

for the voltage wave scattering matrix $\mathbf{S}$ and thus we require

$$\mathbf{S}^*(z^{-1})\mathbf{R}^{-1}\mathbf{S}(z^{-1}) \leq \mathbf{R}^{-1} \qquad \text{for} \qquad |z| \geq 1 \tag{2.20}$$

for passivity. For one-ports, the requirements (2.20) and (2.19) are the same.

Also note that we have, by applying the power wave variable definitions (2.16), and the discrete impedance relation $\hat{\mathbf{v}} = \mathbf{Z}\hat{\mathbf{i}}$ (which is identical to the analog relation from (2.1), except that we now have $\mathbf{Z} = \mathbf{Z}(z^{-1})$), that

$$\mathbf{S} = (\mathbf{Z}\mathbf{R}^{-1} + \mathbf{I})^{-1}(\mathbf{Z}\mathbf{R}^{-1} - \mathbf{I}) \tag{2.21}$$

If the $N$-port is not LTI, then it is possible to apply a similar idea to the expression for the instantaneous pseudopower, from (2.18) in order to derive a passivity condition [46]; In this case, pseudopassivity has also been called ***incremental pseudopassivity*** [125].

### 2.3.4 Wave Digital Elements

We will now present the wave digital equivalents of all the circuit elements mentioned in §2.2.4.

Under the bilinear transform (2.11), the steady-state equation for an inductor becomes

$$\hat{v} = \frac{2L}{T}\left(\frac{1 - z^{-1}}{1 + z^{-1}}\right)\hat{i}$$

or, in the discrete-time domain,

$$v(n) + v(n-1) = \frac{2L}{T}\Big(i(n) - i(n-1)\Big)$$

Applying the definition of wave variables (2.14), we get, in the time domain,

$$a(n)+b(n)+a(n-1)+b(n-1)=\frac{2L}{RT}\Big(a(n)-b(n)-a(n-1)+b(n-1)\Big) \tag{2.22}$$

If we make the choice

$$R=\frac{2L}{T}$$

then (2.22) simplifies to

$$b(n)=-a(n-1) \tag{2.23}$$

Thus the input wave $a$ must undergo a delay and sign-inversion before it is output as $b$. In terms of steady-state quantities, we have

$$\hat{b}=-z^{-1}\hat{a} \qquad \Rightarrow \qquad S(z^{-1})=-z^{-1} \tag{2.24}$$

The reflectance $S(z^{-1})$ is, as expected, LBR (see previous section). The resulting *wave digital one-port* is shown in Figure 2.7(a).

The derivations of the wave digital one-ports corresponding to the resistor and capacitor are similar; their signal-flow graphs also appear in Figure 2.7. We note that the same choice of the port resistance $R$ should be made in the case of power-normalized wave variables. We also note in passing that we have used here the symbol $T$ to represent a unit delay in a wave digital filter[†].

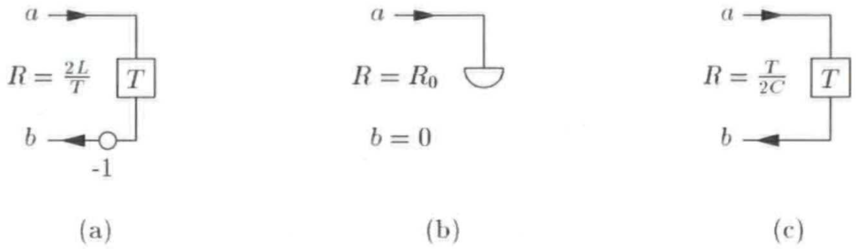

Figure 2.7: *Wave digital one-ports corresponding to the classical one-ports of Figure 2.3*— (a) *the wave digital inductor*, (b) *resistor, and* (c) *capacitor.*

The short-circuit and open-circuit one-ports are, for any choice of the port resistance $R$, perfectly reflecting (with or without sign inversion, respectively). The appearance of the factor $R$ in the definition of the wave digital current source results from our choice of using voltage waves (as opposed to current waves). In all the wave digital one-ports of Figure 2.8, there is an instantaneous dependence of the output wave $b$ on the input wave $a$, and we may expect delay-free loops to appear when these elements are connected with others. On the other hand, the form of these one-ports does not depend on a particular choice of the port resistance $R$ (except in a very minor way for a current source), and remains a free parameter, which can be used, in many cases, to remove delay-free loops.

---

[†] In this chapter, because all elements are LTI, we could equally well use the symbol $z^{-1}$ for the unit delay (as is commonplace in the digital filtering literature). In the next chapter, however, when we will be making use of shifts in multiple dimensions for systems which are not, in general, shift-invariant, then frequency domain signal-flow diagrams may only be used in special cases.

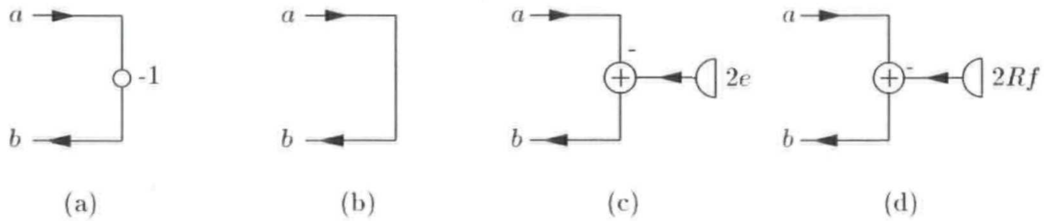

Figure 2.8: *Wave digital one-ports corresponding to the classical one-ports of Figure 2.4*— (a) *short-circuit,* (b) *open-circuit,* (c) *voltage source and* (d) *current source.*

It is also possible to combine resistances and sources [46]; a resistive voltage source, shown in Figure 2.9(a), consists of a voltage source $e$ in series with a resistor of resistance $R_0$. If the port resistance of the combined one-port is chosen to be $R_0$, then the wave digital one-port [46] is as shown in Figure 2.9(b). A wave digital resistive current source can be similarly defined.

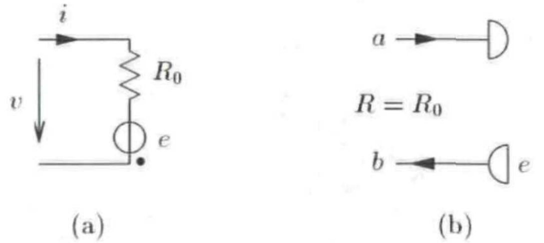

Figure 2.9: (a) *A resistive voltage source, and* (b) *the associated wave digital one-port.*

The classical transformer and gyrator two-ports can be treated in the same way. For example, the gyrator accepts two input waves $a_1$ and $a_2$, and yields two output waves $b_1$ and $b_2$. There are two port resistances, $R_1$ and $R_2$. The instantaneous equations (2.10) relating the voltages and currents in a gyrator become, upon substitution of wave variables,

$$\begin{bmatrix} b_1 \\ b_2 \end{bmatrix} = \frac{1}{R_G^2 + R_1 R_2} \begin{bmatrix} R_G^2 - R_1 R_2 & -2R_G R_1 \\ 2R_G R_2 & R_G^2 - R_1 R_2 \end{bmatrix} \begin{bmatrix} a_1 \\ a_2 \end{bmatrix} \tag{2.25}$$

which simplifies, under the choice of $R_1 = R_G$ and $R_2 = R_G$ to

$$b_1 = -a_2 \qquad\qquad b_2 = a_1 \tag{2.26}$$

If we are using power-normalized wave variables, then the scattering equation for the gyrator becomes

$$\begin{bmatrix}\underline{b}_1\\ \underline{b}_2\end{bmatrix} = \frac{1}{R_G^2 + R_1R_2}\begin{bmatrix}R_G^2 - R_1R_2 & -2R_G\sqrt{R_1R_2}\\ 2R_G\sqrt{R_1R_2} & R_G^2 - R_1R_2\end{bmatrix}\begin{bmatrix}\underline{a}_1\\ \underline{a}_2\end{bmatrix} \tag{2.27}$$

In this case, any choice of the port resistances such that $R_1R_2 = R_G^2$ gives

$$\underline{b}_1 = -\underline{a}_2 \qquad\qquad \underline{b}_2 = \underline{a}_1 \tag{2.28}$$

The ideal transformer also can take on various forms, depending on the choices of the port resistances and on the type of wave variable employed. Under a choice of port resistances $R_1$ and $R_2$ such that $R_2 = n^2R_1$, the equations (2.9) for the ideal transformer of turns ratio $n$ become

$$b_2 = na_1 \qquad\qquad b_1 = \frac{1}{n}a_2 \tag{2.29}$$

For the transformer and gyrator WD two-ports, we adopt general symbols that do not reflect a particular choice of the port resistances. If simplifying choices can be made in either case, than we can write the signal flow graph explicitly (see Figure 2.10). There may be occasions when it is not be possible to make these simplifying choices of the port resistances which yield (2.26) and (2.29). For example, when we approach the numerical integration of beam and plate systems in Chapter 5, as well as certain *balanced forms* (see §3.12) the WD networks contain gyrators whose port resistances are constrained, forcing us to use (2.25). We also mention that these two-ports are both lossless, and in fact *non-energic* [42] (i.e., we have $w_{inst}(n) = 0$, for all $n$).

Numerous other wave digital elements have been proposed, namely circulators, quasi-reciprocal

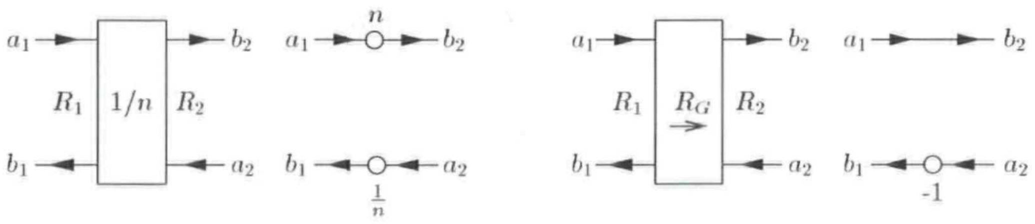

(a) (b)

Figure 2.10: *Wave digital two-ports— (a) a transformer with turns ratio $n$ and its simpler form for $R_2 = n^2R_1$ and (b) a gyrator of gyration coefficient $R_G$ and its simpler form for $R_1 = R_2 = R_G$.*

lines (QUARLS), as well as *unit elements* [46]. All have been applied fruitfully to filter design problems, but the unit element deserves a special treatment.

### The Unit Element

One wave digital two-port, called the unit element, is usually defined in the discrete-time domain, without reference to an analog counterpart; this wave digital two-port is shown in Figure 2.11(a). It was considered by Fettweis to be the "most important two-port element" [46], and was used extensively for realizability reasons in early wave digital filter designs, especially before the appearance of reflection-free ports [57]. It behaves exactly like a transmission line, and is in fact identical to the waveguide or bidirectional delay line which is the key component of the digital waveguide network [166], as we saw in §1.1.2. The unit element is time-invariant, and obviously lossless, though it is reactive (able to store energy). It should be clear, however, that we may simply apply the bilinear transform backwards in order to obtain a representation in the continuous time domain. The scattering relation for the unit element is

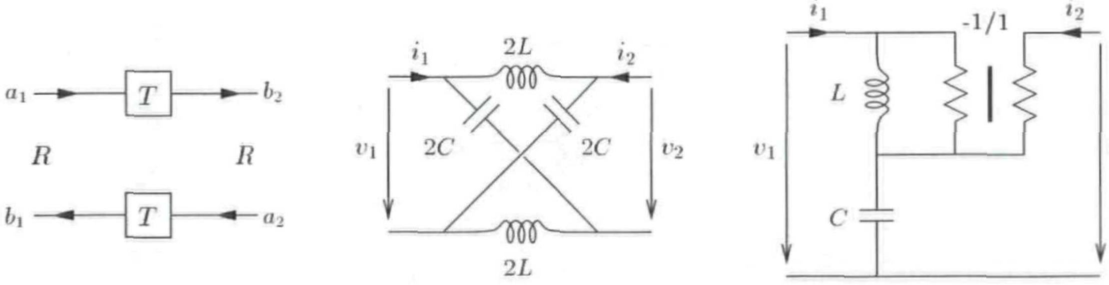

(a) (b) (c)

Figure 2.11: *The unit element and its continuous-time counterparts*— (a) *a unit element, with port resistances $R$ and delays $T$,* (b) *its analog lattice form and* (c) *Jaumann form reference two-ports, with $L = \frac{RT}{4}$ and $C = \frac{T}{R}$.*

$$\begin{bmatrix} \hat{b}_1 \\ \hat{b}_2 \end{bmatrix} = \begin{bmatrix} 0 & z^{-1} \\ z^{-1} & 0 \end{bmatrix} \begin{bmatrix} \hat{a}_1 \\ \hat{a}_2 \end{bmatrix}$$

and transforming from wave variables back to voltages and currents via (2.14) gives

$$\begin{bmatrix} \hat{v}_1 \\ \hat{v}_2 \end{bmatrix} = \frac{R}{1 - z^{-2}} \begin{bmatrix} 1 + z^{-2} & 2z^{-1} \\ 2z^{-1} & 1 + z^{-2} \end{bmatrix} \begin{bmatrix} \hat{i}_1 \\ \hat{i}_2 \end{bmatrix}$$

where $R$ is the port resistance at either port. The bilinear transform (2.11) may be inverted by

$$z^{-1} \rightarrow \frac{2-sT}{2+sT}$$

and we obtain, finally, a relationship between the continuous-time steady-state voltages and currents, with an impedance matrix (dependent on the time step $T$, assumed constant) given by

$$\mathbf{Z}(s,T) = R\begin{bmatrix} \frac{1}{sT}+\frac{sT}{4} & \frac{1}{sT}-\frac{sT}{4} \\ \frac{1}{sT}-\frac{sT}{4} & \frac{1}{sT}+\frac{sT}{4} \end{bmatrix}$$

This defining equation for a two-port may be written as a lattice [55] (or Jaumann [132] equivalent) connection of an inductor and capacitor, each of whose values is now dependent on the choice of the time step, $T$. See Figures 2.11(b) and (c).

We mention this representation because in the distributed case, it will be possible to define multidimensional unit elements which will be very helpful in integrating digital waveguide networks (see Chapter 4) into the multidimensional wave digital filter framework (see Chapter 3). The necessary manipulations, which are quite similar to the ones performed above, are carried out in §4.10.

### 2.3.5 Adaptors

Consider now a series connection of $M$ ports, where we have a port resistance $R_j > 0$, $j = 1, \ldots, M$, associated with each port. In terms of instantaneous quantities, we have

$$\sum_{j=1}^{M} v_j = 0$$

or, in terms of wave variables, using the inverse of the transformation (2.14),

$$\sum_{j=1}^{M} (a_j + b_j) = 0$$

Since the currents at all ports are all equal to $i$, this implies, using $b_j = a_j - 2R_j i$, that

$$\sum_{j=1}^{M} (-2R_j i + 2a_j) = 0$$

and thus

$$i = \frac{1}{\sum_{j=1}^{M} R_j} \sum_{j=1}^{M} a_j \tag{2.30}$$

By applying similar manipulations in the case of a parallel connection of $M$ ports, we can then write down the equations relating the input and output wave variables at the $k$th port for both types of connection as

$$b_k = a_k - \frac{2R_k}{\sum_{j=1}^{M} R_j}\sum_{j=1}^{M} a_j, \qquad k = 1,\dots,M \qquad \text{Series connection} \tag{2.31}$$

$$b_k = -a_k + \frac{2}{\sum_{j=1}^{M} G_j}\sum_{j=1}^{M} G_j a_j, \qquad k = 1,\dots,M \qquad \text{Parallel connection} \tag{2.32}$$

where we recall from (2.15) that $G_j$ is defined as the reciprocal of the port resistance $R_j$. For power-normalized wave variables, we thus have, applying (2.17),

$$\underline{b}_k = \underline{a}_k - \frac{2\sqrt{R_k}}{\sum_{j=1}^{M} R_j}\sum_{j=1}^{M} \sqrt{R_j}\underline{a}_j, \qquad k = 1,\dots,M \qquad \text{Series connection} \tag{2.33}$$

$$\underline{b}_k = -\underline{a}_k + \frac{2\sqrt{G_k}}{\sum_{j=1}^{M} G_j}\sum_{j=1}^{M} \sqrt{G_j}\underline{a}_j, \qquad k = 1,\dots,M \qquad \text{Parallel connection} \tag{2.34}$$

The operator which performs this calculation on the wave variables is called a *series adaptor* or a *parallel adaptor* [46], depending on the type of connection. The graphical representations of three-port adaptors, for either voltage or power-normalized waves, are shown in Figure 2.12.

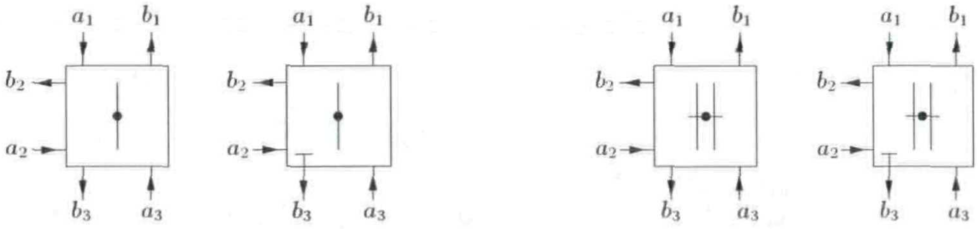

(a) (b)

Figure 2.12: *Three-port adaptors*— (a) *a general three-port series adaptor and one for which port 3 is reflection-free and* (b) *a general three-port parallel adaptor and one for which port 3 is reflection-free.*

A useful simplification occurs when we can choose, for a particular port $q$ (called a *reflection-free* port [57]) of an $M$-port adaptor,

$$R_q = \sum_{j=1,j\neq q}^{M} R_j \qquad \text{Series reflection-free port resistance} \tag{2.35a}$$

$$G_q = \sum_{j=1,j\neq q}^{M} G_j \qquad \text{Parallel reflection-free port conductance} \tag{2.35b}$$

in which case the scattering equations (2.31) yield, for the output wave at port $q$,

$$b_q = -\sum_{j=1, j\neq q}^{M} a_j \qquad \text{Series reflection-free port} \qquad (2.36a)$$

$$b_q = \frac{2}{\sum_{j=1}^{M} G_j} \sum_{j=1, j\neq q}^{M} G_j a_j \qquad \text{Parallel reflection-free port} \qquad (2.36b)$$

Thus, at a reflection-free port $q$, the output wave $b_q$ is independent of the input wave $a_q$; such a port can be connected to any other without risk of a resulting delay-free loop. The same choices of port resistances (2.35) will also give a reflection-free port if power wave variables are employed.

### Scattering Matrices for Adaptors

The adaptor equations for a connection of $M$ ports, in either the series (2.31) or parallel (2.32) case, may be written as

$$\mathbf{b} = \mathbf{S}\mathbf{a} \qquad (2.37)$$

where $\mathbf{b} = [b_1, \ldots, b_M]^T$ and $\mathbf{a} = [a_1, \ldots, a_M]^T$, and where we have

$$\mathbf{S} = \mathbf{I}_M - \boldsymbol{\alpha}_s \mathbf{1}^T \qquad \text{Series adaptor (voltage waves)} \qquad (2.38)$$

$$\mathbf{S} = -\mathbf{I}_M + \mathbf{1}\boldsymbol{\alpha}_p^T \qquad \text{Parallel adaptor (voltage waves)} \qquad (2.39)$$

Here $\mathbf{1}$ is an $M \times 1$ vector containing all ones, $\mathbf{I}_M$ is the $M \times M$ identity matrix, and $\boldsymbol{\alpha}_s$ and $\boldsymbol{\alpha}_p$ are defined by

$$\boldsymbol{\alpha}_s = \frac{2}{\sum_{j=1}^{M} R_j}[R_1, \ldots, R_M]^T \qquad \boldsymbol{\alpha}_p = \frac{2}{\sum_{j=1}^{M} G_j}[G_1, \ldots, G_M]^T$$

The sum of the elements of either $\boldsymbol{\alpha}_s$ or $\boldsymbol{\alpha}_p$ is 2. For power wave variables, we have a similar relationship,

$$\underline{\mathbf{b}} = \underline{\mathbf{S}}\,\underline{\mathbf{a}} \qquad (2.40)$$

where

$$\underline{\mathbf{S}} = \mathbf{I}_M - \sqrt{\boldsymbol{\alpha}_s}\sqrt{\boldsymbol{\alpha}_s}^T \qquad \text{Series adaptor (power-normalized waves)}$$

$$\underline{\mathbf{S}} = -\mathbf{I}_M + \sqrt{\boldsymbol{\alpha}_p}\sqrt{\boldsymbol{\alpha}_p}^T \qquad \text{Parallel adaptor (power-normalized waves)}$$

Here the square root sign indicates an entry-by-entry square root of a vector (all entries of $\boldsymbol{\alpha}_s$ and $\boldsymbol{\alpha}_p$ are non-negative).

Defining the Euclidean norm of a column vector $\mathbf{x}$ as $\|\mathbf{x}\|_2 = \sqrt{\mathbf{x}^T\mathbf{x}}$, it is easy to show that a power normalized scattering matrix $\underline{\mathbf{S}}$ is norm-preserving in either the series or parallel case, i.e., we have

$$\|\underline{\mathbf{b}}\|_2 = \|\underline{\mathbf{a}}\|_2 \tag{2.41}$$

For voltage waves, we have the preservation of a weighted $L_2$ norm, i.e.,

$$\|\mathbf{b}\|_{\mathbf{P},2} = \|\mathbf{a}\|_{\mathbf{P},2} \tag{2.42}$$

where $\|\cdot\|_{\mathbf{P},2} = \sqrt{(\cdot)^T\mathbf{P}(\cdot)}$; in this case, $\mathbf{P}$ is an $M \times M$ positive definite diagonal matrix simply given by $\mathrm{diag}(G_1, \ldots, G_M)$. It should be clear that (2.41) and (2.42) are merely re-statements of power conservation at a memoryless, lossless $M$-port.

Note that multiplying $\mathbf{S}$ or $\underline{\mathbf{S}}$ by a vector requires, in either the series of parallel case, $O(M)$ adds and multiplies; in particular, it is cheaper than a full $M \times M$ matrix multiply.

### 2.3.6 Signal and Coefficient Quantization

In a machine implementation of a wave digital filter, the signals and coefficients must necessarily be represented with a finite number of bits. As such, it is not immediately obvious that the passivity properties for a given WDF, which are framed in terms of real-valued signals (waves) and filter multipliers (related to the port resistances) will hold in a finite word-length computer implementation. All digital filter implementations are vulnerable to a host of undesirable effects which result from signal and coefficient quantization; among them are parasitic oscillations and high sensitivity of filter pole and zero locations (and thus the frequency response). WDFs, however, offer a number of means of combating these problems. The exploration of these means has produced a large body of literature [43, 46, 58, 125, 179, 204]. We give only a brief outline here, for completeness sake.

From the discussion of wave digital elements, it is easy to see that in most cases, the only arithmetic operations in a WDF will occur as signals are scattered from adaptors[†]; the wave digital inductor, capacitor and unit element involve only shifts and possibly sign inversion, and the wave digital resistor, which behaves as a sink, can essentially be ignored by the programmer once its port resistance has been absorbed into the adaptor to which it is connected. Simple quantization procedures [56, 201] were first proposed, and later the concept of incremental pseudopassivity [125] was developed for ensuring that a finite word-length implementation of a wave digital adaptor behaves passively under signal truncation. The most straightforward scheme appears in Figure 2.13, for the case of a three-port adaptor (either series or parallel).

---

[†] Referring to Figure 2.10, it is easy to see that the transformer with $n = \pm 1$ and $R_1 = R_2$, and the gyrator with $R_1 = R_2 = R_G$(their most common forms) also are arithmetic-free. Otherwise, a more detailed treatment is required.

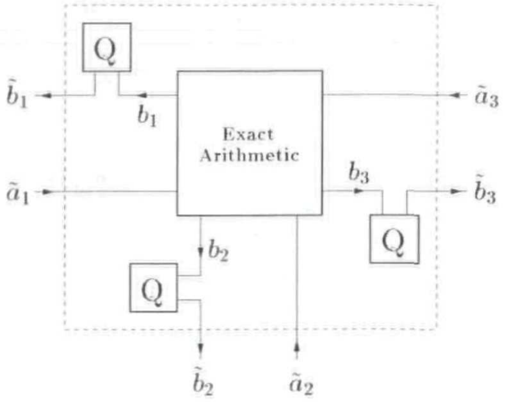

Figure 2.13: *Signal truncation at a three-port adaptor.*

$\tilde{a}_j$ are the input waves (assumed voltage waves) to the junction, for $j = 1, \ldots, M$ (we have $M = 3$ in Figure 2.13), and are assumed to be of some finite word-length. Extended precision is used within the adaptor in order exactly calculate the output waves $b_j$, from (2.37). We have assumed that the multiplier coefficients within the junction are of finite word-length as well—we will discuss this presently. The output waves $b_j$ thus satisfy (2.42), where $\mathbf{a}$ is replaced by $\tilde{\mathbf{a}}$, with $\tilde{\mathbf{a}} = [\tilde{a}_1, \ldots, \tilde{a}_M]^T$. Scattering is lossless. In general, however, the number of bits required to represent $b_j$ will now be greater than the number required for $\tilde{a}_j$; in order to reduce the size of the output word-length, we may apply *magnitude truncation* (represented graphically in Figure 2.13 by boxes labelled "Q", which are *not* wave digital one-ports. Magnitude truncation may be incorporated formally into the scattering picture through the use of *circulators* [125]). A reduced word-length wave $\tilde{b}_j$ is obtained from $b_j$ by truncating it in any way as long as magnitude is decreased. In other words, for any port $j$,

$$\tilde{b}_j^2 \leq b_j^2$$

This implies, then, that

$$\|\tilde{\mathbf{b}}\|_{\mathbf{P},2} \leq \|\mathbf{b}\|_{\mathbf{P},2} = \|\tilde{\mathbf{a}}\|_{\mathbf{P},2}$$

so that passivity is maintained even considering the finite word-length wave variables. In this way (by ensuring a decrease in the overall energy measure of the WD network), both large- and small-scale parasitic oscillations can be completely eliminated, at least the zero-input case [46]. Various types of overflow characteristics have been examined in [56, 125]. Such a quantization rule has also appeared in other contexts [193], and applies equally well to digital waveguide networks [166], which are the subject of Chapter 4.

The quantization of coefficients in WDFs [42, 43, 46, 111] as well as other similar filter structures [193] has been shown to have a minimal effect on the filter response. That is, in many lossless configurations [46], variations in the values of the multiplier coefficients (which are usually the reflection and transmission parameters $\boldsymbol{\alpha}_s$ or $\boldsymbol{\alpha}_p$ at an adaptor) can be shown to have a second-order effect on the filter response. In contrast, when such variations occur in direct-form filter structures, large changes in pole locations can result, and a stable filter may even become unstable [133]. This robustness property of scattering-based filter structures is sometimes called ***structural passivity*** [147, 169, 193]. As a simple example, consider the scattering equations (2.38) for a series adaptor; as mentioned above, the parameters in the vector $\boldsymbol{\alpha}_s$ are the filter multiplier coefficients, and recall also that the sum of the elements in $\boldsymbol{\alpha}_s$ is exactly 2, in infinite-precision arithmetic. Suppose that the elements of $\boldsymbol{\alpha}_s$ are truncated to some finite word-length values, which can be written as the vector $\tilde{\boldsymbol{\alpha}}_s$. If they are truncated such that all elements of $\tilde{\boldsymbol{\alpha}}_s$ are positive, and their sum is still exactly 2, then it is easy to show that there must correspond a set of non-negative port resistances, and thus the quantized adaptor can still be considered as exactly lossless. More generally, it is possible to ensure passivity if the sum of the elements of $\tilde{\boldsymbol{\alpha}}_s$ is less than or equal to 2; this has been discussed in the waveguide filter context in [169].

While most of the approaches to quantization have been concerned with fixed-point implementations, many of the same ideas can be applied in floating-point as well. Floating-point signal truncation rules were proposed in [34], and an early study of coefficient sensitivity and roundoff noise appeared in [111]. More recent developments include a generalized WDF which is simply realized using multiply/accumulate operations [53], and a description of passive coefficient-truncation rules [121] based on scattering matrix factorization.

### 2.3.7 Vector Wave Variables

It is straightforward to extend wave digital filtering principles to the vector case (this has been outlined in [131]; the same idea has apeared in the context of digital waveguide networks in [166, 169]). For a $q$-component vector one-port element with voltage $\mathbf{v} = [v_1, \dots, v_q]^T$ and current $\mathbf{i} = [i_1, \dots, i_q]^T$, it is posible to define wave variables $\mathbf{a}$ and $\mathbf{b}$ by

$$\mathbf{a} = \mathbf{v} + \mathbf{R}\mathbf{i} \tag{2.43a}$$

$$\mathbf{b} = \mathbf{v} - \mathbf{R}\mathbf{i} \tag{2.43b}$$

for a $q \times q$ symmetric positive definite matrix $\mathbf{R}$; power-normalized quantities may be defined by

$$\underline{\mathbf{a}} = \frac{1}{2}\left(\mathbf{R}^{-T/2}\mathbf{v} + \mathbf{R}^{1/2}i\right) \tag{2.44a}$$

$$\underline{\mathbf{b}} = \frac{1}{2}\left(\mathbf{R}^{-T/2}\mathbf{v} - \mathbf{R}^{1/2}i\right) \tag{2.44b}$$

where $\mathbf{R}^{1/2}$ is some right square root of $\mathbf{R}$, and $\mathbf{R}^{T/2}$ is its transpose. The power absorbed by the vector one-port will be

$$w_{inst} = \left(\mathbf{a}^T\mathbf{R}^{-1}\mathbf{a} - \mathbf{b}^T\mathbf{R}^{-1}\mathbf{b}\right) = 4\left(\underline{\mathbf{a}}^T\underline{\mathbf{a}} - \underline{\mathbf{b}}^T\underline{\mathbf{b}}\right) = 4\mathbf{v}^T\mathbf{i} \tag{2.45}$$

Kirchoff's Laws, for a series or parallel connection of $M$ $q$-component vector elements with voltages $\mathbf{v}_j$ and $\mathbf{i}_j$, $j = 1, \ldots, M$ can be written as

$$\mathbf{i}_1 = \mathbf{i}_2 = \ldots = \mathbf{i}_M \qquad \mathbf{v}_1 + \mathbf{v}_2 + \ldots + \mathbf{v}_M = 0 \qquad \text{Series connection} \tag{2.46a}$$

$$\mathbf{v}_1 = \mathbf{v}_2 = \ldots = \mathbf{v}_M \qquad \mathbf{i}_1 + \mathbf{i}_2 + \ldots + \mathbf{i}_M = 0 \qquad \text{Parallel connection} \tag{2.46b}$$

and the resulting scattering equations will be

$$\mathbf{b}_k = \mathbf{a}_k - 2\mathbf{R}_k\left(\sum_{j=1}^{M}\mathbf{R}_j\right)^{-1}\sum_{j=1}^{M}\mathbf{a}_j, \qquad k = 1, \ldots, M \qquad \text{Series connection} \tag{2.47a}$$

$$\mathbf{b}_k = -\mathbf{a}_k + 2\left(\sum_{j=1}^{M}\mathbf{R}_j^{-1}\right)^{-1}\sum_{j=1}^{M}\mathbf{R}_j^{-1}\mathbf{a}_j, \qquad k = 1, \ldots, M \qquad \text{Parallel connection} \tag{2.47b}$$

in terms of the wave variables $\mathbf{a}_k$, $\mathbf{b}_k$ defined as per (2.43) and the port resistance matrices $\mathbf{R}_k$, $k = 1, \ldots, M$. These are the defining equations of a vector adaptor; their schematics are essentially the same as those of Figure 2.12, except that they are drawn in bold—see Figure 2.14. As before, we use the same representation for power-normalized waves.

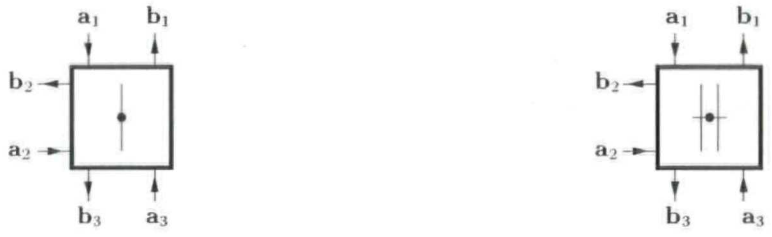

(a) (b)

Figure 2.14: *Three-port vector adaptors—* (a) *a vector series adaptor and* (b) *a vector parallel adaptor.*

### Coupled Inductances and Capacitances

Coupled inductances and capacitances defined, in vector form, by

$$\mathbf{v} = \mathbf{L}\frac{d\mathbf{i}}{dt} \qquad \mathbf{i} = \mathbf{C}\frac{d\mathbf{v}}{dt} \tag{2.48}$$

for symmetric positive definite matrices $\mathbf{L}$ and $\mathbf{C}$ were first introduced in the WDF context by Nitsche [131]; they turn out to be essential to the construction of WDF-based numerical simulation algorithms for stiff distributed systems such as plates (see §5.4) and shells (see §5.5), as well for full three-dimensional elastic solid dynamics (see §5.6). Though these are best thought of as vector elements, they appear within larger scalar circuits, and it is convenient to have a representation for which the vectors of port quantities are separated out into scalar port-wise components.

We show an inductive coupling of $q$ loops in Figure 2.15(a); self-inductances are indicated by directed arrows, accompanied by an inductance $L_{jj}$, $j = 1, \dots, q$ (these are the diagonal elements of $\mathbf{L}$), and a mutual inductance between loops $j$ and $k$, $j \neq k$ is represented by an arrow and the associated inductance $L_{kj}$ (which is the $(k,j)$th or $(j,k)$th element of $\mathbf{L}$, and is not constrained to be positive). A coupled capacitance is shown in Figure 2.15(b).

A coupled inductance can be discretized through the use of the trapezoid rule applied directly to the vector equations of (2.48); in terms of wave variables defined by (2.43), we get

$$\mathbf{b}(n) = -\mathbf{a}(n-1) \qquad \mathbf{R} = 2\mathbf{L}/T$$

which is a direct vector generalization of (2.23). Similarly, for a capacitor, we get

$$\mathbf{b}(n) = \mathbf{a}(n-1) \qquad \mathbf{R} = T(2\mathbf{C})^{-1}$$

In practice, if a coupled inductance (or capacitance) appears in a circuit which is to be discretized using WDFs, we may treat it as a $q$-vector two-port made up of a series (or parallel) junction terminated on a vector wave digital inductor (or capacitor) of port resistance $2\mathbf{L}/T$ (or $T(2\mathbf{C})^{-1}$).

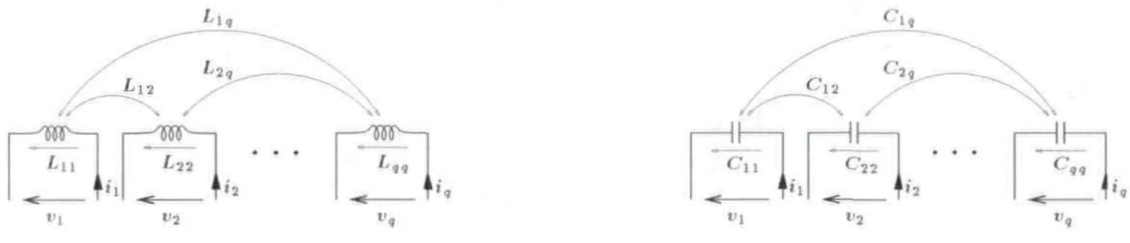

(a) (b)

Figure 2.15: (a) $q$ *coupled inductances and* (b) $q$ *coupled capacitances.*

See Figure 2.16 for the signal flow diagrams for these objects and the simplified representations that we will use. The port resistance at the opposing port will in general be diagonal, so that the vector wave variables entering and leaving the junction may be decomposed into scalar wave variables; this diagonal port resistance will be determined by the rest of the network to which the $q$-vector two-port is connected. See §4.2.6 for more information on this decomposition in the DWN context; we will return to vector/scalar connections in Chapter 5. We note that in the representations in Figure 2.16, we have not explicitly indicated the order in which the $q$ scalar incoming and outgoing vectors should be "packed" and "unpacked" from the vector wave variables at the lower ports of the vector junctions. In the applications in Chapter 5, for a given coupled inductance (say), self-inductances will all be identical, as will all mutual inductances; thus any ordering will do, as long as the $j$th elements of both $\mathbf{a}$ and $\mathbf{b}$ correspond to wave variables at the $j$th scalar port.

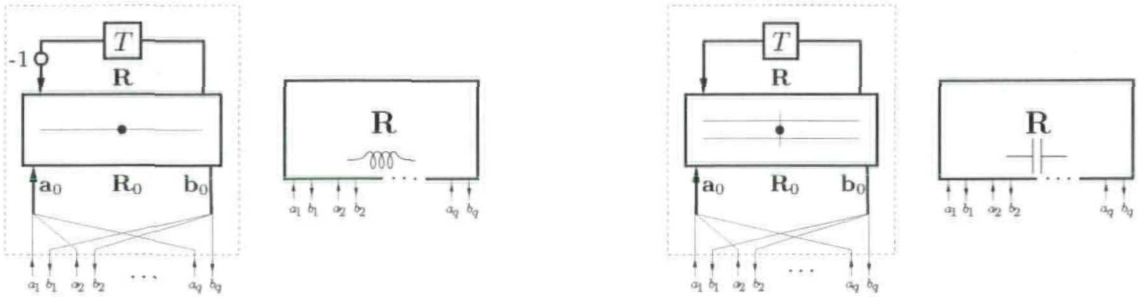
-1
$T$
$\mathbf{R}$
$\mathbf{a}_0$
$\mathbf{R}_0$
$\mathbf{b}_0$
$a_1$ $b_1$ $a_2$ $b_2$ ... $a_q$ $b_q$
$\mathbf{R}$
$a_1$ $b_1$ $a_2$ $b_2$ ... $a_q$ $b_q$
$T$
$\mathbf{R}$
$\mathbf{a}_0$
$\mathbf{R}_0$
$\mathbf{b}_0$
$a_1$ $b_1$ $a_2$ $b_2$ ... $a_q$ $b_q$
$\mathbf{R}$
$a_1$ $b_1$ $a_2$ $b_2$ ... $a_q$ $b_q$

(a) (b)

Figure 2.16: (a) *Signal flow graph for a wave digital coupled inductance and a simplified representation. Here the* $q \times q$ *port resistance* $\mathbf{R} = 2\mathbf{L}/T$, *and* $\mathbf{R}_0$ *is a* $q \times q$ *diagonal matrix; the diagonal entries specify the port resistances at the* $q$ *scalar ports to which the element is connected.* (b) *The signal flow graph for a wave digital coupled capacitance (vector port resistance* $\mathbf{R} = T(2\mathbf{C})^{-1}$*), and its simplified representation. In either case, the wave variables at the lower port of the vector junction are simply defined by* $\mathbf{a}_0 = [a_1, \ldots, a_q]^T$ *and* $\mathbf{b}_0 = [b_1, \ldots, b_q]^T$.

# Chapter 3

# Multidimensional Wave Digital Filters

## 3.1 Introductory Remarks

The last chapter was concerned with techniques for deriving a digital filter design from an analog network. It should be clear that such a digital filter structure can also be considered to be an explicit numerical solver for the system of of ordinary differential equations (ODEs) defined by the analog network which performs the filtering on continuous-time signals. This is perhaps an obvious point, but was apparently first noted in the literature in [65]. It is interesting that this link was not made immediately in the multidimensional case, which is the subject of this chapter.

A multidimensional generalization of wave digital filters (*MDWDFs*) first appeared rather early on [44], and most of the initial work involved applications to 2D filter design [118, 119]. It is itself an outgrowth of earlier work in the area of multidimensional circuits and systems [20, 105, 135] where the emphasis was on the synthesis of so-called variable networks (i.e., lumped passive networks with variable elements). The procedure for deriving a wave digital filter is largely the same in multiple dimensions as for the lumped case: to a given reference circuit, made up of elements connected either in series or parallel, various transformations are applied, specifically a change to wave variables, and spectral mappings. The end product is a wave digital network which has nearly all of the same desirable properties as lumped WD networks, especially recursive computability, and insensitivity to signal and coefficient truncation. The difference in MD, however, is that the reference circuit, usually called a *multidimensional Kirchoff circuit* or *MDKC* is now far more of a mathematical abstraction than a lumped circuit; the circuit state is a function of several variables, which may or may not include time, and the circuit elements (as well as the connections between them) must be interpreted in a distributed sense. In particular, it is not a circuit which can be "built" (except in the case of the variable networks mentioned previously). As such, the major problem confronting the designer of a MDWDF is the construction of this reference circuit [45, 44]. Various techniques were put forth, some involving MD circuits obtained by rotation of a known lumped reference network [46]. A good deal of work went into the related synthesis problem for general multidimensional reactance two-ports [8, 9, 52], which is much more difficult than in the lumped case (and not possible in general).

The first paper to consider MDWDFs from a simulation perspective appeared in 1990 [59], though it was foreshadowed much earlier in [178]. That is to say, in analogy with the lumped case, a closed MDWD network could be considered to be a simulator of a distributed system which is defined by a system of partial differential equations (PDEs) and *represented* by an MDKC. Here, unlike for filtering, there is a clear interpretation of the reference circuit, which is simply a symbolic restatement of the defining equations of a particular model system. The wave digital numerical integration approach is applicable to a wide variety of physical systems, including electromagnetics [50], coupled transmission lines [63, 106] and elastic solid and beam dynamics [131]. Most surprisingly, the method can be applied to highly nonlinear systems [127] such as those of fluid dynamics [16, 49, 70], as well as even more complex hybrids, such as the magnetohydrodynamic system [191]. The method requires that the propagation speeds in the problem to be modeled be bounded; this is equivalent to saying that the system should be of *hyperbolic type*[†][176]. This requirement is important because numerical methods derived in this way from this approach can be interpreted as *explicit finite difference schemes* [82]; as such, they must obey a requirement (the Courant-Friedrichs-Lewy criterion [176]) relating the physical region of dependence for the model problem to a similar region on a numerical grid. We would also like to note that a related approach to numerical integration, based on a transfer function formulation has been taken in [108, 141, 143, 144].

Although this chapter is intended in part as an extended review and compendium of the work to date in the field of numerical integration through the use of wave digital filters, the subtext is certainly that these methods can and should be treated as a particular class of finite difference methods endowed with a special property, namely passivity. This point has not been explored in any depth in the literature, except in the lumped case [131]. Such a treatment will also make it easier to compare wave digital methods to digital waveguide networks (DWNs)[166, 198, 200], which can also be used for numerical integration purposes in a very similar way. Chapter 4, which is devoted to DWNs, will return to the subject of MDWDFs for such a comparison, and eventually, a unification of the two methods. In Chapter 5, we will apply the concepts discussed here to a variety of more complex systems, in particular those describing the vibration of beams, plates, shells and elastic solids.

---

[†] It is possible to extend the MDWD approach to cover *parabolic* systems [176] as well; parabolic systems may not have a bounded propagation velocity, but they can be approximated by hyperbolic systems. This is essentially the path taken by Fettweis in the modeling of the full *Navier-Stokes Equations* [112] which describe the behavior of a general viscous fluid [49]; we remark that a similar idea, termed "second-sound theory," [26, 205] has been used to hyperbolicize parabolic problems (indeed, all time-dependent systems obeying the laws of classical physics *must* be hyperbolic, even if certain models do not reflect this). Elliptic problems, which typically occur in describing steady state potential distributions in both electrostatics and fluid dynamics can be dealt with using MDWDFs using a relaxation-type approach [47].

We refer to §1.3 for a full technical summary of this chapter.

## 3.2 Symmetric Hyperbolic Systems

In the previous chapter, we examined the discretization of lumped analog circuits; by lumped, we mean that the voltages and currents in these circuits are functions of only one independent variable: time. Although the described procedure was originally intended as a means of developing robust digital filtering structures, an equivalent point of view is that such structures in fact *numerically integrate* the set of ordinary differential equations describing the time evolution of these currents and voltages.

In a distributed problem, the dependent variables are functions not only of time $t$, but also of location within an $n$-dimensional spatial domain $\mathcal{D}$, with coordinates $\mathbf{x} = [x_1, \ldots, x_n]^T$. Such a problem is referred to as an $(n + 1)$D problem in the WDF literature [131]. Problems without spatial dependence will be called *lumped* problems. If the equations which define the problem include differential operators, we are faced with solving a set of partial differential equations (PDEs).

A particularly important family of PDE systems are the *symmetric hyperbolic* [74, 82] systems of the form

$$\mathbf{P}\frac{\partial \mathbf{w}}{\partial t} + \sum_{k=1}^{n} \mathbf{A}_k \frac{\partial \mathbf{w}}{\partial x_k} + \mathbf{B}\mathbf{w} + \mathbf{f} = \mathbf{0} \tag{3.1}$$

Here, $\mathbf{w}$, the state, is a $q$-element column vector defined over coordinates $\mathbf{x} \in \mathcal{D} \subset \mathcal{R}^n$ and $t \geq 0$. $\mathbf{P}$ and $\mathbf{A}_k$, $k = 1, \ldots, n$, are real symmetric $q \times q$ matrices[†]; in particular, $\mathbf{P}$ is assumed to be positive definite. $\mathbf{B}$ is a real $q \times q$ matrix (not necessarily symmetric) whose symmetric part models energy loss or growth, and the $q$-element real column vector $\mathbf{f}$ is a *forcing function* or excitation. For all the systems to be discussed in this thesis (except the fluid dynamic systems of Appendix B), the matrices $\mathbf{A}_k$ are assumed to be constant, though $\mathbf{P}$ and $\mathbf{B}$ are allowed to depend on $\mathbf{x}$. These systems are thus linear and time-invariant, but not generally shift-invariant, so that we cannot apply spatial Fourier transforms directly to analyze them. System (3.1) must be complemented by initial and boundary conditions [82], in order for the solution to exist and be unique.

Though it is possible to extend this definition to include cases where the matrices $\mathbf{A}_k$ may depend on $\mathbf{x}$, $t$ or even $\mathbf{w}$ (in which case system (3.1) is nonlinear), this simpler form describes a wide variety of physical systems, from electromagnetics to string, membrane, beam, plate, shell, and elastic solid dynamics, to transmission line systems, to linear acoustics, etc. Symmetric hyperbolic systems are important because they form a subclass of *strongly hyperbolic* systems, for which the initial-value problem is well-posed [176]. Roughly speaking, to say that a system is well-posed is to say that the growth of its solution is bounded in a well-defined way; growth in an $L_2$ norm cannot be faster than exponential. This concept is elaborated in detail in [82, 176]. We can examine this growth in the present case as follows.

---

[†] We will always choose $x_1 = x$, $x_2 = y$, $x_3 = z$, so the matrices $\mathbf{A}_1$, $\mathbf{A}_2$ and $\mathbf{A}_3$ will refer to the matrix coefficients of the partial derivatives in these three directions in (3.1).

First, assume that the problem is defined over an unbounded spatial domain $\mathcal{D} = \mathbb{R}^n$, so that we can drop any consideration of boundary conditions, and also that the forcing function $\mathbf{f} = \mathbf{0}$. We now take the inner product of $\mathbf{w}^T$ (the transpose of $\mathbf{w}$) with (3.1) to get

$$\mathbf{w}^T\mathbf{P}\frac{\partial \mathbf{w}}{\partial t} + \sum_{k=1}^{n}\mathbf{w}^T\mathbf{A}_k\frac{\partial \mathbf{w}}{\partial x_k} + \frac{1}{2}\mathbf{w}^T(\mathbf{B}+\mathbf{B}^T)\mathbf{w} = 0 \tag{3.2}$$

where we have replaced $\mathbf{B}$ by its symmetric part $\frac{1}{2}\left(\mathbf{B}+\mathbf{B}^T\right)$. Due to the symmetry of $\mathbf{P}$ and the $\mathbf{A}_k$, we can then write

$$\frac{1}{2}\frac{\partial}{\partial t}\left(\mathbf{w}^T\mathbf{P}\mathbf{w}\right) + \frac{1}{2}\sum_{k=1}^{n}\frac{\partial}{\partial x_k}\left(\mathbf{w}^T\mathbf{A}_k\mathbf{w}\right) + \frac{1}{2}\mathbf{w}^T\left(\mathbf{B}+\mathbf{B}^T\right)\mathbf{w} = 0 \tag{3.3}$$

Now, integrate (3.3) over $\mathbb{R}^n$, to get

$$\frac{d}{dt}\int_{\mathbb{R}^n}\frac{1}{2}\left(\mathbf{w}^T\mathbf{P}\mathbf{w}\right)dV + \frac{1}{2}\int_{\mathbb{R}^n}\sum_{k=1}^{n}\frac{\partial}{\partial x_k}\left(\mathbf{w}^T\mathbf{A}_k\mathbf{w}\right)dV + \frac{1}{2}\int_{\mathbb{R}^n}\mathbf{w}^T(\mathbf{B}+\mathbf{B}^T)\mathbf{w}dV = 0 \tag{3.4}$$

where $dV = dx_1dx_2\dots dx_n$ is the $n$D differential volume element. The expression $\sum_{k=1}^{n}\frac{\partial}{\partial x_k}\left(\mathbf{w}^T\mathbf{A}_k\mathbf{w}\right)$ is easily seen to be the divergence of a vector field, and by the Divergence Theorem [174], the integral of this quantity can be replaced by a surface integral over the problem boundary—because we have assumed no boundary, this integral vanishes, and we are left with

$$\frac{d}{dt}\int_{\mathbb{R}^n}\frac{1}{2}\left(\mathbf{w}^T\mathbf{P}\mathbf{w}\right)dV + \frac{1}{2}\int_{\mathbb{R}^n}\mathbf{w}^T(\mathbf{B}+\mathbf{B}^T)\mathbf{w}dV = 0 \tag{3.5}$$

The quantity

$$E(t) \triangleq \int_{\mathbb{R}^n}\frac{1}{2}\left(\mathbf{w}^T\mathbf{P}\mathbf{w}\right)dV \tag{3.6}$$

can be interpreted as the total energy of system (3.1) at time $t$. Note that due to the positivity requirement on $\mathbf{P}$, it is a positive definite function of the state, $\mathbf{w}$. If $\mathbf{B}+\mathbf{B}^T$ is positive semi-definite, then we must have, from (3.5), that

$$\frac{d}{dt}E \leq 0$$

which implies that

$$E(t_2) \leq E(t_1) \qquad \text{for} \qquad t_2 \geq t_1 \tag{3.7}$$

In other words, the energy of the system must decrease as time progresses.

In the MD circuit models that we will discuss, what we will be doing, in essence, is dividing this energy up among various reactive MD circuit elements. We will elaborate on this in the sections on the (1+1)D transmission line and (2+1)D parallel-plate system. The passivity condition is essentially equivalent to (3.7). Also, the symmetric nature of the systems will be reflected, in the circuit models, by the use of mainly *reciprocal* [12] circuit elements, though non-reciprocal elements (gyrators) will come into play if **B** is not symmetric (it is not required to be, and note that system (3.1) is well-posed regardless of the form of **B** [82]). We have not explored the application of passive circuit methods to systems which are more generally strongly hyperbolic, for which energy estimates such as (3.7) can also be derived [82]. This would appear to be a worthy direction of future research.

### Note on Boundary Conditions

In the analysis above, the spatial domain is assumed unbounded (i.e., we took $\mathcal{D} = \mathbb{R}^n$). It is useful to examine the energetic behavior of (3.1) if this is not the case. Integrating (3.3) over $\mathcal{D}$, we get

$$\frac{d}{dt}\int_{\mathcal{D}} \frac{1}{2}\left(\mathbf{w}^T\mathbf{P}\mathbf{w}\right) dV + \int_{\mathcal{D}} \nabla \cdot \mathbf{b}\, dV + \frac{1}{2}\int_{\mathcal{D}} \mathbf{w}^T(\mathbf{B}+\mathbf{B}^T)\mathbf{w} dV = 0$$

where $\nabla \triangleq [\frac{\partial}{\partial x_1}, \ldots, \frac{\partial}{\partial x_n}]^T$, and where we have defined

$$\mathbf{b} \triangleq \frac{1}{2}[\mathbf{w}^T\mathbf{A}_1\mathbf{w}, \ldots, \mathbf{w}^T\mathbf{A}_n\mathbf{w}]^T$$

If the boundary of $\mathcal{D}$ is sufficently smooth, then upon applying the Divergence Theorem, we get

$$\frac{d}{dt}\int_{\mathcal{D}} \frac{1}{2}\left(\mathbf{w}^T\mathbf{P}\mathbf{w}\right) dV + \int_{\partial\mathcal{D}} \mathbf{b}^T\mathbf{n}_{\mathcal{D}} d\sigma + \frac{1}{2}\int_{\mathcal{D}} \mathbf{w}^T(\mathbf{B}+\mathbf{B}^T)\mathbf{w} dV = 0$$

where $\partial\mathcal{D}$ is the boundary of $\mathcal{D}$, $\mathbf{n}_{\mathcal{D}}$ is defined as the unit outward normal (assumed unique everywhere on $\mathcal{D}$ except over a set of measure zero), and $d\sigma$ is a surface element of $\mathcal{D}$. If we define the total energy by

$$E(t) \triangleq \int_{\mathcal{D}} \frac{1}{2}\left(\mathbf{w}^T\mathbf{P}\mathbf{w}\right) dV$$

then we have

$$\frac{d}{dt}E = -\int_{\partial\mathcal{D}} \mathbf{b}^T\mathbf{n}_{\mathcal{D}} d\sigma - \frac{1}{2}\int_{\mathcal{D}} \mathbf{w}^T(\mathbf{B}+\mathbf{B}^T)\mathbf{w} dV$$

If $\mathbf{B}+\mathbf{B}^T$ is positive semi-definite, then a simple condition for passivity is

$$\mathbf{b}^T\mathbf{n}_{\mathcal{D}} \geq 0 \tag{3.8}$$

and the system is lossless if $\mathbf{B}$ is antisymmetric and (3.8) holds with equality.

This analysis is grossly incomplete, however, because we have not said anything about which boundary conditions ensure the existence and uniqueness of a solution; this analysis is rather involved, and we refer the reader to [82] for an introduction. The basic issue is the over- or under-specification of $\mathbf{b}$ on the boundary. We will consider only lossless, memoryless boundary conditions in this thesis.

### Phase and Group Velocity

Because the stability of an explicit numerical method (such as those that we will examine in the rest of this thesis) which solves a system of hyperbolic equations is dependent on propagation velocities, it is worthwhile to spend a few moments here to define *phase* and *group* velocities [35, 101] for a system such as (3.1).

Let us return to the unbounded domain problem with $\mathcal{D}=\mathcal{R}^n$. Suppose that the matrices $\mathbf{P}$, $\mathbf{B}$ and $\mathbf{A}_k$, $k=1,\dots,n$ which define system (3.1) are real constants; in particular, we assume that the driving term $\mathbf{f}$ is zero, and that $\mathbf{B}$ is anti-symmetric, so that system (3.1) is lossless. This is then a linear and shift-invariant system, and the solution can be written as a superposition of plane wave solutions of the form

$$\mathbf{w}(\mathbf{x},t)=\mathbf{w}_0e^{j\omega t+\boldsymbol{\beta}\cdot\mathbf{x}}$$

where $\mathbf{w}_0$ is a constant vector, $\omega$ is a real frequency variable, and $\boldsymbol{\beta}=[\beta_1,\dots,\beta_n]^T$ is the $n$-component vector wavenumber defining the direction of propagation of the plane wave. Substituting this plane wave solution into the constant-coefficient system (3.1) gives

$$\left(j\omega\mathbf{P}+\sum_{k=1}^{n}j\beta_k\mathbf{A}_k+\mathbf{B}\right)\mathbf{w}=\mathbf{0} \tag{3.9}$$

Non-trivial solutions to (3.9) can only occur when

$$\chi(\omega,\boldsymbol{\beta})\triangleq\det\left(j\omega\mathbf{P}+\sum_{k=1}^{n}j\beta_k\mathbf{A}_k+\mathbf{B}\right)=0 \tag{3.10}$$

The $n$ solutions to this equation,

$$\omega_k(\boldsymbol{\beta}), \qquad\qquad k=1,\dots,n \tag{3.11}$$

(which are not necessarily distinct) define dispersion relations, from which we can derive much useful information.

All the linear systems to be examined in this thesis are isotropic; propagation characteristics are independent of direction (though not necessarily of location, or frequency). For LSI systems, this implies that the dispersion relations (3.11) can be written as functions of $\|\boldsymbol{\beta}\|_2$ alone, where $\|\boldsymbol{\beta}\|_2$ is simply the Euclidean norm of the vector $\boldsymbol{\beta}$. In this case, we may define the *phase* and *group velocities* for the $k$th relation by

$$\gamma_k^p \triangleq \frac{\omega_k}{\|\boldsymbol{\beta}\|_2} \qquad\qquad \gamma_k^g \triangleq \frac{d\omega_k}{d\|\boldsymbol{\beta}\|_2} \tag{3.12}$$

(For non-isotropic systems, we will need to resort to vector generalizations of these quantities [101, 190].) Phase velocities define the speeds of single sinusoidal plane wave solutions, and the group velocities can be interpreted as the speeds of propagation of a wave packet; from the point of view of the stability of numerical methods, it is the group velocities which are of most importance, because they define the speeds of information or energy transfer [35]. It is interesting to note that if $\mathbf{B}$ is non-zero, phase velocities may become unbounded in the limit as $\boldsymbol{\beta}$ becomes small—this occurs in several of the systems that will be discussed in Chapter 5, though for all these systems, the group velocities will be bounded. This is related to the fact that the system characteristics [74] are independent of $\mathbf{B}$.

In the interest of extending these ideas to spatially inhomogeneous systems (of the form of (3.1) where $\mathbf{P}$ and $\mathbf{B}$ may exhibit a smooth functional dependence on $\mathbf{x} \in \mathcal{D}$), we note that about any location $\mathbf{x} = \mathbf{x}_0 \in \mathcal{D}$, solutions to system (3.1) behave locally as solutions to the *frozen-coefficient* system [82] defined by $\mathbf{P}(\mathbf{x}_0)$ and $\mathbf{B}(\mathbf{x}_0)$. We may then define local group velocities $\gamma_k^g(\|\boldsymbol{\beta}\|_2, \mathbf{x}_0)$, $k = 1, \ldots, n$ in the same way as in (3.12). A quantity which will appear frequently in our subsequent treatment of the stability of numerical methods for these systems will be the maximum global group velocity, defined as

$$\gamma_{max}^g \triangleq \max_{\substack{k \,=\, 1,\ldots,n \\ \mathbf{x}_0 \,\in\, \mathcal{D} \\ \|\boldsymbol{\beta}\|_2 \,\geq\, 0}} \gamma_k^g(\|\boldsymbol{\beta}\|_2, \mathbf{x}_0) \tag{3.13}$$

which, more simply stated, is the maximum propagation velocity over all system modes, wavenumbers, and throughout the entire spatial problem domain.

## 3.3 Coordinate Changes and Grid Generation

Before looking directly at circuits and signal flow diagrams in multiple dimensions, it is useful to introduce coordinate changes, which were first applied in the context of multidimensional wave digital filters in [122]. One might add that it is *useful*, but not strictly *necessary*, since it is possible to develop numerical integration algorithms along the same lines without any explicit reference to new coordinates [61]. It is, however, a very convenient way of understanding causality and grid generation issues, as well as generalizing the passivity concept to MD [48, 85, 131].

Some of the lumped circuit elements we have discussed so far we have seen to be *passive*—that is, they dissipate energy as time progresses, as do Kirchoff networks composed of connections of such elements (by *Tellegen's Theorem* [136]). In the multidimensional setting, many systems possess a similar property; some measure of energy decreases as a function of time. For example, the amplitude of the vibrations in a struck string or membrane will gradually decrease (or at least not increase) as a function of time. We have also seen that, for lumped circuits, application of the trapezoid rule translates this passivity property to a discrete equivalent. When attempting a discretization of a set of PDEs, however, we have to cope not only with the time direction but spatial ones as well, and passivity (usually a result of the conservative nature of the laws from which a system of equations is derived) does not in general hold with respect to space [51].

The idea of Fettweis and Nitsche [62] was to perform a coordinate transformation such that the new coordinates, generally a mixture of time and space, all contain a part of the physical time variable. Traveling in the positive direction along any of the new coordinates implies that one is also moving forward in time (as well as in some spatial direction). More specifically, if

$$(t_1, \ldots, t_{n+1}) = f(x_1, \ldots, x_n, t)$$

are the new coordinates, the authors provide the following conditions:

> Any positive change $\Delta t$ in the variable $t$ must be reflected by a similar positive change $\Delta t_j$ in all the new coordinates $t_j$, $j = 1, \ldots, n+1$. (3.14a)
>
> Conversely, any positive change $\Delta t_j$ in any of the new coordinates must produce a positive change in the old variable $t$. (3.14b)

As a result, *all* the new coordinates have a time-like character; the practical implications of this will become apparent in the next section, when we introduce multidimensional circuit elements.

### 3.3.1 Structure of Coordinate Changes

These same authors provide some more detailed guidelines as to what types of coordinate changes are of interest [62]. In particular, they describe transformations of the form:

$$\mathbf{u} = \mathbf{V}^{-1}\mathbf{H}\mathbf{t} \tag{3.15a}$$

$$\mathbf{t} = \mathbf{H}^{-1}\mathbf{V}\mathbf{u} \tag{3.15b}$$

where $\mathbf{t} = [t_1, \ldots, t_{n+1}]^T$ are the new coordinates and $\mathbf{u} = [x_1, \ldots, x_n, t]^T$ are the old. $\mathbf{V}$ is prescribed to be $\mathrm{diag}(1, 1, \ldots, 1, v_0)$ and can be thought of as a simple scaling of the original coordinates $\mathbf{u}$ to a non-dimensional (or rather, "all-spatial") form. $v_0$ thus plays an important role, as we shall see later in a discrete setting, as the space step/time step ratio on a numerical grid. Its magnitude will be governed by a stability bound [176], sometimes called the *Courant-Friedrichs-Lewy* (CFL) criterion, as in conventional explicit finite difference methods (although the manifestation of the condition in the networks we will derive is of a quite different character). The invertible matrix $\mathbf{H}$ is usually chosen to be orthogonal [62].

Here, we can see that the requirement (3.14a) will be satisfied if the elements in the rightmost column of $\mathbf{H}^{-1}$ are positive; if $\mathbf{H}$ is orthogonal, we have $\mathbf{H}^{-1} = \mathbf{H}^T$. The bottom row of $\mathbf{H}$ then consists of positive elements (often chosen equal, so as to give equal contributions from all components $t_j$ to $t$), in order to satisfy requirement (3.14b).

The differential operators $\nabla_{\mathbf{t}} = [\frac{\partial}{\partial t_1}, \ldots, \frac{\partial}{\partial t_k}]^T$ and $\nabla_{\mathbf{u}} = [\frac{\partial}{\partial x_1}, \ldots, \frac{\partial}{\partial x_n}, \frac{\partial}{\partial t}]^T$ are related by:

$$\nabla_{\mathbf{t}} = \mathbf{H}^T\mathbf{V}^{-1}\nabla_{\mathbf{u}} \qquad\qquad \nabla_{\mathbf{u}} = \mathbf{V}\mathbf{H}^{-T}\nabla_{\mathbf{t}} \tag{3.16}$$

Also, we introduce the scaled time variable

$$t' = v_0 t \tag{3.17}$$

which will necessitate a special treatment in the circuit models to follow. See §3.5.1 for more details.

### 3.3.2 Coordinate Changes in (1+1)D

Solving a set of PDEs numerically nearly always involves sampling the problem domain, and attempting to approximate the solution to the problem at the finite collection of points. Coordinate sampling in the MDWDF context was first examined in [122], and was subsequently addressed in [62] and [7]. In (1+1)D, there is essentially only one useful type of regular grid; it is shown, in the (1+1)D case, in Figure 3.1(a), where the grid spacings or step sizes are assumed equal to $\Delta$ in the scaled time (i.e., $t' = v_0 t$) and space directions. Note that the use of the scaled coordinates allows this uniform sampling, without implying any restriction on the relative grid spacings in the unstretched coordinates, since we have introduced the (as yet) free parameter $v_0$.

Suppose we now change coordinates by:

$$t_1 = \frac{1}{\sqrt{2}}(v_0 t + x) \qquad\qquad t_2 = \frac{1}{\sqrt{2}}(v_0 t - x) \tag{3.18}$$

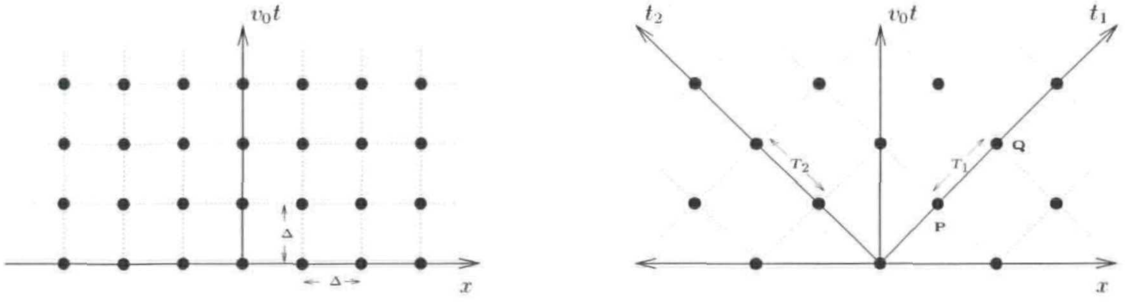

(a) (b)

Figure 3.1: *Sampling grids,* (a) *in rectangular coordinates* $(x, v_0t)$ *and* (b) *in the new coordinates* $(t_1, t_2)$ *defined by* (3.18).

which corresponds to a transformation of type (3.15) with

$$\mathbf{H} = \frac{1}{\sqrt{2}}\begin{bmatrix} 1 & -1 \\ 1 & 1 \end{bmatrix} \tag{3.19}$$

If we now sample the plane in the $(t_1, t_2)$ coordinates, with equal spacings along the two axes, using a step size of $T_1 = T_2$, we obtain the grid in Figure 3.1(b). Notice that if we choose $T_1 = T_2 = \sqrt{2}\Delta$, then our grid aligns perfectly with exactly half of the grid points sampled uniformly along the $(x, v_0t)$ axes, as in Figure 3.1(a). In fact, the grid of Figure 3.1(a) can be decomposed into two grids of the form in Figure 3.1(b), where one of the grids is shifted by $(\Delta, \Delta)$ with respect to the other, in the $(x, v_0t)$ plane. It will be possible in some instances to exploit this decomposition so as to achieve a gain in computational efficiency; the key idea here is that if we begin with a grid such as shown in Figure 3.1(a), and then are able to develop an algorithm such that only one of the two subdomains is used, then we will have halved the amount of computation, at the expense of a decrease in accuracy by a factor of $\sqrt{2}$ (the step size in the $(t_1, t_2)$ plane is $T_1 = T_2 = \sqrt{2}\Delta$ versus $\Delta$ in the $(x, v_0t)$ plane). We will mention this *offset* sampling [61, 211] when we look at the (1+1)D transmission line problem in §3.7, and will examine subgrid decompositions extensively in §4.4.3 and Appendix A. It is important to point out that regardless of the coordinate change, updating in any of the WDF-based algorithms that will subsequently be developed will be done with respect to the *time* variable alone (the direction of data flow is still in the time direction), as per standard explicit finite difference methods for hyperbolic problems.

### 3.3.3 Coordinate Changes in Higher Dimensions

There are more choices for the type of coordinate transformation (and hence the type of grid) that are available when we move to higher dimensional problems. As an example, let us look at the transformation defined by:

$$\mathbf{H} = \begin{bmatrix} \frac{1}{\sqrt{2}} & -\frac{1}{\sqrt{2}} & 0 \\ \frac{1}{\sqrt{6}} & \frac{1}{\sqrt{6}} & -\sqrt{\frac{2}{3}} \\ \frac{1}{\sqrt{3}} & \frac{1}{\sqrt{3}} & \frac{1}{\sqrt{3}} \end{bmatrix} \qquad \mathbf{V} = \begin{bmatrix} 1 & 0 & 0 \\ 0 & 1 & 0 \\ 0 & 0 & v_0 \end{bmatrix} \tag{3.20}$$

which is discussed in [62] and [211]. Uniform sampling in the $(t_1, t_2, t_3)$ coordinates yields the grid arrangement shown in Figure 3.2(a), flattened onto the $(x, y)$ plane. This is, effectively, a cubic lattice of points viewed along its main diagonal. At any given time step, one of three different grids (in Figure 3.2(a) the different grids are marked by grey, white or black points) which are simple translations of each other, is used. In a discrete setting, it is sometimes possible (depending on the system at hand) to design an algorithm such that they are used cyclically—grid variables at white grid points can be updated with reference to variables at the grey points, which in turn were updated using stored variables at the black points, etc. If the separation of the points is as indicated in Figure 3.2(a), then we have used sample steps of $T_1 = T_2 = T_3 = \sqrt{\frac{3}{2}}\Delta$.

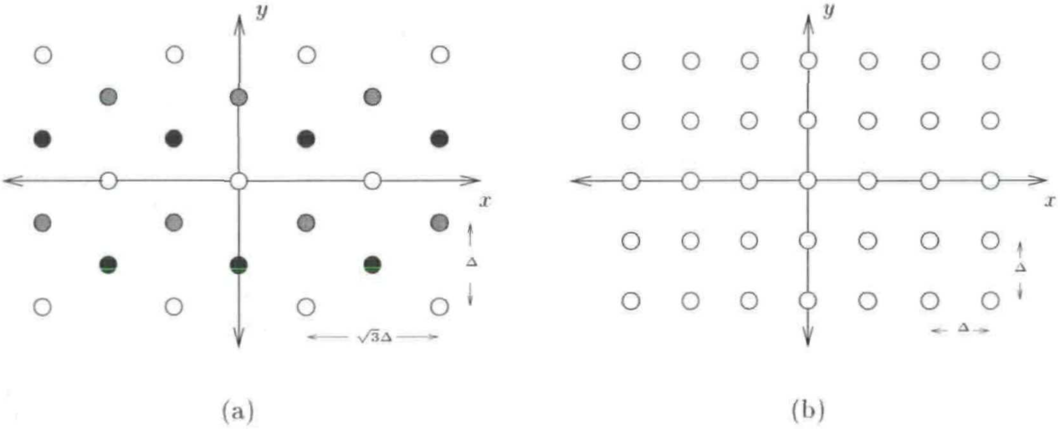

Figure 3.2: *(2+1)D sampling grids,* (a) *in hexagonal and* (b) *rectangular coordinates.*

### Embeddings

In order to obtain a standard rectilinear grid in higher dimensions, it is possible to proceed in the same fashion, but it is in fact more convenient to extend the class of coordinate transformations so as to embed the problem domain in a higher dimensional space. In [62], the following generalization of (3.15) has been put forth:

$$\mathbf{u} = \mathbf{V}^{-1}\mathbf{H}\mathbf{t} \tag{3.21a}$$

$$\mathbf{t} = \mathbf{H}^{-R}\mathbf{V}\mathbf{u} \tag{3.21b}$$

Here, $\mathbf{u}$ is still the $n+1$-dimensional vector $[x_1, \ldots, x_n, t]^T$, but $\mathbf{t}$ is $k$-dimensional, with $k \geq n+1$. $\mathbf{H}$ must be chosen such that the elements in its bottom row are positive. $\mathbf{H}^{-R}$ is a $k \times (n+1)$ right pseudo-inverse [92] of $\mathbf{H}$—in order to satisfy a generalization of the first of conditions (3.14), it must be chosen so that the elements in its rightmost column are all positive. For example, for a (2+1)D problem with $\mathbf{u} = [x, y, t]^T$, in order to generate a rectilinear grid, the following choice is usually made:

$$\mathbf{H} = \begin{bmatrix} 1 & 0 & -1 & 0 & 0 \\ 0 & 1 & 0 & -1 & 0 \\ 1 & 1 & 1 & 1 & 1 \end{bmatrix} \tag{3.22}$$

$\mathbf{H}$ projects five-dimensional coordinates $\mathbf{t} = [t_1, t_2, t_3, t_4, t_5]^T$ back to the three-dimensional space of $\mathbf{u}$. One choice [62] for this right pseudo-inverse is

$$\mathbf{H}^{-R} = \frac{1}{2}\mathbf{H}^T \mathrm{diag}(1,1,\tfrac{2}{5}) \tag{3.23}$$

Uniform sampling in the $\mathbf{t}$ coordinates, with step sizes of $T_j = \Delta$, $j = 1, \ldots, 5$ yields the standard rectangular grid shown in Figure 3.2(b), which is a pattern equivalent to what one would get by sampling uniformly (see comment below) in the $(x, y, v_0 t)$ coordinates, with a spacing of $\Delta$ in all three untransformed variables. It should be clear that to every grid point in the $\mathbf{u}$ coordinates corresponds a two-parameter family of points in the $\mathbf{t}$ coordinates; this fact will not influence the resulting difference schemes. This embedding of the problem domain in a higher dimensional space is simply a means to an end; in particular, we will not be solving a system numerically over a higher-dimensional grid (which would be computationally infeasible). The new coordinate directions are chosen so that they define a grid, and they will also serve as directions of *energy flow* for the MD circuit elements which we will define presently. In effect, the total energy flow in a physical system is broken up among these new coordinate directions; it will sometimes be true (as in the case of a rectilinear grid in (2+1)D) that energy can approach a particular grid location from a number of neighbors which is greater than the dimensionality of the problem (for the (2+1)D parallel-plate problem on a rectilinear grid, at least four: north, south, east and west). We will take a closer a look at this particular transformation, its suitability for calculation on a rectilinear grid in §3.8.

In (3+1)D, in order to obtain a standard rectilinear sampling pattern, Nitsche has proposed seven-dimensional coordinates [62] defined by

$$\mathbf{H} = \begin{bmatrix} 1 & 0 & 0 & -1 & 0 & 0 & 0 \\ 0 & 1 & 0 & 0 & -1 & 0 & 0 \\ 0 & 0 & 1 & 0 & 0 & -1 & 0 \\ 1 & 1 & 1 & 1 & 1 & 1 & 1 \end{bmatrix} \tag{3.24}$$

It is easy to verify that shifts of distance $\Delta$ along the coordinates $t_j$, $j = 1, \ldots, 6$ correspond to shifts of $\Delta$ along the positive and negative $x$, $y$, $z$, $-x$, $-y$ and $-z$ directions accompanied by a shift of $T = \Delta/v_0$ in the time direction. We will make of this coordinate transformation when developing scattering methods for Maxwell's Equations (see §4.10.6) and for the system describing elastic solid dynamics (see §5.6).

The embedding technique has some tricky aspects. We will make some comments here, in order to complement the information provided in [62]. The two relationships given in (3.21) are not equivalent for general rectangular matrices $\mathbf{H}$. (3.21a) serves to define $\mathbf{t}$, but the definition of directional derivatives in the $\mathbf{t}$ coordinates will be given by

$$\nabla_{\mathbf{t}} = \mathbf{H}^T\mathbf{V}^{-1}\nabla_{\mathbf{u}} \tag{3.25}$$

and depends only on $\mathbf{H}$. The question of how sampling in the new coordinates is to be carried out is not well-addressed in the literature. Suppose, for example, that we wish to use embedding (3.22). Grid definition proceeds by letting $\mathbf{t} = \Delta[n_1, n_2, n_3, n_4, n_5]^T$, where $n_j$, $j = 1, \ldots, 5$ are integers. Clearly, then, using (3.21a), grid points in the original coordinates are given by $\mathbf{u} = [\Delta(n_1 - n_3), \Delta(n_2 - n_4), \frac{\Delta}{v_0}(n_1 + n_2 + n_3 + n_4 + n_5)]^T$, and thus any point of the form $\mathbf{u} = [\Delta m_1, \Delta m_2, \frac{\Delta}{v_0} m_3]^T$, for integer $m_1$, $m_2$ and $m_3$ is in the range of $\mathbf{V}^{-1}\mathbf{H}$ for some choice of the $n_j$. This defines the rectilinear grid in the untransformed coordinates. Note, however, that not all of these points can be mapped back to some $\mathbf{t}$ with $\mathbf{t} = \Delta[n_1, n_2, n_3, n_4, n_5]^T$ under (3.21b). This is worthy of note, but will not influence the numerical methods which will depend on discretizing directional derivatives in the $\mathbf{t}$ coordinates, which, as mentioned above, are defined in terms of $\mathbf{H}$ and not $\mathbf{H}^{-R}$. We remark that the inverse relationship for (3.25) will be given by

$$\nabla_{\mathbf{u}} = \mathbf{V}\mathbf{H}^{-RT}\nabla_{\mathbf{t}} \tag{3.26}$$

where $\mathbf{H}^{-RT}$ is the transpose of $\mathbf{H}^{-R}$.

We don't wish to go too much into the formalism of these coordinate transformations here; it seems excessive since the associated circuit manipulations which we will review are quite straightforward. As mentioned earlier, the coordinate changes in this section are introduced in order to aid in understanding the method and MD-passivity, and are not necessary for deriving WDF-based algorithms for numerical integration, though it would appear that some types of reference circuits can only be derived via the transformation approach [130].

## 3.4 MD-passivity

In dealing with networks and circuit elements in multiple dimensions, we must have a means of generalizing their energetic properties accordingly. In particular, the notion of passivity, which in the lumped case played an important role in developing stable digital filters directly from an analog network, must be expanded to include the distributed character of the system to be modeled. The definition of *MD-passivity* was given in [48], and more basic results are provided in [85] and [131]. The idea is nearly the same as in the lumped case—a passive $N$-port cannot produce energy on its own, and hence a well-defined [12] network made up of Kirchoff connections of such passive $N$-ports recirculates and possibly dissipates energy. The difference is that in MD, we would like to be able to take into account that for most physical systems, conservation of energy is a property holding with respect to time alone. We will need to make use of the coordinates defined in §3.3, so as to ensure that passivity holds with respect to all coordinates in the problem. In this section, we recap the main points of the definitions and derivations in [48].

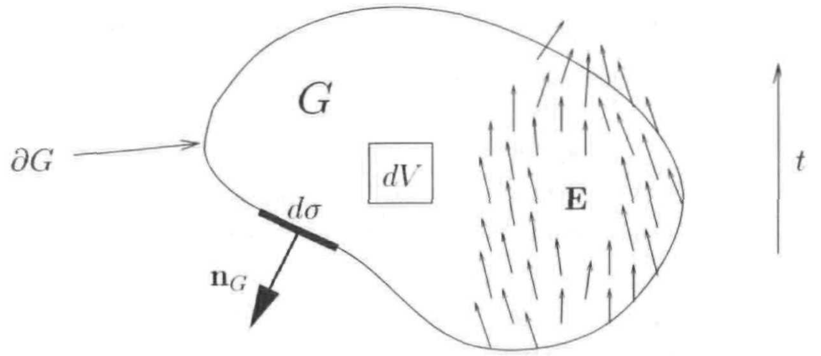

Figure 3.3: *k-dimensional domain G.*

We begin by defining a domain $G$ in the vector space defined by the new coordinates $\mathbf{t} = [t_1, \ldots, t_k]^T$ under a transformation of the type (3.21) (which may be an embedding). Consider an $N$-port defined over the domain $G$, with port voltages $v_j(\mathbf{t})$ and currents $i_j(\mathbf{t})$, for $j = 1, \ldots, N$. The instantaneous absorbed power density, at any point in the interior of $G$ is defined by

$$w_{inst}(\mathbf{t}) = \sum_{j=1}^{N} v_j i_j$$

and the *stored energy flow* as a vector field

$$\mathbf{E} = [E_1, \ldots, E_k]^T$$

In addition, we can define the source and dissipated power densities within $G$ to be $w_s(\mathbf{t})$ and $w_d(\mathbf{t})$.

The energy balance of the $N$-port can then be generalized directly from (2.3):

$$\int_G (w_{inst} + w_s - w_d)\, dV = \int_{\partial G} \mathbf{n}_G \mathbf{E} d\sigma \tag{3.27}$$

where $\mathbf{n}_G$ is the $k$-element row vector outward unit normal to the surface of $G$, $d\sigma$ is a surface element of $G$, and $dV$ is a volume element internal to $G$. See Figure 3.3[†] for a graphical representation of some of the relevant quantities. The $N$-port is called MD-passive if there is a stored energy vector field $\mathbf{E}$, which is a positive semi-definite function of the state of the $N$-port (i.e., all components of $\mathbf{E}$ are non-negative, everywhere in $G$) such that

$$\int_G w_{inst} dV \geq \int_{\partial G} \mathbf{n}_G \mathbf{E} d\sigma \tag{3.28}$$

and MD-lossless if (3.28) holds with equality. The total stored energy lost through the boundary of $G$ must be less than the energy supplied through the ports in $G$; this is equivalent, from (3.27) to saying that the energy dissipated in $G$ must be greater than the energy coming from the source. The previous definition of MD-passivity has been more precisely called *integral* MD-passivity (with respect to a domain $G$) [85]. A corresponding differential (pointwise) definition is

$$w_{inst} \geq \nabla_{\mathbf{t}} \cdot \mathbf{E} \qquad \text{in } G \tag{3.29}$$

An $N$-port which is differentially MD-passive everywhere throughout a domain $G$ will also be integrally MD-passive with respect to $G$. The converse is not necessarily true.

It is also useful to define, for an $N$-port, a scalar total energy [85] by

$$\mathcal{E}(t) = \int_{G_t} \mathbf{e}_t^T \mathbf{E} dx_1 dx_2 \ldots dx_n \tag{3.30}$$

Here $G_t$ a spatial region defined as the cross-section of $G$ at time $t$, and $\mathbf{e}_t$ is a column unit vector in the time direction; note that this definition is framed in terms of the untransformed coordinates $\mathbf{u}$, and $\mathbf{E}$ has been projected onto these coordinates under (3.21a). It can also be used as a measure of the total energy at time $t$ in a given circuit, as we will see in §3.7.4.

Fettweis [44] looks at an extension of the idea of positive realness (see §2.2.2) to two dimensions, for the case of a real linear and shift-invariant $N$-port. This idea generalizes easily to higher dimensions, as per some very early work in MD system theory [135]. Consider a real linear and shift-invariant (LSI) $k$-dimensional $N$-port, where the port quantities are in an exponential state of frequency $\mathbf{s_t}$, where

$$\mathbf{s_t} = [s_1, \ldots, s_k]^T$$

---

[†] Adapted from Figure 2 of [85] and Figure 1 of [48].

are the frequency variables conjugate to $\mathbf{t}$. Thus we have the real instantaneous voltages and currents

$$v_j(\mathbf{t}) = \mathrm{Re}\left(\hat{v}_j e^{\mathbf{s_t}^T\mathbf{t}}\right) \qquad i_j(\mathbf{t}) = \mathrm{Re}\left(\hat{i}_j e^{\mathbf{s_t}^T\mathbf{t}}\right) \qquad j = 1, \ldots, N$$

where $\hat{v}_j$ and $\hat{i}_j$ are complex amplitudes. If there is an impedance relation between the voltages and currents, then we can write

$$\hat{\mathbf{v}} = \mathbf{Z}(\mathbf{s_t})\hat{\mathbf{i}}$$

where $\hat{\mathbf{v}} = [\hat{v}_1, \ldots, \hat{v}_N]^T$ and $\hat{\mathbf{i}} = [\hat{i}_1, \ldots, \hat{i}_N]^T$. The total complex MD power density at frequency $\mathbf{s}_t$ can be defined as

$$w(\mathbf{s_t}) = \hat{\mathbf{i}}^*\hat{\mathbf{v}}$$

and the average or active power density as

$$\bar{w}(\mathbf{s_t}) = \mathrm{Re}\left(\hat{\mathbf{i}}^*\hat{\mathbf{v}}\right)$$

The positive realness condition on $\mathbf{Z}$ for MD-passivity follows immediately, and is similar to (2.5), except that we now must have

$$\mathbf{Z}(\mathbf{s_t}) + \mathbf{Z}^*(\mathbf{s_t}) \geq 0 \qquad \text{for} \qquad \mathrm{Re}(s_j) \geq 0 \quad j = 1, \ldots, k \tag{3.31}$$

Thus the impedance must be positive real in *all* the new coordinates. The $N$-port is MD-lossless if (3.31) holds with equality for $\mathrm{Re}(s_j) = 0$, $j = 1, \ldots, k$. It is important to note that because of (3.26) and (3.25), we have

$$\mathbf{s_u} = \mathbf{V}\mathbf{H}^{-RT}\mathbf{s_t} \qquad \mathbf{s_t} = \mathbf{H}^T\mathbf{V}^{-1}\mathbf{s_u} \tag{3.32}$$

where $\mathbf{s_u} = [s_{x_1}, \ldots, s_{x_n}, s_t]^T$ is the vector of frequencies in the untransformed coordinates $\mathbf{u}$. Thus, due to the positivity condition on the elements of the last row of $\mathbf{H}^{-RT}$ and the last column of $\mathbf{H}^T$, we will have that

$$\mathrm{Re}(s_j) \geq 0 \quad \text{for} \quad j = 1, \ldots, k \qquad \Longleftrightarrow \qquad \mathrm{Re}(s_t) \geq 0$$

so that for an MD-passive $N$-port,

$$\mathbf{Z} + \mathbf{Z}^* \geq 0 \qquad \text{for} \qquad \mathrm{Re}(s_t) \geq 0 \tag{3.33}$$

It is thus seen that MD-passivity can be interpreted as passivity, but spread over a new system of coordinates (regardless of whether the new coordinates number more than the old).

## 3.5 MD Circuit Elements

Beginning from the perspective of the one-port circuit elements described in the last chapter, it is not difficult to see how such elements can be generalized to a multidimensional setting. Consider again the inductance and its WD one-port equivalent, shown in Figure 3.4. The voltage across the inductor is integrated and scaled by a factor $1/L$ to yield a current. The fact that the signal flow graph for the WD one-port equivalent is causal indicates that the inductor one-port is associated with the forward time direction. In the multidimensional case, the concepts of a direction associated with a circuit element and causality become crucial.

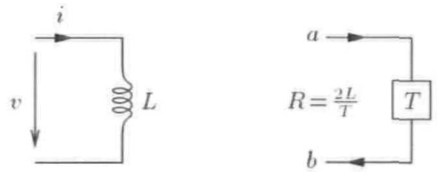

Figure 3.4: *Inductor and its wave digital one-port.*

### 3.5.1 The MD Inductor

Consider the following (partial) differential equation:

$$v = L\frac{\partial i}{\partial t_j} \tag{3.34}$$

where $L$ is a positive constant, and $t_j$, for any $j$, $j = 1, \ldots, k$ is a coordinate defined by transformation (3.21). We now have $v = v(\mathbf{t})$ and $i = i(\mathbf{t})$. Considered as an MD one-port, the instantaneous applied power will be

$$w_{inst} = vi = \frac{\partial}{\partial t_j}\left(\frac{1}{2}Li^2\right) = \nabla_{\mathbf{t}} \cdot \mathbf{E}$$

if we also define the stored energy flux $\mathbf{E}$ to be

$$\mathbf{E} = \frac{1}{2}Li^2\mathbf{e}_j \tag{3.35}$$

where $\mathbf{e}_j$ is a column unit vector in the $t_j$ direction. If $L \geq 0$, this is indeed a positive semi-definite vector function of the current across the one port. (3.34) defines a passive (in fact lossless) element in the sense of (3.29), henceforth called an MD-inductor, of inductance $L$ and *direction* $t_j$.

This equation resembles that which defines the voltage/current relation in an inductor with inductance $L$, the exception being that the integration variable is no longer time, but $t_j$, a mixed space-time variable. In fact, the discretization procedure is identical to that of the lumped case, as we shall see, but for illustrative purposes, we will derive the multidimensional wave digital one-port. The important thing to note here is that even though (3.34) is defined over a $k$-dimensional domain with coordinates $\mathbf{t}$, it is solved (given $v$, say) as a series of one-dimensional integrations (since (3.34) must hold for all values of $\mathbf{t}$).

We can immediately approximate (3.34) by the MD trapezoid rule [62] as

$$\frac{v(\mathbf{t}-\mathbf{T}_j)+v(\mathbf{t})}{2}=\frac{L}{T_j}\Big(i(\mathbf{t})-i(\mathbf{t}-\mathbf{T}_j)\Big)+O(T_j^2) \tag{3.36}$$

where $\mathbf{T}_j = T_j\mathbf{e}_j$. $T_j$ is interpreted as the step-size. Assuming that we have uniformly sampled the $\mathbf{t}$ plane as in §3.3, with grid spacings $T_1, \dots, T_k$, we now define the grid functions $v(\mathbf{n})$ and $i(\mathbf{n})$ where $\mathbf{n} = [n_1, \dots, n_k]^T$ is an integer-valued vector. We intend to use them to approximate $v(\mathbf{t} = [n_1T_1, \dots, n_kT_k]^T)$ and $i(\mathbf{t} = [n_1T_1, \dots n_kT_k]^T)$, so we can immediately write the recursion

$$\frac{v(\mathbf{n})+v(\mathbf{n}-\mathbf{e}_j)}{2}=\frac{L}{T_j}\Big(i(\mathbf{n})-i(\mathbf{n}-\mathbf{e}_j)\Big) \tag{3.37}$$

which approximates (3.34) to $O(T_j^2)$.

We can now introduce the wave variables,

$$\begin{aligned} a(\mathbf{n}) &= v(\mathbf{n})+Ri(\mathbf{n}) \\ b(\mathbf{n}) &= v(\mathbf{n})-Ri(\mathbf{n}) \end{aligned}$$

which are also grid functions defined over $\mathbf{n}$. As in the lumped case, $R$ is an arbitrary positive number (here assumed constant). Inserting these wave variables into (3.37) yields, with the choice $R = 2L/T_1$,

$$b(\mathbf{n}) = -a(\mathbf{n}-\mathbf{e}_j) \tag{3.38}$$

In terms of the untransformed coordinates (where we will perform the updating in a simulation), (3.36) becomes

$$\frac{v(\mathbf{u}-\mathbf{V}^{-1}\mathbf{H}\mathbf{T}_j)+v(\mathbf{u})}{2}=\frac{L}{T_j}\left(i(\mathbf{u})-i(\mathbf{u}-\mathbf{V}^{-1}\mathbf{H}\mathbf{T}_j)\right) \tag{3.39}$$

again to second order in the transformed spacing. The quantity $\mathbf{V}^{-1}\mathbf{H}\mathbf{T}_j$ is the vector corresponding to the same shift, in the untransformed coordinates.

Take, for example the case of an inductor of direction $t_1$ under the coordinate change defined by (3.19). A shift of $\mathbf{T}_1 = T_1\mathbf{e}_1$ of $T_1$ in direction $t_1$ corresponds to a shift in the old coordinates of $(T_1/\sqrt{2})[1, 1/v_0]^T$. Referring to Figure 3.1(b), where we have chosen $T_1 = \sqrt{2}\Delta$, the *instance* of the wave variable $a$ entering the MD-inductor at point $P$ exits, sign-inverted, as $b$ at point $Q$. From this standpoint, MD-losslessness is obvious, since the MD-inductor merely shifts and sign-inverts an array of numbers.

One point requires some clarification; the MD inductor as defined by (3.34) is MD-passive for constant $L \geq 0$, and for a transformed coordinate $t_j$, $j = 1, \ldots, k$. In problems for which material parameters have some spatial variation, some of the MD circuit elements that we will require will, as a rule, have some spatial dependence. If $L$ in (3.34) is a function of $\mathbf{t}$, then in general the equation does not describe an MD-passive one-port. More precisely, if $L$ does not commute with $\frac{\partial}{\partial t_j}$, then the application of the trapezoid rule to (3.34) does not yield the simple wave relationship (3.38). This begs the question, then, of how the trapezoid rule can be applied to circuit elements which are not LSI (which we will require in order to numerically integrate systems with spatial material parameter variation).

For almost all the systems of interest in this thesis, it will be possible to consolidate any material parameter variation in circuit elements defined with respect to the pure time direction (recall that in our general symmetric hyperbolic system (3.1), such variation is confined to the coefficients of the time derivative term). For example, consider an inductor described by

$$v = L\frac{\partial i}{\partial t'} \tag{3.40}$$

in the (1+1)D coordinates defined by (3.18). Here, $L$ is strictly positive, but may be a function of $x$, and note that $t'$ is not among the new coordinates defined by (3.18). Because $L$ does commute with $\frac{\partial}{\partial t'}$, it is still possible to apply the trapezoid rule, in the time direction, in order to get a wave relationship of the form of (3.38). The directional shift will then be along the time direction, and we need to be sure that the shift does in fact refer to another grid point—from Figure 3.1(b), we can see that this is in fact true (it is true for any of the coordinate systems discussed in §3.3). It is of course possible to include a pure time derivative among the new coordinates; this is done, for example, in the case of the embedding defined by coordinates (3.22), for which $t_5$ is simply $t$ multiplied by a scaling factor. Nitsche [62] has called this the *generalized trapezoid rule*. Note, however, that if we write (3.40) as

$$v = \frac{L}{\sqrt{2}}\left(\frac{\partial i}{\partial t_1} + \frac{\partial i}{\partial t_2}\right) \tag{3.41}$$

it is *not* permissible to treat this as a series connection of two MD inductors—neither one is MD-passive, because $L$ does not commute with either of the two directional derivatives.

A more general definition of an inductor, suitable for use in time-varying or nonlinear problems is

$$v = \sqrt{L}\frac{\partial}{\partial t_j}\left(\sqrt{L}i\right) = \frac{1}{2}\left(L\frac{\partial i}{\partial t_j} + \frac{\partial Li}{\partial t_j}\right) \tag{3.42}$$

for any transformed coordinate $t_j$. In this case, $L$ can depend on $\mathbf{t}$ or even on $v$ or $i$; as long as we have $L \geq 0$ and use power-normalized waves, the MD inductor defined by (3.42) is MD passive [48, 85]. For constant $L$, (3.42) reduces to (3.34). Circuit elements of this type appear in circuit networks for fluid dynamical systems [16, 49, 70, 191], as well as in a vector-matrix context when dealing with the linearized Euler Equations [86]. We also note that passivity under time-varying conditions can be enforced as it has been done in digital waveguide networks [166]; it would appear that waveguide networks (to be discussed in depth in Chapter 4) could be generalized to include the nonlinear case in the same manner (see Appendix B for an interesting application of these ideas).

### 3.5.2 Other MD Elements

The inductor and capacitor are the only circuit elements which need a more involved treatment in the MD case[†]. The capacitor is treated as the dual to the inductor, replacing $v$ by $i$ and $L$ by $C$, and needs no further comment, other than that, as with the lumped capacitor, there is no sign inversion in the resulting MD wave one-port. The graphical representations of these MD one-ports and their MDWD equivalents are shown in Figure 3.5. Note that for the sake of compactness, in the circuit diagrams that will follow, we will use the derivative notation of the MDWDF literature [131] where we have

$$D_j \triangleq \frac{\partial}{\partial t_j}$$

for some transformed coordinate $t_j$. In some instances, derivatives with respect to the original untransformed variables appear, and we will write

$$D_t \triangleq \frac{\partial}{\partial t} \quad , \quad D_x \triangleq \frac{\partial}{\partial x} \quad , \quad D_y \triangleq \frac{\partial}{\partial y} \quad \ldots$$

We will also use the notation

$$D_{t'} \triangleq \frac{1}{v_0}\frac{\partial}{\partial t}$$

to refer to the dimensionless time derivative, which appears frequently. Also, in a signal flow graph, we represent the operation of shifting by $T_j$ in direction $t_j$ by the symbol $\mathbf{T}_j$. In cases where the system or $N$-port is linear and shift-invariant, we will be able to replace $\mathbf{T}_j$ by $z_j^{-1}$, the transmittance of a shift in direction $t_j$ (see the next section).

---

[†] We will return to the multidimensional generalization of the unit element in §4.10.

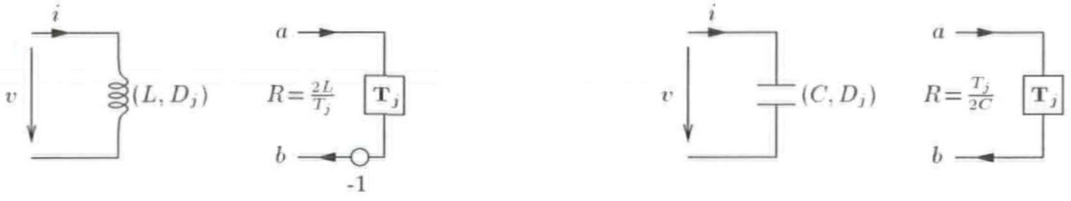

(a) (b)

Figure 3.5: *MDWD one-ports*— (a) *an MD inductor, with inductance $L$, direction $t_j$ and its MDWD counterpart, for step-size $T_j$ and $R = 2L/T_j$ and* (b) *an MD capacitor, of capacitance $C$, direction $t_j$ and its MDWD one-port, with step-size $T_j$ and port resistance $R = T_j/2C$.*

All the other elements for which we will have a use, namely the resistor, transformer and gyrator, as well as scattering junctions are *memoryless* and hence their pointwise behavior in MD is identical to that of their lumped counterparts. Their graphical representations are also identical (see §2.2.4). We must keep in mind however, that these are still distributed elements. For example, a resistor of resistance $R(\mathbf{t})$ in an MDKC represents some resistivity at every point in the domain of the problem.

A network made up of Kirchoff connections of $N$-ports which are individually MD-passive can be shown (through the use of Tellegen's Theorem [136], which is unchanged in multiple dimensions) to be be MD-passive as a whole [44].

### 3.5.3 Discretization in the Spectral Domain

If our network or $N$-port is linear and shift-invariant, it is also possible to view the discretization procedure as a *spectral mapping*, just as in the last chapter. Consider now the case where the problem domain is some $n$-dimensional space, with coordinates $\mathbf{u} = [x_1, \dots, x_n, t]^T$, and where we have changed coordinates to $\mathbf{t} = [t_1, \dots, t_k]^T$, with $k \geq n+1$ via a transformation of type (3.21). The defining equation of an MD inductor of direction $t_j$ for any $j = 1, \dots, k$ is

$$v = L\frac{\partial i}{\partial t_j}$$

and for an exponential state at frequencies $\mathbf{s_t}$, we have

$$\hat{v} = Ls_j\hat{i}$$

where $v = \hat{v}e^{\mathbf{s_t}^T\mathbf{t}}$ and $i = \hat{i}e^{\mathbf{s_t}^T\mathbf{t}}$. The "impedance" is here $Z = Ls_j$ and clearly satisfies MD positive realness criterion given in (3.31) (and furthermore is MD-lossless) if $L \geq 0$ . As in the lumped case, the trapezoid rule, now applied in the $t_j$ direction, can be interpreted as a spectral mapping

$$s_j \rightarrow \psi_j \triangleq \frac{2}{T_j}\frac{1-e^{-s_jT_j}}{1+e^{-s_jT_j}} = \frac{2}{T_j}\frac{1-z_j^{-1}}{1+z_j^{-1}} \tag{3.43}$$

where $T_j$ is some arbitrary step-size in the $t_j$ direction. For notational purposes, we have used

$$z_j^{-1} = e^{-s_jT_j}$$

to represent the frequency domain equivalent of a unit shift in the $t_j$ direction. In complete analogy with the lumped case, (3.43) implies that

$$\mathrm{Re}(s_j) \gtreqless 0 \quad \Longleftrightarrow \quad \mathrm{Re}(\psi_j) \gtreqless 0 \quad \Longleftrightarrow \quad |z_j| \gtreqless 1$$

This shift can of course also be written in terms of delays and shifts in the $\mathbf{u}$ coordinates. For example, consider the coordinate transformation defined in (3.18). In this case we have, in the frequency domain,

$$\begin{aligned} s_1 &= \frac{1}{\sqrt{2}v_0}s_t + \frac{1}{\sqrt{2}}s_x \\ s_2 &= \frac{1}{\sqrt{2}v_0}s_t - \frac{1}{\sqrt{2}}s_x \end{aligned}$$

where $s_t$ and $s_x$ are the frequency variables conjugate to $t$ and $x$ respectively. (We assume that our spatial domain is of infinite extent, so that $s_x$ corresponds to an imaginary Fourier transform variable.) Suppose we have also chosen the step-sizes in the two coordinates such that the grids overlap, that is, $T_1 = \sqrt{2}\Delta = \sqrt{2}v_0T$, where $T$ is the shift in the pure time direction. Then, for a shift of $T_1$ in the $t_1$ direction, we can write

$$e^{-s_1T_1} = e^{-\frac{1}{\sqrt{2}v_0}s_tT_1 - \frac{1}{\sqrt{2}}s_xT_1} = e^{-s_tT - s_x\Delta}$$

or

$$z_1^{-1} = z^{-1}w^{-1} \tag{3.44}$$

where $z^{-1}$ represents a delay of duration $T$ in the time direction, and $w^{-1}$ corresponds to a shift over distance $\Delta$ in the positive space direction. Similarly, we can write

$$z_2^{-1} = z^{-1}w \tag{3.45}$$

For a more complex example, consider again the transformation defined by

$$\mathbf{H} = \begin{bmatrix} 1 & 0 & -1 & 0 & 0 \\ 0 & 1 & 0 & -1 & 0 \\ 1 & 1 & 1 & 1 & 1 \end{bmatrix}$$

which maps coordinates $[x, y, t]^T$ to a five-dimensional coordinates $[t_1, t_2, t_3, t_4, t_5]^T$. A shift of $T_1 = \Delta$ in direction $t_1$ corresponds to a transmittance of the form

$$z_1^{-1} = e^{-s_1 T_1} = e^{-(s_x + \frac{1}{v_0} s_t)\Delta} = e^{-(s_x\Delta + s_t T)} = z^{-1} w_x^{-1}$$

where $w_x$ represents a unit shift (of length $\Delta$) in the $x$-direction, and as before, $z^{-1}$ corresponds to a unit delay of $T = \Delta/v_0$. The other shifts can be written as

$$z_2^{-1} = z^{-1} w_y^{-1} \qquad z_3^{-1} = z^{-1} w_x \qquad z_4^{-1} = z^{-1} w_y \qquad z_5^{-1} = z^{-1}$$

where $w_y$ represents a unit shift (of length $\Delta$) in the $y$ direction. At a given grid point in the old coordinates, the unit delays $z_1^{-1}, \dots, z_4^{-1}$, interpreted as directional shifts, refer to points on the grid at the previous time step, and located one grid point away in the $-x$, $-y$, $x$ and $y$ directions, respectively. The unit delay $z_5^{-1}$ is simply a unit time delay.

It is important to note the manner in which the special character of the coordinate transformation manifests itself here. Due to the positivity requirement on the elements of the last column of **H**, a unit delay in *any* of the directions $t_j$ will always include some delay in the pure time direction. By means of this requirement, and the introduction of wave variables, MDWD networks can, in the same way as their lumped counterparts, be designed in which delay-free loops do not appear. Such networks, when used for simulation, will give rise, in general, to *explicit* numerical schemes [176].

### 3.5.4 Other Spectral Mappings

One could well ask whether the spectral mappings of the form (3.43), which correspond to an application of the trapezoid rule, are the only means of deriving an MD-passive discrete system from a continuous one. The criterion for a passivity-preserving mapping is that it map multidimensional positive real functions (i.e., functions whose real parts are positive when the real parts of *all* of their arguments are positive) to functions which have the same property in a generalized multidimensional outer disk.

In a brief section of one of the original papers on the subject of WD integration [61], a different type of mapping is proposed, in a discussion of boundary conditions for the transmission line equations. Suppose that, in the (1+1)D case, our transformed coordinates are given by (3.18). The alternative mapping can be written as

$$s_1 \rightarrow \phi_1 \qquad\qquad s_2 \rightarrow \phi_2$$

where the frequency variables $\phi_1$ and $\phi_2$ are defined in terms of the variables $\psi_1$ and $\psi_2$ from (3.43) by

$$\phi_1 \triangleq \frac{\psi_1}{1+T_1T_2\psi_1\psi_2/4} = \frac{1}{T_1}\frac{(1-z_1^{-1})(1+z_2^{-1})}{1+z_1^{-1}z_2^{-1}} \tag{3.46a}$$

$$\phi_2 \triangleq \frac{\psi_2}{1+T_1T_2\psi_1\psi_2/4} = \frac{1}{T_2}\frac{(1-z_2^{-1})(1+z_1^{-1})}{1+z_1^{-1}z_2^{-1}} \tag{3.46b}$$

We then have that

$$\mathrm{Re}(\phi_1) = \frac{\mathrm{Re}(\psi_1)+T_1T_2|\psi_1|^2\mathrm{Re}(\psi_2)/4}{|1+T_1T_2\psi_1\psi_2/4|^2} \qquad \mathrm{Re}(\phi_2) = \frac{\mathrm{Re}(\psi_2)+T_1T_2|\psi_2|^2\mathrm{Re}(\psi_1)/4}{|1+T_1T_2\psi_1\psi_2/4|^2}$$

from which we can conclude that

$$\mathrm{Re}(\psi_1) \gtreqless 0 \text{ and } \mathrm{Re}(\psi_2) \gtreqless 0 \qquad \Longrightarrow \qquad \mathrm{Re}(\phi_1) \gtreqless 0 \text{ and } \mathrm{Re}(\phi_2) \gtreqless 0$$

Another simple way of seeing positive realness is by rewriting (3.46) as

$$\phi_1 \triangleq \frac{1}{1/\psi_1+T_1T_2\psi_2/4} \tag{3.47a}$$

$$\phi_2 \triangleq \frac{1}{1/\psi_2+T_1T_2\psi_1/4} \tag{3.47b}$$

in which case $\phi_1$ and $\phi_2$ can be viewed as impedances of parallel combinations of passive (indeed, lossless) elements. For example, $\phi_1$ is equivalent to the impedance of a parallel combination of an inductor of impedance $\psi_1$ and a capacitor of impedance $4/(T_1T_2\psi_2)$. Second-order accuracy is also obtained under these mappings; this should be clear from (3.47) as well. This spectral mapping differs from the trapezoid rule in that the discrete spectral images of the two continuous frequency variables $s_1$ and $s_2$ are now mixtures of the two discrete frequency variables $z_1^{-1}$ and $z_2^{-1}$. In addition, the transformation does not have a unique inverse, but this is of little consequence because we will never have any occasion to invert such a mapping. We mention this particular mapping, because it will serve as the bridge between multidimensional wave digital filters and digital waveguide networks (to be discussed in Chapter 4). We will spend some time in §4.10 elaborating this link. It will also allow us to introduce higher-order accurate methods, which we will discuss in §3.13.

## 3.6 The (1+1)D Advection Equation

Perhaps the simplest hyperbolic partial differential equation imaginable is the so-called scalar *advection* or *one-way wave equation* in (1+1)D, defined by

$$\frac{\partial i}{\partial t}+\alpha\frac{\partial i}{\partial x}=0 \tag{3.48}$$

where $\alpha$ is a real constant [176]. It is complemented by the initial condition

$$i(x,0)=i_0(x), \qquad -\infty<x<\infty \tag{3.49}$$

Here, the solution $i(x,t)$ is assumed continuously differentiable (though it need not be[†]), and is defined over the entire $x$-axis, and for $t\geq 0$. The solution is simply

$$i(x,t)=i_0(x-\alpha t) \tag{3.50}$$

That is, the initial data travels to the left or right (depending on the sign of $\alpha$) with speed $|\alpha|$. Despite its simplicity, it is often used as a model for numerical schemes [95].

### 3.6.1 A Multidimensional Kirchoff Circuit

We first change coordinates via transformation (3.18), which gives

$$\underbrace{\frac{v_0+\alpha}{\sqrt{2}}\frac{\partial i}{\partial t_1}}_{v_1}+\underbrace{\frac{v_0-\alpha}{\sqrt{2}}\frac{\partial i}{\partial t_2}}_{v_2}=0$$

The basis of the WD integration approach is to view this equation as a *loop* equation for a multidimensional circuit, i.e., a circuit in which voltages and currents may depend not only on time but on space as well. The equation above is to be interpreted as describing a series connection of two inductors, where the dependent variable $i$ is considered to be the current passing through them. The MD-inductors have inductances

$$L_1\triangleq\frac{(v_0+\alpha)}{\sqrt{2}} \qquad L_2\triangleq\frac{(v_0-\alpha)}{\sqrt{2}}$$

As explained in §3.3, these two inductors are associated with the directions $t_1$ and $t_2$. The circuit representation of the connection is shown in Figure 3.6(a).

It is important to note that the circuit pictured here is merely a graphical representation of (3.48)—in particular, it represents the point-wise or differential behavior of (3.48) anywhere in the

---

[†] Given the solution (3.50) to (3.48), it is easy to see that it remains unchanged even if $i_0$ is not differentiable everywhere. In this case, $i$ must be considered to be a solution to the integral form of (3.48).

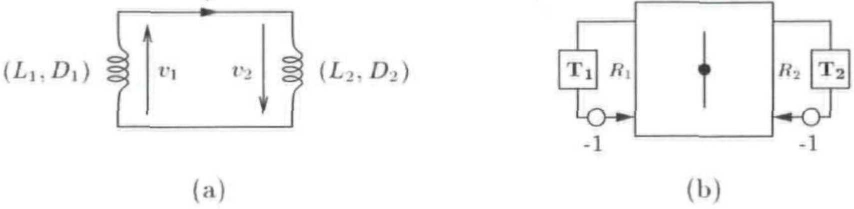

Figure 3.6: *The (1+1)D advection equation*— (a) *MDKC and* (b) *MDWD network.*

$(t_1, t_2)$ plane. It does, however, permit an immediate discretization via wave digital filters, in exactly the same manner as described in the previous chapter on lumped networks. That is, we can replace the circuit by two MDWD inductor one-ports connected through a series adaptor. This complete wave digital network is shown in Figure 3.6(b), where we have defined the port resistances to be:

$$R_1 = \frac{2L_1}{T_1} = \frac{v_0 + \alpha}{\Delta} \qquad\qquad R_2 = \frac{2L_2}{T_2} = \frac{v_0 - \alpha}{\Delta} \tag{3.51}$$

where we have used $T_1 = T_2 = \sqrt{2}\Delta$. Figure 3.6(b) is an abbreviated notation for a numerical integration routine. We can expand out the spatial dependence into a full signal flow graph in order to better perceive the flow of data. This is shown in Figure 3.7, where we have indicated unit time delays by $T$; series scattering junctions are separated by a distance $\Delta$.

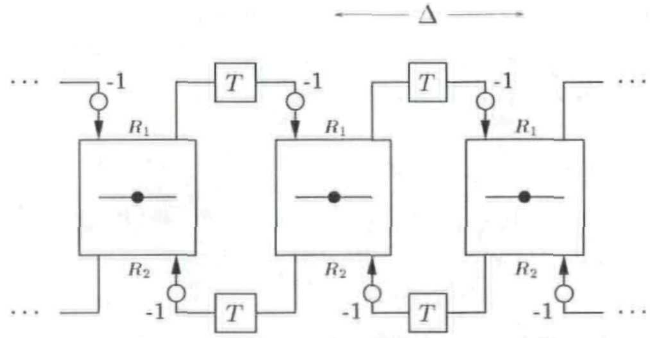

Figure 3.7: *Signal flow graph for Figure 3.6(b).*

This signal flow graph can be interpreted as follows: At every grid point in the domain, and at every time step there are three computational stages:

1. Retrieve the incoming wave variables from the registers. Referring to Figure 3.6(b), this means that for the port of port resistance $R_1$, which accepts a wave variable shifted by $\mathbf{T_1}$, we must use the sign-inverted wave quantity output from the corresponding port, one time step earlier, and one grid point to the *left*. This shifting operation is to applied at every grid point, as

per Figure 3.7. Similarly, the input to the port of port resistance $R_2$ takes the sign-inverted output of its corresponding port one time step earlier, and one grid point to the *right.*

2. Perform scattering operation.

3. Insert output wave variables into registers.

If $v_0 = |\alpha|$, then either $R_1$ or $R_2$ is zero, depending on the sign of $\alpha$. In this case, the associated inductor can be dropped from the network entirely (i.e., we can treat it as a short-circuit). For example, if $\alpha < 0$, then $v_0 = |\alpha|$ implies that $R_1 = 0$, and we get the simplified network of Figure 3.8. Here, we in fact have an exact solution to (3.48); the signals in the delay registers are shifted repeatedly to the left, and directly implement the traveling wave solution given by (3.50). Note that the sign inversion of the inductor is canceled by that of the reflection from the port.

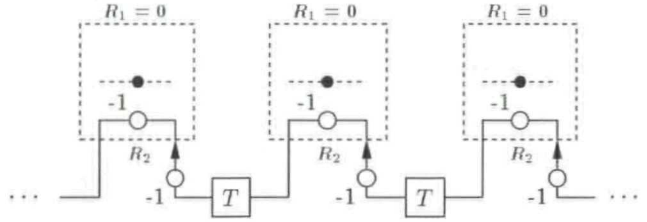

Figure 3.8: *Simplified signal flow graph for Figure 3.6(b), for* $v_0 = |\alpha|$, $\alpha < 0$.

### 3.6.2 Stability

It is easy to see that the MDKC of Figure 3.6(a) will be MD-passive if the inductances $L_1$ and $L_2$, and consequently the port resistances $R_1$ and $R_2$ of the MDWDF in Figure 3.6(b) are non-negative. From (3.51), this gives a constraint on $v_0$, the space step/time step ratio, namely that we must have

$$v_0 = \frac{\Delta}{T} \geq |\alpha| \qquad \text{(for passivity)}$$

Any such value of $v_0$ yields a passive, and thus stable algorithm.

It is important to mention, however, that the *instances* of the MDWDF, sampled at every grid point as in Figure 3.7 are *not* connected port-wise, as must be true for a traditional lumped WD-network. The output wave at the bottom port at spatial location $x = i\Delta$ is sign-inverted and then sent as input to the same port, at location $x = (i-1)\Delta$ at the next time step. Thus the realization of Figure 3.7 can not be analyzed directly as a chain of lumped elements; passivity follows from the multidimensional representations shown in Figure 3.6.

### 3.6.3 An Upwind Form

One of the interesting (and only briefly mentioned [86]) features of the MDKC representation is that it can easily be manipulated to yield what are known as *upwind difference methods*; such methods are usually applied to problems for which there is a directional bias in the propagation speed, and are heavily used in fluid dynamical calculations [89].

We can rewrite the advection equation (3.48), where we assume, without loss of generality, that $\alpha > 0$ as

$$\underbrace{\sqrt{2}\alpha\frac{\partial i}{\partial t_1}}_{v_1}+\underbrace{(v_0-\alpha)\frac{\partial i}{\partial t'}}_{v_2}=0$$

which can be written as the MDKC shown in Figure 3.9(a). We now have

$$L_1=\sqrt{2}\alpha \qquad\qquad L_2=v_0-\alpha$$

In this case, we have left a directional derivative in the pure time (or scaled time) direction in the MDKC; for this inductor, we apply the generalized trapezoid rule discussed in §3.5.1, with a step-size of $T'=\Delta$. The resulting MDWD network is shown in Figure 3.9(b), with port resistances given by

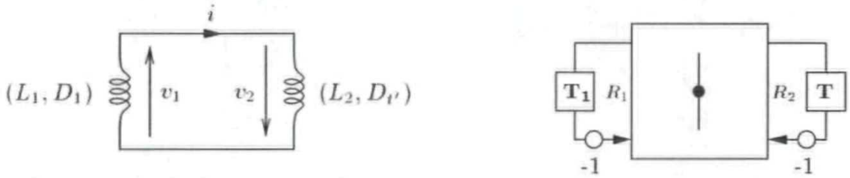

(a) (b)

Figure 3.9: *An upwind-differencing form for the advection equation*— (a) *MDKC and* (b) *MDWD-network.*

$$R_1=\frac{2\alpha}{\Delta} \qquad\qquad R_2=\frac{2}{\Delta}(v_0-\alpha) \tag{3.52}$$

(Note that a directional shift of length $\Delta$ in the scaled time direction $t'=v_0t$ corresponds to a pure time shift of duration $\Delta/v_0=T$, and so we have indicated this shift in Figure 3.9(b) by a **T**). The signal flow graph, with spatial dependence expanded out, is shown in Figure 3.10.

This structure is in a sense, a better model for the advection system; recall that for $\alpha > 0$, the solution at any future time instant $t \geq 0$ will simply be the initial distribution shifted to the right by an amount $\alpha t$. By using upwind differencing, we have dispensed with the unphysical leftward traveling wave which appears in the signal flow diagram in Figure 3.7. As before, the network will

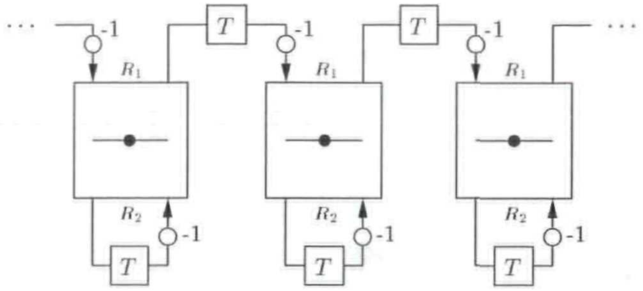

Figure 3.10: *Signal flow graph for Figure 3.9(b), for $\alpha > 0$.*

be MD-passive for $v_0 \geq \alpha$. It also degenerates to a simple delay line when $v_0 = \alpha$ (in which case we will have $R_2 = 0$, and the right-hand inductor in Figure 3.9(b) can be dropped from the network).

Because all the systems that we will subsequently examine do not have any directional disparities in the wave speed, we will not pursue the subject of upwind differencing further here. We do mention, though, that digital waveguide networks [166, 198], which are intimately related to MDWD networks, are incapable of performing upwind differencing for the simple reason that they are constructed from bidirectional delay lines (or unit elements), which carry information symmetrically in opposite directions. In this respect, the two approaches stand in stark contrast; the advantage of having an MD representation is very clear in this case.

## 3.7 The (1+1)D Transmission Line

As a slightly more involved example, which highlights some of the issues which typically arise in the construction of these algorithms, consider the (1+1)D *transmission line* or *telegrapher's* equations [63]:

$$l\frac{\partial i}{\partial t} + \frac{\partial u}{\partial x} + ri + e = 0 \qquad (3.53a)$$

$$c\frac{\partial u}{\partial t} + \frac{\partial i}{\partial x} + gu + h = 0 \qquad (3.53b)$$

Here, $i(x,t)$ and $u(x,t)$ are the current and voltage in the transmission line, $l$, $c$, $r$ and $g$ are inductance, capacitance, resistance and shunt conductance per unit length respectively, and are all non-negative functions of $x$ ($l$ and $c$ are strictly positive[†]). $e(x,t)$ and $h(x,t)$ represent distributed voltage and current source terms. System (3.53) is symmetric hyperbolic; it has the form of (3.1), with $\mathbf{w} = [i, u]^T$, and

---

[†] In fact, $l$ and $c$ should be bounded away from zero, so that the local wave speed (given by $1/\sqrt{lc}$) remains finite everywhere.

$$\mathbf{P} = \begin{bmatrix} l & 0 \\ 0 & c \end{bmatrix} \qquad \mathbf{A}_1 = \begin{bmatrix} 0 & 1 \\ 1 & 0 \end{bmatrix} \qquad \mathbf{B} = \begin{bmatrix} r & 0 \\ 0 & g \end{bmatrix} \qquad \mathbf{f} = \begin{bmatrix} e \\ h \end{bmatrix} \tag{3.54}$$

**Phase and Group Velocity**

In the constant-coefficient case, where $r = g = 0$, the dispersion relation, defined in (3.10), will be

$$\chi_{TL}(\omega, \beta) = -\omega^2 lc + \beta^2 = 0$$

in terms of real frequencies $\omega$ and wavenumbers $\beta$, and has solutions

$$\omega = \pm\frac{\beta}{\sqrt{lc}}$$

The phase and group velocities, from (3.12) are then

$$\gamma_{TL}^{p} = \gamma_{TL}^{g} = \pm\frac{1}{\sqrt{lc}} \tag{3.55}$$

and if $l$ and $c$ are functions of $x$, the maximal group velocity will be

$$\gamma_{TL,max}^{g} = \frac{1}{\sqrt{(lc)_{min}}} \tag{3.56}$$

where $(lc)_{min} = \min_{x\in\mathcal{D}}(lc)$.

### 3.7.1 MDKC for the (1+1)D Transmission Line Equations

In order to put this system into the form of an MDKC, let us first change dependent variables by

$$i_1 \triangleq i \qquad\qquad i_2 \triangleq \frac{u}{r_0} \tag{3.57}$$

where $r_0 > 0$ is a free constant parameter which has dimensions of resistance. The primary reason for introducing this parameter is so that the numerical algorithm may later be tuned to be optimally efficient (in terms of the largest allowable time step for a given grid spacing). After changing variables, and multiplying the second equation by $r_0$, we obtain:

$$l\frac{\partial i_1}{\partial t} + r_0\frac{\partial i_2}{\partial x} + ri_1 + e = 0 \tag{3.58a}$$

$$cr_0^2\frac{\partial i_2}{\partial t} + r_0\frac{\partial i_1}{\partial x} + gr_0^2 i_2 + r_0 h = 0 \tag{3.58b}$$

At this point, it is already possible to write the above system in the form of an MDKC, which is shown in Figure 3.11(a).

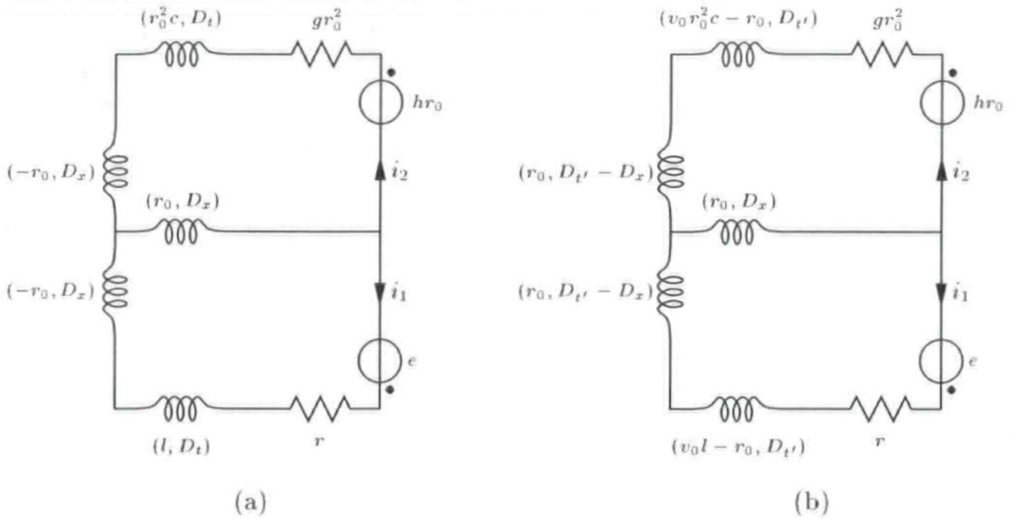

Figure 3.11: *MDKCs for the (1+1)D transmission line system* (3.58)— (a) *a direct representation, and* (b) *after splitting and shifting inductances.*

Kirchoff's node equation tells us the current in the common branch, which is $i_1 + i_2$, then the loop conditions yield system (3.58). This representation, however, can not give an explicit algorithm, because of the purely spatial MD inductors which form a T-junction between the two loops; that is, if one tries to treat these as one-ports, their WD counterparts will be found to contain delay-free paths from input to output; in other words, the algorithm will be implicit. Nor can it be considered to be MD-passive, since there are negative inductances. By performing a few network theoretic transformations to this MDKC, we can obtain a representation which is MD-passive, and which will give rise to an explicit numerical method. The idea here, grossly speaking, is to make sure that each inductance is positive, and that every inductor "points" in the direction of a transformed coordinate, as per conditions (3.14).

First note that we can split and shift the differential operators around at will, as long as the loop equations remain unchanged. In particular, we can redraw the circuit as in Figure 3.11(b), where we have introduced the scaled time coordinate $t' = v_0t$ and its associated derivative $D_{t'}$. Now, examine the three inductors which form a T-junction connecting the two loops. If we are planning to use coordinates defined by (3.19), then the two inductors on the vertical rail can be identified as MD-passive—we have $D_{t'} - D_x = \sqrt{2}D_2$. The inductance in the common branch, however is not yet in proper form. It is now possible to apply transformations from classical network theory so as to ensure that the resulting equivalent two-port is composed of only MD-passive elements. Although the system as a whole does not change under these manipulations, we would like it to be *concretely* passive†, so that it may be decomposed into a connection of simpler passive blocks. Since the two-port containing the T-junction will always be, by itself, linear and shift-invariant (i.e., shift-invariant with respect to any coordinate, because the inductances are constant), we are justified in describing it by means of impedances and applying spectral transformations. When it is connected to the other components which are not shift-invariant, the spectrally transformed two-port may be interpreted in terms of differencing formulae.

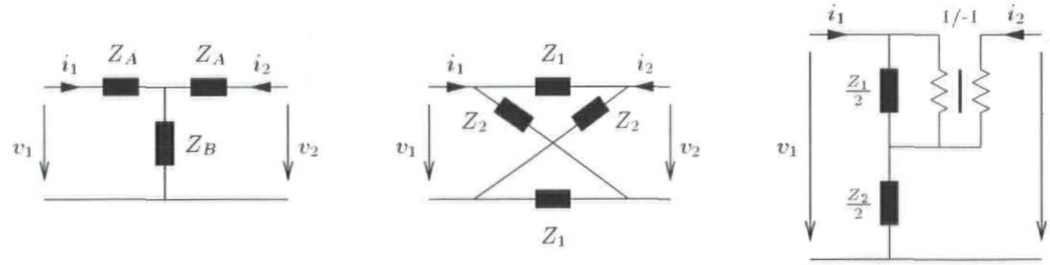

(a) (b) (c)

Figure 3.12: *Equivalent two-ports*— (a) *T-junction, with impedances* $Z_A$ *and* $Z_B$ *and* (b) *and* (c), *lattice and Jaumann equivalent two-ports, both with* $Z_1 = Z_A$ *and* $Z_2 = Z_A + 2Z_B$.

The symmetric T-junction, and its lattice [55, 131] and Jaumann [132] equivalents are shown in Figure 3.12, for arbitrary impedances $Z_A$ and $Z_B$. Replacement of the T-junction in Figure 3.11(b) by either of the two-ports in Figure 3.12(b) and (c) gives an MDKC which is indeed concretely MD-passive; this circuit is shown in Figure 3.14(a). Note that in this representation, we have left inductors (with symbols $D_{t'}$) in the circuit, instead of rewriting them as $D_{t'} = (D_1 + D_2)/\sqrt{2}$. In this case, we must proceed as such because their inductances are possibly spatially-varying (note that they depend on $l$ and $c$); for this reason these elements cannot be split into inductances acting along directions $t_1$ and $t_2$ without giving up passivity. For these inductances, we will apply the generalized trapezoid rule, which was discussed in §3.5.1.

### 3.7.2 Digression: Derivation of an Inductive Lattice Two-port

We have derived the WD equivalents for all the standard circuit elements, but the two-ports pictured in Figure 3.12 need a special treatment. Fettweis and Nitsche find the lattice form to be the most straightforward derivation, but we would especially like to call attention to the fact that the resultant WD two-port is the same regardless of which of the equivalent structures we choose; use of a concretely MD-passive two-port, however, makes the passivity of the resulting circuit obvious. We will continue to use the Jaumann equivalent in all future diagrams (though we could equally well use the lattice form). Basu [10], as well as Fettweis [46] make the point that an electrical network equivalent is a convenient formalism for developing MD-passive discrete networks, but it is by no means necessary.

---

† By concretely passive, we simply mean that all elements in the network should be individually passive. A network (or $N$-port [12]) may be abstractly passive, but not concretely passive; the MDKCs shown in Figure 3.11 are of this type.

Beginning from any of the equivalent two-port structures in Figure 3.12, we can immediately write down the impedance matrix, which we will denote by $\mathbf{Z}$:

$$\mathbf{Z} = \frac{1}{2}\begin{bmatrix} Z_2+Z_1 & Z_2-Z_1 \\ Z_2-Z_1 & Z_2+Z_1 \end{bmatrix} = \frac{1}{2}\begin{bmatrix} 1 & 1 \\ 1 & -1 \end{bmatrix}\begin{bmatrix} Z_2 & 0 \\ 0 & Z_1 \end{bmatrix}\begin{bmatrix} 1 & 1 \\ 1 & -1 \end{bmatrix} = \mathbf{N}^{-1}\mathbf{\Lambda}\mathbf{N}$$

where we have set $\mathbf{N} = \left[\begin{smallmatrix} 1 & 1 \\ 1 & -1 \end{smallmatrix}\right]$ and $\mathbf{\Lambda}=\left[\begin{smallmatrix} Z_2 & 0 \\ 0 & Z_1 \end{smallmatrix}\right]$.

We now introduce a port resistance matrix $\mathbf{R} = \left[\begin{smallmatrix} R & 0 \\ 0 & R \end{smallmatrix}\right] > \mathbf{0}$, where we can choose equal port resistances because the two-port is symmetric. The scattering matrix is then, from (2.21),

$$\mathbf{S} = \left(\mathbf{N}^{-1}\mathbf{\Lambda}\mathbf{N}\mathbf{R}^{-1} + \mathbf{I}_2\right)^{-1}\left(\mathbf{N}^{-1}\mathbf{\Lambda}\mathbf{N}\mathbf{R}^{-1} - \mathbf{I}_2\right)$$

where $\mathbf{I}_2$ is the $2\times 2$ identity matrix. This is easily rearranged to become

$$\mathbf{S} = \mathbf{N}^{-1}\left(\mathbf{\Lambda}\mathbf{R}^{-1} + \mathbf{I}_2\right)^{-1}\left(\mathbf{\Lambda}\mathbf{R}^{-1} - \mathbf{I}_2\right)\mathbf{N}$$

Returning to the problem of the (1+1)D transmission line, for the two-port in question in Figure 3.14(a), we have $Z_1 = \sqrt{2}r_0s_2$ and $Z_2 = \sqrt{2}r_0s_1$. Notice in particular that for these choices of impedance, any of the two-ports of Figure 3.12 are described by MD positive real matrices. We now discretize using the trapezoid rule, i.e.

$$s_j \quad \rightarrow \quad \psi_j = \frac{2}{T_j}\frac{1-z_j^{-1}}{1+z_j^{-1}} \qquad\qquad j = 1,2$$

where we also will set $T_1 = T_2 = \sqrt{2}\Delta$. If we make the choice $R = 2r_0/\Delta$, we obtain the discrete-time, causal scattering matrix

$$\mathbf{S}(z_1,z_2) = \mathbf{N}^{-1}\begin{bmatrix} -z_1^{-1} & 0 \\ 0 & -z_2^{-1} \end{bmatrix}\mathbf{N} \tag{3.59}$$

The resulting MD two-port is shown in Figure 3.13.

It should be clear that the same procedure can be used for arbitrary impedances $Z_1$ and $Z_2$; it should be remarked, however, that we can not always get a simple form without a through path like that pictured in Figure 3.13. Since this two-port is strictly causal, it may easily be connected to other ports without the risk of the appearance of a delay-free loop.

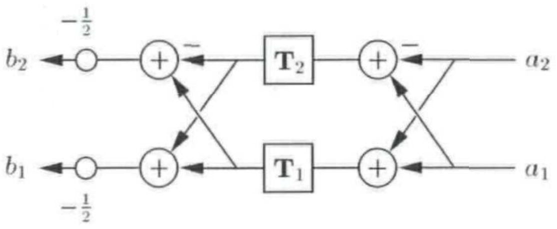
$-\frac{1}{2}$
$b_2$
$\mathbf{T}_2$
$a_2$
$b_1$
$\mathbf{T}_1$
$a_1$
$-\frac{1}{2}$

Figure 3.13: *Signal flow diagram for the MDWD lattice or Jaumann two-port.*

### 3.7.3 A MDWD Network for the (1+1)D Transmission Line

Returning to Figure 3.14(a), and making use of the discrete two-port derived in the last section, we can now write the complete wave digital network. It is shown in Figure 3.14(b).

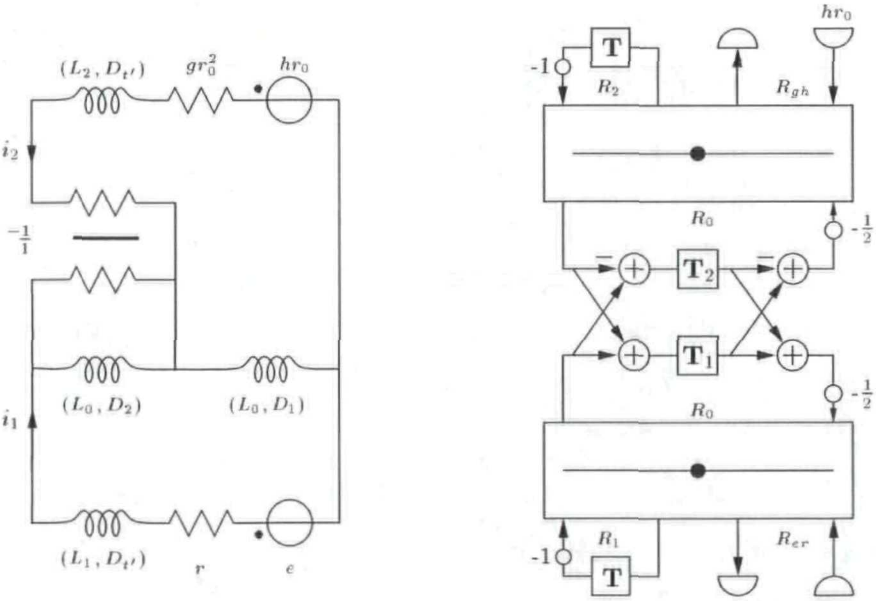
$(L_2, D_{t'})$
$gr_0^2$
$hr_0$
$i_2$
$-\frac{1}{1}$
$(L_0, D_2)$
$(L_0, D_1)$
$i_1$
$(L_1, D_{t'})$
$r$
$e$
$hr_0$
-1
$\mathbf{T}$
$R_2$
$R_{gh}$
$R_0$
$-\frac{1}{2}$
$\mathbf{T}_2$
$\mathbf{T}_1$
$-\frac{1}{2}$
$R_0$
$R_1$
$R_{er}$
-1
$\mathbf{T}$
$e$

(a) (b)

Figure 3.14: (a) *MD-passive network for the (1+1)D transmission line equations and* (b) *its associated MDWD network.*

The inductances in the MDKC of Figure 3.14(a) are

$$L_1 = v_0 l - r_0 \qquad L_2 = v_0 r_0^2 c - r_0 \qquad L_0 = \frac{r_0}{\sqrt{2}} \tag{3.60}$$

and the port resistances of the MDWD network of Figure 3.14(b) are

$$R_0 = \frac{2r_0}{\Delta} \qquad R_1 = \frac{2L_1}{\Delta} \qquad R_2 = \frac{2L_2}{\Delta} \qquad R_{gh} = gr_0^2 \qquad R_{er} = r \tag{3.61}$$

The MDWD network is MD-passive if all the port resistances are non-negative over the entire spatial domain; from (3.60) and (3.61), the only port resistances which are possibly negative are $R_1$ and $R_2$. Requiring their positivity gives the constraints

$$v_0 \geq \frac{r_0}{l_{min}} \qquad\qquad v_0 \geq \frac{1}{r_0 c_{min}}$$

where $l_{min} = \min_x l$ and $c_{min} = \min_x c$. A judicious choice of $r_0 = \sqrt{\frac{l_{min}}{c_{min}}}$ [131] allows the largest possible time step for a given grid spacing; the condition is then

$$v_0 \geq \sqrt{\frac{1}{l_{min}c_{min}}} \geq \gamma^g_{TL,max} \tag{3.62}$$

where $\gamma_{TL,max}$ is defined by (3.56).

If $l$ and $c$ are constant, and (3.62) holds with equality, so that we have

$$v_0 = \sqrt{\frac{1}{lc}} = \gamma^g_{TL,max} \tag{3.63}$$

then the MDWD numerical scheme is said to be operating at the *Courant-Friedrichs-Lewy* (CFL) bound [176]. For varying coefficients, however, $v_0$ is bounded away from $\gamma^g_{TL,max}$, so the time step will have to be chosen smaller than might be expected; we will look at how to improve upon this bound in §3.12.

### 3.7.4 Energetic Interpretation

Let us now reexamine the passive MDKC in Figure 3.14(a). The total stored energy flux in the network is contained in the four inductors and will be, from (3.35),

$$\mathbf{E}_{total} = \frac{1}{2}L_1 i_1^2 \mathbf{e}_{t'} + \frac{1}{2}L_2 i_2^2 \mathbf{e}_{t'} + \frac{1}{2}L_0(i_1+i_2)^2\mathbf{e}_1 + \frac{1}{2}L_0(i_1-i_2)^2\mathbf{e}_2$$

where the $\mathbf{e}_{t'}$ is a unit vector in direction $t'$, and $\mathbf{e}_1$ and $\mathbf{e}_2$ are unit vectors in directions $t_1$ and $t_2$ respectively. Applying the definitions of the inductances, from (3.60), the current definitions from (3.57), and the fact that $\mathbf{e}_1 = (\mathbf{e}_{t'} + \mathbf{e}_x)/\sqrt{2}$ and $\mathbf{e}_2 = (\mathbf{e}_{t'} - \mathbf{e}_x)/\sqrt{2}$, then this total energy flux can be rewritten as

$$\mathbf{E}_{total} = \frac{1}{2}v_0 l i^2 \mathbf{e}_{t'} + \frac{1}{2}v_0 c u^2 \mathbf{e}_{t'} + ui\mathbf{e}_x = \frac{1}{2}li^2\mathbf{e}_t + \frac{1}{2}cu^2\mathbf{e}_t + ui\mathbf{e}_x$$

Here $\mathbf{e}_t = v_0\mathbf{e}_{t'}$ is a unit vector in the time direction. The total scalar energy at time $t$ of this network will, from (3.30), be

$$\mathcal{E}(t) = \int_{-\infty}^{+\infty} \mathbf{e}_t^T \mathbf{E}_{total} dx = \int_{-\infty}^{+\infty} \frac{1}{2}\left(li^2 + cu^2\right) dx = \int_{-\infty}^{+\infty} \frac{1}{2}\mathbf{w}^T\mathbf{P}\mathbf{w}dx$$

and thus coincides with the energy definition of the symmetric hyperbolic system, from (3.6). This is certainly not surprising, but the important point here is that in an MDKC such as that of Figure 3.14(a), the scalar energy has been broken down into contributions from several interacting components (the inductors), each of which is passive individually; this useful energy subdivision has been exploited here as a means of developing passive numerical methods.

### 3.7.5 Simplified Networks

In the particular case for which $l$ and $c$ are constants, and where we do not have sources, the MDWD network shown in Figure 3.14(b) can be simplified considerably. If we pick $v_0 = 1/\sqrt{lc}$ and $r_0 = \sqrt{l/c}$, then $R_1$ and $R_2$ become zero, and their associated inductors may be dropped from the network (that is, they can be treated as short-circuits). The two series adaptors then reduce to simple multiplies of the signals output by the lattice two-port as in Figure 3.15(a) where we have written

$$\beta_1 = \frac{r\Delta - 2r_0}{r\Delta + 2r_0} \qquad\qquad \beta_2 = \frac{gr_0\Delta - 2}{gr_0\Delta + 2}$$

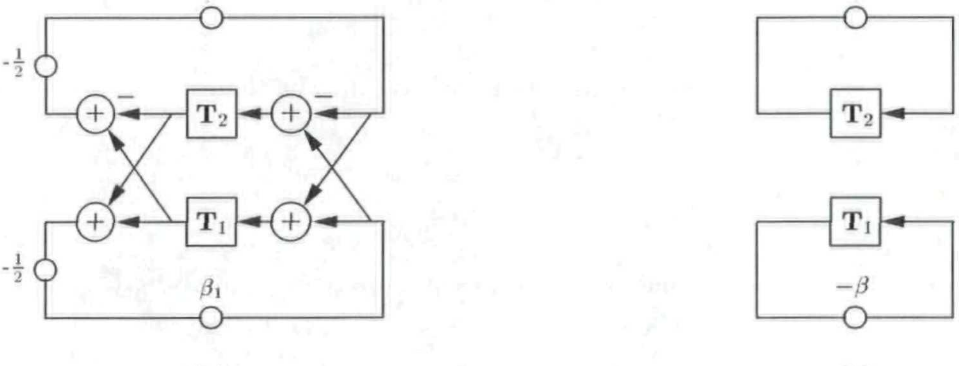

(a) (b)

Figure 3.15: *Simplified MDWD network for the (1+1)D transmission line equations—* (a) *for constant $l$ and $c$ and* (b) *further simplified in the distortionless case.*

If, in addition, the transmission line is *distortionless* [28], so that we have $lg = cr$ for all values of $x$ (though as mentioned above, we require $l$ and $c$ to be constant), then the network can be simplified further giving Figure 3.15(b), where $\beta_1 = \beta_2 = \beta$. Now the MDWD network has decoupled into two independent loops, each comprised of an MD shift and a scaling. Examine the expanded signal flow graph of Figure 3.16, where the value of the multiplier coefficient $-\beta$ at location $x = i\Delta$ is written as $\beta_i$. Values input into the upper array will be shifted repeatedly to the left and attenuated by the factor $-\beta$, and similarly, those in the lower array are shifted to the right and attenuated by the same factor. We thus have a traveling wave formulation of the solution to the transmission line equations, to be compared with the digital waveguide implementation to be discussed in Chapter 4.

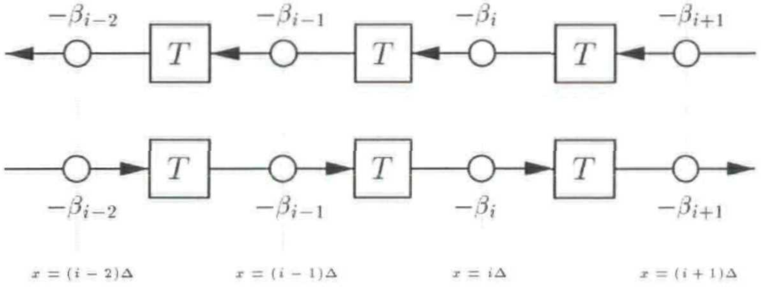

Figure 3.16: *Signal flow graph for the MDWD network of Figure 3.15(b).*

Two special cases are of note here. If the transmission line is lossless, so that $r = g = 0$, then $\beta = -1$. The initial values in the storage registers are shifted without attenuation. We would like to note, however, that if $\Delta > \frac{2}{gr_0}$, then $\beta > 0$, and the traveling waves will be oscillatory, and the solution is thus non-physical. More disturbing is the case $\Delta = \frac{2}{gr_0}$, in which case we have $\beta = 0$, and all energy leaves the network immediately! Though these examples would seem to indicate that the MDWD network is not behaving correctly, it should be kept in mind that, by construction, it is stable and consistent with the continuous time/space transmission line equations, and is convergent in the limit as $\Delta \to 0$, by the *Lax-Richtmeyer Equivalence Theorem* [176]. $\Delta$ can always be chosen small enough so that $\beta$ is negative, and that thus the solution will be well-behaved (i.e., non-oscillatory). This important extra restriction on the grid spacing, which is independent of the time step, is purely a result of the use of the trapezoid rule as our integration method. The lesson here is that passivity, while providing a guarantee of stable numerical methods, does not ensure that we necessarily get a physically acceptable solution in all cases.

## 3.8 The (2+1)D Parallel-plate System

Generalizing the above procedure to several dimensions is straightforward. We examine here, as a practical example, the (2+1)D *parallel-plate system*, which is written as:

$$l\frac{\partial i_x}{\partial t}+\frac{\partial u}{\partial x}+ri_x+e = 0 \tag{3.64a}$$

$$l\frac{\partial i_y}{\partial t}+\frac{\partial u}{\partial y}+ri_y+f = 0 \tag{3.64b}$$

$$c\frac{\partial u}{\partial t}+\frac{\partial i_x}{\partial x}+\frac{\partial i_y}{\partial y}+gu+h = 0 \tag{3.64c}$$

This system was treated using MDWDFs in [62, 211]. Now the dependent variables are a voltage $u$, and current density components $i_x$ and $i_y$; these, and the sources $e$, $f$ and $h$ are functions of time $t$ and two spatial variables, $x$ and $y$. $l$, $c$, $r$ and $g$ are arbitrary smooth positive functions of $x$ and $y$ ($l$ and $c$ are strictly positive). It is worth mentioning that the same equations can be used in the contexts of (2+1)D linear acoustics, the vibration of a membrane, and, with a trivial modification, (2+1)D electromagnetic field problems (involving TE or TM modes).

System (3.64) is symmetric hyperbolic, and thus has the form of (3.1), where $\mathbf{w} = [i_x, i_y, u]^T$, and with

$$\mathbf{P}=\begin{bmatrix} l & 0 & 0\\ 0 & l & 0\\ 0 & 0 & c\end{bmatrix} \quad \mathbf{A}_1=\begin{bmatrix} 0 & 0 & 1\\ 0 & 0 & 0\\ 1 & 0 & 0\end{bmatrix} \quad \mathbf{A}_2=\begin{bmatrix} 0 & 0 & 0\\ 0 & 0 & 1\\ 0 & 1 & 0\end{bmatrix} \quad \mathbf{B}=\begin{bmatrix} r & 0 & 0\\ 0 & r & 0\\ 0 & 0 & g\end{bmatrix} \quad \mathbf{f}=\begin{bmatrix} e\\ f\\ h\end{bmatrix}$$

It will follow, as in the case of the (1+1)D transmission line system (see §3.7.4), that the total energy of the MDKC that we will derive in the next section will be equal to the energy of system (3.64), as per (3.6).

### Phase and Group Velocity

For the constant-coefficient, lossless and source-free case (i.e., $r = g = e = f = h = 0$), the numerical dispersion relation, in terms of the frequency $\omega$ and wavenumber magnitude $\|\boldsymbol{\beta}\|_2 = \sqrt{\beta_x^2+\beta_y^2}$ will be, from (3.10),

$$\omega\left(\omega^2-\frac{1}{lc}\|\boldsymbol{\beta}\|_2^2\right)=0$$

which has roots

$$\omega = 0 \qquad\qquad \omega=\pm\sqrt{\frac{1}{lc}}\|\boldsymbol{\beta}\|_2$$

Discounting the stationary mode with $\omega = 0$, the phase and group velocities are then, from (3.12),

$$\gamma^{p}_{PP} = \gamma^{g}_{PP} = \pm\frac{1}{\sqrt{lc}}$$

and if $l$ and $c$ are functions of $x$ and $y$, the maximal group velocity will be

$$\gamma^{g}_{PP,max} = \frac{1}{\sqrt{(lc)_{min}}} \tag{3.65}$$

where $(lc)_{min} = \min_{(x,y)\in\mathcal{D}}(lc)$. This bound is the same as for the (1+1)D transmission line equations.

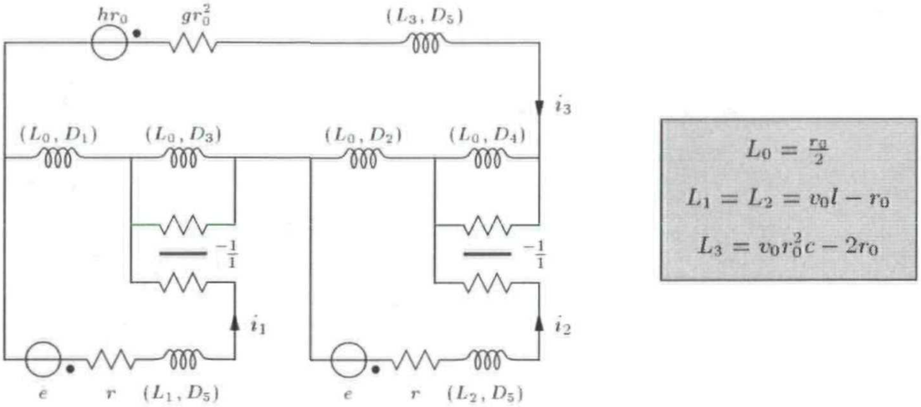

Figure 3.17: *MDKC for the (2+1)D parallel-plate system in rectangular coordinates.*

### 3.8.1 MDKC and MDWD Network

The circuit can be derived along the same lines as for the (1+1)D case; we deal here with the discretization on a rectilinear grid, and will thus apply coordinate transformation defined by the $\mathbf{H}$ of (3.22). Rewriting system (3.64) in terms of the new coordinates $[t_1, \ldots, t_5]^T$ using $\nabla_{\mathbf{u}} = \mathbf{V}\mathbf{H}^{-R}\nabla_{\mathbf{t}}$, with the pseudo inverse (3.23) gives

$$(v_0 l - r_0)\, D_5 i_1 + \frac{r_0}{2} D_1 (i_1 + i_3) + \frac{r_0}{2} D_3 (i_1 - i_3) + r i_1 + e = 0 \tag{3.66a}$$

$$(v_0 l - r_0)\, D_5 i_2 + \frac{r_0}{2} D_2 (i_2 + i_3) + \frac{r_0}{2} D_4 (i_2 - i_3) + r i_2 + f = 0 \tag{3.66b}$$

$$\begin{aligned}\left(v_0 r_0^2 c - 2r_0\right) D_5 i_3 &+ \frac{r_0}{2} D_1 (i_3 + i_1) + \frac{r_0}{2} D_3 (i_3 - i_1)\\ &+ \frac{r_0}{2} D_2 (i_3 + i_2) + \frac{r_0}{2} D_4 (i_3 - i_2) + g r_0^2 i_3 + h r_0 = 0\end{aligned} \tag{3.66c}$$

where we have used the new current-like variables

$$i_1 \triangleq i_x \qquad i_2 \triangleq i_y \qquad i_3 \triangleq \frac{u}{r_0}$$

and $r_0$ is, as in the (1+1)D case, an arbitrary positive constant (which has also been used to scale (3.66c)). $D_5 = D_{t'}$ will be treated as a simple time derivative, according to the generalized trapezoid rule discussed in §3.5.1. Figure 3.17 shows the MDKC that results from the transformed set of equations (3.66). The MDWD network corresponding to the MDKC is shown in Figure 3.18, where we have used step-sizes $T_j = \Delta$, $j = 1, \ldots, 5$.

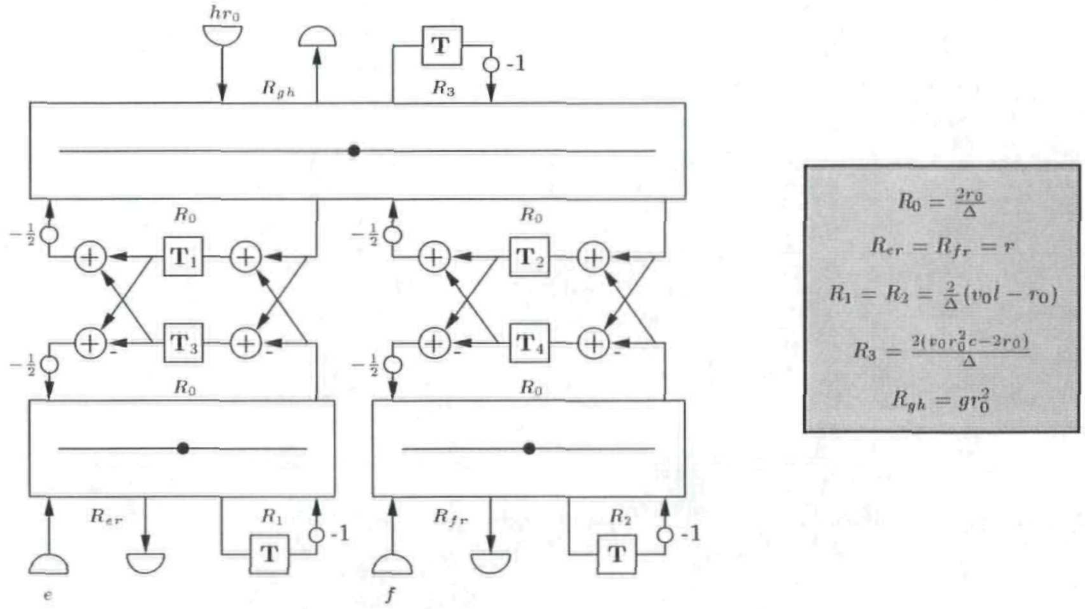
$hr_0$
$R_{gh}$
T
-1
$R_3$
$R_0$
$-\frac{1}{2}$
$\mathrm{T}_1$
$\mathrm{T}_2$
$\mathrm{T}_3$
$\mathrm{T}_4$
$R_{er}$
$R_1$
$R_{fr}$
$R_2$
e
f
$R_0 = \frac{2r_0}{\Delta}$
$R_{er} = R_{fr} = r$
$R_1 = R_2 = \frac{2}{\Delta}(v_0 l - r_0)$
$R_3 = \frac{2(v_0 r_0^2 c - 2r_0)}{\Delta}$
$R_{gh} = gr_0^2$

Figure 3.18: *MDWD network for the (2+1)D parallel-plate system, in rectangular coordinates.*

Passivity follows from a positivity condition on the network inductances, in particular $L_1$, $L_2$ and $L_3$ (the values of which are given in Figure 3.17). These conditions are

$$v_0 \geq \frac{r_0}{l_{min}} \qquad v_0 \geq \frac{2}{r_0 c_{min}} \tag{3.67}$$

The choice of $r_0 = \sqrt{\frac{2l_{min}}{c_{min}}}$, where $l_{min} = \min_{x,y} l$ and $c_{min} = \min_{x,y} c$ gives a stability bound of

$$v_0 \geq \sqrt{\frac{2}{l_{min}c_{min}}} \geq \sqrt{2}\gamma^g_{PP,max} \tag{3.68}$$

which is the best possible bound for this network [61]. Note that $v_0$ is again bounded away from the maximum group velocity, even taking into account the scaling factor ($\sqrt{2}$ in this case), which is a consistent feature of explicit numerical methods in multiple spatial dimensions.

If $l$ and $c$ are constant, and in addition $r$, $g$, $e$, $f$ and $h$ are zero, and (3.68) holds with equality, i.e., we have

$$v_0 = \sqrt{2}\gamma^{g}_{PP,max} \tag{3.69}$$

then the network of Figure 3.18 simplifies to the structure shown in Figure 3.19. This particular structure bears a very strong resemblance to the (2+1)D waveguide mesh [157, 198] which we saw briefly in §1.1.2, and will examine in detail in Chapter 4.

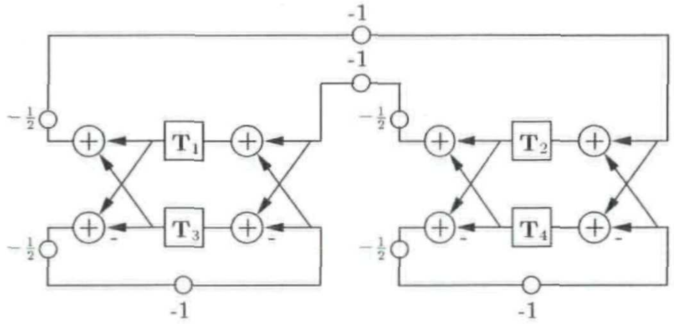

Figure 3.19: *Simplified MDWD network for the (2+1)D transmission line equations, in the lossless, source-free and constant parameter case.*

## 3.9 Finite Difference Interpretation

It should be clear that a MDWD network corresponding to a particular MDKC (and thus to a given set of PDEs) is no more than a particular type of finite difference method, and can be analyzed as such. We will do so here for the case of the (1+1)D transmission line, in order to compare the schemes that arise from the WD approach to the simple centered difference schemes which will be introduced in the next chapter in the waveguide context, and which can also be put into a scattering form.

### 3.9.1 MDWD Networks as Multi-step Schemes

Recall that the discretization step discussed in §3.5.3 consisted of the application of a spectral transformation of the form

$$s_j \rightarrow \frac{2}{T_j}\frac{1-z_j^{-1}}{1+z_j^{-1}}$$

where $s_j$ is the frequency domain transform variable corresponding to any MD-causal coordinate $t_j$, and $z_j^{-1}$ is the frequency domain unit shift in the same direction.

For spatially inhomogeneous problems, this spectral mapping is equivalent to the application of the trapezoid rule in direction $t_j$. We can thus write, using operator notation,

$$\frac{\partial}{\partial t_j} \rightarrow \frac{2}{T_j}(1+\delta_j)^{-1}(1-\delta_j) \tag{3.70}$$

where $\delta_j$ is a shift operator defined by

$$\delta_j p(t_1, \ldots, t_j, \ldots, t_k) = p(t_1, \ldots, t_j - T_j, \ldots, t_k)$$

when applied to any continuous function $p(\mathbf{t})$. Consider again the lossless (1+1)D transmission line equations

$$l\frac{\partial i}{\partial t} + \frac{\partial u}{\partial x} = 0 \tag{3.71a}$$

$$c\frac{\partial u}{\partial t} + \frac{\partial i}{\partial x} = 0 \tag{3.71b}$$

which can be written as

$$(v_0 l - r_0)\frac{\partial i_1}{\partial t'} + \frac{r_0}{\sqrt{2}}\frac{\partial}{\partial t_1}(i_1 + i_2) + \frac{r_0}{\sqrt{2}}\frac{\partial}{\partial t_2}(i_1 - i_2) = 0 \tag{3.72a}$$

$$\left(v_0 c r_0^2 - r_0\right)\frac{\partial i_2}{\partial t'} + \frac{r_0}{\sqrt{2}}\frac{\partial}{\partial t_1}(i_2 + i_1) + \frac{r_0}{\sqrt{2}}\frac{\partial}{\partial t_2}(i_2 - i_1) = 0 \tag{3.72b}$$

under the application of coordinate transformation (3.19) and using scaled variables $i_1 = i$ and $i_2 = u/r_0$, as well as the scaled time variable $t' = v_0 t$. Under the substitution of (3.70), for $j = 1, 2$, and using the generalized trapezoid rule in time, defined by

$$\frac{\partial}{\partial t'} \rightarrow \frac{2}{T'}(1+\delta_{t'})^{-1}(1-\delta_{t'})$$

where $\delta_{t'}$ is a shift in the scaled time direction $t'$ of duration $T'$, we get

$$\begin{aligned}
(v_0 l - r_0)\frac{2}{T'}(1+\delta_{t'})^{-1}(1-\delta_{t'})i_1 \quad &+ \quad \frac{\sqrt{2}r_0}{T_1}(1+\delta_1)^{-1}(1-\delta_1)(i_1+i_2) \\
&+ \quad \frac{\sqrt{2}r_0}{T_2}(1+\delta_2)^{-1}(1-\delta_2)(i_1-i_2) = 0 \\
\left(v_0 c r_0^2 - r_0\right)\frac{2}{T'}(1+\delta_{t'})^{-1}(1-\delta_{t'})i_2 \quad &+ \quad \frac{\sqrt{2}r_0}{T_1}(1+\delta_1)^{-1}(1-\delta_1)(i_2+i_1) \\
&+ \quad \frac{\sqrt{2}r_0}{T_2}(1+\delta_2)^{-1}(1-\delta_2)(i_2-i_1) = 0
\end{aligned}$$

to second order in $\Delta$. This can be rewritten as

$$(1+\delta_1)(1+\delta_2)\frac{R_1}{R_0}(1-\delta_{t'})\,i_1+(1+\delta_{t'})\left(1-\delta_{t'}^2\right)i_1+(1+\delta_{t'})(\delta_2-\delta_1)\,i_2=0 \tag{3.73a}$$

$$(1+\delta_1)(1+\delta_2)\frac{R_2}{R_0}(1-\delta_{t'})\,i_2+(1+\delta_{t'})\left(1-\delta_{t'}^2\right)i_2+(1+\delta_{t'})(\delta_2-\delta_1)\,i_1=0 \tag{3.73b}$$

where we have used $T'=v_0T=\Delta$, $T_1=T_2=\sqrt{2}\Delta$, the fact that $\delta_1\delta_2=\delta_{t'}^2$, and also the definitions of the port resistances of the MDWD network of Figure 3.14(b), given in (3.61)[†]. Upon replacing the quantities $i_1$ and $i_2$ by their respective grid functions $I_{1,i}(n)$ and $I_{2,i}(n)$, which take on values for $n$ and $i$ integer, (3.73a) and (3.73b) define recursions on a regular grid, of spacing $\Delta$. (3.73a) can be written as

$$\begin{aligned}\alpha_iI_{1,i}(n) &+ \beta_{i+1}I_{1,i+1}(n-1)+\beta_{i-1}I_{1,i-1}(n-1)+\gamma_iI_{1,i}(n-1)\\ &- I_{2,i-1}(n-1)+I_{2,i+1}(n-1)\\ &- \beta_{i+1}I_{1,i+1}(n-2)-\beta_{i-1}I_{1,i-1}(n-2)-\gamma_iI_{1,i}(n-2)\\ &- I_{2,i-1}(n-2)+I_{2,i+1}(n-2)\\ &- \alpha_iI_{1,i}(n-3)=0\end{aligned} \tag{3.74}$$

with

$$\alpha_i\triangleq 1+\frac{R_1(i\Delta)}{R_0}\qquad\qquad \beta_i\triangleq\frac{R_1(i\Delta)}{R_0}\qquad\qquad \gamma_i\triangleq 1-\frac{R_1(i\Delta)}{R_0} \tag{3.75}$$

The recursion corresponding to (3.73b) is very similar, under the interchange of $I_1$ and $I_2$. Note that if $l$ and $c$ are constants, and if the difference scheme is operating at the CFL bound (so that $R_1=R_2=0$, then (3.74) can be simplified to

$$I_{1,i}(n)-I_{1,i}(n-2)+I_{2,i+1}(n-1)-I_{2,i-1}(n-1)=0 \tag{3.76}$$

which is a simple centered difference approximation to (3.71a) and which we will see again in the waveguide mesh context in §4.3.2. Unlike the case of the mesh however, away from the passivity bound we have a *multi-step scheme* [176] which involves three steps of "look-back" in order to update a grid variable at a particular location. The introduction of wave variables, then, can be considered to be a means of expanding the state of the system so that using the new state, the recursion (now in the form of the MDWDF of Figure 3.14) requires access only to wave quantities at the time step immediately preceding the current one.

In order to generate a scheme which operates on alternating interleaved grids (called *offset*

---

[†] We have also used the fact that because this system is linear and time-invariant (though not shift-invariant), time-shifting operators such as $\delta_{t'}$ commute with purely spatially-varying quantities such as $R_1$.

*sampling* in [61]), it is possible to use a doubled time step of $T' = 2\Delta$ in order to implement the generalized trapezoid rule applied to the time derivatives in (3.72a) and (3.72b), i.e.,

$$\frac{\partial}{\partial t'} \rightarrow \frac{2}{T'}\left(1-\delta_{t'}^{2}\right)^{-1}\left(1+\delta_{t'}^{2}\right) = \frac{1}{\Delta}\left(1-\delta_{t'}^{2}\right)^{-1}\left(1+\delta_{t'}^{2}\right)$$

in which case we get, as an approximation to (3.71a),

$$\begin{aligned} \alpha_i I_{i,1}(n) \quad &+ \quad \beta_{i+1} I_{1,i+1}(n-1) + \beta_{i+1} I_{1,i-1}(n-1) + I_{2,i+1}(n-1) - I_{2,i-1}(n-1) \\ &- \quad \beta_{i+1} I_{1,i+1}(n-3) - \beta_{i+1} I_{1,i-1}(n-3) + I_{2,i+1}(n-3) - I_{2,i-1}(n-3) \\ &- \quad \alpha_i I_{1,i}(n-4) = 0 \end{aligned} \tag{3.77}$$

where $\alpha$ and $\beta$ are defined as per (3.75), but where $R_1$ is now equal to $\frac{1}{\Delta}\left(v_0 l - r_0\right)$. This form also reduces to simple centered differences when $l$ and $c$ are constant, and when we are operating at the CFL bound.

The computational stencils corresponding to the two different schemes are shown in Figure 3.20; the top black dot in either picture represents the location of the grid variable currently being updated (either $I_1$ or $I_2$), and the other dots cover the discrete region of influence of the difference scheme. Notice in particular that each scheme has a width of only three grid points, corresponding to nearest-neighbor-only updating. Also, because these are multi-step methods, one might expect that we will have to take special care when initializing the scheme; we discuss this issue in §3.10. For the offset scheme of Figure 3.20(b), the stencil can be shifted one step to the left or right without any overlapping; thus such a scheme can subdivided into two mutually exclusive subschemes (operating only for $n+i$ always even or always odd), one of which may be dropped from the calculating scheme entirely. This behavior appears in many of the difference schemes which we will come across subsequently; we will pay particular attention to such schemes during a spectral analysis of finite difference schemes in Appendix A. One of the interesting features of the MDKC representation of a set of PDEs is that the same circuit can give rise to an entire family of MDWD networks, or, in other words, of difference methods, all of which are consistent with the original set of PDEs. In the case of the MDKC for the transmission line equations derived previously, although we have defined the directions of the various inductors (along which we will be integrating), at the circuit stage we have not as yet specified any spectral mapping which will determine the type of differencing to be applied. Any passivity-preserving mapping which is correct in the low frequency limit will give rise to a passive, consistent MDWD algorithm. We will examine the important implications of a more exotic type of mapping in §4.10, but it is also interesting to note that we can apply the trapezoid rule using different step sizes for all the reactive elements. The constraint on our choices of these step sizes is that all shifting operations refer, ultimately, to another grid point (for computability).

Finally, we note that in general, the determination of stability for a multi-step scheme can be quite difficult; even in the constant coefficient case, it will in general be necessary to perform *Von*

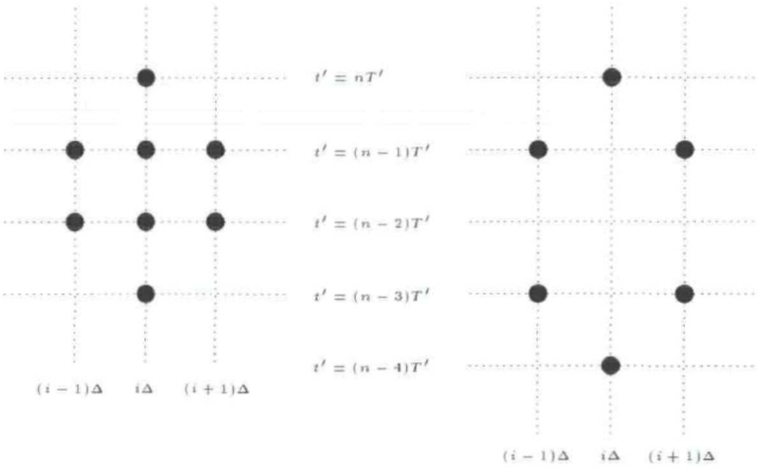

(a) (b)

Figure 3.20: *Computational stencils of the equivalent multi-step schemes of MDWDFs for the (1+1)D transmission line equations—* (a) *scheme* (3.74) *and* (b) *"offset" scheme* (3.77).

*Neumann analysis* [176] (see Appendix A for such an analysis applied to difference schemes for the wave equation in (2+1)D and (3+1)D), which can be quite formidable. Here, however, we are ensured stability through the passivity condition on the network.

### 3.9.2 Numerical Phase Velocity and Parasitic Modes

Because, in general, the image MDWDF of a given MDKC for a system of PDEs is a multi-step numerical integration scheme, it is reasonable to expect that *parasitic modes* [176] will be present in the solution. Energy in such modes often travels at speeds other than the desired wave speed in the medium, and may be highly oscillatory. If the scheme is consistent with the original system of PDEs, and stable, as is an MDWD network derived from the equivalent MDKC under the application of the trapezoid rule, then these parasitic modes must disappear in the limit as the time step is decreased (by the *Lax-Richtmeyer Equivalence Theorem* [176]). They have not as yet been addressed in the wave digital theory, and the subject is related to how initial conditions should be set in a MDWDF. The subject of initialization has been touched on only very briefly in [106].

Analysis of parasitic modes is easiest in the constant-coefficient case. We will examine the simplest possible non-trivial MDWDF, namely that of the constant-coefficient lossless source-free (1+1)D transmission line. Because at the stability limit, this scheme becomes equivalent to simple centered differences (see previous section), for which we do not have parasitic modes at all, we will look at the MDWDF of Figure 3.14(b) away from this limit[†]. We have chosen $r_0 = \sqrt{l/c}$. The

---

[†] Analysis of a numerical method away from its stability limit is useful because it can give some indication of how the scheme will behave in the presence of material variations; if the system does exhibit such variations, then, locally

MDWDF is redrawn in Figure 3.21, where we have

$$R_1 = R_2 = \frac{2}{\Delta}(v_0 l - r_0) \qquad\qquad R_0 = \frac{2r_0}{\Delta}$$

for some $v_0 > 1/\sqrt{lc}$. Note that because the system is now linear and shift-invariant, we have replaced

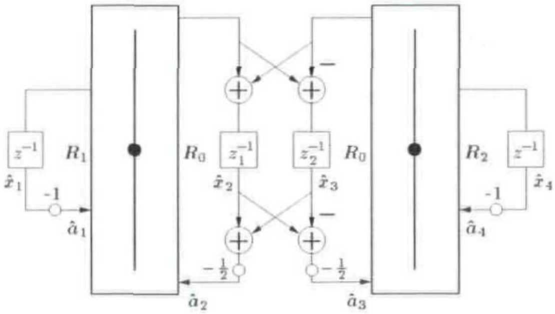

Figure 3.21: *Steady-state MDWD network for the lossless, source-free constant-coefficient (1+1)D transmission-line equations.*

the shifts $\mathbf{T}_1$ and $\mathbf{T}_2$ in the two directions $t_1$ and $t_2$ by their frequency domain counterparts $z_1^{-1}$ and $z_2^{-1}$. Recall also that we have, from (3.44) and (3.45), that

$$z_1^{-1} = z^{-1}w^{-1} \qquad\qquad z_2^{-1} = z^{-1}w$$

where $z^{-1}$ represents a unit delay in the time direction, and $w$ a unit shift in the $x$ direction. We have written the outputs of the delay registers, in an exponential state, as

$$x_j(k\Delta, nT) = \hat{x}_j z^n w^k, \qquad \text{for} \qquad j = 1, \ldots, 4$$

where the $\hat{x}_j$ are complex amplitudes. The updating of the values in the delay registers can be written, in terms of these amplitudes, as

$$\begin{bmatrix} \hat{x}_1 \\ \hat{x}_2 \\ \hat{x}_3 \\ \hat{x}_4 \end{bmatrix} = z^{-1} \begin{bmatrix} -\alpha & \frac{1-\alpha}{2} & \frac{1-\alpha}{2} & 0 \\ \frac{(1+\alpha)}{2}w & \alpha w & 0 & \frac{(1+\alpha)}{2}w \\ \frac{(1+\alpha)}{2}w^{-1} & 0 & \alpha w^{-1} & -\frac{(1+\alpha)}{2}w^{-1} \\ 0 & \frac{1-\alpha}{2} & \frac{\alpha-1}{2} & -\alpha \end{bmatrix} \begin{bmatrix} \hat{x}_1 \\ \hat{x}_2 \\ \hat{x}_3 \\ \hat{x}_4 \end{bmatrix}$$

---

speaking, we will necessarily be operating away from this limit in at least part of the problem domain.

which is parametrized by a reflectance

$$\alpha = \frac{R_0 - R_1}{R_0 + R_1} \tag{3.78}$$

If we introduce the variables

$$y_1 = x_1 + x_4 \qquad\qquad y_4 = x_1 - x_4$$

the updating decouples into two subsystems, namely

$$\begin{bmatrix} \hat{x}_2 \\ \hat{y}_1 \end{bmatrix} = z^{-1} \begin{bmatrix} \alpha w & (1+\alpha)w \\ (1-\alpha) & -\alpha \end{bmatrix} \begin{bmatrix} \hat{x}_2 \\ \hat{y}_1 \end{bmatrix} = z^{-1}\mathbf{A}_{21} \begin{bmatrix} \hat{x}_2 \\ \hat{y}_1 \end{bmatrix} \tag{3.79a}$$

$$\begin{bmatrix} \hat{x}_3 \\ \hat{y}_4 \end{bmatrix} = z^{-1} \begin{bmatrix} \alpha w^{-1} & (1+\alpha)w^{-1} \\ (1-\alpha) & -\alpha \end{bmatrix} \begin{bmatrix} \hat{x}_3 \\ \hat{y}_4 \end{bmatrix} = z^{-1}\mathbf{A}_{34} \begin{bmatrix} \hat{x}_3 \\ \hat{y}_4 \end{bmatrix} \tag{3.79b}$$

$\mathbf{A}_{21}$ and $\mathbf{A}_{34}$ are known as *spectral amplification* matrices (see Appendix A).

The *symbols* [176] of the two subsystems, $\mathbf{Q}_{24}$ and $\mathbf{Q}_{31}$ are defined by

$$\mathbf{Q}_{21} = \mathbf{I}_2 - z^{-1}\mathbf{A}_{21} \qquad\qquad \mathbf{Q}_{34} = \mathbf{I}_2 - z^{-1}\mathbf{A}_{34}$$

where $\mathbf{I}_2$ is the $2 \times 2$ identity matrix. Nontrivial solutions to the update equations (3.79) occur when the determinants of the symbols vanish. In the absence of boundary conditions, we may assume $w = e^{j\beta\Delta}$, where $\beta$ is a real wavenumber, in which case we have four solutions in terms of $z$ given by

$$z_{21,\pm} = e^{\frac{j\beta\Delta}{2}} \left( j\alpha \sin(\frac{\beta\Delta}{2}) \pm \sqrt{1 - \alpha^2 \sin^2(\frac{\beta\Delta}{2})} \right) \tag{3.80a}$$

$$z_{34,\pm} = e^{-\frac{j\beta\Delta}{2}} \left( -j\alpha \sin(\frac{\beta\Delta}{2}) \pm \sqrt{1 - \alpha^2 \sin^2(\frac{\beta\Delta}{2})} \right) \tag{3.80b}$$

which are simply the eigenvalues of the spectral amplification matrices. The corresponding eigenvectors of these same matrices are

$$\mathbf{u}_{21,\pm} = \begin{bmatrix} \alpha\cos(\frac{\beta\Delta}{2}) \pm \sqrt{1 - \alpha^2 \sin^2(\frac{\beta\Delta}{2})} \\ (1-\alpha)e^{-\frac{\beta\Delta}{2}} \end{bmatrix} \qquad \mathbf{u}_{34,\pm} = \begin{bmatrix} \alpha\cos(\frac{\beta\Delta}{2}) \pm \sqrt{1 - \alpha^2 \sin^2(\frac{\beta\Delta}{2})} \\ (1-\alpha)e^{\frac{\beta\Delta}{2}} \end{bmatrix}$$

All four eigenvalues are of unit magnitude, and thus, using $z = e^{j\omega T}$, we can rewrite solutions (3.80) as

$$e^{j\omega_{21\pm}T} = \pm e^{\frac{j\Delta}{2}(\beta\pm\nu)} \qquad\qquad e^{j\omega_{34\pm}T} = \pm e^{-\frac{j\Delta}{2}(\beta\pm\nu)} \tag{3.81}$$

for some real $\nu$ defined by $\sin(\nu\Delta/2) = \alpha\sin(\beta\Delta/2)$. ($\nu$ always exists because we have $|\alpha| \leq 1$, from (3.78).) For small wavenumbers, we have

$$\nu \approx \alpha\beta$$

and we thus have in this limit, for the roots subscripted with + in (3.81),

$$\begin{aligned} e^{j\omega_{21+}T} &\approx e^{\frac{j\Delta(1+\alpha)}{2}\beta} & &\Rightarrow & \frac{\omega_{21+}}{\beta} &\approx \frac{1}{\sqrt{lc}} \\ e^{j\omega_{34+}T} &\approx e^{-\frac{j\Delta(1+\alpha)}{2}\beta} & &\Rightarrow & \frac{\omega_{34+}}{\beta} &\approx -\frac{1}{\sqrt{lc}} \end{aligned}$$

where we have used the fact that $(1+\alpha)/2 = 1/(v_0\sqrt{lc})$, which follows from (3.78) and the definitions of the port resistances in (3.61) as well as $v_0 = \Delta/T$. The quantities $\omega_{21+}/\beta$ and $\omega_{34+}/\beta$ are called *numerical phase velocities* [176]; they approach the propagation speed in the medium, from (3.55), and these two solutions are to be interpreted as approximations to the traveling wave solution to the transmission line equations. The other modes, however, are *parasitic*, in that they do not propagate near the physical velocity. They are not problematic, provided initial conditions are set properly; indeed, in the limit as $\Delta$ becomes small, any reasonable initial conditions tend to align the system with the dominant traveling modes of the system.

Clearly, if we are at the passivity limit, where $v_0 = 1/\sqrt{lc}$, then $R_1 = 0$, and thus $\alpha = 1$, which implies, finally that $\nu = \beta$, so that we have, from (3.81), that $\omega_{21+}/\beta = 1/\sqrt{lc}$ and $\omega_{34+}/\beta = -1/\sqrt{lc}$; wave propagation is thus dispersionless. As mentioned in the previous section, at this limit, the MDWD network reduces to an exact digital traveling wave solution (this was also noted in §3.7.5). It is also interesting to note that when $R_1 = R_2 = R_0$, so that $\alpha$ and $\nu$ are zero, then (3.81) implies that wave propagation is also dispersionless in this case as well. It is easy to see here, from Figure 3.21, that because $R_1 = R_2 = R_0$, there will be no scattering through the adaptors; the pure time delays may thus be shifted directly into the lattice two port, and we can perform a manipulation similar to that of §3.7.5 to give a simplified digital "traveling wave" network, with doubled time delays. Here, we are in effect implementing a traveling wave solution on a different grid, but the implication is that for the corresponding problem with material variation, the MDWD network gives a good approximation to the numerical phase velocity even for certain values of $v_0$ which are far from the local physical wave speed. This is not true for digital waveguide networks, where the numerical phase velocities degrade considerably away from the passivity limit. We will return to these expressions (which provide complete information regarding the *numerical dispersion* properties of the scheme) in §4.3.8 in a comparison with the digital waveguide network for the same system. In anticipation of the discussion in §3.10, we mention that for constant $v_0$, we have for the eigenvectors corresponding to the dominant modes, that

$$\lim_{\Delta\rightarrow 0}\mathbf{u}_{21+} = \lim_{\Delta\rightarrow 0}\mathbf{u}_{34,+} = \begin{bmatrix}\alpha+1\\1-\alpha\end{bmatrix}$$

Because we also have, from Figure 3.21, that $\hat{a}_1 = -\hat{x}_1 = -(\hat{y}_1+\hat{y}_4)/2$, and $\hat{a}_2 = -(\hat{x}_2+\hat{x}_3)/2$, we can also write, for the dominant mode,

$$\lim_{\Delta\rightarrow 0}\begin{bmatrix}\hat{a}_1\\\hat{a}_2\end{bmatrix} = -\frac{1}{2}\lim_{\Delta\rightarrow 0}\left(\mathbf{u}_{21+}+\mathbf{u}_{34,+}\right) = -\begin{bmatrix}\alpha+1\\1-\alpha\end{bmatrix} = -\frac{2}{R_1+R_0}\begin{bmatrix}R_1\\R_0\end{bmatrix}$$

Thus in this limit, the wave variables incident on the left adaptor occur in the same ratio as the port resistances, and are in fact aligned with an eigenvector of the scattering matrix corresponding to the adaptor. A similar statement holds for the quantities incident on the right adaptor. We will return to this observation in the next section.

## 3.10 Initial Conditions

Numerical simulations for time-dependent systems of PDEs must necessarily be initialized; while this is a relatively straightforward matter for WDF-based integration schemes, it has only been addressed in passing [106] in the literature.

We will examine here the initialization of the MDWD network for the source-free transmission line system (3.53) with $e = h = 0$. This system requires initial distributions for both the current and voltage, which we will call $i_0(x)$ and $u_0(x)$, respectively. For the initialization of the MDWD network for this system (shown in Figure 3.22), we will also need their spatial derivatives (assuming they exist), which we will write as $i_0'(x)$ and $u_0'(x)$. We note that in the approach considered in [106], spatial derivative information has not been taken into account. For the MDWD network of Figure 3.22, we must initialize all the wave variables incident upon the scattering junctions, written as $a_j$, $j = 1,\ldots,4$; because we have assumed no sources, no wave enters through the loss/source port. This circuit is a MD representation, and each of these wave variables refers to an array. Assuming that the spatial grid spacing is $\Delta$, and the time step is $T$, we can index the elements of these arrays as $a_{jm}(n)$, for $m$ and $n$ integer; this represents an instance of the MD wave variable $a_j$ at grid location $x = m\Delta$, and at time $t = nT$. For initialization, we must thus set $a_{jm}(0)$, over all grid locations $x = m\Delta$ included in the domain of the problem, in terms of the quantities $i_0(m\Delta)$, $u_0(m\Delta)$ and their spatial derivatives.

We will consider only the settings for the wave variables in the left-hand adaptor; one proceeds

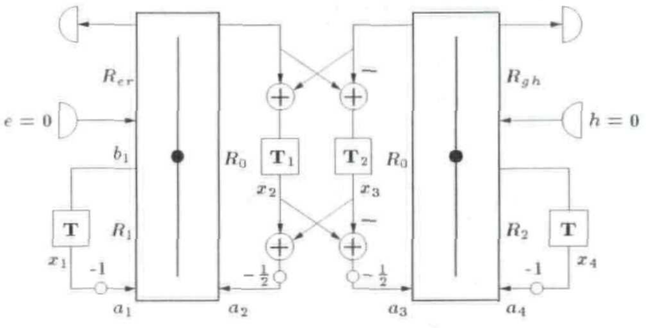

Figure 3.22: *MDWD network for the source-free (1+1)D transmission line equations.*

in the same way for the right adaptor. We recall that the port resistances are defined by

$$R_1 = \frac{2}{\Delta}(v_0 l - r_0) \qquad R_0 = \frac{2r_0}{\Delta} \qquad R_{er} = r$$

Since the port resistances $R_1$ and $R_{er}$ are functions of position, we will write $R_{1m} \triangleq R_1(m\Delta)$ and $R_{erm} \triangleq R_{er}(m\Delta)$. $R_0$ is independent of $x$. It is easy to see, from (2.30), that the initial values $a_{1m}(0)$ and $a_{2m}(0)$ must be arranged such that we produce the initial current $i_0(m\Delta)$. Thus we need

$$i_0(m\Delta) = \frac{1}{R_0 + R_{1m} + R_{erm}}\Big(a_{1m}(0) + a_{2m}(0)\Big) \tag{3.82}$$

Another condition is required to fully specify the wave variable initial values. Referring to the generating MDKC for this MDWD network in Figure 3.14(a), we can see that the voltage across the inductor of inductance $L_1$ will be $L_1\frac{\partial i}{\partial t'}$. We intend to relate this voltage to the associated digital voltage across the inductor of port resistance $R_1$ in Figure 3.22. We have

$$\begin{aligned} L_1\frac{\partial i}{\partial t'} &\overset{(3.17)}{=} \frac{L_1}{v_0}\frac{\partial i}{\partial t} \\ &\overset{(3.60)}{=} \frac{v_0 l - r_0}{v_0}\frac{\partial i}{\partial t} \\ &\overset{(3.53)}{=} \left(\frac{r_0}{v_0 l} - 1\right)\left(\frac{\partial u}{\partial x} + ri\right) \end{aligned} \tag{3.83}$$

At time $t = 0$, and at location $x = m\Delta$, we may write this voltage as

$$L_1\frac{\partial i}{\partial t'}\bigg|_{x=m\delta,t=0} \overset{(3.61)}{=} -\frac{R_{1m}}{R_0 + R_{1m}}\Big(u_0'(m\Delta) + r_m i_0(m\Delta)\Big)$$

The wave digital voltage across the same port, at location $x = m\Delta$ is defined by

$$v_m = \frac{1}{2}\left(a_{1m} + b_{1m}\right) = \frac{1}{R_0 + R_{1m} + R_{erm}}\Big((R_0 + R_{erm})a_{1m} - R_{1m}a_{2m}\Big) \tag{3.84}$$

Thus, for initialization, equating the voltages in (3.84) and (3.83), we must have

$$-\frac{R_{1m}(R_{1m} + R_0 + R_{erm})}{R_{1m} + R_0}\left(u_0'(m\Delta) + R_{erm}i_0(m\Delta)\right) = (R_0 + R_{er})a_{1m}(0) - R_1 a_{2m}(0)$$

This requirement, along with (3.82) fully specifies the initial values of the wave variables at the left adaptor. We thus have

$$a_{1m}(0) = \left(R_{1m} \quad - \quad \frac{R_{erm}R_{1m}}{R_{1m} + R_0}\right) i_0(m\Delta) \quad - \quad \frac{R_{1m}}{R_{1m} + R_0}u_0'(m\Delta) \tag{3.85a}$$

$$a_{2m}(0) = \left(R_0 + R_{erm} + \frac{R_{erm}R_{1m}}{R_{1m} + R_0}\right) i_0(m\Delta) \quad + \quad \frac{R_{1m}}{R_{1m} + R_0}u_0'(m\Delta) \tag{3.85b}$$

We note that $u_0'(m\Delta)$ may be obtained from the initial voltage distribution $u_0(x)$ by any reasonable (i.e., consistent) approximation to the spatial derivative.

It is important to recognize that for constant $v_0$, we have

$$\lim_{\Delta\to 0} a_{1m}(0) = R_{1m}i_0(m\Delta) \qquad\qquad \lim_{\Delta\to 0} a_{2m}(0) = R_0 i_0(m\Delta)$$

These values occur in the same ratio as those of an *eigenvector* of the scattering matrix for the left series adaptor. In particular, they follow the distribution of the principal eigenvector (i.e., the unique eigenvector whose elements are all of the same sign) of the scattering matrix. Thus the proper setting for the initial conditions (except at the loss port) should be aligned with the dominant mode of the numerical scheme in this limit (and the fraction of the initial energy injected into the parasitic modes will vanish)—see §3.9.2 for a discussion of parasitic modes in this particular system†. We also suggest the following very simple "rule of thumb" for setting initial conditions:

---

†We would like to note here that the eigenvectors of the scattering matrix will give extremal values for the quantity $\mathbf{a}^T\mathbf{P}\mathbf{b}$ for an $N$-port with $N$-vector input waves $\mathbf{a}$ and output waves $\mathbf{b}$ and a diagonal weighting matrix $\mathbf{P}$ containing port conductances. This quantity, at least for some simple lumped systems, can be identified with what is called as the *Lagrangian* [190]. Many physics problems (indeed, all the systems treated in this thesis) can be recast as variational problems involving finding an extreme value of the Lagrangian integrated over all possible system states. Though we have not worked out all the details in the distributed case, it would appear that the alignment of the discrete system with an eigenvector of the scattering matrix is the scheme's "attempt" to conform to Lagrangian mechanics (which is to be expected). This is interesting for two reasons; first, the wave digital Lagrangian could form the basis for a new set of quantization rules, which, in addition to (or perhaps instead of) ensuring passivity, nudge the system toward a preferred state. Second, the variational or Lagrangian formulation of a physics problem is a necessary first step in developing what are known as *finite element methods* (FEM) [95]; these methods are not restricted to operating on regular grids, as MDWD methods are. Could MDWD networks operating on unstructured grids be arrived at through such a formulation? This is, admittedly, a very vague notion.

For a given series $M$-port MD-adaptor in a MDWD network, with associated current $i$, port resistances $R_j$ and input wave variables $a_j$, $j = 1, \dots, M$, then if the initial value of $i$ at the adaptor is to be $i_0$, we should set the initial values of the wave variables to be

$$a_j(0) = 0 \qquad \text{at a loss/source port}$$

$$a_j(0) = R_j i_0 \qquad \text{otherwise}$$

This rule is to be interpreted in a distributed sense, i.e., it holds for every instance of an adaptor on the numerical grid. A similar rule holds for a parallel adaptor. These settings ignore spatial derivative information, but give a simple way of proceeding in general, especially during the first stages of programming and debugging, and are correct (to first order) in the limit as $\Delta$ approaches 0. If losses are large, though, one may prefer to use exact conditions like (3.85). This rule applies regardless of the number of dimensions of the problem (but may need to be amended if sources or reflection-free ports are present).

## 3.11 Boundary Conditions

Boundary terminations have been discussed in [61, 107, 131, 211]. We have not done significant work on this problem, but would like to mention the several disparate approaches which have been proposed. The problem of general passive termination of a MD network is very involved, and would probably merit a long treatment in a separate work; termination of a (1+1)D MD circuit, which is all we will be able to discuss here, is a simple matter, and the ideas can be extended to cover certain important cases in higher dimensions. The most straightforward method was put forth in [107]. We will refer here to Figure 3.22, the MDWD network for the source-free transmission line equations. This network represents the signal behavior at any grid point in the domain. In particular, the signals $x_2$ and $x_3$ are obtained at each time step from signals input into the shift registers at grid locations immediately to the left and right, respectively. Suppose now that we have a left boundary termination at $x = 0$, and that the domain has been sampled such that a grid point coincides with this point. Then at this location, $x_2$ cannot be directly obtained because there is no grid point to the left to which the shift register refers.

Let us now examine some simple lossless boundary conditions of the form of (3.8). Suppose that we would like the boundary condition for the transmission line to be that of an *open-circuit* at the left termination, so that we have

$$i(0,t) = 0 \qquad \text{Open-circuit termination}$$

The wave digital approximation to the physical current at any grid point is calculated from the wave variables incident on the left series adaptor, so that we have

$$i = \frac{1}{R_0 + R_{er} + R_1}(a_1 + a_2) = \frac{1}{R_0 + R_{er} + R_1}\left(-x_1 - \frac{1}{2}(x_2 + x_3)\right)$$

If we set, at the left-most grid point,

$$x_2 = -x_3 - 2x_1$$

then the calculated current will be identically zero, and $x_2$ is easily obtained from $x_3$ and $x_1$, both of which are available. A short-circuited termination, i.e.,

$$u(0,t) = 0 \qquad \text{Short-circuit termination}$$

can be accomplished by treating the right-hand adaptor in a similar manner. It is possible to mix these conditions, and to introduce loss and a lumped terminating source as well [107].

This idea is also easily extended to multiple dimensions for rectilinearly sampled grids, if the boundary is parallel to one of the grid axes. We would like to add, however, that such a termination has *never been shown to be passive*, and that there is no general theory applicable to boundary termination of MDWD networks [142](though we will provide a possible foundation for such an approach in §6.2.3). While it is easy to prove that the simple cases above correspond to passive lumped terminations, there are situations in higher dimensions when this approach becomes difficult to apply reliably; in several instances, (see Chapter 5 for some added discussion), this approach has failed in simulation. The difficulty with approaching boundary termination in this way is that the physics of the problem (in particular the passivity at the boundary) is not being taken into account; this method, though easy to apply, is essentially no different from what is done using conventional finite difference methods. Fettweis and Nitsche [61] provided an alternative method which is more satisfying from a physical point of view; in this case, the region beyond the boundary is modeled as a material with extreme parameter values (typically $r = \infty$ or $g = \infty$, for the transmission line or parallel-plate problem). These regions are still passive, though it may now be necessary to employ a "layer" of this material, which will incur extra calculation costs.

Other recent work has involved more general lumped boundary terminations [5, 211, 212], as well as the termination of the (2+1)D parallel-plate problem in hexagonal coordinates; we mention that these approaches are unwieldy in the extreme; in at least one case [210], the proposed modelling of a passive boundary condition requires active elements!

The problem with the termination of MDWD networks is that when spatial dependence is expanded out to get a signal flow graph, we do not end up with a lumped network of portwise-connected elements; see, for example, the flow graph for the simple advective system, shown in Figure 3.7. Such is not the case for digital waveguide networks, which are in fact formulated from the outset as large lumped networks. For this reason, boundary termination is much simpler in a DWN. In Chapter 4, which is devoted to digital waveguide networks, we will discuss boundary termination for the (1+1)D transmission line problem in §4.3.9, and for the parallel-plate problem in §4.4.4. Boundary termination for vibrating beam and plate systems is discussed in detail in Chapter 5.

### Note on Perfectly Matched Layers

An interesting and related direction in current research into boundary termination (and one into which we invested some considerable time and effort) involves the use of so-called *perfectly matched layers* (PMLs) [13, 14] as boundary terminations in problems to be solved over an unbounded spatial domain. The idea, generally speaking, is to surround a numerical problem domain with a layer of a material which creates as little numerical reflection as possible, while also attenuating waves that enter from the problem interior.

Absorbing boundary conditions (ABCs) [185] were long used for this purpose in (2+1)D and (3+1)D electromagnetic problems; in terms of the (2+1)D parallel-plate problem (which is equivalent to (2+1)D TE or TM mode electromagnetics), the layer is chosen to be matched to the characteristic impedance of the plates, namely $\sqrt{l/c}$. As such, it can be thought of as an extension to (2+1)D of the reflectionless matched termination that can be applied to a (1+1)D transmission line. Unfortunately, in higher dimensions, such a termination is reflection-free only for waves at normal incidence, and there will be significant backscatter into the problem interior at oblique incidence; furthermore, the amount of reflection is frequency-dependent.

Berenger [13] solved this problem, at least in theory, by proposing a new unphysical medium as an absorbing material. For the parallel-plate problem, the dependent variables in this new medium are the current density, and two orthogonal ("split") voltage components; if the layer is infinitely thick, then it indeed absorbs and attenuates waves of any frequency or angle of incidence. The problem here, as has been pointed out in [1, 2, 189] is that the proposed medium can be described by a system which, though hyperbolic, is not symmetric hyperbolic and thus not of the form of (3.1), and what is worse, is not even strongly hyperbolic [82]; strong hyperbolicity is the necessary requirement for the initial value problem to be well-posed. As a result, lower-order perturbations such as those that might result from numerical discretization, can render such a system ill-posed, and susceptible to numerical instability. (It is worth noting that the MDKC representations that we have disussed in this chapter have only been applied to symmetric hyperbolic systems of the particular form of (3.1). An MDKC representation of a (3+1)D PML medium has been proposed in [129], but in this case, the asymmetries in the system were lumped into dependent source terms, and MD-passivity does not immediately follow.) Other more physical reformulations of the PML in terms of an anisotropic frequency-dependent medium [153, 216] and stretched complex coordinates [185] do not alleviate this problem significantly, and other similar aproaches, such as sponge layers [138] and the transparent absorbing boundary [137] and Lorentz materials [217] appear to have similar problems.

New PML-type media, which can be described by symmetric hyperbolic systems, were put forth in [2, 189]; they are of the form of (3.1), but for these media the symmetric part of the **B** matrix is not positive semi-definite, so an energy estimate of the form of (3.7) is not available. In particular, though one can indeed develop MDKC representations for these systems, the non-positivity of the symmetric part of **B** leads to active (though purely resistive) coupling between the various circuit loops. This is somewhat curious, because it is shown in [2] that field quantities in the absorbing medium decay as a function of distance from the boundary in any direction, so it would be expected that these media are indeed passive. Several questions arise here which are related to the general issue of the when a passive MDKC representation can be derived from a physically passive system. In particular: what kind of symmetries are required of the various system matrices? Is it possible to represent systems which are not symmetric hyperbolic, but only strongly hyperbolic (in which case non-reciprocal reactive elements would be necessary)?

Finally, we mention that although these absorbing layers have been proposed for use in electromagnetic field simulation problems, they apply equally well to the associated mechanical and acoustic systems; a version of the layer intended for use in fluid dynamic problems was put forth in [93]. Applications in musical and room acoustics would seem to be manifold (calculating the sound fields radiating from the open end of a musical instrument into a large space, or in open-air architectural acoustics problems come to mind as two possible examples).

## 3.12 Balanced Forms

Consider again the (1+1)D transmission line, with spatially-varying coefficients. It has been noted in the past [130, 131] that the restriction on the time step, namely

$$v_0 \geq \frac{1}{\sqrt{l_{min}c_{min}}}$$

with $l_{min} = \min_x l$ and $c_{min} = \min_x c$ is rather unsatisfying; the local group velocity at any point in our domain is given by $\pm 1/\sqrt{lc}$, so we would hope that a more physically meaningful bound such as

$$v_0 \geq \gamma^g_{TL,max} \triangleq \max_x \sqrt{\frac{1}{lc}} \tag{3.86}$$

(which is obtained in using, for example, digital waveguide networks, which will be discussed in Chapter 4) could be attainable. Depending on the variation in $l$ and $c$, the new bound can allow a substantially larger time step. We will show that this is in fact possible via a MDWD approach.

The transmission line equations given in (3.53) can be transformed in the following way: first introduce new dependent variables

$$\tilde{i}_1 = \sqrt{Z}i \qquad\qquad \tilde{i}_2 = u/\sqrt{Z}$$

where $Z$, the local line impedance is defined by

$$Z(x) \triangleq \sqrt{\frac{l}{c}}$$

Such a transformation in fact changes to variables which both have units of *root power*. After a few elementary manipulations (namely scaling (3.53a) by $1/\sqrt{Z}$ and (3.53b) by $\sqrt{Z}$), we have

$$\begin{aligned}
\sqrt{lc}\frac{\partial\tilde{i}_1}{\partial t} + \frac{\partial\tilde{i}_2}{\partial x} + \frac{\partial}{\partial x}(\ln(\sqrt{Z}))\tilde{i}_2 + r\tilde{i}_1/Z + e/\sqrt{Z} &= 0 && (3.87\text{a})\\
\sqrt{lc}\frac{\partial\tilde{i}_2}{\partial t} + \frac{\partial\tilde{i}_1}{\partial x} - \frac{\partial}{\partial x}(\ln(\sqrt{Z}))\tilde{i}_1 + gZ\tilde{i}_1 + h\sqrt{Z} &= 0 && (3.87\text{b})
\end{aligned}$$

System (3.87) is still symmetric hyperbolic; referring to the general system from (3.1), for $\mathbf{w} = [\tilde{i}_1, \tilde{i}_2]^T$, we now have

$$\mathbf{P} = \begin{bmatrix} \sqrt{lc} & 0 \\ 0 & \sqrt{lc} \end{bmatrix} \quad \mathbf{A}_1 = \begin{bmatrix} 0 & 1 \\ 1 & 0 \end{bmatrix} \quad \mathbf{B} = \begin{bmatrix} r/Z & \frac{\partial}{\partial x}(\ln(\sqrt{Z})) \\ -\frac{\partial}{\partial x}(\ln(\sqrt{Z})) & gZ \end{bmatrix} \tag{3.88}$$

Note that because $\mathbf{P}$ is now a multiple of the identity matrix, there is near complete symmetry between the variables $\tilde{i}_1$ and $\tilde{i}_2$. We use the term "balanced" to describe such a system. Note also that new off-diagonal terms have appeared in $\mathbf{B}$ (compare (3.88) with (3.54)), but they appear *antisymmetrically*[†], and thus do not give rise to loss—in other words these terms do not appear in $(\mathbf{B} + \mathbf{B})^T$, which determines the growth or decay of the solution, as per (3.5). In fact, these off-diagonal terms yield a lossless (but non-reciprocal) gyrator in the circuit setting.

In terms of the coordinates defined by (3.18), we can then rewrite (3.87) as

$$\begin{aligned}
L_1 D_{t'}\tilde{i}_1 + L_0 D_1\left(\tilde{i}_1 + \tilde{i}_2\right) + L_0 D_2\left(\tilde{i}_1 - \tilde{i}_2\right) + R_G\tilde{i}_2 + \tilde{r}\tilde{i}_1 + \tilde{e} &= 0\\
L_2 D_{t'}\tilde{i}_2 + L_0 D_1\left(\tilde{i}_2 + \tilde{i}_1\right) + L_0 D_2\left(\tilde{i}_2 - \tilde{i}_1\right) - R_G\tilde{i}_1 + \tilde{g}\tilde{i}_2 + \tilde{h} &= 0
\end{aligned}$$

---

[†] Recall from §3.2 that the term "symmetric hyperbolic" does not refer to the coefficient of the constant-proportional term $\mathbf{B}$, which is not constrained to be of any particular form.

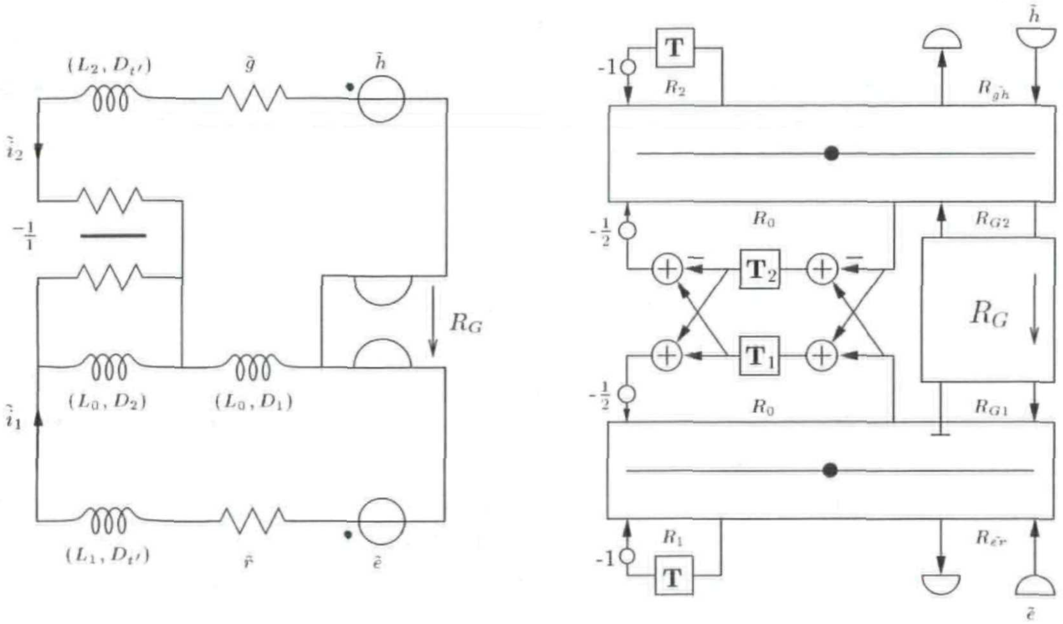
$(L_2, D_{t'})$
$\tilde{g}$
$\tilde{h}$
$\tilde{i}_2$
$-\frac{1}{1}$
$R_G$
$(L_0, D_2)$
$(L_0, D_1)$
$\tilde{i}_1$
$(L_1, D_{t'})$
$\tilde{r}$
$\tilde{e}$
T
-1
$R_2$
$R_{\tilde{g}\tilde{h}}$
$-\frac{1}{2}$
$R_0$
$R_{G2}$
$T_2$
$T_1$
$R_G$
$R_{G1}$
$R_1$
$R_{\tilde{e}\tilde{r}}$

(a) (b)

Figure 3.23: (a) *Balanced MD-passive network for the (1+1)D transmission line equations and* (b) *its associated MDWD network.*

where

$$L_1 = L_2 = v_0\sqrt{lc} - 1 \qquad L_0 = \frac{1}{\sqrt{2}} \qquad R_G = \frac{\partial}{\partial x}\left(\ln(\sqrt{Z})\right)$$

(which should be compared with (3.60), for the standard form), and

$$\tilde{r} = r/Z \quad \tilde{e} = e/\sqrt{Z} \quad \tilde{g} = gZ \quad \tilde{h} = h\sqrt{Z}$$

As mentioned previously, in a MDKC setting, the terms with coefficient $R_G$ can be treated as a *gyrator*. The network and its wave digital counterpart are shown in Figure 3.23. The port resistances are given by

$$R_1 = R_2 = \frac{2}{\Delta}\left(v_0\sqrt{lc} - 1\right) \qquad R_0 = \frac{2}{\Delta} \qquad R_{\tilde{e}\tilde{r}} = \tilde{r} \qquad R_{\tilde{g}\tilde{h}} = \tilde{g}$$

In order to accommodate the gyrator, we have been forced, in order to avoid delay-free loops, to set one of the ports to which it is connected to be *reflection-free* (see §2.3.5). In (1+1)D, we can choose either of these ports, but picking the bottom port in Figure 3.23(b) allows us to extend the idea to (2+1)D easily. This port resistance is then constrained to be

$$R_{G1} = R_1 + R_{\widehat{er}} + R_0$$

We have two simplifying choices for $R_{G2}$; either we can choose it to be reflection-free as well, so that we will have a general gyrator described by (2.25), or we can choose

$$R_{G2} = \frac{R_G^2}{R_{G1}}$$

in which case the gyrator equations (2.25) reduce to a pair of throughs, scaled individually by $R_G/R_{G1}$ and its inverse; this latter choice may be problematic if $R_G$ approaches zero, because one of the multipliers becomes unbounded. If $R_G$ is small over some part of the problem domain, however, it is probably wiser to remove the coupling from the network altogether over these regions (it can be replaced by a simple two-port short-circuit). We have assumed, throughout this development, that $l(x)$ and $c(x)$ (or rather, the local characteristic line impedance $Z(x) = \sqrt{l(x)/c(x)}$) are differentiable. An *offset-sampled* version of this network is also possible, if we halve the port resistances $R_1$ and $R_2$ and double the delays at the same ports.

The stability bound, from a requirement on the positivity of $R_1$ and $R_2$ will be exactly (3.86). In an implementation, there will be of course the slight additional costs due to the extra gyrator and the rescaling of the new dependent variables $\tilde{i}_1$ and $\tilde{i}_2$ at every time step in order to obtain $i$ and $u$. We note that this scaling can be fully incorporated into the MDKC by treating the scaling coefficients as transformer turns-ratios, though there is no advantage in doing so (other than putting one's mind at ease regarding whether such a scaling is a passive operation).

We will examine how this same technique can be applied to more complex systems when we approach the Timoshenko beam equations in §5.2; in that case, the maximum allowable time step can be radically increased for a system with only mild material parameter variation.

### Extension to (2+1)D

We briefly note that the same approach can be easily extended to the parallel-plate problem as well; beginning from system (3.64), we can introduce new variables

$$\tilde{i}_1 = \sqrt{Z}i_x \qquad \tilde{i}_2 = \sqrt{Z}i_y \qquad \tilde{i}_3 = u/\sqrt{Z}$$

where $Z(x,y) \triangleq \sqrt{l(x,y)/c(x,y)}$, and then multiply (3.64a) and (3.64b) by $1/\sqrt{Z}$ and (3.64c) by $\sqrt{Z}$. The new system is again symmetric hyperbolic. We do not show the network here, but we mention that we will require two gyrators; one linking the series adaptors with associated currents $\tilde{i}_1$ and $\tilde{i}_3$, the other between the adaptors for $\tilde{i}_2$ and $\tilde{i}_3$. One reflection-free port must be chosen for each gyrator; choosing both reflection-free ports at the adaptor with current $\tilde{i}_3$ must be ruled out, but other configurations are acceptable.

The stability bound for the balanced (2+1)D network will be

$$v_0 \geq \max_{x,y} \sqrt{\frac{2}{lc}} = \sqrt{2}\gamma^{g}_{PP,max}$$

which is superior to (3.68), the bound for the standard form.

## 3.13 Higher-order Accuracy

WDF-based numerical methods are, in general, second-order accurate in both the time step and the grid spacing. In all the schemes that have been examined in the literature, these quantities occur in a fixed ratio (usually written as $v_0$), so we can say that such schemes are accurate to second order in either one (or of any of the shift lengths in the new coordinates). A numerical approximation to a system of PDEs obtained using a MDWD network will converge to the solution to the model problem with a truncation error [176] proportional to the square of any of these spacings.

While this is true in general, in this section we would like to point out that it is indeed possible to devise MD circuit-based schemes which exhibit a higher-order *spatial* accuracy. Temporal accuracy, however, remains fixed at second-order[†]; for this reason, such schemes must operate using a small time step; this limits their usefulness somewhat. Even more importantly, however, we note that the schemes we will develop here can be rewritten as very simple finite difference schemes of the form corresponding to digital waveguide networks (to be discussed in Chapter 4). We include this section merely to show that higher-order spatial accuracy is not incommensurate with MD-passivity, and to indicate a possible direction for future research.

Consider again the lossless source-free transmission line problem, defined by

$$l\frac{\partial i}{\partial t} + \frac{\partial u}{\partial x} = 0 \tag{3.89a}$$

$$c\frac{\partial u}{\partial t} + \frac{\partial i}{\partial x} = 0 \tag{3.89b}$$

(Losses and sources may be reintroduced at a later stage in these schemes without any difficulty.) Because higher-order spatially accurate explicit methods will require access to grid points other than nearest neighbors, we introduce the following coordinate transformation,

---

[†] We remark here that this restriction may be fundamental. It should be recalled that MD systems are passive with respect to the time coordinate—coordinate transformations are simply a means of distributing this passivity property among all the independent variables of the problem. It is well-known [65] that lumped passive systems of first-order can be approximated by passive numerical methods which are at best second-order accurate. This restriction would appear to carry over in MD, though we have not attempted to prove this. Passivity does not hold, however, with respect to the spatial coordinates, and it may be this distinction which we are able to exploit in this section.

$$\mathbf{H} = \begin{bmatrix} 1 & -1 & 2 & -2 & \dots & q & -q \\ 1 & 1 & 1 & 1 & \dots & 1 & 1 \end{bmatrix} \qquad \mathbf{H}^{-R} = \mathbf{H}^{T} \begin{bmatrix} \frac{3}{q(2q+1)(q+1)} & 0 \\ 0 & \frac{1}{2q} \end{bmatrix} \tag{3.90}$$

for some positive integer $q$ (if $q = 1$, then we get the coordinate transformation defined by (3.18), scaled by a constant factor). $2q$ will shortly be shown to be the order of spatial accuracy of the resulting difference scheme. As before, we have

$$\mathbf{u} = \mathbf{V}^{-1}\mathbf{H}\mathbf{t} \qquad\qquad \mathbf{t} = \mathbf{H}^{-R}\mathbf{V}\mathbf{u}$$

with $\mathbf{u} = [x, t]^T$, and $\mathbf{t} = [t_{1+}, t_{1-}, t_{2+}, t_{2-}, \dots, t_{q+}, t_{q-}]^T$; the coordinate transformation defined by $\mathbf{H}$ thus describes an embedding of the (1+1)D problem in a $2q$-dimensional space. A uniform sampling of the new coordinates with spacings $T_{1+} = T_{1-} = \dots = T_{q+} = T_{q-} = \Delta$ merely regenerates a uniform grid with spacing $\Delta$. The first two pairs of unit shifts are as shown in Figure 3.24.

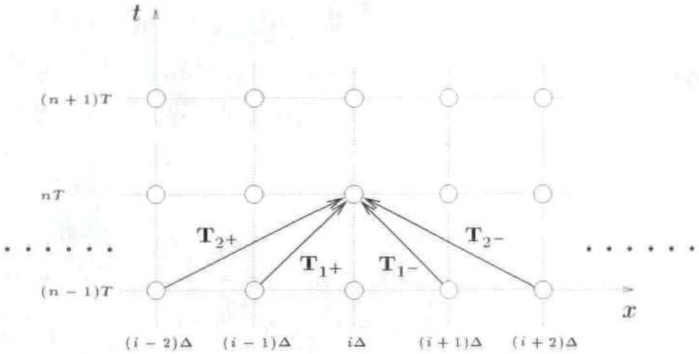

Figure 3.24: *Unit shifts in the coordinates defined by* (3.90).

We now rewrite system (3.89) as

$$\begin{aligned} v_0 l \frac{\partial i_1}{\partial t'} + r_0 \sum_{j=1}^{q} \alpha_{qj} \frac{\partial i_2}{\partial x} &= 0 \\ v_0 c r_0^2 \frac{\partial i_2}{\partial t'} + r_0 \sum_{j=1}^{q} \alpha_{qj} \frac{\partial i_1}{\partial x} &= 0 \end{aligned}$$

where, as before, we have $i_1 = i$, $i_2 = u/r_0$ for some positive constant $r_0$, and $t' = v_0 t$. The $\alpha_{qj}$,

$j = 1, \ldots, q$, are constants which satisfy

$$\sum_{j=1}^{q} \alpha_{qj} = 1 \tag{3.91}$$

We may continue and write

$$\begin{aligned}
\left(v_0 l - r_0 \sum_{j=1}^{q} \frac{|\alpha_{qj}|}{j}\right) \frac{\partial i_1}{\partial t'} + r_0 \sum_{j=1}^{q} \frac{|\alpha_{qj}|}{j} \left(\frac{\partial i_1}{\partial t'} + j\,\mathrm{sgn}(\alpha_{qj}) \frac{\partial i_2}{\partial x}\right) &= 0 \\
\left(v_0 c r_0^2 - r_0 \sum_{j=1}^{q} \frac{|\alpha_{qj}|}{j}\right) \frac{\partial i_2}{\partial t'} + r_0 \sum_{j=1}^{q} \frac{|\alpha_{qj}|}{j} \left(\frac{\partial i_2}{\partial t'} + j\,\mathrm{sgn}(\alpha_{qj}) \frac{\partial i_1}{\partial x}\right) &= 0
\end{aligned}$$

Because, from (3.25), we have that

$$D_{j^+} \triangleq \frac{\partial}{\partial t_{j^+}} = \frac{\partial}{\partial t'} + j\frac{\partial}{\partial x} \qquad D_{j^-} \triangleq \frac{\partial}{\partial t_{j^-}} = \frac{\partial}{\partial t'} - j\frac{\partial}{\partial x} \qquad j = 1, \ldots, q$$

we can immediately write

$$L_{1_q} D_{t'} i_1 + \sum_{j=1}^{q} M_{qj} \left(D_{j^+}(i_1 + \beta_{qj} i_2) + D_{j^-}(i_1 - \beta_{qj} i_2)\right) = 0 \tag{3.92a}$$

$$L_{2_q} D_{t'} i_2 + \sum_{j=1}^{q} M_{qj} \left(D_{j^+}(i_2 + \beta_{qj} i_1) + D_{j^-}(i_2 - \beta_{qj} i_1)\right) = 0 \tag{3.92b}$$

with

$$L_{1_q} = v_0 l - r_0 \sum_{j=1}^{q} \frac{|\alpha_{qj}|}{j} \qquad L_{2_q} = v_0 c r_0^2 - \sum_{j=1}^{q} \frac{r_0 |\alpha_{qj}|}{j} \qquad M_{qj} = \frac{r_0 |\alpha_{qj}|}{2j} \qquad \beta_{qj} = \mathrm{sgn}(\alpha_{qj}) \tag{3.93}$$

The system (3.92) can immediately be identified with an MDKC, as in Figure 3.25.

Each of the Jaumann two-ports can be discretized according to the trapezoid rule; as long as our choice of the constants $\alpha_{qj}$ satisfies the constraint (3.91) and $L_{1_q}$ and $L_{2_q}$ remain positive, the resulting MDWD network will be a second-order stable accurate approximation to system (3.89). Suppose, however, that we apply a different set of discretization rules, namely

$$D_{j^+} \rightarrow \frac{1}{\Delta}\left(1 + \delta_{j^-}\delta_{j^+}\right)^{-1}\left(1 - \delta_{j^+}\right)\left(1 + \delta_{j^-}\right) \tag{3.94a}$$

$$D_{j^-} \rightarrow \frac{1}{\Delta}\left(1 + \delta_{j^-}\delta_{j^+}\right)^{-1}\left(1 - \delta_{j^-}\right)\left(1 + \delta_{j^+}\right) \tag{3.94b}$$

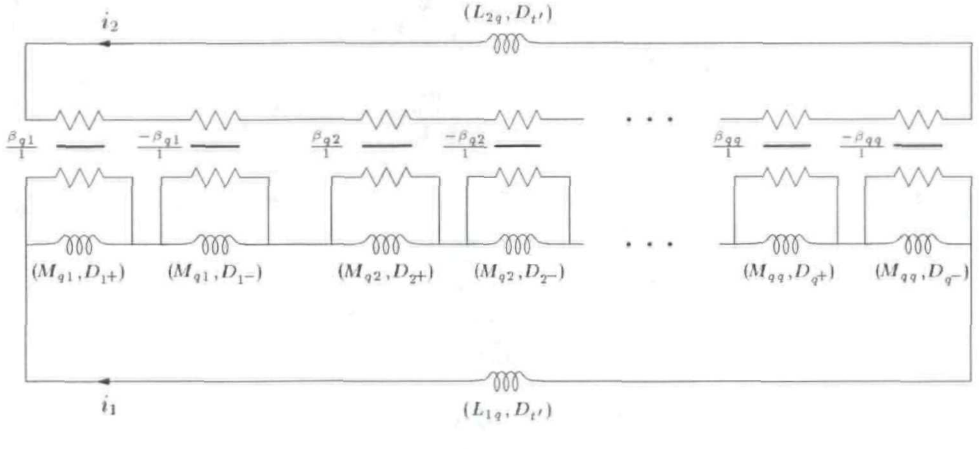

Figure 3.25: *MDKC for the lossless source-free transmission line equations, according to the decomposition given by* (3.92).

for $j = 1, \ldots, q$. Here, $\delta_{j^+}$ and $\delta_{j^-}$ are the shift operators in the directions $t_{j^+}$ and $t_{j^-}$ defined by

$$\delta_{j^+}e(\mathbf{t}) = e(\mathbf{t}-\mathbf{T}_{j^+}) \qquad \delta_{j^-}e(\mathbf{t}) = e(\mathbf{t}-\mathbf{T}_{j^-})$$

for a function $e(\mathbf{t})$, where $\mathbf{T}_{j^+}$ and $\mathbf{T}_{j^-}$ are vectors of length $\Delta$ in directions $t_{j^+}$ and $t_{j^-}$ respectively (see Figure 3.24 for a graphical representation of these shifts on the computational grid). These rules correspond, in the linear shift-invariant case, to pairs of spectral mappings of the type mentioned briefly in §3.5.4, with shift lengths equal to $\Delta$; they are also MD-passivity preserving, and are in general second-order accurate [61]. To the scaled time derivative, we apply the trapezoid rule with a doubled time step $T' = 2\Delta$, as defined by

$$D_{t'} \rightarrow \frac{2}{T'}\left(1+\delta_{t'}^2\right)^{-1}\left(1-\delta_{t'}^2\right) = \frac{1}{\Delta}\left(1+\delta_{t'}^2\right)^{-1}\left(1-\delta_{t'}^2\right)$$

Equation (3.92a) then becomes

$$\begin{aligned} L_{1q}\left(1+\delta_{t'}^2\right)^{-1}\left(1-\delta_{t'}^2\right)i_1 \;&+\; \sum_{j=1}^{q} M_{qj}\left(1+\delta_{j^-}\delta_{j^+}\right)^{-1}\left(1-\delta_{j^+}\right)\left(1+\delta_{j^-}\right)\left(i_1+\beta_{qj}i_2\right) \\ &+\; \sum_{j=1}^{q} M_{qj}\left(1+\delta_{j^-}\delta_{j^+}\right)^{-1}\left(1-\delta_{j^-}\right)\left(1+\delta_{j^+}\right)\left(i_1-\beta_{qj}i_2\right) \\ &=\; O(\Delta^2) \end{aligned} \tag{3.95}$$

Because, however, $\delta_{j^+}\delta_{j^-} = \delta_{t'}^2$ and our system is time-invariant, the operator $1+\delta_{j^+}\delta_{j^-}$ commutes with $L_{1q}$ and $M_{jq}$ and may be factored out of (3.95), giving

$$\begin{aligned} L_{1q}\left(1-\delta_{t'}^{2}\right)i_1 \quad &+ \quad \sum_{j=1}^{q} M_{qj}\left(1-\delta_{j+}\right)\left(1+\delta_{j-}\right)\left(i_1+\beta_{qj}i_2\right) \\ &+ \quad \sum_{j=1}^{q} M_{qj}\left(1-\delta_{j-}\right)\left(1+\delta_{j+}\right)\left(i_1-\beta_{qj}i_2\right) \\ &= \quad O(\Delta^2) \end{aligned}$$

which can be further simplified to

$$v_0 l\left(1-\delta_{t'}^{2}\right)i_1 + r_0\sum_{j=1}^{q}\frac{\alpha_{qj}}{j}\left(\delta_{j-}-\delta_{j+}\right)i_2 = O(\Delta^2)$$

or, writing $\delta_{j-}=\delta_{t'}\delta_x^{-j}$ and $\delta_{j+}=\delta_{t'}\delta_x^{j}$ where $\delta_x$ is a simple shift in the $x$ direction of $\Delta$, as

$$\underbrace{l\,\frac{\left(\delta_{t'}^{-1}-\delta_{t'}\right)}{2\Delta}}_{\approx\frac{\partial}{\partial t}} i_1 + r_0\underbrace{\sum_{j=1}^{q}\alpha_{qj}\frac{\left(\delta_x^{-j}-\delta_x^{j}\right)}{2j\Delta}}_{\approx\frac{\partial}{\partial x}} i_2 = O(\Delta^2)$$

which is easily seen to be a simple difference approximation to (3.89a), The approximation is nominally second-order accurate in $\Delta$, but we have not as yet made any special choice of the $\alpha_{qj}$. This can be done via a conventional finite difference approach [176] in such a way as to yield a higher-order accurate approximation to the spatial derivative.

We can write, expanding the shift operators in Taylor series,

$$\sum_{j=1}^{q}\alpha_{qj}\frac{\left(\delta_x^{-j}-\delta_x^{j}\right)}{2j\Delta} \quad = \quad \sum_{k>0\text{ odd}}\frac{\Delta^{k-1}}{k!}\sum_{j=1}^{q}\alpha_{qj}j^{k-1}\frac{\partial^k}{\partial x^k} \tag{3.96}$$

There are $q$ degrees of freedom, corresponding to the parameters $\alpha_{qj}$, $j=1,\ldots,q$. We require, from (3.91) that the coefficient of the first derivative on the right-hand side of (3.96) equal one. We may then additionally require that the other coefficients, for $k=3,\ldots,2q+1$ be zero; the resulting difference approximation will then be accurate to order $2q$. This yields the linear system

$$\mathbf{C}\boldsymbol{\alpha}_q=\mathbf{e}_q \tag{3.97}$$

where $\mathbf{C}$ is a $q\times q$ matrix with $[\mathbf{C}_{ij}]=j^{2(i-1)}$, $\boldsymbol{\alpha}_q=[\alpha_{q1},\ldots,\alpha_{qq}]^T$, and $\mathbf{e}_q$ is a $q\times 1$ vector whose first entry is one, and whose others are zero. $\mathbf{C}$ is always full rank, so there is a unique solution for any $q$. The same $\boldsymbol{\alpha}_q$ will also give a higher-order approximation to (3.89b), and thus system (3.89) will be approximated to higher-order accuracy as a whole. For a fourth-order approximation, for example,

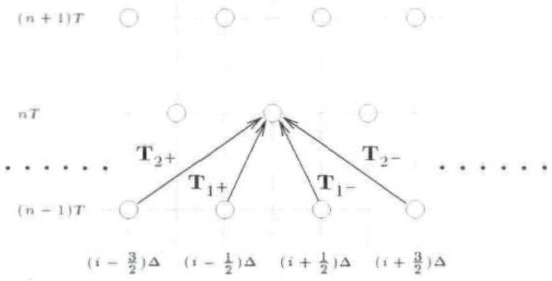

Figure 3.26: *Unit shifts in the coordinates defined by* (3.98).

we obtain $\boldsymbol{\alpha}_2 = [4/3, -1/3]^T$, and for a sixth-order approximation, we get $\boldsymbol{\alpha}_3 = [3/2, -3/5, 1/10]^T$. These values completely determine the MDKC pictured in Figure 3.25.

The passivity requirement is, as before, a condition on the positivity of $L_{1q}$ and $L_{2q}$. Choosing $r_0 = \sqrt{l_{min}/c_{min}}$ gives

$$\begin{array}{rcll} v_0 & \geq & \dfrac{3}{2\sqrt{l_{min}c_{min}}} & \text{Fourth-order accurate scheme} \\ v_0 & \geq & \dfrac{11}{6\sqrt{l_{min}c_{min}}} & \text{Sixth-order accurate scheme} \end{array}$$

It is interesting to note that in the constant-coefficient case, this bound is distinct from the stability bound obtained from *Von Neumann analysis* (see Appendix A) applied to the same difference method. For example, for the fourth-order accurate scheme defined by $\boldsymbol{\alpha}_2$, the stability bound is $v_0 \geq 1.37\gamma$, with $\gamma = 1/\sqrt{lc}$; there is thus a range of values of $v_0$ for which the scheme will be stable, but not MD-passive. We will comment extensively on the distinction between passive and stable methods in Appendix A.

It is also of interest to define a similar scheme with respect to the coordinate transformation defined by

$$\mathbf{H} = \begin{bmatrix} \frac{1}{2} & -\frac{1}{2} & \frac{3}{2} & -\frac{3}{2} & \dots & \frac{2q-1}{2} & -\frac{2q-1}{2} \\ 1 & 1 & 1 & 1 & \dots & 1 & 1 \end{bmatrix} \tag{3.98}$$

Keeping the same notation for the new coordinates, the shifts are as shown in Figure 3.26; now we have a grid ideal for a staggered or interleaved algorithm, with alternating grid points at alternating time steps.

For this coordinate system, we follow through a development very similar to that in the previous pages. We again have an MD circuit representation as in Figure 3.25, where now we have

$$L_{1q} = v_0 l - r_0 \sum_{j=1}^{q} \frac{|\alpha_{qj}|}{j-\frac{1}{2}} \qquad L_{2q} = v_0 c r_0^2 - r_0 \sum_{j=1}^{q} \frac{|\alpha_{qj}|}{j-\frac{1}{2}} \qquad M_{qj} = \frac{r_0|\alpha_{qj}|}{2(j-\frac{1}{2})}$$

for some set of $\alpha_{qj}$, $j = 1, \ldots, q$ which sum to unity. The symbols $D_{j+}$ and $D_{j-}$ in the figure now refer to directional derivatives in the coordinate directions defined by (3.98). For higher-order accuracy, constraint equation (3.97) will apply, now with $[\mathbf{C}_{ij}] = (j-1/2)^{2(i-1)}$. For fourth-order accuracy, we obtain $\boldsymbol{\alpha}_2 = [9/8, -1/8]^T$, and for a sixth-order approximation, we get $\boldsymbol{\alpha}_3 \approx [1.179, -0.195, 0.0234]^T$.

Because here we are using an alternative discretization rule, the resulting MDWD networks are more appropriately discussed in the context of digital waveguide networks (which are the subject of the next chapter). We will return briefly to waveguide network representations of these higher-order accurate methods in §4.10.5.

# Chapter 4

# Digital Waveguide Networks

## 4.1 Introductory Remarks

We now turn our attention to a different approach to numerical integration which is, in many respects, very similar to the multidimensional wave digital filtering technique discussed in the last chapter. *Digital waveguide networks* (DWNs) [166] are also based on ideas of scattering and propagation of wave variables in multiple dimensions; indeed, the basic signal processing block of the DWN, the scattering junction, is identical to the wave digital adaptor. As such, a waveguide network will possess the same discrete passivity properties as a wave digital network, and passivity in finite arithmetic also follows accordingly [165].

The process through which one arrives at a particular DWN intended to simulate the behavior of a distributed physical system has been, to date, quite different. Following the wave digital approach, one first obtains a multidimensional circuit representation (MDKC) of a system of PDEs, then applies a set of coordinate transformations and spectral mappings in order to obtain a discrete time/space algorithm. As discussed in the previous chapter, all MD circuit elements (as well as Kirchoff connections between elements) are to be interpreted as *distributed*, from the outset through to the final wave digital network. The integrity of each multidimensional circuit element (including its energetic properties) is preserved through the discretization step, as is network topology as a whole. As we mentioned in §1.1.2, however, the DWN is usually thought of as a collection of lumped elements, and as such, there has not as yet been a convenient multidimensional representation for such a network. We will address this point in some detail in the last section of this chapter. A DWN always operates on a predefined grid, at the points of which are located scattering junctions. Even though the paired delay elements (*waveguides*) which connect the various scattering junctions behave like transmission lines, we will persist in calling them lumped elements, because they are typically connected between junctions at neighboring grid points, and their behavior is hence localized in a way that that of a MDWD element is not.

A multidimensional WD network will behave consistently with the generating system of PDEs because the continuous-to-discrete spectral mapping applied approximates differential operators consistently; for a DWN, we must first show consistency of a DWN with a particular physical system. For both approaches, convergence of simulation results to the true solution of the physical system follows from this consistency as well as stability implied by passivity [176].

It was shown in [200] and [198] that the DWN structures designed to solve the *wave equation* in (2+1) and (3+1)D could be recast as *finite difference approximations* [176] (and in particular *centered difference approximations*) to these equations; we looked at the (2+1)D waveguide mesh briefly in §1.1.2. In infinite-precision arithmetic, these DWNs and centered differences yield identical results. A similar correspondence holds for the MDWD networks examined in the last chapter, though the equivalent difference methods are more involved (see §3.9). The distinction between a DWN and a finite difference approximation is in the types of signals used. Finite difference methods operate using grid variables which are approximations to the physical dependent variables of the problem at hand, but the DWN propagates wave variables; in this formulation, the solution to a system of PDEs is obtained as a by-product of the scattering of these waves. It is perhaps best to think of the difference between the finite difference scheme and DWN implementations as analogous to the distinction between direct form and lattice/ladder form digital filters [79]—both can be designed to implement the same transfer functions, but for the latter forms, stability is tightly controlled by the range of values which the filter multipliers ("reflection coefficients") can take. And indeed, as we saw in §1.1.1, a particular type of (1+1)D DWN can be shown to be directly related to these lattice/ladder forms [165]. One goal of this chapter and the next is to show how this correspondence between the DWN and centered differences may be extended to a wide variety of physical systems.

The immediate question which arises is then: If the DWN is equivalent to finite differences, then is there a compelling reason for using it? Finite differences, after all, are more straightforward to implement. The answer is two-fold. First, although the approaches are equivalent in infinite precision arithmetic, this is no longer true when we are forced, inevitably, to truncate both the signals and multipliers in a computer implementation; stability of a DWN can be simply maintained even in finite arithmetic. Second, the stability criterion for a DWN is, as for MDWD networks, a *positivity condition* on the values of the elements contained in the network (i.e., the immittances of the transmission line segments). It thus becomes very simple to check stability of a given DWN, even in the presence of boundary conditions. Checking the stability of a finite difference scheme is considerably more involved, especially considering that a difference scheme which is stable over the interior of a domain may become unstable when boundary conditions are applied [82]. There is a theoretical machinery for performing such checks (known as GKSO theory [82, 176]), though it can be formidable even in the (1+1)D case. It is quite possible, of course, to *design* a convergent numerical method using a DWN, and then to *apply* it as a finite difference scheme; as mentioned above, however, its stability in finite arithmetic is then no longer guaranteed.

A full technical summary of this chapter appeared in §1.3.

### 4.1.1 FDTD and TLM

Numerical integration methods for the transmission line equations and electromagnetic field problems have developed along two important directions. The first approach was pioneered by Yee [214] in the mid 1960s, and has since blossomed into what is now known as the ***finite difference time domain*** method, or FDTD [184]. The idea behind the method is a straightforward application of centered differences to (in Yee's case) the defining equations of electromagnetics, namely Maxwell's equations. (2+1)D simplifications of Maxwell's equations which describe the evolution of transverse electric (TE) and transverse magnetic (TM) fields can also be treated as well, and are, with some trivial modifications, equivalent to the (2+1)D parallel-plate problem. The important advantage of Yee's method is that, due to the structure of the system of equations to be modeled, it is not necessary to calculate all the field components simultaneously—the field components are interleaved both temporally and spatially. We will examine FDTD in the (2+1)D case explicitly in §4.4. The literature on FDTD is quite large; we refer to chapters 2 and 3 of [184] for a succinct technical overview.

The ***transmission line matrix*** method, or TLM [4, 29, 90] appeared a bit later, in the early 1970s [97, 100]. It (like the wave digital filtering approach) is a descendant of the ground-breaking work of Kron [109], who developed circuit models of electromagnetic field problems before the widespread availability of electronic computers. TLM is very similar to the DWN, in that it employs a network of discrete transmission lines connected at scattering junctions in order to simulate the behavior of a distributed system. The first formulation, known as the ***expanded node*** formulation was derived from a lumped (RLC) model of the (2+1)D transmission line equations [90], and is identical to the type III DWN we will present in §4.3.6. TLM has developed in numerous ways since its inception; the most significant thrust has been towards formulations for which the various field components are not staggered, but computed together at larger nodes. The ***symmetric condensed node*** [99] and its numerous offspring, such as the ***hybrid symmetrical condensed node*** [159] are the results of this work.

FDTD and TLM have been compared and linked in various ways [38, 98], most significantly through the use of field expansions [110], and new variants of FDTD have been developed using TLM as a starting point [27]. We will take a different approach here. Beginning from the observations that have been made regarding the equivalence of certain DWNs to difference methods [67, 157, 198, 200] we will show that Yee's algorithm is equivalent to a family of scattering structures, some of which appear to be quite different from those that have been proposed in the TLM literature. The correspondence holds for media with spatially-varying material parameters; numerical integration of the equations defining such materials has not, as yet, been approached using DWNs. We also note that the TLM community appears to be aware neither of the many valuable numerical properties which scattering-based numerical methods possess [46, 165], in particular their behavior in finite arithmetic, nor of other useful signal-processing manipulations (such as power-normalization of wave quantities and dynamic range minimization [167]) which have their roots in electrical network theory.

## 4.2 Digital Waveguides

We surveyed the basics of digital waveguide networks in §1.1.2. In this section, we review the main principles of waveguide networks, now in the transmission line setting. For a full treatment, we refer the reader to [166].

### 4.2.1 The Bidirectional Delay Line

The basic element in a waveguide network, and the one which does the work of moving energy from one part of the network to another, is the bidirectional delay line, shown in Figure 4.1. It is no more than a pair of digital delay lines, whose delays are equal length ($m$ samples of duration $T$ in Figure 4.1). It should be understood that, for realizability, all delay lengths in a given network should be multiples of a common smallest ("unit") delay. We will use the terms *waveguide* and *bidirectional delay line* interchangeably in this work.

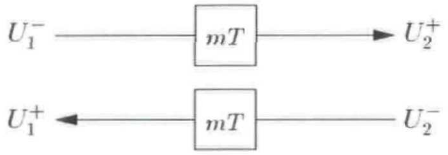

Figure 4.1: *Bidirectional delay line.*

Associated with the bidirectional delay line are two sets of signals, called *waves*: *voltage waves* $U$, and *current waves* $I$. Only voltage waves are shown in Figure 4.1. Waves of either type are indexed with respect to a particular end of the delay line; in Figure 4.1, waves at the left end of the delay line pair are subscripted with a "1", and those at the right end with a "2". In addition, one of the waves at either end *enters* the waveguide, and one *leaves*; the waves are superscripted with − or + respectively[†]. We can immediately read the relationship among the variables from Figure 4.1:

$$U_2^+(n) = U_1^-(n-m) \qquad U_1^+(n) = U_2^-(n-m) \tag{4.1}$$

---

[†] We have chosen here to break with the notational tradition in [167], in which the superscripts are reversed. We choose the above notation so that signal nomenclature in a waveguide network is well-defined. That is, a signal *leaving* a bidirectional delay line, and a signal *entering* a scattering junction (to which each end of the waveguide will ultimately be connected) are both superscripted by a +. This will simplify the derivation of difference schemes later in this chapter. The other indexing method is more useful from the point of view of a unified treatment of both scattering junctions and bidirectional delay lines as digital $n$-port devices (where we would want + and − to denote incoming and outgoing signals, respectively, for any $N$-port).

The delay duration $T$ is implicit, so that a wave variable indexed by $n$ refers to the value of that quantity at time $t = nT$. In terms of $z$-transformed quantities [133] (which we will denote with a hat),

$$\hat{U}_2^+ = z^{-m}\hat{U}_1^- \qquad \hat{U}_1^+ = z^{-m}\hat{U}_2^- \tag{4.2}$$

We also define, at either end of the waveguide, the so-called physical voltage by

$$U_j = U_j^+ + U_j^- \qquad j = 1,2 \tag{4.3}$$

### 4.2.2 Impedance

From the point of view of a programmer, the above description of the operation of an isolated bidirectional delay line is complete. In order to connect one bidirectional delay line to others, however, we must introduce the impedance $Z$, a positive number associated with a particular waveguide. The impedance allows us to define the relationship between the voltage waves and the current waves which were mentioned in the last section, which is:

$$U_j^+ = ZI_j^+ \tag{4.4a}$$

$$U_j^- = -ZI_j^- \tag{4.4b}$$

where $j = 1,2$ referring to Figure 4.1, which implies, from (4.1), that we have

$$I_2^+(n) = -I_1^-(n-m) \qquad I_1^+(n) = -I_2^-(n-m) \tag{4.5}$$

Thus current waves entering a bidirectional delay line are delayed by the same amount as their voltage wave counterparts, but with sign inversion. In view of (4.4), we need only propagate a particular type of wave (i.e., either voltage or current) in a particular waveguide. In a waveguide network, however, we are free to use different types of waves in different waveguides, converting between the different types with (4.4) where necessary.

The *admittance* $Y$ of the waveguide is defined by

$$Y = \frac{1}{Z}$$

and we define the physical current at either end of the waveguide, like the voltage, to be the sum of the wave components. Thus we have

$$I_j = I_j^+ + I_j^- \qquad j = 1,2 \tag{4.6}$$

### 4.2.3 Wave Equation Interpretation

The second-order PDE describing the voltage distribution $u(x,t)$ along an electrical transmission line with constant inductance and capacitance $l$ and $c$ per unit length and which runs parallel to the $x$-axis is

$$\frac{\partial^2 u}{\partial t^2} = \gamma^2 \frac{\partial^2 u}{\partial x^2} \tag{4.7}$$

where the *wave speed* $\gamma$ is $1/\sqrt{lc}$. As we saw in §1.1.1, the solution to this equation, if we set aside boundary conditions for the moment, can be written in terms of *traveling waves*:

$$u(x,t) = u^l(x+\gamma t) + u^r(x-\gamma t) \tag{4.8}$$

That is, the solution at any time $t \geq 0$ is made up of a sum of two shifted copies of the initializing functions $u^l(x)$ and $u^r(x)$, which have traveled to the left and right respectively with velocity $\gamma$ over a distance $\gamma t$. For any $\Delta$ we have, for the leftward-traveling wave, the identity

$$u^l(x+\gamma t) = u^l\big((x+\Delta)+\gamma(t-\Delta/\gamma)\big) \tag{4.9}$$

If we set $\gamma = \Delta/T$, then at time $t = nT$,

$$u^l(x+\gamma nT) = u^l\big((x+\Delta)+\gamma(n-1)T)\big) \tag{4.10}$$

Associate now with a particular waveguide a delay $T$ and a physical length $\Delta$, so that in Figure 4.1 $U_1^+$ represents an outgoing voltage wave quantity at position $x$, and $U_2^-$ an incoming wave at position $x+\Delta$. It is then clear that if we have $\Delta/T = \gamma$, then (4.10) is equivalent to the second equation of (4.1), with $m = 1$, and with $u^l(x+\gamma nT) = U_1^+(n)$ and $u^l(x+\Delta+\gamma(n-1)T) = U_2^-(n-1)$. A similar correspondence holds for the right-going traveling wave component $u^r$ and the wave variables at either end of the rightward waveguide, $U_1^-$ and $U_2^+$. A chain of bidirectional delay lines, connected in cascade will then implement an exact traveling wave solution to the wave equation. The physical voltage $u$ may be obtained (as should be clear from (4.8)) by summing the leftward and rightward traveling components at any particular location in the cascade, as per equation (4.3). Note that because $\gamma = \Delta/T$, the delay period and the waveguide length cannot be chosen independently, if the discrete wave quantities are to behave as traveling wave solutions to (4.7).

### 4.2.4 Note on the Different Definitions of Wave Quantities

Waveguides are sometimes defined in a slightly different way [165], as pictured in Figure 4.2. Now the superscripted + and − refer to a direction of propagation (to the right or left, respectively) rather than to outputs and inputs to the delay line pair. If we still assume (4.4a) and (4.4b) to

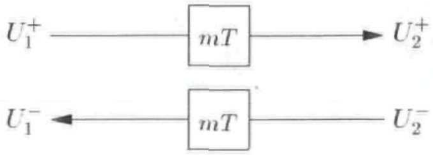

Figure 4.2: *Oriented bidirectional delay line.*

hold for some positive impedance $Z$, then this definition of wave quantities implies that there is a *direction* associated with a particular waveguide—that is, a leftward ($-$) traveling current wave is sign-inverted with respect to the leftward traveling voltage wave, but the same is not true for the rightward traveling waves. It should be obvious that this definition of wave quantities also leads to a traveling wave solution of the wave equation (indeed, the bidirectional delay line of Figure 4.1 is identical to that of Figure 4.2 if we are using only voltage waves). The difference here is that we can now interpret the traveling wave pair $(U, I)$ to be a solution to the ***transmission line*** or telegrapher's equations [28], a set of two first order PDEs (from which the wave equation is often derived):

$$l\frac{\partial i}{\partial t}+\frac{\partial u}{\partial x} = 0 \tag{4.11a}$$

$$c\frac{\partial u}{\partial t}+\frac{\partial i}{\partial x} = 0 \tag{4.11b}$$

which, for constant $l$ and $c$ has a solution

$$\begin{aligned} u(x,t) &= u_l(x+\gamma t)+u_r(x-\gamma t) \\ i(x,t) &= i_l(x+\gamma t)+i_r(x-\gamma t) \end{aligned}$$

where

$$u_l = -\sqrt{\frac{l}{c}}i_l \qquad\qquad u_r = \sqrt{\frac{l}{c}}i_r$$

and $\gamma$ is again given by $1/\sqrt{lc}$. It should be remarked that if we had chosen the relationship between the wave variables to be such that $(+)$ superscripted current wave were to be sign-inverted with respect to the $(+)$ voltage wave, then we would be solving the "mirror-image" PDEs that one would get if one replaced $x$ by $-x$ in system (4.11). The definition of wave variables (which we might call the "input-output" definition) given in §4.2.1 solves the wave equation which results from eliminating variables in system (4.11), or its mirror image, and hence does not have an orientation.

In practice, in order to proceed with numerical methods in systems of PDEs for which direction is important, we can either use the oriented wave variable definition given in this section, or we can use the input-output formulation, and reintroduce directionality into the network where appropriate.

We have chosen the latter course, and we will indicate which changes must be made (usually through the use of *transformers*) explicitly on the signal flow graph. From a programmer's point of view, there is no substantial difference between the algorithms which develop using the different definitions. Both definitions lead to the same scattering equations (to be discussed in the next section) and are identical from a power conservation point of view (that is to say, sign-inversions of wave quantities do not affect the energy measure of the network).

An additional reason for choosing the input-output definition of wave variables is that it will require less notational juggling when we eventually link DWNs to MDWD networks in §4.10.

### 4.2.5 Scattering Junctions

Returning to the "input-output" waveguide defined in §4.2.1 and §4.2.2, we now must deal with connecting bidirectional delay lines; this is done in the same way as in the wave digital filtering framework, namely through the use of Kirchoff's Laws, which conserve instantaneous power at a connection. The resulting equations relating input to output waves at such a connection or *scattering junction* are identical to the adaptor equations for wave digital filters already mentioned in §2.3.5. For completeness sake, we will re-derive the scattering equations for a series connection of $M$ bidirectional delay lines, of impedances $Z_j$, $j = 1, \ldots, M$.

At such a series connection, we must have

$$I_1 = I_2 = \ldots = I_M \triangleq I_J \tag{4.12}$$

$$U_1 + U_2 + \ldots + U_M = 0 \tag{4.13}$$

where $I_J$ is defined to be the *junction current* common to all waveguides.

Thus, we have

$$0 \overset{(4.13)}{=} \sum_{j=1}^{M} U_j \overset{(4.3)}{=} \sum_{j=1}^{M} \left(U_j^+ + U_j^-\right) \overset{(4.4a),(4.4b)}{=} \sum_{j=1}^{M} Z_j \left(I_j^+ - I_j^-\right) \overset{(4.6)}{=} \sum_{j=1}^{M} Z_j \left(2I_j^+ - I_j\right)$$

where the equation numbers appear over the equalities to which they pertain. Using (4.12), we can then write the equation used to calculate the *junction current* from the incoming current waves

$$I_J = \frac{2}{Z_J} \sum_{j=1}^{M} Z_j I_j^+$$

as well as the *scattering equation*

$$I_k^- = -I_k^+ + \frac{2}{Z_J} \sum_{j=1}^{M} Z_j I_j^+, \qquad k = 1, \ldots, M$$

where we have defined the *junction impedance* $Z_J$ by

$$Z_J \triangleq \sum_{j=1}^{M} Z_j$$

In terms of voltage waves, using (4.4a) and (4.4b), the scattering equations can be written as

$$U_k^- = U_k^+ - \frac{2Z_k}{Z_J}\sum_{j=1}^{M} U_j^+, \qquad k = 1, \ldots, M$$

This is identical to the definition of a wave digital series adaptor (2.31) for voltage waves, where we replace $U_k^-$ by $b_k$, $U_k^+$ by $a_k$ and $Z_k$ by $R_k$, for $k = 1, \ldots, M$.

The scattering equations for a dual parallel connection are similar under the replacement of $U_k^+$ and $U_k^-$ by $I_k^+$ and $I_k^-$, $Z_k$ by $Y_k$ and $Z_J$ by the *junction admittance*, defined by

$$Y_J \triangleq \sum_{j=1}^{M} Y_j$$

so that we have

$$U_J = \frac{2}{Y_J}\sum_{j=1}^{M} Y_j U_j^+ \tag{4.14}$$

and

$$U_k^- = -U_k^+ + \frac{2}{Y_J}\sum_{j=1}^{M} Y_j U_j^+, \qquad k = 1, \ldots, M \tag{4.15}$$

The representation we will use for scattering junctions in the waveguide networks in this and the subsequent chapter will usually be as shown in Figure 4.3 (in the case of a connection of four waveguides).

A waveguide's immittance is placed at the port at which it is connected to the junction, and the junction quantity to be calculated from incoming waves appears at the center of the junction. Sometimes, if there is no room in the figure, we will indicate the immittance of a waveguide by an overbrace (see, e.g., Figure 4.8). In the case of electrical variables, a junction current $I_J$ is calculated at a series junction, and a junction voltage $U_J$ at a parallel junction, but when we move to mechanical systems in the next chapter, we will of course use different variable names. A small "s" or "p" is placed in a corner of the junction in order to indicate that the junction is series or parallel, respectively. In addition, because it is only necessary to propagate one type of wave in a bidirectional delay line, *a graphical representation of a waveguide network will always imply the use*

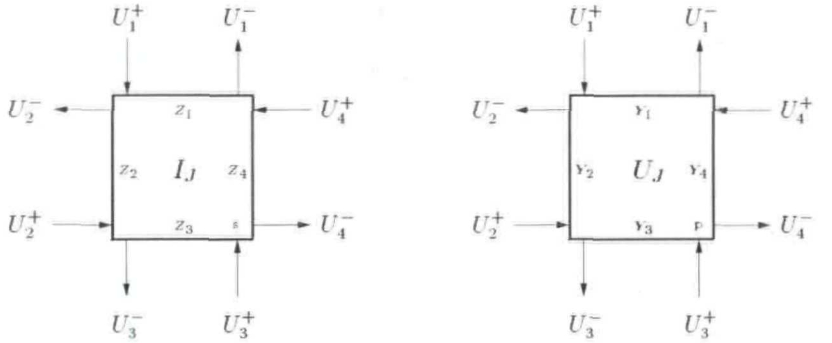

(a) (b)

Figure 4.3: *Graphical representations of scattering 4-port junctions*— (a) *series and* (b) *parallel.*

*of voltage waves everywhere.* This is the same convention that is used in wave digital signal flow graphs. This is important, because it will be recalled from §4.2.2 that current waves require an additional sign inversion that is not shown in the network diagrams.

Instantaneous power is preserved at the scattering junction (here again, as in the WDF case, the scattering junction is no more than a wave variable implementation of Kirchoff's Laws, which preserve power by definition). The power-normalization strategy employed in the wave digital filter setting can also be used here as well, and gives rise to the same orthogonality property of the scattering junction in either the series or parallel case (see §2.3.5). Power-normalized waves can be used in order to construct time-varying passive waveguide networks [165], though for time-invariant problems, the use of such power-normalized quantities involves more arithmetic operations.

### 4.2.6 Vector Waveguides and Scattering Junctions

It is also possible to extend a DWN to the vector case [167, 169]; this has also been done in the WDF framework in [46, 131], as discussed in §2.3.7. We briefly introduce vector waveguides, because it will be necessary to apply them when simulating the behavior of stiff systems and elastic solids; we will examine this problem in depth in Chapter 5.

A vector waveguide accepts two incoming signals $\hat{\mathbf{U}}_1^-$ and $\hat{\mathbf{U}}_2^-$ and outputs $\hat{\mathbf{U}}_1^+$ and $\hat{\mathbf{U}}_2^+$; all are assumed to be $q \times 1$ vectors (note that we have used $z$-transformed quantities here). The waveguide itself, like its scalar counterpart, is described by two parameters: its *impedance* $\mathbf{Z}$, a $q \times q$ matrix, which we will assume to be constant and symmetric positive definite (though it may be generalized to a para-Hermitian matrix function of the unit delay $z^{-1}$ [169]) and its *generalized delay*, $\mathbf{H}(z^{-1})$, a $2q \times 2q$ matrix function of the unit delay, which we assume to be para-unitary (lossless) [193]. The input and output voltage waves are related by

$$\begin{bmatrix}\hat{\mathbf{U}}_1^+(z^{-1})\\ \hat{\mathbf{U}}_2^+(z^{-1})\end{bmatrix} = \mathbf{H}(z^{-1})\begin{bmatrix}\hat{\mathbf{U}}_2^-(z^{-1})\\ \hat{\mathbf{U}}_1^-(z^{-1})\end{bmatrix}$$

(In applications in Chapter 5, where bidirectional delay lines are extracted from an MDKC, we will always set $\mathbf{H}(z^{-1})$ to be a multiple of the $2q \times 2q$ identity matrix.) We can define instantaneous current wave vectors $\mathbf{I}_j^+$ and $\mathbf{I}_j^-$, for $j = 1, 2$, and Ohm's Law becomes, in the vector case,

$$\mathbf{U}_j^+ = \mathbf{Z}\mathbf{I}_j^+ \qquad\qquad \mathbf{U}_j^- = -\mathbf{Z}\mathbf{I}_j^-$$

The scattering equations at a series or parallel junction of $k$ waveguides generalize in a straightforward way to the vector case—we have

$$\mathbf{I}_k^- = -\mathbf{I}_k^+ + 2\mathbf{Z}_J^{-1}\sum_{j=1}^{M}\mathbf{Z}_j\mathbf{I}_j^+ \qquad \text{Series junction} \qquad (4.16a)$$

$$\mathbf{U}_k^- = -\mathbf{U}_k^+ + 2\mathbf{Y}_J^{-1}\sum_{i=1}^{M}\mathbf{Y}_j\mathbf{U}_j^+ \qquad \text{Parallel junction} \qquad (4.16b)$$

for $k = 1, \ldots, M$, where $\mathbf{Y}_j = \mathbf{Z}_j^{-1}$ is the admittance of the $j$th waveguide, which must exist because $\mathbf{Z}_j$ is assumed positive definite (for passivity) [167]. The *vector junction admittance and impedance* are defined by

$$\mathbf{Z}_J \triangleq \sum_{j=1}^{M}\mathbf{Z}_j \qquad \text{Series junction}$$

$$\mathbf{Y}_J \triangleq \sum_{j=1}^{M}\mathbf{Y}_j \qquad \text{Parallel junction}$$

By virtue of the fact that they are sums of positive definite matrices, they will also be positive definite, and thus their inverses, used in the scattering equations (4.16), must exist. Vector waveguides were explored extensively in [169] in the context of artificial reverberation. Power normalization may also be applied by scaling the wave variables by a square root of the impedance (which is non-unique) [167]. Vector junction passivity has been shown to hold in the fixed word-length case in [167].

### Vector/Scalar Waveguide Coupling

In a few cases, it is useful to have a means of connecting vector and scalar network elements. This comes up when designing networks to simulate mixed vector/scalar systems of PDEs; in particular, it will be necessary to use vector methods when working in non-orthogonal coordinate systems (see §4.8) and in the WDF context for some of the mechanical systems of Chapter 5.

We will always assume that for any given scattering junction, the number of components of any approaching wave is the same at every port; it may not be, however, that every junction in the network accepts waves with some universal number of components. In particular, a vector waveguide, one of whose ends is connected to a vector junction may be split into several scalar waveguides, or more generally into a number of vector waveguides each with a smaller number of components. Similarly, it is possible to "bundle" several waveguides into a single larger waveguide.

Let us assume that all splittings and bundlings are from vector to strictly scalar and scalar to vector respectively. An element which splits a single three-component waveguide into three scalar waveguides is shown in Figure 4.4(a), and its simplified graphical representation for arbitrary $q$ in (b). In (b) the admittance of the $j$th scalar waveguide, $j = 1, \dots, q$ is $Y_j$, and the voltage waves entering and leaving the splitter at the connection with this waveguide are $U_j^+$ and $U_j^-$. On the other side of the connection, we have a single $q$-vector waveguide, of matrix admittance $\mathbf{Y}$. The column vector voltage waves entering and leaving the connection are $\mathbf{V}^+$ and $\mathbf{V}^-$. In order for this connection to make sense, we must choose $\mathbf{Y} = \mathrm{diag}(Y_1, \dots, Y_q)$, and order the splitting such that the $j$th components of $\mathbf{V}_-$ and $\mathbf{V}_+$ are equal to $U_j^+$ and $U_j^-$ respectively; such an ordering for a 1:3 splitting is shown in (a). In this case, it is easy to see that energy is conserved across such a connection (indeed, if the scalar waveguides are thought of as acoustic tubes, then the black bar in (b) is merely equivalent to a "rubber band" joining them). The power entering the connection from the vector side can be written as

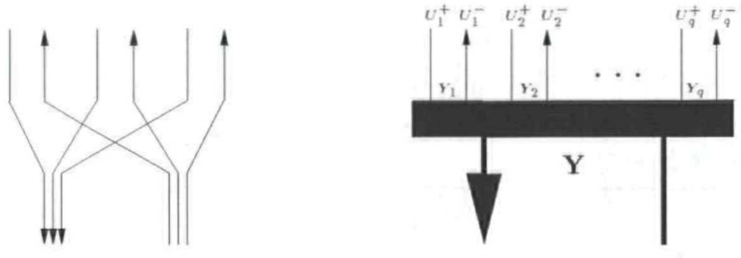

(a) (b)

Figure 4.4: (a) *Element for splitting of a vector waveguide into three scalar waveguides and* (b) *a simplified graphical representation in the general case of $q$ scalar waveguides.*

$$(\mathbf{V}^+ + \mathbf{V}^-)^T \mathbf{Y} (\mathbf{V}^+ - \mathbf{V}^-) = -\sum_{j=1}^{q} (U_j^+ + U_j^-) Y_j (U_j^+ - U_j^-)$$

which is the total power leaving the connection through the scalar waveguides. It is important to note that such a connection can not be viewed as a multi-port element. In addition, passivity is contingent upon this choice of $\mathbf{Y}$. It is easy to generalize this picture to a connection which splits a vector waveguide into various smaller vector waves (instead of scalars). In that case, **Y** should be chosen to be the block diagonal "direct sum" of the various matrix admittances on the other side of the connection.

### 4.2.7 Music and Audio Applications of Digital Waveguides

Digital waveguide networks have been widely applied towards the synthesis of musical sound. Significant portions of many musical instruments can be simply modeled as nearly lossless uniform transmission lines: strings support transverse wave motion, and stiff strings and bars allow longitudinal and torsional motion as well; acoustic waves travel in the tubes that make up brass and wind instruments, organ pipes, as well as the human vocal tract, as we saw in §1.1.1. As such, there is a *traveling wave decomposition* of the motion in these systems.

As we already mentioned in §4.2.3, a bidirectional delay line can be thought of as a discrete-time description of traveling wave propagation in a uniform transmission line. Thus a single waveguide, which is in itself no more than a pair of delay lines, can be used to model an uninterrupted stretch of a tube or string, without requiring any machine arithmetic. Scattering occurs only at the ends of the waveguide, and in fact, it is possible to use bidirectional delay lines to model wave propagation even in lossy [160] or dispersive [199] media by consolidating these effects at the terminations. If the length of the string or tube does not correspond to an integer number of delays at a given sample rate, then it is possible to employ *fractional delay lines* [114, 195], which approximate non-integer delay lengths using all-pass (lossless) filters[†]. A typical situation is shown in Figure 4.5. The string (or tube) is modeled as two bidirectional delay lines; at the extreme left and right, digital filters may be employed which model bridge terminations [164], horn bells and acoustic radiation [15, 160], coupling with an instrument body or resonator such as a stringed instrument body [102], and, conceivably, coupling between different strings, and for a stiff string, even coupling between

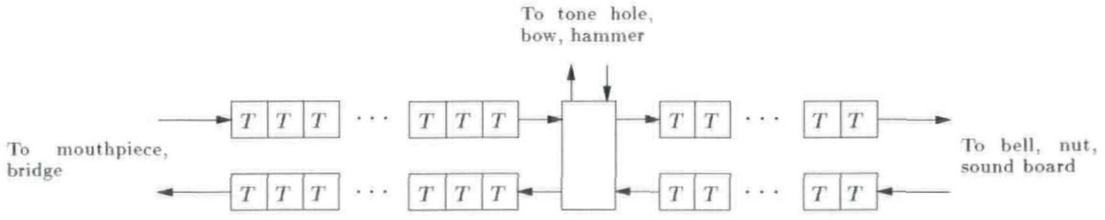

Figure 4.5: *Typical digital waveguide configuration for musical sound synthesis.*

---

[†] This is often essential, because working at the audio sampling rate often forces a large grid spacing. In an acoustic tube, for example, the wave speed is $\gamma = 330$ m/s. At the audio sampling rate we will have a waveguide delay of $T = 1/44100$ s, which implies a waveguide length of $\Delta = 330/44100$ m $= 0.75$ cm. For a woodwind instrument, this distance is on the order of the tone hole separation distance, and will thus be far too crude for good physical modelling.

different types of motion (i.e. transverse, longitudinal and torsional). Excitation mechanisms (such as mouth pressure for a woodwind instrument [164] and lip pressure in brasses [15]) may be modeled as sources, are also used to terminate the waveguide; these may be linearly or nonlinearly coupled to the instrument body. If wave propagation is disturbed along the length of the tube or string, either by an excitation (such as a piano hammer [197] or bow [164]), or by an impedance change (due perhaps to a woodwind tone hole [160, 194, 196], or a change in the cross-sectional area of the vocal tract [30]), then these effects may be modeled at the junction between the two waveguides. In some situations, it may be necessary to employ a larger network of interconnected waveguides, as when the vocal tract is to be coupled with the nasal passageways. A full articulatory model of the human vocal tract has been built in this way to simulate the singing voice [30].

Digital waveguide networks have also been used to simulate wave motion in higher dimensions, in which case they are sometimes called *waveguide meshes* [198, 200]; cases of particular interest have been (2+1)D meshes (see §1.1.2) used to simulate the vibration of a uniform membrane [67], and (3+1)D meshes used to model acoustic spaces [156]. Many different types of mesh have been proposed; they differ chiefly in their numerical dispersion properties [157], and we will analyze these forms in detail in Appendix A. A good deal of recent work has gone into the problem of correcting numerical dispersion by introducing terminating filters at the boundaries, and by using interpolation and frequency warping techniques [157]. A (2+1)D rectilinear mesh is shown in Figure 4.6(a). Unit-sample bidirectional delay lines (here represented by two-headed arrows) are connected to scattering junctions (white circles) located at the nodes of a rectangular lattice. Such a mesh has been used to model drum heads as well as gongs (where a nonlinear mesh termination has been applied) [197]. We mentioned in §1.1.2 that this mesh indeed solves the (2+1)D wave equation numerically [198]. We will elaborate on this idea extensively throughout the rest of the chapter.

Waveguide networks have also been used in a quasi-physical manner in order to effect artificial reverberation [163]. In this case, an unstructured network of waveguides of possibly time-varying impedance is used; such a network is shown in Figure 4.6(b), where the number of samples of delay in each waveguide (integers $a$ through $h$) may be different. Such networks are passive, so that signal energy injected into the network from a dry source signal will produce an output whose amplitude will gradually attenuate, with frequency-dependent decay times dependent on the delays and immittances of the various waveguides—some of the delay lengths can be interpreted as implementing "early reflections."[163]. Such networks provide a cheap and stable way of generating rich impulse responses. Generalizations of waveguide networks to feedback delay networks (FDNs) [149] and circulant delay networks [150] have also been explored, also with an eye towards applications in digital reverberation.

We will call these DWNs used for reverberation *unstructured*; by this we mean that the waveguides and scattering junctions are not necessarily arranged according to a regular grid in any coordinate system. Yet such a network is, by construction, passive. This contrasts sharply with the MDWD networks discussed in the previous chapter. In that case, discretization is performed through the use

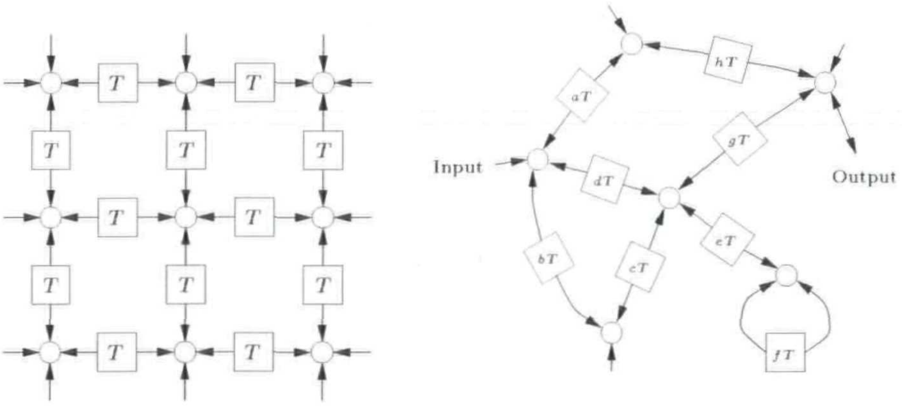

(a) (b)

Figure 4.6: *Other waveguide network configurations*— (a) *a (2+1)D waveguide mesh, and* (b) *an unstructured network suitable for implementing artificial reverberation.*

of a spectral mapping or integration rule; implicit in such an approach is that the algorithm operates on a regular grid in some system of coordinates (and the same will be true of the DWNs that are derived through an MDWD-like discretization procedure, as will be discussed in §4.10). The reason for this is that the DWN, as we have described it in this section, is essentially a large network of lumped elements, whereas the MDWD network is a multidimensional object. In certain cases (see §4.9), unstructured DWNs may come in handy.

### 4.2.8 Transitional Note

We have now finished reviewing the fundamentals of digital waveguide networks. On the more practical level of the implementation of DWNs, there are many more topics which deserve elaboration, including strategies for reducing the numbers of delays, and also various normalization techniques which can be used to vary the number of required arithmetic operations. In this last respect, we note that it is possible to establish formal links between chains of bidirectional delay lines and other similar filter designs such as the normalized ladder form [80], etc. We refer the reader to [166] for an in-depth treatment.

## 4.3 The (1+1)D Transmission Line

We return now to the transmission line, which served as a useful model problem for MDWD network methods in §3.7 of the last chapter, and show that its numerical solution can also be approached using waveguide networks. The material in this section has also appeared in [19].

### 4.3.1 First-order System and the Wave Equation

We recall that the set of PDEs which describes the evolution of the voltage and current distributions along a lossless, source-free transmission line in (1+1)D is:

$$l\frac{\partial i}{\partial t}+\frac{\partial u}{\partial x} = 0 \tag{4.17a}$$

$$c\frac{\partial u}{\partial t}+\frac{\partial i}{\partial x} = 0 \tag{4.17b}$$

where $i(x,t)$ and $u(x,t)$ are, respectively, the current in and voltage across the lines, and $l(x)$ and $c(x)$, both assumed strictly positive everywhere, are the inductance and capacitance per unit length. For the moment, we will leave aside the discussion of boundary conditions, and deal only with the Cauchy problem (i.e., we assume the spatial domain of the problem to be the entire $x$ axis). Note also that this system includes the vocal tract model (1.20) as a special case, under an appropriate set of variable and parameter replacements.

As discussed in §4.2.3, if we assume that $l$ and $c$ are constant, then the set of equations can be reduced to a single second order equation in the voltage alone[†]:

$$\frac{\partial^2 u}{\partial t^2}=\gamma^2\frac{\partial^2 u}{\partial x^2} \tag{4.18}$$

where the *wave speed* $\gamma$ is given by

$$\gamma=\frac{1}{\sqrt{lc}}$$

This equation and its analogues in higher dimensions (see Appendix A) are collectively known as the *wave equation.* The solution, as mentioned in §4.2.3, can be written in terms of traveling waves. In the (1+1)D case, we can write an identical wave equation in the current alone, but this does not hold in higher dimensions.

### 4.3.2 Centered Difference Schemes and Grid Decimation

Suppose we are interested in developing a finite difference scheme to calculate the solution to (4.17) numerically. We first define *grid functions* $I_i(n)$, and $U_i(n)$ which, for convenience, will run over half-integer values of $i$ and $n$, i.e.,

$$i,n=\ldots-1,-\tfrac{1}{2},0,\tfrac{1}{2},1\ldots$$

---

[†] Even if $l$ and $c$ are functions of $x$, it is still possible to reduce system (4.17) to a second order equation in the voltage alone, but it does not have the simple form of (4.18).

They are intended to approximate $i$ and $u$ at the points $(i\Delta, nT)$, where $\Delta$ is the spatial grid step, and $T$ the time step. We note that we have used the same variable, $i$, to stand for both the continuous-time current which solves (4.17), as well as the discrete-valued variable representing the spatial coordinate on the grid.

We have the *centered difference* approximations

$$\left.\frac{\partial w}{\partial t}\right|_{i\Delta,nT} = \frac{w(i\Delta,(n+\frac{1}{2})T)-w(i\Delta,(n-\frac{1}{2})T)}{T}+O(T^2) \tag{4.19a}$$

$$\left.\frac{\partial w}{\partial x}\right|_{i\Delta,nT} = \frac{w((i+\frac{1}{2})\Delta,nT)-w((i-\frac{1}{2})\Delta,nT)}{\Delta}+O(\Delta^2) \tag{4.19b}$$

where $w$ stands for either of $i$ or $u$.

Employing these differences in (4.17), and replacing the continuous time/space variables $i$ and $u$ by their respective grid functions yields the difference scheme

$$I_i(n+\tfrac{1}{2}) - I_i(n-\tfrac{1}{2}) + \frac{1}{v_0\bar{l}_i}\left(U_{i+\frac{1}{2}}(n)-U_{i-\frac{1}{2}}(n)\right)=0 \tag{4.20a}$$

$$U_i(n+\tfrac{1}{2}) - U_i(n-\tfrac{1}{2}) + \frac{1}{v_0\bar{c}_i}\left(I_{i+\frac{1}{2}}(n)-I_{i-\frac{1}{2}}(n)\right)=0 \tag{4.20b}$$

Here, we have chosen

$$\bar{l}_i \triangleq l(i\Delta)+O(\Delta^2) \tag{4.21a}$$

$$\bar{c}_i \triangleq c(i\Delta)+O(\Delta^2) \tag{4.21b}$$

for half-integer $i$. Because the centered difference approximations (4.19) are second-order accurate, $l$ and $c$ may be approximated to the same order without any decrease in accuracy. We leave the exact form of these approximations, $\bar{l}$ and $\bar{c}$ unspecified for the moment, but will return to various settings in §4.3.6. Also, in order to remain consistent with the notation in the MDWD schemes of the last chapter, we have set

$$v_0 \triangleq \frac{\Delta}{T}$$

Thus difference equations (4.20) are consistent with (4.17), and accurate to $O(\Delta^2, T^2)$.

In a difference scheme for a general system of PDEs, it would be necessary to update all the grid functions every time step, and at every grid point—that is to say, at every increment in $n$ and $i$ of one-half, new values of the grid functions would have to be calculated, and indeed, we can proceed in this manner in with the scheme (4.20) as well. In this case, however, it is easy to see that updating $U_k(m)$, for $2k$ and $2m$ even requires access only to $I_k(m)$ at the previous time step, and at *neighboring* grid locations (thus for $2m$ odd and $2k$ odd), as well as $U$ at the same location, two time steps previously ($2m$ and $2k$ again even) [131, 184]. Similarly, updating $I_k(m)$ for $2m$ odd and $2k$ odd involves only values of $U$ for $2m$ even and $2k$ even, and $I$ for $2m$ odd and $2k$ odd. It is then obvious that only values of $U_k(m)$ for which $2m$ is even and $2k$ even (and values of $I_k(m)$ with $2m$ odd and $2k$ odd) need enter into our scheme. We can thus *decimate* the grid in the manner shown in Figure 4.7. We calculate the values of $U_i(n)$ at the grey dots in Figure 4.7, and $I_{i+\frac{1}{2}}(n+\frac{1}{2})$ at the white dots. The difference scheme on the decimated grid can be written as

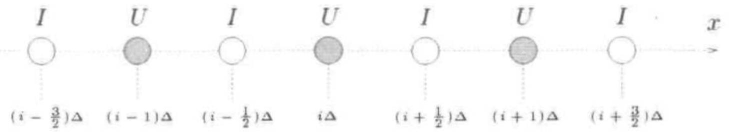

Figure 4.7: *Interleaved sampling grid for the (1+1)D transmission line.*

$$I_{i+\frac{1}{2}}(n+\tfrac{1}{2}) - I_{i+\frac{1}{2}}(n-\tfrac{1}{2}) + \frac{1}{v_0\bar{l}_{i+\frac{1}{2}}}\left(U_{i+1}(n)-U_i(n)\right) = 0 \tag{4.22a}$$

$$U_i(n)-U_i(n-1)+\frac{1}{v_0\bar{c}_i}\left(I_{i+\frac{1}{2}}(n-\tfrac{1}{2})-I_{i-\frac{1}{2}}(n-\tfrac{1}{2})\right) = 0 \tag{4.22b}$$

for $i$, $n$ *integer*. We perform the calculation on the decimated grid with no decrease in accuracy, although we are of course approximating the solution at fewer grid points. In analogy with the continuous case, when $l$ and $c$ are constant it is possible to combine the difference equations (4.22) into a single equation for the voltage grid function $U$, which is

$$U_i(n+1)-2U_i(n)+U_i(n-1)=\frac{\gamma^2}{v_0^2}\left(U_{i+1}(n)-2U_i(n)+U_{i-1}(n)\right) \tag{4.23}$$

and which solves the (1+1)D wave equation (4.18). For the so-called *magic* time step [184],

$$v_0=\gamma\triangleq\frac{1}{\sqrt{lc}}$$

the difference scheme (4.23) reduces to

$$U_i(n+1)+U_i(n-1)=U_{i+1}(n)+U_{i-1}(n) \tag{4.24}$$

a form which has great relevance to the discussion to follow on the waveguide implementation. It is interesting that in this case, the grid may be *further* decimated; we need only calculate $U_i(n)$ for $i+n$ even (or odd), for $i$, $n$ integer. We will examine this point in further detail in higher dimensions in Appendix A.

### 4.3.3 A (1+1)D Waveguide Network

Consider the waveguide network pictured in Figure 4.8. Each scattering junction (in this case parallel) is connected to its two neighbors by unit sample bidirectional delay lines. The spacing of the junctions is $\Delta$ and the waveguide delays are of duration $T$. The voltage at a junction with coordinate $i\Delta$ and at time $nT$ is denoted by $U_{J,i}(n)$ for integer $i$ and $n^{\dagger}$.

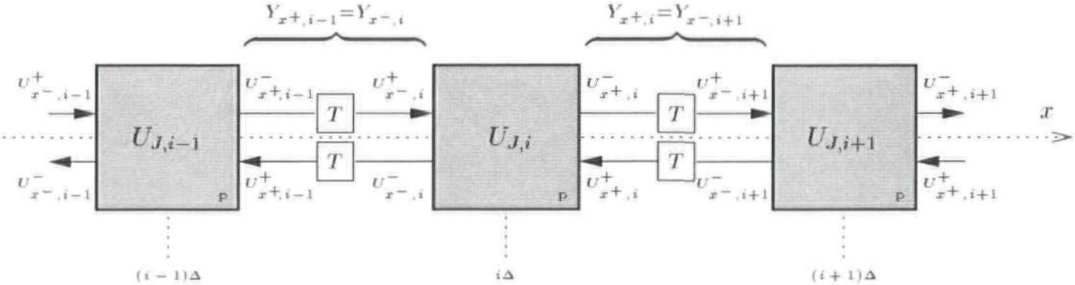

Figure 4.8: *(1+1)D waveguide network.*

We can name the voltages and current flows in individual waveguides in the following way. At junction $i$, the line voltages are:

$$U_{x^+,i} = \text{voltage in waveguide leading east}$$
$$U_{x^-,i} = \text{voltage in waveguide leading west}$$

and the flows are:

$$I_{x^+,i} = \text{current flow in waveguide leading east}$$
$$I_{x^-,i} = \text{current flow in waveguide leading west}$$

The constraints, imposed by Kirchoff's Laws at a parallel junction, are:

$$U_{J,i} = U_{x^+,i} = U_{x^-,i} \qquad\qquad I_{x^+,i} + I_{x^-,i} = 0 \tag{4.25}$$

As discussed in §4.2, the voltages and current flows in the individual waveguides can be further broken up into *incoming* and *outgoing* waves. That is, we have, at a junction at grid location $i$:

$$U_{q,i} = U^+_{q,i} + U^-_{q,i} \qquad\qquad I_{q,i} = I^+_{q,i} + I^-_{q,i}$$

where $q$ is either of $x^+$ or $x^-$. The variables superscripted with a + refer to the incoming waves,

---

[†] In any case where the time index $n$ is omitted, we mean for the statement to hold at any time step.

and those marked $-$ to outgoing waves. In a particular waveguide section, the current and voltage waves are related by:

$$I^{+}_{q,i} = Y_{q,i}U^{+}_{q,i} \qquad\qquad I^{-}_{q,i} = -Y_{q,i}U^{-}_{q,i} \tag{4.26}$$

where $Y_{q,i}$ is the characteristic admittance of the waveguide connected to junction $i$ in direction $q$. In addition, because the junctions at $i$ and $i+1$ are connected to opposite ends of the same waveguide, we have

$$Y_{x^-,i+1} = Y_{x^+,i}$$

As before, we will also define the *impedance* of any waveguide to be

$$Z_{q,i} = \frac{1}{Y_{q,i}}$$

At a particular parallel junction, the junction admittance will thus be

$$Y_{J,i} \triangleq Y_{x^+,i} + Y_{x^-,i}$$

In this case, from (4.14), the junction voltage can be written in terms of incoming wave variables as

$$U_{J,i} = \frac{2}{Y_{J,i}}\left(Y_{x^-,i}U^{+}_{x^-,i} + Y_{x^+,i}U^{+}_{x^+,i}\right) \tag{4.27}$$

and the outgoing voltage waves from any junction are related to the incoming waves by

$$U^{-}_{r,i} = -U^{+}_{r,i} + U_{J,i}$$

where $r$ refers to either of the directions $x^+$ or $x^-$.

The incoming voltage wave entering each junction from a particular waveguide at time step $n$ is simply the outgoing voltage wave leaving a neighboring junction, one time step before. Reading directly from Figure 4.8, we have

$$U^{+}_{x^+,i}(n) = U^{-}_{x^-,i+1}(n-1) \tag{4.28a}$$
$$U^{+}_{x^-,i}(n) = U^{-}_{x^+,i-1}(n-1) \tag{4.28b}$$

The case of flow waves is similar except for a sign inversion—that is, we have

$$I^{+}_{x^+,i}(n) = -I^{-}_{x^-,i+1}(n-1) \tag{4.29a}$$
$$I^{+}_{x^-,i}(n) = -I^{-}_{x^+,i-1}(n-1) \tag{4.29b}$$

As discussed in §4.2, we can perform all calculations using voltage waves; in the waveguide networks pictured in this chapter, we will always assume, without loss of generality, that we are dealing with voltage waves.

### 4.3.4 Waveguide Network and the Wave Equation

Now consider the case in which $Y_{q,i} = Y$ is invariant over $i$ (and thus $q$, where again, $q$ stands for either $x^+$ or $x^-$). At all junctions, then, we have $Y_{J,i} = 2Y$. From (4.3.3) and (4.28), it is possible to obtain a finite difference scheme purely in terms of the junction voltages $U_{J,i}$. Beginning from (4.27), we have

$$\begin{aligned}
U_{J,i}(n+1) &= \frac{2}{Y_{J,i}}\Big(Y_{x^-,i}U^+_{x^-,i}(n+1) + Y_{x^+,i}U^+_{x^+,i}(n+1)\Big) \\
&= U^-_{x^+,i-1}(n) + U^-_{x^-,i+1}(n) \\
&= U_{J,i-1}(n) + U_{J,i+1}(n) - U^+_{x^+,i-1}(n) - U^+_{x^-,i+1}(n) \\
&= U_{J,i-1}(n) + U_{J,i+1}(n) - U^-_{x^-,i}(n-1) - U^-_{x^+,i}(n-1) \\
&= U_{J,i-1}(n) + U_{J,i+1}(n) - U_{J,i}(n-1) \qquad (4.30)
\end{aligned}$$

This is identical to (4.24) if we replace $U_J$ by $U$. In this case of identical impedances in all the waveguides, there is no scattering, so the parallel junctions in Figure 4.8 reduce to simple "throughs," and Figure 4.8 becomes Figure 4.9. Thus we have a discrete equivalent to the traveling wave solution to the wave equation, to be expected when the impedance does not vary spatially along the line. This particular case, which is trivial to implement (as a *single* many sample bidirectional delay line), has enormous applications to (1+1)D problems in homogeneous media, as were mentioned in §4.2.7. We also note that if the impedances do vary from one waveguide to the next, as in Figure 4.8, then we have a useful model of a system such as a tube with varying cross-sectional area or horn [66], a system whose impedance varies along its length, but whose *wave speed* remains constant. (In order

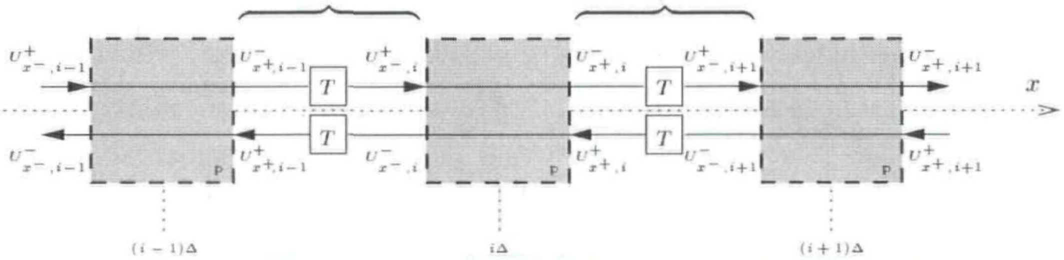

Figure 4.9: *Simplified (1+1)D waveguide network.*

to deal with local changes in the wave speed, we will have to introduce self-loops, which we will do shortly in §4.3.6.) This waveguide network is essentially equivalent to the Kelly-Lochbaum model used in speech synthesis [104], which we discussed in §1.1.1. It is interesting that linear predictive coding (LPC) [124], which is used to design filters to fit the spectrum of an analysis signal, essentially synthesizes a waveguide network like the one shown in Figure 4.8 (in effect it produces, as a by-product of the main calculation of direct-form filter coefficients, the *reflection coefficients* at the scattering junctions, from which impedances can then be deduced).

**Comment on Numerical Instability**

We have just shown, in the derivation ending with (4.30), that scattering in a particular waveguide network can be rewritten as a finite difference scheme purely in terms of the *junction* quantities. Thus all numerical solutions obtained using the waveguide network implementation could also be obtained (at least in infinite-precision arithmetic) using such a scheme. It is interesting to note that certain solutions to the finite difference equation (4.30) can not be obtained using the DWN, if we require that the wave variables in the network be *bounded in magnitude*. As a very simple example, consider initializing scheme (4.24) with $U_i(0) = -1$ and $U_i(1) = 1$, for all $i$. Then we will have $U_i(2) = 3$, $U_i(3) = 5$, and in general, $U_i(n) = 2n - 1$ for all $i$. Similar linear growth will result from setting $U_i(0) = U_i(1) = (-1)^i$. We will then have, at any future time step $n$, $U_i(n) = (2n-1)(-1)^{i+n-1}$.

Though these solutions would appear to be completely unphysical, it is worth mentioning that the (1+1)D wave equation (to which (4.24) is an approximation) admits linear growth as well; $u = t$, for example, is a solution to (4.18). It is possible to view this solution as the sum of two traveling wave solutions $(x/\gamma + t)/2$ and $(-x/\gamma + t)/2$; these, however are unbounded in magnitude, and thus the wave variables used to initialize the DWN will be as well; the finite difference scheme, on the other hand, produces this behavior for the bounded initial conditions mentioned above. It is important to note that this linear growth occurs at the spatial DC and Nyquist frequencies; it is simple to show that these are in fact the only spatial frequencies for which scheme (4.24) will admit such behavior. We will return to this point in some detail in Appendix A, because the analysis is somewhat easier in the frequency domain.

### 4.3.5 An Interleaved Waveguide Network

The simplified waveguide network described above solves the wave equation for voltage, at the magic time step, $T = \Delta/\gamma$. That is, the junction voltages $U_J$ solve the difference equation (4.24), and hence approximate $u$. We would, however, like to be able to have direct access to a discrete equivalent of the other variable as well, the current $i$.

Bearing in mind the discussion in §4.3.2 on interleaved grids, examine the identity pictured in Figures 4.10 and 4.11. We have merely split the unit sample bidirectional delay line into two half-

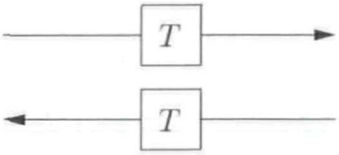

Figure 4.10: *Bidirectional delay line.*

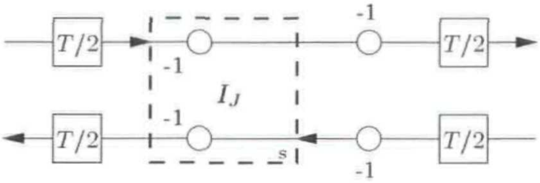
T/2
T/2
T/2
T/2
-1
-1
-1
-1
$I_J$
s

Figure 4.11: *Split equivalent to the bidirectional delay line.*

sample delay lines of equal impedance, and placed a *series* junction (in cascade with sign inverters) in between. In this case, since there is no scattering, the net behavior of the junction and sign inversion is that of a simple "through," with sign inversions exactly canceling those that appear in the signal path (these can be added formally using transformers). Later we will add additional ports to this new junction. We introduce these series junctions so as to be able to associate a junction current with them, which we will identify with the physical current in the transmission line.

If we now replace all the bidirectional delay lines in Figure 4.8 by the split pair of lines, then we get the arrangement in Figure 4.12. As at the parallel junctions, we can define wave voltages

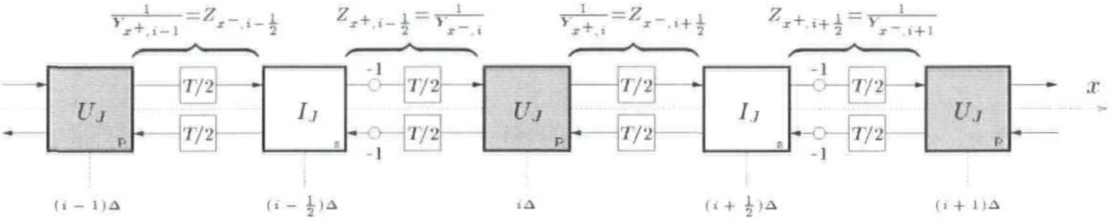
$\frac{1}{Y_{x^+,i-1}}=Z_{x^-,i-\frac{1}{2}}$
$Z_{x^+,i-\frac{1}{2}}=\frac{1}{Y_{x^-,i}}$
$\frac{1}{Y_{x^+,i}}=Z_{x^-,i+\frac{1}{2}}$
$Z_{x^+,i+\frac{1}{2}}=\frac{1}{Y_{x^-,i+1}}$
$U_J$
$I_J$
$U_J$
$I_J$
$U_J$
T/2
-1
p
s
$x$
$(i-1)\Delta$
$(i-\frac{1}{2})\Delta$
$i\Delta$
$(i+\frac{1}{2})\Delta$
$(i+1)\Delta$

Figure 4.12: *(1+1)D interleaved waveguide network.*

and currents at the series junctions, which we will index by $i+\frac{1}{2}$ for $i$ integer. Furthermore, we name the impedances at the left- and right-hand ports of the series junctions $Z_{x^-,i-\frac{1}{2}}$ and $Z_{x^+,i-\frac{1}{2}}$ respectively. As indicated in Figure 4.12, we must also have

$$Z_{x^+,i-\frac{1}{2}}=\frac{1}{Y_{x^-,i}} \qquad\qquad Z_{x^-,i+\frac{1}{2}}=\frac{1}{Y_{x^+,i}}$$

The junction impedance at the series junctions will be

$$Z_{J,i+\frac{1}{2}} \triangleq Z_{x^-,i+\frac{1}{2}}+Z_{x^+,i+\frac{1}{2}}=\frac{1}{Y_{x^+,i}}+\frac{1}{Y_{x^-,i+1}}$$

See Figure 4.13 for a complete picture of the various wave quantities at the interleaved junctions.

Assuming that the impedances in all the delay lines are identical and equal to $Z$ (and so $Z_{J,i-\frac{1}{2}}=$

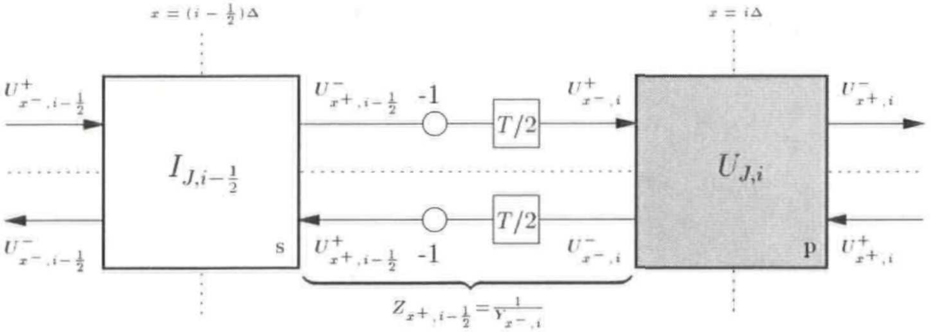
$x=(i-\frac{1}{2})\Delta$
$x=i\Delta$
$U^{+}_{x^-,i-\frac{1}{2}}$
$U^{-}_{x^-,i-\frac{1}{2}}$
$I_{J,i-\frac{1}{2}}$
s
$U^{-}_{x^+,i-\frac{1}{2}}$
-1
$U^{+}_{x^+,i-\frac{1}{2}}$
-1
$T/2$
$T/2$
$U^{+}_{x^-,i}$
$U^{-}_{x^-,i}$
$U_{J,i}$
p
$U^{-}_{x^+,i}$
$U^{+}_{x^+,i}$
$Z_{x^+,i-\frac{1}{2}}=\frac{1}{Y_{x^-,i}}$

Figure 4.13: *Wave quantities in the interleaved network of Figure 4.12.*

$2Z$), we can now define

$$\begin{aligned}
I_{J,i-\frac{1}{2}} &= \frac{2}{Z_{J,i-\frac{1}{2}}}\left(Z_{x^+,i-\frac{1}{2}}I^{+}_{x^+,i-\frac{1}{2}} + Z_{x^-,i-\frac{1}{2}}I^{+}_{x^-,i-\frac{1}{2}}\right)\\
&= I^{+}_{x^+,i-\frac{1}{2}} + I^{+}_{x^-,i-\frac{1}{2}}
\end{aligned}$$

We also have that

$$\begin{aligned}
U^{+}_{x^-,i}(n) &= -U^{-}_{x^+,i-\frac{1}{2}}(n-\tfrac{1}{2})\\
U^{+}_{x^+,i-\frac{1}{2}}(n+\tfrac{1}{2}) &= -U^{-}_{x^-,i}(n)
\end{aligned}$$

and (4.26) holds as before.

We now show that this waveguide network performs a calculation identical to that which we would get for centered differences on a decimated grid, exactly as in Figure 4.7. For integer $i$ and $n$, we have:

$$\begin{aligned}
U_{J,i}(n) &= U^{+}_{x^+,i}(n) + U^{+}_{x^-,i}(n)\\
&= Z\left(I^{+}_{x^+,i}(n) + I^{+}_{x^-,i}(n)\right)\\
&= -Z\left(I^{-}_{x^-,i+\frac{1}{2}}(n-\tfrac{1}{2}) - I^{-}_{x^+,i-\frac{1}{2}}(n-\tfrac{1}{2})\right)\\
&= -Z\left(I_{J,i+\frac{1}{2}}(n-\tfrac{1}{2}) - I_{J,i-\frac{1}{2}}(n-\tfrac{1}{2})\right)\\
&\qquad + Z\left(I^{+}_{x^-,i+\frac{1}{2}}(n-\tfrac{1}{2}) - I^{+}_{x^+,i-\frac{1}{2}}(n-\tfrac{1}{2})\right)\\
&= -Z\left(I_{J,i+\frac{1}{2}}(n-\tfrac{1}{2}) - I_{J,i-\frac{1}{2}}(n-\tfrac{1}{2})\right)\\
&\qquad + U^{-}_{x^+,i}(n-1) + U^{-}_{x^-,i}(n-1)\\
&= -Z\left(I_{J,i+\frac{1}{2}}(n-\tfrac{1}{2}) - I_{J,i-\frac{1}{2}}(n-\tfrac{1}{2})\right) + U_{J,i}(n-1) \qquad (4.31)
\end{aligned}$$

If we now identify $I_J$ with $I$ and $U_J$ with $U$, we get (4.22b) (in the constant-coefficient case), with $Z = 1/(v_0 c)$. A similar derivation beginning from the series (white, in Figure 4.12) junctions yields (4.22a), with $Z = v_0 l$, for constant $l$. Together, these constraints imply that:

$$v_0 = \frac{1}{\sqrt{lc}} \qquad\qquad Z = \sqrt{\frac{l}{c}}$$

so that we are again at the magic time step. Furthermore, the impedance of any waveguide in the network must be set equal to the characteristic impedance of the continuous time/space transmission line described by (4.17), whereas in the network of Figure 4.8, the constant impedance value could be set arbitrarily, since it is *not used* in the simulation. It is important to realize that, at least in this constant-coefficient case, no scattering occurs at any of the junctions. We can still perform all operations at the original sampling rate, and on the original grid (i.e., with grid spacing $\Delta$ and time step $T$). It is, however, possible to see more clearly how initial (and boundary) conditions must be set, and also to extend the network to handle more complex problems. We will deal with one such generalization in the next section.

### 4.3.6 Varying Coefficients

We now return to the more general case in which the material parameters $l$ and $c$ have spatial dependence. The staggered, or interleaved network of delay lines and scattering junctions presented in the last section gives rise to a centered difference method which approximates the solution to system (4.17). Consider the waveguide network in Figure 4.14.

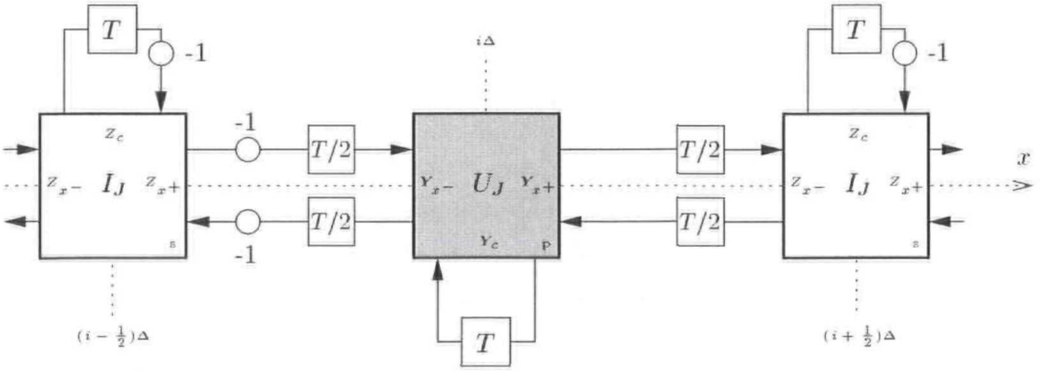

Figure 4.14: *Waveguide network for the (1+1)D transmission line equations with spatially-varying coefficients.*

The picture is the same as in the constant-coefficient case, except that we have added an extra port to each scattering junction, which is connected to a delay line of impedance $Z_c$ (marked as $Y_c$ at the parallel junctions). These *self-loops* [167] are bidirectional delay lines in their own right—since both ends are connected to the same junction, we are free to drop one of the line pairs. Note that the loop connected to the series junction contains a sign inversion (like a lumped wave digital inductor) and the loop at the parallel junction does not (like a capacitor). Also note that the delay in this line is a full sample, so that we are able to operate on the interleaved grid. The reason for this choice should be clear from Figure 4.7. Now, the immittances of the delay lines are in general no longer identical, so we expect non-trivial scattering to occur, due to the spatially-varying material parameters. The admittances of the lines connected to the parallel junction at grid point $i$, $i$ integer, are denoted by $Y_{x^+,i}$, $Y_{x^-,i}$ and $Y_{c,i}$. The impedances of the self-loops at grid points $i+\frac{1}{2}$ for $i$ integer will be called $Z_{c,i+\frac{1}{2}}$. (We have marked these new immittances in Figure 4.14.) The junction immittances are now

$$\begin{aligned} Y_{J,i} &\triangleq Y_{x^+,i} + Y_{x^-,i} + Y_{c,i} && \text{Parallel junction} \\ Z_{J,i+\frac{1}{2}} &\triangleq Z_{x^+,i+\frac{1}{2}} + Z_{x^-,i+\frac{1}{2}} + Z_{c,i+\frac{1}{2}} && \text{Series junction} \\ &= \frac{1}{Y_{x^-,i+1}} + \frac{1}{Y_{x^+,i}} + Z_{c,i+\frac{1}{2}} \end{aligned}$$

at parallel junctions at grid point $i$ and series junctions at grid point $i+\frac{1}{2}$, for integer $i$. We will call the new voltage wave variables entering and leaving the parallel junction from the new port $U^+_{c,i}(n)$ and $U^-_{c,i}(n)$ respectively, and those entering and leaving the series junction from its new port $U^+_{c,i+\frac{1}{2}}(n+\frac{1}{2})$ and $U^-_{c,i+\frac{1}{2}}(n+\frac{1}{2})$, for integer values of $i$ and $n$. In addition, we will adopt the notation

$$l_k \triangleq l(k\Delta) \qquad\qquad c_k \triangleq c(k\Delta)$$

for half-integer values of $k^\dagger$.

One physical interpretation of the need for these self-loops is that if $l$ and $c$ vary over the domain, the effective local wave speed does as well. Thus, if we choose a regular grid spacing, there are necessarily grid points at which the space step/time step ratio is *not* the magic ratio (it must be greater, by the CFL criterion). Thus if we were to try to use a structure such as that pictured in Figure 4.12, regardless of how the waveguide impedances are set, energy would be moving "too fast" through the network. The extra delays at the junctions serve to slow down the propagation of energy, by storing a portion of it for a time step. The amount of slowdown is locally determined by the values of self-loop admittances and impedances. Self-loops are used for the same purpose in TLM [29, 90]—in this context they are called inductive or capacitive stubs, depending on whether or not they invert sign.

Beginning from a parallel junction in Figure 4.14, we can proceed through a derivation similar

---

[†] We take care to distinguish these quantities, which are simply values of the continuous functions $l$ and $c$ from the indeterminate quantities $\bar{l}_i$ and $\bar{c}_i$ defined in (4.21).

to that leading to (4.31):

$$\begin{aligned}
U_{J,i}(n) &= \frac{2}{Y_{J,i}}\left(Y_{x^+,i}U^+_{x^+,i}(n)+Y_{x^-,i}U^+_{x^-,i}(n)+Y_{c,i}U^+_{c,i}(n)\right)\\
&= \frac{2}{Y_{J,i}}\left(I^+_{x^+,i}(n)+I^+_{x^-,i}(n)+Y_{c,i}U^+_{c,i}(n)\right)\\
&= \frac{2}{Y_{J,i}}\left(-I^-_{x^-,i+\frac{1}{2}}(n-\tfrac{1}{2})+I^-_{x^+,i-\frac{1}{2}}(n-\tfrac{1}{2})+I^+_{c,i}(n)\right)\\
&= \frac{2}{Y_{J,i}}\left(-I_{J,i+\frac{1}{2}}(n-\tfrac{1}{2})+I_{J,i-\frac{1}{2}}(n-\tfrac{1}{2})\right)\\
&\qquad + \frac{2}{Y_{J,i}}\left(I^+_{x^-,i+\frac{1}{2}}(n-\tfrac{1}{2})-I^+_{x^+,i-\frac{1}{2}}(n-\tfrac{1}{2})-I^-_{c,i}(n-1)\right)\\
&= \frac{2}{Y_{J,i}}\left(-I_{J,i+\frac{1}{2}}(n-\tfrac{1}{2})+I_{J,i-\frac{1}{2}}(n-\tfrac{1}{2})\right)\\
&\qquad - \frac{2}{Y_{J,i}}\left(I^-_{x^+,i}(n-1)+I^-_{x^-,i}(n-1)+I^-_{c,i}(n-1)\right)\\
&= \frac{2}{Y_{J,i}}\left(-I_{J,i+\frac{1}{2}}(n-\tfrac{1}{2})+I_{J,i-\frac{1}{2}}(n-\tfrac{1}{2})\right)+U_{J,i}(n-1) \qquad (4.32)
\end{aligned}$$

In order to equate this difference relation with (4.22b), we must have, recalling (4.21b),

$$Y_{J,i} = 2v_0\bar{c}_i \tag{4.33}$$

Beginning from the series junctions at $x = (i+\frac{1}{2})\Delta$, for $i$ integer, we obtain similarly an interleaved central difference approximation to (4.17a), under the constraint

$$Z_{J,i+\frac{1}{2}} = 2v_0\bar{l}_{i+\frac{1}{2}} \tag{4.34}$$

Under the further condition that all impedances in the network be positive, these constraints give rise to a family of stable centered difference approximations to (4.17). We can distinguish three special types:

**Type I: Voltage-centered Network**

We set the admittances of the waveguides leading away from a parallel junction to be identical, i.e.,

$$Y_{x^-,i} = Y_{x^+,i} = v_0c_i \tag{4.35}$$

and set

$$Y_{c,i,j} = 0$$

which satisfies (4.33) with $\bar{c}_i = c_i$. From (4.35), we have that

$$Z_{x^+,i+\frac{1}{2}} = \frac{1}{v_0 c_{i+1}} \qquad\qquad Z_{x^-,i+\frac{1}{2}} = \frac{1}{v_0 c_i}$$

Thus the series junction impedance at location $i + \frac{1}{2}$ will be

$$Z_{J,i+\frac{1}{2}} = \frac{1}{v_0 c_i} + \frac{1}{v_0 c_{i+1}} + Z_{c,i+\frac{1}{2}}$$

We can then set

$$Z_{c,i+\frac{1}{2}} = v_0(l_i + l_{i+1}) - \frac{1}{v_0}\left(\frac{1}{c_i} + \frac{1}{c_{i+1}}\right)$$

which satisfies (4.34) with $\bar{l}_{i+\frac{1}{2}} = \frac{1}{2}(l_i + l_{i+1})$.

Only the series self-loop impedances are possibly negative, so the network will be passive if $Z_{c,i+\frac{1}{2}} \geq 0$. This will certainly be true if we choose

$$v_0 \geq \max_i\left(\sqrt{\frac{1}{l_i c_i}}\right) \tag{4.36}$$

Recall that in our earlier discussion of group velocities for symmetric hyperbolic systems in §3.2 and for the transmission line in particular in §3.7, the maximum group velocity for the transmission line is

$$\gamma^g_{TL,max} = \max_{x\in\mathcal{D}} \frac{1}{\sqrt{lc}} \tag{4.37}$$

The optimal space step/time step ratio from (4.36) is exactly the maximum of the local group velocity of the transmission line, at least over the range of values of $l$ and $c$ sampled at the parallel junction locations; thus it approaches the maximum group velocity for the continuous system in the limit as the grid spacing $\Delta$ becomes small.

### Type II: Current-centered Network

This arrangement is the dual to the previous case. We now set

$$Z_{x^+,i+\frac{1}{2}} = Z_{x^-,i+\frac{1}{2}} = v_0 l_{i+\frac{1}{2}} \qquad\qquad Z_{c,i+\frac{1}{2}} = 0$$

and

$$Y_{c,i} = v_0\left(c_{i+\frac{1}{2}} + c_{i-\frac{1}{2}}\right) - \frac{1}{v_0}\left(\frac{1}{l_{i+\frac{1}{2}}} + \frac{1}{l_{i-\frac{1}{2}}}\right) \tag{4.38}$$

We have thus chosen $\bar{c}_i = \frac{1}{2}(c_{i+\frac{1}{2}} + c_{i-\frac{1}{2}})$ and $\bar{l}_{i+\frac{1}{2}} = l_{i+\frac{1}{2}}$. Now we must have

$$v_0 \geq \max_i \left(\sqrt{\frac{1}{l_{i+\frac{1}{2}}c_{i+\frac{1}{2}}}}\right)$$

which is very similar to condition (4.36), except that the maximum is now taken over the series junction locations.

Here, scattering at the series junctions is trivial, since the impedances at the two connecting ports are identical, and the self-loop impedance is zero (and we thus drop entirely any calculation of the value in the self-loop at the series nodes). We can operate at the down-sampled rate, with scattering occurring only at the parallel junctions. In this case, we are directly computing only junction voltages, and are in fact solving the second-order reduction of system (4.17), namely

$$\frac{\partial^2 u}{\partial t^2} = \frac{1}{c}\frac{\partial}{\partial x}\left(\frac{1}{l}\frac{\partial u}{\partial x}\right) \tag{4.39}$$

We could have made a similar statement about scattering at the parallel junctions in the previous case. This efficient configuration, unlike type I, however, generalizes to the (2+1)D case, as we will see in §4.4.2.

### Type III: Mixed Network

Suppose we set all the impedances which connect one grid point to another to be equal to some constant $Z_{const}$ which is independent of position. Thus

$$Y_{x^-,i} = Y_{x^+,i} = 1/Z_{const}$$

We then choose, to satisfy (4.33) and (4.34),

$$\begin{aligned} Y_{c,i} &= 2v_0c_i - \frac{2}{Z_{const}} \\ Z_{c,i+\frac{1}{2}} &= 2v_0l_{i+\frac{1}{2}} - 2Z_{const} \end{aligned}$$

and this leads to the conditions

$$v_0 \geq \max_i \frac{1}{c_iZ_{const}} = \frac{1}{c_{min}Z_{const}} \qquad\qquad v_0 \geq \max_i \frac{Z_{const}}{l_{i+\frac{1}{2}}} = \frac{Z_{const}}{l_{min}}$$

where

$$c_{min} = \min_i c_i \qquad\qquad l_{min} = \min_i l_{i+\frac{1}{2}}$$

The lower bounds on $v_0$ coincide when

$$Z_{const} = \sqrt{l_{min}/c_{min}}$$

in which case we have

$$v_0 \geq \sqrt{\frac{1}{l_{min}c_{min}}}$$

Since in general, $l_{min}c_{min} \leq \min_i(l_ic_i)$, for $2i$ either even or odd, we are no longer at the optimal bound, and are forced to use a smaller time step than in the previous two cases, if we wish the network to remain concretely passive. This arrangement bears a strong resemblance to the MDWD network in [107] and [131], and discussed in §3.7. We will explore this similarity in more detail in §4.10. Many other choices are of the waveguide immittances satisfying (4.33) and (4.34) are of course possible.

**Comment: Passivity and Stability**

At this point, we would like to mention an interesting property of the interleaved waveguide networks discussed in the earlier part of this section. We showed, in the last few pages, that three different types of immittance settings for the waveguide network could be used to solve the (1+1)D transmission line equations, and could, in fact, be interpreted as centered difference approximations. The three types of network integrate system (4.17) using slightly different *effective* inductances $\bar{l}$ and capacitances $\bar{c}$ which converge to $l$ and $c$ in the limit as the grid spacing becomes small. We had, for integer $i$,

$$\begin{array}{lll}
\bar{l}_{i+\frac{1}{2}} = \frac{1}{2}\left(l_i + l_{i+1}\right) & \bar{c}_i = c_i & \text{Type I} \\
\bar{l}_{i+\frac{1}{2}} = l_{i+\frac{1}{2}} & \bar{c}_i = \frac{1}{2}\left(c_{i+\frac{1}{2}} + c_{i-\frac{1}{2}}\right) & \text{Type II} \\
\bar{l}_{i+\frac{1}{2}} = l_{i+\frac{1}{2}} & \bar{c}_i = c_i & \text{Type III}
\end{array}$$

The three types, however, yield different requirements for passivity on the space step/time step ratio $v_0$,

$$v_0 \geq \max_i\left(\sqrt{\frac{1}{l_ic_i}}\right) \qquad \text{Type I} \tag{4.40}$$

$$v_0 \geq \max_{i+\frac{1}{2}}\left(\sqrt{\frac{1}{l_{i+\frac{1}{2}}c_{i+\frac{1}{2}}}}\right) \qquad \text{Type II} \tag{4.41}$$

$$v_0 \geq \sqrt{\frac{1}{\min_{i+\frac{1}{2}} l_i \min_i c_i}} \qquad \text{Type III} \tag{4.42}$$

The first two bounds are roughly the same, and are close to optimal, in the sense that $v_0$ is bounded by(in the limit as $\Delta$ approaches 0) the maximum of the local group velocity over the transmission line. The type III bound, however, may be substantially poorer, and is similar to that which arises in MDWD networks (see §3.7).

If we choose $l(x)$ and $c(x)$ to be positive affine functions (linear in $x$ with a constant offset), then $\bar{l}$ and $\bar{c}$ are the same in all three cases, so the three networks will, in infinite-precision arithmetic, calculate identical solutions. But there will be a range of values of $v_0$ (namely, the range of $v_0$ greater than the bounds given in (4.40) and (4.41), but less than that of (4.42)) for which the type I and II networks are *concretely* passive [12], but for which the type III network is not. Over this range, some immittances in the type III network will necessarily be negative.

We can conclude that there is a large middle ground between passivity and global stability of networks. One important difference would seem to be that wave quantities in a concretely passive network are *power-normalizable*, whereas if a network is only *abstractly* passive—that is, its global behavior is passive, even though it contains elements which are themselves not—may not be. We do not investigate this further here, but comment that it would be of great interest to make clearer the distinction between passive and stable numerical methods for solving PDEs. This subject has been broached in some detail for ODEs [32, 75], and we will see some other interesting examples of this distinction in Appendix A.

### 4.3.7 Incorporating Losses and Sources

We now reconsider the full (1+1)D transmission line equations, including the effects of losses and sources; this system was presented earlier in §3.7, and we repeat its definition here:

$$l\frac{\partial i}{\partial t} + \frac{\partial u}{\partial x} + ri + e = 0 \tag{4.43a}$$

$$c\frac{\partial u}{\partial t} + \frac{\partial i}{\partial x} + gu + h = 0 \tag{4.43b}$$

Here $r(x) \geq 0$ and $g(x) \geq 0$ represent resistance and shunt conductivity at any point in the domain, and $e$ and $h$ are driving terms and can be functions of $x$ and $t$.

In order to add these terms to the centered difference approximation in such a way that we may still use an interleaved scheme, we can use the *semi-implicit* [184] approximations to $i$, and $u$ given by

$$i(x,t) = \frac{1}{2}\left(i(x,t-T/2) + i(x,t+T/2)\right) \; + O(T^2)$$

$$u(x,t) = \frac{1}{2}\left(u(x,t-T/2) + u(x,t+T/2)\right) + O(T^2)$$

We also define

$$r_{i+\frac{1}{2}} \triangleq r\left((i+\tfrac{1}{2})\Delta\right) \qquad g_i \triangleq g(i\Delta)$$

$$e_{i+\frac{1}{2}}(n+\tfrac{1}{2}) \triangleq e\left((i+\tfrac{1}{2})\Delta, (n+\tfrac{1}{2})T\right) \qquad h_i(n) \triangleq h(i\Delta, nT)$$

and use the second-order approximations

$$\begin{aligned} \bar{e}_{i+\frac{1}{2}}(n) &= \frac{1}{2}\left(e_{i+\frac{1}{2}}(n+\tfrac{1}{2}) + e_{i+\frac{1}{2}}(n-\tfrac{1}{2})\right) \\ \bar{h}_i(n-\tfrac{1}{2}) &= \frac{1}{2}\left(h_i(n) + h_i(n-1)\right) \end{aligned}$$

We then get, as an approximation to (4.43),

$$\begin{aligned} I_{i+\frac{1}{2}}(n+\tfrac{1}{2}) &- \rho_{I,i+\frac{1}{2}} I_{i+\frac{1}{2}}(n-\tfrac{1}{2}) \\ &+ \sigma_{I,i+\frac{1}{2}}\left(U_{i+1}(n) - U_i(n)\right) + \Delta\sigma_{I,i+\frac{1}{2}}\bar{e}_{i+\frac{1}{2}}(n) = 0 \qquad (4.44a) \\ U_i(n) &- \rho_{U,i} U_i(n-1) \\ &+ \sigma_{U,i}\left(I_{i+\frac{1}{2}}(n-\tfrac{1}{2}) - I_{i-\frac{1}{2}}(n-\tfrac{1}{2})\right) + \Delta\sigma_{U,i}\bar{h}_i(n-\tfrac{1}{2}) = 0 \qquad (4.44b) \end{aligned}$$

with

$$\rho_{I,i+\frac{1}{2}} \triangleq \frac{2\bar{l}_{i+\frac{1}{2}} - r_{i+\frac{1}{2}}T}{2\bar{l}_{i+\frac{1}{2}} + r_{i+\frac{1}{2}}T} \qquad \rho_{U,i} \triangleq \frac{2\bar{c}_i - g_iT}{2\bar{c}_i + g_iT}$$

$$\sigma_{I,i+\frac{1}{2}} \triangleq \frac{2}{2v_0\bar{l}_{i+\frac{1}{2}} + r_{i+\frac{1}{2}}\Delta} \qquad \sigma_{U,i} \triangleq \frac{2}{2v_0\bar{c}_i + g_i\Delta}$$

Losses and sources can be added to the waveguide network scheme rather easily, by introducing new ports at each series or parallel junction. In fact, as per wave digital filters, each pair of terms $ri + e$, and $gu + h$ can be interpreted as a *resistive source* [46], and only requires the addition of a single new port at each junction. (The resistive voltage source was discussed in §2.3.4.) For any parallel port we will call the new port admittance $Y_{R,i}$, and the voltage wave variable entering the port $U^+_{R,i}$. For a series port, we call the new impedance $Z_{R,i+\frac{1}{2}}$, and the incoming voltage wave variable $U^+_{R,i+\frac{1}{2}}$. The generalized network is shown in Figure 4.15, with the new loss/source port immittances marked. As a result of the addition of this port, the junction admittances and impedances become

$$\begin{aligned} Y_{J,i} &\triangleq Y_{x^-,i} + Y_{x^+,i} + Y_{c,i} + Y_{R,i} \\ Z_{J,i+\frac{1}{2}} &\triangleq Z_{x^+,i+\frac{1}{2}} + Z_{x^-,i+\frac{1}{2}} + Z_{c,i+\frac{1}{2}} + Z_{R,i+\frac{1}{2}} \end{aligned}$$

Beginning again from a parallel junction, and proceeding through a derivation similar to that which

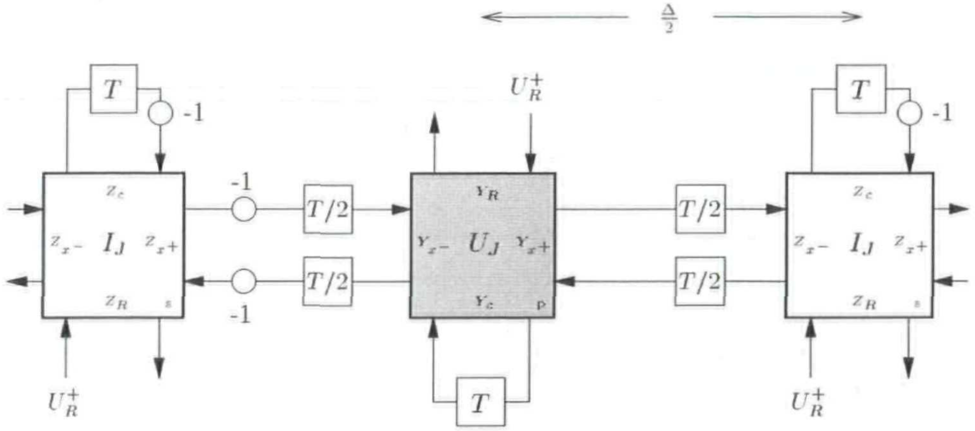

Figure 4.15: *Waveguide network for system* (4.43).

leads to (4.32), we obtain a difference relation among the junction voltages and currents:

$$\begin{aligned} U_{J,i}(n) - \frac{Y_{J,i}-2Y_{R,i}}{Y_{J,i}}U_{J,i}(n-1) \quad &+ \quad \frac{2}{Y_{J,i}}\left(I_{J,i+\frac{1}{2}}(n-\tfrac{1}{2}) - I_{J,i-\frac{1}{2}}(n-\tfrac{1}{2})\right) \\ &- \quad \frac{2Y_{R,i}}{Y_{J,i}}\left(U^{+}_{R,i}(n) + U^{+}_{R,i}(n-1)\right) = 0 \end{aligned}$$

In order to equate this relation with (4.44b), we can set

$$\begin{aligned} Y_{R,i} &= g_i\Delta \\ U^{+}_{R,i}(n) &= -\frac{h_i(n)}{2g_i} \end{aligned}$$

Beginning from a series junction, we obtain an analogous relation, which becomes (4.44a) under the choices

$$\begin{aligned} Z_{R,i+\frac{1}{2}} &= r_{i+\frac{1}{2}}\Delta \\ U^{+}_{R,i+\frac{1}{2}}(n+\tfrac{1}{2}) &= -\frac{\Delta e_{i+\frac{1}{2}}(n+\frac{1}{2})}{2} \end{aligned}$$

Note that in the case where the loss parameter $g$ is zero, or close to zero, $U^{+}_{R,i}(n)$ will become infinite, or very large. For this reason, it will be necessary in this case to use the dual type of wave; i.e., if $g_i$ is small, set $I^{+}_{R,i} = Y_{R,i}U^{+}_{R,i} = -\frac{\Delta}{2}h_i$, and use current waves at the series junctions. The other impedances in the network remain unchanged under the addition of losses and sources; thus all the stability criteria mentioned in §4.3.6 remain the same. It is rather interesting to note, however, that in the case of the current-centered network, for example (type II), scattering at the series junctions is no longer trivial if we have non-zero sources $e$ or loss $r$. That is, the series junctions cannot be treated as simple throughs. A similar statement holds for the dual case of the voltage-centered network (type I) in (1+1)D, but will not be true when we generalize to the (2+1)D mesh (see §4.4).

### 4.3.8 Numerical Phase Velocity and Dispersion

We now make a few comments regarding the spectral properties of these difference methods; a detailed summary of spectral methods is provided in Appendix A.

Consider again the type II DWN for the (1+1)D transmission line equations, as discussed in §4.3.6. In the lossless, source-free case, the difference scheme can be written purely in terms of the junction voltages, and for integer time steps $n$ as

$$U_{J,i}(n+1)+U_{J,i}(n-1)=\frac{2}{Y_{J,i}}\Big(Y_{x^-,i}U_{J,i-1}(n)+Y_{x^+,i}U_{J,i+1}(n)+Y_{c,i}U_{J,i}(n)\Big) \tag{4.45}$$

where $Y_{x^-,i}=1/(v_0 l_{i-\frac{1}{2}})$ and $Y_{x^+,i}=1/(v_0 l_{i+\frac{1}{2}})$, and the self-loop admittance is given by (4.38). In effect, we are numerically solving the reduced form (4.39) of (4.17) obtained by elimination of the current $i$.

If the material parameters are constant, then (4.45) can be rewritten as

$$U_{J,i}(n+1)+U_{J,i}(n-1)=\lambda^2\Big(U_{J,i-1}(n)+U_{J,i+1}(n)\Big)+2(1-\lambda^2)U_{J,i}(n)$$

where $\lambda=\gamma/v_0$ and $\gamma=1/\sqrt{lc}$ is the wave speed. It is possible to examine this scheme in terms of discrete spatial frequencies $\beta$, as per the methods discussed in [176]; the range of spatial frequencies which are available on this grid of spacing $\Delta$ are $-\pi/\Delta\leq\beta\leq\pi/\Delta$. The *spectral amplification factors* (defined in §A.1) for this scheme are given by

$$G_{\beta,\pm}=\frac{1}{2}\left(-B_\beta\pm\sqrt{B_\beta^2-4}\right)$$

where

$$B_\beta=-2\Big(1+\lambda^2(1-\cos(\beta\Delta))\Big)$$

These spectral amplification factors define the numerical phase velocities $v_{\beta,phase}$[176] (see §A.1.4) and thus the numerical dispersion of the scheme (in general, the numerical phase velocity is different from the physical velocity $\gamma$). It is of interest to plot the numerical phase velocity of this scheme versus that of the MDWDF for the same system; the spatial frequency dependence of the various modal frequencies of the MDWDF were discussed in §3.9.2.

In Figure 4.16, the quantity $v_{phase}/\gamma$ is plotted for various values of the parameter $\lambda$. At the stability bound, for $\lambda = 1$ (i.e. $v_0 = \gamma = 1/\sqrt{lc}$), both schemes are dispersionless. For the DWN, all spatial frequencies are slowed increasingly as $\lambda$ is decreased, but for the MDWD network, wave speeds decrease for $\lambda > 1/2$, then are exact again at $\lambda = 1/2$, and finally faster than the physical speed if $\lambda < 1/2$. This curious behavior of the phase velocities in the MDWD network was also mentioned in §3.9.2. In general, the phase velocities of the MDWD network are closer to the correct wave speed over the entire spatial frequency spectrum for a wide range of $\lambda$—this is mitigated, however, by the fact this MDWD network corresponds to a three-step difference method (compared to two-step for the DWN), and is thus more computationally intensive.

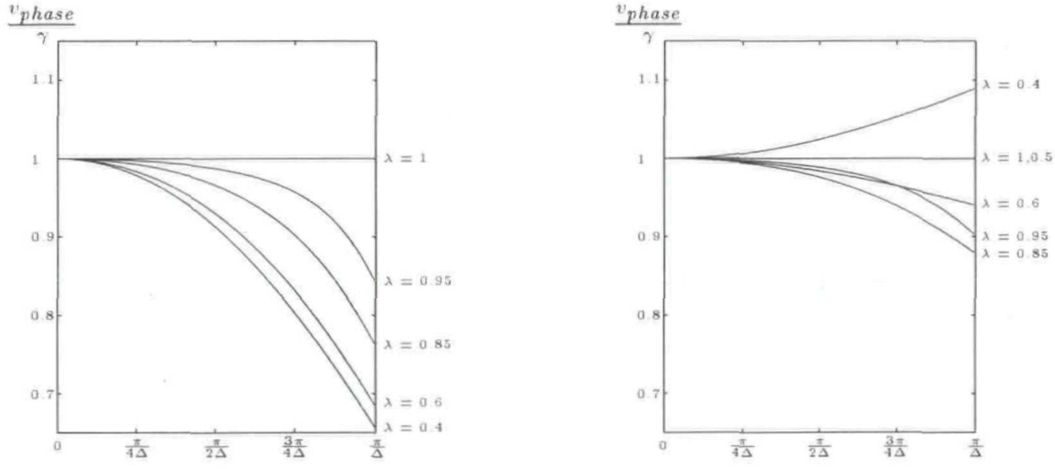

(a) (b)

Figure 4.16: *Numerical dispersion curves for various values of* $\lambda$— (a) *for the DWN and* (b) *for the MDWD network.*

### 4.3.9 Boundary Conditions

The (1+1)D transmission line equations, if they are to be solved on a domain of finite extent, require one supplementary boundary condition at any end point [82]. Suppose that $x = 0$ is such an end point, and furthermore assume that our grid has been constructed such that the point $x = 0$ coincides with one of the parallel (grey) scattering junctions of the interleaved waveguide network shown in Figure 4.15. We now are faced with *terminating* the waveguide network, by replacing the left-hand port of the parallel junction at $x = 0$ with a lumped network. If the lumped network is passive (that is, if its reflectance is *bounded*), then it should be clear that the network as a whole will be passive as well.

The two most important types of boundary condition are

| | |
|---|---|
| $u(0, t) = 0$ | Short-circuit at $x = 0$ |
| $i(0, t) = 0$ | Open-circuit at $x = 0$ |

Both are lossless, and have the form of (3.8). The first of these conditions is easy to deal with by short-circuiting the left-hand port. In this case, we may also remove the self-loop, as well as the combined loss/source port from the junction at $x = 0$. $U_{J,0}$ is forced to zero by the short-circuit condition; this boundary termination is shown in Figure 4.17(a). We have assumed that $Y_{x^+,0} = Y_{x^-,0}$, so that the termination degenerates to a simple sign inversion of the wave incoming from the right-hand side. The other boundary termination requires a bit more analysis, because we do not have access to $I_J$ at a parallel junction. It is sufficient to drop the left hand port entirely in this case (or, equivalently, to terminate the junction with an open circuit, which, when connected in parallel, may be ignored). In this case, though, we must retain the self-loop and the loss/source port. We now show that such a termination does indeed approximate the boundary condition $i(0, t) = 0$. The resulting termination is shown in Figure 4.17(b).

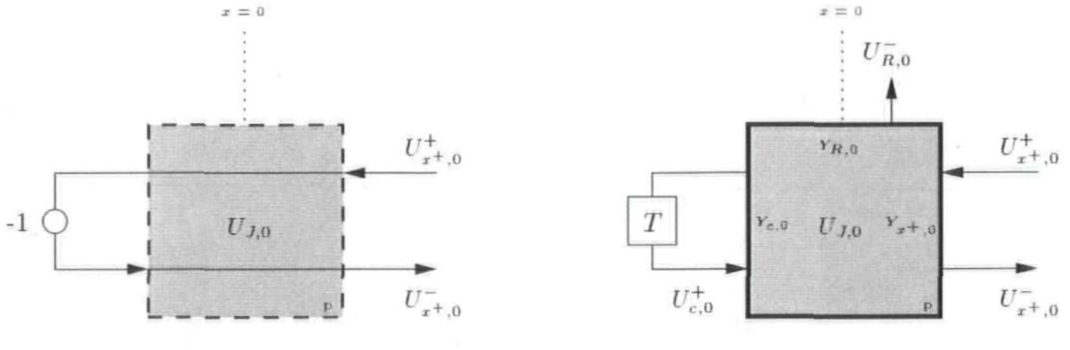

(a) (b)

Figure 4.17: *Boundary terminations of the waveguide network for the (1+1)D transmission line equations at* $x = 0$ *when* (a) $u(0, t) = 0$ *and* (b) $i(0, t) = 0$.

Beginning from system (4.43), where we assume no source (to avoid conflicting conditions at the boundary), we can apply centered differences in time, and use a *one-sided* [176] approximation for the spatial derivative,

$$\begin{aligned} \left.\frac{\partial i}{\partial x}\right|_{x=0, t=(n+\frac{1}{2})T} &= \frac{2}{\Delta}\Big(i(\tfrac{1}{2}, (n+\tfrac{1}{2})T) - i(0, (n+\tfrac{1}{2})T)\Big) + O(\Delta) \\ &= \frac{2}{\Delta} i(\tfrac{1}{2}, (n+\tfrac{1}{2})T) + O(\Delta) \end{aligned}$$

where we have set $i(0, (n+\frac{1}{2})T) = 0$ in accordance with the boundary condition. This yields the difference approximation to (4.43b) given by

$$U_0(n) - \frac{2\bar{c}_0 - g_0T}{2\bar{c}_0 + g_0T}U_0(n-1) + \frac{4}{2v_0\bar{c}_0 + g_0\Delta}I_{\frac{1}{2}}(n-\tfrac{1}{2}) = 0 \tag{4.46}$$

The difference formula obtained from the network termination of Figure 4.17(b) is

$$U_{0,J}(n) - \frac{Y_{J,0} - 2Y_{R,0}}{Y_{J,0}}U_{0,J}(n-1) + \frac{2}{Y_{J,0}}I_{\frac{1}{2},J} = 0$$

where we now have

$$Y_{J,0} \triangleq Y_{x^+,0} + Y_{R,0} + Y_{c,0} \tag{4.47}$$

It is easy to see that if we set

$$Y_{R,0} = \frac{1}{2}g_0\Delta \qquad\qquad Y_J = \frac{1}{2}v_0\left(2\bar{c}_0 + g_0T\right) \tag{4.48}$$

then the waveguide network is indeed performing a calculation equivalent to (4.46). $Y_{c,0}$ and $Y_{x^+,0}$ may be set according to the type of network we are using (i.e., I, II or III in §4.3.6) as long as (4.47) and (4.48) are satisfied; the stability bounds are unchanged. It is important to note that this realization of the boundary condition $i(0,t) = 0$ will be first-order accurate in the grid spacing $\Delta$, due to our use of a one-sided difference approximation. It is recommended, then, to align the waveguide network such that a series junction lies at the left-most grid point, where it can be simply terminated by an open circuit. Such a termination will be second-order accurate.

Because *any* bounded reflectance may be used to terminate the waveguide network, it has been proposed [96] (in the context of the Karplus-Strong algorithm [103], which can be shown to be equivalent to a particular digital waveguide configuration [168]) that one can model wave propagation in a dispersive medium (like a beam [77]) by using a non-dispersive waveguide for the interior with an all-pass terminating reflectance. Such an all-pass filter will introduce a frequency-dependent phase delay which can be chosen so as to match the dispersion of the medium itself, without dissipating energy. It should be kept in mind, however, that one means of synthesizing such an all-pass filter would be by adding an additional chain of junctions on the opposing side of the boundary junction, and terminating it with an open- or short-circuit. Synthesis (for a given dispersion profile) presumably proceeds along the lines of methods used in related filter-design areas [215].

## 4.4 The (2+1)D Parallel-plate System

We return now to the parallel-plate transmission line problem that was discussed in the previous chapter in §3.8. As we mentioned before, this is a useful model problem in that it can be simplified to model the transverse motion of a membrane, and (2+1)D linear acoustics. It can be modified in a trivial way to model transverse electric (TE) or transverse magnetic (TM) fields in a substance of spatially-varying dielectric constant, magnetic permeability, and loss characteristics.

### 4.4.1 Defining Equations and Centered Differences

The set of PDEs describing a lossless, source-free parallel-plate transmission line in (2+1)D is a direct generalization of system (4.17):

$$l\frac{\partial i_x}{\partial t}+\frac{\partial u}{\partial x} = 0 \tag{4.49a}$$

$$l\frac{\partial i_y}{\partial t}+\frac{\partial u}{\partial y} = 0 \tag{4.49b}$$

$$c\frac{\partial u}{\partial t}+\frac{\partial i_x}{\partial x}+\frac{\partial i_y}{\partial y} = 0 \tag{4.49c}$$

Now $i_x(x,y,t)$ and $i_y(x,y,t)$ are the components of the current density vector in the $x$ and $y$ directions, respectively, and $u(x,y,t)$ is the voltage between the plates. $l(x,y)$ and $c(x,y)$, both assumed positive everywhere, are the inductance and capacitance per unit length.

If we assume that $l$ and $c$ are constant, then as in the (1+1)D case, the set of equations can be reduced to a single second order equation in the voltage alone:

$$\frac{\partial^2 u}{\partial t^2}=\gamma^2\left(\frac{\partial^2 u}{\partial x^2}+\frac{\partial^2 u}{\partial y^2}\right) \tag{4.50}$$

and again, the *wave speed* $\gamma$ is given by

$$\gamma=\frac{1}{\sqrt{lc}}$$

The centered difference scheme for system (4.49) also generalizes simply. Define grid functions $I_{x,i,j}(n)$, $I_{y,i,j}(n)$ and $U_{i,j}(n)$ which run over half-integer values of $i$, $j$, and $n$, i.e.,

$$i,j,n=\ldots-1,-\tfrac{1}{2},0,\tfrac{1}{2},1\ldots$$

We will furthermore assume that the spatial step in the $x$ direction and the $y$ direction are the same and equal to $\Delta/2$. As before, the time step will be $T/2$. We can use the approximations (4.19), as well as an approximation to the derivative in the $y$ direction,

$$\left.\frac{\partial w}{\partial y}\right|_{i\Delta,j\Delta,nT} = \frac{w(i,j+\frac{1}{2},n)-w(i,j-\frac{1}{2},n)}{\Delta}+O(\Delta^2)$$

where $w$ stands for either of $i_y$ or $u$. We obtain the difference scheme

$$I_{x,i,j}(n+\tfrac{1}{2}) - I_{x,i,j}(n-\tfrac{1}{2}) + \frac{1}{v_0\bar{l}_{i,j}}\left(U_{i+\frac{1}{2},j}(n) - U_{i-\frac{1}{2},j}(n)\right) = 0 \tag{4.51a}$$

$$I_{y,i,j}(n+\tfrac{1}{2}) - I_{y,i,j}(n-\tfrac{1}{2}) + \frac{1}{v_0\bar{l}_{i,j}}\left(U_{i,j+\frac{1}{2}}(n) - U_{i,j-\frac{1}{2}}(n)\right) = 0 \tag{4.51b}$$

$$\begin{aligned} U_{i,j}(n+\tfrac{1}{2}) - U_{i,j}(n-\tfrac{1}{2}) &+ \frac{1}{v_0\bar{c}_{i,j}}\left(I_{x,i+\frac{1}{2},j}(n) - I_{x,i-\frac{1}{2},j}(n)\right) \\ &+ \frac{1}{v_0\bar{c}_{i,j}}\left(I_{y,i,j+\frac{1}{2}}(n) - I_{y,i,j-\frac{1}{2}}(n)\right) = 0 \end{aligned} \tag{4.51c}$$

where we have written

$$\bar{l}_{i,j} \triangleq l(i\Delta, j\Delta) + O(\Delta^2)$$
$$\bar{c}_{i,j} \triangleq l(i\Delta, j\Delta) + O(\Delta^2)$$

and

$$v_0 \triangleq \frac{\Delta}{T}$$

As in the (1+1)D case, it is possible to subdivide the calculation scheme (4.51) into smaller, mutually exclusive subschemes. Using a decimated grid for the variable coefficient difference scheme amounts to rewriting scheme (4.51) as

$$I_{x,i+\frac{1}{2},j}(n+\tfrac{1}{2}) - I_{x,i+\frac{1}{2},j}(n-\tfrac{1}{2}) + \frac{1}{v_0\bar{l}_{i+\frac{1}{2},j}}\left(U_{i+1,j}(n) - U_{i,j}(n)\right) = 0 \tag{4.52a}$$

$$I_{y,i,j+\frac{1}{2}}(n+\tfrac{1}{2}) - I_{y,i,j+\frac{1}{2}}(n-\tfrac{1}{2}) + \frac{1}{v_0\bar{l}_{i,j+\frac{1}{2}}}\left(U_{i,j+1}(n) - U_{i,j}(n)\right) = 0 \tag{4.52b}$$

$$\begin{aligned} U_{i,j}(n) - U_{i,j}(n-1) &+ \frac{1}{v_0\bar{c}_{i,j}}\left(I_{x,i+\frac{1}{2},j}(n-\tfrac{1}{2}) - I_{x,i-\frac{1}{2},j}(n-\tfrac{1}{2})\right) \\ &+ \frac{1}{v_0\bar{c}_{i,j}}\left(I_{y,i,j+\frac{1}{2}}(n-\tfrac{1}{2}) - I_{y,i,j-\frac{1}{2}}(n-\tfrac{1}{2})\right) = 0 \end{aligned} \tag{4.52c}$$

where we now compute solutions for $i$, $j$ and $n$ integer. The interleaved grid is shown in Figure 4.18; a grey (white) dot at a grid location indicates that the adjacent named variable is to be calculated at times which are even (odd) multiples of $T/2$. This interleaved form was originally put forth by Yee [214] in the context of electromagnetic field problems, and forms the basis of the widely used *finite-difference time domain* (FDTD) family of difference methods [184], which were discussed briefly in §4.1. If system (4.52) is rewritten as a TE or TM system, the interleaved arrangement of the field components also has an interesting physical interpretation as a discrete counterpart to the integral form of Ampere's and Faraday's Laws [184]. This result also extends easily to the discretization of

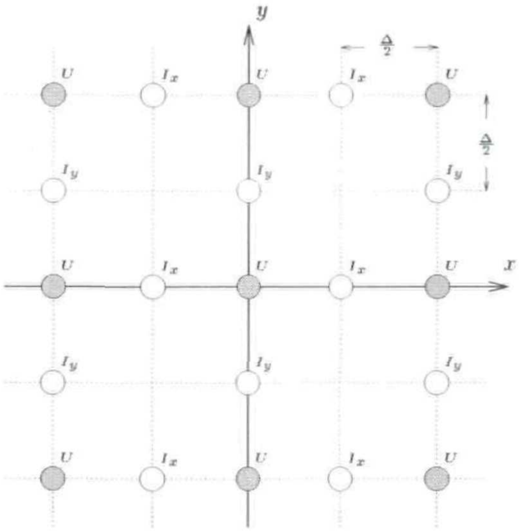

Figure 4.18: *Interleaved computational grid for the (2+1)D parallel-plate system.*

*Maxwell's equations* in (3+1)D [214]; see §4.10.6 for more details.

The (2+1)D analogue of (4.23), which holds in the case where $l$ and $c$ are constant, is

$$\begin{aligned}\frac{v_0^2}{\gamma^2}\Big(U_{i,j}(n+1)+U_{i,j}(n-1)\Big) = U_{i+1,j}(n)+U_{i-1,j}(n) \quad &+ \quad U_{i,j+1}(n)+U_{i,j-1}(n) \\ &+ \quad 2\left(\frac{v_0^2}{\gamma^2}-2\right)U_{i,j}(n) \end{aligned} \tag{4.53}$$

The *magic* time step will now be

$$v_0 = \sqrt{2}\gamma$$

and (4.53) simplifies to

$$U_{i,j}(n+1)+U_{i,j}(n-1) = \frac{1}{2}\Big(U_{i+1,j}(n)+U_{i-1,j}(n)+U_{i,j+1}(n)+U_{i,j-1}(n)\Big) \tag{4.54}$$

As in (1+1)D, when we are solving the wave equation by centered differences at the magic time step (or at CFL), the calculation further decomposes into two independent calculations; we need only update $U_{i,j}(n)$ for $i+j+n$ even (or odd). We will examine this interesting decomposition property in detail in Appendix A.

### 4.4.2 The Waveguide Mesh

Consider the original form (2+1)D waveguide network, or *mesh* [198], operating on a rectilinear grid. Each scattering junction (parallel) is connected to four neighbors by unit sample bidirectional delay

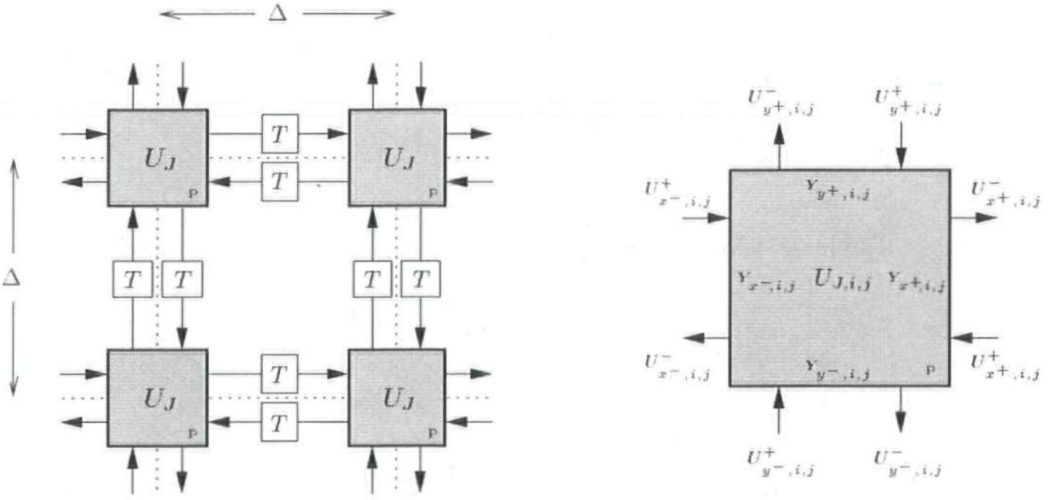

Figure 4.19: *(2+1)D waveguide mesh and a representative scattering junction.*

lines. The spacing of the junctions is $\Delta$ (in either the $x$ or $y$ direction) and the time delay is $T$ in the delay lines (see Figure 4.19). We now index a junction (and all its associated voltages and currents and wave quantities) at coordinates $(i\Delta, j\Delta)$ by the pair $(i, j)$. As in the (1+1)D case, at each parallel junction at location $(i, j)$, we have voltages at every port, given by

$$\begin{aligned} U_{x^+,i,j} &= \text{voltage in waveguide leading east} \\ U_{x^-,i,j} &= \text{voltage in waveguide leading west} \\ U_{y^+,i,j} &= \text{voltage in waveguide leading north} \\ U_{y^-,i,j} &= \text{voltage in waveguide leading south} \end{aligned}$$

and current flows

$$\begin{aligned} I_{x^+,i,j} &= \text{current flow in waveguide leading east} \\ I_{x^-,i,j} &= \text{current flow in waveguide leading west} \\ I_{y^+,i,j} &= \text{current flow in waveguide leading north} \\ I_{y^-,i,j} &= \text{current flow in waveguide leading south} \end{aligned}$$

as well as wave quantities

$$\begin{aligned} U_{q,i,j} &= U^+_{q,i,j} + U^-_{q,i,j} \\ I_{q,i,j} &= I^+_{q,i,j} + I^-_{q,i,j} \end{aligned}$$

where $q$ is any of $x^+$, $x^-$, $y^+$ or $y^-$. The variables superscripted with a $+$ refer to the incoming waves, and those marked $-$ to outgoing waves. The voltage and current waves are related by

$$I^+_{q,i,j} = Y_{q,i,j}U^+_{q,i,j} \qquad\qquad I^-_{q,i,j} = -Y_{q,i,j}U^-_{q,i,j} \tag{4.55}$$

where $Y_{q,i,j}$ is the admittance of the waveguide connected to the junction with coordinates $(i\Delta, j\Delta)$ in direction $q$. The junction admittance is then

$$Y_{J,i,j} \triangleq Y_{x^-,i,j} + Y_{x^+,i,j} + Y_{y^-,i,j} + Y_{y^+,i,j} \tag{4.56}$$

and the scattering equation, for voltage waves, will be, from (4.15),

$$U^-_{r,i,j} = -U^+_{r,i,j} + \frac{2}{Y_{J,i,j}}\left(Y_{x^-,i,j}U^+_{x^-,i,j} + Y_{x^+,i,j}U^+_{x^+,i,j} + Y_{y^+,i,j}U^+_{y^+,i,j} + Y_{y^-,i,j}U^+_{y^-,i,j}\right) \tag{4.57}$$

where $r$ is any of $x^+$, $x^-$, $y^+$, or $y^-$. Voltage waves are propagated by:

$$\begin{aligned} U^+_{x^+,i,j}(n) &= U^-_{x^-,i+1,j}(n-1) \qquad & U^+_{x^-,i,j}(n) &= U^-_{x^+,i-1,j}(n-1) \\ U^+_{y^+,i,j}(n) &= U^-_{y^-,i,j+1}(n-1) \qquad & U^+_{y^-,i,j}(n) &= U^-_{y^+,i,j-1}(n-1) \end{aligned}$$

The case of flow waves is similar except for a sign inversion. The complete picture is shown in Figure 4.19.

Similarly to the (1+1)D case, it is possible to obtain a finite difference scheme purely in terms of the junction voltages $U_{J,i,j}$, under the assumption that the admittances of all the waveguides in the network are identical, and equal to some positive constant $Y$. Thus, from (4.56), $Y_{J,i,j} = 4Y$. We have, for the junction at location $x = i\Delta$, $y = j\Delta$,

$$\begin{aligned} U_{J,i,j}(n+1) &= \frac{2}{Y_{J,i,j}}\sum_q Y_{q,i,j}U^+_{q,i,j}(n+1), \qquad\qquad q = \{x^-, x^+, y^-, y^+\} \\ &= \frac{1}{2}\left(U^-_{x^-,i+1,j}(n) + U^-_{x^+,i-1,j}(n) + U^-_{y^-,i,j+1}(n) + U^-_{y^+,i,j-1}(n)\right) \\ &= \frac{1}{2}\left(U_{J,i+1,j}(n) + U_{J,i-1,j}(n) + U_{J,i,j+1}(n) + U_{J,i,j-1}(n)\right) \\ &- \frac{1}{2}\left(U^+_{x^-,i+1,j}(n) + U^+_{x^+,i-1,j}(n) + U^+_{y^-,i,j+1}(n) + U^+_{y^+,i,j-1}(n)\right) \\ &= \frac{1}{2}\left(U_{J,i+1,j}(n) + U_{J,i-1,j}(n) + U_{J,i,j+1}(n) + U_{J,i,j-1}(n)\right) \\ &- \frac{2}{Y_{J,i,j}}\sum_q Y_{q,i,j}U^-_{q,i,j}(n-1) \\ &= \frac{1}{2}\left(U_{J,i+1,j}(n) + U_{J,i-1,j}(n) + U_{J,i,j+1}(n) + U_{J,i,j-1}(n)\right) - U_{J,i,j}(n-1) \end{aligned}$$

This is identical to 4.54 if we replace $U_J$ by $U$.

If we now replace all the bidirectional delay lines in Figure 4.19 by the same split pair of lines shown in Figure 4.11, then we get the arrangement in Figure 4.20. We have placed the split lines such that the branches containing sign inversions are adjacent to the western and southern ports of the parallel junctions. We also introduce new junction variables $I_{xJ}$ at the series junctions between two horizontal half-sample waveguides, and $I_{yJ}$ at the series junctions between two vertical delay lines, as well as all the associated wave quantities at the ports of the new series junctions. It is straightforward to show that upon identifying $I_{xJ}$, $I_{yJ}$ and $U_J$ with $I_x$ and $I_y$ and $U_J$, the mesh will calculating according to scheme (4.52) with constant coefficients, if we choose

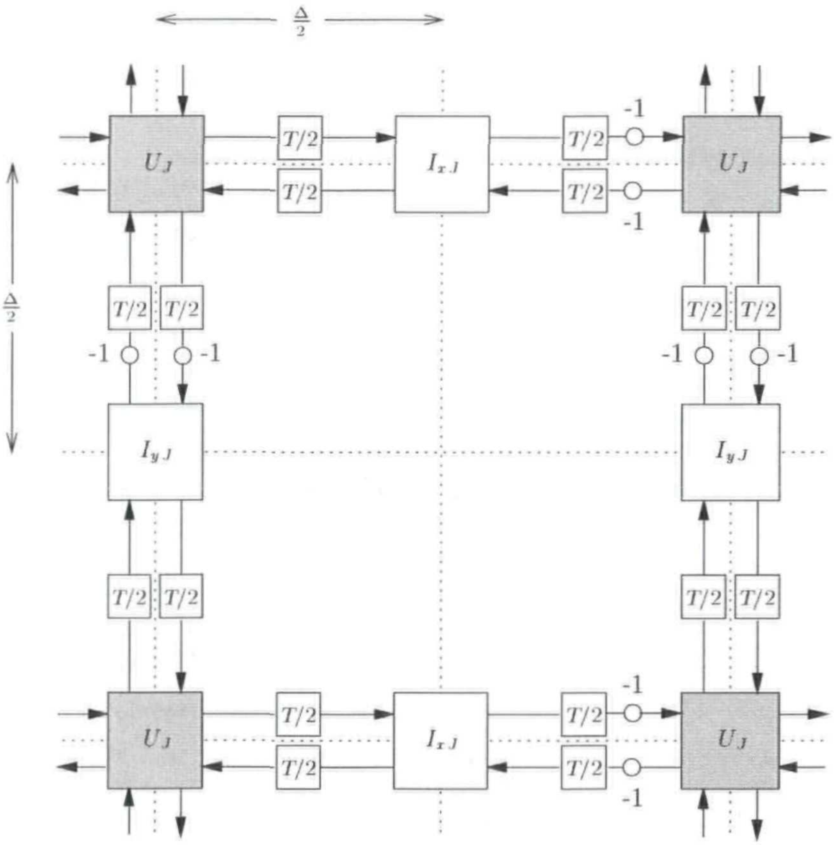

Figure 4.20: *(2+1)D interleaved waveguide mesh.*

$$v_0 = \sqrt{\frac{2}{lc}} \qquad\qquad Z = \sqrt{\frac{2l}{c}}$$

where $Z$ is the impedance in all the delay lines. We are again at the *magic* time step, but the impedance has been set to be *larger* than the characteristic impedance of the medium. Also, notice that the speed of propagation along the delay lines is not the wave speed of the medium, which is $\gamma = 1/\sqrt{lc}$. Such a mesh is called a *slow-wave* structure [90] in the TLM literature. At this point, it is useful to compare Figures 4.20 and 4.18.

**Losses, Sources, and Spatially-varying Coefficients**

We can deal with spatially-varying material parameters as well as losses and sources in a manner similar to the (1+1)D case. The full (2+1)D transmission line equations, as originally presented in §3.8, are

$$\begin{aligned}
l\frac{\partial i_x}{\partial t} + \frac{\partial u}{\partial x} + ri_x + e &= 0 && (4.58a)\\
l\frac{\partial i_y}{\partial t} + \frac{\partial u}{\partial y} + ri_y + f &= 0 && (4.58b)\\
c\frac{\partial u}{\partial t} + \frac{\partial i_x}{\partial x} + \frac{\partial i_y}{\partial y} + gu + h &= 0 && (4.58c)
\end{aligned}$$

where we have $r(x,y) \geq 0$ and $g(x,y) \geq 0$, and $e$, $f$ and $h$ are driving functions of $x$, $y$ and $t$.

The centered difference approximation to (4.58) is

$$\begin{aligned}
I_{x,i+\frac{1}{2},j}(n+\tfrac{1}{2}) - \rho_{I,i+\frac{1}{2},j}I_{x,i+\frac{1}{2},j}(n-\tfrac{1}{2}) &+ \sigma_{I,i+\frac{1}{2},j}\left(U_{i+1,j}(n) - U_{i,j}(n)\right)\\
&+ \Delta\sigma_{I,i+\frac{1}{2},j}\bar{e}_{i+\frac{1}{2},j}(n) = 0 && (4.59a)\\
I_{y,i,j+\frac{1}{2}}(n+\tfrac{1}{2}) - \rho_{I,i,j+\frac{1}{2}}I_{y,i,j+\frac{1}{2}}(n-\tfrac{1}{2}) &+ \sigma_{I,i,j+\frac{1}{2}}\left(U_{i,j+1}(n) - U_{i,j}(n)\right)\\
&+ \Delta\sigma_{I,i,j+\frac{1}{2}}\bar{f}_{i,j+\frac{1}{2}}(n) = 0 && (4.59b)\\
U_{i,j}(n) - \rho_{U,i,j}U_{i,j}(n-1) &+ \sigma_{U,i,j}\left(I_{x,i+\frac{1}{2},j}(n-\tfrac{1}{2}) - I_{x,i-\frac{1}{2},j}(n-\tfrac{1}{2})\right)\\
&+ \sigma_{U,i,j}\left(I_{y,i,j+\frac{1}{2}}(n-\tfrac{1}{2}) - I_{y,i,j-\frac{1}{2}}(n-\tfrac{1}{2})\right)\\
&+ \Delta\sigma_{U,i,j}\bar{h}_{i,j}(n-\tfrac{1}{2}) = 0 && (4.59c)
\end{aligned}$$

where

$$\rho_{I,k,p} = \frac{2\bar{l}_{k,p} - r_{k,p}T}{2\bar{l}_{k,p} + r_{k,p}T} \qquad \sigma_{I,k,p} = \frac{2}{2v_0\bar{l}_{k,p} + r_{k,p}\Delta} \qquad (4.60)$$

$$r_{k,p} = r(k\Delta, p\Delta) \qquad \bar{l}_{k,p} = l(k\Delta, p\Delta) + O(\Delta^2) \qquad (4.61)$$

for $k$, $p$ half-integer such that $2(k+p)$ is odd, and

$$\rho_{U,i,j} = \frac{2\bar{c}_{i,j} - g_{i,j}T}{2\bar{c}_{i,j} + g_{i,j}T} \qquad \sigma_{U,i,j} = \frac{2}{2v_0\bar{c}_{i,j} + g_{i,j}\Delta}$$

$$g_{i,j} = g(i\Delta, j\Delta) \qquad \bar{c}_{i,j} = c(i\Delta, j\Delta) + O(\Delta^2)$$

for $i$, $j$ integer. For the sources, we have used

$$\begin{aligned}\bar{e}_{i+\frac{1}{2},j}(n) &= \frac{1}{2}\Big(e_{i+\frac{1}{2},j}(n+\tfrac{1}{2})+e_{i+\frac{1}{2},j}(n-\tfrac{1}{2})\Big)\\ \bar{f}_{i,j+\frac{1}{2}}(n) &= \frac{1}{2}\Big(f_{i,j+\frac{1}{2}}(n+\tfrac{1}{2})+f_{i,j+\frac{1}{2}}(n-\tfrac{1}{2})\Big)\\ \bar{h}_{i,j}(n-\tfrac{1}{2}) &= \frac{1}{2}\Big(h_{i,j}(n)+h_{i,j}(n-1)\Big)\end{aligned}$$

where

$$\begin{aligned}e_{i+\frac{1}{2},j}(n+\tfrac{1}{2}) &= e\left((i+\tfrac{1}{2})\Delta, j\Delta, (n+\tfrac{1}{2})T\right)\\ f_{i,j+\frac{1}{2}}(n+\tfrac{1}{2}) &= f\left(i\Delta, (j+\tfrac{1}{2})\Delta, (n+\tfrac{1}{2})T\right)\\ h_i(n) &= h\left(i\Delta, j\Delta, nT\right)\end{aligned}$$

Again, we have applied a semi-implicit approximation to the constant-proportional terms of (4.58).

The waveguide network shown in Figure 4.21 is a direct generalization to (2+1)D of Figure 4.15. To the structure of Figure 4.20 we have added an extra port to each scattering junction, series or parallel, which is connected to a self-loop of impedance $Z_c$ and doubled delay length, as well as a port with impedance $Z_R$ to introduce losses and sources. All immittances are indexed by the coordinates of their associated junctions. As before, we set the admittance $Y = 1/Z$ for any impedance $Z$ in the network. In Figure 4.21, the linking admittances of the bidirectional delay lines are indicated only at the parallel junction, since we must have

$$Y_{x^+,i,j} = \frac{1}{Z_{x^-,i+\frac{1}{2},j}} \qquad Y_{x^-,i,j} = \frac{1}{Z_{x^+,i-\frac{1}{2},j}} \qquad Y_{y^+,i,j} = \frac{1}{Z_{y^-,i,j+\frac{1}{2}}} \qquad Y_{y^-,i,j} = \frac{1}{Z_{y^+,i,j-\frac{1}{2}}}$$

The junction admittances and impedances are thus

$$\begin{aligned}Y_{J,i,j} &= Y_{x^-,i,j}+Y_{x^+,i,j}+Y_{y^-,i,j}+Y_{y^+,i,j}+Y_{c,i,j}+Y_{R,i,j}\\ Z_{J,i+\frac{1}{2},j} &= Z_{x^-,i+\frac{1}{2},j}+Z_{x^+,i+\frac{1}{2},j}+Z_{c,i+\frac{1}{2},j}+Z_{R,i+\frac{1}{2},j}\\ Z_{J,i,j+\frac{1}{2}} &= Z_{y^-,i,j+\frac{1}{2}}+Z_{y^+,i,j+\frac{1}{2}}+Z_{c,i,j+\frac{1}{2}}+Z_{R,i,j+\frac{1}{2}}\end{aligned}$$

Beginning from series and parallel junctions, and proceeding through derivations similar to (4.32) yields the difference scheme (4.59) in the junction variables $U_J$, $I_{xJ}$ and $I_{yJ}$, provided we set

$$\begin{aligned}Y_{J,i,j} &= 2v_0\bar{c}_{i,j}+\Delta g_{i,j} & Y_{R,i,j} &= \Delta g_{i,j} & U^+_{R,i,j} &= -h_{i,j}/2g_{i,j}\\ Z_{J,i+\frac{1}{2},j} &= 2v_0\bar{l}_{i+\frac{1}{2},j}+\Delta r_{i+\frac{1}{2},j} & Z_{R,i+\frac{1}{2},j} &= \Delta r_{i+\frac{1}{2},j} & I^+_{R,i+\frac{1}{2},j} &= -e_{i+\frac{1}{2},j}/2r_{i+\frac{1}{2},j}\\ Z_{J,i,j+\frac{1}{2}} &= 2v_0\bar{l}_{i,j+\frac{1}{2}}+\Delta r_{i,j+\frac{1}{2}} & Z_{R,i,j+\frac{1}{2}} &= \Delta r_{i,j+\frac{1}{2}} & I^+_{R,i,j+\frac{1}{2}} &= -e_{i,j+\frac{1}{2}}/2r_{i+\frac{1}{2},j}\end{aligned} \tag{4.62}$$

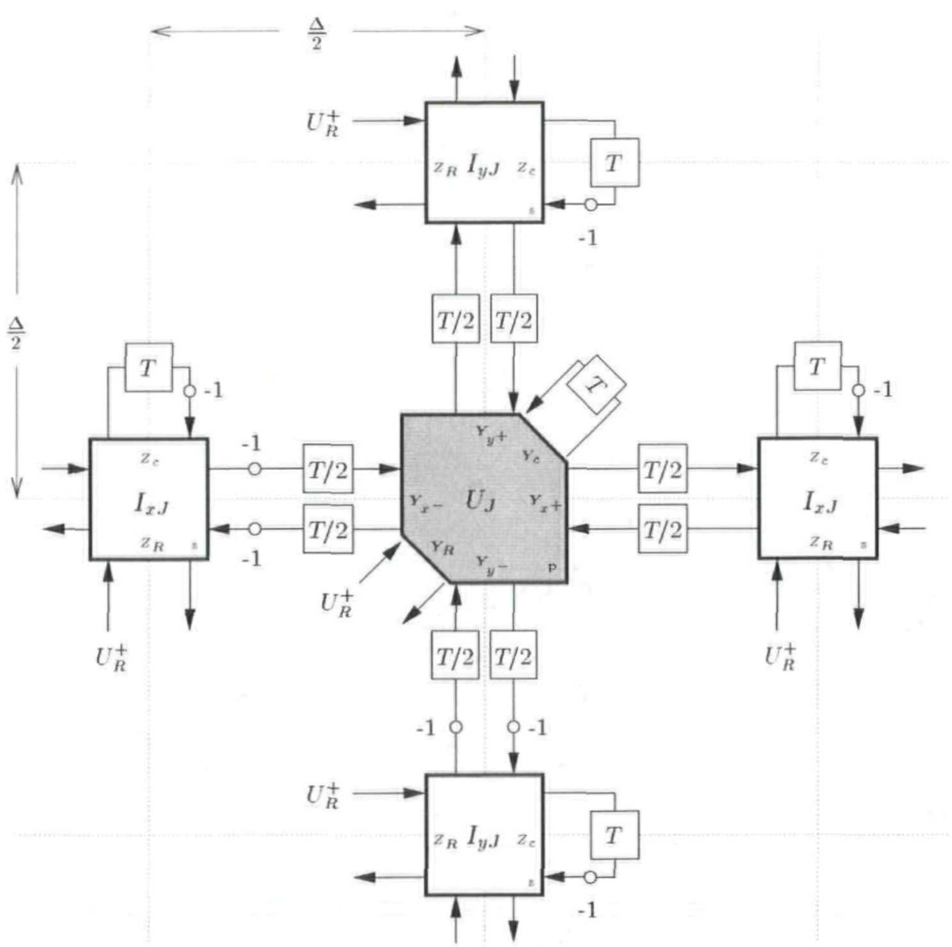

Figure 4.21: *(2+1)D waveguide mesh for the varying-coefficient system* (4.58), *with losses and sources.*

We can again identify three useful ways of setting the immittances:

### Type I: Voltage-centered Mesh

At a parallel junction, we set the self-loop admittance $Y_{c,i,j}$ to zero, and the admittances of the branches leading away from a parallel junction at grid point $(i,j)$ to be identical, thus

$$Y_{c,i,j}=0 \qquad\qquad Y_{x-,i,j}=Y_{x+,i,j}=Y_{y-,i,j}=Y_{y+,i,j}=\frac{v_0}{2}c_{i,j}$$

and set

$$\begin{aligned} Z_{c,i+\frac{1}{2},j} &= v_0(l_{i,j}+l_{i+1,j})-\frac{2}{v_0}\left(\frac{1}{c_{i,j}}+\frac{1}{c_{i+1,j}}\right) \\ Z_{c,i,j+\frac{1}{2}} &= v_0(l_{i,j}+l_{i,j+1})-\frac{2}{v_0}\left(\frac{1}{c_{i,j}}+\frac{1}{c_{i,j+1}}\right) \end{aligned}$$

The positivity requirements on $Z_{c,i+\frac{1}{2},j}$ and $Z_{c,i,j+\frac{1}{2}}$ force us to choose

$$v_0 \geq \max_{i,j}\left(\sqrt{\frac{2}{l_{i,j}c_{i,j}}}\right) \tag{4.63}$$

Thus we have a simple CFL-type bound on the space step/time step ratio, which must be chosen greater than $\sqrt{2}$ times the maximum value of the local group velocity $1/\sqrt{lc}$ over parallel junction locations $(i\Delta, j\Delta)$. The bound (4.63) converges to $\sqrt{2}\gamma^{g}_{PP,max}$, as defined by (3.65), in the limit as the grid spacing $\Delta$ becomes small.

### Type II: Current-centered Mesh

This arrangement is the dual to the previous case. We now set

$$\begin{aligned}
Z_{x^+,i+\frac{1}{2},j} &= Z_{x^-,i+\frac{1}{2},j} = v_0 l_{i+\frac{1}{2},j} && (4.64)\\
Z_{y^+,i,j+\frac{1}{2}} &= Z_{y^-,i,j+\frac{1}{2}} = v_0 l_{i,j+\frac{1}{2}} && (4.65)\\
Z_{c,i+\frac{1}{2},j} &= Z_{c,i,j+\frac{1}{2}} = 0 && (4.66)
\end{aligned}$$

and

$$Y_{c,i,j} = -\frac{1}{v_0}\left(\frac{1}{l_{i+\frac{1}{2},j}}+\frac{1}{l_{i-\frac{1}{2},j}}+\frac{1}{l_{i,j+\frac{1}{2}}}+\frac{1}{l_{i,j-\frac{1}{2}}}\right)+\frac{v_0}{2}\left(c_{i+\frac{1}{2},j}+c_{i-\frac{1}{2},j}+c_{i,j+\frac{1}{2}}+c_{i,j-\frac{1}{2}}\right)$$

We then have

$$v_0 \geq \max_{2(k+p)\ \mathrm{odd}}\left(\sqrt{\frac{2}{l_{k,p}c_{k,p}}}\right) \tag{4.67}$$

for half-integer $k$ and $p$. It is rather interesting that in (2+1)D, if we have $r = 0$ and $e = f = 0$, this arrangement (and not that of type I) allows the series junctions to be treated as throughs (with sign inversion). We may thus operate at a reduced sample rate in this case. This particular choice of immittances, in the constant-coefficient, lossless and source-free case with $v_0 = \sqrt{2/(lc)}$, yields the original form of the waveguide mesh proposed in [198], and mentioned in §4.2.7. We also note that networks such as this and type I, for which the connecting immittances may vary spatially have also been explored in TLM [29, 159].

### Type III: Mixed Mesh

We set

$$Z_{x^-,i+\frac{1}{2},j} = Z_{x^+,i+\frac{1}{2},j} = Z_{y^-,i,j+\frac{1}{2}} = Z_{y^+,i,j+\frac{1}{2}} = Z_{const}$$

where $Z_{const}$ is some positive constant, and then choose

$$\begin{aligned} Y_{c,i,j} &= 2v_0 c_{i,j} - \frac{4}{Z_{const}} \\ Z_{c,i+\frac{1}{2},j} &= 2v_0 l_{i+\frac{1}{2},j} - 2Z_{const} \\ Z_{c,i,j+\frac{1}{2}} &= 2v_0 l_{i,j+\frac{1}{2}} - 2Z_{const} \end{aligned}$$

The optimal value of $Z_{const}$ is easily shown to be

$$Z_{const} = \sqrt{\frac{2\min_{2(k+p)\ \mathrm{odd}} l_{k,p}}{\min_{i,j} c_{i,j}}}$$

and this leads to the constraint

$$v_0 \geq \sqrt{\frac{2}{\min_{2(k+p)\ \mathrm{odd}}(l_{k,p})\min_{i,j}(c_{i,j})}}$$

for $i$, $j$ integer and $k$ and $p$ half-integer. As in (1+1)D, this bound is inferior to those obtained using the type I and type II meshes. Because the immittance settings are simpler, however, this form may be preferable, from a programming standpoint.

### 4.4.3 Reduced Computational Complexity and Memory Requirements in the Standard Form of the Waveguide Mesh

The standard form of the waveguide mesh [198] was proposed as a means of solving the (2+1)D wave equation (4.50). We would like to note that it is possible, in this special case, to reduce both computational complexity and memory requirements by taking advantage of the fact that the mesh calculation can be subdivided into two mutually exclusive schemes. We represent this subdivision graphically in Figure 4.22 by coloring the two subgrids white and grey. Voltages are calculated at all the junctions, at every time step. However, it should be clear from the figure that the calculation of $U_J$ at a grey-colored junction will only depend on wave variables scattered from the white junctions at the previous time step. We then only need calculate half the junction voltages at any given time step: at the grey junctions at even multiples (say) of the time step, and at white junctions for odd multiples.

We can go further as well—if we have dropped half the junction calculations at any given time step, then we are in fact only using one of the two delay registers in any bidirectional delay line (grey or white in Figure 4.22). Thus only one delay register will be required for any waveguide. In addition, because in calculating the junction voltage at a grey junction (say), we make use only of incoming wave variables, and not the junction voltages at the white junctions, calculated one time step previously, one set of registers may be used at alternating time steps to store both the grey and

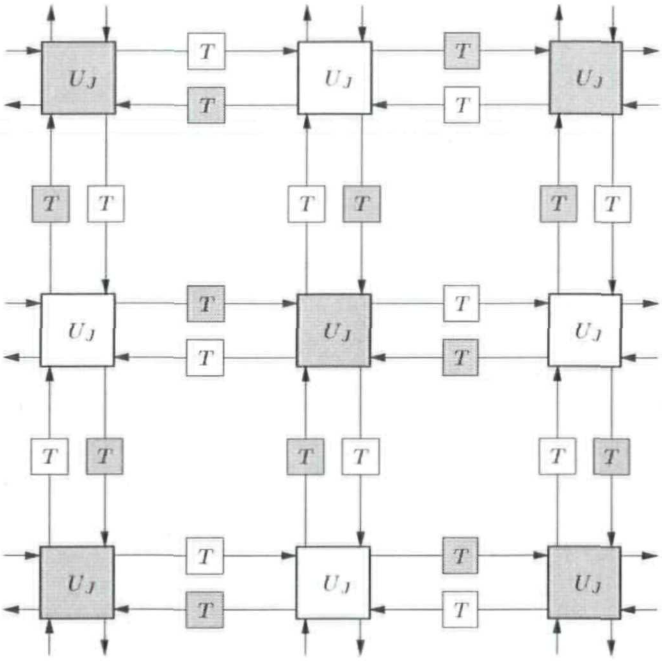

Figure 4.22: *Grid decomposition for the standard waveguide mesh.*

white voltages.

This amounts to a factor-of-two savings in terms of both memory requirements and the operation count. We are, of course, approximating the solution at only half the mesh points at any time step, but there is no reduction in accuracy, because the separate sub-calculation which has been removed operated completely independently. (It is true, however, that we have sacrificed the higher end of the range of spatial frequencies which can be approximated without aliasing.) One additional advantage is that under this simplification, there will be no need for temporary registers (normally necessary during the scattering operation); at a given time step there is no danger of overwriting an incoming wave variable at a particular junction, because if we have just scattered there, we will not scatter there again for two time steps. The savings in terms of memory is of a factor of $14/5$ over the standard mesh implementation, though the reduction in the spatial frequency range should be taken into account. We note that in this implementation, each pass through the main loop in the computer program will contain two time steps worth of scattering operations. Once one has programmed a mesh a few times, the possibility of performing such a computational trick becomes obvious, and for this reason it is rather surprising that it has apparently not been explicitly mentioned in the TLM literature, even in papers specific to parallel computation [170]. We will look at grid decomposition issues in much more detail in Appendix A.

Such memory-sharing ideas also appeared early on in wave digital filters which use unit elements [41] and in WDF-based numerical integration schemes [131]. We note that this idea can be applied here only for the wave equation at CFL; otherwise, if we are using, for example, a type II mesh, we necessarily have unit-delay self-loops at the junctions, so that the mesh calculation can not be similarly decomposed.

### 4.4.4 Boundary Conditions

We now examine the termination of the waveguide mesh which simulates the behavior of the (2+1)D parallel-plate equations. The two most important types of boundary conditions are

$$u = 0 \qquad \text{Short-circuit termination} \qquad (4.68)$$

$$i_n = 0 \qquad \text{Open-circuit termination} \qquad (4.69)$$

where $i_n$ refers to the component of $(i_x, i_y)$ which is normal to the boundary. Condition (4.68) corresponds to a transmission line plate pair which are connected (and thus short-circuited) at the boundary; the same condition holds for a clamped membrane for which $u$ is interpreted as a transverse velocity, and $(i_x, i_y)$ as in-plane forces. Condition (4.69) is an open-circuited termination; current can not leave the plate at the edges. This second condition is analogous to the rigid termination of a (2+1)D acoustic medium, where $(i_x, i_y)$ are interpreted as flow velocities, and $u$ as a pressure. Both conditions are of the form of (3.8), and are lossless. We will examine only the termination of the mesh on a rectangular domain (though the result extends easily to the radial mesh to be discussed in §4.6.2).

In the case of the (1+1)D transmission line, we could treat a staggered mesh terminated by a parallel junction, and through the duality of $i$ and $u$ extend the result to include termination by a series junction (see §4.3.9). This is no longer the case in (2+1)D, and we must treat the two types of termination separately. Consider a bottom (southern) boundary at $y = 0$ of an interleaved mesh of the type shown in Figure 4.21. The two possible types of termination are shown in Figure 4.23.

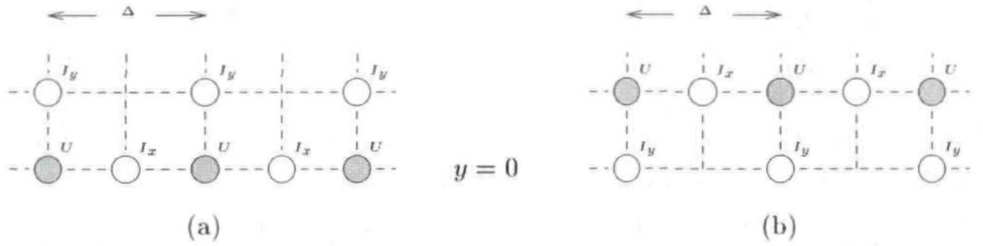

(a) (b)

Figure 4.23: *Grid terminations at a southern boundary.*

### Grid Arrangement Requiring Voltage and Tangential Current Density Component on Boundary

Consider the termination arrangement of Figure 4.23(a). In the source-free case, if for $y = 0$ we have $u(x, 0, t) = 0$, then from (4.58a),

$$l\frac{\partial i_x}{\partial t} + ri_x = 0 \qquad \text{for} \qquad y = 0$$

Thus the current density component tangential to the boundary is uncoupled from the other dependent variables. It is convenient to assume, then, that $i_x(x, 0, t)$ is initially zero, so that it will remain so permanently. In this case, we can drop the series junctions corresponding to $i_x$ on the southern boundary from the network. Otherwise, we may allow the junctions to remain, as lumped damped (by a factor $r/l$) elements, still uncoupled from the rest of the network. In either case, the parallel junctions at the grey points in Figure 4.23(a) may be short-circuited as in the (1+1)D case in order to realize boundary condition (4.68). The waveguide mesh termination corresponding to (4.68) is shown in Figure 4.24(a).

To deal with the boundary condition $i_y(x, 0, t) = 0$, we may proceed as in the (1+1)D case, and write down a difference approximation to (4.58c), where we use the one-sided difference approximation

$$\begin{aligned}\left.\frac{\partial i_y}{\partial y}\right|_{y=0} &= \frac{2}{\Delta}\left(i_y(x, \frac{\Delta}{2}, t) - i_y(x, 0, t)\right) + O(\Delta)\\ &= \frac{2}{\Delta}i_y(x, \frac{\Delta}{2}, t) + O(\Delta)\end{aligned}$$

and centered differences in the time and $x$ directions,

$$\begin{aligned}U_{i,0}(n) - \rho_{U,i,0}U_{i,0}(n-1) &+ \sigma_{U,i,0}\left(I_{x,i+\frac{1}{2},0}(n-\tfrac{1}{2}) - I_{x,i-\frac{1}{2},0}(n-\tfrac{1}{2})\right)\\ &+ 2\sigma_{U,i,0}I_{y,i,\frac{1}{2}}(n-\tfrac{1}{2}) = 0\end{aligned}$$

where $\sigma_{U,i,0}$ and $\rho_{U,i,0}$ are as given in (4.60).

Here, the voltages on the boundary are related to the tangential currents, which, from Figure 4.23(a), are also calculated on the boundary. This implies that the corresponding junctions will be connected to one another by waveguides which lie directly on the boundary. Also notice the doubled weighting of the $I_y$ grid function at the boundary; this requires special care in the DWN implementation, though it also follows from a structurally passive termination, provided we make use of *transformers* along the boundary waveguides. Though we have not discussed transformers in the DWN context [166], they are identical to wave digital transformers, which were mentioned in §2.3.4. In effect, we may introduce multiplies by $\kappa$ and $1/\kappa$, for any real $\kappa$ in the two signal paths of any waveguide without affecting losslessness, provide we scale impedances at both ends of the waveguide accordingly. The DWN termination corresponding to $i_y = 0$ at a southern boundary is shown in Figure 4.24(b). We have used transformers of turns ratio 2, implying that the immittances on the boundary satisfy

$$Y_{x^-,i,0} = \frac{1}{4Z_{x^+,i-\frac{1}{2},0}} \qquad\qquad Y_{x^+,i,0} = \frac{1}{4Z_{x^-,i+\frac{1}{2},0}} \tag{4.70}$$

The corresponding difference equation at a parallel boundary junction is then

$$\begin{aligned} U_{J,i,0}(n) - \frac{Y_{J,i,0} - 2Y_{R,i,0}}{Y_{J,i,0}} U_{J,i,0}(n-1) \quad &+ \quad \frac{1}{Y_{J,i,0}}\left(I_{xJ,i+\frac{1}{2},0}(n-\tfrac{1}{2}) - I_{xJ,i-\frac{1}{2},0}(n-\tfrac{1}{2})\right) \\ &+ \quad \frac{2}{Y_{J,i,0}} I_{y,i,\frac{1}{2}}(n-\tfrac{1}{2}) = 0 \end{aligned}$$

where

$$Y_{J,i,0} \triangleq Y_{x^-,i,0} + Y_{x^+,i,0} + Y_{y^+,i,0} + Y_{c,i,0} + Y_{R,i,0} \tag{4.71}$$

The junction updating will be equavlent to the centered difference scheme if we choose

$$Y_{J,i,0} = v_0\bar{c}_{i,0} + \frac{g_{i,0}\Delta}{2} \qquad\qquad Y_{R,i,0} = \frac{g_{i,0}\Delta}{2} \tag{4.72}$$

Given that the northward immittances at the boundary junctions must be set as interior values, the settings for the remaining immittances for the type I and II meshes discussed in §4.4.2 will be

Type I:

$$\begin{aligned} Y_{x^-,i,0} &= Y_{x^+,i,0} = \frac{v_0c_{i,0}}{4} \qquad Z_{x^+,i+\frac{1}{2},0} = \frac{1}{v_0c_{i+1,0}} \qquad Z_{x^-,i+\frac{1}{2},0} = \frac{1}{v_0c_{i-1,0}} \\ Y_{c,i,0} &= 0 \qquad Z_{c,i+\frac{1}{2},0} = v_0l_{i+1,0} + v_0l_{i,0} - \frac{1}{v_0c_{i+1,0}} - \frac{1}{v_0c_{i,0}} \end{aligned}$$

Type II:

$$\begin{aligned} Z_{x^-,i+\frac{1}{2},0} &= Z_{x^-,i+\frac{1}{2},0} = v_0l_{i+\frac{1}{2},0} \qquad Y_{x^+,i,0} = \frac{1}{4v_0l_{i+\frac{1}{2},0}} \qquad Y_{x^-,i,0} = \frac{1}{4v_0l_{i-\frac{1}{2},0}} \\ Z_{c,i+\frac{1}{2},0} &= 0 \qquad Y_{c,i,0} = \frac{v_0c_{i,\frac{1}{2}}}{2} + \frac{v_0c_{i+\frac{1}{2},0}}{4}\frac{+v_0c_{i-\frac{1}{2},0}}{4} - \frac{1}{v_0l_{i,\frac{1}{2}}} - \frac{1}{4v_0l_{i+\frac{1}{2},0}} - \frac{1}{4v_0l_{i-\frac{1}{2},0}} \end{aligned}$$

The passivity conditions which follow from the positivity of the boundary self-loop immittances will be

$$\begin{aligned} v_0 &\geq \max_i \sqrt{\frac{1}{l_{i,0}c_{i,0}}} && \text{Type I} \\ v_0 &\geq \max\left(\max_i \sqrt{\frac{2}{l_{i,\frac{1}{2}}c_{i,\frac{1}{2}}}},\ \max_{i+\frac{1}{2}} \sqrt{\frac{1}{l_{i+\frac{1}{2},0}c_{i+\frac{1}{2},0}}}\right) && \text{Type II} \end{aligned}$$

and clearly are *less restrictive* than the conditions (4.63) and (4.67) over the mesh interior, and hence do not affect the overall stability bound on $v_0$.

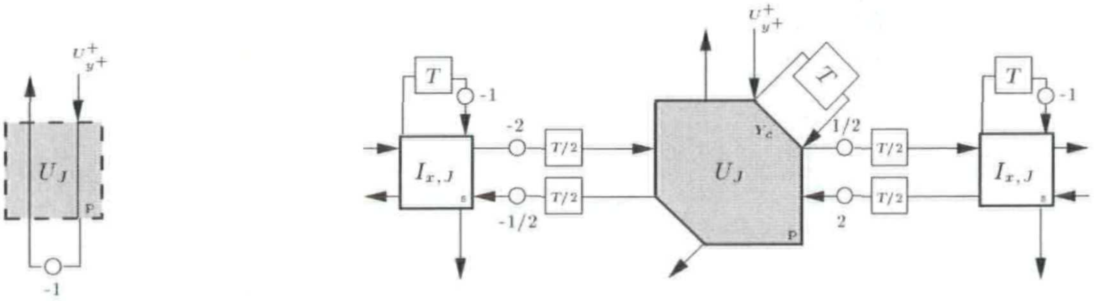

(a) (b)

Figure 4.24: *(2+1)D waveguide mesh terminations at a southern boundary, for the grid arrangement of Figure 4.23(a)*— (a) *for* $u(x,0,t)=0$ *and* (b) $i(x,0,t)=0$.

### Grid Arrangement with Normal Current Density Component Required on Boundary

Termination of the other type of mesh, as shown in Figure 4.23(b) is comparatively simple, because the series junctions are isolated from one another along the boundary itself. Terminations for both types of boundary conditions are shown in Figure 4.25. The boundary condition $i_y = 0$ can be simply implemented by terminating the series boundary junctions in open circuits. The condition $u = 0$ can be ensured by through proper adjustment of the self-loop impedance, depending on the type of waveguide mesh. The settings will be

$$\begin{aligned} Z_{c,i+\frac{1}{2},0} &= v_0 l_{i+\frac{1}{2},\frac{1}{2}} - \frac{2}{v_0 c_{i+\frac{1}{2},\frac{1}{2}}} && \text{Type I} \\ Z_{c,i+\frac{1}{2},0} &= 0 && \text{Type II} \end{aligned}$$

The positivity condition on the boundary self-loop impedances for the type I mesh again does not degrade the stability bound over the mesh interior. As for interior series junctions, we will have $Z_R = r\Delta/2$ at the boundary junctions.

This type of mesh possesses an additional advantage—if we are working on a rectangular domain,

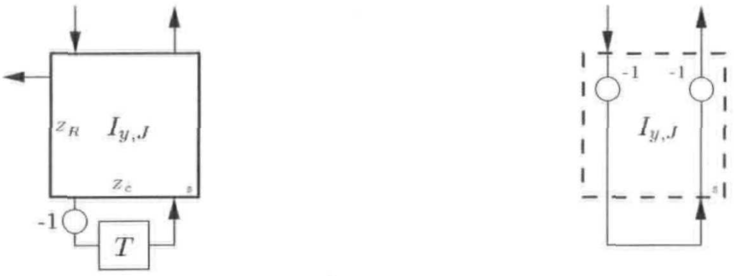

(b)

Figure 4.25: *(2+1)D waveguide mesh terminations at a southern boundary, for the grid of Figure 4.23(b)— for* (a) $u(x,0,t)=0$ *and* (b) $i_y(x,0,t)=0$.

then the "holes" in the staggered grid (that is, those points at which neither $U$ nor $I$ is calculated, as per Figure 4.18) may be placed at the corners of the domain. The extra programming task of specializing the waveguide mesh at the corners can then be safely ignored.

All results can of course be extended, by symmetry, to any edge of a rectangular domain.

## 4.5 Initial Conditions

We have dealt, so far, with a method of integrating the transmission line and parallel-plate transmission line systems, but have not examined the necessary initialization of the algorithm. We will deal, here, with the lossless source-free cases.

In (1+1)D, the hyperbolic system (4.17) requires two initial conditions. That is, we require the knowledge of initial current and voltage distributions along the line. We would like to enter the discrete equivalent of this data into the delay registers somehow at the first time step $n=0$. From Figure 4.14, it should be clear that four sets of data are required: $U^{+}_{x^-,i}(0)$, $U^{+}_{x^+,i}(0)$, $U^{+}_{c,i}(0)$, which are the initial incoming waves at the parallel junctions, and $I^{+}_{c,i+\frac{1}{2}}(\frac{1}{2})$, the values initially stored in the self-loops at the series junctions.

The first problem we encounter is that, on our decimated grid, we calculate values of $U_J$ and $I_J$, the grid functions corresponding to voltage and current, at alternating time steps. We have chosen our grid such that for $k$ and $m$ half-integer, $I_k(m)$ is calculated for odd values of $2m$, and $U_k(m)$ for $2m$ even; at time zero, then, $U_J$ is accessible (as a combination of wave variables). How then do we enter the current initial data into the algorithm? It turns out that this problem is rather simply addressed. We can do one of two things: set the value of $I_J$ at time step $\frac{1}{2}$ to be equal to a sampled version of $i(x,0)$, and accept the error that this introduces, which will be $O(T)$, or we can use any available numerical method (i.e. one which does not operate on a staggered grid) to propagate the initial data $i_0(x)$ forward by $T/2$. Such a method should be at least $O(T^2)$ accurate, but it is allowed to even be ***unstable***, since we will only be using it to update once [176].

Assume then, that our initial data are $U_i^*(0) = u(i\Delta, 0)$, and $I^*_{i+\frac{1}{2}}(\frac{1}{2})$, some approximation to $i((i+\frac{1}{2})\Delta, \frac{T}{2})$ obtained by either of the methods mentioned above. At time step $n = 0$, we can write the junction voltages $U_{J,i}(0)$ as

$$U_{J,i}(0) = \frac{2}{Y_{J,i}}\left(Y_{x^+,i}U^+_{x^+,i}(0) + Y_{x^-,i}U^+_{x^-,i}(0) + Y_{c,i}U^+_{c,i}(0)\right) \tag{4.73}$$

and $I_{J,i+\frac{1}{2}}(\frac{1}{2})$ as

$$\begin{aligned}
I_{J,i+\frac{1}{2}}(\tfrac{1}{2}) =& \frac{2}{Z_{J,i+\frac{1}{2}}}\left(Z_{x^+,i+\frac{1}{2}}I^+_{x^+,i+\frac{1}{2}}(\tfrac{1}{2}) + Z_{x^-,i+\frac{1}{2}}I^+_{x^-,i+\frac{1}{2}}(\tfrac{1}{2}) + Z_{c,i+\frac{1}{2}}I^+_{c,i+\frac{1}{2}}(\tfrac{1}{2})\right)\\
=& \frac{2}{Z_{J,i+\frac{1}{2}}}\left(U^+_{x^+,i+\frac{1}{2}}(\tfrac{1}{2}) + U^+_{x^-,i+\frac{1}{2}}(\tfrac{1}{2}) + Z_{c,i+\frac{1}{2}}I^+_{c,i+\frac{1}{2}}(\tfrac{1}{2})\right)\\
=& \frac{2}{Z_{J,i+\frac{1}{2}}}\left(-U^-_{x^-,i+1}(0) + U^-_{x^+,i}(0) + Z_{c,i+\frac{1}{2}}I^+_{c,i+\frac{1}{2}}(\tfrac{1}{2})\right)\\
=& \frac{2}{Z_{J,i+\frac{1}{2}}}\left(-U_{J,i+1}(0) + U_{J,i}(0) + U^+_{x^-,i+1}(0) - U^+_{x^+,i}(0) + Z_{c,i+\frac{1}{2}}I^+_{c,i+\frac{1}{2}}(\tfrac{1}{2})\right)
\end{aligned} \tag{4.74}$$

The safest and most general way of proceeding, given that the immittances $Z_{c,i+\frac{1}{2}}$ and $Y_{c,i}$ may be zero, depending on the type of network we are using, is to set the initial values in the self-loops to zero. In this case, we can set

$$U^+_{c,i}(0) = I^+_{c,i+\frac{1}{2}}(\tfrac{1}{2}) = 0 \tag{4.75a}$$

$$U^+_{x^-,i}(0) = \frac{1}{4}\left(\frac{Y_{J,i}U_i^*(0)}{Y_{x^-,i}} + Z_{J,i-\frac{1}{2}}I^*_{i-\frac{1}{2}}(\tfrac{1}{2})\right) \tag{4.75b}$$

$$U^+_{x^+,i}(0) = \frac{1}{4}\left(\frac{Y_{J,i}U_i^*(0)}{Y_{x^+,i}} - Z_{J,i+\frac{1}{2}}I^*_{i+\frac{1}{2}}(\tfrac{1}{2})\right) \tag{4.75c}$$

It can be easily verified that with these initial values for the wave variables, the junction voltages $U_{J,i}(0)$ and currents $I_{J,i+\frac{1}{2}}(\frac{1}{2})$ calculated from the DWN by (4.73) and (4.74) respectively will be consistent with the initial values of the continuous problem to first order in $\Delta$. These settings may be used with any of the three types of network mentioned in §4.3.6.

We may ask, however, whether there is a way of setting the initial values such that we achieve better initial accuracy. For a network of type I, say, we have $Y_{c,i} = 0$. Then, if $Z_{c,i+\frac{1}{2}}$ is non-zero everywhere (this can always be arranged by operating slightly away from CFL), we may use

$$\begin{aligned}
U^+_{x^-,i}(0) &= U^+_{x^+,i}(0) = \frac{1}{2}U_i^*(0)\\
I^+_{c,i+\frac{1}{2}}(\tfrac{1}{2}) &= \frac{1}{2Z_{c,i+\frac{1}{2}}}\left(Z_{J,i+\frac{1}{2}}I^*_{i+\frac{1}{2}}(\tfrac{1}{2}) - U_i^*(0) + U^*_{i+1}(0)\right)
\end{aligned}$$

in which case the waveguide network reproduces the initial currents and voltages with no error. Similarly, for a type II network, we may set

$$\begin{aligned}
U^+_{x^+,i}(0) &= U^*_i(0) - \frac{1}{2Y_{x^+,i}} I^*_{i+\frac{1}{2}}(\tfrac{1}{2}) \\
U^+_{x^-,i}(0) &= U^*_i(0) + \frac{1}{2Y_{x^-,i}} I^*_{i-\frac{1}{2}}(\tfrac{1}{2}) \\
U^+_{c,i}(0) &= \frac{1}{2Y_{c,i}} \left( (Y_{c,i} - Y_{x^-,i} - Y_{x^+,i}) U^*_i(0) + I^*_{i+\frac{1}{2}}(\tfrac{1}{2}) - I^*_{i-\frac{1}{2}}(\tfrac{1}{2}) \right)
\end{aligned}$$

which also yields an exact calculation. Either of these two means of initializing wave variables may also be used in the type III DWN.

These initialization procedures generalize simply to (2+1)D, where the parallel-plate equations require three initial conditions $u(x,y,0)$, $i_x(x,y,0)$ and $i_y(x,y,0)$. In general, we now have seven wave variables to set: the waves approaching any parallel junction with coordinates $(i,j)$ at $n=0$, namely $U^+_{x^-,i,j}(0)$, $U^+_{x^+,i,j}(0)$, $U^+_{y^-,i,j}(0)$, $U^+_{y^+,i,j}(0)$ and $U^+_{c,i,j}(0)$, as well as the values stored in the self-loop registers at the series junctions, $I^+_{x,c,i+\frac{1}{2},j}(\frac{1}{2})$ and $I^+_{y,c,i,j+\frac{1}{2}}(\frac{1}{2})$. For the sake of brevity, we provide only the settings for the general case, analogous to (4.75):

$$\begin{aligned}
U^+_{x^-,i,j}(0) &= \frac{1}{4}\left( \frac{Y_{J,i,j} U^*_{i,j}(0)}{2Y_{x^-,i,j}} + Z_{J,i-\frac{1}{2},j} I^*_{x,i-\frac{1}{2},j}(\tfrac{1}{2}) \right) \\
U^+_{x^+,i,j}(0) &= \frac{1}{4}\left( \frac{Y_{J,i,j} U^*_{i,j}(0)}{2Y_{x^+,i,j}} - Z_{J,i+\frac{1}{2},j} I^*_{x,i+\frac{1}{2},j}(\tfrac{1}{2}) \right) \\
U^+_{y^-,i,j}(0) &= \frac{1}{4}\left( \frac{Y_{J,i,j} U^*_{i,j}(0)}{2Y_{y^-,i,j}} + Z_{J,i,j-\frac{1}{2}} I^*_{y,i,j-\frac{1}{2}}(\tfrac{1}{2}) \right) \\
U^+_{y^+,i,j}(0) &= \frac{1}{4}\left( \frac{Y_{J,i,j} U^*_{i,j}(0)}{2Y_{y^+,i,j}} - Z_{J,i,j+\frac{1}{2}} I^*_{y,i,j+\frac{1}{2}}(\tfrac{1}{2}) \right)
\end{aligned}$$

with, in addition,

$$U^+_{c,i,j}(0) = I^+_{x,i+\frac{1}{2},j}(\tfrac{1}{2}) = I^+_{y,i,j+\frac{1}{2}}(\tfrac{1}{2}) = 0$$

where

$$\begin{aligned}
U^*_{i,j}(0) &= u(i\Delta, j\Delta, 0) \\
I^*_{x,i+\frac{1}{2},j}(\tfrac{1}{2}) &= i_x((i+\tfrac{1}{2})\Delta, j\Delta, \tfrac{1}{2}) \\
I^*_{y,i,j+\frac{1}{2}}(\tfrac{1}{2}) &= i_y(i\Delta, (j+\tfrac{1}{2})\Delta, \tfrac{1}{2})
\end{aligned}$$

Because DWNs of the forms discussed in the previous sections are equivalent to two-step finite difference methods, problems with parasitic modes do not arise as they do in wave digital networks which simulate the same systems. This problem was discussed in detail in §3.9.

## 4.6 Alternative Grids in (2+1)D

We have looked, so far, at waveguide mesh solutions to the (2+1)D parallel-plate equations on a rectilinear grid. We now mention some other possible grid arrangements, first hexagonal and triangular regular grids, then a radial grid. Because Appendix A is devoted to an in-depth exploration of the various types of mesh which have appeared in the literature, we will only take a brief look at these meshes here, with an emphasis on spatially-varying media.

### 4.6.1 Hexagonal and Triangular Grids

Two other ways of regularly sampling the $(x, y)$ plane are shown in Figure 4.26. It was shown in [157] and [200] that a waveguide mesh can be constructed which solves the (2+1)D wave equation on a grid of either type. We will extend this result to include the lossless, source-free but varying-coefficient parallel-plate problem (4.49).

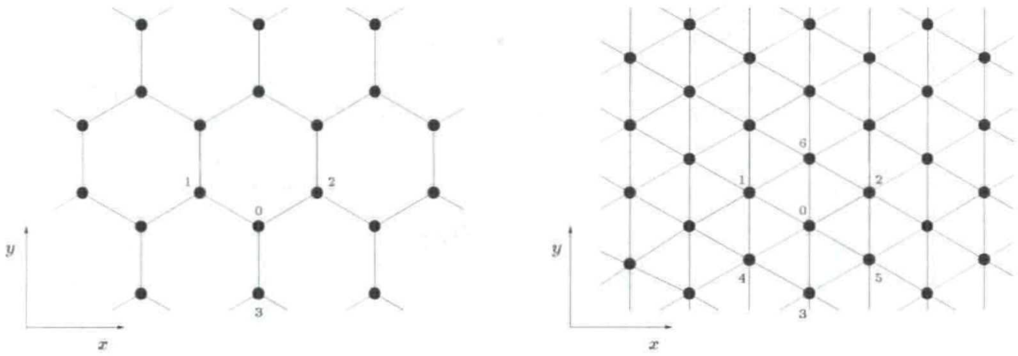

(a) (b)

Figure 4.26: *Alternative sampling grids*— (a) *hexagonal and* (b) *triangular.*

For both types of grid, lines between the grid points (marked by black dots in Figure 4.26) indicate that the points are to be connected by bidirectional delay lines. Connected points are separated by a distance $\Delta$. We will look at meshes of the type II form—that is, meshes for which we will need to calculate using only parallel junctions (recall that if we did not have losses or sources in (4.58a) and (4.58b) for the type II mesh of §4.4.2, the impedances of the bidirectional delay lines were set so that the series junctions degenerated to simple throughs) located at the grid points. We still allow $l$ and $c$ to vary smoothly over the domain. Additionally, we could allow sources and losses in (4.58c), but as mentioned above, we consider only the fully lossless source-free case here. We remark that we now have a mesh for which all delays are of equal duration (i.e., in both connecting waveguides and self-loops), unlike the interleaved mesh of type I or III.

The derivation of the waveguide mesh equivalent difference schemes on a hexagonal or triangular grid is very similar to the rectilinear case, and we will omit most steps. Referring to Figure 4.26(a), for the hexagonal mesh we have a four-port parallel junction at each grid point. At grid point 0, for example, we have unit sample bidirectional delay lines connecting the junction to those at locations 1, 2, and 3, and we will name the admittances of the three connecting lines $Y_{01}$, $Y_{02}$ and $Y_{03}$ respectively. In order to allow variation in local wave speed, we also add a self-loop of admittance $Y_{c,0}$. The junction voltages at points 0, 1, 2, and 3 will be named $U_{J,0}$, $U_{J,1}$, $U_{J,2}$ and $U_{J,3}$, and we have, for the junction admittance at point 0,

$$Y_{J,0} \triangleq Y_{01} + Y_{02} + Y_{03} + Y_{c,0}$$

The scattering junction at grid location 0 is shown in Figure 4.27(a). It should be clear from Figure 4.26(a) that the scattering junctions will be upside-down with respect to that of grid point 0 at half the grid points in the domain, but the waveguide mesh we will develop holds, by symmetry, at such points as well[†].

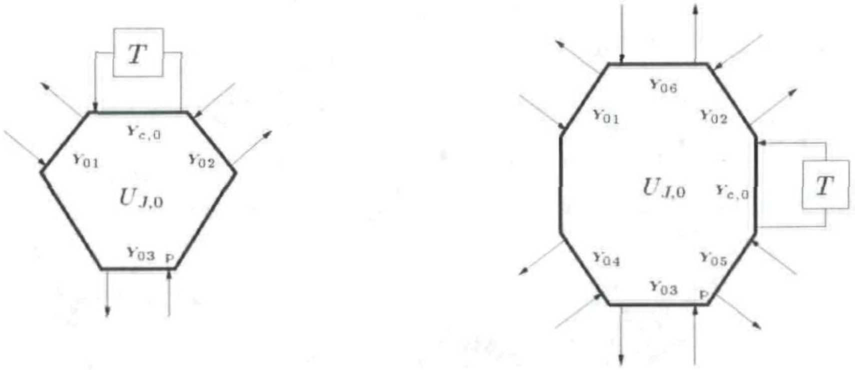

(a) (b)

Figure 4.27: *Scattering junctions*— (a) *on a hexagonal grid, and* (b) *on a triangular grid.*

Beginning at junction 0, and performing manipulations similar to those on a rectilinear grid (i.e., breaking the junction voltage into wave components, and tracing their movement through the network), we get a difference relation among the voltages at point 0 and its neighbors:

$$U_{J,0}(n+1) + U_{J,0}(n-1) = \frac{2}{Y_{J,0}}\left(Y_{01}U_{J,1}(n) + Y_{02}U_{J,2}(n) + Y_{03}U_{J,3}(n) + Y_{c,0}U_{J,0}(n)\right) \qquad (4.76)$$

which we would like to identify with

$$\frac{\partial^2 u}{\partial t^2} = \frac{1}{c}\left(\frac{\partial}{\partial x}\left(\frac{1}{l}\frac{\partial u}{\partial x}\right) + \frac{\partial}{\partial y}\left(\frac{1}{l}\frac{\partial u}{\partial y}\right)\right) \qquad (4.77)$$

---

[†] *In fact, we are being somewhat cavalier here (as we will be again when we look at the tetrahedral mesh in §4.7), because the updating is not the same at every junction. We will deal with this aspect in full detail in Appendix A.*

which is simply the reduced form of system (4.49) where we have eliminated $i_x$ and $i_y$. If we were to identify this mesh with the type II mesh of §4.4, we might guess that we should set the impedances of the bidirectional delay lines to be equal to $v_0$ times the value of $l$ at the midpoint of the line, where we again have $v_0 = \Delta/T$. That is, if grid point 0 is situated at coordinates $(x, y)$, then we should set

$$Y_{01} = \frac{1}{v_0 l_{01}} \qquad Y_{02} = \frac{1}{v_0 l_{02}} \qquad Y_{03} = \frac{1}{v_0 l_{03}}$$

with

$$l_{01} = l(x - \frac{\sqrt{3}\Delta}{4}, y + \frac{\Delta}{4}) \qquad l_{02} = l(x + \frac{\sqrt{3}\Delta}{4}, y + \frac{\Delta}{4}) \qquad l_{03} = l(x, y - \frac{\Delta}{2})$$

With this choice of the waveguide admittances, we must have, in order to force consistency of (4.76) with (4.77),

$$Y_{J,0} = \frac{3}{2} v_0 \bar{c}_0 \tag{4.78}$$

where $\bar{c}_0$ is some second order approximation to $c$ at the location of junction 0. We can now choose, in order to satisfy (4.78),

$$Y_{c,0} = \frac{v_0}{2}(c_{01} + c_{02} + c_{03}) - \frac{1}{v_0 l_{01}} - \frac{1}{v_0 l_{02}} - \frac{1}{v_0 l_{03}}$$

where $c_{01}$ and $c_{02}$ and $c_{03}$ are values of $c(x, y)$ at the midpoints of the waveguides connecting the junction at point 0 to its neighbors.

The stability bound for this mesh, resulting from a positivity condition on the self-loop admittance $Y_{c,X}$ over all grid points $X$ is

$$v_0 \geq \max_{\text{waveguide midpoints}} \sqrt{\frac{2}{lc}} \tag{4.79}$$

The approach to the triangular mesh is very similar. We now have, at each grid point, a seven-port junction, to accommodate waves incoming from six directions and a self-loop (see Figure 4.27(b)). We now make the choices, at a grid point 0, of

$$Y_{0j} = \frac{1}{v_0 l_{0j}}, \qquad j = 1, \ldots, 6$$

where $l_{0j}$, $j = 1, \ldots, 6$ are the values of the inductance at the midpoints of the attached waveguides in directions 1 through 6. The relevant condition for consistency with (4.77) can be shown to be

$$Y_{J,0} = 3v_0\bar{c}$$

and we choose

$$Y_{c,0} = \sum_{j=1}^{6} \left( \frac{1}{2} v_0 c_{0j} - \frac{1}{v_0 l_{0j}} \right)$$

where $c_{0j}$, $j = 1, \ldots, 6$ are the values of the capacitance at the adjacent waveguide midpoints. The stability bound is again

$$v_0 \geq \max_{\text{waveguide midpoints}} \sqrt{2/lc} \tag{4.80}$$

If $l$ and $c$ are constant, and we are operating at the CFL bound (i.e., $v_0 = \sqrt{\frac{2}{lc}}$), then in both the hexagonal or the triangular meshes $Y_{c,0}$ vanishes, and we have, respectively, three-port and six-port scattering junctions, all of whose port admittances are identical. These meshes, although they are slightly more difficult to program than the rectilinear mesh, possess better numerical dispersion properties [157]; a comparison of the directional dispersion of various types of (2+1)D meshes in the constant-coefficient case is given in §A.2. We also note that in this same constant-coefficient case, when we are at CFL, the hexagonal mesh, like the rectilinear mesh, can be decomposed into two meshes which operate on half the grid points, and thus a cut in computational and memory costs of a factor of two is possible (see §4.4.3). This is not true for the triangular mesh—see Appendix A.

We do not include any material about boundary termination of hexagonal or triangular grids, although we do conjecture that it should be comparatively less tricky than the termination of MDWDF networks in the same coordinate systems (we mentioned a hexagonal coordinate system in passing in §3.3.3), where the available results are extremely unsatisfactory [211, 212].

### 4.6.2 The Waveguide Mesh in Radial Coordinates

We will look at waveguide meshes in general curvilinear coordinates in §4.8, but radial coordinates are an important special case, especially for musical instrument physical modelling applications (considering how many instruments exhibit some form of radial symmetry).

In terms of radial coordinates $(\rho, \theta)$, where

$$x = \rho \cos\theta \qquad\qquad y = \rho \sin\theta \tag{4.81}$$

the parallel-plate system (4.58) becomes

$$l_\rho \frac{\partial i_\rho}{\partial t} + \frac{\partial u}{\partial \rho} + r_\rho i_\rho + e_\rho = 0 \tag{4.82a}$$

$$l_\theta \frac{\partial i_\theta}{\partial t} + \frac{\partial u}{\partial \theta} + r_\theta i_\theta + e_\theta = 0 \tag{4.82b}$$

$$c_u \frac{\partial u}{\partial t} + \frac{\partial i_\rho}{\partial \rho} + \lambda \frac{\partial i_\theta}{\partial \theta} + g_u u + e_u = 0 \tag{4.82c}$$

where we define radial and angular current densities by

$$i_{\rho} = \rho\left(i_x \cos\theta + i_y \sin\theta\right) \qquad i_{\theta} = \frac{1}{\lambda}\left(-i_x \sin\theta + i_y \cos\theta\right) \tag{4.83}$$

and the effective radial material parameters and sources by

$$\begin{aligned} l_{\rho} &= \frac{l}{\rho} & l_{\theta} &= \rho l \lambda & c_u &= \rho c \\ r_{\rho} &= \frac{r}{\rho} & r_{\theta} &= \rho r \lambda & g_u &= \rho g \\ e_{\rho} &= e\cos\theta + f\sin\theta & e_{\theta} &= \rho\left(-e\sin\theta + f\cos\theta\right) & e_u &= \rho h \end{aligned} \tag{4.84}$$

$\lambda$ is a scaling coefficient which we will set, in anticipation of discretization, equal to $\frac{\Delta_{\theta}}{\Delta_{\rho}}$, the ratio of the grid spacings in the $\theta$ and $\rho$ directions. We will allow these spacings to be, in general, different.

It is evident that system (4.82) has a form similar to its counterpart in rectilinear coordinates, apart from the extra factor of $\lambda$ in (4.82c). The chief difference is that we now have different effective inductances $l_{\rho}$ and $l_{\theta}$ in the two coordinate directions, but, as we shall see, this anisotropy is easily taken care of (indeed, we could have defined anisotropic inductances $l_x$ and $l_y$ in the rectilinear case without greatly complicating matters). We can see immediately that when centered differences are applied to system (4.82), we will be able to operate on an interleaved grid in the $(\rho, \theta)$ coordinates. A version of Yee's algorithm in arbitrary curvilinear coordinates first appeared in [91], and is also discussed in [209]. The interleaved grid, viewed in rectilinear coordinates, is shown in Figure 4.28, where, as before, the dependent variable to be calculated at a particular grid point is indicated next to the point. Grey and white coloring of points indicates operation at alternating time steps. Centered differencing yields a scheme nearly identical to (4.59), with, again, the difference that the inductance has a directional character. We can thus proceed directly to the waveguide mesh, and, furthermore, can use the same indexing as in the rectilinear case; now, the grid indices $(i, j, n)$ will refer to points $(\rho, \theta, t) = (i\Delta_r, j\Delta_{\theta}, nT)$. Due to the interleaved nature of the resulting difference approximations, we will have series junctions at locations $(i+\frac{1}{2}, j, n+\frac{1}{2})$ and $(i, j+\frac{1}{2}, n+\frac{1}{2})$ for $i > 0$, $j$ and $n$ integer (with associated junction currents $I_{\rho J, i+\frac{1}{2}, j}(n+\frac{1}{2})$ and $I_{\theta J, i, j+\frac{1}{2}}(n+\frac{1}{2})$) and parallel junctions at locations $(i, j, n)$ where we will calculate junction voltages $U_{J,i,j}(n)$, for $i > 0$, $j$ and $n$ integer (we return to the central grid point at $i = 0$ later in this section). The computational molecule of the mesh is shown in Figure 4.29.

Referring to Figure 4.30, which gives the immittance nomenclature in the waveguide network, and where in addition we have the junction immittances defined by

$$\begin{aligned} Y_{J,i,j} &\triangleq Y_{\rho^-,i,j} + Y_{\rho^+,i,j} + Y_{\theta^+,i,j} + Y_{\theta^-,i,j} + Y_{c,i,j} + Y_{R,i,j} \\ Z_{J,i+\frac{1}{2},j} &\triangleq Z_{\rho^+,i+\frac{1}{2},j} + Z_{\rho^-,i+\frac{1}{2},j} + Z_{c,i+\frac{1}{2},j} + Z_{R,i+\frac{1}{2},j} \\ Z_{J,i,j+\frac{1}{2}} &\triangleq Z_{\rho^+,i,j+\frac{1}{2}} + Z_{\rho^-,i,j+\frac{1}{2}} + Z_{c,i,j+\frac{1}{2}} + Z_{R,i,j+\frac{1}{2}} \end{aligned}$$

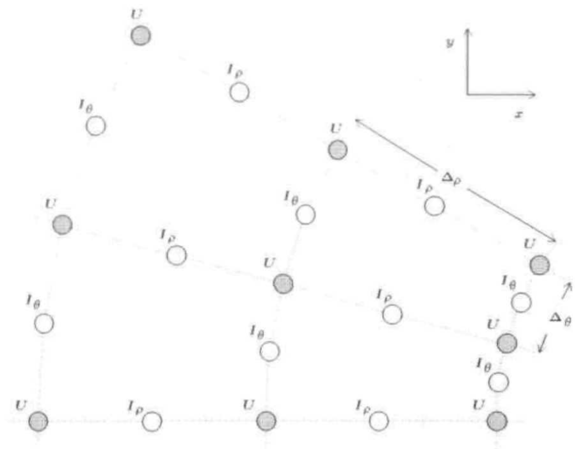

Figure 4.28: *Interleaved grid in radial coordinates.*

for $i > 0$ and $j$ integer, we can perform an analysis similar to the rectilinear case in order to determine that we must have

$$\begin{aligned}
Y_{J,i,j} &= 2\Delta_\rho\left(\frac{\bar{c}_{u,i,j}}{T}+\frac{1}{2}g_{u,i,j}\right) & Y_{R,i,j} &= \Delta_\rho g_{u,i,j}\\
Z_{J,i+\frac{1}{2},j} &= 2\Delta_\rho\left(\frac{\bar{l}_{\rho,i+\frac{1}{2},j}}{T}+\frac{1}{2}r_{\rho,i+\frac{1}{2},j}\right) & Z_{R,i+\frac{1}{2},j} &= \Delta_\rho r_{\rho,i+\frac{1}{2},j}\\
Z_{J,i,j+\frac{1}{2}} &= 2\Delta_\theta\left(\frac{\bar{l}_{\theta,i,j+\frac{1}{2}}}{T}+\frac{1}{2}r_{\theta,i,j+\frac{1}{2}}\right) & Z_{R,i,j+\frac{1}{2}} &= \Delta_\theta r_{\theta,i,j+\frac{1}{2}}
\end{aligned}$$

(The junction admittance $Y_{J,0,0}$ will be dealt with shortly.) The source waves should be chosen as

$$\begin{aligned}
U^{+}_{R,i,j}(n) &= -\frac{e_{u,i,j}(n)}{2g_{u,i,j}}\\
I^{+}_{R,i+\frac{1}{2},j}(n+\tfrac{1}{2}) &= -\frac{e_{\rho,i+\frac{1}{2},j}(n+\frac{1}{2})}{2r_{\rho,i+\frac{1}{2},j}}\\
I^{+}_{R,i,j+\frac{1}{2}}(n+\tfrac{1}{2}) &= -\frac{e_{\theta,i,j+\frac{1}{2}}(n+\frac{1}{2})}{2r_{\theta,i,j+\frac{1}{2}}}
\end{aligned}$$

where we may of course use the dual type of wave in regions where the loss parameters become small, as discussed in §4.3.7. Just as in the rectilinear case, these conditions define a family of waveguide networks which solve the radial transmission line equations. We here provide the impedance settings for voltage- and current-centered meshes, as well as stability bounds.

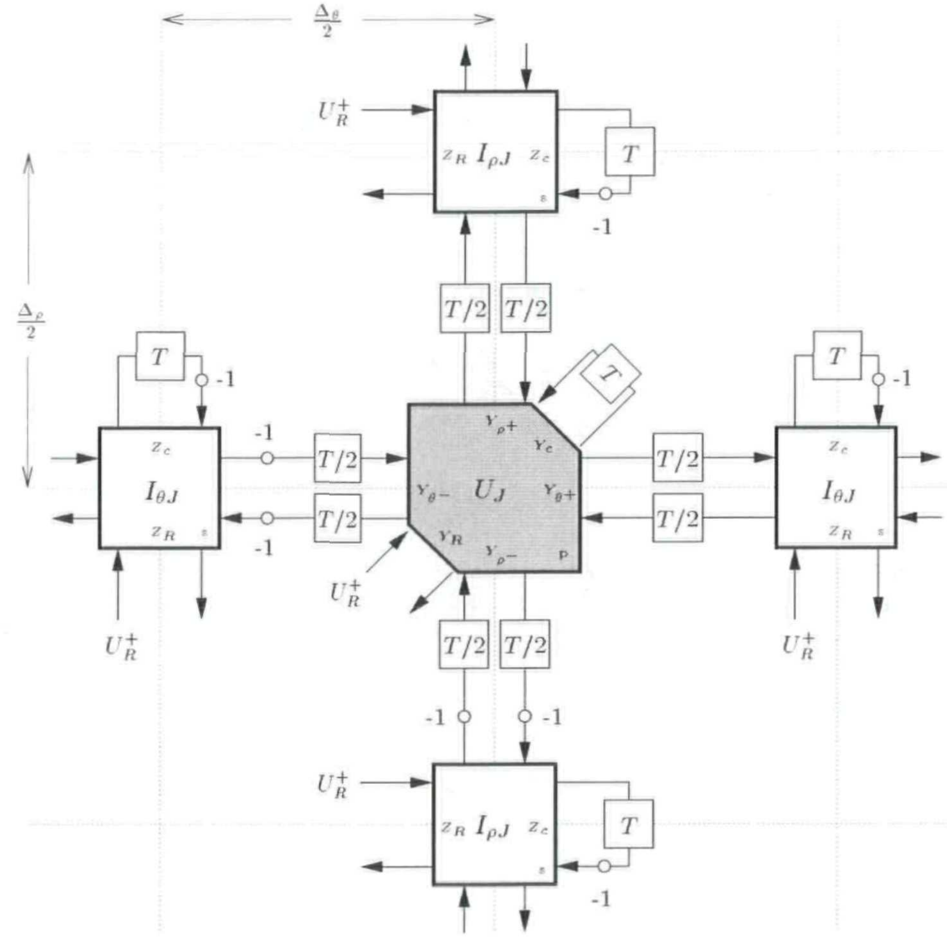
$\frac{\Delta_\theta}{2}$
$U_R^+$
$z_R$ $I_{\rho J}$ $z_c$
T
s
-1
$\frac{\Delta_\rho}{2}$
T/2
T/2
T
T
-1
T
-1
-1
$z_c$
$I_{\theta J}$
$z_R$
s
-1
$Y_{\rho+}$
$Y_c$
$Y_{\theta-}$
$U_J$
$Y_{\theta+}$
$Y_R$
$Y_{\rho-}$
P
T/2
T/2
T/2
T/2
$z_c$
$I_{\theta J}$
$z_R$
s
$U_R^+$
$U_R^+$
$U_R^+$
T/2
T/2
-1
-1
$U_R^+$
$z_R$ $I_{\rho J}$ $z_c$
T
s
-1

Figure 4.29: *Waveguide mesh for the (2+1)D parallel-plate system, in radial coordinates.*

### Type I: Voltage-Centered Mesh

$$Y_{\rho^+,i,j} = Y_{\rho^-,i,j} = Y_{\theta^+,i,j} = Y_{\theta^-,i,j} = \frac{\Delta_\rho c_{u,i,j}}{2T} \qquad Y_{c,i,j} = 0 \tag{4.85}$$

$$\begin{aligned} Z_{c,i+\frac{1}{2},j} &= \frac{\Delta_\rho l_{\rho,i,j}}{T} - \frac{2T}{\Delta_\rho c_{u,i,j}} + \frac{\Delta_\rho l_{\rho,i+1,j}}{T} - \frac{2T}{\Delta_\rho c_{u,i+1,j}} & (4.86)\\ Z_{c,i,j+\frac{1}{2}} &= \frac{\Delta_\theta l_{\theta,i,j}}{T} - \frac{2T}{\Delta_\rho c_{u,i,j}} + \frac{\Delta_\theta l_{\theta,i,j+1}}{T} - \frac{2T}{\Delta_\rho c_{u,i,j+1}} & (4.87) \end{aligned}$$

The stability constraints (which follow from the requirement of positivity of $Z_c$ everywhere) are

$$\frac{\Delta_\rho}{T} \geq \max_{i,j} \sqrt{\frac{2}{l_{i,j}c_{i,j}}} \qquad \frac{\Delta_\theta}{T} \geq \max_{i,j} \left( \frac{1}{\rho_i} \sqrt{\frac{2}{l_{i,j}c_{i,j}}} \right) \tag{4.88}$$

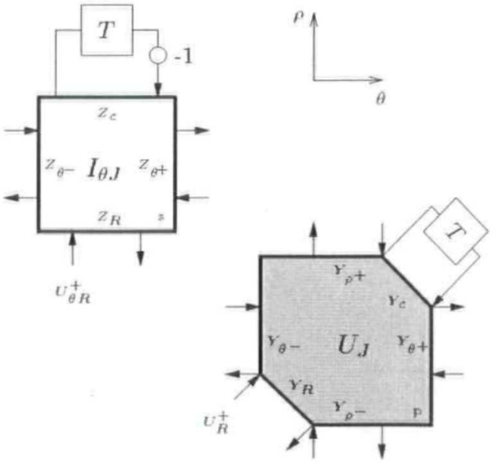

Figure 4.30: *Representative scattering junctions for the waveguide mesh for the (2+1)D parallel-plate system, in radial coordinates.*

There is thus a dependence on $\rho$ in the second condition (relating the angular spacing $\Delta_\theta$ to $T$), which we expect, since the spacing between the junctions at a given radius now varies linearly with the radius. Stability bounds are, for a radial mesh, necessarily more severe than in the rectilinear case, due to this variation in grid spacing.

**Type II: Current-Centered Mesh**

$$Z_{\rho^+,i+\frac{1}{2},j} = Z_{\rho^-,i+\frac{1}{2},j} = \frac{\Delta_\rho l_{\rho,i+\frac{1}{2},j}}{T} \tag{4.89}$$

$$Z_{\theta^+,i,j+\frac{1}{2}} = Z_{\theta^-,i,j+\frac{1}{2}} = \frac{\Delta_\theta l_{\theta,i,j+\frac{1}{2}}}{T} \tag{4.90}$$

$$Z_{c,i+\frac{1}{2},j} = 0 \tag{4.91}$$

$$Z_{c,i,j+\frac{1}{2}} = 0 \tag{4.92}$$

$$\begin{aligned} Y_{c,i,j} &= \frac{2\Delta_\rho c_{u,i+\frac{1}{2},j}}{T} - \frac{T}{\Delta_\rho l_{\rho,i+\frac{1}{2},j}} + \frac{2\Delta_\rho c_{u,i-\frac{1}{2},j}}{T} - \frac{T}{\Delta_\rho l_{\rho,i-\frac{1}{2},j}} \\ &+ \frac{2\Delta_\rho c_{u,i,j+\frac{1}{2}}}{T} - \frac{T}{l_{\theta,i,j+\frac{1}{2}}} + \frac{2\Delta_\rho c_{u,i,j-\frac{1}{2}}}{T} - \frac{T}{l_{\theta,i,j-\frac{1}{2}}} \end{aligned}$$

The stability bound is the same as given by (4.88), except that we take maxima over the series junction locations.

We leave out a discussion of the type III mesh because it was already shown in §4.4.2 to be relatively inefficient in terms of the maximum allowable time step for a given grid spacing (when compared to types I and II).

### Central Gridpoint in a Radial Mesh

We have so far restricted our attention to interior points of the grid (for which $i > 0$). If the center of the $(\rho, \theta)$ coordinate system is to be contained in the grid, a special treatment is required. We have indexed the grid variables such that, in our interleaved mesh, a single parallel junction lies at the origin (for $i = 0$). If the problem domain includes a full circle, we also must assume that $\Delta_\theta$ divides $2\pi$ evenly so that we have a positive integer $N$ such that

$$N = \frac{2\pi}{\Delta_\theta}$$

Thus the central parallel junction will be connected to $N$ series junctions at locations $(\frac{\Delta_\rho}{2}, j\Delta_\theta)$, $j = 0, \ldots, N-1$. We will name the admittances of the $N$ waveguides radiating from the central hub $Y_{j,0,0}$, $j = 0, \ldots, N-1$, and the admittance of the self-loop and loss/source ports will be $Y_{c,0,0}$ and $Y_{R,0,0}$ respectively (see Figure 4.31).

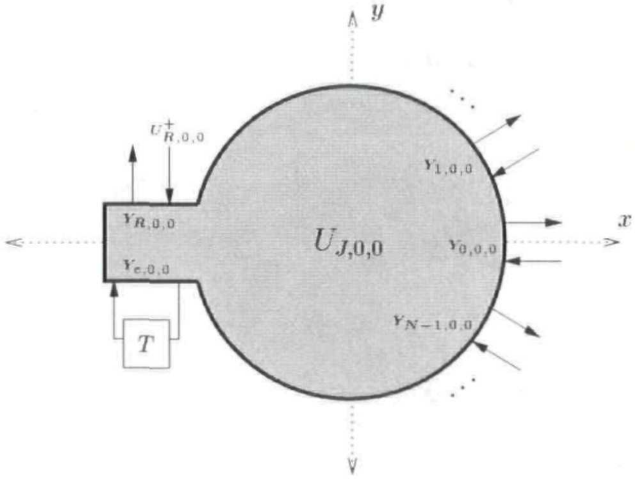

Figure 4.31: *Central scattering junction for the waveguide mesh in radial coordinates.*

The difference scheme relating the junction voltage at the central grid point to the radial currents at the surrounding junctions will then be

$$\begin{aligned} U_{J,0,0}(n) &- \frac{Y_{J,0,0} - 2Y_{R,0,0}}{Y_{J,0,0}} U_{J,0,0}(n-1) + \frac{2}{Y_{J,0,0}} \sum_{j=0}^{N-1} I_{\rho J,\frac{1}{2},j}(n - \frac{1}{2}) \\ &- \frac{2Y_{R,0,0}}{Y_{J,0,0}} \left( U^+_{R,0,0}(n) + U^+_{R,0,0}(n-1) \right) = 0 \end{aligned} \tag{4.93}$$

The sum over the junction currents, which we now look at in the continuous time/space domain so as to develop a series approximation) may be rewritten using (4.83) in terms of the rectilinear current variables as

$$\begin{aligned}
\sum_{j=0}^{N-1} i_\rho(\frac{\Delta_\rho}{2}, j\Delta_\theta) &= \sum_{j=0}^{N-1} \frac{\Delta_\rho}{2}\left(i_x(\frac{\Delta_\rho}{2}, j\Delta_\theta)\cos(j\Delta_\theta) + i_y(\frac{\Delta_\rho}{2}, j\Delta_\theta)\sin(j\Delta_\theta)\right)\\
&= \frac{\Delta_\rho}{2} i_x(0,0)\sum_{j=0}^{N-1}\cos(j\Delta_\theta) + \frac{\Delta_\rho}{2} i_y(0,0)\sum_{j=0}^{N-1}\sin(j\Delta_\theta)\\
&\quad + \frac{\Delta_\rho^2}{4}\sum_{j=0}^{N-1}\left(\left.\frac{\partial i_x}{\partial x}\right|_{(0,0)}\cos^2(j\Delta_\rho) + \left.\frac{\partial i_y}{\partial y}\right|_{(0,0)}\sin^2(j\Delta_\rho)\right)\\
&= \frac{N\Delta_\rho^2}{8}\left(\left.\frac{\partial i_x}{\partial x}\right|_{(0,0)} + \left.\frac{\partial i_y}{\partial y}\right|_{(0,0)}\right) \qquad (4.94)
\end{aligned}$$

where we have neglected higher order terms in $\Delta_\rho$ and used, in the last line, the identities

$$\sum_{j=0}^{N-1}\cos\left(\frac{2\pi j}{N}\right) = \sum_{j=0}^{N-1}\sin\left(\frac{2\pi j}{N}\right) = 0 \qquad \sum_{j=0}^{N-1}\cos^2\left(\frac{2\pi j}{N}\right) = \sum_{j=0}^{N-1}\sin^2\left(\frac{2\pi j}{N}\right) = \frac{N}{2}$$

which hold for $N > 2$. Using approximation (4.94) and by comparing (4.93) with (4.82c), we must choose the junction and loss/source port admittance to be

$$Y_{J,0,0} = \frac{1}{4}N\Delta_\rho^2\left(\frac{\bar{c}_{0,0}}{T} + \frac{g_{0,0}}{2}\right) \qquad Y_{R,0,0} = \frac{1}{8}N\Delta_\rho^2 g_{0,0}$$

and the source wave variable $U_{R,0,0}^+(n)$ to be

$$U_{R,0,0}^+(n) = -\frac{h_{0,0}(n)}{g_{0,0}}$$

A mesh of type I is infeasible because it would require access to $l_{\rho,0,0}$ in order to set $Z_{c,\frac{1}{2},j}$ as prescribed in (4.86), but $l_\rho$ as defined in (4.84) is singular at the origin (although if we are working with a radial geometry which does not contain the origin, this problem does not arise). For a mesh of type II, we have, from (4.89),

$$Y_{j,0,j} = \frac{1}{Z_{\rho^-,\frac{1}{2},j}} = \frac{T}{\Delta_\rho l_{\rho,\frac{1}{2},j}} = \frac{T}{2l_{\frac{1}{2},j}}$$

and so we may set, for the self-loop admittance at the central junction,

$$Y_{c,0,0} = \sum_{j=0}^{N-1}\left(\frac{\Delta_\rho^2 c_{\frac{1}{2},j}}{4T} - \frac{T}{2l_{\frac{1}{2},j}}\right)$$

which is positive when

$$\frac{\Delta_\rho}{T} \geq \max_{j=0,\ldots,N-1} \sqrt{\frac{2}{l_{\frac{1}{2},j}c_{\frac{1}{2},j}}}$$

Thus the stability requirement at the central junction does not interfere with the requirements over the interior of the mesh given for the type II mesh.

We note that a different type of central node, proposed for use in radial TLM simulations, is described in [24].

**Simulation: Circular Region with Varying Inductance**

We show here a simulation of the parallel-plate problem over a circular region, radius 1, with short-circuited boundary conditions ($u = 0$ on the outer rim). The capacitance is 1 everywhere, as is the inductance except over four circular regions of radius 0.2 with centers at radius 0.5 and equally spaced around the circle (circled in black in Figure 4.32). In these smaller regions, the inductance has the form of a 2D raised cosine distribution—$l$ takes on a maximum value of 3 at the centers, and decreases to 1 at the edges. The initial voltage distribution is a raised 2D cosine of radius 0.15 and amplitude 1, centered at radius 0.5, directly between two of the circular regions of higher inductance. The grid spacings are $\Delta_\rho = \frac{1}{60}$ and $\Delta_\theta = \frac{2\pi}{100}$, and we use a radial waveguide mesh of type II.

The time evolution of the voltage distribution is shown in Figure 4.32, where light- and dark-colored areas indicate regions of positive and negative voltage respectively. The plot is normalized to show voltages between $-0.3$ (black) and $0.3$ (white). We remark that the voltage distribution on this pair of plates will behave identically to the transverse velocity distribution on a clamped membrane which has regions of increased density. Interpolation has been performed for better plotting results.

## 4.7 The (3+1)D Wave Equation and Waveguide Meshes

In this brief section we summarize, for completeness sake, (3+1)D waveguide meshes, introduced in [200] and [156]. We will return to these mesh formulations in §4.9.5, where we will discuss interfaces between meshes of different grid densities. We will also analyze the spectral characteristics of these methods in some detail in Appendix A.

The transmission line problem with spatially-varying material parameters does not generalize in a meaningful way to (3+1)D; there is no commonly-known physical system that would behave according to such a set of equations (though linear acoustics in non-Cartesian coordinates might serve as one example). Physical systems of interest in (3+1)D generally have a more complex form than would be implied by such a straightforward generalization. We will have occasion to examine two such systems in detail, namely the (3+1)D equations describing the vibration of a linear, isotropic elastic solid, in §5.6, and Maxwell's equations (see §4.10.6).

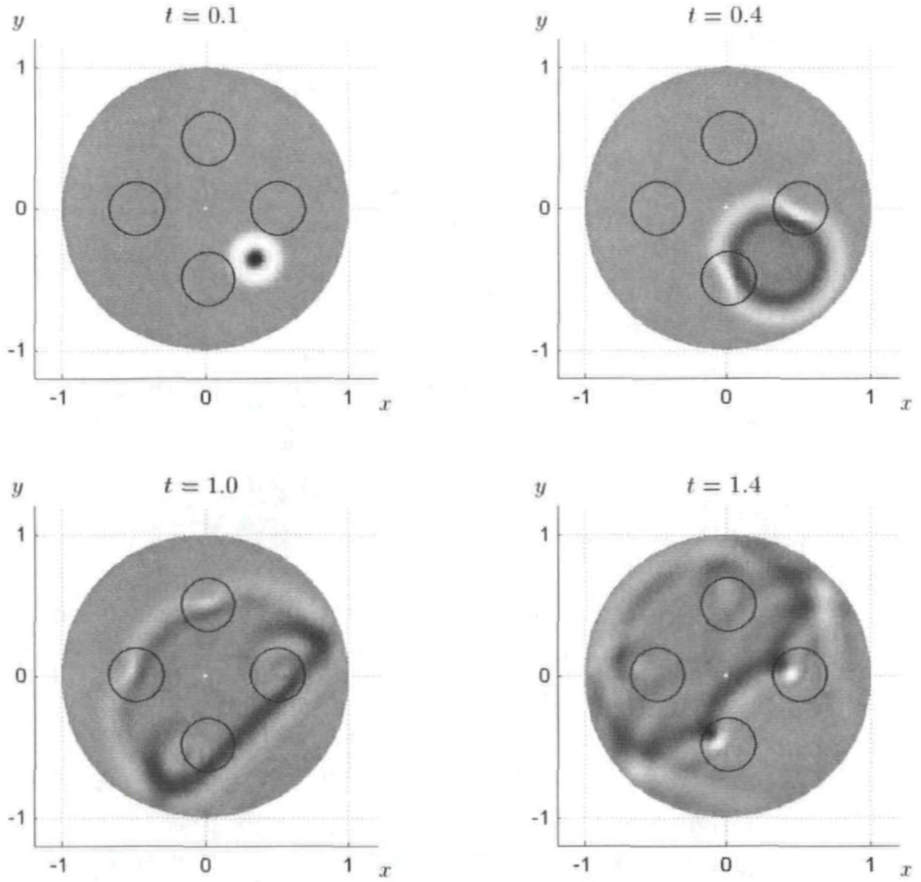

Figure 4.32: *Simulation of a circular parallel-plate system using a radial waveguide mesh.*

The (3+1)D wave equation, however, is of interest in linear acoustics (and it is arrived at by linearizing a system of conservation laws, namely *Euler's equations* [112], to which we will return briefly in Appendix B). It is written as

$$\frac{1}{\gamma^2}\frac{\partial^2 p}{\partial t^2} = \frac{\partial^2 p}{\partial x^2} + \frac{\partial^2 p}{\partial y^2} + \frac{\partial^2 p}{\partial z^2} \tag{4.95}$$

where $p(x, y, z, t)$ is pressure deviation from ambient pressure, and $\gamma = \sqrt{K/\rho}$ is the wave speed ($K$ and $\rho$ are the bulk modulus and density of the medium [15, 66]). In order to enforce notational consistency, we will assume that we can write $\gamma^2 = 1/lc$, for some positive constants $l$ and $c$. Obviously, any such choices of $l$ and $c$ will be appropriate, if we are only interested in solving for the pressure. (In particular, a reasonable choice would be $l = \rho$ and $c = 1/K$.)

Three regular grids are shown in Figure 4.33, and we have indicated waveguide couplings between

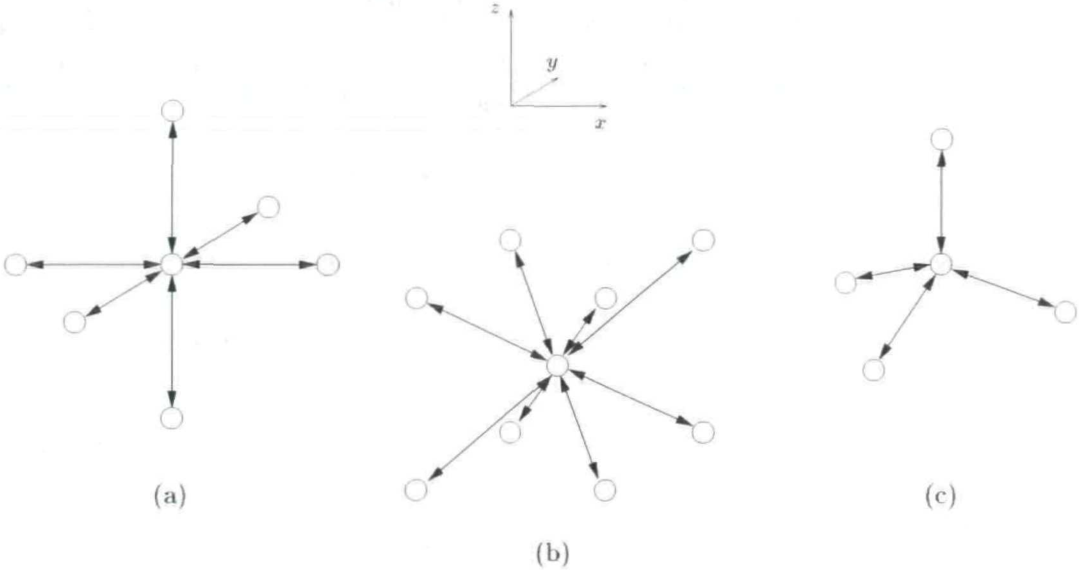

Figure 4.33: *Regular grids in (3+1)D*— (a) *rectilinear,* (b) *octahedral and* (c) *tetrahedral.*

neighboring points (where scattering junctions will be placed) by double-headed arrows. Delays in these bidirectional delay lines are assumed to be of length $T$, and are identical over the entire network, in all three cases. Junctions are separated by a distance $\Delta$. The first, shown in (a), is the standard rectilinear mesh [156, 198], and the second, shown in (b) is a mesh obtained by superimposing one rectilinear grid on top of a shifted copy of itself, then connecting each point to its eight nearest neighbors; an appropriate name for such a configuration might be an "octahedral mesh." A third structure, the so-called tetrahedral mesh [200], is shown in (c). Self-loops, necessary when we are operating away from the CFL bound, are not shown, and the immittances of the connecting waveguides are assumed to all be identical. Other structures are also conceivable.

We remark here on a computational aspect of these junctions—as mentioned in [200], if we are at CFL (and so do not need self-loops), it is useful to have the number of waveguides connected to a particular junction be a power of two; if this can be arranged, then all multiplies carried out during the scattering step may be implemented as simple bit-shifting operations in a fixed-point implementation. Because this is not true for the rectilinear mesh, (i.e., there are six waveguides connected to each junction), the tetrahedral mesh was proposed as a more efficient structure. We note, however, that the octahedral mesh, with eight waveguides connected to each junction, also can be implemented efficiently in fixed-point. Furthermore, it may be easier to deal with from the programmer's point of view, because unlike the tetrahedral mesh, it will not involve any special indexing strategy (for a tetrahedral mesh, half of the junctions will have an inverse orientation with respect to the other half).

If we are at the CFL bound—that is if we have

$$v_0 = \sqrt{3}\gamma \tag{4.96}$$

where $\Delta$ is the physical length of a waveguide in any of the three types of mesh, then we may choose any constant to be the admittance of the connecting waveguide. In this case, all three types of mesh can be decomposed into two meshes, to be used at alternating time steps; as in (2+1)D, this can be exploited to increase computational efficiency (see §4.4.3). If we are away from CFL (as we may be in a multi-grid setting—see §4.9), then we must set, for the self-loop admittances,

$$\begin{aligned}
Y_c &= 2v_0c - \frac{6}{v_0l} && \text{Rectilinear mesh}\\
Y_c &= \frac{4}{\sqrt{3}}v_0c - \frac{4\sqrt{3}}{v_0l} && \text{Octahedral mesh}\\
Y_c &= \frac{4}{3}v_0c - \frac{4}{v_0l} && \text{Tetrahedral mesh}
\end{aligned}$$

where the connecting waveguide admittance has been chosen as $\frac{1}{v_0l}$.

## 4.8 The Waveguide Mesh in General Curvilinear Coordinates

A generalization of the waveguide mesh to arbitrary curvilinear coordinates is useful in that it becomes possible to model boundary conditions which may not be simply aligned with a rectilinear grid. The resulting structure is quite similar to the interleaved forms discussed earlier, and for this reason we will give only a brief description of the coordinate transformation procedure. Consider the following system:

$$l_{\mathbf{x}}\frac{\partial \mathbf{i}_{\mathbf{x}}}{\partial t} + \nabla_{\mathbf{x}}u + r_{\mathbf{x}}\mathbf{i}_{\mathbf{x}} + \mathbf{e}_{\mathbf{x}} \quad = \quad \mathbf{0} \tag{4.97a}$$

$$c_x\frac{\partial u}{\partial t} + \nabla_{\mathbf{x}}\cdot\mathbf{i}_{\mathbf{x}} + g_{\mathbf{x}}u + h_{\mathbf{x}} \quad = \quad 0 \tag{4.97b}$$

Here we may assume any number $k$ of physical spatial coordinates $\mathbf{x} = [x_1, \ldots, x_k]^T$, so that $\nabla_{\mathbf{x}} = \frac{\partial}{\partial \mathbf{x}} = [\frac{\partial}{\partial x_1}, \ldots, \frac{\partial}{\partial x_k}]^T$. $\mathbf{i}_{\mathbf{x}}$ and $\mathbf{e}_{\mathbf{x}}$ are both assumed to be $k$-dimensional column vectors. $l_{\mathbf{x}}$, $c_{\mathbf{x}}$, $r_{\mathbf{x}}$ and $g_{\mathbf{x}}$ are all positive functions of $\mathbf{x}$ ($l_{\mathbf{x}}$ and $c_{\mathbf{x}}$ are strictly positive), and $\mathbf{e}_{\mathbf{x}}$ and $h_{\mathbf{x}}$ are the source terms. If $k$ is 1 or 2, then we have the transmission line or parallel-plate transmission line system respectively, and if $k = 3$, we have the system describing linear acoustic phenomena (assuming that the material parameters are constant).

Consider the mapping

$$\mathbf{x} = \boldsymbol{\zeta}(\mathbf{w})$$

where $\mathbf{w} = [w_1, \ldots, w_k]^T$ are the transformed coordinates. A rectilinear grid in the $\mathbf{w}$ coordinates can be mapped to a curvilinear grid in the physical $\mathbf{x}$ coordinates. We can then define the $k \times k$ matrix of partial derivatives $\mathbf{J}$ by

$$[\mathbf{J}_{\alpha,\beta}] = \frac{\partial \zeta_\alpha}{\partial w_\beta} \qquad \alpha, \beta = 1, \ldots, k$$

where $\zeta_\alpha$ is the $\alpha$th component of $\boldsymbol{\zeta}$. We assume $\mathbf{J}$ to be nonsingular everywhere in the problem domain (though this assumption may be relaxed as will mention later in this section) . Defining the differential operator $\nabla_{\mathbf{w}}$ by $\nabla_{\mathbf{w}} = \frac{\partial}{\partial \mathbf{w}} = [\frac{\partial}{\partial w_1}, \ldots, \frac{\partial}{\partial w_k}]^T$, it then follows [69] that

$$\nabla_{\mathbf{w}} = \mathbf{J}^T \nabla_{\mathbf{x}} \qquad \nabla_{\mathbf{x}} \cdot \mathbf{a} = \frac{1}{|\mathbf{J}|} \nabla_{\mathbf{w}} \cdot (|\mathbf{J}|\mathbf{J}^{-1}\mathbf{a})$$

for any $k \times 1$ column vector $\mathbf{a}$. Here, $|\mathbf{J}|$ is the so-called *Jacobian determinant* [172]. Using these relationships, the system (4.97) may be rewritten as

$$\begin{aligned} l_{\mathbf{x}}\mathbf{J}^T \frac{\partial \mathbf{i}_{\mathbf{x}}}{\partial t} + \nabla_{\mathbf{w}} u + r_{\mathbf{x}}\mathbf{J}^T \mathbf{i}_{\mathbf{x}} + \mathbf{J}^T \mathbf{e}_{\mathbf{x}} &= \mathbf{0} \\ c_{\mathbf{x}}|\mathbf{J}|\frac{\partial u}{\partial t} + \nabla_{\mathbf{w}} \cdot (|\mathbf{J}|\mathbf{J}^{-1}\mathbf{i}_{\mathbf{x}}) + |\mathbf{J}|g_{\mathbf{x}}u + |\mathbf{J}|h_{\mathbf{x}} &= 0 \end{aligned}$$

or

$$\mathbf{L}_{\mathbf{w}} \frac{\partial \mathbf{i}_{\mathbf{w}}}{\partial t} + \nabla_{\mathbf{w}} u + \mathbf{R}_{\mathbf{w}} \mathbf{i}_{\mathbf{w}} + \mathbf{e}_{\mathbf{w}} = \mathbf{0} \qquad (4.98a)$$

$$c_{\mathbf{w}} \frac{\partial u}{\partial t} + \nabla_{\mathbf{w}}^T \cdot \mathbf{i}_{\mathbf{w}} + g_{\mathbf{w}} u + h_{\mathbf{w}} = 0 \qquad (4.98b)$$

where

$$\mathbf{i}_{\mathbf{w}} = |\mathbf{J}|\mathbf{J}^{-1}\mathbf{i}_{\mathbf{x}}$$

and

$$\mathbf{L}_{\mathbf{w}} = \frac{l_{\mathbf{x}}}{|\mathbf{J}|}\mathbf{J}^T\mathbf{J} \qquad \mathbf{R}_{\mathbf{w}} = \frac{r_{\mathbf{x}}}{|\mathbf{J}|}\mathbf{J}^T\mathbf{J} \qquad \mathbf{e}_{\mathbf{w}} = \mathbf{J}^T\mathbf{e}_{\mathbf{x}}$$

$$c_{\mathbf{w}} = |\mathbf{J}|c_{\mathbf{x}} \qquad g_{\mathbf{w}} = |\mathbf{J}|g_{\mathbf{x}} \qquad h_{\mathbf{w}} = |\mathbf{J}|h_{\mathbf{x}}$$

System (4.98) is similar to (4.97), except that we now have "vector" inductance and resistance coefficients (note that both $\mathbf{L_w}$ and $\mathbf{R_w}$ are positive definite matrices, if $\mathbf{J}$ is non-singular). In particular, it is still symmetric hyperbolic (see §3.2), so we may expect that it is possible to derive a waveguide structure.

Consider now the transformed system (4.98) in (2+1)D. If $\mathbf{J}^T\mathbf{J}$ is diagonal, then $\mathbf{L_w}$ and $\mathbf{R_w}$ will be as well; in this case, system (4.98) is in the same form[†] as the parallel-plate system in radial coordinates (4.82), so we need not discuss this case further here. Indeed, the radial system is a special case of (4.98) with $\mathbf{w} = [\rho, \theta]^T$ and

$$\mathbf{J} = \begin{bmatrix} \cos\theta & -\rho\sin\theta \\ \sin\theta & \rho\cos\theta \end{bmatrix}$$

On the other hand, if $\mathbf{J}^T\mathbf{J}$ is not diagonal (so that we are working in non-orthogonal or oblique coordinates), then the situation is more complex. Due to the cross-coupling between the components of $\mathbf{i_w}$ through the matrices $\mathbf{L_w}$ and $\mathbf{R_w}$, it will no longer be possible to stagger all the components of the solution; in particular, it will be necessary to use *vector* scattering junctions. Let us look at the case $k = 2$, so that (4.98) are the equations of the parallel-plate system in the curvilinear coordinates $\mathbf{w}$. Furthermore, we will set $w_1 = p$ and $w_2 = q$. A centered difference approximation to (4.98), over grid points with coordinates $p = i\Delta$ and $q = j\Delta$, and at times $t = nT$ for $i$, $j$ and $n$ half-integer is

$$\begin{aligned} v_0\bar{\mathbf{L}}_{\mathbf{w},i+\frac{1}{2},j}\Big(\mathbf{I}_{i+\frac{1}{2},j}(n+\tfrac{1}{2}) &- \mathbf{I}_{i+\frac{1}{2},j}(n-\tfrac{1}{2})\Big) + \begin{bmatrix} U_{i+1,j}(n) - U_{i,j}(n) \\ U_{i,j+\frac{1}{2}}(n) - U_{i,j-\frac{1}{2}}(n) \end{bmatrix} \\ &+ \frac{\Delta}{2}\mathbf{R}_{\mathbf{w},i+\frac{1}{2},j}\Big(\mathbf{I}_{i+\frac{1}{2},j}(n+\tfrac{1}{2}) + \mathbf{I}_{i+\frac{1}{2},j}(n-\tfrac{1}{2})\Big) \\ &+ \frac{\Delta}{2}\Big(\mathbf{e}_{\mathbf{w},i+\frac{1}{2},j}(n+\tfrac{1}{2}) + \mathbf{e}_{\mathbf{w},i+\frac{1}{2},j}(n-\tfrac{1}{2})\Big) = \mathbf{0} \qquad (4.99a) \\ v_0\bar{c}_{\mathbf{w},i,j}\Big(U_{i,j}(n) - U_{i,j}(n-1)\Big) &+ I_{p,i+\frac{1}{2},j}(n-\tfrac{1}{2}) - I_{p,i-\frac{1}{2},j}(n-\tfrac{1}{2}) \\ &+ I_{q,i,j+\frac{1}{2}}(n-\tfrac{1}{2}) - I_{q,i,j-\frac{1}{2}}(n-\tfrac{1}{2}) \\ &+ \frac{\Delta}{2}g_{\mathbf{w},i,j}\Big(U_{i,j}(n) + U_{i,j}(n-1)\Big) \\ &+ \frac{\Delta}{2}\Big(h_{\mathbf{w},i,j}(n) + h_{\mathbf{w},i,j}(n-1)\Big) = 0 \qquad (4.99b) \end{aligned}$$

Here, we have the vector grid function $\mathbf{I}_{i+\frac{1}{2},j}(n+\frac{1}{2})$, which is a two-vector with components $I_{p,i+\frac{1}{2},j}(n+\frac{1}{2})$ and $I_{q,i+\frac{1}{2},j}(n+\frac{1}{2})$ as well as the scalar grid function $U_{i,j}(n)$. $\bar{\mathbf{L}}_{\mathbf{w},i+\frac{1}{2},j+\frac{1}{2}}$ and $\bar{c}_{\mathbf{w},i,j}$ are second-order approximations to $\mathbf{L_w}$ and $c_\mathbf{w}$ at the indicated grid points. The scheme above has been written so that it is clear that it can operate for $n$ integer, and for $i$ and $j$ such that $i+j$ is integer; notice that $U$ and $\mathbf{I}$ are calculated at alternating time instants and grid locations,

---

[†] It is in the same form except for the scaling parameter $\lambda$ which was introduced so as to allow a different grid spacing in the two radial coordinate directions; such a scaling parameter may be used here to exactly the same effect.

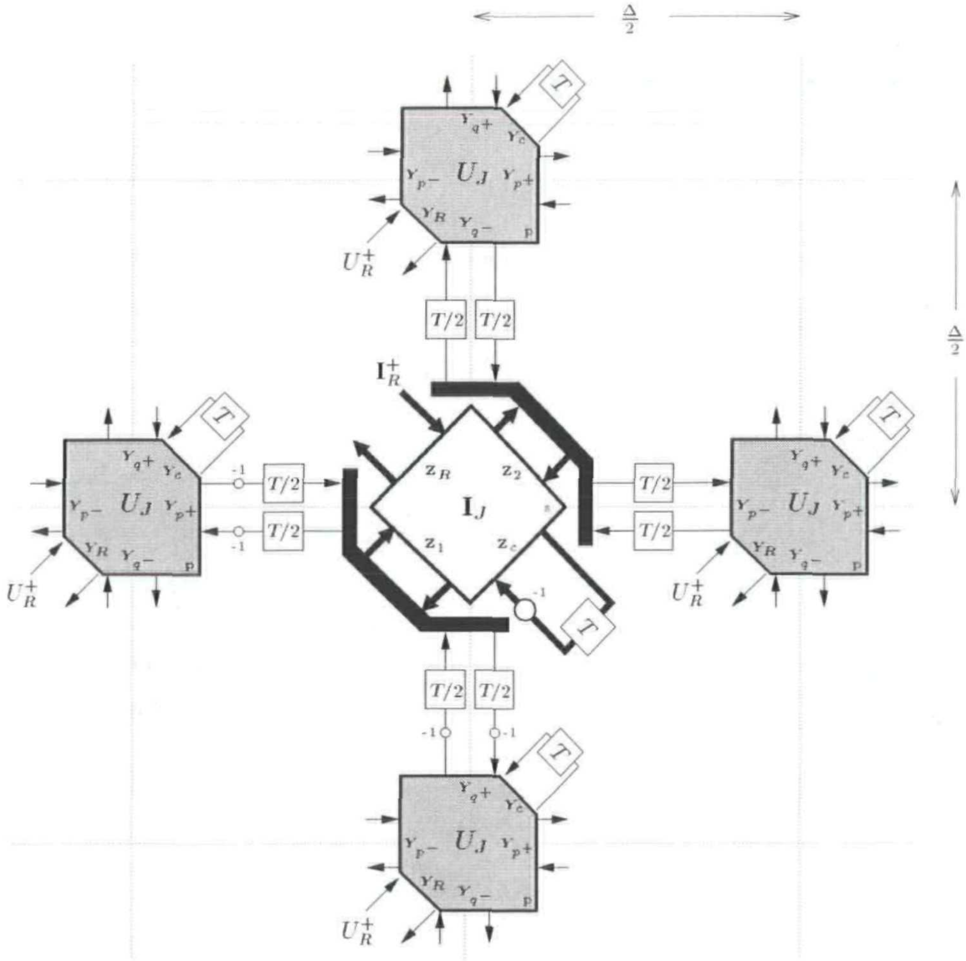

Figure 4.34: *(2+1)D DWN for the parallel-plate system* (4.98) *in general non-orthogonal curvilinear coordinates.*

but the components of **I** can not, in general, be calculated at separate locations. $v_0$, again, is equal to $\Delta/T$, and (4.99) will be a second-order accurate approximation to (4.98).

We will skip the tedious procedure of deriving a waveguide mesh, and simply present the resulting structure in Figure 4.34. Junction vector currents $\mathbf{I}_J$ are calculated at the series vector scattering junctions; the black bars surrounding this junction in the figure are the splitting elements that were discussed in §4.2.6. Although we have not drawn them in the figure, there will be similar vector junctions at the four grid points neighboring any of the parallel junctions where the voltages $U_J$ are calculated. This vector junction has four $2 \times 2$ matrix impedances associated with it: $\mathbf{Z}_c$, the self-loop impedance, $\mathbf{Z}_R$, the loss/source impedance, and $\mathbf{Z}_1$ and $\mathbf{Z}_2$, which are constrained (see

§4.2.6) to be

$$\mathbf{Z}_{1,i+\frac{1}{2},j} = \begin{bmatrix} \frac{1}{Y_{p+,i,j}} & 0 \\ 0 & \frac{1}{Y_{q+,i+\frac{1}{2},j-\frac{1}{2}}} \end{bmatrix} \qquad \mathbf{Z}_{2,i+\frac{1}{2},j} = \begin{bmatrix} \frac{1}{Y_{p-,i+1,j}} & 0 \\ 0 & \frac{1}{Y_{q-,i+\frac{1}{2},j+\frac{1}{2}}} \end{bmatrix} \tag{4.100}$$

The junction impedance $\mathbf{Z}_J$ is defined to be the sum of these four matrices. The admittances at the parallel junctions are defined in a manner similar to those of the DWN in rectilinear coordinates. Also, we have the source voltage waves $U^+_{R,i,j}$ at the parallel junctions and vector source current waves $\mathbf{I}^+_{R,i+\frac{1}{2},j}$ at the series junctions.

This DWN can be identified with the difference system (4.99) if we set

$$\begin{aligned} \mathbf{Z}_J &= 2v_0\bar{\mathbf{L}}_{\mathbf{w}} + \Delta\mathbf{R}_{\mathbf{w}} & \mathbf{Z}_R &= \Delta\mathbf{R}_{\mathbf{w}} & \mathbf{I}^+_R &= -\Delta\mathbf{R}^{-1}_{\mathbf{w}}\mathbf{e}_{\mathbf{w}}/2 \\ Y_J &= 2v_0\bar{c}_{\mathbf{w}} + \Delta g_{\mathbf{w}} & Y_R &= \Delta g_{\mathbf{w}} & U^+_R &= -\Delta g_{\mathbf{w}} h_{\mathbf{w}}/2 \end{aligned}$$

at the grid points for which such quantities are defined.

There are, of course, various realizations, depending on how the self-loop and connecting immittances are chosen. First, note that because $\mathbf{Z}_J$ is not diagonal, it will not be possible to distribute it equally among the two connecting impedances $\mathbf{Z}_1$ and $\mathbf{Z}_2$, which are constrained to be diagonal from (4.100). Thus a type II (current-centered) realization analogous to that which was discussed in the case of the rectilinear mesh will not be possible, even in the absence of losses and sources. A type I realization is certainly possible, but for brevity sake, we will only provide the settings for the type III DWN. Here all the connecting impedances are all set to be some constant value $Z_{const}$. This then implies that

$$\mathbf{Z}_c = 2v_0\bar{\mathbf{L}}_{\mathbf{w}} - 2Z_{const}\mathbf{I}_2 \qquad Y_c = 2v_0\bar{c}_{\mathbf{w}} - 4/Z_{const}$$

where $\mathbf{I}_2$ is the $2 \times 2$ identity matrix. Requiring the positivity of $Y_c$ and the positive definiteness of $\mathbf{Z}_c$ gives the constraint

$$v_0 \geq \sqrt{\frac{2}{\mathbf{L}_{\mathbf{w},min} c_{\mathbf{w},min}}}$$

for $c_{\mathbf{w},min}$ the minimum of $c_{\mathbf{w}}$ over parallel junction locations and $\mathbf{L}_{\mathbf{w},min}$ the minimum of the eigenvalues of $\mathbf{L}_{\mathbf{w}}$ over series junction locations, and where we have made the choice

$$Z_{const} = \sqrt{\frac{2\mathbf{L}_{\mathbf{w},min}}{c_{\mathbf{w},min}}}$$

In general, this bound will depend on the choice of coordinates.

FDTD in general curvilinear coordinates has developed in a similar way; most formulations are slightly different in that they are based on a tensor density formulation [91, 209] and employ a double set of variables (covariant and contravariant) in the non-orthogonal case; differencing involves interleaving these two sets of components at alternating time steps. They have also been used as a starting point for developing FDTD methods in "local" coordinates defined with respect to an automatically generated grid [72, 73]. Curvilinear coordinate systems have been touched upon in the MDWD framework as well; An approach similar to the above is discussed in [69], and a tensor density formulation is given in [131].

## 4.9 Interfaces Between Grids

In (2+1)D, we have looked so far at numerically solving the parallel-plate transmission line system over *regular* grids—that is to say, grids whose points can be indexed with respect to some regular coordinate system. We now examine ways of connecting grids of different types, and in particular grids of differing densities of points. The ability to decompose a domain into regions of different grid point densities is especially useful when dealing with boundaries and irregular features (i.e., variations in material parameters) throughout the problem domain; we may use a fine grid to calculate the solution to a problem in such regions, and then a coarse grid everywhere else. The problem, then, is in connecting the various subgrids so that consistency of a numerical method with the original set of equations to be solved can be maintained at the boundaries between the regions. The use of multi-grid techniques in numerical integration had developed into a very large field recently, and we can not hope to summarize the many developments that have taken place, nor even the basic theory. Unfortunately, there is not as yet a single good basic reference; we refer the reader to [140] for an general introduction. Multi-grid methods have been used in the TLM framework, but the structures there employed are somewhat different. In particular, the methods proposed in [88] and [87] (and reviewed in [29]) do not, in general, enforce passivity at an interface between a coarse and fine grid, though they are capable of operating using different time steps in the coarse and fine meshes. The method of [207] is perhaps closer in spirit to that presented here, in that the time step is everywhere the same, but in that case, certain *a priori* assumptions are made about the fields at the interface.

We will show that it is in fact possible to devise passive connections between waveguide networks (themselves generally passive, unless sources are present) which operate on different types of grids, so that passivity can be maintained in a global sense—there is, as before, an energy measure for the network which can be expressed as a weighted sum of the squares of the wave variables in the network. In this section, we will look in particular at the lossless, source-free parallel-plate equations in (2+1)D (system (4.58) with $r = g = e = f = h = 0$ everywhere). Furthermore, for simplicity, we will confine our attention to waveguide networks of type II as described in §4.4; it will be recalled that for type II networks, when $r = e = f = 0$, there is no scattering at the series junctions, and we need only calculate voltages at the parallel junctions. $l$ and $c$ will still be allowed to vary over the problem domain. (It may be possible to extend the multi-grid methods to be described here to the full lossy system including sources, but we will not pursue this direction here.)

### 4.9.1 Doubled Grid Density Across an Interface

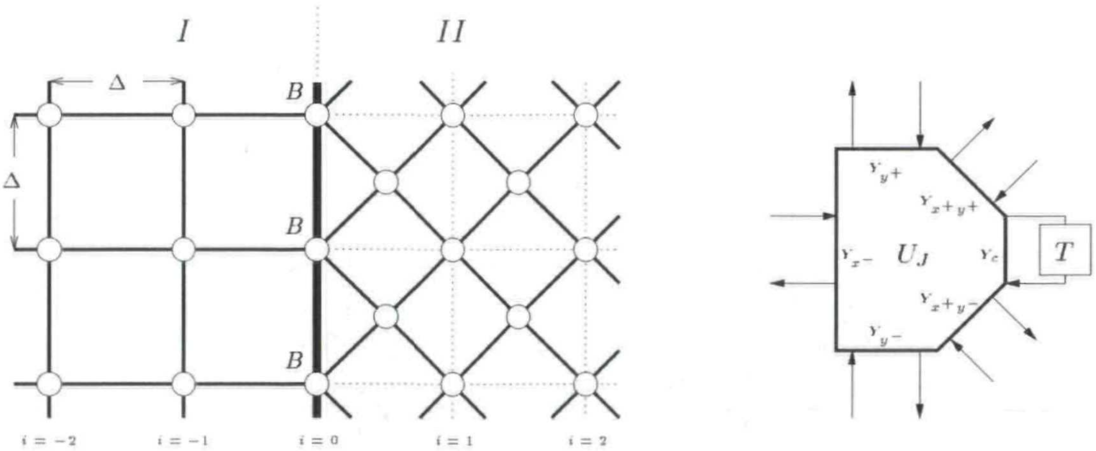

(a) (b)

Figure 4.35: *Interface between mesh and mesh with doubled grid density*— (a) *grid arrangement, where boundary junctions are labelled $B$, and* (b) *scattering junction at such a boundary junction.*

In Figure 4.35(a) is shown an interface between a regular rectilinear grid with spacing $\Delta$ (region $I$) and a grid with spacing $\Delta/\sqrt{2}$ (region $II$) whose orientation is rotated by 45 degrees with respect to that of region $I$. Clearly then, the density of grid points in region $II$ is double that of region $I$. At any point in the interior of either regions $I$ or $II$, if we are interested in solving the parallel-plate transmission line equations, we can use the rectilinear mesh described in §4.4. We indicate waveguide connections between junctions located at the gridpoints by black lines. At points lying on the interface between the two regions (labelled $B$) however, we need to develop special scattering junctions. The most straightforward arrangement requires a six-port junction at a boundary point (waves enter the junction from five irregularly spaced directions, as well as through a self-loop). Such a junction is shown in Figure 4.35(b). The problem, then, is in finding the correct admittance settings for the waveguides connected to such boundary points. If these admittances can be chosen positive and in such a way that the resulting scheme is consistent with the parallel-plate system, then we are assured convergence over the entire problem domain. We note that such interfaces bear a resemblance to the very early work of MacNeal [123], who developed asymmetric resistive networks as a means of solving elliptic problems via relaxation.

We assume that the boundary is aligned with the $y$-axis, so that the boundary junctions are located at coordinates $(0, j\Delta)$, for $j$ integer. We also assume, for the moment, that all delays in the network will be unit sample delays (we will return to interfaces between grids with differing delay lengths in the next section). As before, we will set $v_0 = \Delta/T$. At a boundary junction at coordinates $(0, j\Delta)$, we will have six port admittances: $Y_{x^-,0,j}$, $Y_{y^-,0,j}$ and $Y_{y^+,0,j}$ corresponding to waveguide connections with junctions to the west, south and north respectively, $Y_{x^+y^+,0,j}$ and $Y_{x^+y^-,0,j}$ for connections to junctions to the northeast and southeast, respectively in region $II$ and a self-loop admittance $Y_{c,0,j}$. The junction admittance at a boundary point $B$ is then

$$Y_{J,0,j} \triangleq Y_{x^-,0,j} + Y_{y^-,0,j} + Y_{y^+,0,j} + Y_{x^+y^+,0,j} + Y_{x^+y^-,0,j} + Y_{c,0,j}$$

Because this waveguide mesh is an extension of the type II mesh described in §4.4.2, we might expect that the waveguide admittances will be related to values of the material parameters $l$ and $c$ at the midpoints of the waveguides. This is, in fact, true, even at the boundary junctions, though because of the asymmetric nature of these junctions with respect to the coordinate axes, we must perform a judicious scaling of some of these admittances. In fact, we must only scale the admittances of the waveguides which lie along the boundary itself, and that of the self-loop. The admittances of waveguides connected to interior points in region $I$ or $II$ should be treated as "interior," so that the scattering will be correct at junctions neighboring the boundary).

The difference scheme operating at a junction on the boundary will be

$$\begin{aligned}\frac{Y_{J,0,j}}{2}\left(U_{J,0,j}(n+1) + U_{J,0,j}(n-1)\right) = \; & Y_{x^+y^+,0,j}U_{J,\frac{1}{2},j+\frac{1}{2}}(n) + Y_{x^+y^-,0,j}U_{J,\frac{1}{2},j-\frac{1}{2}}(n)\\ & + Y_{x^-,0,j}U_{J,-1,j}(n) + Y_{y^+,0,j}U_{J,0,j+1}(n)\\ & + Y_{y^-,0,j}U_{J,0,j-1}(n) + Y_{c,0,j}U_{J,0,j}(n)\end{aligned}$$

If we now treat the junction voltages as samples of a continuous function $u$, then the difference scheme above can be expanded in a Taylor series about $(0, j\Delta, nT)$ to give

$$\begin{aligned}Y_{J,0,j}T^2\frac{\partial^2 u}{\partial t^2} = \; & 2\Delta\left(-Y_{x^-,0,j} + \frac{1}{2}(Y_{x^+y^-,0,j} + Y_{x^+y^+,0,j})\right)\frac{\partial u}{\partial x}\\ & + 2\Delta\left(Y_{y^+,0,j} - Y_{y^-,0,j} + \frac{1}{2}(Y_{x^+y^+,0,j} - Y_{x^+y^-,0,j})\right)\frac{\partial u}{\partial y}\\ & + \Delta^2\left(Y_{x^-,0,j} + \frac{1}{4}(Y_{x^+y^-,0,j} + Y_{x^+y^+,0,j})\right)\frac{\partial^2 u}{\partial x^2}\\ & + \Delta^2\left(Y_{y^-,0,j} + Y_{y^+,0,j} + \frac{1}{4}(Y_{x^+y^-,0,j} + Y_{x^+y^+,0,j})\right)\frac{\partial^2 u}{\partial y^2}\\ & + \frac{\Delta^2}{2}\left(Y_{x^+y^+,0,j} - Y_{x^+y^-,0,j}\right)\frac{\partial^2 u}{\partial x \partial y}\\ & + O(\Delta^3, T^4)\end{aligned} \tag{4.101}$$

In order to associate this expansion with the reduced form of the parallel-plate equations of (4.77), we may set

$$Y_{x^-,0,j}=\frac{1}{v_0l_{-\frac{1}{2},j}}\qquad Y_{y^+,0,j}=\frac{1}{2v_0l_{0,j+\frac{1}{2}}}\qquad Y_{y^-,0,j}=\frac{1}{2v_0l_{0,j-\frac{1}{2}}}$$

$$Y_{x^+y^+,0,j}=\frac{1}{v_0l_{\frac{1}{4},j+\frac{1}{4}}}\qquad Y_{x^+y^+,0,j}=\frac{1}{v_0l_{\frac{1}{4},j-\frac{1}{4}}}$$

and for the self-loop admittance, we set

$$\begin{aligned}Y_{c,0,j} &= \frac{3}{16}v_0\left(2c_{-\frac{1}{2},j}+2c_{\frac{1}{4},j+\frac{1}{4}}+2c_{\frac{1}{4},j-\frac{1}{4}}+c_{0,j+\frac{1}{2}}+c_{0,j-\frac{1}{2}}\right)\\ &\quad -Y_{x^-,0,j}-Y_{y^-,0,j}-Y_{y^+,0,j}-Y_{x^+y^+,0,j}-Y_{x^+y^-,0,j}\end{aligned}\tag{4.102}$$

These settings yield a difference scheme which is consistent with the transmission line equations, and which is first-order accurate in the grid spacing $\Delta$. It is important to note that the admittances of the waveguides connecting two junctions on the boundary itself are set to be *half* what they would be in the interior of region $I$. Also note that the mixed derivative term in (4.101) becomes $O(\Delta^3)$ (because $Y_{x^+y^+,0,j}$ and $Y_{x^+y^-,0,j}$ are the same to zeroth-order, and hence their difference, which is the coefficient of the mixed-derivative term, will be $O(\Delta)$).

The additional stability requirement, from (4.102) is

$$v_0\geq\max_{\substack{\text{boundary waveguide}\\ \text{midpoints}}}\sqrt{\frac{8}{3lc}}$$

which is marginally more restrictive than the requirement on the interior of region $I$ (by a factor of $\sqrt{\frac{4}{3}}$). This deterioration in the stability bound is offset, however, by the fact in region $II$, the grid spacing is $\Delta/\sqrt{2}$ we must have

$$\frac{\Delta}{\sqrt{2}T}\geq\max_{\substack{\text{waveguide midpoints in}\\ \text{region II}}}\sqrt{\frac{2}{lc}}\qquad\Rightarrow\qquad v_0\geq\max_{\substack{\text{waveguide midpoints in}\\ \text{region II}}}2\sqrt{\frac{1}{lc}}$$

because we are by necessity operating away from the CFL bound in this particular multi-grid setting, which incorporates different grid spacings and yet maintains the same time step throughout the mesh.

The choice of $Y_{x^-,0,j}=\frac{1}{v_0l_{-\frac{1}{2},j}}$ means that all other admittances in region $I$ may be set as previously discussed in §4.4.2 for a type II mesh.

### Corners

If we are interested in using a grid of doubled density over a particular region of the problem domain (in order to surround a particular feature or an irregular part of the boundary), then we are faced with corners, and must develop special scattering junctions for them. An example of an irregular partitioning of the problem domain into two regions, $I$ and $II$, is shown in Figure 4.36(a). Boundary

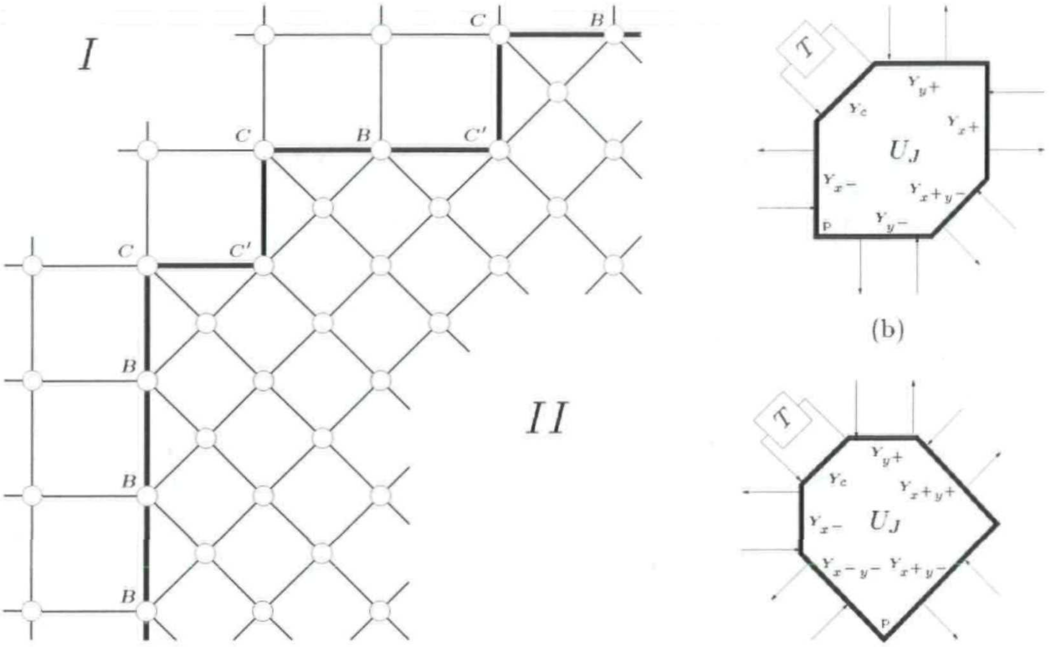

(a) (b) (c)

Figure 4.36: (a) *A particular grid arrangement between a rectilinear mesh I and one of doubled grid density II*, (b) *a scattering junction at a corner point (labelled C)*, and (c) *a scattering junction at another type of corner point (labelled C′)*.

points (labelled $B$) were treated previously, and it was found that waveguides connected to points $B$ which lie along the boundary must have their admittances set to one-half what they would be in the interior of region $I$ (i.e., to $\frac{1}{2v_0 l}$, where $l$ is the inductance at the center of the particular boundary waveguide).

There are two types of corners which can arise in an irregular domain decomposition of this kind: those which are concave with respect to region $I$ (the grid point at such a corner is labelled $C$ in Figure 4.36(a)), and those which are concave with respect to region $II$ (labelled $C'$). There are obviously four possible orientations for each type of corner, though, by symmetry, we need only treat the type shown. Because the admittances of the boundary waveguides (represented by thick lines connecting boundary points) are now prescribed, then for a corner junction the linking admittances are fixed; only the self-loop admittance may be varied. Scattering junctions corresponding to corners of type $C$ and $C'$ are shown in Figure 4.36(b) and (c).

Suppose we have a corner point of type $C$ located at coordinates $(0, 0)$. Then, from the results previously given in this section, the admittances of the five waveguides connecting this corner to its neighbors will be

$$Y_{y^+,0,0} = \frac{1}{v_0 l_{0,\frac{1}{2}}} \qquad Y_{x^-,0,0} = \frac{1}{v_0 l_{-\frac{1}{2},0}} \qquad Y_{x^+y^-,0,0} = \frac{1}{v_0 l_{\frac{1}{4},-\frac{1}{4}}}$$

$$Y_{x^+,0,0} = \frac{1}{2v_0 l_{\frac{1}{2},0}} \qquad Y_{y^-,0,0} = \frac{1}{2v_0 l_{0,-\frac{1}{2}}}$$

and the difference equation relating the corner junction voltage $U_{J,0,0}$ to those of its neighbors is

$$\begin{aligned}\frac{Y_{J,0,0}}{2}\left(U_{J,0,0}(n+1) + U_{J,0,0}(n-1)\right) = {} & \frac{1}{v_0 l_{-\frac{1}{2},0}} U_{J,-1,0} + \frac{1}{v_0 l_{0,\frac{1}{2}}} U_{J,0,1} \\ & + \frac{1}{2v_0 l_{\frac{1}{2},0}} U_{J,1,0} + \frac{1}{2v_0 l_{0,-\frac{1}{2}}} U_{J,0,-1} \\ & + \frac{1}{v_0 l_{\frac{1}{4},-\frac{1}{4}}} U_{J,\frac{1}{2},-\frac{1}{2}} + Y_{c,0,0} U_{J,0,0}\end{aligned}$$

where we have yet not specified $Y_{c,0,0}$ or $Y_{J,0,0}$. A Taylor expansion about $(0,0)$ gives, in terms of the continuous variable $u$ and neglecting higher-order terms,

$$\begin{aligned}\frac{4Y_{J,0,0}}{7v_0}\frac{\partial^2 u}{\partial t^2} = {} & \left(\frac{\partial}{\partial x}\left(\frac{1}{l}\right) - \frac{1}{7}\frac{\partial}{\partial y}\left(\frac{1}{l}\right)\right)\frac{\partial u}{\partial x} + \left(\frac{\partial}{\partial y}\left(\frac{1}{l}\right) - \frac{1}{7}\frac{\partial}{\partial x}\left(\frac{1}{l}\right)\right)\frac{\partial u}{\partial y} \\ & + \frac{1}{l}\left(\frac{\partial^2 u}{\partial x^2} + \frac{\partial^2 u}{\partial y^2}\right) + \frac{2}{7l}\frac{\partial^2 u}{\partial x \partial y}\end{aligned}$$

We can thus conclude that the differencing occurring at the corner junction is *not* consistent with the lossless source-free parallel-plate system, regardless of our choice of the self-loop admittance. The coefficients of the spatial first derivative terms are incorrect, and there is an extra mixed-derivative term; neither vanishes in the limit as $\Delta \to 0$ (although if $l$ is constant in a neighborhood surrounding the corner, then the first derivative terms vanish).

The corner junction is, however, still *lossless*, as are all junctions in this waveguide network, and hence a simulation of the parallel-plate system using such a mesh will be stable, regardless of inconsistencies at the corners. It is possible to argue, loosely speaking, that if the number of corners in the interface does not grow as the grid spacing is decreased (an example of this would be an enclosed rectangular doubled density grid, for which the number of corners will be four, independently of the grid spacing), then the error at the corners will become negligible. Although we will make no attempt to prove this, the simulation which we will present later in this section concurs readily with this assertion; indeed, in all tests we have run, any anomalous scattering at the corners is certainly far less important than the first-order scattering error (i.e., numerical reflection) along the interface itself. In the interest, however, of making any scattering error at the corner junctions as small as possible, we should set, at a corner with coordinates $C$ (in order that the wave speed at the corner is correct, in a gross sense)

$$Y_{c,C} = \frac{7}{4}v_0c_C - \frac{4}{v_0l_C}$$

where $l_C$ and $c_C$ are the inductance and capacitance at a corner point $C$. The stability requirement at such a corner is then

$$v_0 \geq \sqrt{\frac{16}{7l_Cc_C}} \qquad \text{Corner } C$$

which is, like the stability condition at boundary points $B$, only marginally worse than the CFL bound, and mitigated by the somewhat worse bound to be found in region $II$ (due to the decreased inter-junction spacing). See the discussion earlier in this section.

A similar argument follows for points $C'$, and we also ideally have $l$ constant in the neighborhood of such points. The setting of the self-loop admittance $Y_{c,C'}$ should be

$$Y_{c,C'} = \frac{5}{4}v_0c_{C'} - \frac{4}{v_0l_{C'}}$$

The resulting stability bound is

$$v_0 \geq \sqrt{\frac{16}{5l_{C'}c_{C'}}} \qquad \text{Corner } C'$$

### Simulation

To demonstrate the behavior of the interface discussed above, we will simulate the parallel-plate system (4.58), assuming no losses or sources, over a square region with side-length 1, with short-circuited boundary conditions (i.e., $u = 0$). Over a central square region with side lengths of $\frac{1}{2}$ (bounded by the white square in Figure 4.37), we use a mesh of doubled density with respect to the outer region, where a simple rectilinear mesh is in place. The grid spacing in the outer region is $\Delta = 0.01$. We set the capacitance per unit length $c = 1$ everywhere, and the inductance per unit length $l$ is equal to 1 in the outer region. In the inner region, it also takes the value 1, except in the interior of the black circle in Figure 4.37(radius 0.1, center at $x = 0.6$, $y = 0.5$), where it rises, in a 2D raised cosine distribution, to a maximal value of $l = 11$.

The initial voltage distribution takes the form of a 2D raised cosine over a circular region of radius 0.07, centered at coordinates $x = 0.4$ and $y = 0.5$. The initial voltage takes a maximum of 1, and is zero everywhere outside this circle.

The voltage distribution is shown at three successive time instants, with light and dark coloring indicating areas of positive and negative plate voltage, respectively; the plots have been normalized and interpolated for better plotting results. At time $t = 0.15$, the voltage distribution has spread and begun to scatter from the inductive region inside the black circle. Note that the local wave

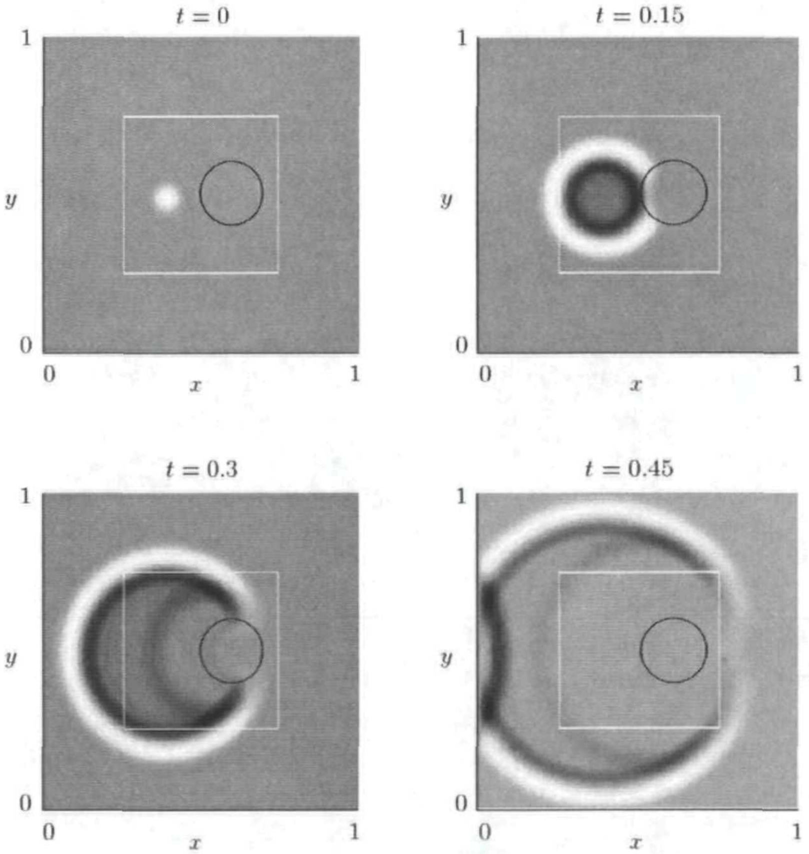

Figure 4.37: *Simulation of a parallel-plate system, with an inductive feature surrounded by a region of doubled grid density.*

speed decreases in the interior of the circle. By $t = 0.3$, it has progressed through the interface, with little visible numerical reflection, and by $t = 0.45$, the outward moving voltage distribution has reflected with inversion from the boundary at $x = 0$.

### 4.9.2 Progressive Grid Density Doubling

The delays in the bidirectional delay lines of the combined coarse/fine grid of the previous section were everywhere identical. In this section, we will look at networks for which this is not true—all delay line lengths, though, will be multiples of a common smallest unit delay, in order that the network remain synchronous [46]. It should be said, though, that even in a portion of the network where the delay line lengths are longer than a single sample delay, we will still be scattering at the rate of the smallest delay line length in the system as a whole. We will, however, be performing scattering operations at fewer points in the coarse regions. We will call such structures (for lack of a better word) multi-rate, though it should be understood that such networks are not multi-rate in the sense of [193] (see above comment). Specifically, we will focus on the use of such structures in order to extend the grid refinement technique introduced in the previous section.

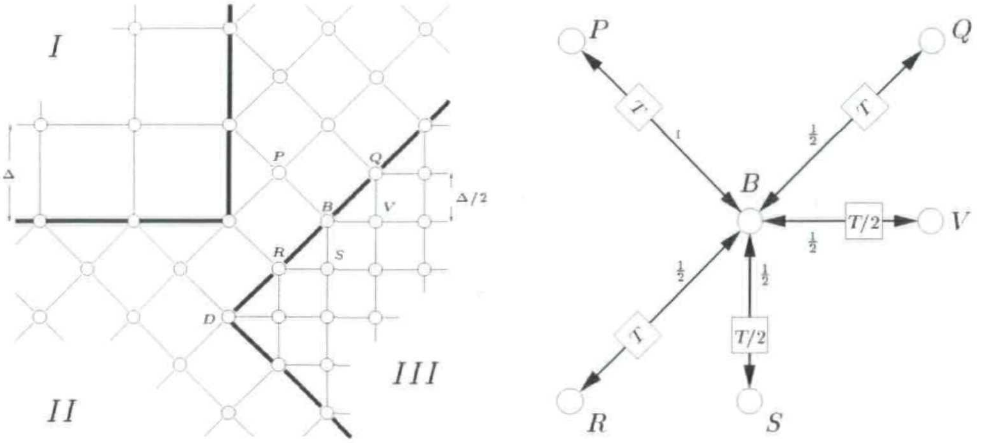

(a) (b)

Figure 4.38: (a) *Mesh $I$, with grid spacing $\Delta$, is adjoined to a doubled density mesh $II$, which is in turn adjoined to a quadrupled density mesh $III$, with grid spacing $\frac{\Delta}{2}$ and a halved waveguide delay.* (b) *A scattering junction at a point $B$ on the boundary between layers $II$ and $III$.*

Consider the grid arrangement of Figure 4.38(a). The interface between region $I$ and region $II$ was discussed in the previous section; in that case, we assumed the waveguide delays to be identical everywhere in regions $I$ and $II$, including the boundary. We can, of course, apply the same idea again in order to introduce a grid of quadrupled point density, by adjoining it to region $II$. In this case, however, we would like to take advantage of the fact that waveguide lengths in region $III$ are half those of region $I$; it is more natural, then, to use a delay of half that of region $I$ throughout the interior of region $III$. Waveguides which run along the boundary will still operate at the rate of regions $I$ and $II$, as will the self-loop (of admittance $Y_c$, not shown). A scattering junction at a typical point $B$ on the boundary between regions $II$ and $III$ is shown in Figure 4.38(b). Here, we have abbreviated the depiction of a bidirectional delay line to a single double-headed arrow, and have omitted the self-loop (which contains a full unit delay). Note in particular that for such a boundary junction, the delays of the connecting waveguides are now not all identical. As might be expected, the difference scheme relating the junction voltage at such a point to those of its neighbors is no longer a simple two-step difference method, but a four-step scheme, where each time step is now $\frac{T}{2}$; a full derivation of this difference scheme is very lengthy but rewarding, in the sense that it becomes clear why it takes four steps for the wave variables to fully "recombine" into junction voltages. We will, however, only present the resulting difference equation for a boundary junction at location $B$ as in Figure 4.38(b). Here the junction voltage will be $U_{J,B}$, and the junction voltages at the neighboring points are, referring to Figure 4.38(b), $U_{J,P}, \dots, U_{J,V}$. The admittances of the connecting waveguides will be called $Y_{PB}, \dots, Y_{VB}$, the self-loop admittance $Y_{c,B}$ and the junction admittance at point $B$ is defined as

$$Y_{J,B} = Y_{PB} + Y_{QB} + Y_{RB} + Y_{SB} + Y_{VB} + Y_{c,B}$$

We have

$$\begin{aligned}\frac{Y_{J,B}}{2}U_{J,B}(n+1) = & \; Y_{VB}U_{J,V}(n+\tfrac{1}{2}) + Y_{SB}U_{J,S}(n+\tfrac{1}{2}) \\ & + Y_{QB}U_{J,Q}(n) + Y_{PB}U_{J,P}(n) + Y_{RB}U_{J,R}(n) \\ & + (Y_{c,B} - Y_{SB} - Y_{VB})\,U_{J,B}(n) \\ & + Y_{VB}U_{J,V}(n-\tfrac{1}{2}) + Y_{SB}U_{J,S}(n-\tfrac{1}{2}) \\ & - \frac{Y_{J,B}}{2}U_{J,B}(n-1)\end{aligned}$$

A Taylor series expansion allows us to set the admittances of the waveguides to be

$$\begin{gathered}Y_{PB} = \frac{1}{v_0 l_{PB}} \qquad Y_{QB} = \frac{1}{2v_0 l_{QB}} \qquad Y_{RB} = \frac{1}{2v_0 l_{RB}} \\ Y_{SB} = \frac{1}{2v_0 l_{SB}} \qquad Y_{VB} = \frac{1}{2v_0 l_{VB}}\end{gathered}$$

where $l_{XY}$ is the material inductance at the point midway between points $X$ and $Y$. Note in particular that the setting of $Y_{PB}$ coincides with an interior point setting of a connecting waveguide admittance in the interior of region $II$, from (4.64) and (4.65). These relative strengths of the connecting waveguide admittances are indicated by adjacent small numbers in Figure 4.38(b).

Because we now have a four-step scheme, the determination of $Y_{c,B}$ is no longer as simple as in the two-step case, but it can be found, nevertheless, to be

$$\begin{aligned}Y_{c,B} = & \; \frac{v_0}{8}\left(2c_{PB} + c_{QB} + c_{RB} + c_{SB} + c_{VB}\right) \\ & - \frac{5}{12v_0}\left(\frac{2}{l_{PB}} + \frac{1}{l_{QB}} + \frac{1}{l_{RB}} + \frac{1}{l_{SB}} + \frac{1}{l_{VB}}\right)\end{aligned}$$

where $c_{XY}$ signifies a waveguide midpoint evaluation of $c$ between any points $X$ and $Y$.

The positivity requirement yields the bound

$$v_0 \geq \max_{\substack{\text{II/III boundary} \\ \text{waveguide midpoints}}} \sqrt{\frac{10}{3lc}}$$

Corners present essentially the same problems as before, and we will not discuss them further, other than to repeat that, given the settings derived above for the waveguide admittances at the $II/III$ boundary, which determine completely the scattering behavior at the corners (an example of which is point $D$ in Figure 4.38(a)), the mesh will not be consistent with the parallel-plate system at these points.

### 4.9.3 Grid Density Quadrupling

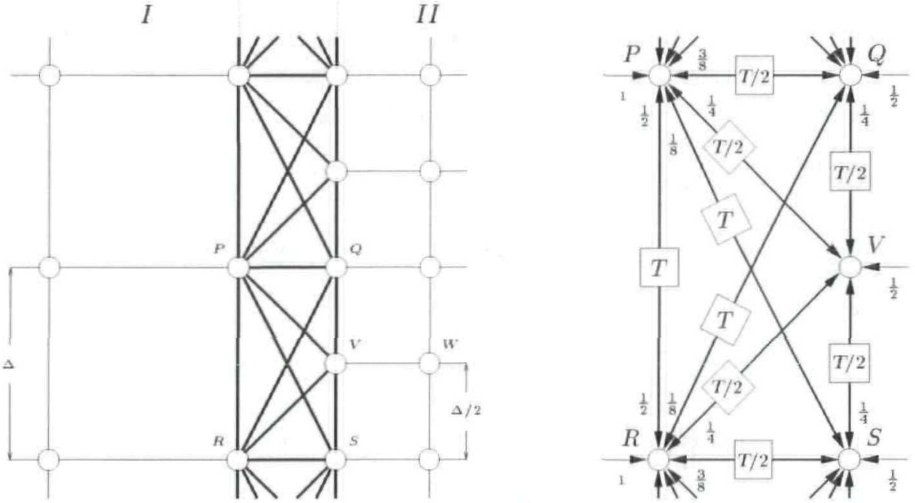

(a) (b)

Figure 4.39: (a) *Grid I, with grid spacing* $\Delta$, *is adjoined to a quadrupled density region II with grid spacing* $\frac{\Delta}{2}$. (b) *Detail of the interface.*

Instead of progressing, in two steps, from a grid to one of quadrupled point density, as we did in the last section, we might ask whether it is possible to design a direct passive interface in order to quadruple grid density in one step. Such an arrangement is shown in Figure 4.39(a): a quadrupled density region ($II$), for which the delay in all waveguides is one-half time step, or $\frac{T}{2}$ is adjoined to a rectilinear mesh ($I$) via a matching layer composed of various waveguides connecting each point on the boundary of region $I$ with five neighboring points in region $II$. The admittances and delays of the waveguides in the matching layer must be set to particular values relative to the values in the interiors of regions $I$ and $II$ so as to satisfy the transmission line equations at all grid points (junctions). These delays and admittance settings are shown in Figure 4.39(b), where we have used the following notation for the admittance settings: first suppose that admittances in the interior of region $I$ are set to the normal values for a type II mesh—namely, the admittance of a particular connecting waveguide is equal to $\frac{1}{v_0 l}$, where $l$ is evaluated at the midpoint of the waveguide. All other connecting admittances in the network, including those in region $II$ and in the matching later, will also be set to $\frac{1}{v_0 l}$, where $l$ is evaluated at the center of the particular waveguide, and multiplied by a scaling coefficient. In Figure 4.39(b), this scaling coefficient is shown next to the waveguide. For example, for the waveguide connecting point $P$ to point $S$, the admittance should be set to

$$Y_{PS} = \frac{1}{8}\frac{1}{v_0 l_{PS}}$$

where $l_{PS}$ is the inductance evaluated midway between points $P$ and $S$. Note in particular that even though the space step/time step ratio is the same in region $II$ (both quantities are halved), the admittances of the interior waveguides should be scaled by a factor of $\frac{1}{2}$. This, however, has no bearing on stability, since scaling all connecting waveguide admittances in a network by the same factor does not affect the *reflection coefficients* (though we must change the self-loop admittance settings in region $II$; we provide this setting shortly).

It is simple (after some tedious algebra) to set the self-loop admittances at the junctions in the matching layer such that the transmission line equations are approximated at these points. We first define average capacitances and inverse inductances at a junction at point $X$ by:

$$\left(\overline{\frac{1}{l}}\right)_X = \frac{1}{\sum_j \beta_{Xj}}\sum_j \frac{\beta_{Xj}}{l_{Xj}} \qquad \bar{c}_X = \frac{1}{\sum_j \beta_{Xj}}\sum_j \beta_{Xj}c_{Xj}$$

where the index $j$ runs over all the junctions to which the junction at point $X$ is connected and where $\beta_{Xj}$ is the scaling factor of the waveguide connecting point $X$ to point $j$. $l_{Xj}$ and $c_{Xj}$ are the inductance and capacitance at the midpoint of the same waveguide. Obviously, we have $\left(\overline{\frac{1}{l}}\right)_X = \frac{1}{l_X}$ and $\bar{c}_X = c_X$ to first order in $\Delta$. For example, we would have, from Figure 4.39,

$$\bar{c}_V = \left(\frac{1}{2}+\frac{1}{4}+\frac{1}{4}+\frac{1}{4}+\frac{1}{4}\right)^{-1}\left(\frac{1}{2}c_{VW}+\frac{1}{4}c_{VQ}+\frac{1}{4}c_{VS}+\frac{1}{4}c_{VP}+\frac{1}{4}c_{VR}\right)$$

Referring to Figure 4.39(a), it is easy to see that we need only examine self-loop admittances $Y_{c,P}$, $Y_{c,V}$ and $Y_{c,Q}$ at points $P$, $V$ and $Q$; all other junctions in the matching layer will behave similarly (because they map to these three points under translation in the vertical direction). We set

$$Y_{c,P} = \frac{3}{2}v_0\bar{c}_P - \frac{43}{16v_0}\left(\overline{\frac{1}{l}}\right)_P \qquad Y_{c,V} = v_0\bar{c}_V - \frac{3}{2v_0}\left(\overline{\frac{1}{l}}\right)_V$$
$$Y_{c,Q} = \frac{1}{2}v_0\bar{c}_Q - \frac{15}{8v_0}\left(\overline{\frac{1}{l}}\right)_Q$$

and, at an interior point in region $II$ (such as point $W$),

$$Y_{c,W} = v_0\bar{c}_W - 2\left(\overline{\frac{1}{l}}\right)_W$$

It is interesting that, in contrast to situation at the grid-doubling interface presented in the last section, the positivity conditions that arise from these self-loop admittances do not degrade the stability bound which arises from self-loop admittances in the interior of either region $I$ or $II$. We note that it would appear (through trial and error) that this is the simplest density-quadrupling layer possible.

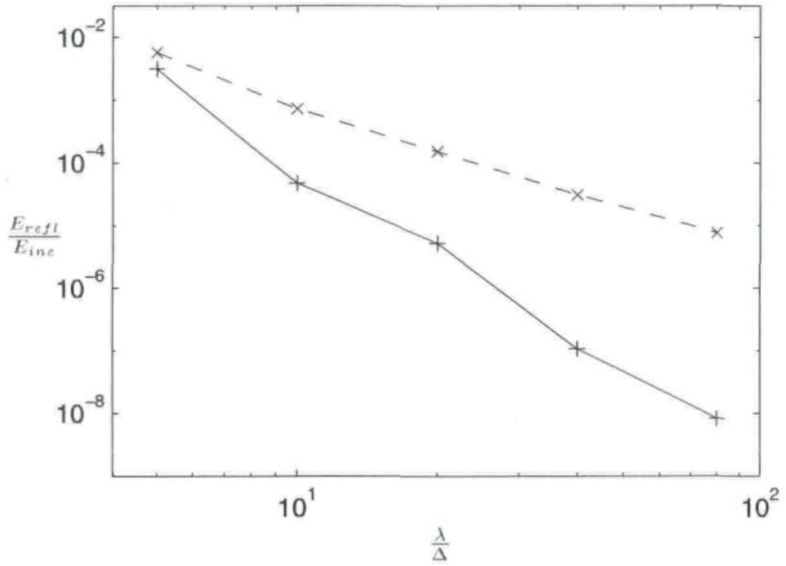

Figure 4.40: *Log plot of the ratio of reflected energy to incident energy versus number of grid points per wavelength, for a wave normally incident from a region containing a standard rectilinear mesh on two types of interface—density-doubling (solid line) and density quadrupling (dashed line).*

We also show some numerical results, comparing the numerical reflection error of the density doubling and quadrupling layers for normally incident waves. Waves (one period of a raised cosine) impinge on the layer from the side of smaller grid density (region $I$) in both cases. In Figure 4.40, we have plotted the log of the ratio of the reflected energy to the incident energy ($\frac{E_{refl}}{E_{inc}}$) versus the log of the number of grid spacings $\Delta$ per wavelength $\lambda$. $E_{refl}$ and $E_{inc}$ were computed by taking the sum of the squares of the junction quantities $U_J$ over region $I$, before and after the passage of the wave through the interface.

The density doubling layer (solid line in Figure 4.40) leads to a smaller reflected energy than the quadrupling layer (dashed line). This is to be expected—in general, the more abrupt a change in grid density, the more numerical reflection will result. As exemplified by Figure 4.40, however, the reflected energy will always tend to zero as grid density is increased on both sides of the interface. The case of oblique incidence has not been examined; it would appear, also, to be possible to derive an analytic expression for the numerical reflectance, though we have not done so here.

It would be very interesting to know whether the coarse/fine mesh arrangements discussed in this section and the last could be made truly multi-rate—that is, could we have scattering operations which recur with period $T$ in the coarse mesh, and period $\frac{T}{2}$ in the fine mesh? As mentioned earlier, there are TLM structures which are capable of this, but they in general perform time-averaging of wave quantities which may render the interface non-passive [87, 88].

We also note that because interfaces between grids operating at different rates by necessity correspond to multi-step methods, we may also see parasitic modes [176] appearing along the interface (though we are assured convergence in the limit as the grid spacing becomes small). A discussion of parasitic modes in MDWDFs appears in §3.9.2.

### 4.9.4 Connecting Rectilinear and Radial Grids

As another example of a passive interface between different types of waveguide meshes, we examine the means by which grids defined in different coordinate systems may be connected, for the special (but quite practically important) case of the connection between a rectilinear and radial grid. Such a grid would be useful in cases where it is desired to solve the parallel-plate system or wave equation over some region which has boundaries which are are straight in some places, but circularly curved in others. One could in general proceed by attempting to find a global coordinate transformation which maps an irregular region to a regular one (like a rectangle), and then developing a waveguide mesh in the new coordinates, as per the methods discussed in §4.8. It is perhaps simpler, however, to use rectilinear and radial meshes at appropriate places in the domain, and then define a matching layer at the boundary between the regions, which should also be locally consistent with the equations to be solved. Consider the grid arrangement of Figure 4.41. We have a type II radial waveguide mesh in

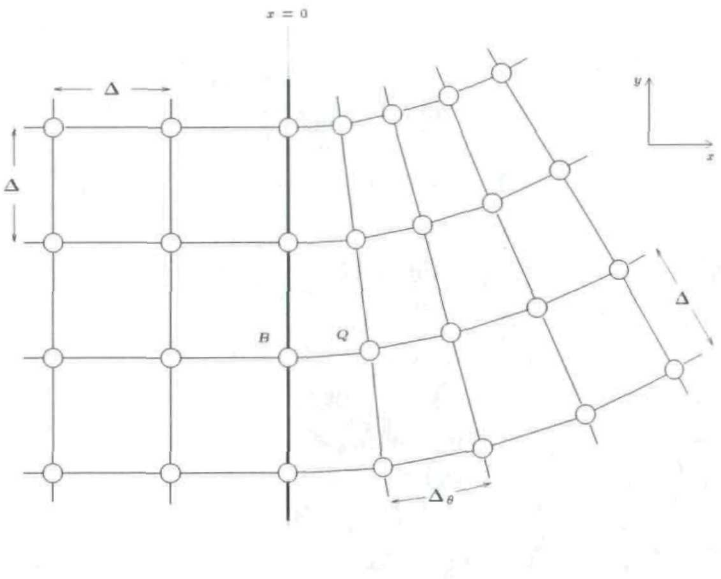

Figure 4.41: *Interface between radial and rectilinear meshes.*

$x > 0$ and a type II rectilinear mesh in $x < 0$; parallel junctions are to be placed at all the grid points, and waveguide connections (bidirectional delay lines of delay $T$) are indicated by connecting lines. Special boundary waveguides, which lie along the $y$ axis, are drawn in bold. All interior waveguide admittances in either region (i.e., all admittances except for those of the boundary waveguides) are assumed to be set to the values that they must take in the interior in order to solve the lossless source-free transmission line equations, as given in (4.64)—(4.66) and (4.89)—(4.92). Self-loops are of course required in general at all junctions, though for simplicity, they are not represented in Figure 4.41. The spacing $\Delta$ between junctions in the rectilinear mesh is assumed to be equal to the radial grid spacing in the radial mesh. The angular spacing in this same grid, $\Delta_\theta$, may be set independently. We will use $v_0 = \Delta/T$ here.

In order to derive the admittance and self-loop settings at the boundary, we may examine a junction at coordinates $(0, j\Delta)$, $j$ integer (one such point is labelled $B$ in Figure 4.41). In keeping with the notation for a rectilinear mesh (used in $x < 0$), we call the admittances of the four connecting waveguides at such a point $Y_{x^-,0,j}$, $Y_{x^+,0,j}$, $Y_{y^-,0,j}$ and $Y_{y^+,0,j}$, and the self-loop admittance $Y_{c,0,j}$. The junction admittance $Y_{J,0,j}$ is then the sum of these five admittances. The junction voltage at point $B$ will be called $U_{J,0,j}$, and we will call the junction voltage at point $Q$ directly to the right $U_{J,Q}$. The difference scheme in the junction voltages resulting from such a mesh is then

$$\begin{aligned}\frac{Y_{J,0,j}}{2}\left(U_{J,0,j}(n+1)+U_{J,0,j}(n-1)\right) = \; & Y_{x^-,0,j}U_{J,-1,j}(n)+Y_{x^+,0,j}U_{J,Q}(n)\\ & +Y_{y^-,0,j}U_{J,0,j-1}(n)+Y_{y^+,0,j}U_{J,0,j+1}(n)\\ & +Y_{c,0,j}U_{J,0,j}(n)\end{aligned}$$

Expansion in terms of a Taylor series about $(0, j\Delta, nT)$ gives, in terms of the continuous function $u(x, y, t)$,

$$\begin{aligned}\frac{Y_{J,0,j}T^2}{2}\frac{\partial^2 u}{\partial t^2} = \; & \Delta\left(Y_{y^+,0,j}-Y_{y^-,0,j}\right)\frac{\partial u}{\partial y}+\Delta\left(\rho_j\lambda Y_{x^+,0,j}-Y_{x^-,0,j}\right)\frac{\partial u}{\partial x}\\ & +\frac{\Delta^2}{2}\left(Y_{y^+,0,j}+Y_{y^-,0,j}\right)\frac{\partial^2 u}{\partial y^2}\\ & +\frac{\Delta^2}{2}\left(Y_{x^-,0,j}+\rho_j^2\lambda^2 Y_{x^+,0,j}\right)\frac{\partial^2 u}{\partial x^2}\end{aligned} \tag{4.103}$$

where we have discarded higher-order terms in $\Delta$, and used $\lambda = \Delta_\theta/\Delta$ and $\rho_j$ as in §4.6.2.

First examine, in (4.103), the coefficient of $\frac{\partial u}{\partial x}$ on the right-hand side. Notice that in order for this term to behave as $O(\Delta^2)$, we must have $Y_{x^-,0,j} = \rho_j\lambda Y_{x^+,0,j} + O(\Delta)$. Since $Y_{x^+,0,j}$ is assumed set as an interior admittance in the type II radial waveguide mesh, namely, from (4.90) as

$$Y_{x^+,0,j} = \frac{1}{\lambda^2 v_0 l_{BQ}\rho_j}$$

where $l_{BQ}$ is the value of the inductance at the midpoint of the waveguide connecting points $B$ and $Q$, we may choose

$$Y_{x^-,0,j} = \frac{1}{\lambda v_0 l_{-\frac{1}{2},j}}$$

Because $Y_{x^-,0,j}$ is to be interpreted as an interior admittance in the rectilinear mesh, it is clear that all connecting admittances in this mesh should incorporate this same scaling factor of $\lambda$.

Since a boundary waveguide can be interpreted as lying in *both* waveguide meshes, a good initial guess as to its admittance might be a simple linear average of the admittances of interior radial and rectilinear waveguides located at the same position. This would give:

$$Y_{y^+,0,j} = Y_{y^-,0,j+1} = \frac{1}{2v_0\lambda} l_{0,j+\frac{1}{2}} \left(1 + \frac{1}{\rho_{j+\frac{1}{2}}\lambda}\right)$$

It is straightforward (but tedious) to show that these admittances do indeed yield a difference scheme which is consistent with the lossless source-free parallel-plate system, provided that we set

$$\begin{aligned} Y_{c,0,j} = \; & \frac{c_{-\frac{1}{2},j}v_0}{2\lambda} + \frac{c_{0,j+\frac{1}{2}}v_0}{4\lambda}\left(\rho_{j+\frac{1}{2}} + \frac{1}{\lambda}\right) + \frac{c_{0,j-\frac{1}{2}}v_0}{4\lambda}\left(\rho_{j-\frac{1}{2}} + \frac{1}{\lambda}\right) + \frac{v_0 c_{BQ}\rho_j}{2} \\ & - Y_{x^-,0,j} - Y_{x^+,0,j} - Y_{y^-,0,j} - Y_{y^+,0,j} \end{aligned}$$

where $c_{BQ}$ is the capacitance at the midpoint of the waveguide joining points $B$ and $Q$, for any $j$. The stability bound is identical to that obtained in the interior of the radial mesh, and this type of matching layer requires very little extra programming effort in an implementation .

#### Simulation: Solving the Acoustic Wave Equation in a U-Shaped Tube

As a simple application of an interface between radial and rectilinear meshes, we solve the (2+1)D acoustic wave equation (1.18) in a U-shaped tube—that is, a tube consisting of two straight segments connected by a semicircular radial tube; we note that the (3+1)D version of this problem was first solved using a waveguide mesh by Tim Stilson at CCRMA, in the context of physical modeling of brass instruments [200]. In that case, a rectilinear mesh was used over the entire domain, which forces a staircase-type approximation to the radial boundary. Here, however, because we are modeling the semicircular tube in radial coordinates, boundary conditions can be implemented in a well-defined manner; the trade-off will be in the added numerical reflection at the radial/rectilinear mesh interface.

We assume a wave speed of 1 throughout the interior, and an open-circuited boundary condition ($i_n$, the normal current density component is zero everywhere on the boundary). The thickness of the tube is 0.2, the inner radius of the circular portion is 0.1, and the lengths of the two straight tube segments are each 0.3. The grid spacing is set to $\Delta = 0.005$, and white lines indicate the

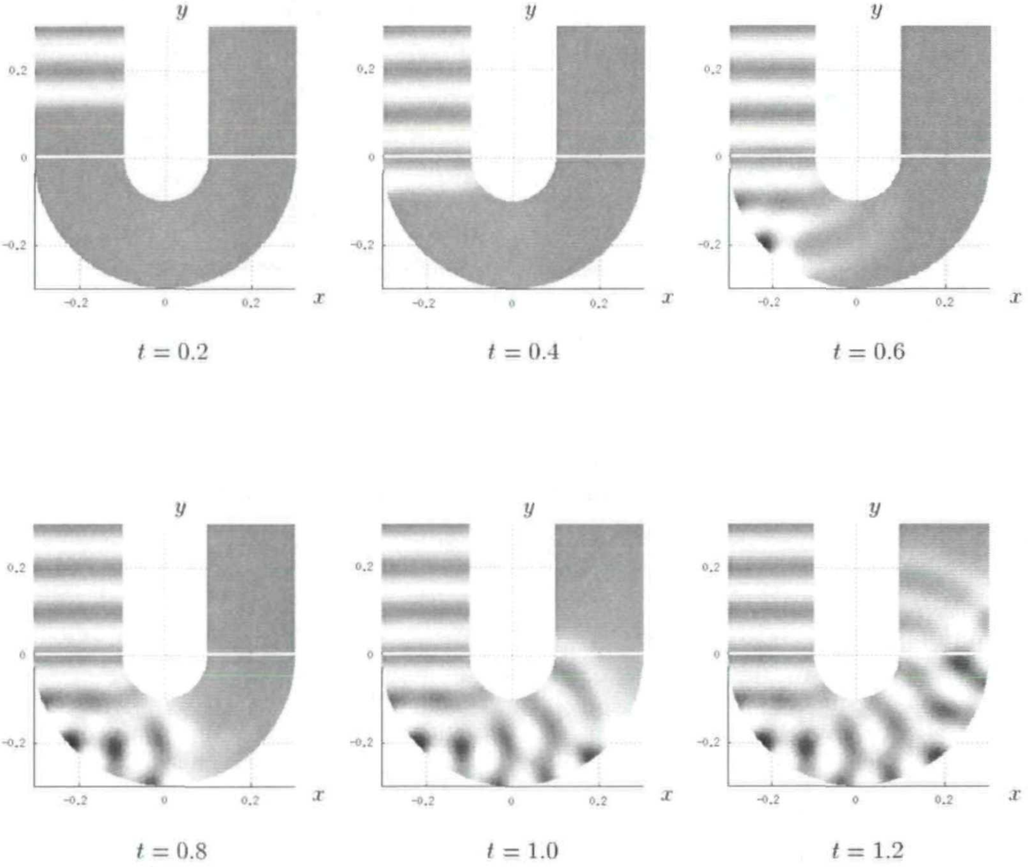

$t = 0.2$ $t = 0.4$ $t = 0.6$

$t = 0.8$ $t = 1.0$ $t = 1.2$

Figure 4.42: *Simulation of wave propagation in a U-shaped tube.*

interfaces between the radial mesh and the adjacent rectilinear meshes. The input signal is a raised cosine voltage of period 0.2 at the upper left-hand entrance to the tube. The evolution of the voltage in the tube is shown in Figure 4.42. Here, $u$ can be interpreted as a pressure in a tube with hard boundaries; this situation comes up in the modelling of brass instruments, in particular in curved sections of tubes, such as trombone slides or crooks (though we have used, for illustrative purposes, an unnaturally short wavelength; longer wavelengths in the musical range can be modeled more cheaply using a coarse grid, and numerical reflections will be even smaller as the number of grid points per wavelength increases).

### 4.9.5 Grid Density Doubling in (3+1)D

It is straightforward to extend the grid density doubling technique presented in §4.9.1 to (3+1)D. As in §4.7, we will assume that our mesh is to simulate the (3+1)D wave equation (4.95). If we have a rectilinear mesh (region $I$ in Figure 4.43(a)) with inter-junction spacing $\Delta$ to which we would like

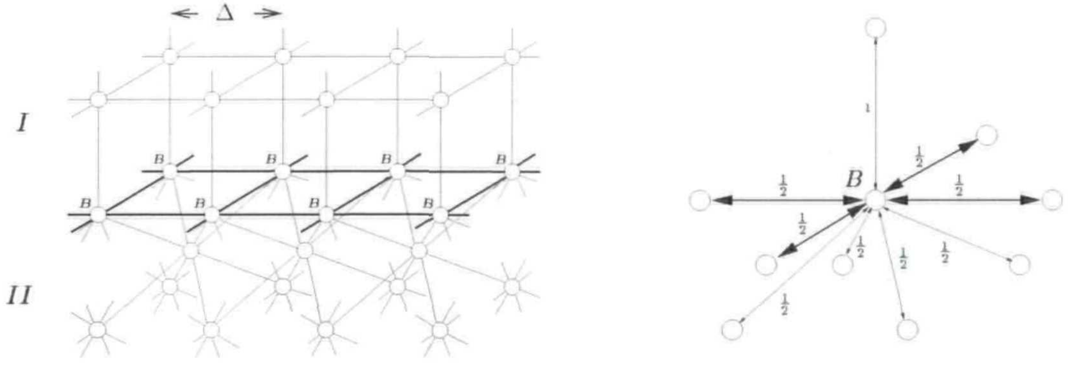

(a) (b)

Figure 4.43: (a) *Grid $I$, with grid spacing $\Delta$, is adjoined to a doubled density region $II$ with grid spacing* $\frac{\sqrt{3}\Delta}{2}$. (b) *a junction at the interface.*

to adjoin a mesh of doubled grid density, we may introduce an octahedral mesh (region $II$) with a grid spacing of $\sqrt{\frac{3}{4}}\Delta$, to be connected to region $I$ across an interface; special matching waveguide connections at this interface are shown in bold in Figure 4.43(a). The spacing of $\sqrt{\frac{3}{4}}\Delta$ in region $II$ is chosen so that the octahedral grid may be decomposed into two offset rectilinear grids of spacing $\Delta$, and may hence be aligned with region $I$ at the interface.

The relative admittances at the special boundary 10-ports (nine connecting waveguides and a self-loop) are shown in Figure 4.43(b); only the waveguides in bold in (a) take on special values; all others may be set as interior admittances. For consistency with the wave equation, we must choose the admittances in region $I$ to be double those in region $II$. In addition, the self-loop admittance at a boundary junction (labelled $B$ in Figure 4.43) must be chosen to be

$$Y_{c,B} = \frac{3}{2}v_0c - \frac{5}{v_0l} \qquad \text{Boundary junction}$$

where we have chosen the connecting admittance in region $I$ to be $\frac{1}{v_0l}$, and where we must have $\gamma = \sqrt{\frac{1}{lc}}$ as discussed in §4.7. The stability requirement at such a boundary junction $B$ is then

$$v_0 \geq \sqrt{\frac{10}{3}}\gamma \qquad \text{Boundary junction}$$

which is worse than the bound over the interior of region $I$, as given in (4.96). On the other hand, because the grid spacing is $\sqrt{\frac{3}{4}}\Delta$ in region $II$, we must set, at an interior point in region $II$,

$$Y_c = cv_0 - \frac{4}{v_0l} \qquad \Rightarrow \qquad v_0 \geq 2\gamma \qquad \text{in region } II$$

This bound is, as expected, worse still than the boundary requirement, and hence boundary scattering, as in the (2+1)D case, does not compromise the overall requirement on space step/time step ratio which is forced by the settings in region *II*.

We briefly mention that at edges and corners of a doubled density region, the waveguide mesh cannot be made consistent with the wave equation. We may invoke the same argument that was ventured in the (2+1)D case, namely that numerical reflection should be minimal, and should vanish in the limit as the grid spacing becomes small. Special admittance values for the connecting waveguides along such edges, and for the self-loops at both edges and corners may be chosen such that numerical reflection is made as small as possible, though we do not provide here those values, due to the ease with which they can be calculated, and relatively large number of cases that must be considered (two edge types and four corner types).

We have not investigated ways of redoubling (quadrupling) grid density as was done in the (2+1)D case, though we would conjecture that it should be possible, either via a direct quadrupling layer with a special interface (analogous to the scheme of §4.9.3) or via successive redoubling (as per §4.9.2).

### 4.9.6 Note

We would like to add that an interesting future direction of development of waveguide meshes might involve the use of fully unstructured grids—that is, grids whose points cannot be ordered according to some regular indexing system. An unstructured DWN is certainly conceivable (and has been used for artificial reverberation [163]), though it is difficult to design a structure which is locally consistent with the continuous parallel-plate problem (though it will be passive, regardless). Such a structure would, of course, be very useful for dealing with the irregular geometries which typically arise in almost all musical instrument bodies. On the other hand, FDTD has evolved in this direction, specifically by making use of the *finite volume method* [89, 140], long known in the fluid dynamics community. The FVTD (*finite volume time domain*) method is the result—the general idea is that instead of using finite differences to approximate derivative terms, the integral forms of the governing equations (Maxwell's, for the FDTD people, but mechanical systems can be treated equally easily) are discretized over cells of finite size which may not have any particular ordering. For a look at some recent work in this area, we refer the reader to [21] and [148].

## 4.10 Incorporating the DWN into the MDWD Framework

At this point, the reader may have noticed more than a few similarities between the treatment of transmission lines in this chapter and the last. It should be recalled from Chapter 3 that the multidimensional wave digital networks that numerically integrate the parallel-plate system are derived

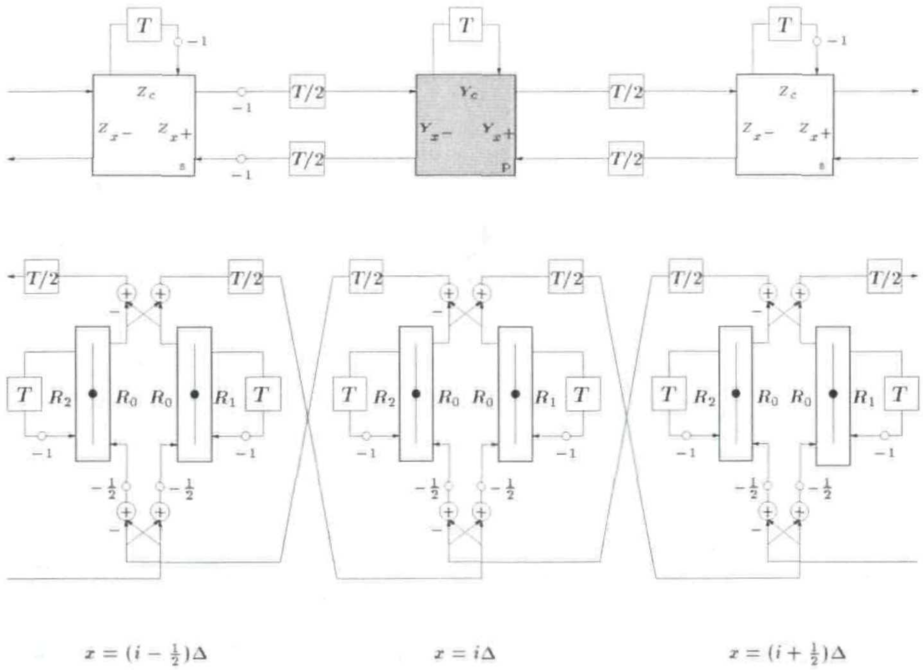

Figure 4.44: *Signal flow diagrams of the DWN and MDWD networks for the (1+1)D lossless source-free transmission line.*

from multidimensional Kirchoff circuits under a set of coordinate transformations and spectral mappings from the continuous to discrete domain. A DWN, on the other hand, is constructed entirely in the discrete time and space domain, and is then identified with a finite difference method consistent with the problem.

It will be shown in this section that certain DWNs may in fact be derived from an MDKC under an alternative spectral mapping (also passivity-preserving), provided new wave digital circuit elements (*multidimensional unit elements*) are also defined. In this way, the DWN may be considered to be a multidimensional wave digital network in its own right, depending on how attached one feels to the trapezoid rule as an integration method. The behavior of TLM and wave-digital numerical integration methods have been previously compared in [131] and [71], and the material in this section also appears in [18].

It is instructive to first reconsider the (1+1)D transmission line system in the lossless source-free case. In Figure 4.44 are presented both the type III DWN, and the MDWD network for the same system using offset sampling, with spatial dependence expanded out. For the MDWD network, we have chosen a grid spacing of $\Delta/2$, and a time step of $T/2$ so as to align it with the DWN. (In other words, we have used $T_1 = T_2 = \Delta/\sqrt{2}$— see §3.7 for details.)

First, notice that for the DWN, we have one three-port scattering junction at each grid point, and that parallel junctions are interleaved with series junctions. Approximations to $i$ and $u$ are calculated at alternating grid points, and at alternating multiples of the time step, $T/2$. For the MDWDF, we have two two-port series adaptors at each grid point; we are approximating both $i$ and $u$ *together* at the same locations, though due to offset sampling, these locations alternate from one time step to the next. Both variables are treated as *currents*. For both networks, all the material variation of the transmission line is expressed in the immittances of self-loops at every junction or adaptor, the delay in which is twice that of the linking delay between adjacent grid points. It is also useful to compare the waveguide immittances to the port resistances of the MDWDF. We have

$$R_1 = \frac{2}{\Delta}\left(v_0 l - r_0\right) \qquad R_2 = \frac{2}{\Delta}\left(v_0 r_0^2 c - r_0\right) \qquad R_0 = \frac{4r_0}{\Delta}$$

and

$$Z_c = 2\left(v_0 l - r_0\right) \qquad Y_c = 2\left(v_0 c - \frac{1}{r_0}\right) \qquad Z_{x^-} = Z_{x^+} = \frac{1}{Y_{x^-}} = \frac{1}{Y_{x^+}} = r_0$$

where we recall, from the discussion of the type III waveguide network in §4.3.6, that the connecting impedances were chosen to be some constant $Z_{const}$, in this case $Z_{const} = r_0$.

Enforcing the positivity of $R_1$ and $R_2$ or $Z_c$ and $Y_c$ leads to identical stability conditions, and the self-loop immittances and inductances are simply related to one another by

$$Z_c = \Delta R_1 \qquad Y_c = \Delta R_2 / r_0^2$$

at locations for which both quantities coexist in their respective discrete networks.

Most important, though, is the observation that, whereas the DWN can be considered to be made up of an array of lumped two-port bidirectional delay lines, the signal flow diagram of the MDWD network in Figure 4.44 does not have such an interpretation—the port in this setting is defined only as a multidimensional object, and instances of this port in the discrete domain are *not* connected port-wise. It is crucial to recognize that passivity of such a discrete network is reflected by the power conservation of the scattering operation, and not by where wave variables go in the network after they have been scattered; in particular, they need not be paired as they are for waveguide networks, as long as the shifting operation which they undergo subsequently does not increase energy in the network. On the other hand, as we shall see in Chapter 5, boundary conditions are much easier to implement in a lumped network.

### 4.10.1 Multidimensional Unit Elements

As a first step towards reintroducing this port structure to a MDWD network (and hence towards relating the DWN to the MDWDF), we can extend the definition of the unit element (and recall from §4.2.1 that the unit element is a wave digital two-port which is equivalent to a single bidirectional delay line) to multi-D in the following way[†]. Suppose that we are dealing with a (1+1)D system, and new coordinates $t_1$ and $t_2$ are as defined by (3.18). We thus have two transform frequencies $s_1$ and $s_2$, as well as two frequency-domain shift-operators $z_1^{-1}$ and $z_2^{-1}$ in the two directions $t_1$ and $t_2$. The multidimensional two-port defined, at steady-state, by

$$\begin{bmatrix}\hat{b}_1\\ \hat{b}_2\end{bmatrix} = \begin{bmatrix}0 & z_2^{-1}\\ z_1^{-1} & 0\end{bmatrix}\begin{bmatrix}\hat{a}_1\\ \hat{a}_2\end{bmatrix} \tag{4.104}$$

and shown in Figure 4.45(a) bears some resemblance to the lumped unit element discussed initially in §2.3.4; it is clearly lossless (because it merely implements a pair of shifts), but, unlike the unit element, it is no longer reciprocal. In this last respect, we remark that a multidimensional element so defined is perhaps closer in spirit to a generalization of the so-called quasi-reciprocal line (QUARL) proposed by Fettweis [46]. The two port resistances are assumed identical and equal to some positive constant $R$. When the spatial dependence is expanded out, it appears as an entire array of unit elements, as in Figure 4.45(b), where we have assumed

$$z_1^{-1} = z^{-\frac{1}{2}}w^{-\frac{1}{2}} \qquad\qquad z_2^{-1} = z^{-\frac{1}{2}}w^{\frac{1}{2}}$$

where $z^{-\frac{1}{2}}$ and $w^{-\frac{1}{2}}$ correspond, respectively, to unit shifts in time and space by $T/2$ and $\Delta/2$. We have thus chosen $T_1 = T_2 = \Delta/\sqrt{2}$.

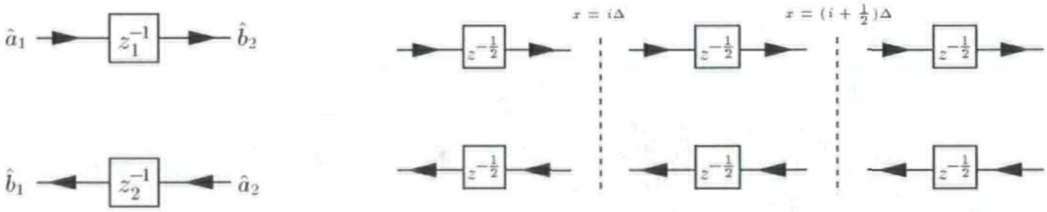

(a) (b)

Figure 4.45: (a) *Multidimensional unit element at steady state making use of shifts in directions* $t_1$ *and* $t_2$ *and* (b) *its steady state schematic when spatial dependence is expanded out.*

This element, like the standard unit element, is defined in the discrete (time and space) domain, and using wave variables. Rewriting the scattering relation in terms of steady-state discrete voltage and current amplitudes, (4.104) becomes the impedance relationship

$$\begin{bmatrix}\hat{v}_1\\ \hat{v}_2\end{bmatrix} = \frac{R}{1-z_1^{-1}z_2^{-1}}\begin{bmatrix}1+z_1^{-1}z_2^{-1} & 2z_2^{-1}\\ 2z_1^{-1} & 1+z_1^{-1}z_2^{-1}\end{bmatrix}\begin{bmatrix}\hat{i}_1\\ \hat{i}_2\end{bmatrix} \tag{4.105}$$

---

[†] Fettweis has already defined a multidimensional unit element in [44], but in that case, shifts in a single direction were used in both delay paths; the multidimensional unit element defined here can be thought of as a simple generalization of this structure.

### 4.10.2 Hybrid Form of the Multidimensional Unit Element

We now have an impedance relationship describing the multidimensional unit element in terms of the discrete frequency variables $z_1^{-1}$ and $z_2^{-1}$. It is of interest, however, to introduce a particular type of *hybrid form* [12]. The reason for doing this ultimately has to do with the fact that in a DWN in interleaved form, such as that shown in Figure 4.14 or 4.21, a typical linking waveguide (or unit element) is connected in parallel at one port and in series at the other; it is somewhat easier to make the transition from wave digital filters to digital waveguide networks if we take account of this asymmetry.

Suppose we have a two-port which is defined, at steady-state, by the relationship $\hat{\mathbf{v}} = \mathbf{Z}\hat{\mathbf{i}}$, or

$$\begin{bmatrix}\hat{v}_1\\ \hat{v}_2\end{bmatrix} = \begin{bmatrix}Z_{11} & Z_{12}\\ Z_{21} & Z_{22}\end{bmatrix}\begin{bmatrix}\hat{i}_1\\ \hat{i}_2\end{bmatrix}$$

This can be rewritten in a so-called hybrid form as

$$\begin{bmatrix}\hat{v}_1\\ \hat{i}_2\end{bmatrix} = \frac{1}{Z_{22}}\begin{bmatrix}Z_{11}Z_{22} - Z_{12}Z_{21} & Z_{12}\\ -Z_{21} & 1\end{bmatrix}\begin{bmatrix}\hat{i}_1\\ \hat{v}_2\end{bmatrix}$$

or as

$$\hat{\mathbf{p}} \quad = \quad \mathbf{K} \quad \hat{\mathbf{q}}$$

For the multidimensional unit element defined by (4.104), the hybrid matrix is, given the impedance relation (4.105),

$$\mathbf{K}_{ue}(z_1^{-1}, z_2^{-1}) = \frac{1}{1 + z_1^{-1}z_2^{-1}}\begin{bmatrix}R(1 - z_1^{-1}z_2^{-1}) & 2z_2^{-1}\\ -2z_1^{-1} & \frac{1}{R}(1 - z_1^{-1}z_2^{-1})\end{bmatrix}$$

It should be clear that the definition of the unit element holds regardless of which complex frequencies we choose. In particular, the delays $z_1^{-1}$ and $z_2^{-1}$ could be replaced by delays in higher dimensional spaces (we will make use of this in §4.10.4, §4.10.5 and §4.10.6). We will enforce the order of the arguments of $\mathbf{K}_{ue}$ so that, for example, $\mathbf{K}_{ue}(z_1^{-1}, z_2^{-1})$ and $\mathbf{K}_{ue}(z_2^{-1}, z_1^{-1})$ refer to unit elements of mirror-image orientation.

Suppose now that we have $N$ two-ports defined by their impedance and hybrid relationships

$$\hat{\mathbf{v}}_k = \mathbf{Z}_k\hat{\mathbf{i}}_k \qquad \hat{\mathbf{p}}_k = \mathbf{K}_k\hat{\mathbf{q}}_k \qquad k = 1, \ldots, N$$

If we are interested in connecting the first ports of all $N$ two-ports to each other in series, and the

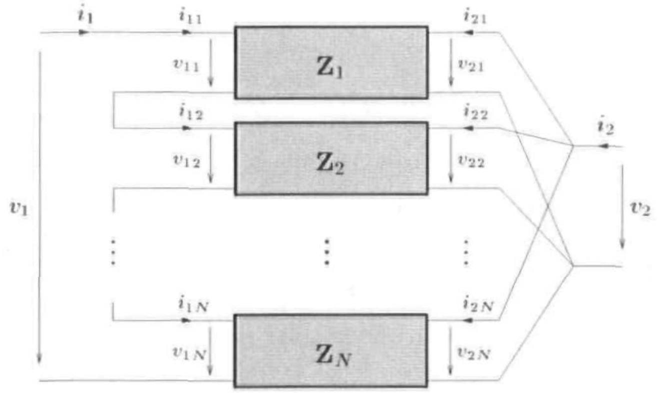

Figure 4.46: *Series/parallel connection of $N$ two-ports.*

second ports in parallel as in Figure 4.46, then we will have, for the total voltages and currents

$$v_1 = \sum_{k=1}^{N} v_{1k} \qquad i_2 = \sum_{k=1}^{N} i_{2k}$$

and

$$i_{1k} = i_1 \qquad v_{2k} = v_2 \qquad k = 1, \ldots, N$$

which hold instantaneously, and thus, in order to describe the two-port resulting from the connection, we may write

$$\hat{\mathbf{p}} = \sum_{k=1}^{N} \hat{\mathbf{p}}_k = \sum_{k=1}^{N} \mathbf{K}_k \hat{\mathbf{q}}_k = \left(\sum_{k=1}^{N} \mathbf{K}_k\right) \hat{\mathbf{q}}$$

Thus for such a series/parallel combination of two-ports, the hybrid matrix of the connection is simply the sum of the hybrid matrices of the individual two-ports, and thus

$$\mathbf{K} = \sum_{k=1}^{N} \mathbf{K}_k \qquad \text{Series/parallel combination of } N \text{ two-ports}$$

### 4.10.3 Alternative MDKC for the (1+1)D Transmission Line

We now reexamine the lossless, source-free (1+1)D transmission line equations and show that how, after a simple network manipulation and under the alternative spectral mappings mentioned in

§3.5.4, we end up with an interleaved DWN identical to that discussed in §4.3.6.

We begin by first scaling the (1+1)D transmission line equations by a factor of $\Delta$, and where, as before, we introduce a scaled time variable defined by $t' = v_0 t$, giving

$$\Delta v_0 l \frac{\partial i}{\partial t'} + \Delta \frac{\partial u}{\partial x} = 0 \tag{4.106a}$$

$$\Delta v_0 c \frac{\partial i}{\partial t'} + \Delta \frac{\partial u}{\partial x} = 0 \tag{4.106b}$$

It should be clear that the scaling by $\Delta$ will have no effect on the solution to equations (4.106), even in the limit as $\Delta \to 0$. The MDKC for this system is shown in Figure 4.47(a), where we have used the coordinate transformation defined by (3.18). Aside from the scaling of the element values by $\Delta$, this is identical to the MDKC of Figure 3.14(a), where the resistors and voltage sources (corresponding to loss and source terms) have been omitted (they can be simply reintroduced at a later stage).

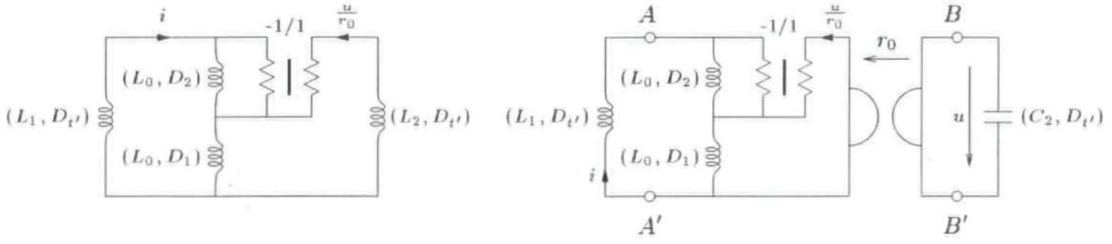

(a) (b)

Figure 4.47: *MDKCs for the lossless source-free (1+1)D transmission line equations— (a) the standard representation and (b) a modified form.*

The element values are given by

$$L_1 = \Delta\left(v_0 l - r_0\right) \qquad L_2 = \Delta\left(v_0 c r_0^2 - r_0\right) \qquad L_0 = \Delta r_0/\sqrt{2}$$

In this representation, the transmission line voltage $u$ is considered, after a scaling by $1/r_0$, to be a *current*. This is somewhat unsatisfying from a physical point of view; it is easy, however, to rectify this: by a simple network transformation, the inductor in the right-hand loop (through which current $u/r_0$ flows) may be replaced by a *gyrator* of gyration constant $r_0$ terminated on a *capacitor*. The voltage across this capacitor of capacitance $C_2 = \Delta\left(v_0 c - \frac{1}{r_0}\right)$ will then be exactly $u$. See Figure 4.47(b).

Consider now the two-port of Figure 4.47(b), with terminals $A$, $A'$, $B$ and $B'$. The hybrid matrix for this linear shift-invariant two-port is, in terms of the frequencies $s_1$ and $s_2$,

$$\mathbf{K}(s_1, s_2) = \frac{\Delta}{\sqrt{2}}\begin{bmatrix} r_0\,(s_1+s_2) & s_1-s_2 \\ s_1-s_2 & \frac{1}{r_0}\,(s_1+s_2)\end{bmatrix}$$

We now apply the alternative spectral mapping introduced in §3.5.4, namely

$$s_1 \rightarrow \frac{1}{T_1}\frac{(1-z_1^{-1})(1+z_2^{-1})}{1+z_1^{-1}z_2^{-1}} \qquad s_2 \rightarrow \frac{1}{T_2}\frac{(1-z_2^{-1})(1+z_1^{-1})}{1+z_1^{-1}z_2^{-1}} \tag{4.107}$$

with $T_1 = T_2 = \Delta/\sqrt{2}$ (recall that the for the interleaved scheme, we will have increments in the time step of $T/2$ and in the space step of $\Delta/2$, and thus we have chosen $T_1$ and $T_2$ to be half the values they previously took). It will be recalled that this mapping, like the trapezoidal rule, is passivity-preserving. The hybrid matrix becomes

$$\mathbf{K}(z_1^{-1}, z_2^{-1}) = \frac{2}{1+z_1^{-1}z_2^{-1}}\begin{bmatrix} r_0\left(1-z_1^{-1}z_2^{-1}\right) & z_2^{-1}-z_1^{-1} \\ z_2^{-1}-z_1^{-1} & \frac{1}{r_0}\left(1-z_1^{-1}z_2^{-1}\right)\end{bmatrix} \tag{4.108}$$

which, upon inspection, can be written as the sum

$$\mathbf{K}(z_1^{-1}, z_2^{-1}) = \mathbf{K}_{ue}(z_1^{-1}, z_2^{-1}) + \mathbf{K}_{ue}(-z_2^{-1}, -z_1^{-1})$$

where it will be recalled that $\mathbf{K}_{ue}(z_1^{-1}, z_2^{-1})$ is the hybrid matrix for the multidimensional unit element defined in (4.104), with $R = r_0$. Because for a series/parallel connection of two-ports, hybrid matrices sum, we have thus decomposed our connecting two-port into two multidimensional unit elements of opposing directions, one of which incorporates a sign-inversion in both of its signal paths. The MDWD network can then immediately be constructed as in Figure 4.48. The port resistances are

$$R_1 = \frac{2}{\Delta}L_1 = 2v_0 l - 2r_0 \qquad R_2 = \frac{\Delta}{2C_2} = \frac{1}{2v_0 c - 2/r_0} \qquad R_0 = r_0$$

We have chosen here a doubled delay length (of $T' = \Delta$) in the self-loops, according to the *offset* scheme mentioned in §3.9 (for these one-ports, we use the trapezoid rule as for MDWD networks).

This network is, when spatial dependence is expanded out, identical to the DWN shown in Figure 4.44, under the replacement of the series and parallel adaptor symbols by series and parallel scattering junction symbols—recall that they perform identical operations. This MDWD network, then, (if it can be called that) operates on a decimated grid, unlike the standard form shown in Figure 4.44. Losses and sources can easily be added back in to the alternative MDKC of Figure 4.47(b), and the resulting MDWD network will be identical to that of Figure 4.15.

We would conjecture that it is possible to find similar equivalences for the type I and II DWNs for

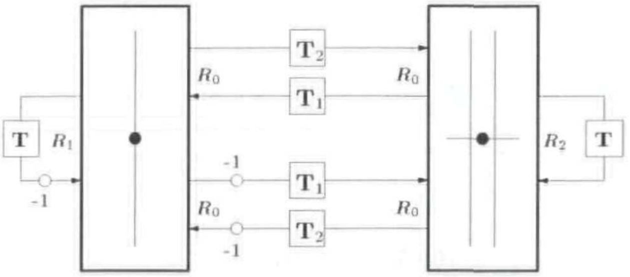

Figure 4.48: *MD network equivalent to type III DWN for the lossless source-free (1+1)D transmission line equations under an alternative spectral mapping.*

the same system (which have better stability bounds); in these cases however, recall from §4.3.6 that the immittances of the connecting waveguides did indeed vary from one grid location to the next. In order to design a MDKC corresponding to such a network, it would be necessary to extend the definition of the multidimensional unit element to include spatially-varying port-resistances (indeed, this extension is automatic, since the port resistances do not appear explicitly in the definition of this element in (4.104)). The problem, then, is that the two-port connecting the series and parallel adaptors will no longer be shift-invariant, so we must take special care with application of the discretization rule, which can no longer be treated as a spectral mapping.

### 4.10.4 Alternative MDKC for (2+1)D Parallel-plate System

The same idea extends simply to the (2+1)D parallel-plate equations (3.64). In this case, we again look at the lossless source-free system, scaled by a factor of $\Delta$, and can develop an MDKC along the lines of Figure 4.47(b), with $u$ now treated as a voltage instead of a current as in Figure 3.17. We remind the reader that we use the notation $D_k$, $k = 1, \dots, 5$ in circuit diagrams to indicate directional derivatives in the directions $t_k$ defined by the coordinate transformation (3.22). Also, we have written $i_1$ and $i_2$ for $i_x$ and $i_y$, in keeping with the WDF literature [62]. The alternative MDKC is shown in Figure 4.49, and the element values are given by

$$L_1 = L_2 = \Delta\left(v_0 l - r_0\right) \qquad C_3 = \Delta\left(v_0 c - \frac{2}{r_0}\right) \qquad L_0 = \Delta r_0/2$$

$r_0 > 0$ is, as before, a free parameter which can be scaled to achieve an optimal space step/time step ratio.

The two two-ports with terminals $A_1$, $A_1'$, $B$, $B'$ and $A_2$, $A_2'$, $B$, $B'$ are both linear and shift-invariant, and their right-hand pairs of terminals are both connected in parallel with the capacitor.

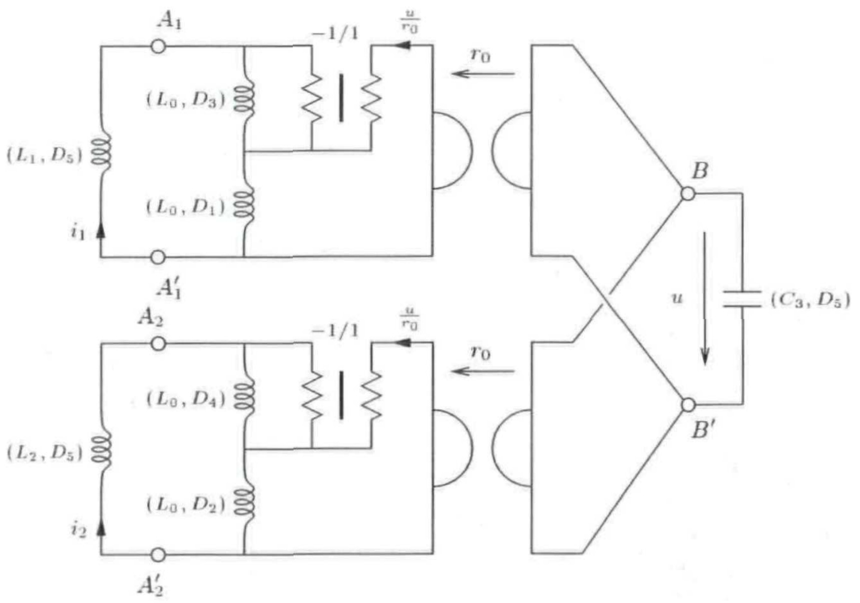

Figure 4.49: *Alternative MDKC for the (2+1)D parallel-plate system in rectangular coordinates.*

The hybrid matrices for these two-ports are

$$\mathbf{K}_1(s_1, s_3) = \frac{\Delta}{2}\begin{bmatrix} r_0\,(s_1+s_3) & s_1-s_3 \\ s_1-s_3 & \frac{1}{r_0}\,(s_1+s_3)\end{bmatrix} \qquad \text{Two-port} \quad A_1A_1'BB'$$

$$\mathbf{K}_2(s_2, s_4) = \frac{\Delta}{2}\begin{bmatrix} r_0\,(s_2+s_4) & s_2-s_4 \\ s_2-s_4 & \frac{1}{r_0}\,(s_2+s_4)\end{bmatrix} \qquad \text{Two-port} \quad A_2A_2'BB'$$

and under the spectral mappings

$$s_1 \to \frac{1}{T_1}\frac{(1-z_1^{-1})(1+z_3^{-1})}{1+z_1^{-1}z_3^{-1}} \qquad s_3 \to \frac{1}{T_3}\frac{(1-z_3^{-1})(1+z_1^{-1})}{1+z_1^{-1}z_3^{-1}} \tag{4.109a}$$

$$s_2 \to \frac{1}{T_2}\frac{(1-z_2^{-1})(1+z_4^{-1})}{1+z_2^{-1}z_4^{-1}} \qquad s_4 \to \frac{1}{T_4}\frac{(1-z_4^{-1})(1+z_2^{-1})}{1+z_2^{-1}z_4^{-1}} \tag{4.109b}$$

with $T_1 = T_2 = T_3 = T_4 = \Delta/2$, we again have a decomposition of the discrete hybrid two-ports into pairs of multidimensional unit elements (impedance $r_0$) connected in series/parallel, i.e.

$$\begin{aligned}\mathbf{K}_1(z_1^{-1}, z_3^{-1}) &= \mathbf{K}_{ue}(z_1^{-1}, z_3^{-1}) + \mathbf{K}_{ue}(-z_3^{-1}, -z_1^{-1}) \\ \mathbf{K}_2(z_2^{-1}, z_4^{-1}) &= \mathbf{K}_{ue}(z_2^{-1}, z_4^{-1}) + \mathbf{K}_{ue}(-z_4^{-1}, -z_2^{-1})\end{aligned}$$

The MDWD network, corresponding to "checkerboard"-type sampling, is as shown in Figure 4.50, and where $\mathbf{T_1}, \ldots, \mathbf{T_4}$ are the shifts in the coordinate directions $t_1, \ldots, t_4$, and the port resistances are given by

$$R_1 = R_2 = 2\,(v_0 l - r_0) \qquad R_3 = \frac{1}{2\,(v_0 c - 2/r_0)} \qquad R_0 = r_0$$

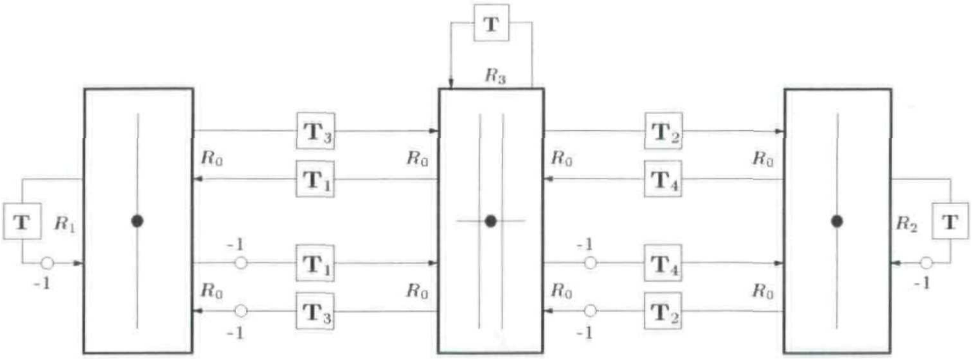

Figure 4.50: *MD network equivalent to type III DWN for the lossless source-free (2+1)D parallel-plate system under an alternative spectral mapping.*

For the one-port inductors and the capacitor, we have again applied the trapezoid rule, with a step-size of $T_5 = \Delta$ (implying a delay of $T$, written as $\mathbf{T}$ in Figure 4.50).

When spatial dependence is expanded out, the signal flow graph is identical to the interleaved type III DWN for the parallel-plate equations shown in Figure 4.21, without the loss/source ports. As in (1+1)D, loss and source elements can be reintroduced into the MDKC of Figure 4.49 without difficulty.

It should also be possible to derive DWNs from MDKCs for the same system on alternative grids, such as the hexagonal and triangular grids mentioned in §4.6.1, though we have not investigated this in any detail. In this case, one would presumably begin from the MDKC under the appropriate coordinate transformation. One of these coordinate transformations (which generates a hexagonal grid under uniform sampling in the new coordinates), was discussed briefly in §3.3.3. The full MDKC for the parallel-plate equations in these coordinates is given in [62].

### 4.10.5 Higher-order Accuracy Revisited

Recall that in §3.13, we derived two MDKCs that were suitable for solving the transmission line equations to higher-order spatial accuracy; we were forced, however, to employ a set of alternative spectral mappings very similar to those that have appeared earlier in this section. For this reason, we postponed showing the full scattering network until now. This is a good opportunity to see the flexibility of having a multidimensional representation of a DWN.

The MDKC in Figure 3.25 represents the lossless source-free (1+1)D transmission line equations, in a set of $2q$ coordinates defined by (3.21) using the transformation matrix of (3.90). These new coordinates allow us to define directional shifts that refer to points other than nearest neighbors. The general approach to deriving a DWN for this MDKC is the same as in the previous sections; first we perform some network manipulations on the MDKC, and then we apply alternative spectral mappings or integration rules to the connecting LSI two-ports, which then reduce to multidimensional unit elements, which are then interpreted as arrays of digital waveguides. The circuit manipulations in this case are slightly more involved; skipping several steps, we note that we can rewrite the MDKC as shown in Figure 4.51.

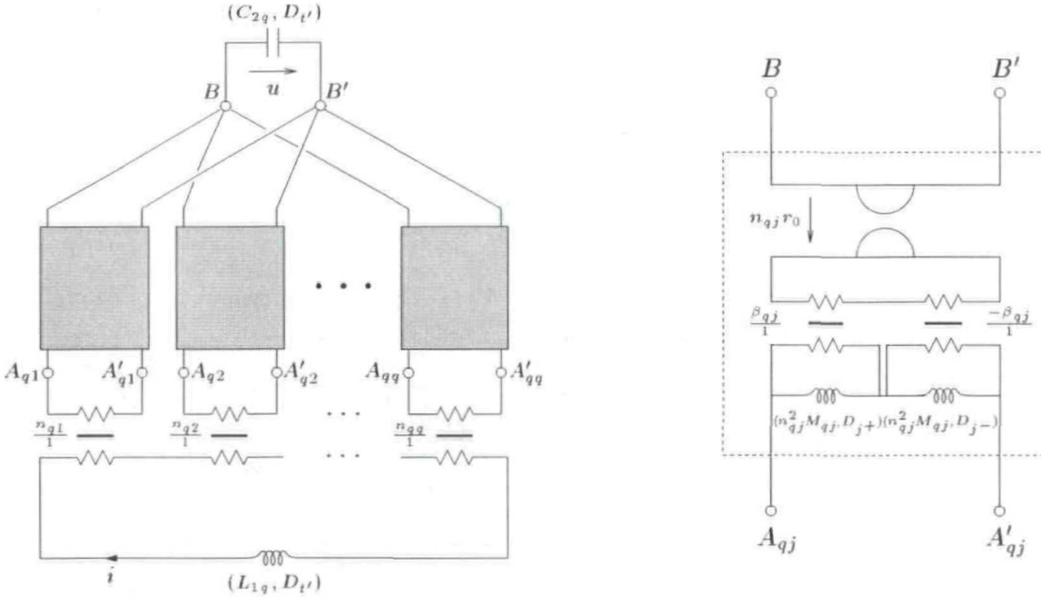

(a) (b)

Figure 4.51: (a) *A modified MDKC for the lossless, source-free(1+1)D transmission line system and* (b) *a detail of connecting two-ports* $A_{qj}$,$A'_{qj}$,$B$, $B'$ *for any* $j$, $j = 1, \ldots, q$ *from* (a).

As before, we treat $u$ as the voltage across a capacitor, and have introduced a gyrator in each of the connecting two-ports with terminals $A_{qj}$, $A'_{qj}$, $B$ and $B'$, $j = 1, \ldots, q$. In addition, we have extracted a transformer, of turns ratio $n_{qj}$ for each of these two-ports; the gyrator constant is similarly scaled in order to compensate. The effect of this extracted transformer will be to weight the port resistances of the various multidimensional unit elements that result (and hence the waveguide impedances in the resulting DWN). In addition, we will also need to re-scale the inductances from (3.93) by a factor of $\Delta$, giving

$$L_{1q} = \Delta\left(v_0 l - r_0 \sum_{j=1}^{q} \frac{|\alpha_{qj}|}{j}\right) \qquad C_{2q} = \Delta\left(v_0 c - \sum_{j=1}^{q} \frac{|\alpha_{qj}|}{r_0 j}\right) \qquad M_{qj} = \frac{\Delta r_0 |\alpha_{qj}|}{2j}$$

The two-port shown in Figure 4.51(b) contains two inductors of inductances $M_{qj}$ defined with respect to the directions $t_{j+}$ and $t_{j-}$. Its continuous hybrid matrix will be, in terms of the two associated complex frequencies $s_{j+}$ and $s_{j-}$,

$$\mathbf{K}_{qj}(s_{j+}, s_{j-}) = \begin{bmatrix} M_{qj}n_{qj}^2\left(s_{j+}+s_{j-}\right) & \frac{M_{qj}n_{qj}\beta_{qj}}{r_0}\left(s_{j+}-s_{j-}\right) \\ \frac{M_{qj}n_{qj}\beta_{qj}}{r_0}\left(s_{j+}-s_{j-}\right) & \frac{M_{qj}}{r_0^2}\left(s_{j+}+s_{j-}\right) \end{bmatrix}$$

Under the spectral mappings from $s_{j+}$ and $s_{j-}$ to the frequency domain unit shifts $z_{j+}^{-1}$ and $z_{j-}^{-1}$ given by

$$s_{j+} \rightarrow \frac{1}{\Delta}\frac{(1-z_{j+}^{-1})(1+z_{j-}^{-1})}{1+z_{j+}^{-1}z_{j-}^{-1}} \qquad s_{j-} \rightarrow \frac{1}{\Delta}\frac{(1-z_{j-}^{-1})(1+z_{j+}^{-1})}{1+z_{j+}^{-1}z_{j-}^{-1}}$$

(which are passive and correspond to the integration rules (3.94), with a shift length of $\Delta$), the discrete hybrid matrix becomes

$$\mathbf{K}_{qj}(z_{j+}^{-1}, z_{j-}^{-1}) = \frac{2}{\Delta(1+z_{j+}^{-1}z_{j-}^{-1})}\begin{bmatrix} M_{qj}n_{qj}^2\left(1-z_{j+}^{-1}z_{j-}^{-1}\right) & \frac{M_{qj}n_{qj}\beta_{qj}}{r_0}\left(z_{j-}^{-1}-z_{j+}^{-1}\right) \\ \frac{M_{qj}n_{qj}\beta_{qj}}{r_0}\left(z_{j-}^{-1}-z_{j+}^{-1}\right) & \frac{M_{qj}}{r_0^2}\left(1-z_{j+}^{-1}z_{j-}^{-1}\right) \end{bmatrix}$$

It should be clear that in general, this hybrid matrix does not reduce to a pair of series/parallel connected multidimensional unit elements (in which case it should have the form of (4.108), with $z_{j-}^{-1}$ and $z_{j+}^{-1}$ in place of $z_2^{-1}$ and $z_1^{-1}$). Under the special choice of $n_{qj} = 2j/\alpha_{qj}$, however, it does reduce to such a connection, so we have

$$\mathbf{K}_{qj}(z_{j+}^{-1}, z_{j-}^{-1}) = \mathbf{K}_{ue}(z_{j+}^{-1}, z_{j-}^{-1}) + \mathbf{K}_{ue}(-z_{j-}^{-1}, -z_{j+}^{-1})$$

where the port resistances of the unit elements are

$$R_{qj} = \frac{2jr_0}{|\alpha_{qj}|}$$

The two-port multidimensional unit elements are connected to transformers, of turns ratio $n_{qj}$, as per Figure 4.51(a). The port resistance at one end of each transformer can be set to that of the unit element to which it is connected, which is $R_{qj}$. It is possible to implement these transformers as multiplies by $n_{qj}$ and $1/n_{qj}$ directly in the signal paths, if we make the choice of the other port resistance (which we call $R'_{qj}$) according to the rule discussed in §2.3.4; we thus choose

$$R'_{qj} = R_{qj}/n_{qj}^2 = \frac{r_0|\alpha_{qj}|}{2j}$$

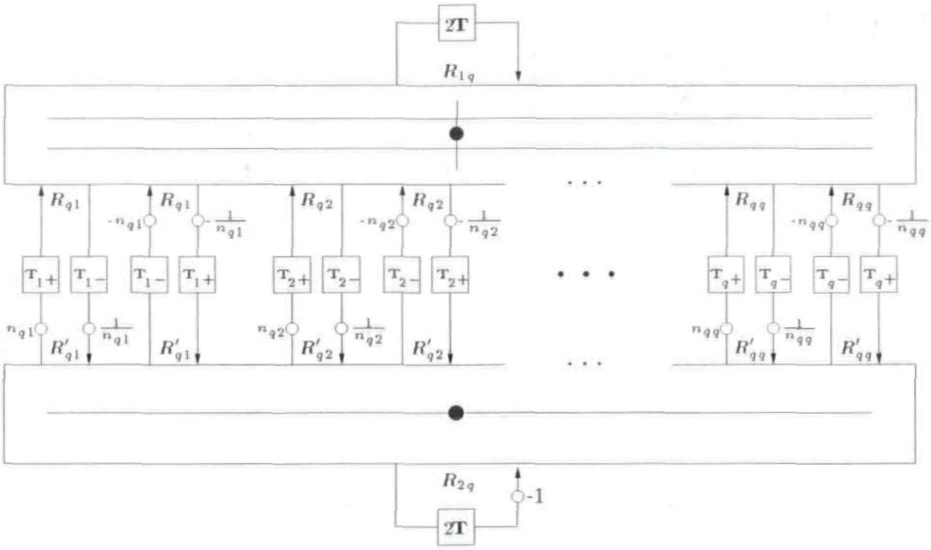

Figure 4.52: *Multidimensional DWN suitable for a qth-order spatially accurate solution to the (1+1)D transmission line equations.*

For the one-port inductor and capacitor (of inductance $L_{1q}$ and $C_{2q}$ respectively), we use the trapezoid rule with a doubled time step $T' = 2\Delta$, and the wave digital one-ports (of port resistances $R_{1q} = L_{1q}/\Delta$ and $R_{2q} = \Delta/C_{2q}$) result. The multidimensional network shown in Figure 4.52 can be interpreted as a DWN, and if the parameters $\alpha_{qj}$ are chosen according to the method discussed in §3.13, then the DWN will give a $q$th-order spatially accurate solution to the (1+1)D lossless source-free transmission line system. In order not to belabor this point any further, we leave the explicit construction of the expanded signal flow graph for this multidimensional DWN from Figure 4.52 (as well as the interleaved DWN which results from the use of coordinates defined by (3.98)) as an exercise to the reader.

It is interesting that not all DWN topologies permit a higher-order spatially accurate scheme; in §A.2.5, we will look at a stable fourth-order accurate difference scheme for the (2+1)D wave equation which cannot be realized in a straightforward way as a DWN. The topology of the DWN in this section follows directly from a passive MD circuit representation.

### 4.10.6 Maxwell's Equations

We now take a brief look at Maxwell's equations, the (3+1)D system of PDEs which describes the time evolution of electromagnetic fields. This system was the original motivation behind the development of FDTD [184, 214], and MDWD network methods for Maxwell's system were explored early on in [50]. In the interest of solidifying the link between these two types of methods, we show how a passive circuit representation yields a DWN, which is no more than a scattering form of FDTD.

Maxwell's Equations, for a linear isotropic (though not necessarily spatially homogeneous) medium, are usually written in vector form[†] as

$$\epsilon\frac{\partial \mathbf{E}}{\partial t} = \nabla \times \mathbf{H} \qquad \mu\frac{\partial \mathbf{H}}{\partial t} = -\nabla \times \mathbf{E} \tag{4.110}$$

where $\mathbf{E} = [E_x, E_y, E_z]^T$ and $\mathbf{H} = [H_x, H_y, H_z]^T$ are, respectively, the electric and magnetic field vectors, $\epsilon(x, y, z)$ and $\mu(x, y, z)$ are the dielectric constant and magnetic permeability of the medium, assumed positive and bounded away from 0. (We have left out losses here.) This system has the form of (3.1), with $\mathbf{w} = [\mathbf{E}^T, \mathbf{H}^T]^T$, and

$$\mathbf{P} = \begin{bmatrix} \epsilon\mathbf{I}_3 & \cdot \\ \cdot & \mu\mathbf{I}_3 \end{bmatrix} \qquad \mathbf{A}_j = \begin{bmatrix} \cdot & \mathbf{A}_{j\times} \\ \mathbf{A}_{j\times}^T & \cdot \end{bmatrix} \qquad j = 1, 2, 3$$

where $\mathbf{I}_3$ is the $3 \times 3$ identity matrix, $\cdot$ stands for zero entries, and where we also have

$$\mathbf{A}_{1\times} = \begin{bmatrix} 0 & 0 & 0 \\ 0 & 0 & 1 \\ 0 & -1 & 0 \end{bmatrix} \qquad \mathbf{A}_{2\times} = \begin{bmatrix} 0 & 0 & -1 \\ 0 & 0 & 0 \\ 1 & 0 & 0 \end{bmatrix} \qquad \mathbf{A}_{3\times} = \begin{bmatrix} 0 & 1 & 0 \\ -1 & 0 & 0 \\ 0 & 0 & 0 \end{bmatrix}$$

### Phase and Group Velocity

If $\epsilon$ and $\mu$ are constant, then from (3.10), the dispersion relation for Maxwell's Equations has the form

$$\omega^2 \left(\epsilon\mu\omega^2 - ||\beta||_2^2\right)^2 = 0$$

in terms of frequencies $\omega$ and wavenumber magnitudes $||\beta||_2$. This equation has solutions

$$\omega = 0 \qquad \omega = \pm\frac{||\beta||_2}{\sqrt{\epsilon\mu}}$$

---

[†] We leave out the supplemental relations

$$\nabla \cdot \mathbf{E} = \rho \qquad \nabla \cdot \mathbf{H} = 0$$

where $\rho$ is the charge density. These can be viewed as extra restrictions on the allowed solutions to (4.110).

Leaving aside the non-propagating mode with $\omega = 0$, the phase and group velocities will then be given by

$$\gamma^p_{Maxwell} = \gamma^g_{Maxwell} = \pm\frac{1}{\sqrt{\epsilon\mu}}$$

For spatially inhomogeneous problems, the maximum group velocity will be

$$\gamma^g_{Maxwell,max} = \frac{1}{\sqrt{(\epsilon\mu)_{min}}}$$

**Scattering Networks for Maxwell's Equations**

This system has been represented by an MDKC in [50, 131], where the coordinate transformation defined by (3.24) has been employed, and the current variables are defined by

$$(i_1, i_2, i_3, i_4, i_5, i_6) = (E_x/r_0, E_y/r_0, E_z/r_0, H_x, H_y, H_z)$$

for some positive constant $r_0$. We have reproduced this MDKC in Figure 4.53. This network can be viewed as two coupled (2+1)D parallel-plate networks (see §3.8), and this is not surprising, given that the (2+1)D parallel-plate system is essentially equivalent to the *transverse electric* (TE) or *transverse magnetic* (TM) system alone. The resulting MDWD network is shown, at bottom, in Figure 4.53; here, we have assumed the directional shifts $\mathbf{T}_j$, $j = 1, \ldots, 7$ to be of length $\Delta$. (And thus $T_7 = T' = \Delta/v_0 \triangleq T$.) The passivity condition is again a condition on the positivity of the network inductances in the MDKC; these values are given in Figure 4.53, and the resulting conditions are

$$v_0 \geq \frac{2}{r_0\epsilon_{min}} \qquad\qquad v_0 \geq \frac{2r_0}{\mu_{min}}$$

Under the choice of $r_0 = \sqrt{\frac{\mu_{min}}{\epsilon_{min}}}$, the stability condition becomes

$$v_0 \geq \frac{2}{\sqrt{\mu_{min}\epsilon_{min}}} \geq 2\gamma^g_{Maxwell,max} \tag{4.111}$$

with

$$\epsilon_{min} = \min_{x,y,z} \epsilon \qquad\qquad \mu_{min} = \min_{x,y,z} \mu$$

and the numerical scheme is passive and hence stable over this range of $v_0$.

In order to generate a digital waveguide network, we may proceed as for the (1+1)D transmission line and (2+1)D parallel-plate systems discussed in §4.10.3 and §4.10.4, and apply the by now familiar network transformations to yield the modified circuit shown in Figure 4.54. Electric field quantities are now treated as voltages across capacitors, and the six LSI connecting two-ports will all become multidimensional unit elements under the application of alternative spectral mappings.

The coordinate transformation from coordinates $\mathbf{u} = [x, y, z, t]^T$ to coordinates $\mathbf{t} = [t_1, \ldots, t_7]^T$ defined by (3.21), using the transformation matrix of (3.24) gives us, in the LSI case, seven frequencies $s_1, \ldots, s_7$. For the connecting two-ports, we may use pairwise spectral mappings defined by

$$s_j \to \frac{1}{T_j}\frac{(1-z_j^{-1})(1+z_{j+3}^{-1})}{1+z_j^{-1}z_{j+3}^{-1}} \qquad s_{j+3} \to \frac{1}{T_{j+3}}\frac{(1-z_{j+3}^{-1})(1+z_j^{-1})}{1+z_{j+3}^{-1}z_j^{-1}} \qquad j = 1, 2, 3 \quad (4.112)$$

where $z_j^{-1}$, $j = 1, \ldots, 6$ corresponds to a unit shift in direction $t_j$, and the step-sizes $T_j$, $j = 1, \ldots, 6$ are all chosen equal to $\Delta/2$. For the one-port time inductors and capacitors, we use the trapezoid rule with a step-size of $T_7 = T' = \Delta$. The resulting multidimensional DWN is shown at bottom in Figure 4.54, and the stability bound is unchanged from (4.111).

When the spatial dependence is expanded out, we have a DWN operating on an interleaved numerical grid as shown in Figure 4.55, with the electric and magnetic field components calculated at parallel (white) and series (grey) junctions respectively. The connecting waveguide impedances (of delay $T/2$, shown as solid lines) are all equal to $r_0$, and the self-loops (of delay $T$, not shown) have impedances $2v_0\mu - 2r_0$ and admittances $2v_0\epsilon - 2/r_0$ at the series and parallel junctions respectively, where these expressions are evaluated at the junction location. It is also possible to derive DWNs of the type I and II forms (see §4.3.6), for which the stability bound is improved to CFL.

It is easy to verify that this scheme is indeed a scattering form of FDTD. Referring to Figure 4.55, we will have six sets of junction quantities: at the parallel junctions, we will have $E_{xJ,i,j+\frac{1}{2},k+\frac{1}{2}}(n+\frac{1}{2})$, $E_{yJ,i,j+\frac{1}{2},k}(n+\frac{1}{2})$ and $E_{zJ,i+\frac{1}{2},j+\frac{1}{2},k}(n+\frac{1}{2})$, and at the series junctions, we will have $H_{xJ,i+\frac{1}{2},j,k}(n)$, $H_{yJ,i,j+\frac{1}{2},k}(n)$ and $H_{zJ,i,j,k+\frac{1}{2}}(n)$. The indices $i$, $j$, $k$ and $n$ take on integer values. Examine the DWN at a parallel junction with "voltage" $E_{xJ,,i,j+\frac{1}{2},k+\frac{1}{2}}(n+\frac{1}{2})$. The DWN updates this grid function according to

$$\begin{aligned}
E_{xJ,i,j+\frac{1}{2},k+\frac{1}{2}}(n+\tfrac{1}{2}) \;=\;& E_{xJ,i,j+\frac{1}{2},k+\frac{1}{2}}(n-\tfrac{1}{2}) \\
&+\frac{1}{v_0\epsilon_{i,j+\frac{1}{2},k+\frac{1}{2}}}\Big(H_{zJ,i,j+1,k+\frac{1}{2}}(n) - H_{zJ,i,j,k+\frac{1}{2}}(n) \\
&\qquad -H_{yJ,i,j+\frac{1}{2},k+1}(n) + H_{yJ,i,j+\frac{1}{2},k}(n)\Big)
\end{aligned}$$

with $\epsilon_{i,j+\frac{1}{2},k+\frac{1}{2}} \triangleq \epsilon(i\Delta, (j+\frac{1}{2})\Delta, (k+\frac{1}{2})\Delta)$. This is exactly centered differences applied to the equation in $E_x$, $H_y$ and $H_z$. according to the Yee algorithm [184]. It is also worth comparing this DWN to the TLM version, discussed in [4].

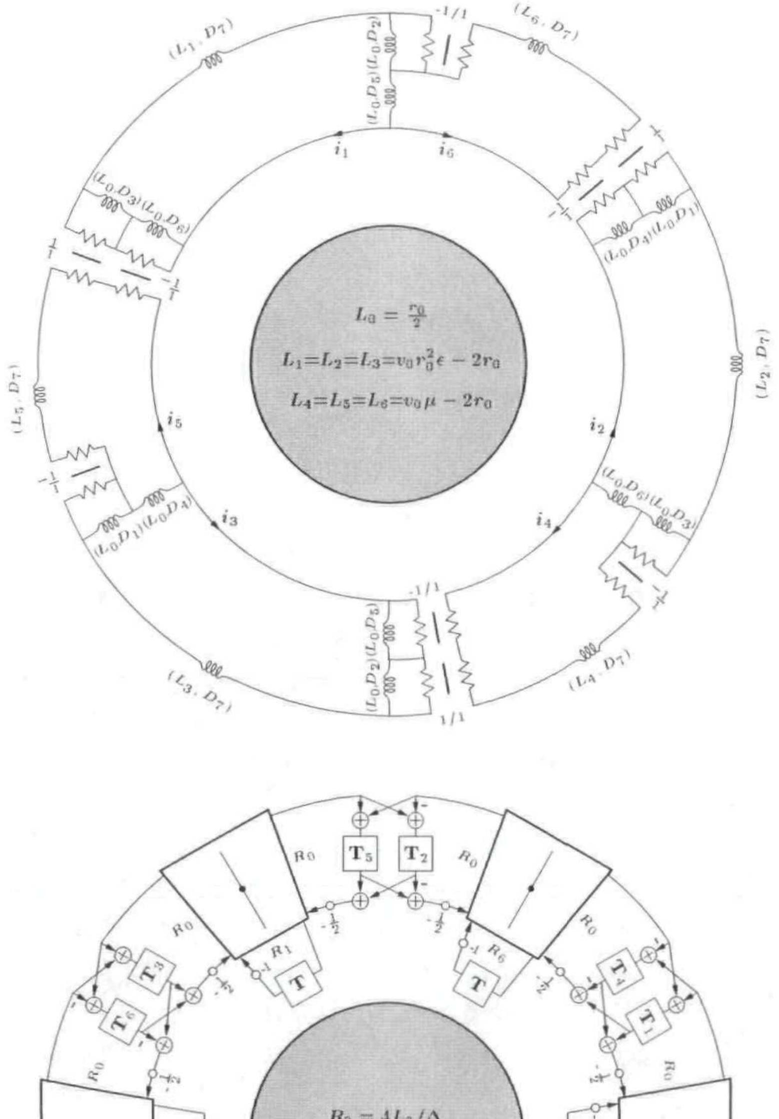
$L_0 = \frac{r_0}{2}$
$L_1=L_2=L_3=v_0 r_0^2 \epsilon - 2r_0$
$L_4=L_5=L_6=v_0 \mu - 2r_0$
$(L_1, D_7)$
$(L_2, D_7)$
$(L_3, D_7)$
$(L_4, D_7)$
$(L_5, D_7)$
$(L_6, D_7)$
$(L_0 D_5)(L_0 D_2)$
$(L_0 D_3)(L_0 D_6)$
$(L_0 D_4)(L_0 D_1)$
$(L_0 D_1)(L_0 D_4)$
$(L_0 D_6)(L_0 D_3)$
$(L_0 D_2)(L_0 D_5)$
-1/1
1/1
$i_1$
$i_2$
$i_3$
$i_4$
$i_5$
$i_6$
$R_0 = 4L_0/\Delta$
$R_j = 2L_j/\Delta, \quad j = 1, \ldots, 6$
$R_0$
$R_1$
$R_2$
$R_3$
$R_4$
$R_5$
$R_6$
$\mathbf{T}$
$\mathbf{T}_1$
$\mathbf{T}_2$
$\mathbf{T}_3$
$\mathbf{T}_4$
$\mathbf{T}_5$
$\mathbf{T}_6$
$-\frac{1}{2}$
-1

Figure 4.53: *MDKC and MDWD network for Maxwell's equations* (4.110).

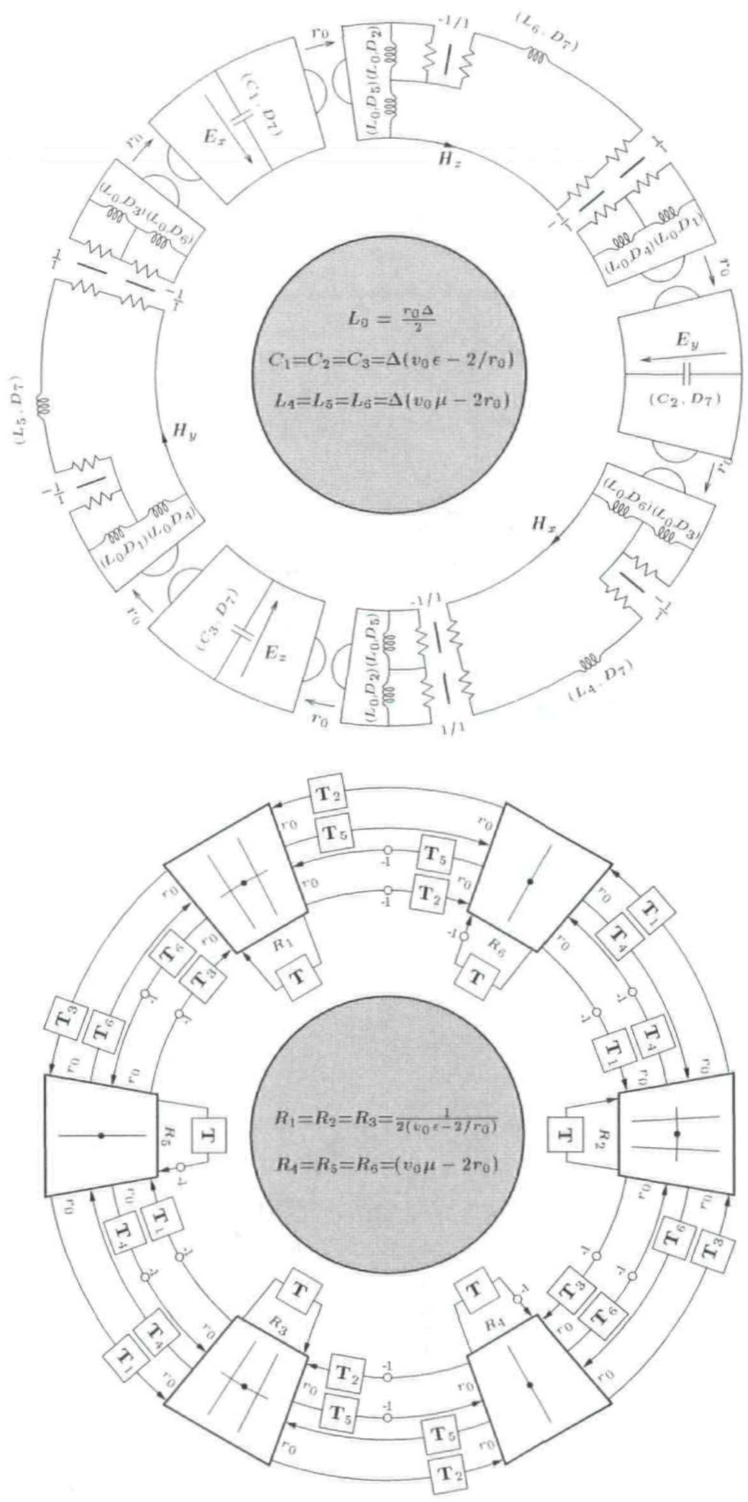
$L_0 = \frac{r_0\Delta}{2}$
$C_1=C_2=C_3=\Delta(v_0\epsilon - 2/r_0)$
$L_4=L_5=L_6=\Delta(v_0\mu - 2r_0)$
$E_x$
$E_y$
$E_z$
$H_x$
$H_y$
$H_z$
$(C_1, D_7)$
$(C_2, D_7)$
$(C_3, D_7)$
$(L_4, D_7)$
$(L_5, D_7)$
$(L_6, D_7)$
$(L_0D_5)(L_0D_2)$
$(L_0D_3)(L_0D_6)$
$(L_0D_4)(L_0D_1)$
$(L_0D_1)(L_0D_4)$
$(L_0D_6)(L_0D_3)$
$(L_0D_2)(L_0D_5)$
-1/1
1/1
$r_0$
$R_1=R_2=R_3=\frac{1}{2(v_0\epsilon-2/r_0)}$
$R_4=R_5=R_6=(v_0\mu - 2r_0)$
$R_1$
$R_2$
$R_3$
$R_4$
$R_5$
$R_6$
$\mathbf{T}$
$\mathbf{T}_1$
$\mathbf{T}_2$
$\mathbf{T}_3$
$\mathbf{T}_4$
$\mathbf{T}_5$
$\mathbf{T}_6$
-1

Figure 4.54: *Modified MDKC and multidimensional DWN for Maxwell's equations* (4.110).

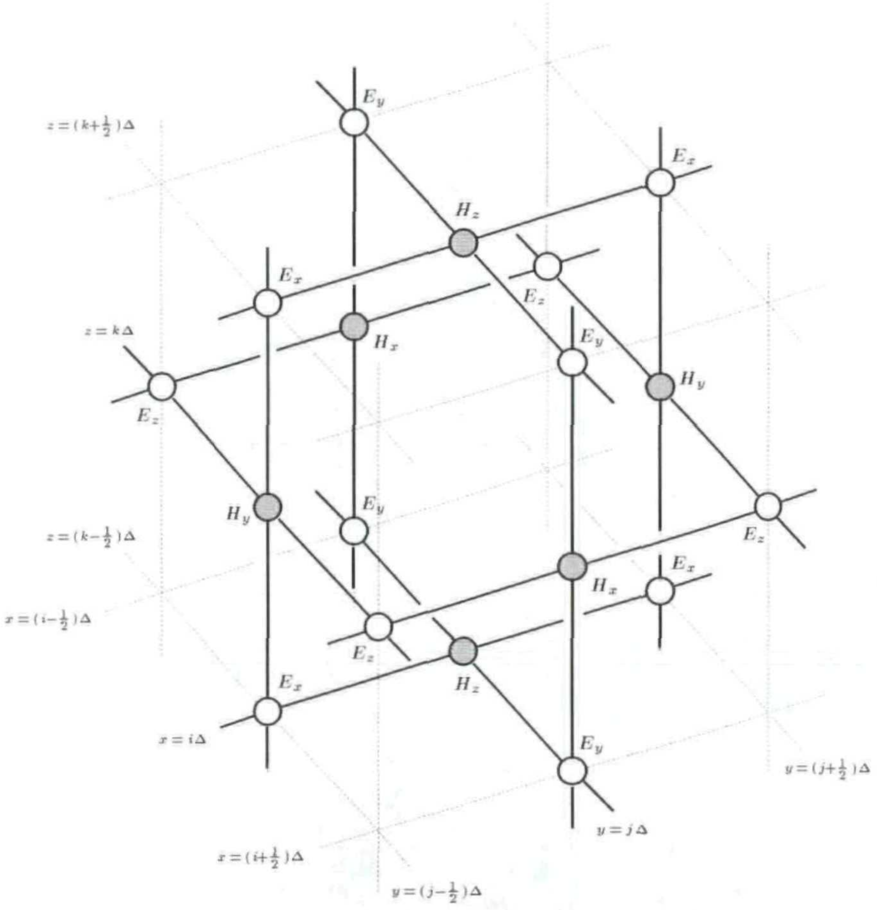
$z=(k+\frac{1}{2})\Delta$
$z=k\Delta$
$z=(k-\frac{1}{2})\Delta$
$x=(i-\frac{1}{2})\Delta$
$x=i\Delta$
$x=(i+\frac{1}{2})\Delta$
$y=(j-\frac{1}{2})\Delta$
$y=j\Delta$
$y=(j+\frac{1}{2})\Delta$
$E_y$
$E_x$
$H_z$
$E_x$
$E_z$
$H_x$
$E_z$
$E_y$
$E_z$
$H_y$
$H_y$
$E_y$
$E_z$
$E_x$
$H_x$
$E_z$
$E_x$
$H_z$
$E_y$

Figure 4.55: *Computational grid for FDTD applied to Maxwell's equations* (4.110)*; electric and magnetic field quantities are calculated at alternating multiples of* $T/2$*, and at alternating grid locations. In the DWN implementation, waveguide connections (of delay length* $T/2$*) between series junctions (grey) and parallel junctions (white) are shown as dark lines; waveguide sign inversions and self-loops are not shown here.*

# Chapter 5

# Applications in Vibrational Mechanics

In the previous chapters, we dealt with the numerical integration of systems of PDEs that were all, in some sense, generalizations of the *wave equation*. In the case where the material parameters ($l$ and $c$ in the case of the transmission line) have no spatial variation, this amounts to saying that wave propagation in these media is *dispersionless*; a plane wave travels at a fixed speed, regardless of its wavelength. We now turn to sets of equations which fundamentally engender some degree of dispersion, namely those describing the motion of stiff systems such as beams, plates and shells. As a result, we move toward the use of mechanical quantities, as opposed to electrical, but the analogy should be clear. We will show how waveguide and wave digital filter principles can be used in order to obtain numerical solutions of such equations.

We will develop these algorithms in order of increasing dimensionality of the system; first we look at classical beam dynamics, and then proceed to the more modern beam theory devised by Timoshenko. We then look at stiff plates, and in particular the thick plate formulation of Mindlin, and then at two types of cylindrical shell theories, first the so-called membrane shell, then the thick shell system of Naghdi and Cooper. Finally, we look at the general (3+1)D system which describes the motion of a linear elastic solid.

It will be necessary to introduce several new techniques in order to develop numerical methods for such systems, which are considerably more complex than the transmission line test problems which we examined in the previous chapters. First, although these systems are all (with the exception of Euler-Bernoulli beam system) symmetric hyperbolic, we will need to make use of non-reciprocal circuit elements in order to model some asymmetric couplings that occur. Second, we may have to perform some additional initial work on these same systems in order to symmetrize them, as they are not always symmetric hyperbolic in their commonly encountered forms. Third, in some cases we will be forced to make use of vector-valued wave variables and scattering junctions [131] (see §2.3.7).

A full technical summary of this chapter appeared in §1.3.

## 5.1 Transverse Motion of the Ideal Beam

Consider a thin beam, or rod, aligned parallel to the $x$ axis. We will be interested in the transverse motion of the beam, which we will assume to be restricted to one perpendicular direction; we will call the deflection of the beam from the $x$ axis $w(x,t)$. The relevant material parameters of the beam are the mass density $\rho$, the cross-sectional area $A$, Young's modulus $E$ and $I$, the moment of inertia of the beam about the perpendicular axis. The material parameters are, in general, allowed to be slowly-varying functions of $x$. Under the further assumptions that the beam deflection $w(x,t)$ is small, and that the beam cross-section remains perpendicular to the so-called "neutral axis", it is possible to arrive at the *Euler-Bernoulli* equation [77]:

$$\rho A\frac{\partial^2 w}{\partial t^2} = -\frac{\partial^2}{\partial x^2}\left(EI\frac{\partial^2 w}{\partial x^2}\right) \tag{5.1}$$

Notice that this equation contains a fourth order spatial derivative, resulting from the fact that the beam provides its own restoring stiffness, proportional to its curvature, in marked contrast to the equation for a string, which requires externally applied tension in order to support wave motion. In particular, it does not result from the elimination of variables in a hyperbolic system (see §3.2). If the material properties of the beam do not vary spatially, then (5.1) reduces to the more familiar form

$$\frac{\partial^2 w}{\partial t^2} = -b^2\frac{\partial^4 w}{\partial x^4} \tag{5.2}$$

where $b = \sqrt{\frac{EI}{\rho A}}$. In what follows, however, we will deal with the more general case.

### Phase and Group Velocity

Though equation (5.2) is not hyperbolic, it is simple to obtain a dispersion relationship by considering wave-like solutions of the form $e^{j(\omega t+\beta x)}$, where $\omega$ is the frequency variable, and $\beta$ is the spatial wavenumber. The relationship can be written as

$$\omega^2 - b^2\beta^4 = 0$$

which has solutions

$$\omega = \pm b\beta^2$$

The phase and group velocities can then be written, from (3.12), as

$$\gamma^p_{EB} = \pm b\beta \qquad\qquad \gamma^g_{EB} = \pm 2b\beta$$

These velocities are now dependent on the spatial wavenumbers, and hence wave propagation is *dispersive*. Notice also that the group velocities are unbounded, so we will expect to run into some numerical difficulties (recall that for all the systems dealt with in the previous chapters, stability bounds on $v_0$, the space step/time step ratio were dependent on a maximum group velocity).

We also mention that a good model for the piano string is based on the wave equation, and complemented by several perturbation terms, among which are a fourth spatial derivative term like the above [25]; such a term models frequency-dependent dispersion in the string.

### 5.1.1 Finite Differences

There are many ways to approach the numerical integration of (5.1). If the material parameters are constant, then a simple explicit method can be obtained by applying centered difference approximations to both the time and space derivatives, yielding the scheme

$$\begin{aligned} W_i(n+1) + W_i(n-1) &= -\frac{T^2b^2}{\Delta^4}\left(W_{i+2}(n) - 4W_{i+1}(n) - 4W_{i-1}(n) + W_{i-2}(n)\right) \\ &\quad + \left(2 + \frac{6T^2b^2}{\Delta^4}\right)W_i(n) \end{aligned} \tag{5.3}$$

where $W_i(n)$ is a grid function defined for integer $i$ and $n$, and represents an approximation to $w(i\Delta, nT)$, where $\Delta$ is a uniform grid spacing, and $T$ is the time step. This scheme is accurate to $O(\Delta^2, T^2)$, but is stable only for $2b\frac{T}{\Delta^2} \leq 1$, so it is effectively only first-order accurate; this is typical of explicit methods for systems with some parabolic character [176].

In order to deal more effectively with the varying-coefficient problem, we can divide (5.1) into a system of two PDEs, and differentiate with respect to time, to get

$$\frac{\partial v}{\partial t} = -\frac{1}{\rho A}\frac{\partial^2 m}{\partial x^2} \tag{5.4a}$$

$$\frac{\partial m}{\partial t} = EI\frac{\partial^2 v}{\partial x^2} \tag{5.4b}$$

Here, $v \triangleq \frac{\partial w}{\partial t}$ is the beam transverse velocity, and $m$ can be interpreted as a bending moment. We have chosen these variables in order to make clear the relationship of the classical beam theory with the more modern Timoshenko theory (see §5.2). Applying centered differences to this system yields

$$\begin{aligned} V_i(n+1) - V_i(n) &= -\frac{\mu}{(\overline{\rho A})_i}\left(M_{i+1}(n+\tfrac{1}{2}) - 2M_i(n+\tfrac{1}{2}) + M_{i-1}(n+\tfrac{1}{2})\right) && (5.5a) \\ M_i(n+\tfrac{1}{2}) - M_i(n-\tfrac{1}{2}) &= \mu(\overline{EI})_i\left(V_{i+1}(n) - 2V_i(n) + V_{i-1}(n)\right) && (5.5b) \end{aligned}$$

where $V$ and $M$ are the grid functions corresponding to $v$ and $m$. Similarly to the case of the transmission line (see §4.3.6), we have used

$$\begin{aligned} (\overline{\rho A})_i &= \rho(i\Delta)A(i\Delta) + O(\Delta^2) \\ (\overline{EI})_i &= E(i\Delta)I(i\Delta) + O(\Delta^2) \end{aligned}$$

and in keeping with the literature [176], we have also defined

$$\mu \triangleq \frac{T}{\Delta^2}$$

As for the transmission line, we can evaluate the grid functions $V$ and $M$ at alternating time steps. Due to the nature of the difference approximation, however, we cannot interleave these variables on the spatial grid. That is, we are forced to calculate both $V$ and $M$ at every grid location (at their respective time steps). We have written the difference scheme above such that temporal interleaving is evident, i.e. $V_k(m)$ and $M_k(m)$, $m$ half-integer, are calculated only for (say) $2m$ even and odd, respectively.

### 5.1.2 Waveguide Network for the Euler-Bernoulli System

It is possible to design a waveguide network which simulates the behavior of equation (5.1), but there are some extra features we must add which were not necessary in the case of the transmission line. In addition, the overloaded symbols for the wave variables become even more overloaded, due to the fact that we can no longer interleave the two dependent variables spatially, and are faced with a double set of wave variables at every grid point. (This can be remedied with recourse to other more involved difference methods, but we will not pursue this subject here.) The structure of interest is shown in Figure 5.1. This is still a (1+1)D waveguide network, like that which simulates the (1+1)D transmission line equations, but we have drawn the junctions which calculate $V_J$ and $M_J$ separately; it should be kept in mind that they operate at the same spatial locations. As before, we use grey/white coloring of junctions to signify operation at different time steps. Here we have interpreted $V_J$ (which we will identify with $V$ of difference scheme (5.5), and thus with $v$) as a *voltage-like* variable, and $M_J$ as the current-flow. Also as before, the diagram above is correct when we are using voltage-like wave variables as our signals. Figure 5.2 gives the complete picture of the wave quantities and immittances in the network.

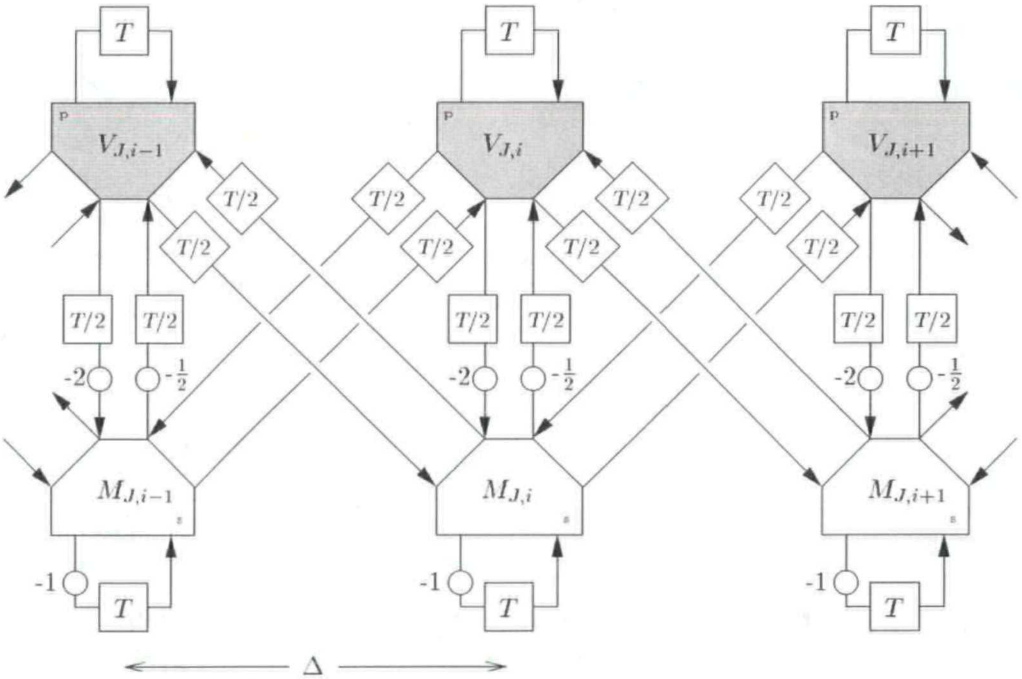

Figure 5.1: *(1+1)D DWN for the Euler-Bernoulli system* (5.4).

We note that the wave variables at the series scattering junction at location $x = i\Delta$ are indicated by a tilde, to distinguish them from those at the parallel junction at the same location, even though the two sets of variables are calculated at alternate time steps. As for the (1+1)D transmission line, we index wave variables and immittances at the left and right ports of any junction by $x^-$ and $x^+$ respectively, and the same such quantities associated with any self-loop are subscripted with $c$. We also have new waveguides connecting parallel and series junctions at the same grid point; immittances and wave variables are subscripted with a $t$ in this case. With reference to Figure 5.2, we can define the junction admittance at the parallel junction, and the junction impedance at the series junction to be

$$Y_{J,i} \triangleq Y_{x^-,i} + Y_{x^+,i} + Y_{c,i} + Y_{t,i} \tag{5.6}$$

$$\tilde{Z}_{J,i} \triangleq \tilde{Z}_{x^-,i} + \tilde{Z}_{x^+,i} + \tilde{Z}_{c,i} + \tilde{Z}_{t,i} \tag{5.7}$$

It should be clear that this waveguide network is really a pair of coupled (1+1)D transmission lines; the coupling is via the waveguide connecting the series and parallel junctions at the same grid location (the vertical waveguide in Figure 5.1). The factors of -2 and $-\frac{1}{2}$ in the "coupling" waveguide in Figure 5.3 deserve some extra commentary. Figure 5.3 shows an equivalence between two waveguide configurations. On the left, we have two identical waveguides with delay $m$ time steps and impedance

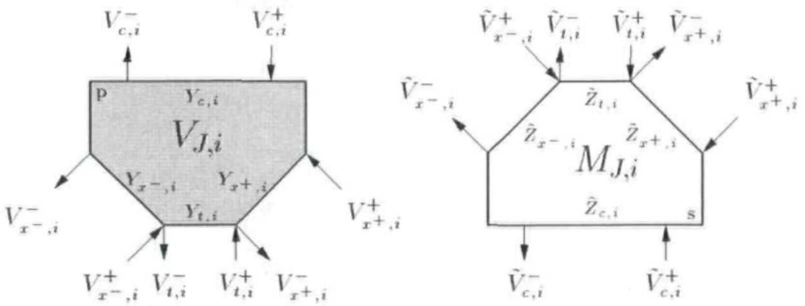
$V^-_{c,i}$
$V^+_{c,i}$
P
$Y_{c,i}$
$V_{J,i}$
$Y_{x^-,i}$
$Y_{x^+,i}$
$Y_{t,i}$
$V^-_{x^-,i}$
$V^+_{x^+,i}$
$V^+_{x^-,i}$
$V^-_{t,i}$
$V^+_{t,i}$
$V^-_{x^+,i}$
$\tilde{V}^+_{x^-,i}$
$\tilde{V}^-_{t,i}$
$\tilde{V}^+_{t,i}$
$\tilde{V}^-_{x^+,i}$
$\tilde{V}^-_{x^-,i}$
$\tilde{V}^+_{x^+,i}$
$\tilde{Z}_{t,i}$
$\tilde{Z}_{x^-,i}$
$\tilde{Z}_{x^+,i}$
$M_{J,i}$
$\tilde{Z}_{c,i}$
s
$\tilde{V}^-_{c,i}$
$\tilde{V}^+_{c,i}$

Figure 5.2: *Scattering junctions of Figure 5.1, with incoming and outgoing voltage waves indicated.*

$Z$ connected between a parallel junction and a series junction; in approximating a second derivative by centered differences, as we are indeed doing in (5.5), we need such a configuration so as to double the strength of the wave variable coming from the same grid location at the previous time step relative to that of those entering from the neighboring junctions. The equivalent form on the right, which introduces a transformer with turn ratio -2, serves to reduce the pair of waveguides to a single one, accompanied by two multiplications (the waveguide transformer is identical to the wave digital transformer, discussed in §2.3.4). This implies that the port impedance $Y_{t,i}$ at a parallel junction at grid point $i$ in Figure 5.1 and the port admittance $\tilde{Z}_{t,i}$ at the series junction at the same point must be related by

$$Y_{t,i} = \frac{4}{\tilde{Z}_{t,i}} \tag{5.8}$$

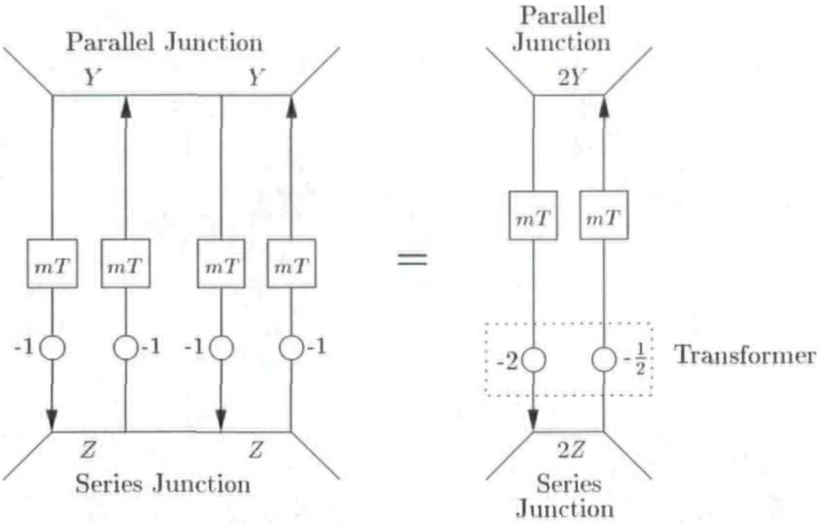
Parallel Junction
$Y$
$Y$
$mT$
$mT$
$mT$
$mT$
-1
-1
-1
-1
$Z$
$Z$
Series Junction
=
Parallel Junction
$2Y$
$mT$
$mT$
-2
$-\frac{1}{2}$
Transformer
$2Z$
Series Junction

Figure 5.3: *An equivalent form for duplicate bidirectional delay lines running between a parallel and a series junction.*

(This equivalence can easily be derived through the manipulation of *hybrid matrices* for bidirectional delay lines, as per the methods discussed in §4.10.2.) Also note the sign inversions in this central coupling waveguide with respect to the left- and right-going waveguides.

We now trace the signal flow in the network to show that it does indeed solve the Euler Bernoulli system. Beginning from a series junction at grid point $i$, we have:

$$\begin{aligned}
M_{J,i}(n+\tfrac{1}{2}) &= \frac{2}{\tilde{Z}_{J,i}}\left(\tilde{V}^{+}_{x^-,i}(n+\tfrac{1}{2})+\tilde{V}^{+}_{x^+,i}(n+\tfrac{1}{2})+\tilde{V}^{+}_{t,i}(n+\tfrac{1}{2})+\tilde{V}^{+}_{c,i}(n+\tfrac{1}{2})\right)\\
&= \frac{2}{\tilde{Z}_{J,i}}\left(V^{-}_{x^+,i-1}(n)+V^{-}_{x^-,i+1}(n)-2\tilde{V}^{-}_{t,i}(n)-V^{-}_{c,i}(n-\tfrac{1}{2})\right)\\
&= \frac{2}{\tilde{Z}_{J,i}}\left(V_{J,i-1}(n)+V_{J,i+1}(n)-2V_{J,i}(n)+\tilde{V}^{-}_{c,i}(n-\tfrac{1}{2})\right)\\
&\qquad -\frac{2}{\tilde{Z}_{J,i}}\left(V^{+}_{x^+,i-1}(n)+V^{+}_{x^-,i+1}(n)-2V^{+}_{t,i}(n)\right)\\
&= \frac{2}{\tilde{Z}_{J,i}}\left(V_{J,i-1}(n)+V_{J,i+1}(n)-2V_{J,i}(n)\right)\\
&\qquad -\frac{2}{\tilde{Z}_{J,i}}\left(\tilde{V}^{-}_{x^+,i}(n-\tfrac{1}{2})+\tilde{V}^{-}_{x^-,i}(n-\tfrac{1}{2})+\tilde{V}^{-}_{t,i}(n-\tfrac{1}{2})+\tilde{V}^{-}_{c,i}(n-\tfrac{1}{2})\right)\\
&= \frac{2}{\tilde{Z}_{J,i}}\left(V_{J,i-1}(n)+V_{J,i+1}(n)-2V_{J,i}(n)\right)+M_{J,i}(n-\tfrac{1}{2})
\end{aligned}$$

which is identical to (5.5b) if we replace $V_J$ by $V$ and $M_J$ by $M$, and if we have

$$\tilde{Z}_{J,i}=\frac{2}{(\overline{EI})_i\mu} \tag{5.9}$$

Beginning from the series junction, we arrive at a similar requirement for $Y_{J,i}$, namely

$$Y_{J,i}=\frac{2(\overline{\rho A})_i}{\mu} \tag{5.10}$$

As in the case of the transmission line, three families of waveguide networks are distinguishable:

### Type I: Voltage-centered Network

In order to satisfy (5.10), with $Y_J$ defined by (5.6) we set

$$Y_{x^-,i}=Y_{x^+,i}=\frac{(\rho A)_i}{2\mu}\qquad\qquad Y_{t,i}=\frac{(\rho A)_i}{\mu}\qquad\qquad Y_{c,i}=0$$

Now, we have, recalling (5.7) and (5.8),

$$\tilde{Z}_{J,i}=\frac{2\mu}{(\rho A)_{i+1}}+\frac{2\mu}{(\rho A)_{i-1}}+\frac{4\mu}{(\rho A)_i}+\tilde{Z}_{c,i}$$

and in order to satisfy (5.9), we set

$$\tilde{Z}_{c,i} = \left(\frac{1}{2\mu(EI)_{i+1}} + \frac{1}{2\mu(EI)_{i-1}} + \frac{1}{\mu(EI)_i}\right) - \left(\frac{2\mu}{(\rho A)_{i+1}} + \frac{2\mu}{(\rho A)_{i-1}} + \frac{4\mu}{(\rho A)_i}\right)$$

We have written here $h_i \triangleq h(i\Delta)$, where $h$ is either of $\rho A$ or $EI$. In this case, $\tilde{Z}_{c,i}$ will be positive if

$$\mu \leq \frac{1}{2}\min_i \sqrt{\frac{(\rho A)_i}{(EI)_i}} \tag{5.11}$$

and we have an upper bound on the time step in terms of the grid spacing. In the constant-coefficient case, we note that this is the same requirement as for the stability of scheme (5.3).

### Type II: Current-centered Network

This is the dual to the previous arrangement. Now we set

$$\tilde{Z}_{x^-,i} = \tilde{Z}_{x^+,i} = \frac{1}{2\mu(EI)_i} \qquad \tilde{Z}_{t,i} = \frac{1}{\mu(EI)_i} \qquad \tilde{Z}_{c,i} = 0$$

and we thus choose

$$Y_{c,i} = \left(\frac{(\rho A)_{i+1}}{2\mu} + \frac{(\rho A)_{i-1}}{2\mu} + \frac{(\rho A)_i}{\mu}\right) - (2\mu(EI)_{i+1} + 2\mu(EI)_{i-1} + 4\mu(EI)_i)$$

and we have the same stability condition as the previous case,

$$\mu \leq \frac{1}{2}\min_i \sqrt{\frac{(\rho A)_i}{(EI)_i}}$$

### Type III: Mixed Network

We set

$$Y_{x^-,i} = Y_{x^+,i} = Y_{const} \qquad Y_{t,i} = 2Y_{const}$$

(5.10) and (5.9) then require that we set

$$Y_{c,i} = \frac{2(\overline{\rho A})_i}{\mu} - 4Y_{const} \qquad \tilde{Z}_{c,i} = \frac{2}{\mu(\overline{EI})_i} - \frac{4}{Y_{const}}$$

The optimal choice of $Y_{const} = \sqrt{\min_i(\overline{\rho A})_i)\max_i(\overline{EI})_i}$ yields the stability bound

$$\mu \leq \frac{1}{2}\sqrt{\frac{\min_i(\overline{\rho A})_i)}{\max_i(\overline{EI})_i)}} \leq \frac{1}{2}\min_i\sqrt{\frac{(\rho A)_i}{(EI)_i}}$$

and we are thus forced to use a smaller time step than is required by either of the above arrangements.

### 5.1.3 Boundary Conditions in the Waveguide Network

If the ideal beam is of finite length, then we are required to supply boundary conditions at the termination; we show here how to apply such conditions in the waveguide mesh described in the previous section. We will assume that one end of the beam is positioned at $x = 0$; all discussion of boundary conditions applies equally at the other end (or we may assume that the beam is of semi-infinite extent). It is of note that because the Euler-Bernoulli Equation (5.1) is of fourth order in the spatial variable, we are required to provide two boundary conditions at each termination [176]. The simplest boundary conditions for the ideal beam are correspondingly simple to implement in the waveguide mesh. From [77], the most physically relevant such boundary conditions are the following:

**Fixed End, Allowed to Pivot**

In this simple case, we have

$$w(0,t) = 0 \qquad \Longrightarrow \qquad v(0,t) = 0 \tag{5.12a}$$

$$\frac{\partial^2 w(0,t)}{\partial x^2} = 0 \qquad \Longrightarrow \qquad m(0,t) = 0 \tag{5.12b}$$

$v(0,t) = 0$ is ensured by terminating the parallel junction at $i = 0$ with a short-circuit, so that $V_{J,0}$ is forced to zero. From Figure 5.4(a), we see that as a result (really by construction), we have $V^{+}_{x^+,0} = -V^{-}_{x^+,0}$. The second boundary condition, $m(0,t) = 0$ can be enforced in a similar manner by terminating the series junction at grid location zero with an open circuit.

**Fixed Clamped End**

Here the boundary conditions are

$$w(0,t) = 0 \qquad \Longrightarrow \qquad v(0,t) = 0 \tag{5.13a}$$

$$\frac{\partial w(0,t)}{\partial x} = 0 \qquad \Longrightarrow \qquad \frac{\partial v(0,t)}{\partial x} = 0 \tag{5.13b}$$

The boundary condition $w = 0$ is implemented as in the previous case. The condition $\frac{\partial v(0,t)}{\partial x} = 0$ requires some discussion.

Consider difference scheme (5.5) operating at the grid point $i = 0$. By condition (5.13a), $V_0(n)$ will be set to zero, so we do not need to use (5.5a) at all. The difference scheme used to update $M_0$ would be

$$M_0(n+\tfrac{1}{2}) - M_0(n-\tfrac{1}{2}) = \mu(\overline{EI})_0\big(V_1(n) - 2V_0(n) + V_{-1}(n)\big)$$

if we had access to $V_{-1}(n)$, a value of the grid function $V$ at the grid location to the left of the boundary point. Since we don't, we eliminate it by use of the numerical boundary condition

$$V_1(n) = V_{-1}(n)$$

which is a second-order accurate approximation to $\frac{\partial v(0,t)}{\partial x} = 0$. This leaves us with

$$M_0(n+\tfrac{1}{2}) - M_0(n-\tfrac{1}{2}) = 2\mu(\overline{EI})_0 V_1(n) \tag{5.14}$$

Figure 5.4(b) shows the series junction terminated with a self-loop of impedance $\tilde{Z}_{c,0}$. We now show that with the proper setting of this impedance, this termination satisfies a numerical condition identical to (5.14). At this junction, there will only be two incoming waves, $\tilde{V}^{+}_{x^+,0}$ and $\tilde{V}^{+}_{c,0}$, and we thus have:

$$\begin{aligned}
M_{J,0}(n+\tfrac{1}{2}) &= \frac{2}{\tilde{Z}_{J,0}}\Big(\tilde{V}^{+}_{x^+,0}(n+\tfrac{1}{2}) + \tilde{V}^{+}_{x^+,c}(n+\tfrac{1}{2})\Big)\\
&= \frac{2}{\tilde{Z}_{J,0}}\Big(V^{-}_{x^-,1}(n) - \tilde{V}^{-}_{c,0}(n-\tfrac{1}{2})\Big)\\
&= \frac{2}{\tilde{Z}_{J,0}}\Big(V_{J,1}(n) - V^{+}_{x^-,1}(n) - \tilde{V}^{-}_{c,0}(n-\tfrac{1}{2})\Big)\\
&= \frac{2}{\tilde{Z}_{J,0}}V_{J,1}(n) - \frac{2}{\tilde{Z}_{J,0}}\Big(\tilde{V}^{-}_{x^+,0}(n-\tfrac{1}{2}) + \tilde{V}^{-}_{x^+,c}(n-\tfrac{1}{2})\Big)\\
&= \frac{2}{\tilde{Z}_{J,0}}W_{J,1}(n) + M_{J,0}(n-\tfrac{1}{2})
\end{aligned}$$

Thus, by identification with (5.14), we require

$$\tilde{Z}_{J,0} \triangleq \tilde{Z}_{c,0} + \tilde{Z}_{x^+,0} = \frac{1}{\mu(\overline{EI})_0}$$

and we can set

$$\tilde{Z}_{c,0} = \frac{1}{\mu(\overline{EI})_0} - \tilde{Z}_{x^+,0}$$

where the value of $\tilde{Z}_{x^+,0}$ depends on the type of network we are using (see previous section). For a network of type II or III (see previous section), $\tilde{Z}_{c,0}$ as defined above is automatically positive, if the stability conditions over the interior network junctions are satisfied, respectively (this is easily checked). For mesh of type I, we can show that it will be positive if it is true that

$$\mu \leq \sqrt{\frac{(\rho A)_1}{2(EI)_0}}$$

Since, for a Type I network, we already must have condition (5.11) for stability over the problem interior, then assuming that the material parameters do not vary greatly from one grid point to the next (In the limit as $\Delta \to 0$, they *must* not), this boundary condition is stable for the type I mesh as well.

In this case it can be seen that one of the benefits of the waveguide formulation is that it is remarkably easy to check the compatibility of a particular type of boundary condition with a particular scheme. That is to say, the passivity condition, framed in terms of the positivity of the network immittances, even at the boundary, tells us immediately which boundary condition implementations will be stable. Compatibility can be checked directly in the finite difference framework, but the procedure (which form part of what is known as GKSO theory [176]) may be quite involved.

### Free End

The boundary conditions are now

$$\frac{\partial^2 w(0,t)}{\partial x^2} = 0 \qquad \Longrightarrow \qquad m(0,t) = 0 \tag{5.15a}$$

$$\frac{\partial^3 w(0,t)}{\partial x^3} = 0 \qquad \Longrightarrow \qquad \frac{\partial m(0,t)}{\partial x} = 0 \tag{5.15b}$$

The condition $m = 0$ is the same as for the fixed end which is allowed to pivot. Thus we terminate the series junction in the same way as in that case. For the other condition, $\frac{\partial m(0,t)}{\partial x} = 0$, there is complete symmetry with the case of the fixed clamped end, where the condition was $\frac{\partial v(0,t)}{\partial x} = 0$. The junction can be terminated as in Figure 5.4(c), and we choose $Y_{c,0} = Y_{J,0} - Y_{x^+,0}$, where $Y_{J,0} = \frac{(\bar{\rho A})_0}{\mu}$, and $Y_{x^+,0}$ follows from the particular type of mesh configuration that we are using. Stability of this boundary condition for the three types of mesh follows as before as well.

## 5.2 Timoshenko's Beam Equations

Timoshenko's theory of beams constitutes an improvement over the Euler-Bernoulli theory, in that it incorporates shear and rotational inertia effects [77]. This is one of the few cases in which a more refined modeling approach allows more tractable numerical simulation; the reason for this is that Timoshenko's theory gives rise to a *hyperbolic* system, unlike the Euler-Bernoulli system, for which

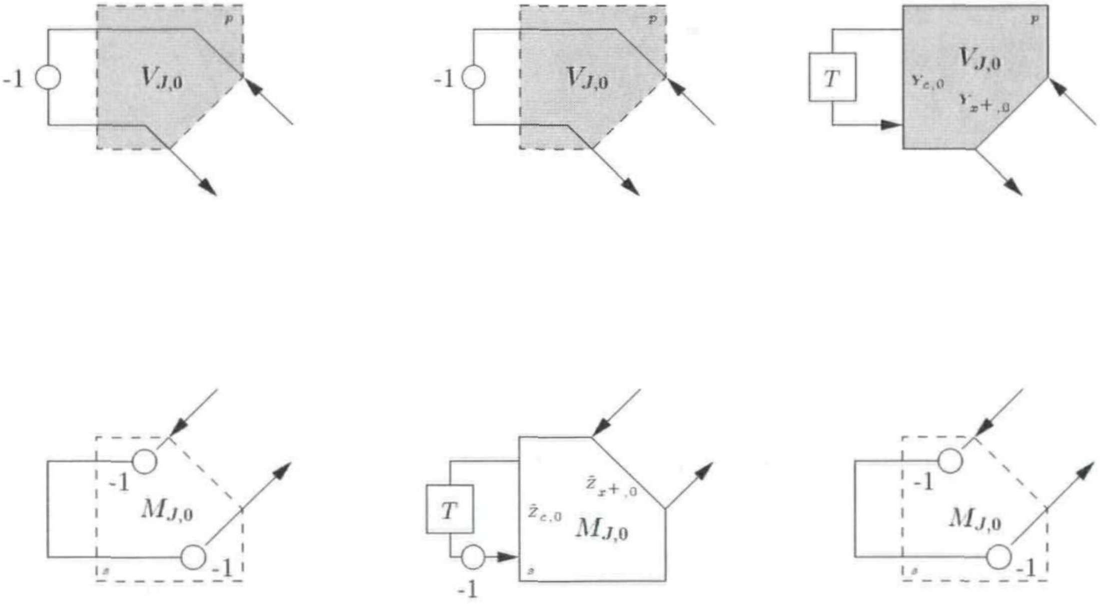

(a) (b) (c)

Figure 5.4: *Boundary terminations for the Euler-Bernoulli system*— (a) *fixed end, allowed to pivot;* (b) *fixed, clamped end;* (c) *free end.*

propagation velocity is unbounded. It is this partially parabolic character of the Euler-Bernoulli system which engenders severe restrictions on the maximum allowable time step (at least in the case of explicit methods, of which type are all the scattering-based methods included in this work). For a physical derivation of Timoshenko's system, we refer the reader to [77, 146, 152, 187, 188], and simply present it here:

$$\rho A\frac{\partial^2 w}{\partial t^2} = \frac{\partial}{\partial x}\left(A\kappa G(\frac{\partial w}{\partial x}-\psi)\right) \tag{5.16a}$$

$$\rho I\frac{\partial^2 \psi}{\partial t^2} = \frac{\partial}{\partial x}\left(EI\frac{\partial \psi}{\partial x}\right)+A\kappa G\left(\frac{\partial w}{\partial x}-\psi\right) \tag{5.16b}$$

As before, $w(x,t)$ represents the transverse displacement of the beam from an equilibrium state, and the new dependent variable $\psi(x,t)$ is the angle of deflection of the cross-section of the beam with respect to the vertical direction. Here, the quantities $\rho$, $A$, $E$ and $I$ are as for the Euler-Bernoulli Equation (5.1). $G$ is the shear modulus (usually called $\mu$ in other contexts) and $\kappa$ is a constant which depends on the geometry of the beam. For generality, we assume that all these material parameters are functions of $x$. Losses or sources are not modeled.

Nitsche [131], in his MDWD network-based approach preferred to use the more fundamental set of four first order PDEs from which system (5.16) is condensed:

$$\begin{aligned} \rho A\frac{\partial v}{\partial t} &= \frac{\partial q}{\partial x} && \text{(5.17a)} & \rho I\frac{\partial \omega}{\partial t} &= \frac{\partial m}{\partial x}+q && \text{(5.18a)} \\ \frac{1}{A\kappa G}\frac{\partial q}{\partial t} &= \frac{\partial v}{\partial x}-\omega && \text{(5.17b)} & \frac{1}{EI}\frac{\partial m}{\partial t} &= \frac{\partial \omega}{\partial x} && \text{(5.18b)} \end{aligned}$$

We have introduced here the quantities

$$v \triangleq \frac{\partial w}{\partial t} \qquad \omega \triangleq \frac{\partial \psi}{\partial t} \qquad m \triangleq EI\frac{\partial \psi}{\partial x} \qquad q \triangleq A\kappa G\left(\frac{\partial w}{\partial x}-\psi\right)$$

$v$ is interpreted as transverse velocity, $\omega$ as an angular velocity, $m$ as the bending moment, and $q$ as the shear force on the cross-section. Each of the subsystems (5.17) and (5.18) has the form of a lossless (1+1)D transmission line system; they are coupled by constant-proportional terms, and it is this coupling that gives the Timoshenko system its dispersive character. The Euler-Bernoulli system (5.4) is recovered in the limit as $A\kappa G \to \infty$ and $\rho I \to 0$ [131].

This is a symmetric hyperbolic system of the form given in (3.1), with $\mathbf{w} = [v, q, \omega, m]^T$, $\mathbf{f} = \mathbf{0}$ and

$$\mathbf{P} = \begin{bmatrix} \rho A & 0 & 0 & 0 \\ 0 & \frac{1}{A\kappa G} & 0 & 0 \\ 0 & 0 & \rho I & 0 \\ 0 & 0 & 0 & \frac{1}{EI} \end{bmatrix} \qquad \mathbf{A}_1 = \begin{bmatrix} 0 & -1 & 0 & 0 \\ -1 & 0 & 0 & 0 \\ 0 & 0 & 0 & -1 \\ 0 & 0 & -1 & 0 \end{bmatrix} \qquad \mathbf{B} = \begin{bmatrix} 0 & 0 & 0 & 0 \\ 0 & 0 & 1 & 0 \\ 0 & -1 & 0 & 0 \\ 0 & 0 & 0 & 0 \end{bmatrix}$$

### Dispersion

The characteristic polynomial equation, from (3.10) with the system matrices given above, in the case of constant coefficients, is

$$\omega^4 - \frac{\omega^2}{\rho}\left(\frac{A\kappa G}{I} + \beta^2\left(E + G\kappa\right)\right) + \frac{E\kappa G}{\rho^2}\beta^4 = 0 \tag{5.19}$$

where $\omega$ and $\beta$ are frequency and spatial wavenumber, respectively. There are two pairs of solutions to this equation, which can be written as

$$\begin{aligned} \omega_{1\pm} &= \pm\sqrt{\frac{1}{2\rho}\left(\frac{A\kappa G}{I} + \beta^2\left(E+G\kappa\right) + \sqrt{\left(\frac{A\kappa G}{I} + \beta^2\left(E+G\kappa\right)\right)^2 - 4E\kappa G\beta^4}\right)} \\ \omega_{2\pm} &= \pm\sqrt{\frac{1}{2\rho}\left(\frac{A\kappa G}{I} + \beta^2\left(E+G\kappa\right) - \sqrt{\left(\frac{A\kappa G}{I} + \beta^2\left(E+G\kappa\right)\right)^2 - 4E\kappa G\beta^4}\right)} \end{aligned}$$

and it is simple to show that in contrast with the Euler-Bernoulli beam, the group velocities will be bounded. Indeed, we have in particular that

$$\lim_{\beta\to\infty} \omega_{1\pm} = \pm\beta\frac{E}{\rho} \qquad\qquad \lim_{\beta\to\infty} \omega_{2\pm} \pm \beta\frac{G\kappa}{\rho}$$

the first of these relations is similar to that which describes longitudinal wave propagation in a bar, and the second corresponds to shear vibration [77]. For the full varying-coefficient problem, the maximum group velocity, as defined in (3.13), will be

$$\gamma^{g}_{T,max} = \max_{x\in\mathcal{D}} \sqrt{\frac{E}{\rho}} \tag{5.20}$$

### 5.2.1 MDKC and MDWDF for Timoshenko's System

Nitsche [131] showed how to write a MDKC and MDWD network corresponding to Timoshenko's system. In order to deal with the asymmetric coupling of the system of equations, he constructed a network using both MD capacitors and inductors, but here we will take the more conventional approach, and use a gyrator (For computational purposes, there is no essential difference between this representation and his.)

Consider again the Timoshenko system of (5.17) and (5.18). We can scale the variables just as for the transmission line (see §3.7). That is, we can write

$$v = r_1 i_1 \qquad q = i_2 \qquad \omega = i_3 \qquad m = r_2 i_4 \tag{5.21}$$

where the constants $r_1$ and $r_2$, are strictly positive. We introduce, as before, the scaled time variable $t' = v_0 t$ where $v_0$ is the space step/time step ratio. Then the Timoshenko system can be rewritten as

$$\begin{aligned} v_0 r_1^2 \rho A \frac{\partial i_1}{\partial t'} &= r_1 \frac{\partial i_2}{\partial x} && (5.22\text{a}) & \qquad v_0 \rho I \frac{\partial i_3}{\partial t'} &= r_2 \frac{\partial i_4}{\partial x} + i_2 && (5.23\text{a}) \\ \frac{v_0}{A\kappa G}\frac{\partial i_2}{\partial t'} &= r_1 \frac{\partial i_1}{\partial x} - i_3 && (5.22\text{b}) & \qquad \frac{v_0 r_2^2}{EI}\frac{\partial i_4}{\partial t'} &= r_2 \frac{\partial i_3}{\partial x} && (5.23\text{b}) \end{aligned}$$

The constant proportional terms on the right-hand side appear anti-symmetrically, and can be interpreted as a lossless gyrator coupling. We can now write down a MDKC for the scaled system of equations; it is shown, along with element values in Figure 5.5. Its MDWD counterpart is pictured in Figure 5.6. Here, we have used the coordinate transformation defined in (3.18) with step sizes $T_1 = T_2 = \sqrt{2}\Delta$. We have used $T' = \Delta$ for the one-port time inductors. An MDWD network can obviously also be designed to operate on alternating grids, just as in the case of the (1+1)D transmission line.

A comment is necessary regarding the gyrator in Figure 5.6. In order to deal with the delay-free

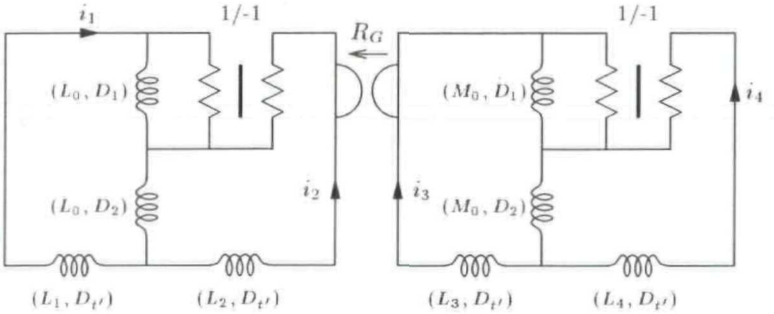
$i_1$
1/-1
$R_G$
1/-1
$(L_0, D_1)$
$(M_0, D_1)$
$i_4$
$i_2$
$i_3$
$(L_0, D_2)$
$(M_0, D_2)$
$(L_1, D_{t'})$
$(L_2, D_{t'})$
$(L_3, D_{t'})$
$(L_4, D_{t'})$

$$\begin{aligned} L_0 &= r_1/\sqrt{2} \\ M_0 &= r_2/\sqrt{2} \\ L_1 &= v_0 r_1^2 \rho A - r_1 \\ L_2 &= v_0/(A\kappa G) - r_1 \\ L_3 &= v_0 \rho I - r_2 \\ L_4 &= v_0 r_2^2/(EI) - r_2 \\ R_G &= 1 \end{aligned}$$

Figure 5.5: *MDKC for Timoshenko's system.*

loop which arises from the placement of a gyrator between two series junctions, we have set the corresponding ports of the series junctions on either side of the gyrator to be reflection-free. This, however, means that the two port resistances of the gyrator are not, in general, equal to the gyrator constant, which, in this case, will be 1. In terms of wave variables, the signal flow diagram of the gyrator will not be of the simple form of (2.26), but takes the more general form of (2.25) mentioned in §2.3.4. It is of course also possible to set only one of the ports connected to the gyrator to be reflection-free, (say $R_5 = R_0 + R_2$), and then the other port resistance to be $R_6 = R_5$, in which case the general gyrator form degenerates to a pair of scalings. As for the parameters $r_1$ and $r_2$, an optimal choice can be shown to be

$$\begin{aligned} r_1 &= \left(\max_x(AG\kappa)\min_x(\rho A)\right)^{-\frac{1}{2}} \\ r_2 &= \left(\max_x(EI)\min_x(\rho I)\right)^{\frac{1}{2}} \end{aligned}$$

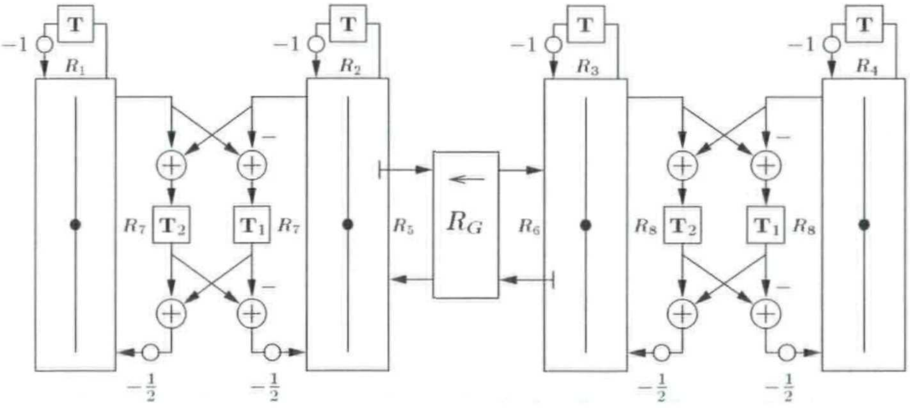
T
T
T
T
−1
−1
−1
−1
$R_1$
$R_2$
$R_3$
$R_4$
−
−
−
−
$R_7$
$\mathbf{T}_2$
$\mathbf{T}_1$
$R_7$
$R_5$
$R_G$
$R_6$
$R_8$
$\mathbf{T}_2$
$\mathbf{T}_1$
$R_8$
$-\frac{1}{2}$
$-\frac{1}{2}$
$-\frac{1}{2}$
$-\frac{1}{2}$

$$\begin{aligned} R_1 &= 2L_1/\Delta \\ R_2 &= 2L_2/\Delta \\ R_3 &= 2L_3/\Delta \\ R_4 &= 2L_4/\Delta \\ R_5 &= R_0 + R_2 \\ R_6 &= R_0 + R_3 \\ R_7 &= 2r_1/\Delta \\ R_8 &= 2r_2/\Delta \end{aligned}$$

Figure 5.6: *MDWD network for Timoshenko's system.*

which yields the bound

$$v_0 \geq \max\left(\sqrt{\frac{\max_x(AG\kappa)}{\min_x(\rho A)}}, \sqrt{\frac{\max_x(EI)}{\min_x(\rho I)}}\right) \geq \gamma^g_{T,max} \tag{5.24}$$

which is the same as that which is derived in [131]. We will show how to improve upon this bound in §5.2.6.

### 5.2.2 Waveguide Network for Timoshenko's System

Recall, from §4.10, that for the (1+1)D transmission line problem, it is possible to obtain a DWN from an MDKC after a few network manipulations, and under the application of an alternative spectral mapping, or integration rule. We may proceed in the same way for Timoshenko's system, and we will skip most of the steps that were detailed in the earlier treatment. We do recall, however, that the original system of equations should be scaled by a factor of $\Delta$, the grid spacing, before making the switch to DWNs.

We first transform the MDKC of Figure 5.5 such that the quantities $v$ and $m$ represent voltages across capacitors, instead of currents through inductors. The transformed MDKC is shown in Figure 5.7.

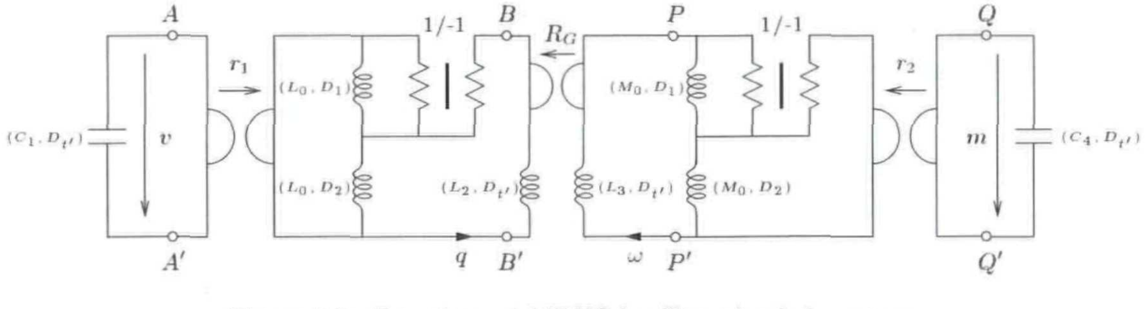

Figure 5.7: *Transformed MDKC for Timoshenko's system.*

The inductances are all as in Figure 5.5, except scaled by $\Delta$, and the new capacitance values will be

$$C_1 = \Delta\left(v_0\rho A - \frac{1}{r_1}\right) \qquad C_4 = \Delta\left(\frac{v_0}{EI} - \frac{1}{r_2}\right)$$

and the gyration coefficient $R_G$ will be equal to $\Delta$. As before, it is possible to interpret the two two-ports $AA'BB'$ and $PP'QQ'$ as MD representations of digital waveguide pairs, if we apply the alternative spectral mapping or integration rule as in §4.10. The MD waveguide network is shown in Figure 5.8.

Here we have chosen the step sizes such that an interleaved algorithm results, just as for the transmission line problem, as discussed in §4.10. Thus, we have $T_1 = T_2 = \Delta/\sqrt{2}$ and $T' = \Delta$ so

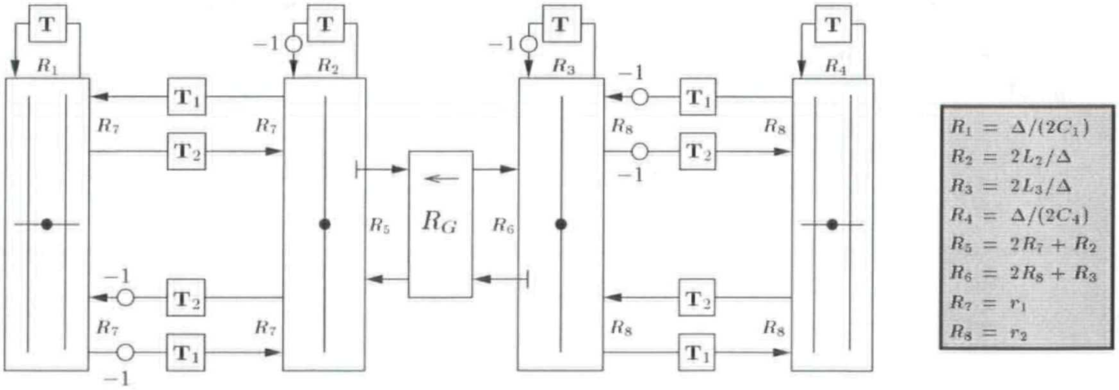
T
T
T
T
$R_1$
$R_2$
$R_3$
$R_4$
$T_1$
$T_2$
$T_1$
$T_2$
$T_1$
$T_2$
$T_1$
$T_2$
$R_7$
$R_8$
$R_5$
$R_6$
$R_G$
-1
$R_1 = \Delta/(2C_1)$
$R_2 = 2L_2/\Delta$
$R_3 = 2L_3/\Delta$
$R_4 = \Delta/(2C_4)$
$R_5 = 2R_7 + R_2$
$R_6 = 2R_8 + R_3$
$R_7 = r_1$
$R_8 = r_2$

Figure 5.8: *Waveguide network for Timoshenko's system, in a multidimensional form.*

that in a computer implementation, approximations to $v$ and $m$ are alternated with those of $q$ and $\omega$. The signal flow diagram corresponding to Figure 5.8 is shown, as a DWN, in Figure 5.9. The junction

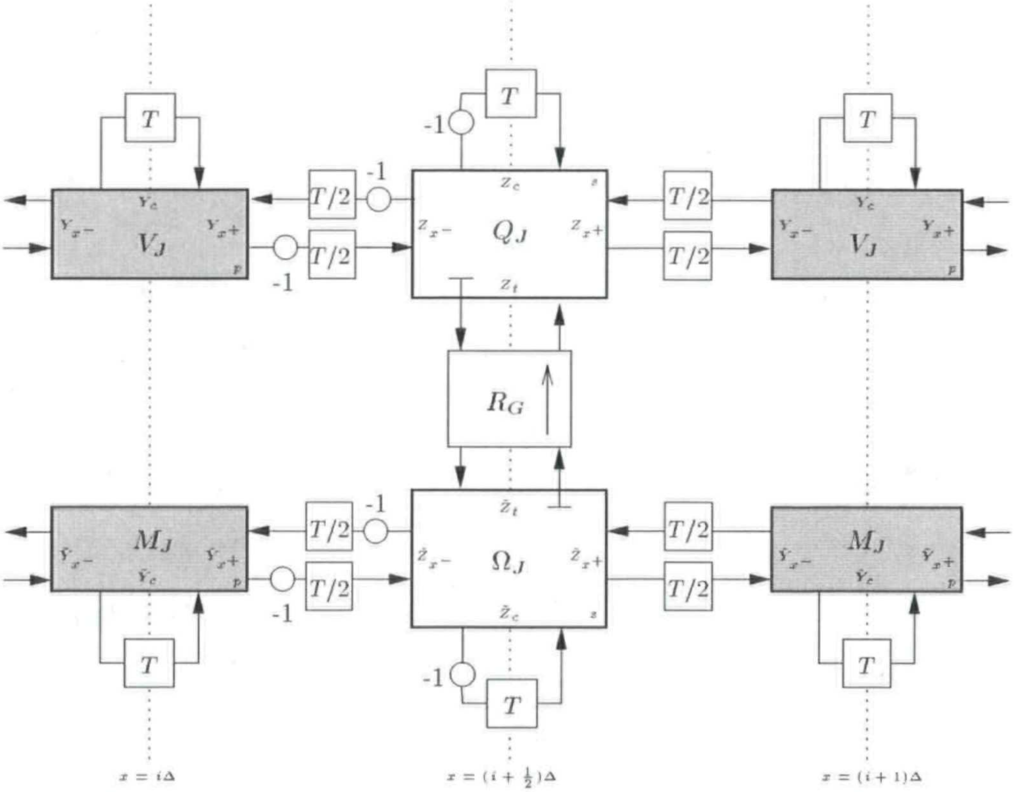
T
T/2
-1
$V_J$
$Q_J$
$R_G$
$M_J$
$\Omega_J$
$x = i\Delta$
$x = (i+\frac{1}{2})\Delta$
$x = (i+1)\Delta$

Figure 5.9: *DWN for Timoshenko's system.*

quantities $V_J$, $Q_J$, $\Omega_J$ and $M_J$ approximate $v$, $q$, $\omega$ and $m$ respectively and for consistency with the DWN notation of Chapter 4, we have replaced the port resistances by waveguide admittances (at the parallel junctions) and impedances (at the series junctions). Because there are now two sets of immittances at any grid point (corresponding to the upper and lower rails in Figure 5.9), we have indexed half of them with a tilde. Referring to Figure 5.9, the self-loop immittances will be given by

$$Y_{c,i} = 2v_0(\rho A)_i - \frac{2}{r_1} \qquad \tilde{Y}_{c,i} = \frac{2v_0}{(EI)_i} - \frac{2}{r_2}$$

$$Z_{c,i+\frac{1}{2}} = \frac{2v_0}{(AG\kappa)_{i+\frac{1}{2}}} - 2r_1 \qquad \tilde{Z}_{c,i+\frac{1}{2}} = 2v_0(\rho I)_{i+\frac{1}{2}} - 2r_2$$

at alternating grid locations indexed by integer $i$. The connecting immittances will be, referring to the series junctions,

$$Z_{x^-,i+\frac{1}{2}} = Z_{x^+,i+\frac{1}{2}} = r_1 \qquad \tilde{Z}_{x^-,i+\frac{1}{2}} = \tilde{Z}_{x^+,i+\frac{1}{2}} = r_2$$

The DWN incorporates a gyrator between the two series junctions, and as such, we must employ reflection-free ports at at least one of the two connected junction ports. Though reflection-free ports and gyrators have not as yet appeared in the DWN context, it is straightforward (indeed immediate, if we are considering DWNs derived from MDKCs), to transfer them from wave digital filters. These port impedances (subscripted with a $t$) at the series junctions can be chosen to be

$$Z_{t,i+\frac{1}{2}} = Z_{c,i+\frac{1}{2}} + Z_{x^-,i+\frac{1}{2}} + Z_{x^+,i+\frac{1}{2}} \qquad \tilde{Z}_{t,i+\frac{1}{2}} = \tilde{Z}_{c,i+\frac{1}{2}} + \tilde{Z}_{x^-,i+\frac{1}{2}} + \tilde{Z}_{x^+,i+\frac{1}{2}}$$

This is a structure of the type III form (i.e., the connecting immittances are spatially invariant; see §4.3.6), and the bound on $v_0$ is suboptimal (and the same as that for the MDWDF structure discussed in the last section). The possible interleaving of the calculated junction quantities in this structure is indicated, as in Chapter 4, by grey/white coloring of scattering junctions.

### 5.2.3 Other Waveguide Networks for Timoshenko's System

For completeness sake, we mention two other DWNs for the Timoshenko system for which there is no need for the coupling reflection-free ports; all junctions are isolated from one another by delays. They were derived separately, and not through the manipulation of an MDKC. In fact, they can be arrived at in this manner, but we will present only the resulting structures. We mention them primarily because although they are quite similar to the DWN of the last section, the passivity condition on the immittance values leads to a radically different bound on $v_0$, the space step/time step ratio.

The difference between the two forms presented here is only in the coupling between the two lines, each type of which gives rise to a different type of offset sampling. For example, in the configuration shown in Figure 5.10, we calculate $Q_J$ and $M_J$ at the same time instant, and at the same grid location, whereas in Figure 5.11, the updating of $Q_J$ with respect to $M_J$ is staggered in both time and space.

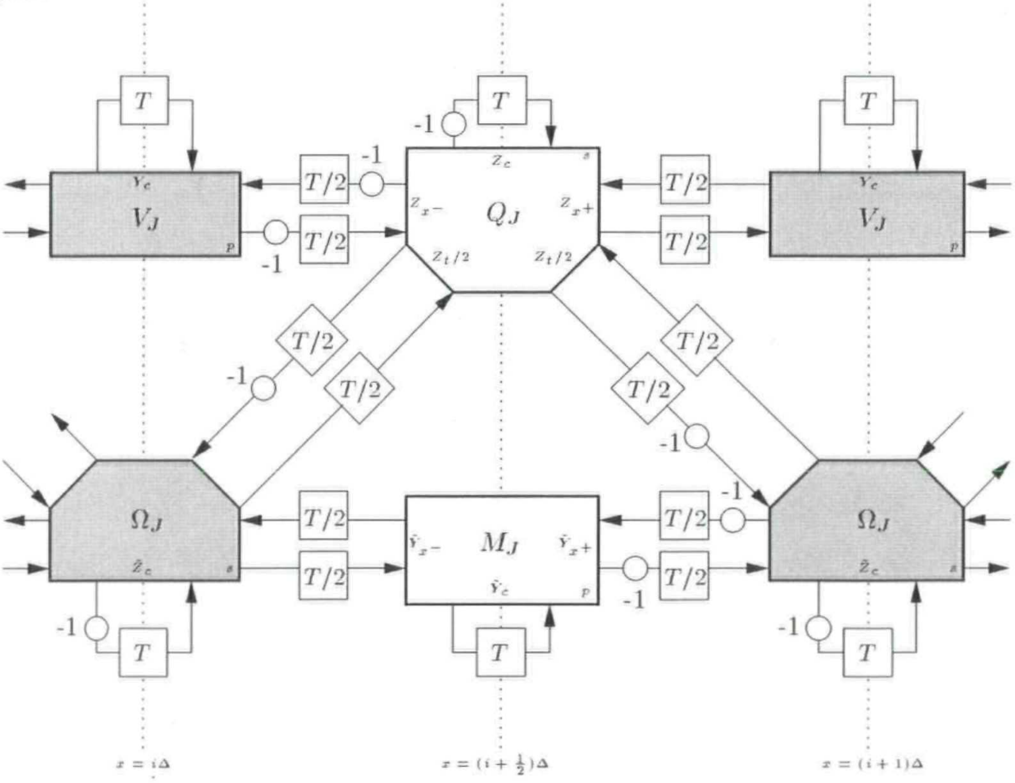
T
T
T
-1
-1
T/2
T/2
-1
$Y_c$
$V_J$
$p$
$z_c$
$s$
$Q_J$
$z_{x}-$
$z_{x}+$
$z_t/2$
$z_t/2$
T/2
T/2
$Y_c$
$V_J$
$p$
T/2
T/2
-1
T/2
T/2
-1
-1
$\Omega_J$
$\tilde{z}_c$
$s$
T/2
T/2
$M_J$
$\tilde{Y}_{x}-$
$\tilde{Y}_{x}+$
$\tilde{Y}_c$
$p$
T/2
T/2
-1
-1
$\Omega_J$
$\tilde{z}_c$
$s$
-1
T
T
-1
T
$x = i\Delta$
$x = (i+\frac{1}{2})\Delta$
$x = (i+1)\Delta$

Figure 5.10: *An alternate DWN for Timoshenko's system.*

There are many ways of setting the network immittances so as to approximate the Timoshenko system. Since both networks are simply just pairs of coupled (1+1)D transmission lines, the derivation of the constraints on the junction immittances is familiar. Because the two networks are so similar, we will state these constraints only for the network shown in Figure 5.11:

$$Z_{J,i+\frac{1}{2}} = \frac{2v_0}{(\overline{AG\kappa})_{i+\frac{1}{2}}} \qquad \tilde{Z}_{J,i+\frac{1}{2}} = 2v_0(\overline{\rho I})_{i+\frac{1}{2}} \qquad Y_{J,i} = 2v_0(\overline{\rho A})_i \qquad \tilde{Y}_{J,i} = \frac{2v_0}{(\overline{EI})_i}$$

We use the bar notation again to indicate an approximation to at least second-order accuracy in the spatial step $\Delta$, and the tilde to distinguish between the immittances in the two transmission

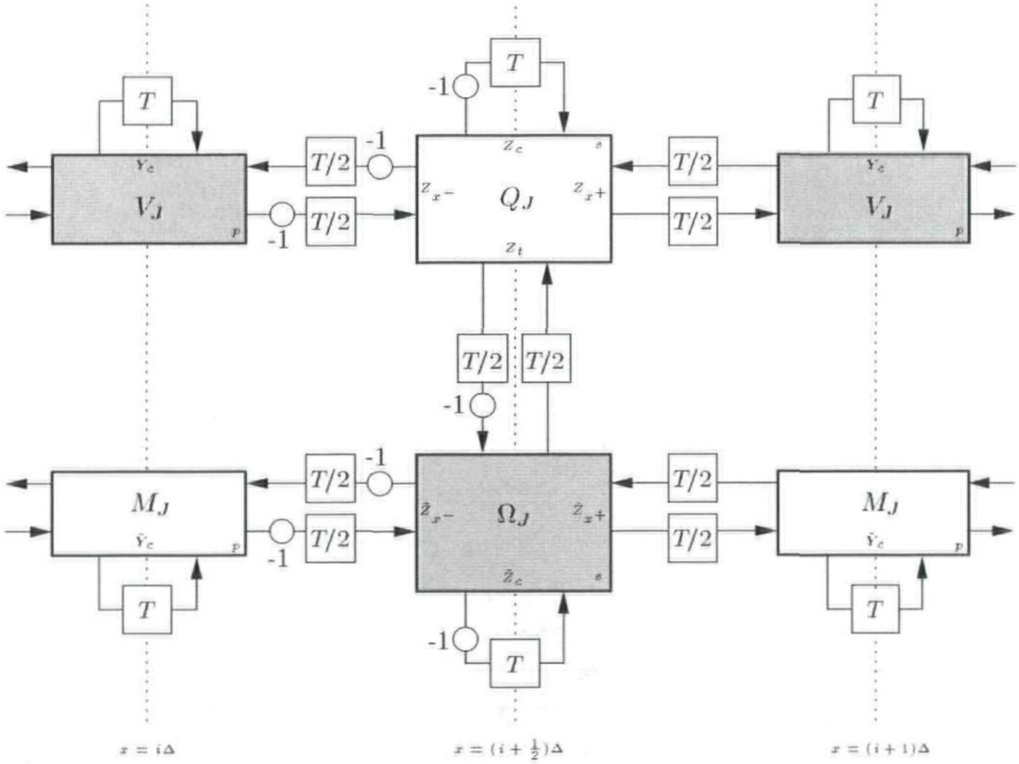

Figure 5.11: *Another alternate DWN for Timoshenko's system.*

lines. Before we begin setting the immittances values, however, we must comment on the coupling waveguides which run between the parallel junctions which calculate $Q_J$ and $\Omega_J$; each such waveguide has a non-reciprocal character (as evidenced by the sign inversion in only one of the two signal paths). We have left the admittance of this coupling waveguide independent of position. The reason for this is seen from the difference equations in the junction variables. For example, in the configuration of Figure 5.11, we have, after following through familiar manipulations,

$$Q_{J,i+\frac{1}{2}}(n+\tfrac{1}{2}) = Q_{J,i+\frac{1}{2}}(n-\tfrac{1}{2}) + \frac{2}{Z_{J,i+\frac{1}{2}}}\Big(V_{J,i+1}(n) - V_{J,i}(n) - Z_t\Omega_{J,i+\frac{1}{2}}(n)\Big)$$

which will approximate (5.17b) only if $Z_t = \Delta$. The same statement is true of the other configuration as well (where the admittance of each coupling waveguide is set to $Z_t/2$).

It is convenient to set the immittances such that the self-loops at the parallel junctions (recall the transmission line) can be dropped entirely from the calculation; in fact, in this lossless case, we can drop the explicit calculation of $V_J$ and $M_J$ altogether if we wish, since when the self-loops at these junctions disappear, we are left with simple "through" junctions which do not scatter (recall Figure 4.14). Eventually, though, we may wish to have access to this variable because it is indeed the time derivative of $w$, the primary dependent variable of interest. We thus set

$$Z_{x^-,i+\frac{1}{2}} = Z_{x^+,i-\frac{1}{2}} = \frac{1}{v_0\rho_iA_i} \qquad \tilde{Z}_{x^-,i+\frac{1}{2}} = \tilde{Z}_{x^+,i-\frac{1}{2}} = \frac{E_iI_i}{v_0} \qquad Z_{t,i+\frac{1}{2}} = \tilde{Z}_{t,i+\frac{1}{2}} = \Delta$$

and

$$\begin{aligned} Z_{c,i+\frac{1}{2}} &= \frac{v_0}{(AG\kappa)_i} + \frac{v_0}{(AG\kappa)_{i+1}} - \frac{1}{v_0\rho_iA_i} - \frac{1}{v_0\rho_{i+1}A_{i+1}} - \Delta \\ \tilde{Z}_{c,i+\frac{1}{2}} &= v_0(\rho I)_i + v_0(\rho I)_{i+1} - \frac{(EI)_i}{v_0} - \frac{(EI)_{i+1}}{v_0} - \Delta \end{aligned}$$

It is quite interesting to examine the positivity conditions on the self-loop admittances. For example, $Z_{c,i+\frac{1}{2}}$ will be positive if, for all integer $i$, we have

$$\frac{v_0}{(AG\kappa)_i} - \frac{1}{v_0(\rho A)_i} - \frac{\Delta}{2} \geq 0$$

which, using $v_0 = \Delta/T$, is equivalent to

$$\Delta^2\left(\frac{1}{(AG\kappa)_i} - \frac{T}{2}\right) \geq \frac{T^2}{(\rho A)_i}$$

It is easy to see that, in contrast to the stability conditions we derived for the various transmission lines, for the ideal beam, and for Timoshenko's system in §5.2.1, for a passive realization there is now a *maximum time step* for the scheme regardless of the spatial step. That is, the above condition can be true only when

$$T \leq \min_i \frac{2}{(AG\kappa)_i}$$

Assuming that this condition is met, we then must have

$$\Delta \geq T\max_i\sqrt{\frac{1}{(\frac{\rho}{G\kappa})_i - \frac{T(\rho A)_i}{2}}}$$

A positivity requirement on $\tilde{Z}_{c,i}$ yields a similar set of conditions,

$$T \leq \min_i\,(2\rho I)_i \qquad \text{and} \qquad \Delta \geq T\max_i\sqrt{\frac{(EI)_i}{(\rho I)_i - \frac{T}{2}}}$$

In the limit as $T$ becomes small, both conditions on the spatial step size $\Delta$ approach conventional CFL-type bounds (recall the wave speeds implied by Timoshenko's system, mentioned in the beginning of this section); both must be satisfied for the waveguide network to be *concretely passive*, though they may be stable in the Von Neumann sense (see Appendix A). It would appear that the special character of these passivity conditions on the scheme are the direct result of the approximation of the memoryless asymmetric line coupling by a reactive waveguide coupling.

### 5.2.4 Boundary Conditions in the DWN

The three common types of boundary conditions used to terminate a Timoshenko beam are similar to the classical beam conditions [146] which were discussed in §5.1.3.

$$w = m = 0 \qquad \text{Fixed end, allowed to pivot} \qquad (5.25a)$$

$$w = \psi = 0 \qquad \text{Fixed clamped end} \qquad (5.25b)$$

$$q = m = 0 \qquad \text{Free end} \qquad (5.25c)$$

All of these conditions are of the form of (3.8), and are lossless.

There are several possibilities for the implementation of these boundary conditions (5.25) at a boundary grid point in the MDWD network or any of the mentioned DWN structures. Through simulation, we have determined that the use of reflection-canceling waves at the boundary, as per the method of [107], does *not* lead to a passive termination. This statement also holds for the termination of the plate and shell models that we will discuss shortly; violent instabilities may appear in these systems, even though the termination of the simpler transmission line and parallel-plate networks by this method is not problematic. At present, the termination of a MDWD network is very poorly understood, even by experts [115]. Indeed, as we mentioned in §3.11, there is not, as yet, a general theory of boundary termination of MDWD networks [142]. We refer to §6.2.3 for a discussion of a possible avenue of approach.

For this reason, we decided to retreat from this problem, and work with the termination of the DWN, in its conventional lumped form. When a network is viewed in this way, it is much simpler to see how boundary conditions may be set such that passivity may be maintained. The difficulty in working with the expanded signal flow diagram for a MDWD network is that unlike the DWN, there is no port structure in this case; in the DWN, applying lumped terminations to junctions on the boundary is straightforward.

Because we looked at the termination of the (1+1)D transmission line, (2+1)D parallel-plate and Euler-Bernoulli systems in this way in §4.3.9, §4.4.4 and §5.1.3 respectively, we simply present the terminations corresponding to boundary conditions (5.25). We have chosen here to work with the DWN shown in Figure 5.9, although the termination of the networks of Figures 5.10 and 5.11 is equally simple. In addition, we align the parallel junctions (at which $V_J$ and $M_J$ are calculated) with the left end point (say) of the beam, located at $x = 0$. In this way, we avoid the slight additional complication of the coupling that occurs if the series junctions are placed at the boundary (though we will be forced to face this issue when we set boundary conditions in the Mindlin plate network in §5.4.2). The three terminations are shown in Figure 5.12.

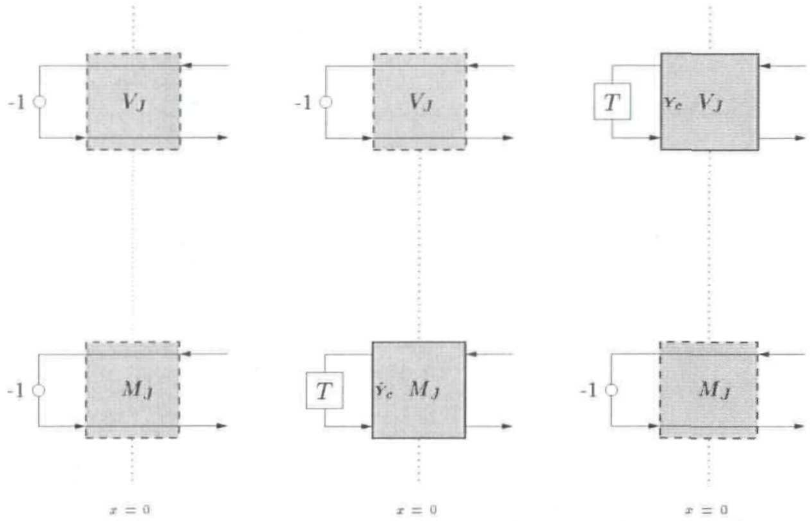

(a) (b) (c)

Figure 5.12: *Boundary terminations for the DWN for Timoshenko's system*—(a) *fixed end, allowed to pivot,* (b) *fixed clamped end, and* (c) *free end.*

A condition $w = 0$ (implying $v = 0$) or $m = 0$ is easily implemented by short-circuiting the appropriate junction. For the condition $\psi = 0$, it is easy to show that we should choose the self-loop admittance to be $\tilde{Y}_c = v_0/(EI) - 1/r_2$ at the terminating junction at which $M_J$ is calculated. Similarly, for the condition $q = 0$, we should choose $Y_c = v_0\rho A - 1/r_1$ at the junction at which $V_J$ is calculated.

### 5.2.5 Simulation: Timoshenko's System for Beams of Uniform and Varying Cross-sectional Areas

We present here some two simple DWN simulations of the Timoshenko beam equations. In both cases, we have made use of the DWN of Figure 5.9, which was derived directly from an MDKC (shown in Figure 5.7). We simulate the behavior of a square prismatic steel beam, of length $L = 1$m, under the application of an initial transverse velocity distribution at the beam center which has the form of one period of a raised cosine, of wavelength 5cm and amplitude 0.0005 m/s. In the first simulation, the beam is assumed to have a uniform thickness of 2 cm, and the boundary conditions are of the free type at either end; the evolution of the velocity distribution is shown in Figure 5.13. In the second simulation, the beam is assumed to be of linearly-varying thickness, from 1 cm at the left end to 3 cm

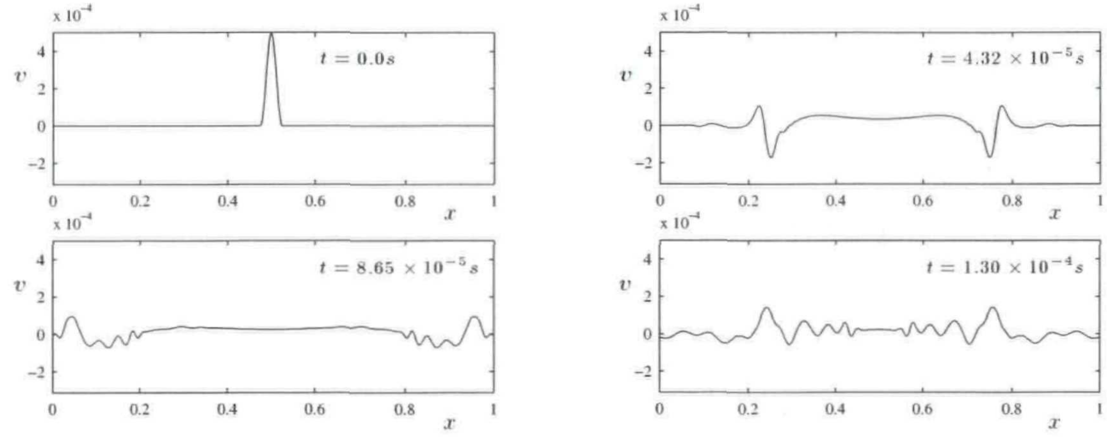

Figure 5.13: *Simulation: evolution of the transverse velocity distribution along a Timoshenko beam of uniform thickness, with free ends.*

at the right end. The area $A$ thus varies quadratically, and the moment of inertia quartically. In this second case (shown in Figure 5.14), the boundary conditions are assumed clamped. The material parameters for steel are taken to be $\rho = 5.38\times10^4\text{kg/m}^3$, $E = 1.4\times10^{12}\text{N/m}^2$, $G = 5.39\times10^{11}\text{N/m}^2$, and Timoshenko's coefficient for a beam of square cross-section is $\kappa = 5/6$ [83]. In both simulations, we operate using a grid spacing of $1/400$ m, and the time step is chosen to be at the passivity limit. From (5.24), and given the above values of the material parameters of the beam, $v_0$ is chosen to be $5.1\times10^3$ m/s for the uniform beam, and $4.59\times10^4$ m/s for the beam of varying thickness.

In both simulations, it is easy to see that due to dispersion, the coherence of the initial velocity

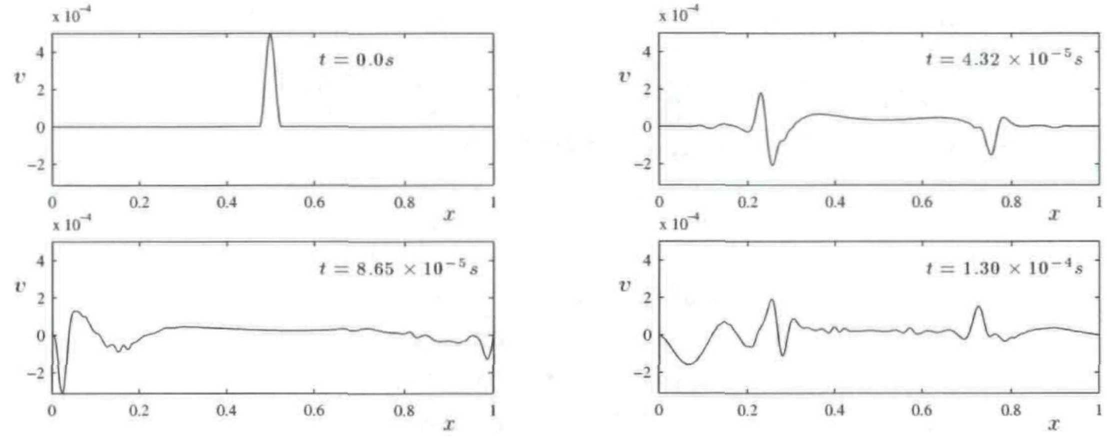

Figure 5.14: *Simulation: evolution of the transverse velocity distribution along a Timoshenko beam of linearly-varying thickness, with clamped ends.*

distribution is lost; short wavelengths tend to move faster (and hence reflect first from the boundary), as can be seen in the plot at $t = 8.65 \times 10^{-5}$s. In the beam with linearly-varying thickness, velocities are amplified in the thin region of the beam, and attenuated in the thick region; the propagation velocities themselves, however, are not significantly altered.

### 5.2.6 Improved MDKC for Timoshenko's System Via Balancing

In the preceding simulation of the steel beam of rectangular cross-section and linearly-varying thickness, we have, from (5.24), $v_0 = 4.59 \times 10^4$; the time step is thus restricted to be quite small. We will now show how the balancing or preconditioning approach applied to the (1+1)D transmission line problem in §3.12 can be used to drastically increase the maximum allowable time step for a given grid spacing.

Suppose we scale the dependent variables according to

$$v = r_1 i_1 \qquad q = r_2 i_2 \qquad \omega = r_3 i_3 \qquad m = r_4 i_4$$

and allow the scaling parameters $r_1, \ldots, r_4$ to be arbitrary smooth functions of $x$. Timoshenko's system (5.17)–(5.18) can then be rewritten as

$$\begin{aligned}
v_0 \left(\frac{r_1}{r_2}\right) \rho A \frac{\partial i_1}{\partial t'} &= \frac{\partial i_2}{\partial x} + \frac{r_2'}{r_2} i_2 && (5.26a)\\
v_0 \left(\frac{r_2}{r_1}\right) \frac{1}{A\kappa G} \frac{\partial i_2}{\partial t'} &= \frac{\partial i_1}{\partial x} + \frac{r_1'}{r_1} i_1 - \frac{r_3}{r_1} i_3 && (5.26b)\\
v_0 \left(\frac{r_3}{r_4}\right) \rho I \frac{\partial i_3}{\partial t'} &= \frac{\partial i_4}{\partial x} + \frac{r_4'}{r_4} i_4 + \frac{r_2}{r_4} i_2 && (5.26c)\\
v_0 \left(\frac{r_4}{r_3}\right) \frac{1}{EI} \frac{\partial i_4}{\partial t'} &= \frac{\partial i_3}{\partial x} + \frac{r_3'}{r_3} i_3 && (5.26d)
\end{aligned}$$

where primes above the $r_i$, $i = 1, \ldots, 4$ indicate $x$-differentiation. If we choose:

$$r_1 = \left(\rho A^2 G\kappa\right)^{-\frac{1}{4}} \qquad r_2 = \left(\rho A^2 G\kappa\right)^{\frac{1}{4}} \qquad r_3 = \left(\rho E I^2\right)^{-\frac{1}{4}} \qquad r_4 = \left(\rho E I^2\right)^{\frac{1}{4}} \qquad (5.27)$$

Then system (5.26) becomes

$$\begin{aligned}
v_0 \sqrt{\frac{\rho}{G\kappa}} \frac{\partial i_1}{\partial t'} &= \frac{\partial i_2}{\partial x} + \frac{r_2'}{r_2} i_2 && (5.28a)\\
v_0 \sqrt{\frac{\rho}{G\kappa}} \frac{\partial i_2}{\partial t'} &= \frac{\partial i_1}{\partial x} - \frac{r_2'}{r_2} i_1 - \frac{r_3}{r_1} i_3 && (5.28b)\\
v_0 \sqrt{\frac{\rho}{E}} \frac{\partial i_3}{\partial t'} &= \frac{\partial i_4}{\partial x} + \frac{r_4'}{r_4} i_4 + \frac{r_2}{r_4} i_2 && (5.28c)\\
v_0 \sqrt{\frac{\rho}{E}} \frac{\partial i_4}{\partial t'} &= \frac{\partial i_3}{\partial x} - \frac{r_4'}{r_4} i_3 && (5.28d)
\end{aligned}$$

and the constant-proportional terms appear anti-symmetrically (note, from (5.27), that $r_2/r_4 = r_3/r_1$). In the MDKC shown in Figure 5.15, these terms are all interpreted as gyrator couplings, where the gyrator coefficients are spatially varying. It is easy to check that this system is still symmetric hyperbolic according to definition (3.1).

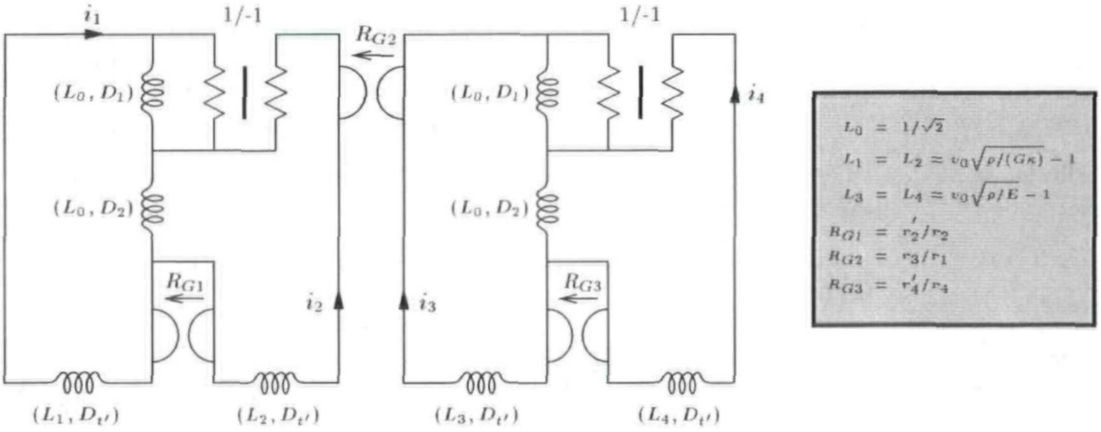

$$\begin{aligned} L_0 &= 1/\sqrt{2} \\ L_1 &= L_2 = v_0\sqrt{\rho/(G\kappa)} - 1 \\ L_3 &= L_4 = v_0\sqrt{\rho/E} - 1 \\ R_{G1} &= r_2'/r_2 \\ R_{G2} &= r_3/r_1 \\ R_{G3} &= r_4'/r_4 \end{aligned}$$

Figure 5.15: *Balanced MDKC for Timoshenko's system.*

The MDWD network (not shown) implied by the MDKC will be slightly more difficult to program, because of the additional reflection-free ports which will necessarily be introduced, but it has the same memory requirements, and the operation count is slightly larger (due chiefly to the post-scaling of the MDKC currents which must now be performed in order to obtain the physical dependent variables). We now have, however, that

$$v_0 \geq \max\left(\max_{x\in\mathcal{D}}\sqrt{\frac{E}{\rho}}, \max_{x\in\mathcal{D}}\sqrt{\frac{G\kappa}{\rho}}\right) = \gamma^g_{T,max}$$

where $\gamma^g_{T,max}$ is the maximum group velocity given in (5.20). $v_0$ is now optimal (in the CFL sense), for a constant grid spacing. Referring to the simulation of §5.2.5, it is easy to see that that due to the quartic dependence of the moment of inertia $I$ on $x$ (for a beam of linearly varying thickness), the maximum time step allowed by the previous approach (also the maximum time step allowed in [131]) will be severely constrained. Using a balanced formulation and MDKC, we now have $v_0 = 5.10 \times 10^3$. Thus for a given grid spacing, the maximum time step is now 9 times larger. From a practical standpoint, this is a huge computational advantage.

We repeat that balancing is unnecessary if there is no spatial variation in the problem parameters, and that in a region of the material for which the parameters do not vary, we may simply drop the additional gyrator couplings $R_{G1}$ and $R_{G3}$ from the network entirely. We also note that it is possible to incorporate the scaling of the dependent variables into the MDKC itself by introducing transformers with turn ratios $r_1, \ldots, r_4$ in all the circuit loops; while useful for showing the MD-passivity of the system under scaling, there is no practical reason for doing so.

## 5.3 Longitudinal and Torsional Waves in Rods

In addition to transverse waves, a one-dimensional stiff medium can support *longitudinal* and *torsional* waves [66, 77]. In these cases, the medium is usually referred to as a *rod* or *bar* instead of a beam [83, 146].

When a bar aligned with the $x$-axis is vibrating longitudinally, motion within the medium will only occur in the $x$ direction. If $u(x,t)$ represents the longitudinal displacement of the medium at position $x$ and time $t$, the equation of motion of the bar [146] is

$$\rho A \frac{\partial^2 u}{\partial t^2} = \frac{\partial}{\partial x}\left(EA\frac{\partial u}{\partial x}\right) \tag{5.29}$$

which is easily identified the second-order equation describing the behavior of current or voltage in the (1+1)D transmission line, as per (4.39). Thus all methods applicable to the (1+1)D transmission line discussed in this work are applicable to this case as well. Note that in the case of constant material parameters and cross-sectional area, (5.29) becomes the (1+1)D wave equation, and thus longitudinal waves travel non-dispersively (in contrast to transverse waves). Here, lateral inertia effects have been neglected—that is, even though the medium undergoes axial compression and expansion, the bar is not allowed to compensate for this by becoming "fatter" or "thinner" respectively. The so-called *Love theory* [77] is an attempt to account for this important effect; it should be possible to apply scattering-based numerical methods to the Love theory, although we have not attempted to do so.

Torsional motion involves the propagation of a twisting disturbance along the length of the bar. For a bar of constant cross-section, the equation of motion here is

$$\rho J \frac{\partial^2 \theta}{\partial t^2} = C\frac{\partial^2 \theta}{\partial x^2}$$

where $\theta(x,t)$ is the angle at which the bar is twisted relative to its equilibrium state, $J$ is the polar moment of inertia, and $C$ is a constant which depends on the geometry of the cross section [77]. Here again, we have the basic (1+1)D transmission line form, and the comments made regarding longitudinal waves apply equally well here.

## 5.4 Plates

The equations of motion of a stiff plate are the (2+1)D generalization of those of a beam. We assume the plate to lie, when at rest, in the $(x,y)$ plane, and to be of thickness $h(x,y)$; the deflection $w(x,y)$ of the plate from its equilibrium state is assumed to be perpendicular to the $(x,y)$ plane. The plate material has density $\rho$, as well as Young's modulus $E$ and Poisson's ratio $\nu$, all of which are assumed, for the sake of generality, to be smooth positive functions of $x$ and $y$. In particular, $\nu$ must be less than one-half. The classical development depends on neglecting rotational inertia effects and makes various assumptions analogous to the "plane sections remain plane and perpendicular to the neutral axis" hypothesis that was used as the basis for the Euler-Bernoulli beam model [77]. The resulting equation of motion [6, 113] can be written as

$$\rho h\frac{\partial^2 w}{\partial t^2} \quad = \quad -\nabla^2\left(D\nabla^2 w\right)+(1-\nu)\left(\frac{\partial^2 D}{\partial x^2}\frac{\partial^2 w}{\partial y^2}-2\frac{\partial^2 D}{\partial x\partial y}\frac{\partial^2 w}{\partial x\partial y}+\frac{\partial^2 D}{\partial y^2}\frac{\partial^2 w}{\partial x^2}\right)$$

where

$$D=\frac{Eh^3}{12(1-\nu^2)}$$

and used $\nabla^2=\frac{\partial^2}{\partial x^2}+\frac{\partial^2}{\partial y^2}$. If the material parameters and the thickness are constant, then

$$\frac{\partial^2 w}{\partial t^2}=-\frac{D}{\rho h}\nabla^2\nabla^2 w \tag{5.30}$$

which is easily seen to be a direct generalization of (5.2). As such, we expect to find the same anomalous behavior of the resulting propagation velocities, which can become infinitely large in the high-frequency limit. Numerical integration of these equations via a waveguide mesh proceeds along exactly the same lines as in the case of the Euler-Bernoulli beam; in particular, we find a restriction on the space step/time step ratio similar to those that resulted in §5.1.2.

Because the development is so similar to the (1+1)D case, we will proceed directly to the more refined model of plate motion, which is a direct generalization of the Timoshenko theory for beams. First proposed by Mindlin, the model [77, 120], can be written as system of eight PDEs [173]:

$$\begin{aligned}
\rho h\frac{\partial v}{\partial t} &= \frac{\partial q_x}{\partial x}+\frac{\partial q_y}{\partial y} && \text{(5.31a)}\\
\frac{1}{\kappa^2 Gh}\frac{\partial q_x}{\partial t} &= \frac{\partial v}{\partial x}+\omega_x && \text{(5.31b)}\\
\frac{1}{\kappa^2 Gh}\frac{\partial q_y}{\partial t} &= \frac{\partial v}{\partial y}+\omega_y && \text{(5.31c)}
\end{aligned}$$

$$\begin{aligned}
\frac{\rho h^3}{12}\frac{\partial \omega_x}{\partial t} &= \frac{\partial m_x}{\partial x}+\frac{\partial m_{xy}}{\partial y}-q_x && \text{(5.32a)}\\
\frac{\rho h^3}{12}\frac{\partial \omega_y}{\partial t} &= \frac{\partial m_{xy}}{\partial x}+\frac{\partial m_y}{\partial y}-q_y && \text{(5.32b)}\\
\frac{1}{D}\frac{\partial m_x}{\partial t} &= \frac{\partial \omega_x}{\partial x}+\nu\frac{\partial \omega_y}{\partial y} && \text{(5.32c)}\\
\frac{1}{D}\frac{\partial m_y}{\partial t} &= \frac{\partial \omega_y}{\partial y}+\nu\frac{\partial \omega_x}{\partial x} && \text{(5.32d)}\\
\frac{2}{D(1-\nu)}\frac{\partial m_{xy}}{\partial t} &= \frac{\partial \omega_y}{\partial x}+\frac{\partial \omega_x}{\partial y} && \text{(5.32e)}
\end{aligned}$$

Here, we have written

$$\omega_x=\frac{\partial \psi_x}{\partial t} \qquad \omega_y=\frac{\partial \psi_y}{\partial t} \qquad v=\frac{\partial w}{\partial t}$$

where $w$ is the transverse displacement of the plate, and $(\psi_x, \psi_y)$ is the pair of angles giving the orientation of the sides of a deformed differential element of the plate with respect to the perpendicular. (In the classical theory, for which cross-sections of the plate are assumed to remain parallel to the plate normal, we have $(\psi_x, \psi_y) = (-\frac{\partial w}{\partial x}, -\frac{\partial w}{\partial y})$.) In addition, we have the shear forces $(q_x, q_y)$ and moments $(m_x, m_y, m_{xy})$, which are the (2+1)D generalizations of $q$ and $m$. The system (5.31)–(5.32) as a whole is known as *Mindlin's system*, although it is more commonly written s a system of three second-order equations in the variables $w$, $\psi_x$ and $\psi_y$ [77]. We have written Mindlin's system so that it is easy to see the decomposition into two separate subsystems, one in $(v, q_x, q_y)$ and the other in $(\omega_x, \omega_y, m_x, m_y, m_{xy})$, with the coupling occurring via constant-proportional terms in $\omega_x$, $\omega_y$, $q_x$ and $q_y$. In particular, subsystem (5.31) is similar to the lossless parallel-plate system (see §4.4), except for the coupling terms.

It is easy to see that this system is not, as written, symmetric hyperbolic. It is easy to symmetrize it by taking sums and differences of (5.32c) and (5.32d), in which case we get, in terms of the variable $\mathbf{w} = [v, q_x, q_y, \omega_x, \omega_y, m_x, m_y, m_{xy}]^T$,

$$\mathbf{P} = \mathbf{P}_M = \begin{bmatrix} \mathbf{P}_M^+ & \cdot \\ \cdot & \mathbf{P}_M^- \end{bmatrix} \quad \mathbf{A}_1 = \mathbf{A}_{M1} = \begin{bmatrix} \mathbf{A}_{M1}^+ & \cdot \\ \cdot & \mathbf{A}_{M1}^- \end{bmatrix} \quad \mathbf{A}_2 = \mathbf{A}_{M2} = \begin{bmatrix} \mathbf{A}_{M2}^+ & \cdot \\ \cdot & \mathbf{A}_{M2}^- \end{bmatrix}$$
$$\mathbf{B} = \mathbf{B}_M = \begin{bmatrix} \cdot & \mathbf{B}_{M\times} \\ -\mathbf{B}_{M\times}^T & \cdot \end{bmatrix} \tag{5.33}$$

where the $\cdot$ stands for zero entries, and

$$\mathbf{P}_M^+ = \begin{bmatrix} \rho h & 0 & 0 \\ 0 & \frac{1}{\kappa^2 Gh} & 0 \\ 0 & 0 & \frac{1}{\kappa^2 Gh} \end{bmatrix} \qquad \mathbf{P}_M^- = \begin{bmatrix} \frac{\rho h^3}{12} & 0 & 0 & 0 & 0 \\ 0 & \frac{\rho h^3}{12} & 0 & 0 & 0 \\ 0 & 0 & \frac{12}{Eh^3} & \frac{-12\nu}{Eh^3} & 0 \\ 0 & 0 & \frac{-12\nu}{Eh^3} & \frac{12}{Eh^3} & 0 \\ 0 & 0 & 0 & 0 & \frac{2}{D(1-\nu)} \end{bmatrix}$$

$$\mathbf{A}_{M1}^+ = \begin{bmatrix} 0 & -1 & 0 \\ -1 & 0 & 0 \\ 0 & 0 & 0 \end{bmatrix} \qquad \mathbf{A}_{M1}^- = \begin{bmatrix} 0 & 0 & -1 & 0 & 0 \\ 0 & 0 & 0 & 0 & -1 \\ -1 & 0 & 0 & 0 & 0 \\ 0 & 0 & 0 & 0 & 0 \\ 0 & -1 & 0 & 0 & 0 \end{bmatrix} \tag{5.34}$$

$$\mathbf{A}_{M2}^+ = \begin{bmatrix} 0 & 0 & -1 \\ 0 & 0 & 0 \\ -1 & 0 & 0 \end{bmatrix} \qquad \mathbf{A}_{M2}^- = \begin{bmatrix} 0 & 0 & 0 & 0 & -1 \\ 0 & 0 & 0 & -1 & 0 \\ 0 & 0 & 0 & 0 & 0 \\ 0 & -1 & 0 & 0 & 0 \\ -1 & 0 & 0 & 0 & 0 \end{bmatrix} \tag{5.35}$$

$$\mathbf{B}_{M\times} = \begin{bmatrix} 0 & 0 & 0 & 0 & 0 \\ -1 & 0 & 0 & 0 & 0 \\ 0 & -1 & 0 & 0 & 0 \end{bmatrix}$$

The system defined by (5.33) is lossless, due to the anti-symmetry of $\mathbf{B}_M$. Also, note that $\mathbf{P}_M$ is positive definite (recall that $\nu$ is positive, and less than one-half), but not diagonal[†]; this did not come up in any of the systems we have looked at previously, and will have interesting consequences in the circuit representations in the next section.

### Maximum Group Velocity

For the constant coefficient problem, the characteristic polynomial relating frequencies $\omega$ to spatial wavenumber $\|\beta\|_2 = \sqrt{\beta_x^2 + \beta_y^2}$, from (3.10), will be

$$\left(\omega^4 - \frac{\omega^2}{\rho}\left(\frac{12\kappa^2 G}{h^2} + \|\beta\|_2^2\left(\frac{E}{1-\nu^2} + G\kappa^2\right)\right) + \frac{E\kappa^2 G}{\rho^2(1-\nu^2)}\|\beta\|_2^4\right)\left(\omega^2 - \frac{G}{\rho}\|\beta\|_2^2 - \frac{12G\kappa^2}{\rho h^2}\right)\omega^2 = 0$$

The first factor, which is similar in form to that which defines the Timoshenko system, from (5.19), has four roots, $\omega_{1\pm}$, $\omega_{2\pm}$ which behave as

$$\lim_{\|\beta\|_2\to\infty} \omega_{1\pm} = \pm\|\beta\|_2\sqrt{\frac{E}{\rho(1-\nu^2)}} \qquad \lim_{\|\beta\|_2\to\infty} \omega_{2\pm} = \pm\|\beta\|_2\sqrt{\frac{G\kappa^2}{\rho}}$$

and the second factor has a pair of roots $\omega_{3\pm}$, which have the limiting behavior

$$\lim_{\|\beta\|_2\to\infty} \omega_{3\pm} = \pm\|\beta\|_2\sqrt{\frac{G}{\rho}}$$

All phase and group velocities are thus bounded. For the varying-coefficient problem, the maximum global group velocity will be

$$\gamma^g_{M,max} = \max_{\mathbf{x}\in\mathcal{D}} \sqrt{\frac{E}{\rho(1-\nu^2)}}$$

---

[†] It is possible to write a symmetric hyperbolic form of Mindlin's system for which the $\mathbf{P}$ matrix is diagonal by introducing the variables $m_1 = (m_x + m_y)/2$ and $m_2 = (m_x - m_y)/2$. Though the resulting MDKC will be simpler, boundary conditions become over-determined and difficult to set properly, because $\mathbf{A}_1$ and $\mathbf{A}_2$ are consequently less sparse (implying greater network connectivity). The form described by the matrices in (5.33) is more fundamental in this respect.

### 5.4.1 MDKCs and Scattering Networks for Mindlin's System

We now introduce scaled dependent variables

$$(i_1, i_2, i_3, i_4, i_5, i_6, i_7, i_8) = (r_1 v, q_x, q_y, \omega_x, \omega_y, r_2 m_x, r_2 m_y, r_3 m_{xy})$$

where again, $r_1$, $r_2$ and $r_3$ are positive constants, as well as the scaled time variable $t' = v_0 t$. The MD-passive circuit representation of Mindlin's system is shown in Figure 5.16, where we have used the coordinates defined by (3.21) with the transformation matrix (3.22). Here, the port with terminals $A$ and $A'$ is assumed to be short-circuited (we will return to this port in §5.5.2). It is best to view this as a three-loop network (on the left, in Figure 5.16) corresponding to the subsystem (5.31), coupled to a five-loop network on the right (subsystem (5.32)).

Because $\mathbf{P}_M$ from (5.33) is not diagonal, the coupling between the loops with currents $i_6$ and $i_7$ (corresponding to the moments $m_x$ and $m_y$) is of a type not previously encountered in the systems examined in this thesis. It can be interpreted in terms a coupled inductance between the loops (see §2.3.7); in Figure 5.16, self-inductances are indicated by directed arrows, and mutual inductance by bidirectional arrows. The element values are as indicated in the figure.

Optimal choices of $r_1$, $r_2$ and $r_3$, and the optimal stability bound on $v_0$ are a little more difficult to find in this case. As before, however, they follow from a positivity requirement on the inductance values defined in Figure 5.16. This requirement is simply applied to $L_1$, $L_2$, $L_3$, $L_4$, $L_5$ and $L_8$, but $L_6$ and $L_7$ define a coupled inductance between the loops with currents $i_6$ and $i_7$. The coupling matrix will be

$$\begin{bmatrix} L_6 & L_7 \\ L_7 & L_6 \end{bmatrix}$$

and is required to be positive semi-definite for passivity. This is true if

$$L_6 \geq |L_7| \tag{5.36}$$

An optimal choice for $r_1$ is easily shown to be

$$r_1 = \sqrt{\frac{2}{\min_{x,y}(\rho h)\max_{x,y}(\kappa^2 G h)}} \tag{5.37}$$

and gives a first bound on $v_0$, which is

$$v_0 \geq v_{M^+} \triangleq \sqrt{\frac{2\max_{x,y}(\kappa^2 G h)}{\min_{x,y}(\rho h)}} \tag{5.38}$$

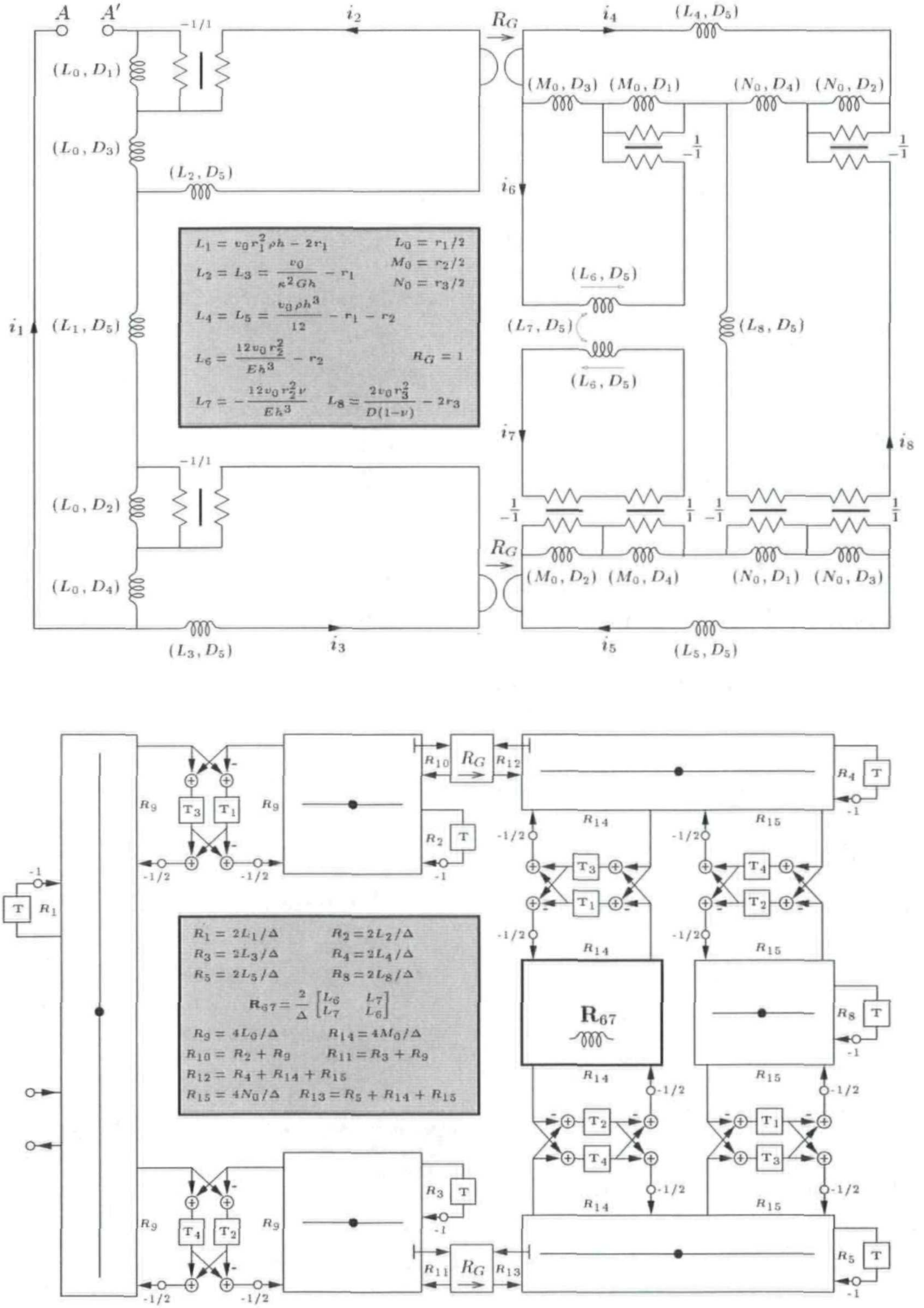
$A$
$A'$
$-1/1$
$i_1$
$i_2$
$i_3$
$i_4$
$i_5$
$i_6$
$i_7$
$i_8$
$R_G$
$(L_0, D_1)$
$(L_0, D_3)$
$(L_0, D_2)$
$(L_0, D_4)$
$(L_1, D_5)$
$(L_2, D_5)$
$(L_3, D_5)$
$(L_4, D_5)$
$(L_5, D_5)$
$(L_6, D_5)$
$(L_7, D_5)$
$(L_8, D_5)$
$(M_0, D_3)$
$(M_0, D_1)$
$(M_0, D_2)$
$(M_0, D_4)$
$(N_0, D_4)$
$(N_0, D_2)$
$(N_0, D_1)$
$(N_0, D_3)$
$\frac{1}{-1}$
$L_1 = v_0 r_1^2 \rho h - 2r_1$
$L_0 = r_1/2$
$L_2 = L_3 = \frac{v_0}{\kappa^2 G h} - r_1$
$M_0 = r_2/2$
$N_0 = r_3/2$
$L_4 = L_5 = \frac{v_0 \rho h^3}{12} - r_1 - r_2$
$L_6 = \frac{12 v_0 r_2^2}{E h^3} - r_2$
$R_G = 1$
$L_7 = -\frac{12 v_0 r_2^2 \nu}{E h^3}$
$L_8 = \frac{2 v_0 r_3^2}{D(1-\nu)} - 2r_3$
T
$T_1$
$T_2$
$T_3$
$T_4$
$R_1$
$R_2$
$R_3$
$R_4$
$R_5$
$R_8$
$R_9$
$R_{10}$
$R_{11}$
$R_{12}$
$R_{13}$
$R_{14}$
$R_{15}$
$\mathbf{R}_{67}$
-1
-1/2
$R_1 = 2L_1/\Delta$
$R_2 = 2L_2/\Delta$
$R_3 = 2L_3/\Delta$
$R_4 = 2L_4/\Delta$
$R_5 = 2L_5/\Delta$
$R_8 = 2L_8/\Delta$
$\mathbf{R}_{67} = \frac{2}{\Delta}\begin{bmatrix} L_6 & L_7 \\ L_7 & L_6 \end{bmatrix}$
$R_9 = 4L_0/\Delta$
$R_{14} = 4M_0/\Delta$
$R_{10} = R_2 + R_9$
$R_{11} = R_3 + R_9$
$R_{12} = R_4 + R_{14} + R_{15}$
$R_{15} = 4N_0/\Delta$
$R_{13} = R_5 + R_{14} + R_{15}$

Figure 5.16: *MDKC and MDWD network for Mindlin's system.*

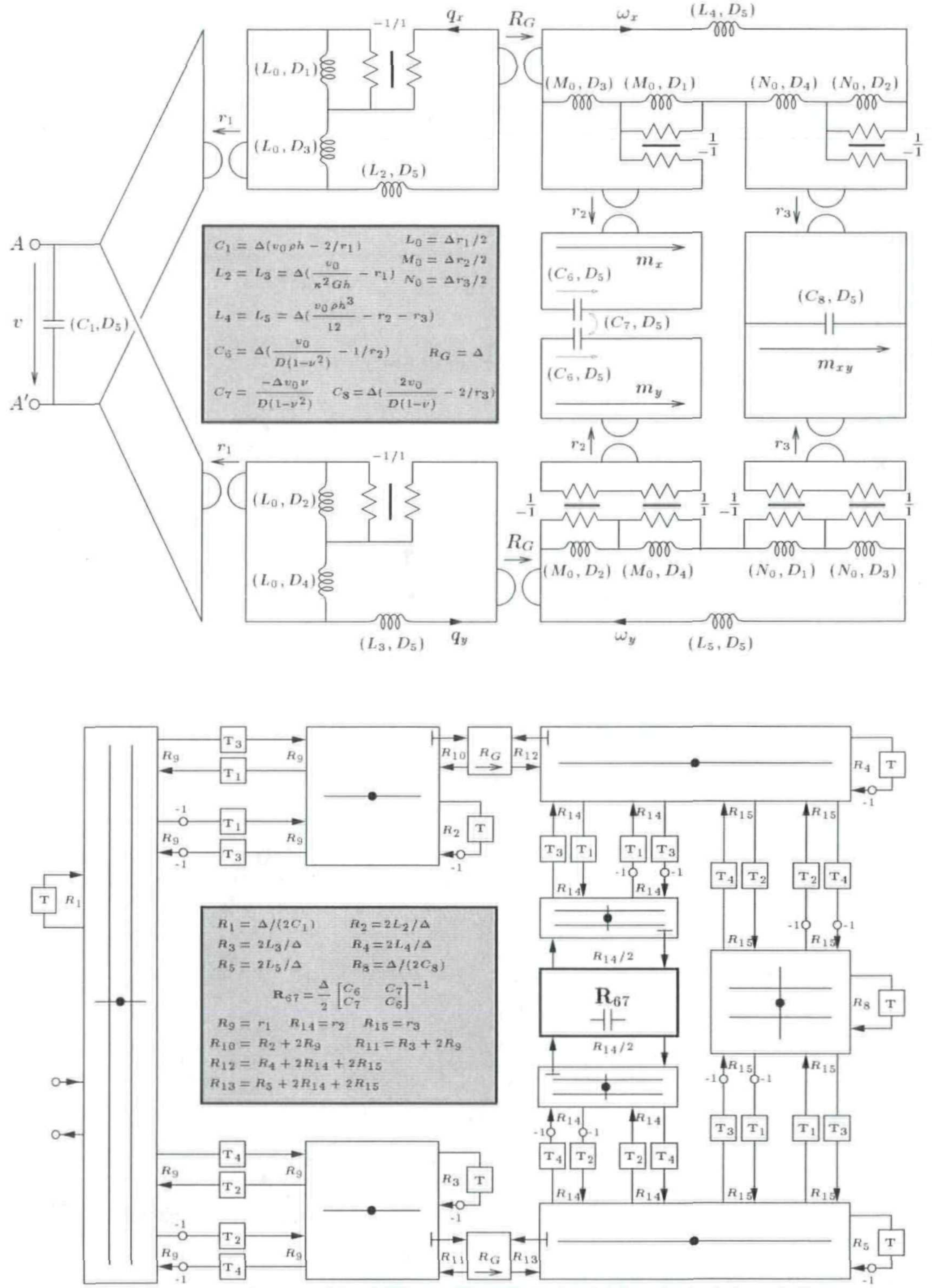
$q_x$
$R_G$
$\omega_x$
$(L_4, D_5)$
$-1/1$
$(L_0, D_1)$
$(L_0, D_3)$
$(L_2, D_5)$
$r_1$
$(M_0, D_3)$
$(M_0, D_1)$
$(N_0, D_4)$
$(N_0, D_2)$
$r_2$
$r_3$
$A$
$v$
$(C_1, D_5)$
$A'$
$C_1 = \Delta(v_0 \rho h - 2/r_1)$
$L_0 = \Delta r_1/2$
$M_0 = \Delta r_2/2$
$L_2 = L_3 = \Delta(\frac{v_0}{\kappa^2 G h} - r_1)$
$N_0 = \Delta r_3/2$
$L_4 = L_5 = \Delta(\frac{v_0 \rho h^3}{12} - r_2 - r_3)$
$C_6 = \Delta(\frac{v_0}{D(1-\nu^2)} - 1/r_2)$
$R_G = \Delta$
$C_7 = \frac{-\Delta v_0 \nu}{D(1-\nu^2)}$
$C_8 = \Delta(\frac{2 v_0}{D(1-\nu)} - 2/r_3)$
$m_x$
$(C_6, D_5)$
$(C_7, D_5)$
$(C_6, D_5)$
$m_y$
$(C_8, D_5)$
$m_{xy}$
$(L_0, D_2)$
$(L_0, D_4)$
$(M_0, D_2)$
$(M_0, D_4)$
$(N_0, D_1)$
$(N_0, D_3)$
$(L_3, D_5)$
$q_y$
$\omega_y$
$(L_5, D_5)$
$R_1 = \Delta/(2C_1)$
$R_2 = 2L_2/\Delta$
$R_3 = 2L_3/\Delta$
$R_4 = 2L_4/\Delta$
$R_5 = 2L_5/\Delta$
$R_8 = \Delta/(2C_8)$
$\mathbf{R}_{67} = \frac{\Delta}{2}\begin{bmatrix} C_6 & C_7 \\ C_7 & C_6 \end{bmatrix}^{-1}$
$R_9 = r_1$
$R_{14} = r_2$
$R_{15} = r_3$
$R_{10} = R_2 + 2R_9$
$R_{11} = R_3 + 2R_9$
$R_{12} = R_4 + 2R_{14} + 2R_{15}$
$R_{13} = R_5 + 2R_{14} + 2R_{15}$
$\mathbf{R}_{67}$
$R_{14}/2$
T
$T_1$
$T_2$
$T_3$
$T_4$
$R_1$
$R_2$
$R_3$
$R_4$
$R_5$
$R_8$
$R_9$
$R_{10}$
$R_{11}$
$R_{12}$
$R_{13}$
$R_{14}$
$R_{15}$
-1

Figure 5.17: *Modified MDKC and multidimensional DWN for Mindlin's system.*

From the positivity requirement on $L_4$, $L_5$, $L_8$, as well as condition (5.36), we have a second bound on $v_0$,

$$v_0 \geq \max_{r2,r3>0}\left(\frac{12(r_2+r_3)}{\min_{x,y}(\rho h^3)}, \frac{\max_{x,y}(\frac{Eh^3}{1-\nu})}{12r_2}, \frac{\max_{x,y}(\frac{Eh^3}{1+\nu})}{12r_3}\right) \tag{5.39}$$

This is a simple minimax-type problem—we would like to minimize the bound on $v_0$, which is the maximum of three quantities as per (5.39), with respect the parameters $r_2$ and $r_3$. The solution is

$$r_2 = \frac{1}{12}\max_{x,y}\left(\frac{Eh^3}{1-\nu}\right)\sqrt{\frac{\min_{x,y}(\rho h^3)}{\max_{x,y}(\frac{Eh^3}{1-\nu})+\max_{x,y}(\frac{Eh^3}{1+\nu})}} \tag{5.40}$$

$$r_3 = \frac{1}{12}\max_{x,y}\left(\frac{Eh^3}{1+\nu}\right)\sqrt{\frac{\min_{x,y}(\rho h^3)}{\max_{x,y}(\frac{Eh^3}{1-\nu})+\max_{x,y}(\frac{Eh^3}{1+\nu})}} \tag{5.41}$$

which gives the second bound

$$v_0 \geq v_{M^-} \triangleq \sqrt{\frac{\max_{x,y}(\frac{Eh^3}{1-\nu})+\max_{x,y}(\frac{Eh^3}{1-\nu})}{\min_{x,y}(\rho h^3)}} \tag{5.42}$$

and the overall stability bound for the combined network will be

$$v_0 \geq v_M \triangleq \max(v_{M^-}, v_{M^+}) \tag{5.43}$$

When the material parameters and the thickness are constant, this bound reduces to

$$v_0 \geq \sqrt{2}\max\left(\sqrt{\frac{G\kappa}{\rho}}, \sqrt{\frac{E}{\rho(1-\nu^2)}}\right) = \sqrt{2}\gamma^g_{M,max}$$

The MDWD network, shown at bottom in Figure 5.16, follows immediately from the MDKC; here, as for the parallel-plate problem discussed in §3.8.1, we have used step sizes $T_j = \Delta$, $j = 1,\ldots,5$. Recall that because coordinate $t_5 = t' = v_0 t$, a step size of $T_5 = \Delta$ implies a time step of $\Delta/v_0 = T$, and we have indicated pure time delays of duration $T$ by $\mathbf{T}$. As for the Timoshenko network of Figure 5.6, reflection-free ports will be necessary due to the memoryless gyrator couplings between the loops with currents $i_2$ and $i_4$, and $i_3$ and $i_5$ in the MDKC. The coupled inductance has been treated as a vector scattering junction terminated on a vector inductor, as discussed in §2.3.7. We also note in passing that this network may be balanced in the same way as the Timoshenko system (see §5.2.6) in order to obtain a much better bound on $v_0$ (at the expense of increased network complexity).

It is also of course possible to put the MDKC into a form which yields, upon discretization, a DWN. This new form is shown in Figure 5.17; now the transverse velocity $v$ and bending moments

$m_x$, $m_y$ and $m_{xy}$ are treated as voltages, and inductors in these loops are replaced by gyrators terminated on capacitances. In particular, the coupled inductance in Figure 5.16 is replaced by a coupled capacitance. In order to discretize this MDKC, we apply the trapezoid rule to all the inductances and capacitances with direction $t_5$ (using a step size of $T_5 = \Delta$), and to the Jaumann two-ports, we make use of the alternative spectral mappings defined by (4.109), with step sizes $T_j = \Delta/2$, $j = 1, \ldots, 4$. We have chosen these step sizes such that an interleaved algorithm results; the computational grid is shown in Figure 5.18. Grid quantities (capitalized) are shown next to the points at which they are to be calculated. The grid on the right, which operates on grid functions $V$, $Q_x$ and $Q_y$ is identical to the grid for the DWN for the (2+1)D parallel-plate problem (see Figure 4.18), which is to be expected, since the related subnetwork of the MDKC shown in Figure 5.17 is the same as that for the parallel-plate problem (see Figure 4.49). It is coupled via gyrators (these couplings are indicated by curved arrows) to a second grid, over which grid functions $\Omega_x$, $\Omega_y$, $M_x$, $M_y$ and $M_{xy}$ are calculated. In particular, $M_x$ and $M_y$ are calculated together as a vector quantity at a vector parallel junction—this vector is written as **M** in Figure 5.18. Waveguide connections (of delay $T/2$) are represented by solid lines, and self-loops and sign-inversions in the signal paths are not shown. Note that at the grey dots, we will have parallel scattering junctions, and at the white dots we will have series junctions; junction quantities are calculated at alternating multiples of $T/2$.

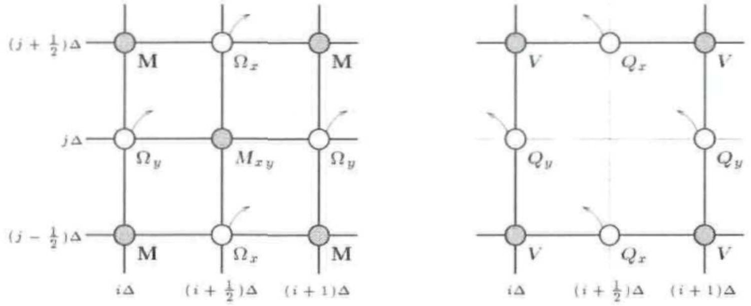

Figure 5.18: *Computational grid for the multidimensional DWN shown in Figure 5.17.*

### 5.4.2 Boundary Termination of the Mindlin Plate

There are four common types of conditions applied at a plate boundary [94]. At a southern boundary, parallel to the $x$ axis, the four conditions can be written as

$$q_y = m_y = m_{xy} = 0 \qquad \text{Free edge} \tag{5.44a}$$

$$v = \omega_x = m_y = 0 \qquad \text{Simply supported edge (1)} \tag{5.44b}$$

$$v = m_{xy} = m_y = 0 \qquad \text{Simply supported edge (2)} \tag{5.44c}$$

$$v = \omega_x = \omega_y = 0 \qquad \text{Clamped edge} \tag{5.44d}$$

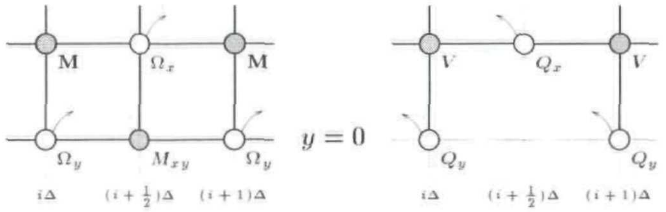

Figure 5.19: *Southern computational grid boundary at $y = 0$ for the DWN for Mindlin's system.*

These conditions are again lossless, and of the form of (3.8). (We note that conditions on $v$, $\omega_x$ and $\omega_y$ in (5.44) are usually written in terms of their time integrals $w$, $\psi_x$ and $\psi_y$, but the formulation above is equivalent.) The same conditions also reduce to a similar set of conditions which can be applied to the classical plate, as defined by [17].

As we mentioned in §5.2.4, the passive boundary termination of an MDWD network, such as that shown in Figure 5.16, is not at all straightforward. Indeed, it is somewhat complicated by the fact that we must approximate all the system variables at any given grid point on the boundary, and we were not able to implement a stable termination for this network. The "wave-canceling" method [107] discussed in §3.11 becomes exceedingly complex when vector wave variables and reflection-free ports are involved; passivity is not easy to ensure.

Termination of the DWN derived from the MDKC of Figure 5.17, operating on the computational grid of Figure 5.18, however, is simpler, because we are able to work directly with the termination of the lumped mesh representation. Suppose we choose our southern boundary at $y = 0$ according to Figure 5.19. The only quantities to be calculated in this arrangement will be $Q_y$ and $\Omega_y$, at coincident series scattering junctions, and $M_{xy}$ at parallel scattering junctions. This arrangement is to be preferred, because we do not need to worry about the termination of the vector scattering junctions at which $\mathbf{M} = [M_x, M_y]$ is calculated.

The southern boundary terminations corresponding to the four conditions (5.44) are shown in Figure 5.20. The conditions $q_y = 0$ and $\omega_y = 0$ that appear in (5.44a) and (5.44d) can be dealt with rather simply, by terminating the boundary series junctions at which the junction currents $Q_{y,J}$ and $\Omega_{y,J}$ are calculated in an open circuit[†]. For these conditions, the gyrator coupling between the two subnetworks (indicated by curved arrows in Figure 5.19) may be dropped entirely. Similarly, the condition $m_{xy} = 0$ can be implemented by short-circuiting the appropriate parallel boundary junctions.

The other conditions, involving variables not calculated directly on the boundary require a slightly more involved treatment; the analysis is similar to that performed in §4.4.4, and the termination problem becomes (for the most part) that of setting the self-loop immittances at the boundary junctions which can not be trivially terminated in an open or short circuit. To this end, we provide the waveguide immittances at the junctions in the problem *interior* at which $M_{xyJ}$, $\Omega_{yJ}$ and $Q_{yJ}$ are calculated. From Figure 5.17, it is possible to read off these values directly. As for the DWN for the Timoshenko system in §5.2.2, immittances in the two overlapped networks are distinguished by a tilde ( $\tilde{}$ ). For example, at a parallel junction in the five-variable grid at location $x = (i+\frac{1}{2})\Delta$, $y = j\Delta$, for $i$ and $j$ integer, where we calculate $M_{xyJ,i+\frac{1}{2},j}$ (see Figure 5.18), there are waveguide connections to the north, south, east and west; their admittances are defined as

---

[†] *In keeping with the notation of Chapter 4, we have appended a "J" to the subscript of any grid function, to indicate that it is to be calculated as a junction current or voltage.*

$$\tilde{Y}_{y^+,i+\frac{1}{2},j} = \tilde{Y}_{y^-,i+\frac{1}{2},j} = \tilde{Y}_{x^+,i+\frac{1}{2},j} = \tilde{Y}_{x^-,i+\frac{1}{2},j} = \frac{1}{R_{15}} = \frac{1}{r_3}$$

respectively, which are simply the admittances of the multidimensional unit elements from Figure 5.17. Similarly, the four connecting waveguide impedances at series junctions at locations $x = i\Delta$, $j = i\Delta$ (at which $\Omega_{yJ,i,j}$ are calculated) will have impedances

$$\tilde{Z}_{y^+,i,j} = \tilde{Z}_{y^-,i,j} = R_{14} = r_2 \qquad\qquad \tilde{Z}_{x^+,i,j} = \tilde{Z}_{x^-,i,j} = R_{15} = r_3$$

In the other waveguide mesh (on the right in Figure 5.18), the connecting northward and southward impedances at the series junctions at which $Q_{yJ,i,j}$ is calculated will be

$$Z_{y^+,i,j} = Z_{y^-,i,j} = R_9 = r_1$$

The self-loop immittances at the three types of junctions will be

$$\tilde{Y}_{c,i+\frac{1}{2},j} = \frac{1}{R_8} = \frac{4v_0}{(D(1-\nu))_{i+\frac{1}{2},j}} - \frac{4}{r_3} \tag{5.45a}$$

$$\tilde{Z}_{c,i,j} = R_4 = \frac{v_0(\rho h^3)_{i,j}}{6} - 2r_2 - 2r_3 \tag{5.45b}$$

$$Z_{c,i,j} = R_2 = \frac{2v_0}{(\kappa^2 Gh)_{i,j}} - 2r_1 \tag{5.45c}$$

We assume $r_1$, $r_2$ and $r_3$ to be chosen according to (5.37), (5.40) and (5.41) respectively.

**Free Edge**

Referring to Figure 5.20(a), the conditions $q_y = 0$ and $m_{xy} = 0$ are rather simply dealt with by open- or short-circuiting the respective junctions. In this case, the gyrator connection between the two waveguide meshes can be severed at the boundary junctions, and in order to get a lossless numerical condition equivalent to $m_y = 0$ we need only set, for $j = 0$,

$$\tilde{Z}_{c,i,0} = \frac{v_0(\rho h^3)_{i,0}}{12} - r_2$$

which is less restrictive than (5.45b), and does not degrade the bound from (5.38) and (5.42).

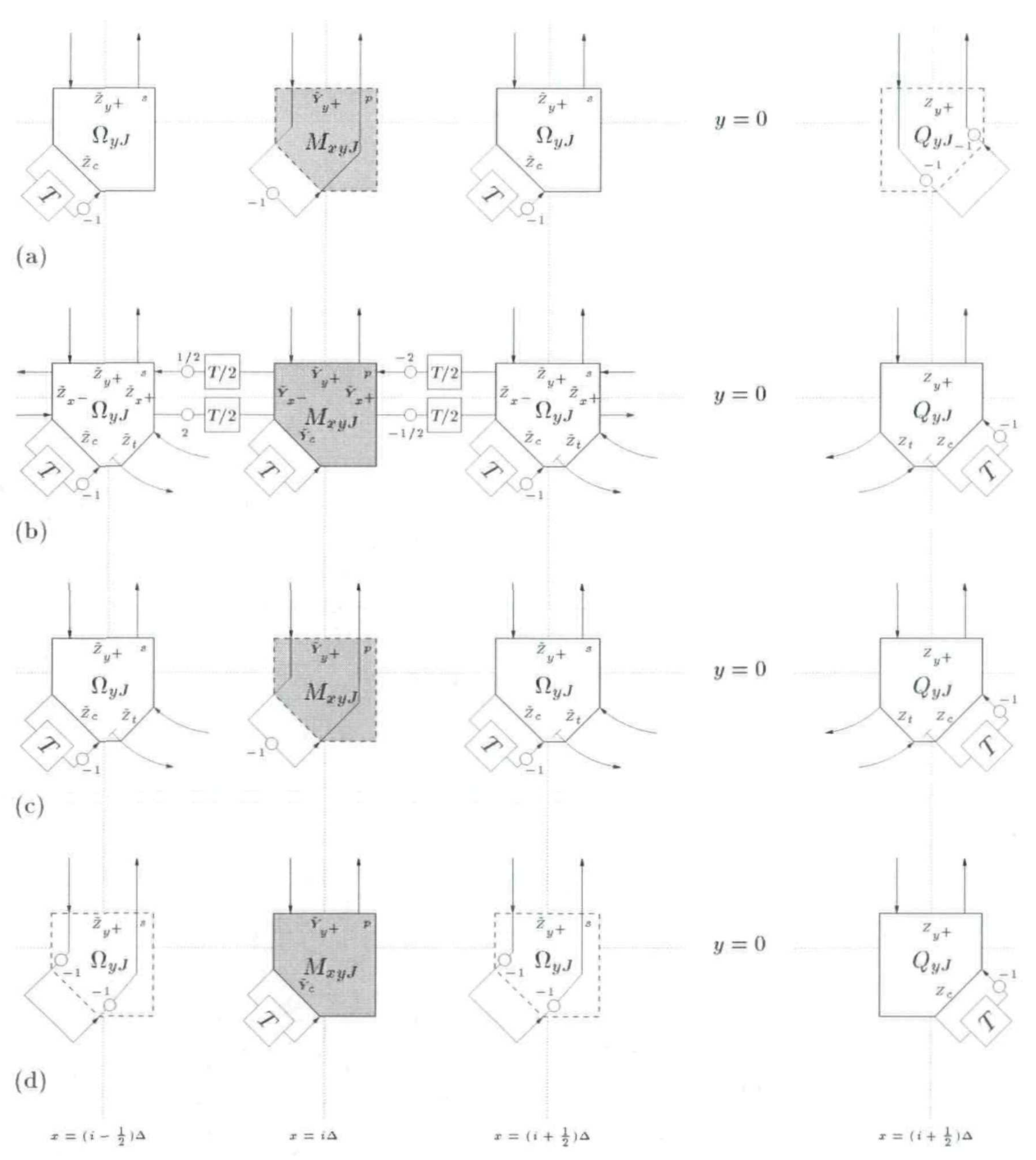
(a)
(b)
(c)
(d)
$\Omega_{yJ}$
$M_{xyJ}$
$Q_{yJ}$
$y = 0$
T
T/2
1/2
2
−2
−1/2
−1
$\hat{Z}_{y+}$
$\hat{Z}_{x-}$
$\hat{Z}_{x+}$
$\hat{Z}_c$
$\hat{Z}_t$
$\hat{Y}_{y+}$
$\hat{Y}_{x-}$
$\hat{Y}_{x+}$
$\hat{Y}_c$
$Z_{y+}$
$Z_t$
$Z_c$
s
p
$x = (i - \frac{1}{2})\Delta$
$x = i\Delta$
$x = (i + \frac{1}{2})\Delta$
$x = (i + \frac{1}{2})\Delta$

Figure 5.20: *Various lossless boundary terminations for the DWN for Mindlin's system*—(a) *free boundary;* (b) *simply supported edge (1);* (c) *simply supported edge (2);* (d) *clamped edge.*

### Simply Supported Edge (1)

Conditions (5.44b) are somewhat more complicated to implement than the others, because none of the variables calculated on the boundary can be zeroed out by short- or open-circuiting. From Figure 5.20(b), we can see that in addition to the gyrator coupling between the two meshes that must be maintained, we also must keep the waveguides which lie along the boundary.

In the problem interior, parallel and series junctions in the five-variable mesh are connected, through waveguides, to four neighboring junctions; on the southern boundary, however, each is connected to three—two to the east and west) and one to the north. Due to this asymmetry, we might suspect that it will be necessary to adjust the boundary waveguide impedances away from the values that they would take on the interior (which is $r_3$). In fact, it is possible to show that by introducing transformers, with turns ratios of $n = 2$ in these waveguides, we indeed have a lossless termination which satisfies conditions (5.44b). We must set the boundary immittances to

$$\tilde{Y}_{x^-,i+\frac{1}{2},0} = \tilde{Y}_{x^+,i+\frac{1}{2},0} = \frac{1}{2r_3} \qquad\qquad Z_{x^-,i,0} = Z_{x^+,i,0} = \frac{r_3}{2}$$

Notice that each waveguide now includes scaling factors (of 2 and 1/2), and that the impedances at either end are no longer identical, due to the transformer impedance matching. The self-loop immittances should be set according to

$$\begin{aligned} \tilde{Y}_{c,i+\frac{1}{2},0} &= \frac{2v_0}{(D(1-\nu))_{i+\frac{1}{2},0}} - \frac{2}{r_3} \\ \tilde{Z}_{c,i,0} &= \frac{v_0(\rho h^3)_{i,0}}{12} - r_2 - r_3 \\ Z_{c,i,0} = &= \frac{v_0}{(\kappa^2 Gh)_{i,0}} - r_1 \end{aligned}$$

which are precisely half the values they would take at interior junctions, from (5.45) (and thus the positivity condition on these immittances is no different from the condition over interior self-loop immittances). We also mention that the gyrator coefficient, which takes on a value of $R_G = \Delta$ over the interior, should also be halved to $R_G = \Delta/2$ at the boundary junctions.

### Simply Supported Edge (2)

The condition $m_{xy} = 0$ from (5.44c) can be set by short-circuiting the parallel boundary junctions. The condition $v = 0$ can be dealt with as for the preceding case, and we will again require

$$Z_{c,i,0} = \frac{v_0}{(\kappa^2 Gh)_{i,0}} - r_1$$

and the gyrator coefficient at the boundary junctions should be set to $R_G = \Delta/2$. The self-loop impedances at the series junctions in the five-variable mesh should be set, in order to ensure $m_y = 0$, as

$$\tilde{Z}_{c,i,0} = \frac{v_0(\rho h^3)_{i,0}}{12} - r_2$$

The positivity requirement on this impedance is again less restrictive than condition (5.45b) on the mesh interior.

**Clamped Edge**

For conditions (5.44d), we may immediately terminate the series junctions in the five-variable mesh with an open-circuit, and the gyrator coupling can be dropped entirely, as for the case of the free boundary condition. The remaining self-loop immittances should be set as

$$\begin{aligned} \tilde{Y}_{c,i+\frac{1}{2},0} &= \frac{2v_0}{(D(1-\nu))_{i+\frac{1}{2},0}} - \frac{1}{r_3} \\ Z_{c,i,0} = &= \frac{v_0}{(\kappa^2 Gh)_{i,0}} - r_1 \end{aligned}$$

which, as before, are less restrictive settings than those over the mesh interior, from (5.45).

### 5.4.3 Simulation: Mindlin's System, for Plates of Uniform and Varying Thickness

For the sake of illustration, we present two DWN simulations of the vibration of a Mindlin plate. In both cases, the plate is assumed to be square, with side length 1m and to be made of steel; the material parameters are thus $\rho = 5.38 \times 10^4 \text{kg/m}^3$, $E = 1.4 \times 10^{12} \text{N/m}^2$, $G = 5.39 \times 10^{11} \text{N/m}^2$. $\kappa$ is taken to be 5/6, and Poisson's ratio $\nu$ is set to 0.3. In both cases, the DWN is initialized with a transverse velocity distribution which takes the form of a single lobe of a 2D raised cosine, of radius 0.1m, amplitude 0.0005m/s, and centered at coordinates $x = 0.3$m, $y = 0.3$m, where $x = 0$m, $y = 0$m are the coordinates of the bottom left-hand plate corner. The grid spacing is set to be $\Delta = 1$cm in the DWN in both cases.

In the first simulation (see Figure 5.21), the plate thickness is 1cm, over the entire plate surface. Boundary conditions are of the free type, given by (5.44a), and implemented as per the DWN termination discussed in the previous section, and shown in Figure 5.20(a). In the second simulation, shown in Figure 5.22, the plate thickness is variable—over most of the plate, it is a constant 1cm, but over the circular region outlined in black (radius 0.2m, and centered at $x = 0.6$m, $y = 0.6$m), it rises in a raised 2D cosine distribution to a peak of 6cm. In both simulations, snapshots of the transverse velocity distribution are taken every $2.875\times10^{-5}$s. The boundary termination is of the clamped type (5.44d) in this case, and has been implemented in the DWN according to Figure 5.20(d).

Light- and dark-colored regions correspond to positive and negative velocities, respectively. The plots have been normalized and interpolated for better visibility. Notice in particular the numerical directional dependence of the propagation velocities at short wavelengths.

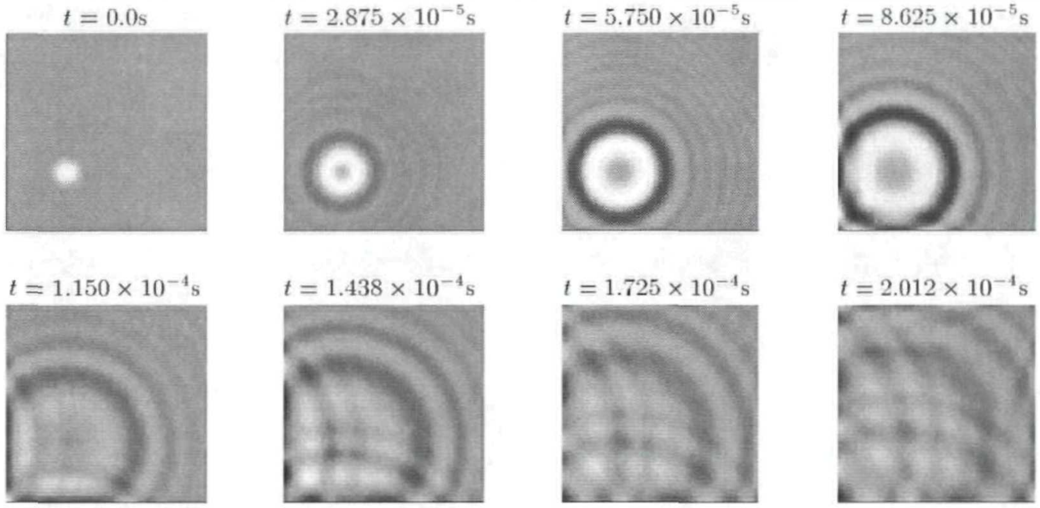

Figure 5.21: *DWN simulation of Mindlin's system, for a steel plate of uniform thickness, with free edges.*

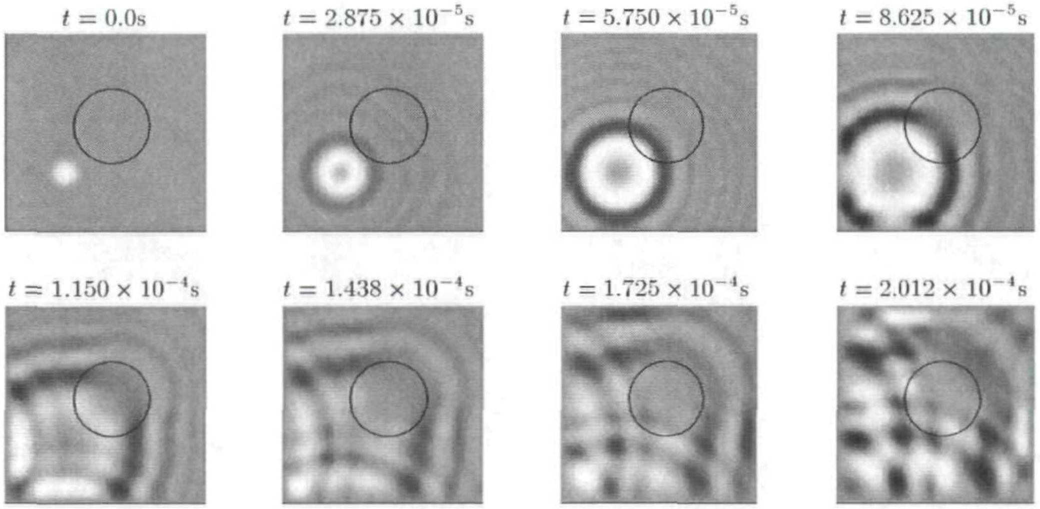

Figure 5.22: *DWN simulation of Mindlin's system, for a steel plate of varying thickness. The variation is limited to the interior of the black circles. Boundary conditions are of the clamped type.*

## 5.5 Cylindrical Shells

A shell is simply a plate with some curvature; it also supports wave motion, but the curvature complicates the motion considerably. As we will see, however, certain types of shell systems can also be represented by (2+1)D MDKCs. We will look first at the so-called cylindrical *membrane shell* formulation [77], then at a more modern (and elaborate) cylindrical shell formulation due to Naghdi and Cooper [31, 128].

### 5.5.1 The Membrane Shell

The simplest type of cylindrical shell theory is the *membrane shell* formulation of Rayleigh [77]. In this very basic theory, the shell is assumed to behave somewhat like a membrane, in that the restoring stiffness is assumed negligible. The shell is assumed to lie parallel to the $x$ axis, and has radius $a$. We define $\theta = a\theta'$, where $\theta'$ is the angular coordinate. This theory models the displacement of the shell from its equilibrium position; in contrast to Mindlin's plate system, however, displacements in all three directions are modeled as a function of time, and we will write these three displacements as $w_z$ (transverse), $w_x$ (axial) and $w_\theta$ (tangential). In the membrane theory, the three displacements complemented by three in-surface stresses $n_x$ (axial), $n_\theta$ (tangential) and $n_{x\theta}$ (shear) form a closed system; bending moments and transverse shear stresses are not modeled. This system can be written as

$$\rho h\frac{\partial^2 w_z}{\partial t^2} = -\frac{1}{a}n_\theta \tag{5.46}$$

$$\begin{aligned}
\rho h\frac{\partial^2 w_x}{\partial t^2} &= \frac{\partial n_x}{\partial x} + \frac{\partial n_{x\theta}}{\partial \theta} && (5.47a)\\
\rho h\frac{\partial^2 w_\theta}{\partial t^2} &= \frac{\partial n_\theta}{\partial \theta} + \frac{\partial n_{x\theta}}{\partial x} && (5.47b)\\
n_x &= \frac{Eh}{1-\nu^2}\left(\frac{\partial w_x}{\partial x} + \nu\frac{\partial w_\theta}{\partial \theta} + \frac{\nu}{a}w_z\right) && (5.47c)\\
n_\theta &= \frac{Eh}{1-\nu^2}\left(\nu\frac{\partial w_x}{\partial x} + \frac{\partial w_\theta}{\partial \theta} + \frac{1}{a}w_z\right) && (5.47d)\\
n_{x\theta} &= \frac{Eh}{2(1+\nu)}\left(\frac{\partial w_\theta}{\partial x} + \frac{\partial w_x}{\partial \theta}\right) && (5.47e)
\end{aligned}$$

The material constants $E$, $\nu$, $\rho$ and the shell thickness $h$ are as discussed in §5.4, and are now assumed to be smooth functions of $x$ and $\theta$. If we define the velocities $v_z$, $v_\theta$ and $v_x$ by

$$v_z = \frac{\partial w_z}{\partial t} \qquad v_\theta = \frac{\partial w_\theta}{\partial t} \qquad v_x = \frac{\partial w_x}{\partial t}$$

then we again have a symmetric hyperbolic system of the form of (3.1) in the dependent variable $\mathbf{w} = [v_z, v_x, v_\theta, n_x, n_\theta, n_{x\theta}]^T$, where the system matrices are

$$\mathbf{P} = \mathbf{P}_R = \begin{bmatrix} P_R^+ & \cdot \\ \cdot & \mathbf{P}_R^- \end{bmatrix} \qquad \mathbf{A}_1 = \mathbf{A}_{R1} = \begin{bmatrix} \cdot & \cdot \\ \cdot & \mathbf{A}_{M1}^- \end{bmatrix} \qquad \mathbf{A}_2 = \mathbf{A}_{R2} = \begin{bmatrix} \cdot & \cdot \\ \cdot & \mathbf{A}_{M2}^- \end{bmatrix}$$

$$\mathbf{B} = \mathbf{B}_R = \begin{bmatrix} \cdot & \mathbf{b}_\times \\ -\mathbf{b}_\times^T & \cdot \end{bmatrix}$$

where

$$P_R^+ = \rho h \qquad \mathbf{P}_R^- = \begin{bmatrix} \rho h & 0 & 0 & 0 & 0 \\ 0 & \rho h & 0 & 0 & 0 \\ 0 & 0 & \frac{1}{Eh} & \frac{-\nu}{Eh} & 0 \\ 0 & 0 & \frac{-\nu}{Eh} & \frac{1}{Eh} & 0 \\ 0 & 0 & 0 & 0 & \frac{2(1+\nu)}{Eh} \end{bmatrix} \qquad \mathbf{b}_\times = \begin{bmatrix} 0 & 0 & 0 & \frac{1}{a} & 0 \end{bmatrix}$$

and $\mathbf{A}_{M1}^-$ and $\mathbf{A}_{M2}^-$ are as defined in (5.34) and (5.35). The lower 5 variable system described by $\mathbf{P}_R^-$, $\mathbf{A}_{R1}^-$ and $\mathbf{A}_{M2}^-$, when uncoupled from the 1 variable system in $P_R^+$ is essentially equivalent to the lower subsystem in the Mindlin plate theory, except that our independent variables are now $x$ and $\theta$ instead of $x$ and $y$. (In fact, if we replace any occurrence of $h^3/12$ in $\mathbf{P}_M^-$ by $h$, we get exactly $\mathbf{P}_R^-$.) We thus expect the MDKC to be very similar to that of the right-hand network in Figure 5.16.

We again introduce current-like variables[†]

$$(i_1, i_9, i_{10}, i_{11}, i_{12}, i_{13}) = (r_1 v_z, v_x, v_\theta, r_4 n_x, r_4 n_\theta, r_5 n_{x\theta})$$

and make use of coordinates defined by (3.22) in terms of the physical coordinates $[x, \theta, t]^T$. $r_1$, $r_4$ and $r_5$ are, as before, positive constants which we will later use for optimization. The MDKC for the membrane shell system is shown in Figure 5.23. (We have marked the points $B$ and $B'$ in the figure in anticipation of the shell model in the next section.)

Optimal settings for $r_4$ and $r_5$, which follow from positivity constraints on the inductances $L_9, \ldots, L_{13}$, can be shown (through an analysis identical to that performed on the Mindlin plate system) to be

$$r_4 = \max_{x,\theta}\left(\frac{Eh}{1-\nu}\right)\sqrt{\frac{2\min_{x,\theta}(\rho h)}{\max_{x,\theta}(\frac{Eh}{1-\nu}) + \max_{x,\theta}(\frac{Eh}{1+\nu})}} \tag{5.48}$$

$$r_5 = \max_{x,\theta}\left(\frac{Eh}{1+\nu}\right)\sqrt{\frac{2\min_{x,\theta}(\rho h)}{\max_{x,\theta}(\frac{Eh}{1-\nu}) + \max_{x,\theta}(\frac{Eh}{1+\nu})}} \tag{5.49}$$

---

[†] The reason for the unusual numbering of these variables will be made clear in the next section.

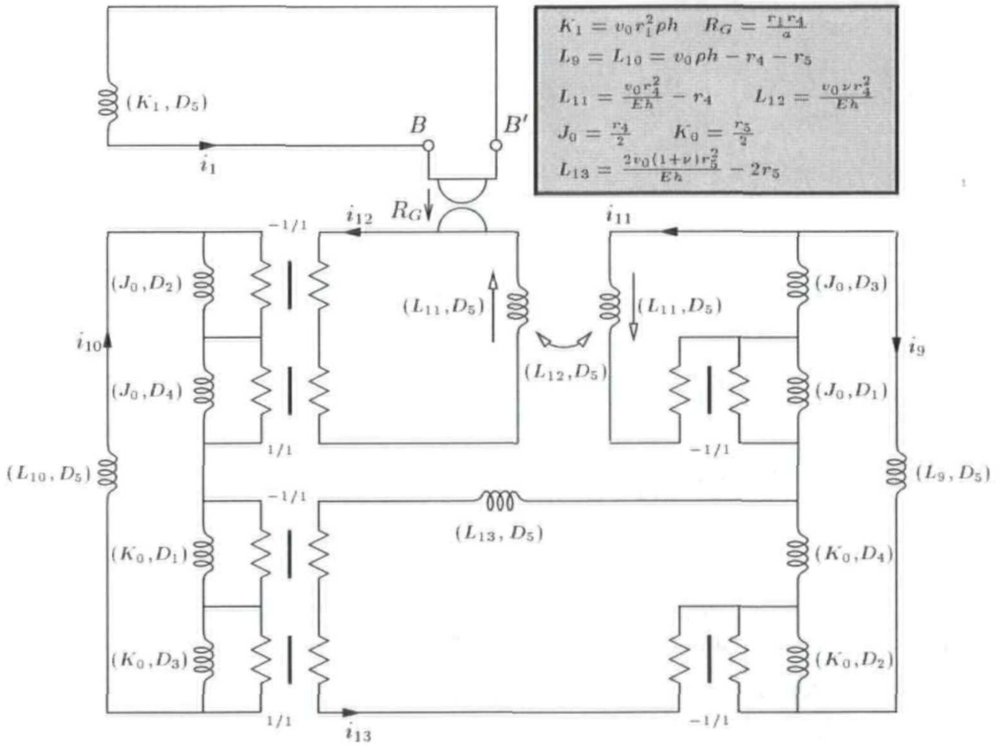
$K_1 = v_0 r_1^2 \rho h$ $R_G = \frac{r_1 r_4}{a}$
$L_9 = L_{10} = v_0 \rho h - r_4 - r_5$
$L_{11} = \frac{v_0 r_4^2}{Eh} - r_4$ $L_{12} = \frac{v_0 \nu r_4^2}{Eh}$
$J_0 = \frac{r_4}{2}$ $K_0 = \frac{r_5}{2}$
$L_{13} = \frac{2v_0(1+\nu)r_5^2}{Eh} - 2r_5$
$(K_1, D_5)$
$B$
$B'$
$i_1$
$R_G$
$i_{12}$
$i_{11}$
$-1/1$
$(J_0, D_2)$
$(J_0, D_4)$
$i_{10}$
$(L_{11}, D_5)$
$(L_{11}, D_5)$
$(L_{12}, D_5)$
$(J_0, D_3)$
$(J_0, D_1)$
$i_9$
$1/1$
$-1/1$
$(L_{10}, D_5)$
$(L_9, D_5)$
$-1/1$
$(L_{13}, D_5)$
$(K_0, D_1)$
$(K_0, D_3)$
$(K_0, D_4)$
$(K_0, D_2)$
$1/1$
$i_{13}$
$-1/1$

Figure 5.23: *MDKC for the cylindrical membrane shell system.*

in which case we must have, for passivity

$$v_0 \geq v_R \triangleq \sqrt{\frac{\max_{x,\theta}(\frac{Eh}{1-\nu}) + \max_{x,\theta}(\frac{Eh}{1+\nu})}{\min_{x,\theta}(\rho h)}} \tag{5.50}$$

The parameter $r_1$ is as yet unconstrained (notice that the inductance $K_1$ is non-negative for any choice of $v_0 \geq 0$).

We have presented the MDKC for the membrane shell because it is an important building block in the more modern theory, which we now present. It should be obvious, from this MDKC, we can immediately arrive at an MDWD network, and after applying network transformations, we can get a multidimensional DWN as well.

### 5.5.2 The Naghdi-Cooper System II Formulation

As we mentioned, the membrane model of the cylindrical shell neglects certain important effects, in particular the crucial transverse shear effects. Many so-called higher-order shell theories have appeared in the literature; for a good survey of these theories, we refer to [77, 81]. We have decided to focus on the Naghdi-Cooper system II shell model [31, 77, 128] because it can be simply interpreted as a passive circuit. We note in passing that not all shell theories have this property—Mirsky-Herrmann theory [77], for example, does not, and Naghdi and Cooper's system II, for example, is simplified from their proposed system I which also does not. The problem, more specifically, is that these systems can apparently not be written in the special symmetric hyperbolic form of (3.1), for which the matrices $\mathbf{A}_1$ and $\mathbf{A}_2$ will be independent of $x$ and $\theta$. This property is essential here in that such dependence considerably complicates the inter-loop coupling in an MDKC (notice that the port-resistances of the Jaumann two-ports which realize this coupling been constant for every system we have looked at so far).

Another reason for choosing this particular shell model is that it can be simply written as Mindlin's plate system (in coordinates $x$ and $\theta$ instead of $x$ and $y$) coupled with the membrane shell. We can write this system in the form of (3.1), where the dependent variable $\mathbf{w}$ is defined by

$$\mathbf{w} = [v_z, q_x, q_\theta, \omega_x, \omega_\theta, m_x, m_y, m_{xy}, v_x, v_\theta, n_x, n_\theta, n_{x\theta}]^T \tag{5.51}$$

Here, the first 8 variables are precisely those that appear in the Mindlin theory (see §5.4), but in cylindrical coordinates; we have changed subscripts $y$ to $\theta$, and written the $v_z$ instead of $v$ for the radial transverse velocity. The other five variables appear in subsystem (5.47) of the membrane shell theory (see §5.5.1). The system matrices are

$$\mathbf{P} = \mathbf{P}_{NC} = \begin{bmatrix} \mathbf{P}_M & \cdot \\ \cdot & \mathbf{P}_{\bar{R}} \end{bmatrix} \quad \mathbf{A}_1 = \mathbf{A}_{NC1} = \begin{bmatrix} \mathbf{A}_{M1} & \cdot \\ \cdot & \mathbf{A}_{\bar{M}1} \end{bmatrix} \quad \mathbf{A}_2 = \mathbf{A}_{NC2} = \begin{bmatrix} \mathbf{A}_{M2} & \cdot \\ \cdot & \mathbf{A}_{\bar{M}2} \end{bmatrix}$$

$$\mathbf{B} = \mathbf{B}_{NC} = \begin{bmatrix} \mathbf{B}_M & \mathbf{B}_{NC\times} \\ -\mathbf{B}_{NC\times}^T & \cdot \end{bmatrix}$$

where $\mathbf{P}_M$, $\mathbf{A}_{M1}$, $\mathbf{A}_{\bar{M}1}$, $\mathbf{A}_{M2}$, $\mathbf{A}_{\bar{M}2}$ and $\mathbf{B}_M$ are as defined in §5.4, and $\mathbf{P}_{\bar{R}}$ appears in §5.5.1. The coupling matrix is

$$\mathbf{B}_{NC\times} = \begin{bmatrix} 0 & 0 & 0 & 0 & 0 & 0 & 0 & 0 \\ 0 & 0 & 0 & 0 & 0 & 0 & 0 & 0 \\ 0 & 0 & 0 & 0 & 0 & 0 & 0 & 0 \\ \frac{1}{a} & 0 & 0 & 0 & 0 & 0 & 0 & 0 \\ 0 & 0 & 0 & 0 & 0 & 0 & 0 & 0 \end{bmatrix}^T$$

Note that this coupling disappears in the limit as the shell radius $a$ becomes large (effectively leaving us with with the Mindlin system). $\mathbf{B}_{NC}$ is indeed anti-symmetric, so we are guaranteed a lossless MDKC network; in fact, this network can be directly constructed from the two networks shown in Figures 5.16 and 5.23, by attaching terminals $A$ and $A'$ in the former to $B$ and $B'$ in the latter. The scaling parameters $r_1$, $r_2$ and $r_3$ can be chosen optimally according to (5.37), (5.40) and (5.41), and

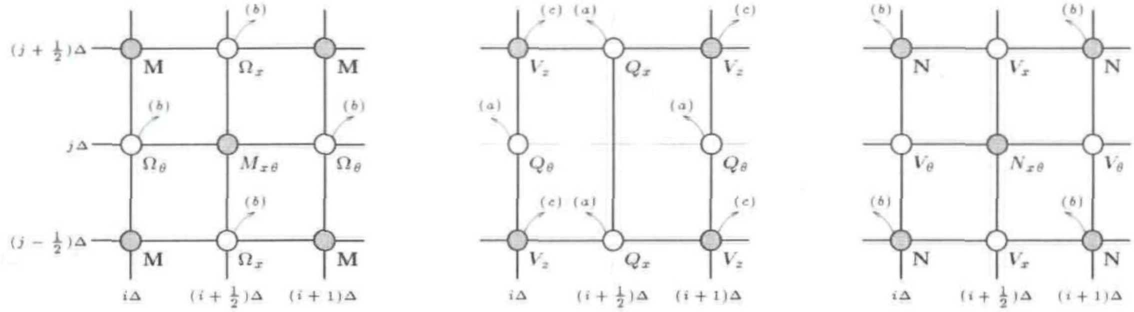
(b)
$(j+\frac{1}{2})\Delta$
M
$\Omega_x$
M
(b)
(b)
$j\Delta$
$\Omega_\theta$
$M_{x\theta}$
$\Omega_\theta$
(b)
$(j-\frac{1}{2})\Delta$
M
$\Omega_x$
M
$i\Delta$
$(i+\frac{1}{2})\Delta$
$(i+1)\Delta$
(c) (a)
(c)
$V_z$
$Q_x$
$V_z$
(a)
(a)
$Q_\theta$
$Q_\theta$
(c) (a)
(c)
$V_z$
$Q_x$
$V_z$
$i\Delta$
$(i+\frac{1}{2})\Delta$
$(i+1)\Delta$
(b)
(b)
N
$V_x$
N
$V_\theta$
$N_{x\theta}$
$V_\theta$
(b)
(b)
N
$V_x$
N
$i\Delta$
$(i+\frac{1}{2})\Delta$
$(i+1)\Delta$

(a) (b) (c)

Figure 5.24: *Computational grid for the DWN for Naghdi and Cooper's system II. Grids (a) and (b) correspond to a DWN for a Mindlin-type subsystem, and are coupled to a membrane shell-type DWN operating on grid (c). Grid functions (capitalized versions of the dependent variables* (5.51)*) are indicated next to the grid points at which they are calculated. Grey/white coloring of grid points indicates calculation at parallel/series junctions at alternating time steps.*

$r_4$ and $r_5$ can be set as in (5.48) and (5.49), giving a bound for passivity on the combined network,

$$v_0 \geq v_{NC} \triangleq \max(v_M, v_R)$$

where $v_M$ is the bounding space step/time step ratio for the Mindlin network, from (5.43) (in cylindrical coordinates), and $v_R$ is the same quantity for the membrane shell system, from (5.50).

Because this system can be constructed entirely by connecting subnetworks that we have already examined in detail, it seems unnecessary to show the discrete MDWD network or the alternate MDKC and its discrete form suitable for DWN implementation. The MDWD network will be exactly the combination of the "Mindlin" system, shown at bottom in Figure 5.16, and the MDWD network corresponding to the MDKC for the membrane shell, shown in Figure 5.23; recall that the MDKC for the membrane shell system (with a free port with terminals $B$ and $B'$) is identical in form to that of the uncoupled five-variable Mindlin subsystem, and thus its MDWD counterpart will be of the same form as well.

For the transformed network to be used to generate a DWN, a few comments are in order. For the Mindlin system, we first applied network theoretic rules in order to arrive at a modified form, shown at top in Figure 5.17. In this case, the transverse velocity $v$ (renamed $v_z$ in this section) and the bending moments $m_x$, $m_y$ and $m_{xy}$ (renamed $m_x$, $m_\theta$ and $m_{x\theta}$) have been interpreted as voltages instead of currents. This transformed network can then be connected (via terminals $A$ and $A'$ in Figure 5.17) to a transformed form of the membrane shell system, shown in Figure 5.23; for the shell subsystem, $n_x$, $n_\theta$ and $n_{x\theta}$ will be treated as voltages, and $v_x$ and $v_\theta$ as currents.

After connecting these transformed subnetworks, and applying the usual alternative discretization rules, we end up with a DWN that will operate on an interleaved grid as shown in Figure 5.24. Grids (a) and (b) are precisely the Mindlin grid shown in Figure 5.18, and are coupled instantaneously to a third grid (c), which adds the effect of curvature to the system.

## 5.6 Elastic Solids

The system defining the behavior of a (3+1)D linear, isotropic, elastic solid is somewhat easier to handle numerically than the (2+1)D plate and (1+1)D beam systems which are derived from it; the physics is less obscured by modeling assumptions. Numerical simulation of the full (3+1)D system is, of course, much more computationally expensive.

Such a medium is characterized by its density, $\rho$, and two material parameters $\lambda$ and $\mu$, called the *Lamé* coefficients, which describe its resilience; there are two parameters because an solid will resist compressional and shear forces to different degrees. Other elastic parameters, which we have already made use of earlier in this chapter, can be defined in terms of these two constants. *Young's modulus* $E$ and *Poisson's ratio* $\nu$ can be written as

$$E = \frac{\mu(3\lambda + 2\mu)}{\lambda + \mu} \qquad \nu = \frac{\lambda}{2(\lambda + \mu)}$$

We remark that $\mu$ is the same as $G$ that was used in the treatment of the Timoshenko beam (see §5.2), the Mindlin plate (see §5.4), and the Naghdi-Cooper shell model of §5.5.2. For the sake of generality, we allow all these parameters to be functions of $x$, $y$ and $z$.

The equations of motion of the solid can be written in terms of stress and displacement fields [77]. There are nine stresses: $\sigma_{xx}$, $\sigma_{yy}$ and $\sigma_{zz}$ are *normal stresses* in the direction indicated by the double subscript, and $\sigma_{xy}$, $\sigma_{xz}$, $\sigma_{yz}$, $\sigma_{yx}$, $\sigma_{zx}$, and $\sigma_{zy}$ are *shear stresses*. The displacements of a point in the medium from its equilibrium position are given by $\mathbf{d} = [w_x, w_y, w_z]^T$. If the material is assumed to be in rotational equilibrium, then we have

$$\sigma_{xy} = \sigma_{yx} \qquad \sigma_{xz} = \sigma_{zx} \qquad \sigma_{yz} = \sigma_{zy}$$

so that there are a total of six independent stresses acting at a given point in the solid [190].

*Newton's Laws* for a solid (neglecting body forces) are written as

$$\rho\frac{\partial^2 w_x}{\partial t^2} = \frac{\partial \sigma_{xx}}{\partial x} + \frac{\partial \sigma_{xy}}{\partial y} + \frac{\partial \sigma_{xz}}{\partial z} \tag{5.52a}$$

$$\rho\frac{\partial^2 w_y}{\partial t^2} = \frac{\partial \sigma_{xy}}{\partial x} + \frac{\partial \sigma_{yy}}{\partial y} + \frac{\partial \sigma_{yz}}{\partial z} \tag{5.52b}$$

$$\rho\frac{\partial^2 w_z}{\partial t^2} = \frac{\partial \sigma_{xz}}{\partial x} + \frac{\partial \sigma_{yz}}{\partial y} + \frac{\partial \sigma_{zz}}{\partial z} \tag{5.52c}$$

The stress-strain relation, or *Hooke's Law* [77] is expressed as a linear proportionality between the six stresses and spatial derivatives of the displacements (the strain):

$$\sigma_{xx} = 2\mu\frac{\partial w_x}{\partial x} + \lambda\nabla\cdot\mathbf{d} \tag{5.53a}$$
$$\sigma_{yy} = 2\mu\frac{\partial w_y}{\partial y} + \lambda\nabla\cdot\mathbf{d} \tag{5.53b}$$
$$\sigma_{zz} = 2\mu\frac{\partial w_z}{\partial z} + \lambda\nabla\cdot\mathbf{d} \tag{5.53c}$$

$$\sigma_{xy} = \mu\left(\frac{\partial w_x}{\partial y} + \frac{\partial w_y}{\partial x}\right) \tag{5.54a}$$
$$\sigma_{xz} = \mu\left(\frac{\partial w_x}{\partial z} + \frac{\partial w_z}{\partial x}\right) \tag{5.54b}$$
$$\sigma_{yz} = \mu\left(\frac{\partial w_y}{\partial z} + \frac{\partial w_z}{\partial y}\right) \tag{5.54c}$$

The systems (5.52), (5.53) and (5.54) taken together are sometimes called the *Navier* system [77, 131]. By introducing velocities defined by

$$v_x \triangleq \frac{\partial w_x}{\partial t} \qquad v_y \triangleq \frac{\partial w_y}{\partial t} \qquad v_z \triangleq \frac{\partial w_z}{\partial t}$$

it is possible to manipulate these equations into the symmetric hyperbolic form of (3.1), with $\mathbf{w} = [v_x, v_y, v_z, \sigma_{xx}, \sigma_{yy}, \sigma_{zz}, \sigma_{xy}, \sigma_{xz}, \sigma_{yz}]^T$, and

$$\mathbf{P} = \begin{bmatrix} \mathbf{P}_N^+ & \cdot \\ \cdot & \mathbf{P}_N^- \end{bmatrix} \qquad \mathbf{A}_1 = \begin{bmatrix} \cdot & \mathbf{A}_{N1\times} \\ \mathbf{A}_{N1\times}^T & \cdot \end{bmatrix} \qquad \mathbf{A}_2 = \begin{bmatrix} \cdot & \mathbf{A}_{N2\times} \\ \mathbf{A}_{N2\times}^T & \cdot \end{bmatrix} \qquad \mathbf{A}_3 = \begin{bmatrix} \cdot & \mathbf{A}_{N3\times} \\ \mathbf{A}_{N3\times}^T & \cdot \end{bmatrix}$$

with

$$\mathbf{P}_N^+ = \mathrm{diag}(\rho, \rho, \rho) \qquad \mathbf{P}_N^- = \begin{bmatrix} \frac{1}{E} & \frac{-\nu}{E} & \frac{-\nu}{E} & 0 & 0 & 0 \\ \frac{-\nu}{E} & \frac{1}{E} & \frac{-\nu}{E} & 0 & 0 & 0 \\ \frac{-\nu}{E} & \frac{-\nu}{E} & \frac{1}{E} & 0 & 0 & 0 \\ 0 & 0 & 0 & \frac{1}{\mu} & 0 & 0 \\ 0 & 0 & 0 & 0 & \frac{1}{\mu} & 0 \\ 0 & 0 & 0 & 0 & 0 & \frac{1}{\mu} \end{bmatrix}$$

and

$$\mathbf{A}_{N1\times} = \begin{bmatrix} -1 & 0 & 0 \\ 0 & 0 & 0 \\ 0 & 0 & 0 \\ 0 & -1 & 0 \\ 0 & 0 & -1 \\ 0 & 0 & 0 \end{bmatrix}^T \qquad \mathbf{A}_{N2\times} = \begin{bmatrix} 0 & 0 & 0 \\ 0 & -1 & 0 \\ 0 & 0 & 0 \\ -1 & 0 & 0 \\ 0 & 0 & 0 \\ 0 & 0 & -1 \end{bmatrix}^T \qquad \mathbf{A}_{N2\times} = \begin{bmatrix} 0 & 0 & 0 \\ 0 & 0 & 0 \\ 0 & 0 & -1 \\ 0 & 0 & 0 \\ -1 & 0 & 0 \\ 0 & -1 & 0 \end{bmatrix}^T$$

### Phase and Group Velocities

The characteristic polynomial relation for the Navier system, in terms of frequencies $\omega$ and wavenumbers $\|\beta\|_2 = \sqrt{\beta_x^2 + \beta_y^2 + \beta_z^2}$, will be

$$\omega^3 \left(\omega^2 - \frac{\lambda + 2\mu}{\rho}\|\beta\|_2^2\right)\left(\omega^2 - \frac{\mu}{\rho}\|\beta\|_2^2\right)^2 = 0$$

and has roots

$$\omega = 0, \qquad \pm\sqrt{\frac{\lambda + 2\mu}{\rho}}, \qquad \pm\sqrt{\frac{\mu}{\rho}}$$

Ignoring the non-propagating modes with frequency $\omega = 0$, and the multiplicities of the other modes, we can see that wave propagation is dispersionless, at least for the constant-coefficient problem. There are two wave speeds,

$$\gamma_{N,P}^{p} = \gamma_{N,P}^{g} = \sqrt{\frac{\lambda + 2\mu}{\rho}} \qquad \geq \qquad \gamma_{N,S}^{p} = \gamma_{N,S}^{g} = \sqrt{\frac{\mu}{\rho}}$$

which are also known as the P-wave and S-wave (or compressional and shear wave) speeds [35].

For the varying-coefficient problem, the global maximum group velocity is then

$$\gamma_{N,max}^{g} = \max_{\mathbf{x}\in\mathcal{D}} \sqrt{\frac{\lambda + 2\mu}{\rho}}$$

## 5.6.1 Scattering Networks for the Navier System

Nitsche has represented this system as an MDKC in [131]. Choosing current-like variables

$$(i_1, i_2, i_3, i_4, i_5, i_6, i_7, i_8, i_9) = (v_x, v_y, v_z, r_1\sigma_{xx}, r_1\sigma_{yy}, r_1\sigma_{zz}, r_2\sigma_{xy}, r_2\sigma_{xz}, r_2\sigma_{yz})$$

he derived an MDKC for the Navier system, which we have reproduced (with some minor changes) at top in Figure 5.25, where coordinates defined by the transformation matrix (3.24) have been used. Notice that again, because $\mathbf{P}$ is not diagonal, the time derivatives of the components $\sigma_{xx}$, $\sigma_{yy}$ and $\sigma_{zz}$ are coupled. In the circuit representation, this is represented by a three-port coupled inductance of the form of (2.48), with a matrix inductance $\mathbf{L}_{456}$ defined by

$$\mathbf{L}_{456} = \begin{bmatrix} L_4 & -L_\times & -L_\times \\ -L_\times & L_5 & -L_\times \\ -L_\times & -L_\times & L_6 \end{bmatrix}$$

where the inductances $L_4$, $L_5$, $L_6$ and $L_\times$ appear in the figure.

The positivity condition on the inductances $L_1$, $L_2$, $L_3$, $L_7$, $L_8$ and $L_9$, as well as a positive definiteness condition on the matrix $\mathbf{L}_{456}$ gives, as optimal choices of the parameters $r_1$ and $r_2$,

$$\begin{aligned} r_1 &= \max_{x,y,z}\left(\frac{E}{1-2\nu}\right)\sqrt{\frac{\min_{x,y,z}(\rho)}{\max_{x,y,z}\left(\frac{E}{1-2\nu}\right)+2\max_{x,y,z}(2\mu)}} \\ r_2 &= \max_{x,y,z}(2\mu)\sqrt{\frac{\min_{x,y,z}(\rho)}{\max_{x,y,z}\left(\frac{E}{1-2\nu}\right)+2\max_{x,y,z}(2\mu)}} \end{aligned}$$

and a bound on $v_0$,

$$v_0 \geq v_N \triangleq \sqrt{\frac{\max_{x,y,z}\left(\frac{E}{1-2\nu}\right)+2\max_{x,y,z}(2\mu)}{\min_{x,y,z}(\rho)}}$$

When the material parameters are constant, $v_N$ reduces to

$$v_N = \sqrt{\frac{3(\lambda+2\mu)}{\rho}} = \sqrt{3}\gamma^g_{N,max}$$

A modified MDKC is shown at top in Figure 5.26, where velocities are treated as currents, and stresses as voltages; as such, the coupled inductance in Figure 5.25 has become a coupled capacitance. This network may be discretized in a way very similar to the network for Maxwell's Equations, as described in §4.10.6. Under the spectral mappings defined by (4.112) (with step sizes of $T_j = \Delta/2$, $j = 1,\ldots,6$), the connecting LSI two-ports decompose into series/parallel connections of multidimensional unit elements. The one-port inductances and capacitances, as well as the coupled capacitance are discretized using the trapezoid rule, with a step size of $T_7 = \Delta$. The resulting multidimensional DWN is shown at bottom in Figure 5.26, and the interleaved computational grid in Figure 5.27 (which is very similar to the grid for the DWN for Maxwell's Equations, as shown in Figure 4.55).

### 5.6.2 Boundary Conditions

The simplest boundary conditions for the Navier system are of the free type, i.e., all stresses normal to the boundary are zero [77]. For a "bottom" boundary $z = 0$, these conditions can be written as

$$\sigma_{xz} = \sigma_{yz} = \sigma_{zz} = 0 \tag{5.55}$$

This condition is lossless and of the form of (3.8).

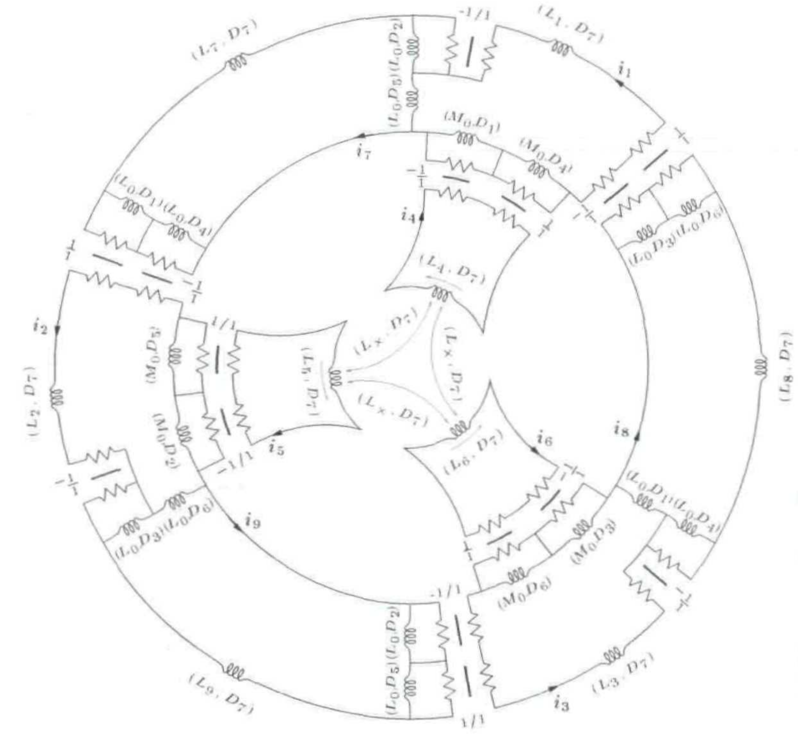
(L_7, D_7)
(L_0D_5)(L_0D_2)
-1/1
(L_1, D_7)
i_1
(M_0D_1)
(M_0D_4)
i_7
i_4
(L_0D_1)(L_0D_4)
(L_0D_3)(L_0D_6)
i_2
(L_4, D_7)
(L_x, D_7)
(L_5, D_7)
(M_0D_5)
1/1
(L_8, D_7)
(L_2, D_7)
(M_0D_2)
i_5
(L_6, D_7)
i_6
i_8
i_9
(M_0D_3)
(M_0D_6)
(L_9, D_7)
(L_3, D_7)
i_3

$$L_0 = \tfrac{r_2}{2} \qquad M_0 = \tfrac{r_1}{2}$$

$$L_1 = L_2 = L_3 = v_0\rho - 2r_2 - r_1$$

$$L_4 = L_5 = L_6 = v_0 r_1^2/E - r_1$$

$$L_\times = v_0 r_1^2 \nu/E$$

$$L_7 = L_8 = L_9 = v_0 r_2^2/\mu - 2r_2$$

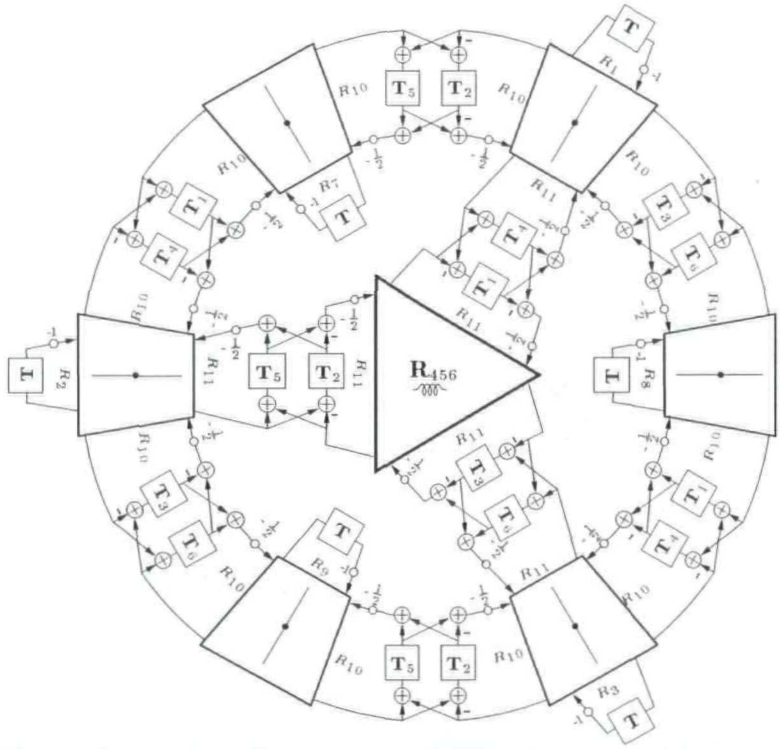
T
R_1
-1
R_10
T_5
T_2
R_7
T_1
T_4
T_3
T_6
-1/2
R_11
R_456
R_2
R_8
R_9
R_3

$$R_1 = \tfrac{2L_1}{\Delta} \quad R_2 = \tfrac{2L_2}{\Delta} \quad R_3 = \tfrac{2L_3}{\Delta}$$

$$\mathbf{R}_{456} = \tfrac{2}{\Delta}\begin{bmatrix} L_4 & -L_\times & -L_\times \\ -L_\times & L_5 & -L_\times \\ -L_\times & -L_\times & L_6 \end{bmatrix}$$

$$R_7 = \tfrac{2L_7}{\Delta} \quad R_8 = \tfrac{2L_8}{\Delta} \quad R_9 = \tfrac{2L_9}{\Delta}$$

$$R_{10} = \tfrac{4L_0}{\Delta} \qquad R_{11} = \tfrac{4M_0}{\Delta}$$

Figure 5.25: *MDKC and MDWD network for the Navier system.*

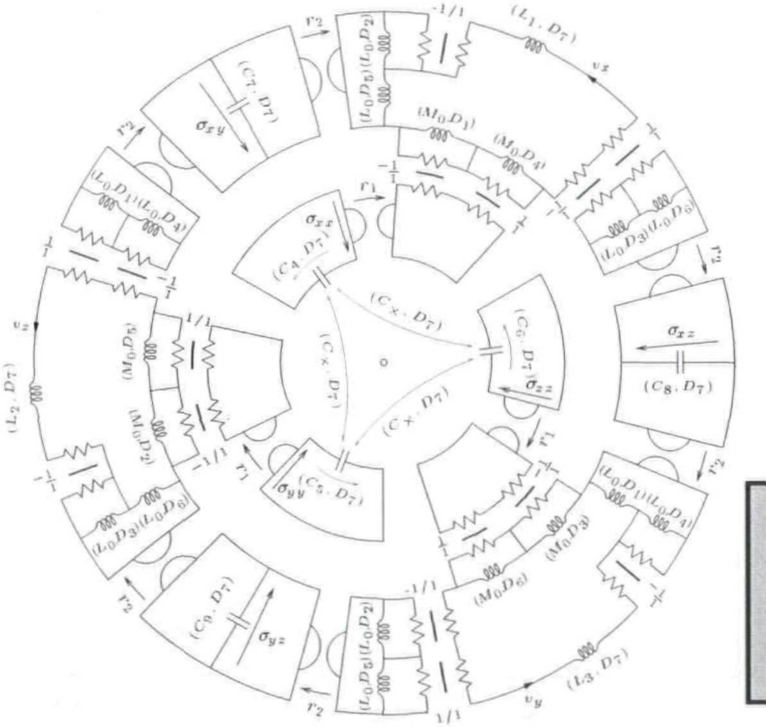
$r_2$
$r_1$
-1/1
1/1
$(L_1, D_7)$
$(L_2, D_7)$
$(L_3, D_7)$
$v_x$
$v_y$
$v_z$
$(L_0D_5)(L_0D_2)$
$(L_0D_1)(L_0D_4)$
$(L_0D_3)(L_0D_6)$
$(M_0D_1)$
$(M_0D_4)$
$(M_0D_2)$
$(M_0D_5)$
$(M_0D_3)$
$(M_0D_6)$
$\sigma_{xy}$
$(C_7, D_7)$
$\sigma_{xx}$
$(C_4, D_7)$
$(C_\times, D_7)$
$(C_6, D_7)$
$\sigma_{zz}$
$\sigma_{xz}$
$(C_8, D_7)$
$\sigma_{yy}$
$(C_5, D_7)$
$(C_9, D_7)$
$\sigma_{yz}$

$$L_0 = \frac{\Delta r_2}{2} \qquad M_0 = \frac{\Delta r_1}{2}$$

$$L_1 = L_2 = L_3 = \Delta(v_0\rho - 2r_2 - r_1)$$

$$C_4 = C_5 = C_6 = \Delta(v_0/E - 1/r_1)$$

$$C_\times = \Delta v_0 \nu / E$$

$$C_7 = C_8 = C_9 = \Delta(v_0/\mu - 2/r_2)$$

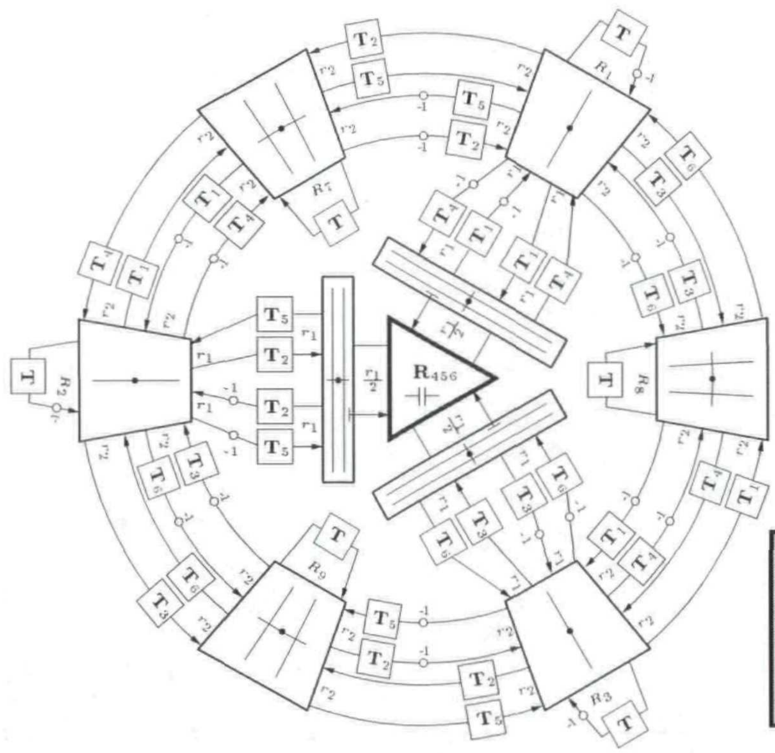
T
$\mathbf{T}_1$
$\mathbf{T}_2$
$\mathbf{T}_3$
$\mathbf{T}_4$
$\mathbf{T}_5$
$\mathbf{T}_6$
$R_1$
$R_2$
$R_3$
$R_7$
$R_8$
$R_9$
$\mathbf{R}_{456}$
$r_1$
$r_2$
-1
$\frac{r_1}{2}$

$$R_1 = \frac{2L_1}{\Delta} \quad R_2 = \frac{2L_2}{\Delta} \quad R_3 = \frac{2L_3}{\Delta}$$

$$\mathbf{R}_{456} = \frac{\Delta}{2}\begin{bmatrix} C_4 & -C_\times & -C_\times \\ -C_\times & C_5 & -C_\times \\ -C_\times & -C_\times & C_6 \end{bmatrix}^{-1}$$

$$R_7 = \frac{\Delta}{2C_7} \quad R_8 = \frac{\Delta}{2C_8} \quad R_9 = \frac{\Delta}{2C_9}$$

Figure 5.26: *Modified MDKC and multidimensional DWN for the Navier system.*

Considering the DWN shown at bottom in Figure 5.26, and the associated computational grid shown in Figure 5.27, it is easy to see that in this case, it best to arrange the grid such that parallel junctions (at which approximations to $\sigma_{xz}$ and $\sigma_{yz}$ are calculated) lie on this bottom boundary. The first two of conditions (5.55) can be ensured by short-circuiting the parallel junctions. As a result, the remaining series junctions on the boundary (at which approximations to $v_z$ are calculated) are decoupled from the parallel junctions, and it remains only to set a self-loop impedance at these junctions so as to approximate the condition $\sigma_{zz} = 0$. We leave the determination of these self-loop impedances as an exercise to the reader.

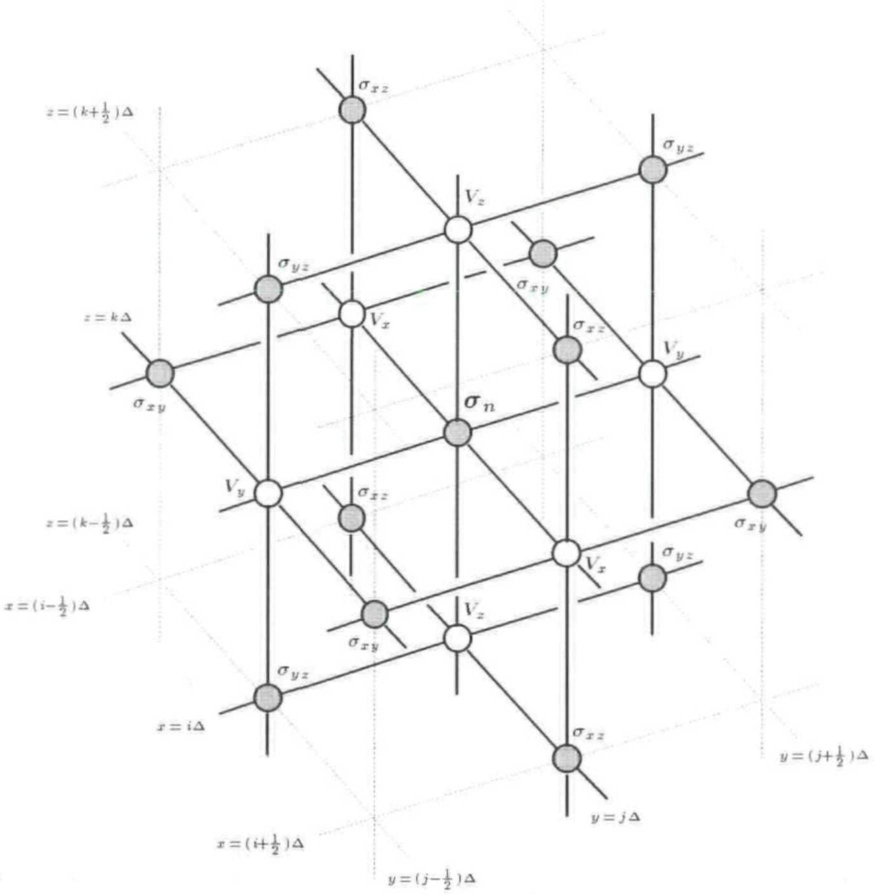

$\sigma_{xz}$
$z=(k+\frac{1}{2})\Delta$
$\sigma_{yz}$
$V_z$
$\sigma_{yz}$
$\sigma_{xy}$
$z=k\Delta$
$V_x$
$\sigma_{xz}$
$V_y$
$\sigma_{xy}$
$\boldsymbol{\sigma}_n$
$V_y$
$\sigma_{xz}$
$\sigma_{xy}$
$z=(k-\frac{1}{2})\Delta$
$V_x$
$\sigma_{yz}$
$x=(i-\frac{1}{2})\Delta$
$V_z$
$\sigma_{xy}$
$\sigma_{yz}$
$x=i\Delta$
$\sigma_{xz}$
$y=(j+\frac{1}{2})\Delta$
$y=j\Delta$
$x=(i+\frac{1}{2})\Delta$
$y=(j-\frac{1}{2})\Delta$

Figure 5.27: *Computational grid for the DWN for Navier's system; stresses and velocities are calculated at alternating multiples of $T/2$, and at alternating grid locations. In the DWN implementation, waveguide connections (of delay length $T/2$) between series junctions (white) and parallel junctions (grey) are shown as dark lines; waveguide sign inversions and self-loops are not shown here. At the center grid point, a vector parallel junction calculates the vector $\boldsymbol{\sigma}_n = (\sigma_{xx}, \sigma_{yy}, \sigma_{zz})$ of normal stresses.*

# Chapter 6

# Conclusions and Future Directions

An extended summary of the technical results in this thesis appeared in §1.3. We will mention these results only as they touch upon the general questions of §1.2, which we now address.

## 6.1 Answers

- *To what types of systems can wave digital and digital waveguide network simulation approaches be applied?*

Let us first confine our attention to numerical methods which result from the passive discretization of an MDKC; all the methods discussed in this thesis are of this form, except for the multigrid methods of §4.9, the type I and II DWNs for the transmission-line and parallel-plate problems (see §4.3.6 and §4.4.2, respectively), the DWN for the Euler-Bernoulli beam system (see §5.1) and the Timoshenko beam systems of §5.2.3. We can then rephrase our question as: *For which types of systems do there exist passive MDKC representations?*

In general, MDKC representations follow directly only for $(n+1)$D symmetric hyperbolic systems of the form of (3.1), and we repeat this definition here.

$$\mathbf{P}\frac{\partial \mathbf{w}}{\partial t}+\sum_{k=1}^{n}\mathbf{A}_k\frac{\partial \mathbf{w}}{\partial x_k}+\mathbf{B}\mathbf{w}+\mathbf{f}=\mathbf{0} \tag{6.1}$$

Recall that the coupling matrices $\mathbf{A}_k$ are constrained to be symmetric and constant, so all material parameter variation is confined to the symmetric positive-definite matrix coefficient $\mathbf{P}$ of the time derivatives, and the coefficient $\mathbf{B}$ of the constant-proportional terms. (Indeed, $\mathbf{B}$ can be *time-varying* without affecting the network representation of any system in which it appears. We will look at the more useful case of time variation of $\mathbf{P}$, which occurs in, e.g., time-varying vocal tract models [145], in §6.2.7.) For passivity, we generally require that the symmetric part of $\mathbf{B}$ be positive semi-definite. The *symmetry* of the $\mathbf{A}_k$ implies a network representation involving only *reciprocal* reactive MD circuit elements[†]. In fact, the structure of the $\mathbf{A}_k$ directly specifies the MD network topology; if any of the $\mathbf{A}_k$ contains a non-zero entry in the $(p,q)$th position, then we will necessarily have some coupling between the $p$th and $q$th loops in the network representation. The constancy of the $\mathbf{A}_k$ has important implications for the energetic analysis of the system, as we saw in §3.2, and also ensures that all inter-loop couplings can be accomplished through the use of linear and shift-invariant (LSI) coupling elements (generally the Jaumann or lattice two-ports introduced in §3.7.2 for MDWDFs, or the alternative hybrid form of §4.10 for DWNs). This is crucial, because the spatial derivative information is concentrated in these coupling elements; discretization of a reactive element is usually only passive if its defining parameters (usually inductances) are independent of the integration directions. (The main exceptions here are the reactive elements discussed at the end of §3.5.1; such elements can be used in the time-varying case, as mentioned above, or in nonlinear problems, which we will discuss at length in Appendix B.) In fact, all the MD-passive systems we have examined have networks which can be decomposed into two networks as in Figure 6.1. The subnetwork on the left is made up of a set of time inductors (or capacitors) with spatially-varying inductances (or capacitances), and perhaps resistances and can be discretized through the trapezoid rule in time. In the expanded signal-flow graphs, these always give rise to *self-loops*. The right-hand subnetwork is linear and shift-invariant, and contains all the spatial derivative terms, in the form of Jaumann or lattice connections, for MDWDFs, or the hybrid form for DWNs, discussed in §4.10. It can be discretized by the MD trapezoid rule (or alternative spectral mappings, for DWNs), and the full discrete network will be passive if the subnetworks are MD-passive separately.

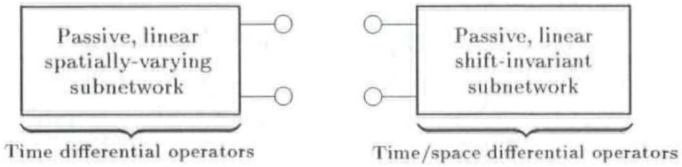

Figure 6.1: *Network decomposition of passive symmetric hyperbolic systems.*

A few other features are worthy of comment. First, although the $\mathbf{P}$ matrix is diagonal for many of the systems we have looked at, it is *not* for any of the vibrating elastic systems in (2+1)D and (3+1)D of Chapter 5 (nor will it be for, say, Maxwell's equations in anisotropic media, or mutually inductive coupled transmission lines, or systems in general curvilinear coordinate systems). The non-diagonal elements of $\mathbf{P}$ are modeled in an MDKC as mutual inductances or capacitances, and subsequently require vector scattering junctions, as discussed in §2.3.7. This leads to more complex "block" scattering matrices, but passivity is not compromised. Second, consider the $\mathbf{B}$ matrix, which is not constrained to be of any particular form. If the symmetric part of **B** is positive semi-definite, then it always implies *loss*, and can be realized as a purely resistive coupling network. The anti-symmetric part of **B**, which does not produce loss, gives rise to ***dispersion*** (as for the Timoshenko beam in §5.2, the Mindlin plate in §5.4 and the shell models of §5.5), and corresponds to lossless gyrator couplings among the circuit loops. In general, if the **B** matrix is not sparse, the resulting resistive and gyrator couplings in the MDKC may considerably complicate the resulting discrete network (i.e., various reflection-free ports will be required). Third, the system (6.1) forms a subclass of what are called ***strongly hyperbolic*** systems, for which the initial value problem is well-posed [82]. A general strongly hyperbolic also can be written in the form of (6.1), but the matrices $\mathbf{A}_k$ are not constrained to be symmetric (any real linear combination of the $\mathbf{A}_k$ must, however, possess a set of real distinct eigenvalues). If the $\mathbf{A}_k$ can not be simultaneously symmetrized by some change of variables, then it is clear that the set of reactive reciprocal circuit elements does not suffice for a passive circuit representation, even though energy estimates of the type discussed in §3.2 may be available. It would be quite interesting to know how a network could be designed for such strongly, but not symmetric hyperbolic systems. Furthermore, system (6.1) is not even the most general form of symmetric hyperbolic system. The matrices $\mathbf{A}_k$ may be functions of space or time variables, though the simple energetic analysis of §3.2 becomes more involved; passivity does not immediately follow. Fourth, we included a discussion of a DWN for the Euler-Bernoulli system in §5.1, in order to indicate that such networks may be available even if the physical system is not hyperbolic (group velocities are ***unbounded*** for the classical beam model). Such extensions of scattering methods have also been discussed in the MDWD context in [202]. Fifth, for nonlinear systems, the natural extension of symmetric hyperbolicity which leads to circuit representations is ***skew self-adjointness.*** We will examine such extensions in Appendix B.

---

[†] Recall that a reciprocal circuit element is one whose impedance matrix (more generally, its hybrid matrix) is Hermitian.

- *What features do the two methods share, and what distinguishes them?*

The most basic difference between the two methods is, as we emphasized early on in Chapter 1, that a DWN can always be viewed as a large network of scattering junctions, connected to one another ***port-wise*** by bidirectional delay lines; a MDWD network is better thought of as the discrete image of a multidimensional Kirchoff circuit representation (MDKC). Though a signal flow graph for a MDWD network follows immediately, it can not be decomposed into a collection of discrete transmission lines, or bidirectional delay lines. Both methods, however, operate using exclusively scattering and shifting operations—it may be useful to flip to Figure 4.44, which shows the expanded signal flow graphs for the DWN and MDWD networks for the (1+1)D transmission line equations. Notice that the port-wise connectivity of the MDWD network is always lost in this (and all) expanded forms; for certain adaptors, the two wave signal paths entering the "port" are not connected to the two terminals of another single port. We have seen, of course, in §4.10, that many DWN forms operating on regular grids can also be derived from MD circuit representations; DWNs are more general in the sense they may be constructed completely *locally*, and in irregular arrangements (recall the general discussion of DWNs in §1.1.2), without using an MDKC.

We have also seen, in the first few sections of Chapter 4, that DWNs are in general equivalent to simple two-step centered finite difference schemes of the FDTD variety. In §3.9, we showed that MDWD simulation methods also correspond to finite difference schemes, but they are in general multi-step methods. In both cases, the calculations have been rearranged (using wave variables) in a *one-step* form. If the underlying system is lossless, and power-normalized wave variables are employed, then at any time step the discrete network recursion involves an *orthogonal transformation* (scattering) applied to the entire set of wave variables stored in memory, followed by a *permutation* (shifting) operation. Losslessness, and thus stability is thus ensured in a very direct way. The two methods possess distinct spectral properties, which we examined briefly in the case of the (1+1)D transmission line in §4.3.8.

There is another more subtle distinction. For almost all first-order PDE systems that follow from physical laws, the state variables can be separated into two types which are *dual* to one another. To be more precise, in all the systems of the form of (6.1) which we have examined in this thesis, the time derivative of a variable of one type is always related to spatial derivatives of variables of the other type; for example, voltages and currents are dual variables in the transmission line and parallel-plate problems, as are electric and magnetic field components described by Maxwell's equations (4.110), etc. This duality implies a certain structure in the coupling matrices $\mathbf{A}_k$. In the MDKCs developed by Fettweis et al., however, this structure is ignored, and all variables are treated generally as *currents*. In the resulting numerical methods, this usually implies that all the dependent variables are computed *together* at the same spatial locations, and at all time steps. (As we mentioned in §3.9, however, it is possible to design MDWD simulation methods operate on "checkerboard" grids; the variables are all computed together, but at locations interleaved in time and space.) For the DWNs we discussed in Chapters 4 and 5, we have made use of this duality in order to design networks in which the two sets of variables are computed at alternating time instants and spatial locations. One set is interpreted as *current-like*, and the other as *voltage-like*. The resulting alternations are generally indicated by grey/white junction colorings in the signal flow graphs. (It is worth calling attention, at this point, to the analogous distinction between so-called "expanded" and "condensed" node TLM formulations [29].)

- *What are their relative advantages?*

The answers to the previous question have several practical implications.

Because any DWN always can be written in the form of a large network of port-wise connected scattering junctions, passive (and thus stable) boundary termination is straightforward. For the transmission line (see §4.3.9), the parallel-plate problem (see §4.4.4), beams (see §5.1.3 and §5.2.4) and plates (see §5.4.2), many useful lossless boundary conditions can be effected through the use of simple short- or open-circuit, or self-loops connected to scattering junctions which lie on the boundary. In fact, the termination of any boundary junction with an *all-pass* (more generally *bounded real*) scattering one-port will *always* yield a numerical scheme which is guaranteed *lossless* (more generally *passive*), though the physical interpretation of such an arbitrary termination may not be obvious. It is worth emphasizing that the ease with which passivity (or exact losslessness, if so desired) can be ensured in the presence of boundary conditions is one great benefit of a scattering formulation. It can be quite difficult to ensure the stability of a boundary condition applied to a finite difference scheme. The same is not true of MDWD networks; because port-wise connectivity is lost in the expanded signal-flow graph, passive termination is no longer simple or straightforward. We indicated in §3.11 and §5.2.4 the severe difficulties inherent in the "wave-canceling" termination approach described in the literature [107], and will look at a possible theoretical foundation for passive distributed network termination shortly in §6.2.3.

An MDKC is always mapped, via spectral transformations or integration rules, to a discrete time and space MDWD image network. As we mentioned above, the resulting numerical method always operates on a regular grid in some coordinate system. It is thus impossible, through the approach of Fettweis et al., to arrive at structures which operate on irregular grids. As we have seen in §4.9, because DWNs may be constructed locally, multigrid methods become a possibility—DWNs of differing densities or in different coordinate systems may be simply connected to one another, in such a way that passivity is maintained across the interface. Such interfaces can be designed so as to be locally consistent with the underlying model problem; as a result, numerical reflection vanishes as the grid spacings become small. The applications to numerical integration over irregular problem domains should be self-evident.

- *Can they be unified in a formal way?*

The single most satisfying result in this thesis was the successful "merging" of waveguide networks and MDWDFs in §4.10. A passive MDKC representation of a system of PDEs is no more than that—a representation. It illustrates, however, how the system can be decomposed into simpler elements, each of which is passive in its own right, and immediately suggests a stable numerical scheme. Each element can be discretized through the application of one or a set of spectral mappings, or multidimensional integration rules, in such a way that this passivity is preserved (this is discussed in §3.5.3) in a discrete network, which can then be directly implemented as a computer simulation routine. The MD trapezoid rule, or bilinear transform, which gives rise to wave digital networks, is one such rule but is by no means the only way of proceeding; in multiple dimensions, the family of such mappings is large and diverse. Digital waveguide networks are the result of the application of another member of this family. As we have seen, especially in Chapter 5, digital waveguide networks are now applicable to any system that has been approached using MDWDFs (we have covered most of them in this thesis). We will make some more comments on this subject in the §6.2.5, but at this stage, the author feels justified in lumping these techniques together as simply "wave" or "scattering" methods.

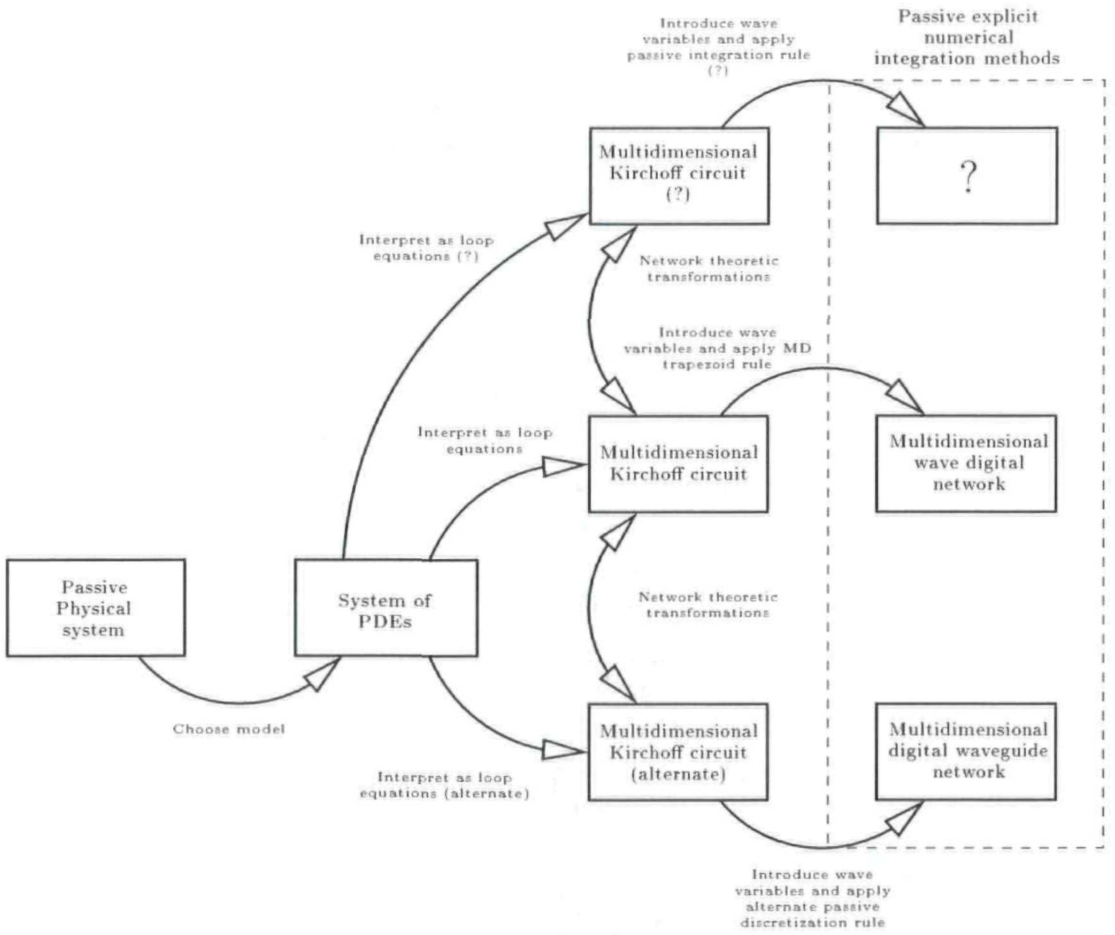
Introduce wave variables and apply passive integration rule (?)
Passive explicit numerical integration methods
Multidimensional Kirchoff circuit (?)
?
Interpret as loop equations (?)
Network theoretic transformations
Introduce wave variables and apply MD trapezoid rule
Interpret as loop equations
Multidimensional Kirchoff circuit
Multidimensional wave digital network
Passive Physical system
System of PDEs
Network theoretic transformations
Choose model
Multidimensional Kirchoff circuit (alternate)
Multidimensional digital waveguide network
Interpret as loop equations (alternate)
Introduce wave variables and apply alternate passive discretization rule

Figure 6.2: *The generalized family of passive numerical methods.*

As indicated in Figure 6.2, the unification of these two methods also implies their membership within a larger class of passive numerical methods; indeed, *any* set of passive spectral mappings or integration rules may be applied to *any* circuit representation of a system of PDEs, and the result is necessarily a stable numerical method built of the same basic scattering and shifting operations as the DWN or an MDWD network. We refer to §6.2.5 for a few further comments on this subject.

- *What extensions and improvements can be made to the existing forms of these methods?*

For all stable explicit numerical methods for hyperbolic systems, a CFL-type condition must necessarily be obeyed. That is, if the time step is $T$, and the grid spacing is $\Delta$, then we will require

$$T \leq \kappa\gamma_{max}\Delta \tag{6.2}$$

where $\gamma_{max}$ is the maximum local group velocity of the system, as defined in §3.2. In other words, the physical region of dependence of the problem must be contained within the region of dependence of the recursion. The parameter $\kappa$ is some constant which depends on problem specifics, such as the number of spatial dimensions, the width of the computational stencil of the scheme, etc., but not the material parameter values themselves. One serious shortcoming of the MDWD numerical methods proposed by Fettweis et al. is that for a given grid spacing, the maximum time-step allowed may be a good deal smaller than the optimal CFL bound, if there are spatial variations in the physical medium. As we have seen in §5.2.1, this constraint on the time step becomes especially severe for stiff vibrating systems. We showed in §3.12 and §5.2.6 how *balancing* approaches may be used to derive networks which give rise to numerical methods which are optimal in that a bound of the type (6.2) is satisfied. Certain DWNs (in particular, the type I and II forms for the transmission line, parallel-plate systems) also exhibit this optimality property, though such forms do not follow directly from MDKC representations that we have discussed.

The DWN has been applied, in the past, to problems in musical acoustics and physical modeling. In particular, DWNs have been used to solve the wave equation in one, (uniform strings and acoustic tubes) two (membranes), or three (room acoustic) spatial dimensions. We have looked at numerous ways of extending the DWN to deal with more realistic problems. First, from the result in §4.10, the DWN is now applicable to a wide class of physical systems, and in particular, those which may exhibit material parameter variation. Among them are the transmission line and parallel-plate problems (which are analogous to strings and membranes, of varying density), and the many elastic solid systems discussed in Chapter 5. In fact, DWNs are fully as general as the MDWD simulation networks of Fettweis, and possess all the same good numerical properties; because boundary conditions are easier to deal with, one might go so far as to say that they are a superior form of scattering method. Second, we examined ways of dealing with boundary and initial conditions in a systematic way (as we mentioned above, this has not been done for MDWD networks). Third, we introduced DWN formulations appropriate for problems with irregular boundary configurations; waveguide meshes in transformed coordinates and multigrid forms are two possibilities. Fourth, we examined the possibilities of higher-order spatially accurate DWNs which follow directly from an MDKC representation. Fifth, we will spend some time in Appendix A cataloging the many forms of waveguide mesh which have been proposed, and looking into ways of improving their numerical dispersion behavior.

## 6.2 Future Directions

In this section, we provide a short list of some possible avenues of future research in the area of numerical integration using wave and scattering methods; several of these topics will be presented in technical detail. (Although this is perhaps not the place for such a treatment, we will do so because this material of a speculative character, and a bit too general in scope to appear in the main chapters.) Some of the more promising directions are discussed in the appendices, namely applications to fluid dynamics systems (see Appendix B), and especially, the spectral analysis of digital waveguide networks for the wave equation (see Appendix A).

### 6.2.1 Passivity vs. Stability

Perhaps the single most interesting question resulting from this thesis can be simply stated: For a given stable finite difference scheme, where "stable" is to be taken in the sense of Von Neumann (see Appendix A), is there *always* a concretely passive network realization? Because the difference scheme coefficients and network element values are usually parametrized by $v_0$, the space step/time step ratio, the question is often one of the *range* of values of $v_0$ for which a given scheme is stable or passive. As we have seen, a distinction between passivity and stability manifests itself in various ways in many very different settings. We saw, for example, in Section 4.3.6, that several different waveguide networks for the transmission line problem, though all equivalent in infinite-precision arithmetic to the same simple centered difference approximation, are passive over quite different ranges of $v_0$, depending on material parameter variation. Even more striking examples will be seen in Appendix A, in the case of the triangular scheme for the (2+1)D wave equation, and in particular for so-called "interpolated" difference schemes for the wave equation in (2+1)D and (3+1)D; these are rudimentary constant-coefficient difference schemes, and yet the difference between the stability condition and the passivity condition for the equivalent waveguide mesh is already quite complex; for the other mesh structures examined in Appendix A, Von Neumann stability and passivity imply one-another. Other instances appear throughout this work. The question is one of network topology—that is, there are many network topologies corresponding to a given difference scheme, and though the stability bound on $v_0$ will be the same for all of them, the bounds for passivity will be, in general, distinct (see §A.2.3 and §A.2.4 for some interesting examples). In sum, passivity is a sufficient, but not necessary condition for numerical stability; it may well be, however, that it is always possible to find a particular topology such that these conditions imply one-another. This author would like very much to make sense of the "grey area" between the two conditions.

### 6.2.2 Higher-order Accuracy

It is known that for lumped systems (i.e., those described by sets of ODEs), *A-stable* methods [32, 65, 75] such as WDF network simulators can be at best second-order accurate; that is, the truncation error between the solution to the difference scheme and the exact solution will behave as $O(T^2)$, where $T$ is the time step. In §3.13 and §4.10.5, however, we showed that it is possible to construct networks that behave as higher-order *spatially* accurate difference schemes, at least for the (1+1)D transmission line equations. The question remains open, however, as to whether it is possible to obtain higher-order time-accurate scattering methods. (One of the originators of the

MDWD simulation method remarked [130] that he had spent an inordinate amount of time trying to design higher-order time accurate methods with no success.) It would be of great use to have a firm answer to this question, mainly because it would provide a clue to answering the question in the previous paragraph; rather, it would encourage us to rephrase it as: "Is there any stable difference scheme which can *not* be written in a scattering form?"

### 6.2.3 MDKC Modeling of Boundaries

One of the big hurdles yet to be overcome in the MDWD simulation method is the implementation of boundary conditions. As we mentioned briefly in §3.11, this is a very tricky business, and the approaches in the literature for simple model problems do not generalize to more complex systems. Setting boundary conditions for systems such as beams and plates was a time-consuming, and ultimately fruitless venture. We were forced to turn to DWNs, for which appropriate boundary conditions are much easier to find, because the DWN can be interpreted as a lumped network. The problem is that there is not, as yet, a general theory of boundary conditions for MDWD simulation methods [142]. In this section, we briefly mention a possible foundation for such a theory which is based on the ideas presented initially in [48, 85, 131] and outlined in §3.4.

Suppose that the problem of interest is $(n+1)$D, and defined with respect to coordinates $\mathbf{u} = [x_1, \ldots, x_n, t]^T$, or equivalently, to $k$ transformed coordinates $\mathbf{t} = [t_1, \ldots, t_k]^T$, with $k \geq n+1$. We will assume that the problem has one spatial boundary, namely the hyperplane $x_1 = 0$, and is defined over a time interval $[0, t_f]$. As such, the problem domain $G$ is then

$$G = \{\mathbf{u} |\ 0 \leq t \leq t_f, x_1 \geq 0\}$$

or its equivalent in the $\mathbf{t}$ coordinates, obtained under a transformation of the form (3.21). We restate the energy balance for an $N$-port defined over $G$, which is

$$\int_G (w_{inst} + w_s)\, dV_{\mathbf{t}} = \int_G (w_d + \nabla_{\mathbf{t}} \cdot \mathbf{E})\, dV_{\mathbf{t}}$$

where $w_{inst}$ is the instantaneous applied power at the ports, $w_s$ is an internal source power, $w_d$ is dissipated power, and $\mathbf{E}$ is a column $k$-vector representing stored energy flux; $dV_{\mathbf{t}}$ is the differential volume element. As mentioned previously, the $N$-port is *integrally MD-passive* over $G$ if

$$\int_G w_{inst} dV_{\mathbf{t}} \geq \int_G \nabla_{\mathbf{t}} \cdot \mathbf{E} dV_{\mathbf{t}} = \int_{\partial G} \mathbf{n}_G \cdot \mathbf{E} d\sigma_G \tag{6.3}$$

for some $\mathbf{E}$, all of whose components in the $\mathbf{t}$ coordinates are positive everywhere in $G$. Here, $\partial G$ is the boundary of $G$, $\mathbf{n}_G$ is the unit outward normal, and $d\sigma_G$ is a differential surface element on the boundary.

Note that $\partial G$ consists of the union of three sets of points, i.e.,

$$\partial G = \partial G_0 \cup \partial G_f \cup \partial G_b$$

where, in terms of the physical $\mathbf{u}$ coordinates

$$\begin{aligned}
\partial G_0 &= \{\mathbf{u}|\ t = 0, x_1 \geq 0\} \\
\partial G_f &= \{\mathbf{u}|\ t = t_f, x_1 \geq 0\} \\
\partial G_b &= \{\mathbf{u}|\ 0 \leq t \leq t_f, x_1 = 0\}
\end{aligned}$$

We can thus rewrite (6.3) as

$$\int_G w_{inst} dV_{\mathbf{t}} \geq \int_{\partial G_0} \mathbf{n}_G \cdot \mathbf{E} d\sigma_G + \int_{\partial G_f} \mathbf{n}_G \cdot \mathbf{E} d\sigma_G + \int_{\partial G_b} \mathbf{n}_G \cdot \mathbf{E} d\sigma_G$$

For a *closed network*—that is, an $N$-port with no free terminals (corresponding to a complete system of PDEs)—the instantaneous applied power is zero, so we are left with

$$0 \geq \int_{\partial G_0} \mathbf{n}_G \cdot \mathbf{E} d\sigma_G + \int_{\partial G_f} \mathbf{n}_G \cdot \mathbf{E} d\sigma_G + \int_{\partial G_b} \mathbf{n}_G \cdot \mathbf{E} d\sigma_G \tag{6.4}$$

In other words, the stored power flux leaving the boundary must be negative (the $N$-port is passive).

Suppose, now, that there is an $n$D $N$-port defined on the spatial boundary $\partial G_b$ of $G$. Renaming this region $G^{(b)}$, we have another energy balance

$$\int_{G^{(b)}} \left( w_{inst}^{(b)} + w_s^{(b)} \right) dV_{\mathbf{t}^{(b)}} = \int_{G^{(b)}} \left( w_d^{(b)} + \nabla_{\mathbf{t}^{(b)}} \cdot \mathbf{E}^{(b)} \right) dV_{\mathbf{t}^{(b)}}$$

over coordinates $\mathbf{t}^{(b)}$ derived from physical coordinates $\mathbf{u} = [x_2, \ldots, x_n, t]^T$ on $G^{(b)}$. The quantities $w_{inst}^{(b)}$, $w_s^{(b)}$, $w_d^{(b)}$ and $\mathbf{E}^{(b)}$ are the applied power, source power, dissipated power, and stored energy flux in the boundary network. Again, if the boundary network is passive, we have

$$\int_{G^{(b)}} w_{inst}^{(b)} dV_{\mathbf{t}^{(b)}} \geq \int_{G^{(b)}} \nabla_{\mathbf{t}^{(b)}} \cdot \mathbf{E}^{(b)} dV_{\mathbf{t}^{(b)}} = \int_{\partial G^{(b)}} \mathbf{n}_{G^{(b)}} \cdot \mathbf{E}^{(b)} d\sigma_{G^{(b)}} \tag{6.5}$$

where $\partial G^{(b)}$ is the boundary of the region $G^{(b)}$, and consists of the union of the two regions

$$\begin{aligned}
\partial G_0^{(b)} &= \{\mathbf{t}^{(b)}|\ t = 0\} \\
\partial G_f^{(b)} &= \{\mathbf{t}^{(b)}|\ t = t_f\}
\end{aligned}$$

so that we have, finally,

$$\int_{G^{(b)}} w_{inst}^{(b)} dV_{\mathbf{t}^{(b)}} \geq \int_{\partial G_0^{(b)}} \mathbf{n}_{G^{(b)}} \cdot \mathbf{E}^{(b)} d\sigma_{G^{(b)}} + \int_{\partial G_f^{(b)}} \mathbf{n}_{G^{(b)}} \cdot \mathbf{E}^{(b)} d\sigma_{G^{(b)}} \tag{6.6}$$

The boundary network is intended to model a passive distributed termination to the problem defined over the region $G$. It should be clear that if both networks are passive, then if the transfer of energy between them is passive, then the terminated system as a whole will be passive. See Figure 6.3 for a representation of the relevant regions.

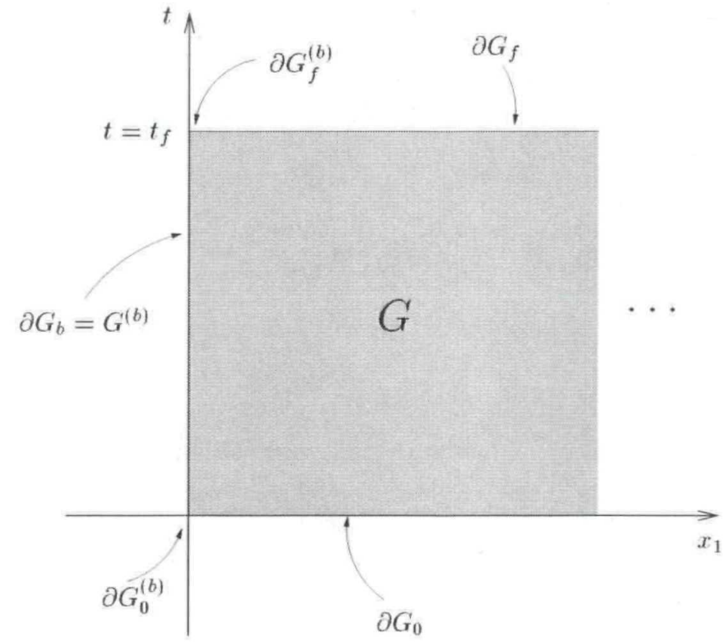

Figure 6.3: *A region with one spatial boundary.*

We can ensure this by requiring that the power applied through the ports of the boundary network over the region $G^{(b)}$ is equal to the stored energy flux of the interior network leaving through its spatial boundary (recall that we have set $G^{(b)} = \partial G_b$). In other words, we require

$$w_{inst}^{(b)} = \mathbf{n}_G \cdot \mathbf{E} \qquad \text{on} \qquad \partial G_b = G^{(b)}$$

Inequality (6.4) can then be rewritten as

$$0 \geq \int_{\partial G_0} \mathbf{n}_G \cdot \mathbf{E} d\sigma_G + \int_{\partial G_f} \mathbf{n}_G \cdot \mathbf{E} d\sigma_G + \int_{G^{(b)}} w_{inst}^{(b)} dV_{G^{(b)}}$$

or, by employing (6.6), as

$$0 \geq \int_{\partial G_0} \mathbf{n}_G \cdot \mathbf{E} d\sigma_G + \int_{\partial G_f} \mathbf{n}_G \cdot \mathbf{E} d\sigma_G + \int_{\partial G_0^{(b)}} \mathbf{n}_{G^{(b)}} \cdot \mathbf{E}^{(b)} d\sigma_{G^{(b)}} + \int_{\partial G_f^{(b)}} \mathbf{n}_{G^{(b)}} \cdot \mathbf{E}^{(b)} d\sigma_{G^{(b)}} \quad (6.7)$$

From (3.30), the quantities in (6.7) have the following interpretation:

$$\begin{aligned}
\mathcal{E}(0) &\triangleq -\int_{\partial G_0} \mathbf{n}_G \cdot \mathbf{E} d\sigma_G &&= \text{Energy of interior network at time } t = 0 \\
\mathcal{E}^{(b)}(0) &\triangleq -\int_{\partial G_0^{(b)}} \mathbf{n}_{G^{(b)}} \cdot \mathbf{E}^{(b)} d\sigma_{G^{(b)}} &&= \text{Energy of boundary network at time } t = 0 \\
\mathcal{E}(t_f) &\triangleq \int_{\partial G_f} \mathbf{n}_G \cdot \mathbf{E} d\sigma_G &&= \text{Energy of interior network at time } t = t_f \\
\mathcal{E}^{(b)}(t_f) &\triangleq \int_{\partial G_f^{(b)}} \mathbf{n}_{G^{(b)}} \cdot \mathbf{E}^{(b)} d\sigma_{G^{(b)}} &&= \text{Energy of boundary network at time } t = t_f
\end{aligned}$$

The negative signs in the definitions of the initial energies result from the fact that the outward normal to $\partial G_0$ and $\partial G_0^{(b)}$ points in the negative time direction. As such, (6.7) can be restated simply as

$$\mathcal{E}(t_f) + \mathcal{E}^{(b)}(t_f) \leq \mathcal{E}(0) + \mathcal{E}^{(b)}(0)$$

or, in other words: the total energy stored in the interior and boundary networks must not increase as time progresses.

It is straightforward to extend this idea to more complex boundaries. For example, if the region $G$ were to be defined by

$$G = \{\mathbf{u} | x_1 \geq 0, x_2 \geq 0, 0 \leq t \leq t_f\}$$

so that there is a corner at $x_1 = x_2 = 0$, we could model passive boundary conditions using four networks: an $(n+1)$D network for the interior of $G$, two $n$D networks for the two "faces," and a $(n-1)$D network for the corner itself; an energy inequality similar to (6.7) results.

Here, we have said absolutely nothing about discretization (and indeed, we have not investigated this problem in any detail). We have, however, indicated the possibility for arbitrary *distributed* passive boundary termination of a given MDKC; only lumped conditions have been examined so far in the literature.

### 6.2.4 Multi-grid Methods Using MDKCs

One of the advantages of the MDWDF approach is that discrete numerical integration routines are arrived at by applying coordinate transformations and spectral mappings (or integration rules along the transformed coordinate directions) to the MD circuit form of the original model problem. Indeed, the principal result of Chapter 4, in §4.10 is that digital waveguide networks on regular grids can be constructed by essentially the same means.

On the other hand, the expanded signal flow graph for a digital waveguide network is a network of lumped $N$-ports in its own right; in fact, the original formulation of the DWN (and TLM structures) is lumped. In the flow graph for a MDWD network, however, the port structure is lost. We showed in §4.9 how several DWNs, differing perhaps in grid density or the choice of coordinate could be joined through the use of passive interfaces. Here Fettweis' approach falters, because it is not clear how to generate an structure on an irregular grid from a MD representation (a similar problem, that of terminating a MDWD network in hexagonal coordinates (see §3.3.3) at a straight boundary has been discussed in great detail in [210], but in that case, it was necessary to resort to active elements even for a passive termination!)

A possible direction here might make use of boundary network modeling, as outlined immediately previously; i.e., treat an interface as a MD boundary network in its own right between two separate MDWD networks operating using different grid arrangements.

### 6.2.5 Spectral Mappings and Network Transformations

The transmission line matrix method (TLM) has developed in many interesting directions that we have not been able to discuss in this thesis. Many different types of structures have been proposed, in particular those for which the dependent variables are not interleaved. Given that we have shown that certain DWNs can be derived from MDKCs, just as MDWD networks are, it would be interesting to know whether the various TLM structures can be arrived at in a similar way. A compact circuit representation would empower an algorithm designer enormously, and would almost certainly make a useful tool for designing new structures which are potentially more efficient and which may have better numerical properties.

We note, however, that for a given circuit representation of a system of PDEs, it is not at all obvious which spectral mappings should be applied in order to give rise to a useful structure; indeed, in the case of the DWN discussed in §4.10, the correct spectral mappings were arrived through a chance encounter with formulae buried in the dark basement of an old paper [61]. It should be possible to elucidate the link to a certain degree; does a particular network topology imply a particular integration rule or mapping? This is important, because for a given system of PDEs, there is not a single MDKC representation; any rules or transformations from classical network theory can be used to manipulate the MDKC into an infinite number of new topologies, each of which, upon discretization, gives rise to a distinct numerical method.

### 6.2.6 Finite Arithmetic Testing

One of the greatest benefits of a scattering formulation is its guaranteed stability even under the highly nonlinear quantization operations that must be applied to both signals and multipliers in a computer implementation (see §2.3.6). To date, however, there have been no published comparisons of quantization effects in scattering structures vs. standard finite difference schemes.

This is, of course, a huge research problem, and certainly worth a dissertation or two by itself. The time is, however, ripe for such work since (a), there is large body of work devoted to quantization strategies in wave digital and other related filter designs, and (b), it is a necessary first step towards building special-purpose simulation hardware, which is the ultimate goal of all this work (such hardware has in fact already been built [202], but as mentioned above, there has been no attempt at any comparison with the performance of standard difference methods). The principal question is of how much there is to gain, in terms of memory savings, using a scattering implementation which employs small word lengths.

We would recommend a comparison of signal quantization effects in a simple (2+1)D structure such as the rectangular mesh for the (2+1)D wave equation, and its finite difference counterpart (to be discussed in Appendix A), subject to various boundary conditions. Because coefficient truncation effects will probably be most noticeable in a problem with material variation, it would be worthwhile to examine such effects in the (1+1)D transmission line problem under very simple conditions (losslessness, and spatial variation of a very simple form in one of the line parameters $l$ or $c$). By "comparison," we mean that the error between the exact solution to the problem and a numerical solution should be computed for various signal and coefficient word lengths.

### 6.2.7 Time-varying Systems

Time-varying distributed systems have not been examined in any detail in the scattering simulation literature, though time-varying WDFs [177] and DWNs [166] have both been proposed, with a focus on vocal tract modelling. Though it is true that time-variations in material parameters generally render a system non-passive, we will show here how passive network representations may be developed for an important class of systems.

Consider a system of the form

$$\frac{\partial}{\partial t}\left(\mathbf{P}(\mathbf{x},t)\mathbf{w}\right)+\sum_{j=1}^{n}\mathbf{A}_j\frac{\partial \mathbf{w}}{\partial x_j}+\mathbf{B}(\mathbf{x},t)\mathbf{w}+\mathbf{f}(\mathbf{x},t)=\mathbf{0} \tag{6.8}$$

which is a simple generalization of the $(n+1)$D symmetric hyperbolic form (3.1) to the case where $\mathbf{P}$ and $\mathbf{B}$ depend on both the spatial coordinates $\mathbf{x}$ and time $t$; $\mathbf{P}$ is assumed to be positive definite for all values of these coordinates and smoothly-varying. The matrices $\mathbf{A}_j$ are again assumed to be constant and symmetric, and $\mathbf{B}$ is not required to have any particular structure. It is easy to show that in this form, it is not possible to arrive immediately at an energy condition such as (3.5). In order to put system (6.8) into more useful form, note that we can factor $\mathbf{P}$ as $\mathbf{P} = \mathbf{P}^{\frac{T}{2}}\mathbf{P}^{\frac{1}{2}}$ where $\mathbf{P}^{\frac{T}{2}}$ is some left matrix square root of $\mathbf{P}$. We can then rewrite (6.8) as

$$\mathbf{P}^{\frac{T}{2}}\frac{\partial \mathbf{P}^{\frac{1}{2}}\mathbf{w}}{\partial t} + \frac{\partial \mathbf{P}^{\frac{T}{2}}}{\partial t}\mathbf{P}^{\frac{1}{2}}\mathbf{w} + \sum_{j=1}^{n}\mathbf{A}_j\frac{\partial \mathbf{w}}{\partial x_j} + \mathbf{B}\mathbf{w} + \mathbf{f} = \mathbf{0}$$

Now introduce a new dependent variable $\mathbf{z}$ defined by $\mathbf{w} = e^{\kappa}\mathbf{z}$, where $\kappa = \kappa(t)$ and is assumed differentiable. Then, in terms of the new variable $\mathbf{z}$, we have

$$\mathbf{P}^{\frac{T}{2}}\frac{\partial \mathbf{P}^{\frac{1}{2}}\mathbf{z}}{\partial t} + \left(\frac{\partial \kappa}{\partial t}\mathbf{P} + \frac{\partial \mathbf{P}^{\frac{T}{2}}}{\partial t}\mathbf{P}^{\frac{1}{2}} + \mathbf{B}\right)\mathbf{z} + \sum_{j=1}^{n}\mathbf{A}_j\frac{\partial \mathbf{z}}{\partial x_j} + \tilde{\mathbf{f}} = \mathbf{0}$$

with $\tilde{\mathbf{f}} = e^{-\kappa}\mathbf{f}$. Assuming that this source term is zero, we can then take the inner product of this expression with $\mathbf{z}^T$ to get

$$\frac{\partial}{\partial t}\left(\frac{1}{2}\mathbf{z}^T\mathbf{P}\mathbf{z}\right) + \frac{1}{2}\sum_{j=1}^{n}\frac{\partial}{\partial x_j}\left(\mathbf{z}^T\mathbf{A}_j\mathbf{z}\right) = -\mathbf{z}^T\mathbf{Q}\mathbf{z}$$

where

$$\mathbf{Q} = \frac{\partial \kappa}{\partial t}\mathbf{P} + \frac{1}{2}\frac{\partial \mathbf{P}}{\partial t} + \frac{1}{2}\left(\mathbf{B} + \mathbf{B}^T\right)$$

If $\mathbf{Q}$ is positive semi-definite, then integrating over $\mathbb{R}^n$ gives the energy condition

$$\frac{d}{dt}\int_{\mathbb{R}^n}\frac{1}{2}\mathbf{z}^T\mathbf{P}\mathbf{z}d\mathbf{x} \le 0$$

which is identical to the condition derived in §3.2, under the replacement of $\mathbf{w}$ with $\mathbf{z}$. As long as $\mathbf{B}$ and the time derivative of $\mathbf{P}$ are bounded, it is always possible to make a choice of $\kappa$ such that $\mathbf{Q}$ is positive semi-definite. For instance, we can choose $\kappa = \kappa_0 t$, with

$$\kappa_0 \ge -\frac{1}{2}\min_{\mathbf{x}\in\mathbb{R}^n, t\ge 0}\frac{\lambda_{min}\left(\frac{\partial \mathbf{P}}{\partial t} + \mathbf{B} + \mathbf{B}^T\right)}{\lambda_{min}(\mathbf{P})}$$

where $\lambda_{min}(\cdot)$ signifies "minimum eigenvalue of." Here, we essentially have a passivity condition in an exponentially-weighted norm.

Consider a generalization of the source-free (1+1)D transmission line system,

$$\frac{\partial(li)}{\partial t} + \frac{\partial u}{\partial x} + ri = 0 \tag{6.9a}$$

$$\frac{\partial(cu)}{\partial t} + \frac{\partial i}{\partial x} + gu = 0 \tag{6.9b}$$

where $l$, $c$, $r$ and $g$, are all smooth positive functions of $x$ and $t$. Introducing the variables

$$i_1 = ie^{-\kappa_0 t} \qquad\qquad i_2 = ue^{-\kappa_0 t}/r_0$$

where $r_0$ is a positive constant as well as the scaled time variable $t' = v_0 t$, and transformed coordinates as per (3.18), we can rewrite this system as

$$\begin{aligned}
\sqrt{L_1}\frac{\partial}{\partial t'}\left(\sqrt{L_1}i_1\right) + r_1 i_1 + \frac{r_0}{\sqrt{2}}\frac{\partial}{\partial t_1}(i_1 + i_2) + \frac{r_0}{\sqrt{2}}\frac{\partial}{\partial t_2}(i_1 - i_2) &= 0 \\
\sqrt{L_2}\frac{\partial}{\partial t'}\left(\sqrt{L_2}i_2\right) + r_2 i_2 + \frac{r_0}{\sqrt{2}}\frac{\partial}{\partial t_1}(i_1 + i_2) + \frac{r_0}{\sqrt{2}}\frac{\partial}{\partial t_2}(i_1 - i_2) &= 0
\end{aligned}$$

with

$$L_1 = v_0 l - r_0 \qquad\qquad L_2 = v_0 c r_0^2 - r_0$$

and

$$r_1 = \kappa_0 l + \frac{1}{2}\frac{\partial l}{\partial t} + r \qquad r_2 = r_0^2\left(\kappa_0 c + \frac{1}{2}\frac{\partial c}{\partial t} + g\right)$$

Under the choices

$$r_0 = \sqrt{l_{min}/c_{min}} \qquad\qquad v_0 \geq 1/\sqrt{l_{min}c_{min}}$$

where now we have

$$l_{min} = \min_{x\in\mathbb{R},t\geq 0} l \qquad\qquad c_{min} = \min_{x\in\mathbb{R},t\geq 0} c$$

then $L_1$ and $L_2$ are non-negative, and the terms involving them can be interpreted as voltages across passive inductors, if power-normalized waves are employed (see §3.5.1 for more information on this definition of inductors). If we also choose

$$\kappa_0 \geq -\frac{1}{2}\min\left(\min_{x\in\mathbb{R},t\geq 0}\left(\frac{1}{l}\frac{\partial l}{\partial t} + r/l\right), \min_{x\in\mathbb{R},t\geq 0}\left(\frac{1}{c}\frac{\partial c}{\partial t} + g/c\right)\right) \tag{6.10}$$

then $r_1$ and $r_2$ are non-negative and can be interpreted as passive resistances. The resulting MDKC is shown in Figure 6.4; an MDWD network can be immediately obtained through the methods discussed in Chapter 3, or network manipulations and alternative integration rules may be employed to get a DWN. A balanced form (see §3.12) is also possible, and gives a less strict bound on $v_0$, but the bound on $\kappa_0$ remains unchanged.

A direct application of this MDKC to an important music synthesis problem would be the

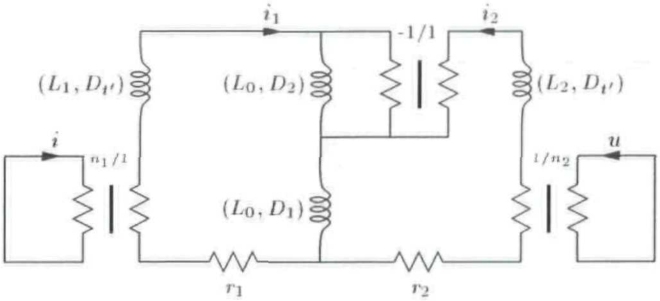

$$L_1 = v_0 l - r_0 \qquad L_2 = v_0 c r_0^2 - r_0$$
$$L_0 = r_0/\sqrt{2}$$
$$r_1 = \kappa_0 l + \tfrac{1}{2}\tfrac{\partial l}{\partial t} + r$$
$$r_2 = r_0^2\left(\kappa_0 c + \tfrac{1}{2}\tfrac{\partial c}{\partial t} + g\right)$$
$$n_1 = e^{-\kappa_0 t} \qquad n_2 = \frac{1}{r_0}e^{-\kappa_0 t}$$

Figure 6.4: *MDKC for time-varying (1+1)D transmission line system* (6.9). *The exponential weighting of the current variables can be viewed (formally) as a time-varying transformer coupling.*

simulation of acoustic wave propagation in the vocal tract, under time-varying conditions. Such a system of PDEs is mentioned in [145], and has the exact form of (6.9), with $r = g = 0$, and under the replacements

$$l \rightarrow \frac{\rho}{A} \qquad c \rightarrow \frac{A}{\rho\gamma^2} \qquad i \rightarrow v \qquad u \rightarrow p + \rho\gamma^2$$

where $\rho$ is the air density, $\gamma$ is the speed of sound, $A(x,t)$ is the surface area of the tube, $v(x,t)$ is the volume velocity and $p(x,t)$ is the pressure variation. The condition (6.10) then reduces to

$$\kappa_0 \geq \max_{\mathbf{x}\in\mathbb{R},t\geq 0}\left|\frac{\partial \ln(\sqrt{A})}{\partial t}\right|$$

If the time variation in $A$ is slow, then $\kappa_0$ will be close to zero, and the exponential weighting will not be overly severe. The problems, for real-time synthesis applications, are that we will need to have an *a priori* estimate of the maximal time variation of the vocal tract area, and that we will apply an exponential weighting to the signal output from the scattering simulation. This exponential weighting may be viewed as a passive operation involving time-varying transformers (as shown in Figure 6.4).

# Afterword

As we mentioned early on, the greater goal of this thesis was to provide a unified and comprehensive treatment of numerical integration methods based on wave and scattering concepts; indeed, published results are dispersed across a wide variety of journals and fields, and assembling them has been somewhat of a challenge in itself. Although as we have seen, wave digital filtering methods and digital waveguide networks are two sides of the same coin (and a more apt metaphor might be that they are but two facets among many on a large, unexplored crystal), the research communities are more than a little isolated from one another. The author has fallen victim to this kind of parochialism as well—one huge regret we have is that we were not made aware of the TLM method earlier in this project, because of its similarity to DWNs, and the richness of the family of structures that has been proposed. In the spirit of Fettweis et al., we have tried to keep the scope as general as possible, treating physical systems that appear across a wide range of disciplines: MDWDFs are just as applicable to musical acoustics and plate vibration problems as the DWN is to electromagnetic field simulation. The unambiguously rosy part of the story, however, ends here.

An interesting remark appears in the preface to a recent book [33] on the transmission line matrix method (TLM). (It was mentioned in §4.1.1 that TLM structures, in that they are constructed from discrete transmission lines, are very similar to digital waveguide networks, though in the case of TLM, apparently no link with digital filtering structures has been made.) The author of this book makes a few comments in a eulogy to J. B. Johns, the originator of this method:

> *...Before his death Johns worried much about whether TLM would ever become accepted. He saw finite difference and finite element methods as the giants which would swallow up his baby...*

One immediately gets a sense of the partisan spirit that must have been predominant at the time of the method's inception. In particular, TLM was seen (and still is, judging from this book, which dates from 1998) as a competitor to FDTD; the same could be said for wave digital filtering approaches. While going through most of the scattering simulation literature, one is bound to feel uneasy at times about the short shrift given to finite difference methods, especially in the WDF arena, where they have been almost willed out of existence; with the notable exception of [131], there has been almost no attempt to view MDWD networks as finite difference schemes (which they are). This is unfortunate, because there is a wealth of well-developed and powerful theory surrounding difference methods which has been in place for many years[†]. It may be that the lack of commentary is due to the self-evident nature of the link—what could these scattering methods be *but* finite difference schemes? The real reason, perhaps, is that difference methods are seen by some as old, crude, and worse, not a physically motivated means of performing a simulation. This point of view, while prejudicial, is partly justified, but begs the question: what is special about scattering methods? A thesis would seem to be the right place to least ask (if not fully answer) this question. While this was not the major "research" goal of this project, it was the most significant source of motivation behind its undertaking, and every effort has been made to make clear the strengths and weaknesses of scattering methods.

With a clearer picture of the relationship between difference and scattering methods at hand, one may get the feeling that somewhere behind the scenes, Rube Goldberg has been busy at work. Indeed, some of the strong features of MDWDFs, according to Fettweis [47], such as local interconnectedness and parallelizeability are possessed by simple finite difference methods such as FDTD as well, and difference methods are undeniably easier on the programmer. Some DWN researchers are even moving away from wave implementations in favor of difference realizations [157]. In balance, however, these circuit-based scattering methods do offer a uniquely physical approach to numerical simulation, especially in the wave digital framework (though as we saw in §4.10, the relationship between MDWD networks and DWNs is now firmly established). Having access to a passivity condition offers the algorithm designer the most simple means imaginable of ensuring numerical stability for complex problems even in the presence of boundary conditions. These stability properties carry over in finite arithmetic as well; this is as sure an indicator as any of the essential correctness of a numerical simulation approach (circuit-based or otherwise) that pays close attention to physics.

Still, this author feels, more now than at the beginning of this project, that proponents of scattering methods have more to learn from straight-ahead finite difference practitioners than they realize (and perhaps more than vice-versa as well, though the balance is probably slight).

---

[†] Spectral, or Von Neumann analysis [176], which we will discuss in Appendix A, and the *energy method* [82] are two branches of this theory which have great bearing on the subject of this thesis. We have not, unfortunately, had the time to fully explore the latter direction, which will surely be more than a little enlightening.

# Appendix A

# Finite Difference Schemes for the Wave Equation

In this appendix, we reexamine the finite difference schemes corresponding to the waveguide meshes discussed in Chapter 4, in the special case for which the underlying model problem is lossless, source-free and does not exhibit any material parameter variation. In this case, these finite difference schemes will solve the wave equation, given by

$$\frac{\partial^2 u}{\partial t^2} = \gamma^2 \nabla^2 u \tag{A.1}$$

in either (2+1)D or (3+1)D, depending on the type of mesh. Here, $\gamma$ is the *wave speed*, and $\nabla^2$ is the *Laplacian* [174]. These schemes will be linear and shift-invariant, and as such, it is possible to analyze them in the frequency domain, through what is called *Von Neumann analysis* [176]. We will apply these methods to the rectilinear, interpolated rectilinear, triangular, hexagonal and fourth-order accurate schemes in (2+1)D, then to the cubic rectilinear, interpolated cubic rectilinear, octahedral and tetrahedral schemes in (3+1)D.

## A.1 Von Neumann Analysis of Difference Schemes

In this section, we summarize the basics of Von Neumann analysis provided in [176]. Consider the $(N+1)$D real-valued grid function $U_{\mathbf{m}}(n)$, defined for integer $n$ and for $\mathbf{m} = [m_1, \ldots, m_N] \in \mathbb{Z}^N$, the set of all integer $N$-tuples. Such a grid function will be used, in a finite difference scheme, as an approximation to the continuous solution $u(\mathbf{x}, t)$ to some problem, at the location $\mathbf{x} = \mathbf{m}\Delta$, and at time $t = nT$, where $\Delta$ is the grid spacing, and $T$ is the time step. Here, and henceforth in this appendix, we have assumed that the grid spacing is uniform in all the spatial coordinates, and that the spatial domain is unbounded. As in Chapters 3 and 4, we define the space step/time step ratio to be

$$v_0 \triangleq \frac{\Delta}{T}$$

The spatial Fourier transform of $U_{\mathbf{m}}(n)$ is defined by

$$\hat{U}_{\boldsymbol{\beta}}(n) = \frac{1}{(2\pi)^{N/2}} \sum_{\mathbf{m}\in\mathbb{Z}^N} e^{-i\Delta\mathbf{m}\cdot\boldsymbol{\beta}} U_{\mathbf{m}}(n)\Delta^N$$

and is a periodic function of $\boldsymbol{\beta} = [\beta_1, \ldots, \beta_N]^T$, a vector of spatial wavenumbers. The transform can be inverted by

$$U_{\mathbf{m}}(n) = \frac{1}{(2\pi)^{N/2}} \int_{[-\pi/\Delta,\pi/\Delta]^N} e^{i\Delta\mathbf{m}\cdot\boldsymbol{\beta}} \hat{U}_{\boldsymbol{\beta}}(n) d\beta_1 d\beta_2 \ldots d\beta_N$$

where $\boldsymbol{\beta} \in [-\pi/\Delta, \pi/\Delta]^N$ refers to the space enclosed by the intervals $-\pi/\Delta \leq \beta_j \leq \pi/\Delta$, for $j = 1, \ldots, N$. If, for a given grid spacing $\Delta$, we define the discrete spatial $L_2$ norm of $U_{\mathbf{m}}(n)$ by

$$\|U(n)\|_2 = \left( \sum_{\mathbf{m}\in\mathbb{Z}^N} U_{\mathbf{m}}^2(n)\Delta^N \right)^{1/2}$$

and the corresponding spectral $L_2$ norm of $\hat{U}_{\boldsymbol{\beta}}(n)$ by

$$\|\hat{U}(n)\|_2 = \left( \int_{[-\pi/\Delta,\pi/\Delta]^N} |\hat{U}_{\boldsymbol{\beta}}(n)|^2 d\beta_1 d\beta_2 \ldots d\beta_N \right)^{1/2}$$

then if $U_{\mathbf{m}}(n)$ and $\hat{U}_{\boldsymbol{\beta}}(n)$ are in their respective $L_2$ spaces, *Parseval's relation* gives

$$\|U(n)\|_2 = \|\hat{U}(n)\|_2$$

### A.1.1 One-step Schemes

Consider the following *one-step* explicit difference scheme, which relates values of the grid function $U_{\mathbf{m}}(n+1)$ to values at the previous time step:

$$U_{\mathbf{m}}(n+1) = \sum_{\mathbf{k}\in\mathbb{K}} \alpha_{\mathbf{k}} U_{\mathbf{m}-\mathbf{k}}(n)$$

where $\mathbb{K}$ is some subset of $\mathbb{Z}^N$, and the parameters $\alpha_{\mathbf{k}}$ are constants; it is initialized by setting $U_{\mathbf{m}}(0)$ equal to some function $U_{\mathbf{m},0}$ (assumed to be in $L_2$). Taking the spatial Fourier transform of this recursion gives

$$\begin{aligned} \hat{U}_{\boldsymbol{\beta}}(n+1) &= \left(\sum_{\mathbf{k}\in\mathbb{K}} \alpha_{\mathbf{k}} e^{-j\Delta\mathbf{k}\cdot\boldsymbol{\beta}}\right)\hat{U}_{\boldsymbol{\beta}}(n) \\ &= \qquad G_{\boldsymbol{\beta}} \qquad \hat{U}_{\boldsymbol{\beta}}(n) \end{aligned} \tag{A.2}$$

$G_{\boldsymbol{\beta}}$ so defined is called the *spectral amplification factor* for a one-step finite difference scheme. (A.2) implies that we have, in particular, that

$$\hat{U}_{\boldsymbol{\beta}}(n+1) = G_{\boldsymbol{\beta}}^{n+1}\hat{U}_{\boldsymbol{\beta},0} \tag{A.3}$$

where $\hat{U}_{\boldsymbol{\beta},0}$ is the spatial Fourier transform of the initial condition $U_{\mathbf{m},0}$. (A.3) further implies that

$$\|\hat{U}(n+1)\|_2 \leq \left(\max_{\boldsymbol{\beta}}|G_{\boldsymbol{\beta}}|\right)^{n+1} \|\hat{U}_0\|_2$$

and finally, through Parseval's relation, that

$$\|U(n+1)\|_2 \leq \left(\max_{\boldsymbol{\beta}}|G_{\boldsymbol{\beta}}|\right)^{n+1} \|U_0\|_2$$

If the $\alpha_{\mathbf{k}}$ which define the difference scheme are independent of the grid spacing and the time step, then such a difference scheme is called *stable* if

$$\max_{\boldsymbol{\beta}}|G_{\boldsymbol{\beta}}| \leq 1$$

The $L_2$ norm of the solution to the difference equation will thus not increase as the simulation progresses.

### A.1.2 Multi-step Schemes

*Multi-step methods* can be treated in a very similar way. An explicit $M$-step method is defined by

$$U_{\mathbf{m}}(n+1) = \sum_{r=1}^{M}\sum_{\mathbf{k}\in\mathbb{K}_r} \alpha_{\mathbf{k}} U_{\mathbf{m}-\mathbf{k}}(n+1-r)$$

for constant coefficients $\alpha_{\mathbf{k}}$ contained in subsets $\mathbb{K}_r$ of $\mathbb{Z}^N$. Taking the Fourier transform of this recursion gives

$$\hat{U}_{\boldsymbol{\beta}}(n+1) = \sum_{r=1}^{M}\sum_{\mathbf{k}\in\mathbb{K}_r} \alpha_{\mathbf{k}} e^{-i\Delta\mathbf{k}\cdot\boldsymbol{\beta}}\hat{U}_{\boldsymbol{\beta}}(n+1-r) \tag{A.4}$$

A simple way of examining (A.4) is to look for solutions of the form $\hat{U}_{\boldsymbol{\beta}}(q) = G_{\boldsymbol{\beta}}^{q}\hat{U}_{\boldsymbol{\beta}}(0)$. This gives the *amplification polynomial equation*

$$G_{\boldsymbol{\beta}}^{M} = \sum_{r=1}^{M}\sum_{\mathbf{k}\in\mathbb{K}_r} \alpha_{\mathbf{k}} e^{-i\Delta\mathbf{k}\cdot\boldsymbol{\beta}} G_{\boldsymbol{\beta}}^{M-r}$$

the solutions of which, $G_{\boldsymbol{\beta},\nu}$, $\nu = 1, \ldots, M$ must be bounded by unity for stability (though in general, this is not sufficient, as we will show presently for a special case).

A particular form of the amplification polynomial equation which will appear frequently in our subsequent treatment of finite difference schemes for the wave equation is that of a simple two-step centered difference approximation, namely

$$G_{\boldsymbol{\beta}}^{2} + B_{\boldsymbol{\beta}}G_{\boldsymbol{\beta}} + 1 = 0 \tag{A.5}$$

for some real function $B_{\boldsymbol{\beta}}$. This expression has solutions

$$G_{\boldsymbol{\beta},\pm} = \frac{1}{2}\left(-B_{\boldsymbol{\beta}} \pm \sqrt{B_{\boldsymbol{\beta}}^{2} - 4}\right) \tag{A.6}$$

which will be bounded by (and in fact equal to) unity in magnitude if we have $|B_{\boldsymbol{\beta}}| \leq 2$ for all $\boldsymbol{\beta}$. Furthermore, if $|B_{\boldsymbol{\beta}}| > 2$ for some $\boldsymbol{\beta}$, then we will necessarily have an amplification factor with magnitude greater than one at that frequency. For any $\boldsymbol{\beta}$ for which $G_{\boldsymbol{\beta},\pm}$ are not equal, we can write

$$\hat{U}_{\boldsymbol{\beta}}(n+1) = \frac{G_{\boldsymbol{\beta},-}\hat{U}_{\boldsymbol{\beta},0} - \hat{U}_{\boldsymbol{\beta},1}}{G_{\boldsymbol{\beta},-} - G_{\boldsymbol{\beta},+}}G_{\boldsymbol{\beta},+}^{n+1} + \frac{G_{\boldsymbol{\beta},+}\hat{U}_{\boldsymbol{\beta},0} - \hat{U}_{\boldsymbol{\beta},1}}{G_{\boldsymbol{\beta},+} - G_{\boldsymbol{\beta},-}}G_{\boldsymbol{\beta},-}^{n+1}$$

where $\hat{U}_{\boldsymbol{\beta},0}$ and $\hat{U}_{\boldsymbol{\beta},1}$ are the spatial frequency spectra of the two grid functions (at time steps $n = 0$ and $n = 1$) used to initialize the two-step method. It is easy to show that the $L_2$ norm of $U_{\mathbf{m}}(n)$ can be bounded in terms of the norms of the initial conditions if the spectral amplification factors are distinct and bounded by 1 in magnitude at all wavenumbers.

It is important to realize, however, that the condition that these roots $G_{\boldsymbol{\beta},\pm}$ be bounded by unity is necessary, but not sufficient to ensure no growth in the $L_2$ norm of the solution; this point has not been addressed in the finite difference treatment of waveguide meshes. In fact, as shown in §4.3.4, the simple centered difference approximation to the wave equation admits linearly growing solutions.

This behavior can be examined in the spectral domain as we will now show, as per [176]. Notice that the solutions (A.6) of the amplification polynomial equation for the two-step scheme can coincide if, and only if at some frequency $\boldsymbol{\beta} = \boldsymbol{\beta}_0$, $B_{\boldsymbol{\beta}_0} = \pm 2$, in which case we have $G_{\boldsymbol{\beta}_0,+} = G_{\boldsymbol{\beta}_0,-} = \mp 1$.

The evolution of the particular spatial frequency component at frequency $\beta_0$ can be written as

$$\hat{U}_{\beta_0}(n) = (\mp 1)^n \hat{U}_{\beta_0,0} + n(\mp 1)^{n-1}\left(\hat{U}_{\beta_0,1} \pm \hat{U}_{\beta_0,0}\right)$$

We can thus expect some linear growth at any such frequency $\beta_0$ if we do not properly initialize the algorithm, so as to cancel the linearly growing part of the solution. It also follows that in employing such a method, one may need to be particularly careful when applying an excitation which contains such frequency components, and that nonlinear signal quantization may pump energy into such modes, even if none is originally present there.

Strikwerda does not classify such linear growth as unstable, because the wave equation itself admits, in addition to traveling wave solutions, a solution which grows linearly with time[†]. For the physical modeling of musical instruments and acoustic spaces, however (the problems to which finite difference schemes of the form to be discussed shortly are often applied), such solutions are nonphysical and definitely not acceptable. These comments concerning this mild linear instability apply to schemes in unbounded domains; when boundary conditions are present, further analysis will be required.

In order to simplify the analysis of these schemes, we mention that for difference schemes for the wave equation, it is often possible to write

$$B_\beta = -2\lambda^2 F_\beta - 2 \tag{A.7}$$

where $\lambda^2 \triangleq \gamma^2/v_0^2$ and $F_\beta$ is independent of $\lambda$. In this case, the stability condition can be rewritten as

$$\max_\beta |B_\beta| \leq 2 \qquad \Longleftrightarrow \qquad \max_\beta |\lambda^2 F_\beta + 1| \leq 1$$

This new condition on $F_\beta$ is easier to analyze: we first require

$$\max_\beta F_\beta \leq 0 \tag{A.8}$$

and if (A.8) holds, we get a further bound on $\lambda$, namely

$$\lambda \leq \sqrt{\frac{-2}{\min_\beta F_\beta}} \qquad \Longrightarrow \qquad T \leq \frac{\Delta}{\gamma}\sqrt{\frac{-2}{\min_\beta F_\beta}} \tag{A.9}$$

Thus the stability of these schemes can be simply analyzed in terms of the global maximum and minimum of $F_\beta$.

For certain schemes (in particular, the interpolated schemes to be discussed in §A.2.2 and §A.3.3), the function $F_{\beta}$ depends on several parameters. Condition (A.8) tells us the the range of parameters over which our scheme is stable, and over the stability region, condition (A.9) gives us a maximum time step $T$, in terms of the grid spacing $\Delta$.

---

[†] $u = t$, for instance, satisfies (A.1).

### A.1.3 Vector Schemes

For two of the schemes that we will examine (hexagonal and tetrahedral), it will be necessary to analyze a vectorized system of difference equations. In general, the analysis of vector forms is considerably more difficult; the typical approach will invoke the *Kreiss Matrix Theorem* [176], which is a set of equivalent conditions which can be used to check the boundedness of a particular amplification matrix. In the general vector case we will be analyzing the evolution of a $q$-element vector $\hat{\mathbf{U}}_{\beta}(n) = [\hat{U}_{1,\beta}(n), \ldots, \hat{U}_{q,\beta}(n)]^{T}$ of spatially Fourier-transformed functions of $\boldsymbol{\beta}$. The $L_2$ norm is defined by

$$\|\hat{\mathbf{U}}(n)\|_2 = \left(\int_{[\pi/\Delta,\pi/\Delta]^N} \hat{\mathbf{U}}_{\beta}^{*}(n)\hat{\mathbf{U}}_{\beta}(n)d\beta_1 d\beta_2 \ldots d\beta_N\right)^{1/2}$$

where $^{*}$ denotes transpose conjugation.

The schemes for the wave equation that we will examine, however, have a relatively simple form. The column vector of grid spatial frequency spectra $\hat{\mathbf{U}}_{\beta}(n)$ satisfies an equation of the form

$$\hat{\mathbf{U}}_{\beta}(n+1) + \mathbf{B}_{\beta}\hat{\mathbf{U}}_{\beta}(n) + \hat{\mathbf{U}}_{\beta}(n-1) = \mathbf{0} \tag{A.10}$$

for some Hermitian matrix function of $\boldsymbol{\beta}$, $\mathbf{B}_{\beta}$. Because $\mathbf{B}_{\beta}$ is Hermitian, we may write $\mathbf{B}_{\beta} = \mathbf{J}_{\beta}^{*}\boldsymbol{\Lambda}_{\beta}\mathbf{J}_{\beta}$, for some unitary matrix $\mathbf{J}_{\beta}$, and a real diagonal matrix $\boldsymbol{\Lambda}_{\beta}$ containing the eigenvalues of $\mathbf{B}_{\beta}$. As such, we may change variables via $\hat{\mathbf{V}}_{\beta}(n) = \mathbf{J}_{\beta}\hat{\mathbf{U}}_{\beta}(n)$, to get

$$\hat{\mathbf{V}}_{\beta}(n+1) + \boldsymbol{\Lambda}_{\beta}\hat{\mathbf{V}}_{\beta}(n) + \hat{\mathbf{V}}_{\beta}(n-1) = \mathbf{0} \tag{A.11}$$

The system thus decouples into a system of scalar two-step spectral update equations; because $\hat{\mathbf{U}}_{\beta}(n)$ and $\hat{\mathbf{V}}_{\beta}(n)$ are related by a unitary transformation, we have $\|\hat{\mathbf{U}}(n)\|_2 = \|\hat{\mathbf{V}}(n)\|_2$, and we may apply stability tests to the uncoupled system (A.11). We thus require that the eigenvalues of $\mathbf{B}_{\beta}$, namely $\Lambda_{\beta,j}$ for $j = 1, \ldots, q$, which are the elements on the diagonal of $\boldsymbol{\Lambda}_{\beta}$, all satisfy

$$\max_{\beta} |\Lambda_{\beta,j}| \leq 2 \tag{A.12}$$

At frequencies $\boldsymbol{\beta}_0$ for which any of the eigenvalues satisfies (A.12) with equality, then we may again have the same problem with mild linear growth in the solution.

### A.1.4 Numerical Phase Velocity

For a given amplification factor $G_{\boldsymbol{\beta}}$, the *numerical phase velocity* at frequency $\boldsymbol{\beta}$ is defined by

$$v_{\boldsymbol{\beta},phase} = \left|\frac{\log(G_{\boldsymbol{\beta}}/|G_{\boldsymbol{\beta}}|)}{i\|\boldsymbol{\beta}\|_2 T}\right|$$

where $\|\boldsymbol{\beta}\|_2$ is the Euclidean norm of the vector $\boldsymbol{\beta}$. This expression gives the speed of propagation for a plane wave of wavenumber $\boldsymbol{\beta}$, according to the numerical scheme for which $G_{\boldsymbol{\beta}}$ is an amplification factor. For the wave equation model problem, the speed of any plane wave solution will simply be $\gamma$, but the numerical phase velocity will in general be different, and in particular, wave speeds will be directionally-dependent to a certain degree, depending on the type of scheme used. For all these schemes, the numerical phase velocity for at least one of the amplification factors will approach the correct physical velocity near the spatial DC frequency, by *consistency* of the numerical scheme with the wave equation†.

## A.2 Finite Difference Schemes for the (2+1)D Wave Equation

Waveguide meshes of rectilinear [198], interpolated rectilinear [157], triangular [157, 200] and hexagonal [200] forms have all been applied to solve the (2+1)D wave equation. Though they have often been written as scattering forms, they can also be written as finite difference schemes. There are quite a few computational issues that arise which serve to distinguish between these difference schemes. Among them are the density of grid points, the possibility of decomposing a given scheme into more computationally efficient subschemes, the operation count, spectral characteristics, the ease with which boundary conditions can be implemented, as well as the maximum allowable time step. The stability issue discussed in §A.1.2 may also be a concern, and thus favor a waveguide mesh implementation instead of a straightforward difference scheme. It is, of course, impossible to say which is best, without knowing problem specifics. The following is intended partly as a catalog, as well as an indication of certain features which probably deserve more attention, in particular the distinction between passivity and stability which becomes apparent in the cases of the triangular and interpolated meshes.

It is worthwhile introducing two new quantities at this point. In addition to $\Delta$, the "nearest-neighbor" grid spacing, or inter-junction spacing, $T$ the time step, $v_0$, which will always be equal to $\Delta/T$, and $\lambda = \gamma/v_0$, we also define $\rho_S$, the *computational density* of a particular scheme $S$ to be number of grid points at which the the difference scheme is operative, per unit volume and per unit time. Thus if the $N$-dimensional volume of the spatial domain $\mathcal{D}$ of a particular problem is $|\mathcal{D}|$ and the total time over which we wish to obtain a solution is $\mathcal{T}$, then the total number of grid point calculations which will need to be made will be $|\mathcal{D}|\mathcal{T}\rho_S$. Similarly, we can define the *add density* $\sigma_S$ to be $A_S\rho_S$ if scheme $S$ requires $A_S$ adds in order to update at any given grid point. A multiply density could be defined similarly, though we will not, for reasons of space, do so here.

---

† Regrettably, a full discussion of consistency of difference schemes would take us too far afield, and we refer to [176] for a full exposition. The idea, grossly speaking, is that for a stable difference scheme, consistency is our guarantee that the numerical solution to the difference scheme converges to the solution of the continuous model problem as the grid spacing and time step are decreased. It is usually checked via a Taylor expansion of the difference scheme.

### A.2.1 The Rectilinear Scheme

The finite difference scheme corresponding to a rectilinear mesh is obtained by applying centered differences to the wave equation, over a rectangular grid with indices $i$ and $j$ (which refer to points with spatial coordinates $x = i\Delta$ and $y = j\Delta$). The difference scheme, given originally as (4.53) is

$$\begin{aligned} U_{i,j}(n+1) + U_{i,j}(n-1) = \lambda^2 \Big(U_{i+1,j}(n) + U_{i-1,j}(n) + U_{i,j+1}(n) + U_{i,j-1}(n)\Big) \\ + \left(2 - 4\lambda^2\right) U_{i,j}(n) \end{aligned} \tag{A.13}$$

and the amplification polynomial equation is of the form (A.5), with

$$B_{\boldsymbol{\beta}} = -2\Big(1 + \lambda^2 \left(\cos(\beta_x\Delta) + \cos(\beta_y\Delta) - 2\right)\Big)$$

for $\boldsymbol{\beta} = [\beta_x, \beta_y]^T$. From (A.7), we thus have

$$F_{\boldsymbol{\beta}} = \cos(\beta_x\Delta) + \cos(\beta_y\Delta) - 2$$

and we have

$$\max_{\boldsymbol{\beta}} F_{\boldsymbol{\beta}} = 0 \qquad\qquad \min_{\boldsymbol{\beta}} F_{\boldsymbol{\beta}} = -4$$

Condition (A.8) is thus satisfied, and condition (A.9) gives the bound

$$\lambda \leq \frac{1}{\sqrt{2}} \qquad\qquad \text{for stability}$$

which implies that the amplification factor $|G_{\boldsymbol{\beta},\pm}| = 1$ for such values of $\lambda$. Because $\lambda = \gamma/v_0$, this bound is the same as the bound for passivity of the associated mesh scheme, given in (4.63). The amplification factors, however, are distinct at all spatial frequencies only for $\lambda < 1/\sqrt{2}$. If $\lambda = 1/\sqrt{2}$, then the factors are degenerate for $\beta_x = \beta_y = 0$, and for $\beta_x = \beta_y = \pm\pi/\Delta$ and we are then in the situation discussed in §A.1.2 where linear growth of the solution may occur. This is an important special case, because it corresponds to the standard finite difference scheme for the rectilinear waveguide mesh (i.e., the realization without self-loops). The waveguide mesh implementation does not allow such growth at these frequencies[†]. As far as assessing the computational requirements of the finite difference scheme, first consider the case $\lambda < 1/\sqrt{2}$. Five adds are required at each grid point in order to update. Given that $T = \Delta/v_0$, we can write the computational and add densities for the scheme as

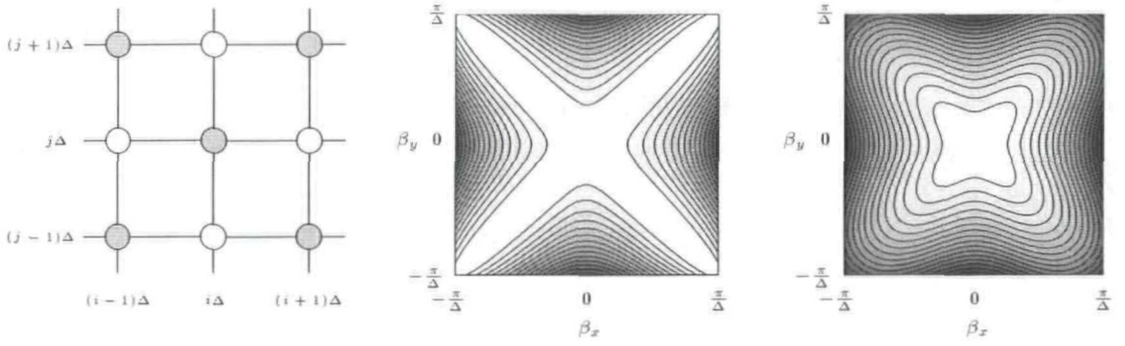

(a) (b) (c)

Figure A.1: *The rectilinear scheme* (A.13)— (a) *grid, of spacing* $\Delta$, *where grey/white coloring indicates a subgrid decomposition possible when* $\lambda = 1/\sqrt{2}$. (b) $v_{\beta,phase}/\gamma$ *for* $\lambda = 1/\sqrt{2}$. *Contour lines are drawn, representing successive deviations of 2 per cent from the ideal value of 1 which is obtained at spatial DC.* (c) $v_{\beta,phase}/\gamma$ *away from the stability bound, for* $\lambda = 1/2$.

$$\rho_{rect} = \frac{v_0}{\Delta^3} \qquad \sigma_{rect} = \frac{5v_0}{\Delta^3} \qquad \text{for} \qquad v_0 > \sqrt{2}\gamma$$

For $\lambda = 1/\sqrt{2}$, however, scheme (A.13) simplifies to

$$U_{i,j}(n+1) + U_{i,j}(n-1) = \frac{1}{2}\Big(U_{i+1,j}(n) + U_{i-1,j}(n) + U_{i,j+1}(n) + U_{i,j-1}(n)\Big) \tag{A.14}$$

which may be operated on alternating grids, i.e., $U_{i,j}(n)$ need only be calculated for $i+j+n$ even (or odd). The computational and add densities, for $\lambda = 1/\sqrt{2}$ are then

$$\rho^{s}_{rect} = \frac{v_0}{2\Delta^3} \qquad \sigma^{s}_{rect} = \frac{2v_0}{\Delta^3} \qquad \text{for} \qquad v_0 = \sqrt{2}\gamma$$

where we note that the reduced scheme (A.14) requires only four adds for updating at a given grid point; in addition, the multiplies by 1/2 may be accomplished, in a fixed-point implementation, by simple bit-shifting operations. The increased efficiency of this scheme must be weighed against the danger of instability, and the fact that because grid density is reduced, the scheme is now applicable over a smaller range of spatial frequencies. The numerical phase velocities of the schemes, at the stability limit, and away from it, at $\lambda = 1/2$, are plotted in Figure A.1. It is interesting to note that away from the stability limit, the numerical dispersion is somewhat less directionally-dependent; this important factor may be useful from the point of view of frequency-warping techniques [157] which may be used to reduce numerical dispersion effects for schemes which are relatively directionally-independent. This idea has been discussed in the waveguide mesh context (where self-loops will be present) in [175].

---

[†] As an example of such growth at the spatial DC frequency, consider initializing the scheme (A.14) using $U_{i,j}(0) = 1$ for $i+j$ even and $U_{i,j}(1) = -1$ for $i+j$ odd. Then we will have $U_{i,j}(n) = 2n-1$, for $i+j+n$ even. It is simple to show that a waveguide implementation does not allow us to choose bounded wave variable initial conditions which yield these values for $U_{i,j}(0)$ and $U_{i,j}(1)$.

### A.2.2 The Interpolated Rectilinear Scheme

This scheme, like the standard rectilinear scheme, is defined over a grid with indices $i$ and $j$, for points with $x = i\Delta$ and $y = j\Delta$. Updating, in this case, at a given point, requires access to values of the grid function at the previous time step at nearest-neighbor grid points to the north, east, west and south, as well as those to the north-east, north-west, south-east and south-west, which are more distant by a factor of $\sqrt{2}$. The scheme is referred to as "interpolated" in [157] because it is derived as an approximation to a hypothetical (and non-realizable) multi-directional difference scheme with minimally directionally-dependent numerical dispersion. (It is perhaps more useful to think of the scheme as interpolating between two rectilinear schemes operating on grids with a relative angle of 45 degrees.) The difference scheme will have the form

$$\begin{aligned} U_{i,j}(n+1) + U_{i,j}(n-1) = {} & \lambda^2 a\Big(U_{i,j+1}(n) + U_{i,j-1}(n) + U_{i+1,j}(n) + U_{i-1,j}(n)\Big) \\ & + \lambda^2 b\Big(U_{i+1,j+1}(n) + U_{i+1,j-1}(n) + U_{i-1,j+1}(n) + U_{i-1,j-1}(n)\Big) \\ & + \lambda^2 c U_{i,j}(n) \end{aligned} \tag{A.15}$$

for constants $a$, $b$ and $c$ which satisfy the constraints

$$a + 2b = 1 \qquad\qquad 4a + 4b + c = \frac{2}{\lambda^2} \tag{A.16}$$

for consistency with the wave equation. If $b = 0$, we get the standard rectilinear scheme, and if $a = 0$, we get a rectilinear scheme operating on a grid of spacing $\sqrt{2}\Delta$, which is rotated by 45 degrees with respect to that of the standard scheme. This general form was put forth in [157], and the free parameter $a$ may be adjusted to give a less directionally-dependent numerical phase velocity; it may thus be used in conjunction with frequency-warping methods for reducing dispersion error. In general, the interpolated scheme cannot be decomposed into mutually exclusive subschemes.

It is possible to examine the stability of this method as in the previous case. We again have an

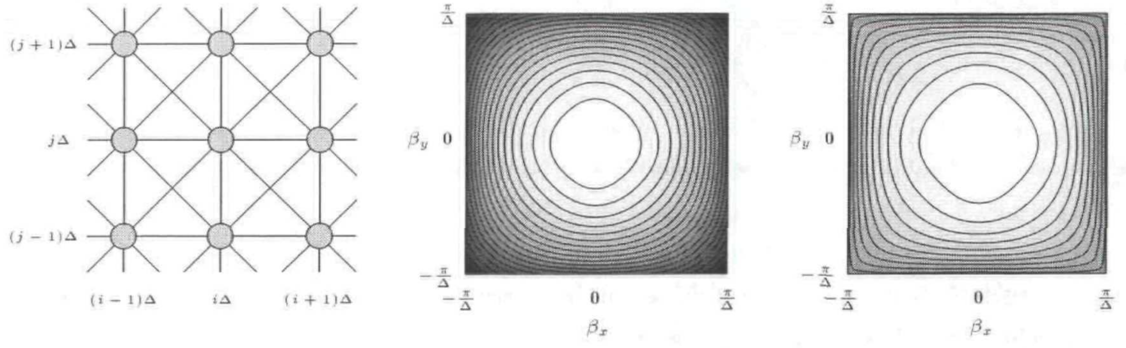

(a) (b) (c)

Figure A.2: *The interpolated rectilinear scheme* (A.15)— (a) *numerical grid and connections for the interpolated rectilinear scheme* (A.15); (b) $v_{\boldsymbol{\beta},phase}/\gamma$ *of the scheme for* $a = 0.62$ *at the "passivity" bound,* $\lambda = 1/\sqrt{1+a}$; (c) $v_{\boldsymbol{\beta},phase}/\gamma$ *for* $a = 0.62$, *at the stability bound, for* $\lambda = 1/\sqrt{2a}$.

amplification polynomial equation of the form of (A.5), with

$$B_{\boldsymbol{\beta}} = -2\lambda^2\Big(a(\cos(\beta_x\Delta)+\cos(\beta_y\Delta))+(1-a)\cos(\beta_x\Delta)\cos(\beta_y\Delta)-1-a\Big)-2$$

and thus

$$F_{\boldsymbol{\beta}} = a\big(\cos(\beta_x\Delta)+\cos(\beta_y\Delta)\big)+(1-a)\cos(\beta_x\Delta)\cos(\beta_y\Delta)-1-a$$

Note that $F_{\boldsymbol{\beta}}$ is *multilinear* [3] in $\cos(\beta_x\Delta)$ and $\cos(\beta_y\Delta)$, so that any extrema must occur at the corners of the region in the spatial frequency plane defined by $|\cos(\beta_x\Delta)| \leq 1$, and $|\cos(\beta_y\Delta)| \leq 1$. Thus, we need evaluate $F_{\boldsymbol{\beta}}$ only for $\boldsymbol{\beta}^T = [\beta_x, \beta_y] = [0,0]$, $[\pi/\Delta, 0]$, $[0, \pi/\Delta]$ and $[\pi/\Delta, \pi/\Delta]$:

$$F_{\boldsymbol{\beta}^T=[0,0]} = 0 \qquad F_{\boldsymbol{\beta}^T=[\pi/\Delta,0]} = F_{\boldsymbol{\beta}^T=[0,\pi/\Delta]} = -2 \qquad F_{\boldsymbol{\beta}^T=[\pi/\Delta,\pi/\Delta]} = -4a$$

The global maximum of $F_{\boldsymbol{\beta}}$ is non-positive (and thus condition (A.8) is satisfied) only if $a \geq 0$. The global minimum of $F_{\boldsymbol{\beta}}$, over this range of $a$ will then be

$$\min_{\boldsymbol{\beta}} F_{\boldsymbol{\beta}} = \begin{cases} -2, & 0 \leq a \leq \frac{1}{2} \\ -4a, & a \geq \frac{1}{2} \end{cases}$$

and the stability bound on $\lambda$ will be

$$\lambda \leq \begin{cases} 1, & 0 \leq a \leq \frac{1}{2} \\ \frac{1}{\sqrt{2a}}, & a \geq \frac{1}{2} \end{cases} \qquad \text{(for Von Neumann stability)} \tag{A.17}$$

It is interesting to look at the interpolated scheme from a waveguide mesh point of view (see Chapter 4 for details). At each grid point we will have a nine-port parallel scattering junction; four connections are made to neighboring points to the north, south, east and west, through a unit-delay bidirectional delay line of admittance $Y_a$, four more connections are made to the points to the north-east, south-east, north-west and south-west using waveguides of admittance $Y_b$, and there will be a self-loop of admittance $Y_c$. If the junction voltage is written as $U_{i,j}(n)$, then the difference scheme corresponding to this waveguide mesh will be exactly (A.15), with

$$\lambda^2 a = \frac{2Y_a}{Y_J} \qquad \lambda^2 b = \frac{2Y_b}{Y_J} \qquad \lambda^2 c = \frac{2Y_c}{Y_J}$$

where the junction admittance $Y_J$ (assumed positive) will be given by

$$Y_J = 4Y_a + 4Y_b + Y_c$$

The passivity condition will then be a condition on the positivity of $Y_a$, $Y_b$ and $Y_c$. From the previous discussion, we already require $a \geq 0$, so this ensures that $Y_a \geq 0$. Requiring $Y_b \geq 0$ is equivalent to requiring $b \geq 0$; from the first of constraints (A.16), this is true only for $a \leq 1$. Requiring $Y_c \geq 0$ is equivalent to requiring finally, from the second of constraints (A.16), that

$$\lambda \leq \frac{1}{\sqrt{1+a}}, \qquad 0 \leq a \leq 1 \qquad \text{(for passivity)}$$

The difference between the constraints for stability from (A.17) and the passivity constraint above is striking; these bounds are graphed in Figure A.3. This is not the last time that we will find a discrepancy between Von Neumann stability of a scheme and passivity of the related mesh structure; it will come up again in the following section during a discussion of the triangular scheme, and in §A.3.3 when we look at the (3+1)D interpolated scheme. It is interesting to note that for a given value of $a$, with $0 \leq a \leq 1$, the numerical dispersion properties can always be improved if we are willing to forgo passivity (and a mesh implementation). We have plotted the numerical phase velocities of this scheme for $a = 0.62$, at both the stability limit and the passivity limit in Figure A.2.

Finally, we mention that the computational and add densities for this scheme will be, in general,

$$\rho_{interp} = \frac{v_0}{\Delta^3} \qquad\qquad \sigma_{interp} = \frac{10v_0}{\Delta^3}$$

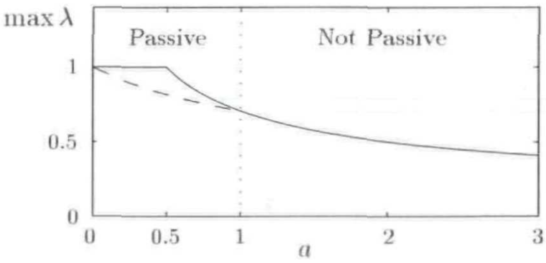

Figure A.3: *Stability bounds for the interpolated rectilinear scheme, as a function of the free parameter a. The solid line indicates the maximum value of $\lambda$ for a given value of a, and the dashed line the maximum value of $\lambda$ allowed in a passive waveguide mesh implementation. Note that there is a passive realization only for $0 \leq a \leq 1$.*

over the range of $v_0$ allowed by the stability constraint (A.17). For the scheme at the passivity bound (for $\lambda = 1/\sqrt{1+a}$, with $0 < a < 1$), we have

$$\rho^{p}_{interp} = \frac{\gamma\sqrt{1+a}}{\Delta^3} \qquad \sigma^{p}_{interp} = \frac{9\gamma\sqrt{1+a}}{\Delta^3}$$

We recall that for $a = 0$ or $a = 1$, at the stability limit, we again have the standard rectilinear scheme, for which a grid decomposition is possible; this was discussed in the previous section.

### Optimally direction-independent numerical dispersion

Although the choice of the free parameter $a$ which gives a maximally direction-independent numerical dispersion profile has been made, in the past, through computerized optimization procedures [157], we note here that it is possible to make a theoretical choice as well, based on a Taylor series expansion of the spectrum.

The spectral amplification factors for the interpolated scheme can be written in terms of the function $B_{\boldsymbol{\beta}}$, or, equivalently, in terms of the function $F_{\boldsymbol{\beta}}$. It should be clear, then, that if $F_{\boldsymbol{\beta}}$ is directionally-independent, then so are the amplification factors, and thus the numerical phase velocity (see §A.1.4) as well. Ideally, we would like $F_{\boldsymbol{\beta}}$ to be a function of the spectral radius $\|\boldsymbol{\beta}\|_2 = (\beta_x^2 + \beta_y^2)^{1/2}$ alone. Now examine the Taylor expansion of $F_{\boldsymbol{\beta}}$ about $\boldsymbol{\beta} = \mathbf{0}$:

$$F_{\boldsymbol{\beta}} = -\Delta^2\|\boldsymbol{\beta}\|_2^2 + \Delta^4\left(\frac{1}{4!}\left(\beta_x^4 + \beta_y^4\right) + \frac{1-a}{4}\beta_x^2\beta_y^2\right) + O(\Delta^6)$$

The directionally-independent $O(\Delta^2)$ term reflects the fact that the scheme is consistent with the wave equation; higher order terms in general show directional dependence. The choice of $a = 2/3$, however, gives

$$F_{\beta} = -\Delta^{2}\|\beta\|_{2}^{2} + \frac{1}{4!}\Delta^{4}\|\beta\|_{2}^{4} + O(\Delta^{6}) \qquad \text{for} \quad a = 2/3$$

and the directional dependence is confined to higher-order powers of $\Delta$. Thus for this choice of $a$, the numerical scheme is maximally direction independent about spatial DC. Note that this value of $a$ does fall within the required bounds for a passive waveguide mesh implementation. The value of 0.62 (for which the numerical dispersion profile is plotted in Figure A.2), which is very close to 2/3, was chosen by visual inspection of dispersion profiles for various values of $a$.

### A.2.3 The Triangular Scheme

The simplest difference scheme which can be used to solve the wave equation on a triangular grid, and which corresponds to the waveguide mesh discussed in §4.6.1 in the constant-coefficient case, is given by

$$\begin{aligned} U_{i,j}(n+1) + U_{i,j}(n-1) = \frac{2}{3}\lambda^{2}\Big(&U_{i,j+2}(n) + U_{i,j-2}(n) + U_{i+1,j+1}(n) + U_{i+1,j-1}(n) \\ &+ U_{i-1,j+1}(n) + U_{i-1,j-1}(n)\Big) \\ &+ 2\left(1-2\lambda^{2}\right)U_{i,j}(n) \end{aligned} \tag{A.18}$$

for a grid defined by points at indices $(i, j)$, for integer $i$ and $j$ such that $i + j$ is even. These coordinates refer to grid points at locations $x = \sqrt{3}i\Delta/2$ and $y = j\Delta/2$, so that a given grid point is equidistant from its six neighbors. This arrangement is shown in Figure A.4(a) and can be considered to be a rectilinear grid under a coordinate transformation; we refer to [193] for a discussion of the range of allowable spatial frequencies for such a grid.

In this case, we will again have an amplification polynomial of the form (A.5), with

$$\begin{aligned} B_{\beta} &= -2\left(1+\frac{2}{3}\lambda^{2}\left(\cos(\beta_{y}\Delta) + 2\cos(\frac{\beta_{y}\Delta}{2})\cos(\frac{\sqrt{3}\beta_{x}\Delta}{2}) - 3\right)\right) \\ F_{\beta} &= \frac{2}{3}\left(\cos(\beta_{y}\Delta) + 2\cos(\frac{\beta_{y}\Delta}{2})\cos(\frac{\sqrt{3}\beta_{x}\Delta}{2}) - 3\right) \end{aligned}$$

Because $F_{\beta}$ is not multilinear (see §A.2.2) in the cosines, finding the extrema is not as simple as in the interpolated case—one can proceed either through some tedious algebra, change to stretched rectilinear coordinates, in which $F_{\beta}$ becomes multilinear again, or make use of a computer. In any case, these extrema can be shown to be

$$\max_{\beta} F_{\beta} = 0 \qquad \min_{\beta} F_{\beta} = -3$$

and thus, from (A.9),

$$\lambda \leq \sqrt{\frac{2}{3}} \qquad \text{for stability}$$

This is surprising, because the bound for passivity, from (4.80), of the triangular mesh is $\lambda \leq 1/\sqrt{2}$. That is to say, for a given inter-junction spacing of $\Delta$, a triangular waveguide mesh, of the type mentioned in §4.6.1, is concretely passive for time steps $T$ with $T \leq \Delta/(\sqrt{2}\gamma)$. The corresponding difference equation, namely (A.18), is *stable* (in the sense of Von Neumann), for $T \leq \sqrt{2}\Delta/(\sqrt{3}\gamma)$. The waveguide mesh can of course operate in a non-passive mode for $1/\sqrt{2} < \lambda \leq \sqrt{2/3}$ (where we will require negative self-loop immittances, and will not have a simple positive definite energy measure for the network in terms of the wave quantities). The numerical dispersion characteristics of the scheme at the two bounds are considerably different, and are plotted in Figure A.4(b) and (c); the phase velocities are near the correct physical velocity over a much wider range of spatial frequencies at the stability bound, though the dispersion is also more directional.

The question which arises here is of the distinction between passive and stable numerical methods (this was also seen for the mesh for the transmission line equations in §4.3.6, as well as in the previous section on the interpolated rectilinear scheme). Is it always possible to find a passive realization of a stable numerical method? The discussion on the hexagonal mesh will help to answer this question. To this end, we note that at the stability limit, we can rewrite $B_{\boldsymbol{\beta}}$ as

$$B_{\boldsymbol{\beta}} = 2(1 - \frac{2}{9}|\psi_{\boldsymbol{\beta}}|^2) \qquad \text{for} \qquad \lambda = \sqrt{\frac{2}{3}}$$

for a function $\psi_{\boldsymbol{\beta}}$ whose squared magnitude is given by

$$|\psi_{\boldsymbol{\beta}}|^2 = 1 + 4\cos^2(\frac{\beta_y\Delta}{2}) + 4\cos(\frac{\beta_y\Delta}{2})\cos(\frac{\sqrt{3}\beta_x\Delta}{2})$$

The spectral amplification factors at the stability limit will then be, from (A.6),

$$G_{\boldsymbol{\beta},\pm} = -1 + \frac{2}{9}|\psi_{\boldsymbol{\beta}}|^2 \pm \frac{2}{3}|\psi_{\boldsymbol{\beta}}|\left(\frac{1}{9}|\psi_{\boldsymbol{\beta}}|^2 - 1\right)^{\frac{1}{2}} \tag{A.19}$$

For $\lambda = \sqrt{2/3}$ (its limiting value), the triangular scheme has the same potential for instability as the rectilinear scheme. Linear growth may occur for this scheme at the seven spatial frequency pairs

$$\boldsymbol{\beta}^T = [0,0], \quad [0, \pm 4\pi/3\Delta], \quad [2\pi/\sqrt{3}\Delta, \pm 2\pi/3\Delta], \quad [-2\pi/\sqrt{3}\Delta, \pm 2\pi/3\Delta]$$

The computational and add densities for the triangular scheme in general, and at the stability

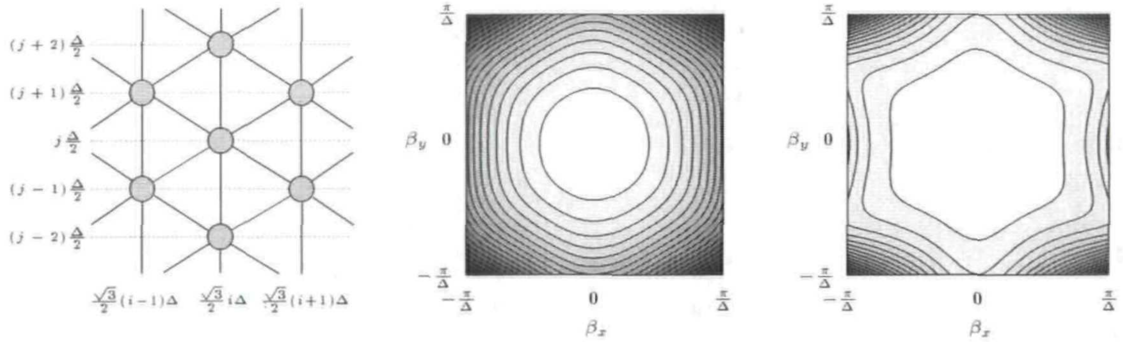

(a) (b) (c)

Figure A.4: *The triangular scheme* (A.18)— (a) *numerical grid and connections;* (b) $v_{\boldsymbol{\beta},phase}/\gamma$ *for the scheme at the passivity bound,* $\lambda = 1/\sqrt{2}$; (c) $v_{\boldsymbol{\beta},phase}/\gamma$ *at the stability bound, for* $\lambda = \sqrt{2/3}$.

($\lambda = \sqrt{2/3}$) and passivity bounds ($\lambda = 1/\sqrt{2}$) will be

$$\rho_{tri} = \frac{2v_0}{\sqrt{3}\Delta^3} \qquad \sigma_{tri} = \frac{14v_0}{\sqrt{3}\Delta^3}$$

$$\rho_{tri}^{s} = \frac{\sqrt{2}\gamma}{\Delta^3} \qquad \sigma_{tri}^{s} = \frac{7\sqrt{2}\gamma}{\Delta^3}$$

$$\rho_{tri}^{p} = \frac{2\sqrt{2}\gamma}{\sqrt{3}\Delta^3} \qquad \sigma_{tri}^{p} = \frac{4\sqrt{6}\gamma}{\Delta^3}$$

Here we have taken into account the fact that at the passivity bound, we require one less add per point (in the waveguide mesh implementation, the self-loop disappears). We also mention that the triangular difference scheme is doubly pathological, in the sense that not only do its passivity and stability regimes not coincide (and aside from the interpolated rectilinear schemes, it is the only scheme examined in this appendix that exhibits this behavior), but it also can not be decomposed into even/odd mutually exclusive subschemes, as can all the other schemes to be discussed here (again, excepting the interpolated scheme). It seems reasonable to conjecture that these two "symptoms" are related (somehow).

### A.2.4 The Hexagonal Scheme

The hexagonal scheme is different from those previously discussed in that updating is not the same at every point on the grid. Indeed, one-half the grid points have a "mirror-image" orientation with respect to the other half, as shown in Figure A.5(a). For this reason, we will take special care in the analysis of this system; first suppose that we have two grid functions $U_1(n)$ and $U_2(n)$

defined over the two subgrids (labeled 1 and 2, in Figure A.5). We index these two grid functions as $U_{1,i,j}(n)$ and $U_{2,i+2,j}(n)$, for $i$ and $j$ integer such that $i = 3m$, for integer $m$, and $j + i/3$ is even. $U_{1,i,j}(n)$ will serve as an approximation to some continuous function $u_1$ at the point $(x = \Delta i/2, y = \sqrt{3}j\Delta/2, t = nT)$, and $U_{2,i+2,j}(n)$ will approximate a function $u_2$ at a point with coordinates $(x = \Delta i/2+\Delta, y = \sqrt{3}j\Delta/2, t = nT)$. As before the distance between any grid point and its nearest neighbors (three in this case) is $\Delta$. The difference scheme for the hexagonal waveguide mesh can then be written as the system

$$\begin{aligned} U_{1,i,j}(n+1) + U_{1,i,j}(n-1) &= \frac{4}{3}\lambda^2\Big(U_{2,i+2,j}(n) + U_{2,i-1,j+1}(n) + U_{2,i-1,j-1}(n)\Big) \\ &\quad +2\left(1-2\lambda^2\right)U_{1,i,j}(n) \qquad \text{(A.20a)} \\ U_{2,i+2,j}(n+1) + U_{2,i+2,j}(n-1) &= \frac{4}{3}\lambda^2\Big(U_{1,i,j}(n) + U_{1,i+3,j+1}(n) + U_{1,i+3,j-1}(n)\Big) \\ &\quad +2\left(1-2\lambda^2\right)U_{2,i+2,j}(n) \qquad \text{(A.20b)} \end{aligned}$$

Consistency of (A.20) with the wave equation is not immediately apparent. We can check it as follows. First expand (A.20) in a Taylor series in terms of the continuous functions $u_1$ and $u_2$ to get

$$\begin{aligned} \left(T^2\frac{\partial^2}{\partial t^2} + 4\lambda^2\right)u_1 &= \lambda^2\left(4+\Delta^2\nabla^2\right)u_2 \\ \left(T^2\frac{\partial^2}{\partial t^2} + 4\lambda^2\right)u_2 &= \lambda^2\left(4+\Delta^2\nabla^2\right)u_1 \end{aligned}$$

to $O(\Delta^4, T^4)$. This system can then be reduced to

$$\left(T^2\frac{\partial^2}{\partial t^2} + 4\lambda^2\right)^2 u = \lambda^4\left(4+\Delta^2\nabla^2\right)^2 u$$

where $u$ is either of $u_1$ or $u_2$. Discarding higher order terms in $T$ and $\Delta$ gives the wave equation.

In terms of the spatial Fourier spectra of the grid functions $U_1$ and $U_2$, we may write the differencing system (A.20) in the vector form of (A.10) with

$$\hat{\mathbf{U}}_{\beta} = \begin{bmatrix}\hat{U}_{1,\beta}\\ \hat{U}_{2,\beta}\end{bmatrix} \qquad \mathbf{B}_{\beta} = \begin{bmatrix}-2(1-2\lambda^2) & -\frac{4}{3}\lambda^2\psi_{\beta}\\ -\frac{4}{3}\lambda^2\psi_{\beta}^{*} & -2(1-2\lambda^2)\end{bmatrix}$$

where

$$\psi_{\beta} = e^{i\beta_x\Delta} + 2e^{-i\beta_x\Delta/2}\cos(\sqrt{3}\beta_y\Delta/2)$$

Because $\mathbf{B}_{\beta}$ is Hermitian, we can then change variables so that the system is the form of (A.11), with

$$\mathbf{\Lambda}_{\beta} = \begin{bmatrix} -2(1-2\lambda^2)+\frac{4}{3}\lambda^2|\psi_{\beta}| & 0 \\ 0 & -2(1-2\lambda^2)-\frac{4}{3}\lambda^2|\psi_{\beta}| \end{bmatrix}$$

The necessary stability condition, from (A.12) will then be

$$\max_{\beta}|-2(1-2\lambda^2)\pm\frac{4}{3}\lambda^2|\psi_{\beta}||\leq 2 \tag{A.21}$$

It is easy to check that $|\psi_{\beta}|$ takes on a maximum of 3 when $\beta_x=\beta_y=0$, and is minimized for $\beta_x=0$, $|\beta_y|=4\pi/(3\sqrt{3}\Delta)$ and for $|\beta_x|=2\pi/3$, $|\beta_y|=2\pi/(3\sqrt{3}\Delta)$, where it takes on the value 0. It is then easy to show that we require $\lambda\leq 1/\sqrt{2}$ in order to satisfy (A.21). This coincides with the passivity bound, from (4.79).

An analysis of numerical dispersion is more complex in the vector case. Beginning from the uncoupled system defined by $\mathbf{\Lambda}_{\beta}$, whose upper and lower diagonal entries we will call $\Lambda_{\beta,1}$ and $\Lambda_{\beta,2}$ respectively, we can see that we will thus have two pairs of spectral amplification factors, one for each uncoupled scalar equation. These will be given by

$$G_{\beta,1,\pm}=\frac{1}{2}\left(-\Lambda_{\beta,1}\pm\sqrt{\Lambda_{\beta,1}^2-4}\right) \qquad G_{\beta,2,\pm}=\frac{1}{2}\left(-\Lambda_{\beta,2}\pm\sqrt{\Lambda_{\beta,2}^2-4}\right)$$

It is useful to check the values of the amplification factors at the spatial DC frequency, and at the stability bound, where we have $\Lambda_{\beta,1}=2$, $\Lambda_{\beta,2}=-2$. At this frequency, the spectral amplification factors take on the values

$$G_{\beta=0,1,\pm}=-1 \qquad G_{\beta=0,2,\pm}=1 \tag{A.22}$$

Clearly, the pair of spectral amplification factors $G_{\beta=0,2,\pm}$ correctly represents wave propagation at spatial DC, but the factors $G_{\beta=0,1,\pm}$ will be responsible for *parasitic oscillations* [176] in the hexagonal scheme; they will not, in general, be overly problematic, since the energy allowed into such modes must vanish as the grid spacing $\Delta$ is decreased; this is a result of the consistency of the numerical scheme (A.20) with the wave equation, as was shown earlier in this subsection. In order to clarify this point, it is useful to examine the diagonalizing transformation defined by $\mathbf{J}_{\beta}$, which takes the Fourier-transformed hexagonal scheme in the form of (A.10), in the variable $\hat{\mathbf{U}}_{\beta}$, to that of (A.11), in $\hat{\mathbf{V}}_{\beta}$. At $\boldsymbol{\beta}=0$, and for $\lambda=1/\sqrt{2}$, we have

$$\mathbf{B}_{\beta=0}=\begin{bmatrix}0 & -2\\ -2 & 0\end{bmatrix} \qquad \mathbf{\Lambda}_{\beta=0}=\begin{bmatrix}2 & 0\\ 0 & -2\end{bmatrix} \qquad \mathbf{J}_{\beta=0}=\frac{1}{\sqrt{2}}\begin{bmatrix}-1 & 1\\ 1 & 1\end{bmatrix}$$

and thus $\hat{V}_{1,\beta=0}=(-\hat{U}_{1,\beta=0}+\hat{U}_{2,\beta=0})/\sqrt{2}$ and $\hat{V}_{2,\beta=0}=(\hat{U}_{1,\beta=0}+\hat{U}_{2,\beta=0})/\sqrt{2}$. Because scheme

(A.20) is consistent with the wave equation, then for any reasonable choice of initial conditions, we must have that $\hat{U}_{1,\beta=0} \approx \hat{U}_{2,\beta=0}$, as $\Delta$ becomes small. Thus $\hat{V}_{1,\beta=0}$, the component of the numerical solution whose spectral amplification is governed by the parasitic factor $G_{\beta=0,1,\pm}$ must vanish in this limit as well.

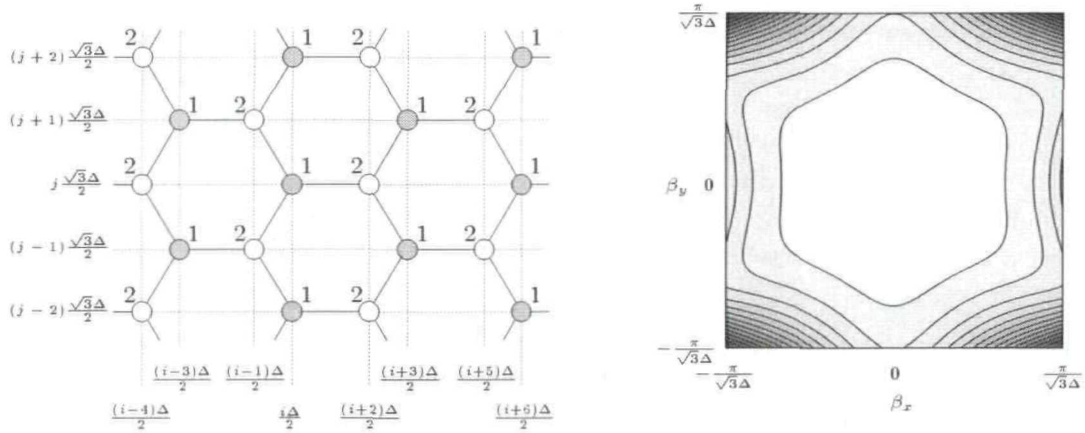

$(j+2)\frac{\sqrt{3}\Delta}{2}$
$(j+1)\frac{\sqrt{3}\Delta}{2}$
$j\frac{\sqrt{3}\Delta}{2}$
$(j-1)\frac{\sqrt{3}\Delta}{2}$
$(j-2)\frac{\sqrt{3}\Delta}{2}$
1
2
$\frac{(i-3)\Delta}{2}$
$\frac{(i-1)\Delta}{2}$
$\frac{(i+3)\Delta}{2}$
$\frac{(i+5)\Delta}{2}$
$\frac{(i-4)\Delta}{2}$
$\frac{i\Delta}{2}$
$\frac{(i+2)\Delta}{2}$
$\frac{(i+6)\Delta}{2}$
$\frac{\pi}{\sqrt{3}\Delta}$
$\beta_y$
0
$-\frac{\pi}{\sqrt{3}\Delta}$
$-\frac{\pi}{\sqrt{3}\Delta}$
0
$\frac{\pi}{\sqrt{3}\Delta}$
$\beta_x$

(a) (b)

Figure A.5: *The hexagonal scheme* (A.20)— (a) *numerical grid and connections, where grey/white coloration of points indicates a division into mutually exclusive sub schemes at the stability bound;* (b) $v_{\beta,phase}/\gamma$ *for the scheme at the passivity bound,* $\lambda = 1/\sqrt{2}$, *for the dominant mode.*

The computational and add densities, for the general scheme (A.20), and at the stability limit for $\lambda = 1/\sqrt{2}$ will be given by

$$\rho_{hex} = \frac{4v_0}{3\sqrt{3}\Delta^3} \qquad \sigma_{hex} = \frac{16v_0}{3\sqrt{3}\Delta^3}$$

$$\rho^s_{hex} = \frac{2\sqrt{2}\gamma}{3\sqrt{3}\Delta^3} \qquad \sigma^s_{hex} = \frac{2\sqrt{2}\gamma}{\sqrt{3}\Delta^3}$$

As in the rectilinear scheme, we have used the fact that the hexagonal scheme decouples into two independent subschemes at the stability limit.

One other point is worthy of comment. Consider again the vector equation which describes the time evolution of the spatial spectra for the hexagonal scheme, which, in diagonalized form, is exactly (A.11). At the stability limit, then, for $\lambda = 1/\sqrt{2}$, we will have

$$\mathbf{\Lambda}_{\beta} = \begin{bmatrix} \frac{2}{3}|\psi_{\beta}| & 0 \\ 0 & -\frac{2}{3}|\psi_{\beta}| \end{bmatrix}$$

Let us examine the second uncoupled subsystem. From (A.22), the spectral amplification factors will then be

$$G_{\beta,2,\pm} = \frac{1}{3}|\psi_{\beta}| \pm \left(\frac{1}{9}|\psi_{\beta}|^2 - 1\right)^{\frac{1}{2}}$$

It is of interest to see the effect of the amplification factors after *two* time steps; these will simply be the squares of $G_{\beta,2,\pm}$, which are

$$G^2_{\beta,2,\pm} = -1 + \frac{2}{9}|\psi_{\beta}|^2 \pm \frac{2}{3}|\psi_{\beta}|\left(\frac{1}{9}|\psi_{\beta}|^2 - 1\right)^{\frac{1}{2}} \tag{A.23}$$

The important point here is that the ***two-step*** spectral amplification factors for scheme (A.20) are identical to the one-step factor for the triangular scheme with grid spacing $\sqrt{3}\Delta$ at its own stability limit; these factors were given in (A.19). This is perhaps not surprising, given that, from Figure A.5(a), it is clear that that either of the two sub grids for the hexagonal scheme forms a triangular grid of spacing $\sqrt{3}\Delta$. What is surprising is that a triangular waveguide mesh at the stability limit is ***not a concretely passive structure*** (see previous section). That is to say, it will still operate stably (in the Von Neumann sense), but will require negative self-loop immittances. Thus a hexagonal waveguide mesh, at its passivity/stability bound can be seen as a ***passive realization*** of the stable difference scheme on a triangular grid. The question as to whether there is always a passive realization for any stable difference scheme remains open[†].

### A.2.5 A Fourth-order Scheme

The schemes examined so far have all been spatially accurate to second-order. That is, at any time step, the $L_2$ norm of the difference between the numerical solution and the solution to the model problem will be proportional to $\Delta^2$. In this section, we examine a family of explicit two-step schemes which are fourth-order spatially accurate. This family is more computationally intensive, due to the fact that updating the grid function requires access to past values which are two grid points away; in addition, we will see that a passive waveguide mesh implementation will not be possible in this case. These disadvantages are mitigated by the fact that the numerical dispersion is greatly reduced, so that the use of a coarse grid may be possible.

This scheme is, like the standard rectilinear scheme, defined over a grid with indices $i$ and $j$ which refer to a location with coordinates $x = i\Delta$ and $y = j\Delta$. Updating, in this case, at a given point, requires access to values of the grid function at the previous time step at the set of 25 grid points which are located at most $2\Delta$ away in either the $x$ or $y$ directions, as shown in Figure A.7(a).

---

[†] We consider this to be the single most important issue raised in this thesis.

The difference scheme will have the general form

$$\begin{aligned}U_{i,j}(n+1)+U_{i,j}(n-1) = {} & \lambda^2 a\big(U_{i,j+1}(n)+U_{i,j-1}(n)+U_{i+1,j}(n)+U_{i-1,j}(n)\big)\\ & +\lambda^2 b\big(U_{i+1,j+1}(n)+U_{i+1,j-1}(n)+U_{i-1,j+1}(n)+U_{i-1,j-1}(n)\big)\\ & +\lambda^2 c\big(U_{i+2,j}(n)+U_{i-2,j}(n)+U_{i,j+2}(n)+U_{i,j-2}(n)\big)\\ & +\lambda^2 d\big(U_{i+2,j+1}(n)+U_{i+2,j-1}(n)+U_{i-2,j+1}(n)+U_{i-2,j-1}(n)\\ & \qquad +U_{i+1,j+2}(n)+U_{i+1,j-2}(n)+U_{i-1,j+2}(n)+U_{i-1,j-2}(n)\big)\\ & +\lambda^2 e\big(U_{i+2,j+2}(n)+U_{i+2,j-2}(n)+U_{i-2,j+2}(n)+U_{i-2,j-2}(n)\big)\\ & +\lambda^2 f U_{i,j}(n)\end{aligned} \tag{A.24}$$

In order for (A.24) to approximate the wave equation, we first require that the constants $a$, $b$, $c$, $d$, $e$ and $f$ satisfy the constraints

$$a+2b+4c+10d+8e=1 \qquad 4a+4b+4c+8d+4e+f=\frac{2}{\lambda^2} \tag{A.25}$$

Then, to ensure that the scheme is fourth-order spatially accurate, we additionally require

$$b+8d+16e=0 \qquad a+2b+16c+34d+32e=0 \tag{A.26}$$

We can then write all the parameters in terms of $d$, $e$ and $\lambda$, as

$$a = 14d+32e+4/3 \tag{A.27a}$$

$$b = -8d-16e \tag{A.27b}$$

$$c = -2d-2e-1/12 \tag{A.27c}$$

$$f = 2/\lambda^2-24d-60e-5 \tag{A.27d}$$

These constraints are all arrived at through a tedious but straightforward Taylor series expansion of the scheme. As for the interpolated scheme discussed in §A.2.2, passivity is guaranteed by a simple positivity condition on the scheme parameters, in this case $a, \dots, f$. From (A.27c), it should be clear that if $d \geq 0$ and $e \geq 0$, then we must necessarily have $c \leq -1/12$, and a passive waveguide mesh implementation for this scheme is ruled out. This is not to say that fourth-order spatially accurate DWNs do not exist; we showed, in §4.10.5 that such a network does exist, at least in the case of the (1+1)D transmission line system (the wave equation is a special case of this system). The conclusion is that the topology of the form discussed in this section does not permit a mesh realization, but there are other forms that do.

The amplification polynomial for this scheme is of the form of (A.5), with $B_{\boldsymbol{\beta}} = -2\lambda^2 F_{\boldsymbol{\beta}} - 2$ and

$$\begin{aligned}F_{\boldsymbol{\beta}} = {} & (14d + 32e + 4/3)\big(\cos(\beta_x\Delta) + \cos(\beta_y\Delta)\big) + (-16d - 32e)\cos(\beta_x\Delta)\cos(\beta_y\Delta)\\ & + (-2d - 2e - 1/12)\big(\cos(2\beta_x\Delta) + \cos(2\beta_y\Delta)\big)\\ & + 2d\big(\cos(\beta_x\Delta)\cos(2\beta_y\Delta) + \cos(2\beta_x\Delta)\cos(\beta_y\Delta)\big)\\ & + 2e\cos(2\beta_x\Delta)\cos(2\beta_y\Delta) - 12d - 30e - 5/2\end{aligned}$$

In order to determine stability bounds, we are faced with finding the extrema of $F_{\boldsymbol{\beta}}$ in terms of the parameters $d$ and $e$. Because $F_{\boldsymbol{\beta}}$ is not multilinear in the cosines, finding these extrema explicitly is a challenging problem.

Let us first simplify the class of difference schemes by looking for those which exhibit maximally direction-independent numerical dispersion. As in §A.2.2, we expand $F_{\boldsymbol{\beta}}$ in a Taylor series about $\boldsymbol{\beta} = \mathbf{0}$, to get

$$F_{\boldsymbol{\beta}} = -\frac{\Delta^2}{2}\|\boldsymbol{\beta}\|_2^2 + \Delta^6\Big(\frac{1}{180}\left(\beta_x^6 + \beta_y^6\right) - (d/2 + 2e)\left(\beta_x^2\beta_y^4 + \beta_x^4\beta_y^2\right)\Big) + O(\Delta^8)$$

The absence of a term in $\Delta^4$ reflects the fourth-order accuracy of the scheme. If we choose $d/2+2e = -1/60$, however, we get

$$F_{\boldsymbol{\beta}} = -\frac{\Delta^2}{2}\|\boldsymbol{\beta}\|_2^2 + \frac{\Delta^6}{180}\|\boldsymbol{\beta}\|_2^6 + O(\Delta^8) \qquad \text{for} \qquad d/2 + 2e = -1/60$$

and the scheme is direction-independent to sixth order in $\Delta$.

Making use of this setting for $e$ in terms of $d$, $F_{\boldsymbol{\beta}}$ now depends only on the free parameter $d$; through a computer analysis, it is possible to show that condition (A.8) is satisfied for $d > -0.134$. The upper bound on $\lambda$, from condition (A.9) is plotted as a function of $d$ in Figure A.6.

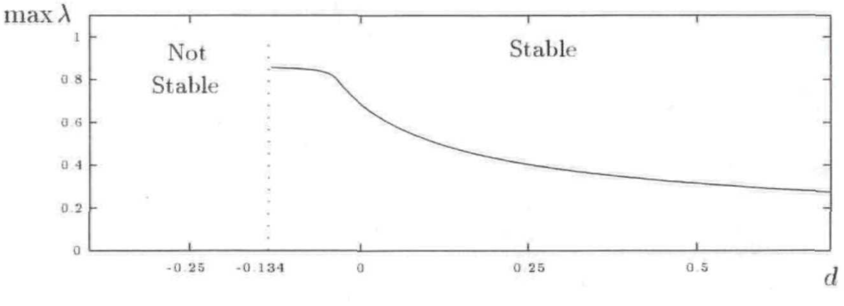

Figure A.6: *Stability bound for the fourth-order scheme* (A.24), *as a function of the free parameter* $d$, *in the optimally direction-independent case. The solid line indicates the maximum value of* $\lambda$ *for a given value of* $d$. *The scheme is stable only for* $d > -0.134$.

We have plotted a numerical dispersion profile in Figure A.7(b). It is interesting to note that the maximum value of $v_{\beta,phase}/\gamma$ for this family of schemes would always appear to be slightly greater than 1, although the numerical phase velocity does indeed approach the physical velocity at spatial DC (as it will for any consistent scheme).

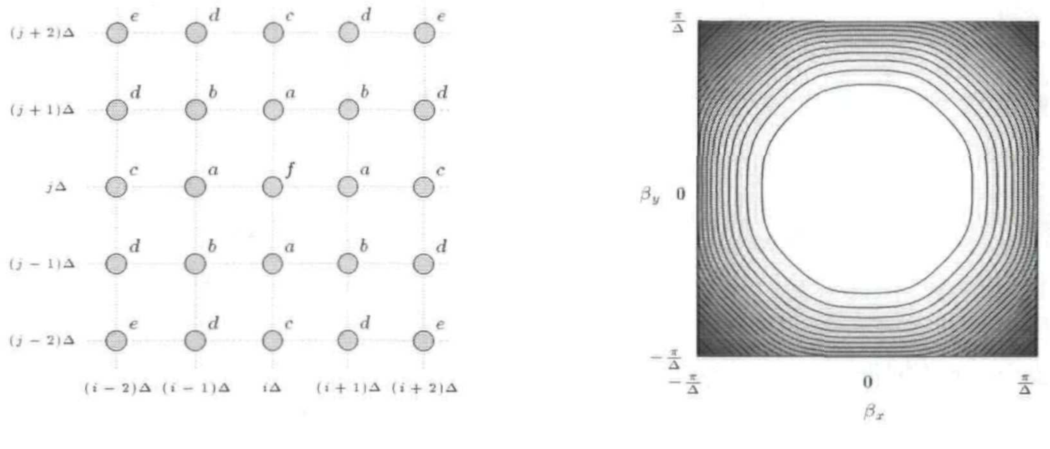

(a) (b)

Figure A.7: *The fourth-order spatially accurate scheme* (A.24)— (a) *numerical grid, where the letters a through f refer to the related coefficients from* (A.24); (b) $v_{\beta,phase}/\gamma$ *for the scheme at for* $d = -0.044$ *and* $\lambda = 0.6174$, *which is away from the bound shown in Figure A.6.* $v_{\beta,phase}/\gamma$ *takes on a maximum of 1.0144 (not shown).*

The computational and add densities for this scheme are, in general,

$$\rho_{fourth} = \frac{v_0}{\Delta^3} \qquad\qquad \sigma_{fourth} = \frac{25v_0}{\Delta^3}$$

There are several ways of cutting down on computational costs; for example, because $d$ and $e$ are free parameters, we may simply set them to zero, and the add density is significantly reduced. There is, however, no decomposition of this scheme into mutually exclusive subschemes.

## A.3 Finite Difference Schemes for the (3+1)D Wave Equation

We now look at several difference schemes which solve the wave equation in (3+1)D, in particular schemes which operate on a rectilinear grid; all the schemes which have appeared in the DWN literature are of this type. We will pay special attention to the interpolated scheme, for which the requirements for stability and passivity become even more distinct than they were in the (2+1)D case (see §A.2.2).

### A.3.1 The Cubic Rectilinear Scheme

This is the simplest scheme for the (3+1)D wave equation. The grid points, indexed by $i$, $j$ and $k$ are located at coordinates $(x, y, z) = (i\Delta, j\Delta, k\Delta)$. The finite difference scheme is written as

$$\begin{aligned} U_{i,j,k}(n+1) + U_{i,j,k}(n-1) = \lambda^2 \Big( & U_{i+1,j,k}(n) + U_{i-1,j,k}(n) + U_{i,j+1,k}(n) + U_{i,j-1,k}(n) \\ & + U_{i,j,k+1}(n) + U_{i,j,k-1}(n) \Big) \\ & + \left(2 - 6\lambda^2\right) U_{i,j,k}(n) \end{aligned} \tag{A.28}$$

If the grid points are located at the corners of a cubic lattice, then updating the scheme requires access to the grid function at the six neighboring corners; see Figure A.8(a). The stability analysis is very similar to that of the (2+1)D rectilinear scheme, except that we now have a 3-tuple of spatial frequencies, $\boldsymbol{\beta} = [\beta_x, \beta_y, \beta_z]^T$. The amplification polynomial equation is again of the form of (A.5), with

$$B_{\boldsymbol{\beta}} = -2\left(1 + \lambda^2\left(\cos(\beta_x \Delta) + \cos(\beta_y \Delta) + \cos(\beta_x \Delta) - 3\right)\right)$$

and thus

$$F_{\boldsymbol{\beta}} = \cos(\beta_x \Delta) + \cos(\beta_y \Delta) + \cos(\beta_x \Delta) - 3$$

Because $F_{\boldsymbol{\beta}}$ is multilinear in the cosines, it is simple to show that

$$\max_{\boldsymbol{\beta}} F_{\boldsymbol{\beta}} = 0 \qquad \min_{\boldsymbol{\beta}} F_{\boldsymbol{\beta}} = -6$$

and so, from (A.9),

$$\lambda \leq \frac{1}{\sqrt{3}} \qquad \text{(for Von Neumann stability)}$$

When $\lambda = 1/\sqrt{3}$, the amplification factors become degenerate and linear growth of the solution may occur for $\beta_x = \beta_y = \beta_z = 0$, and for $|\beta_x| = |\beta_y| = |\beta_z| = \pi/\Delta$. The computational and add densities are

$$\rho_{cub} = \frac{v_0}{\Delta^4} \qquad \sigma_{cub} = \frac{7v_0}{\Delta^4}$$

for $v_0 > \sqrt{3}\gamma$, and

$$\rho^s_{cub} = \frac{\gamma}{2\Delta^4} \qquad \sigma^s_{cub} = \frac{3\gamma}{\Delta^4}$$

at the stability limit $v_0 = \sqrt{3}\gamma$. At this limit, the scheme may, like the (2+1)D scheme, be divided into two mutually exclusive subschemes. See Figure A.8(b) and (c) for plots of the numerical dispersion properties of the cubic rectilinear scheme.

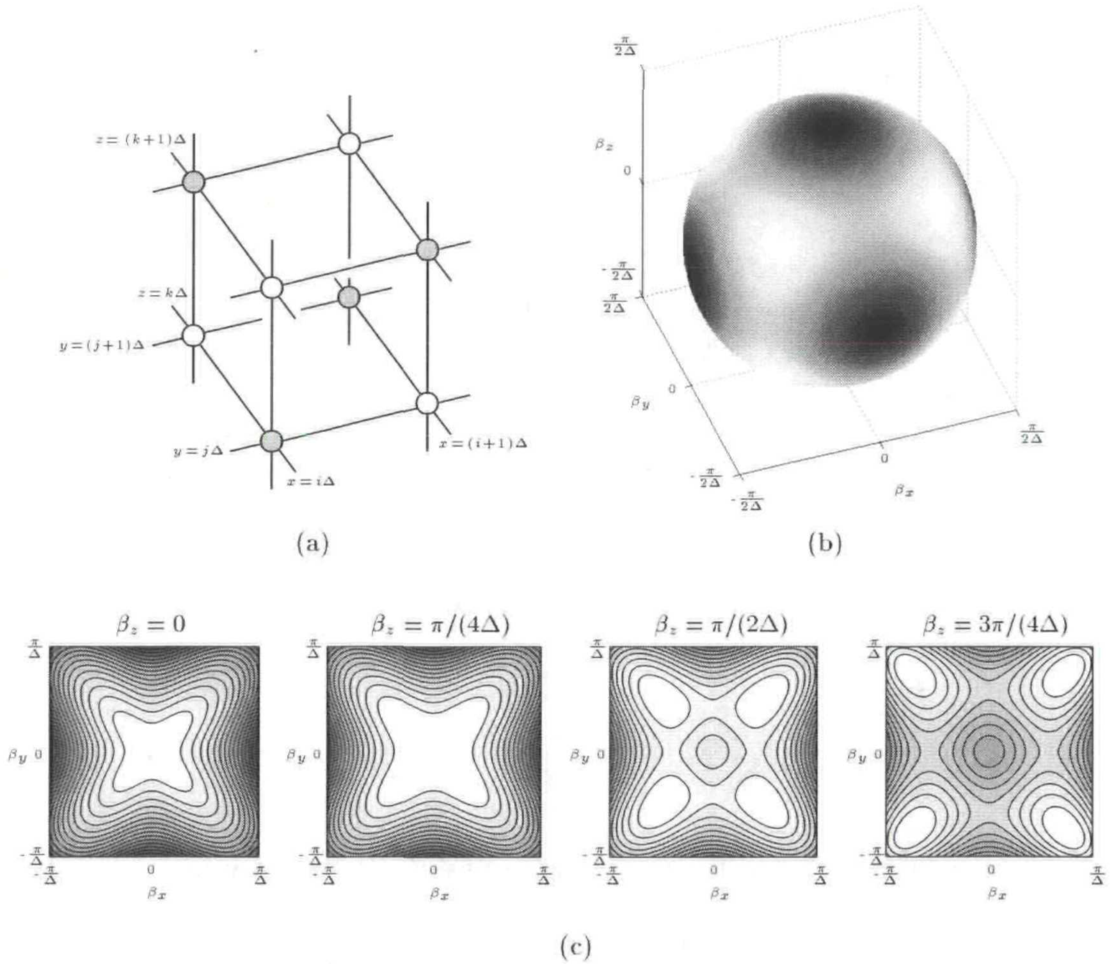

(a) (b)

$\beta_z = 0$ $\beta_z = \pi/(4\Delta)$ $\beta_z = \pi/(2\Delta)$ $\beta_z = 3\pi/(4\Delta)$

(c)

Figure A.8: *The cubic rectilinear scheme* (A.28)— (a) *numerical grid and connections, where grey/white coloring of points indicates a division into mutually exclusive subschemes at the stability bound;* (b) $v_{\boldsymbol{\beta},phase}/\gamma$ *for the scheme at the stability bound* $\lambda = 1/\sqrt{3}$, *for a spherical surface with* $\|\boldsymbol{\beta}\|_2 = \pi/(2\Delta)$*—the shading is normalized over the surface so that white corresponds to no dispersion error, and black to the maximum error over the surface (which is 7 per cent in this case).* (c) *Contour plots of* $v_{\boldsymbol{\beta},phase}/\gamma$ *for various cross-sections of the space of spatial frequencies* $\boldsymbol{\beta}$*; contours indicate successive deviations of 2 per cent from the ideal value of 1 which is obtained at spatial DC.*

### A.3.2 The Octahedral Scheme

The grid for an octahedral scheme is constructed from two superimposed rectilinear grids; if the points of the first grid are located at cube corners, then the points of the second will occur at the centers of the cubes defined by the first. The relevant difference scheme on an octahedral grid can be written as

$$\begin{aligned} U_{i,j,k}(n+1) + U_{i,j,k}(n-1) = \frac{3}{4}\lambda^2 \Big( & U_{i-1,j+1,k+1}(n) + U_{i+1,j+1,k+1}(n) + U_{i-1,j-1,k+1}(n) \\ & + U_{i+1,j-1,k+1}(n) + U_{i-1,j-1,k-1}(n) + U_{i-1,j+1,k-1}(n) \\ & + U_{i+1,j+1,k-1}(n) + U_{i+1,j-1,k-1}(n)\Big) \\ & + \left(2 - 8\lambda^2\right) U_{i,j,k}(n) \end{aligned} \tag{A.29}$$

for $i$, $j$ and $k$ which are either all even or all odd integers. Now, we have taken the spacing between nearest neighbors to be $\Delta$, so the indices $i$, $j$ and $k$ refer to a point with coordinates $x = i\Delta/\sqrt{3}$, $y = j\Delta/\sqrt{3}$ and $z = k\Delta/\sqrt{3}$. The amplification polynomial equation is again of the form (A.5), with

$$B_{\boldsymbol{\beta}} = -2\left(1 + 3\lambda^2\left(\cos(\frac{\beta_x\Delta}{\sqrt{3}})\cos(\frac{\beta_y\Delta}{\sqrt{3}})\cos(\frac{\beta_x\Delta}{\sqrt{3}}) - 1\right)\right)$$

and

$$F_{\boldsymbol{\beta}} = 3\left(\cos(\frac{\beta_x\Delta}{\sqrt{3}})\cos(\frac{\beta_y\Delta}{\sqrt{3}})\cos(\frac{\beta_x\Delta}{\sqrt{3}}) - 1\right)$$

and it is again easy to determine that

$$\max_{\boldsymbol{\beta}} F_{\boldsymbol{\beta}} = 0 \qquad\qquad \min_{\boldsymbol{\beta}} F_{\boldsymbol{\beta}} = -6$$

which are the same as the bounds in the cubic rectilinear case. We again have that

$$\lambda \leq \frac{1}{\sqrt{3}} \qquad\qquad \text{(for Von Neumann stability)}$$

Thus the stability bound coincides with the passivity bound for the mesh implementation. For $\lambda = 1/\sqrt{3}$, instabilities may appear at any spatial frequency triplets $\boldsymbol{\beta} = [\beta_x, \beta_y, \beta_z]^T$ where each component is either 0 or $\pm\sqrt{3}\pi/\Delta$.

The computational and add densities are given by

$$\begin{aligned} \rho_{oct} &= \frac{3\sqrt{3}v_0}{4\Delta^4} & \sigma_{oct} &= \frac{27\sqrt{3}v_0}{4\Delta^4} & &\text{for} \quad v_0 > \sqrt{3}\gamma \\ \rho^s_{oct} &= \frac{9\gamma}{8\Delta^4} & \sigma^s_{oct} &= \frac{9\gamma}{\Delta^4} & &\text{for} \quad v_0 = \sqrt{3}\gamma \end{aligned}$$

At the stability limit, the scheme can be divided into two mutually exclusive subschemes; plots of numerical dispersion are shown in Figure A.9(b) and (c). It is interesting to note that there is no dispersion error along the six axial directions; this should be compared with the cubic rectilinear scheme, for which wave propagation is dispersionless along the diagonal directions (there are eight such directions).

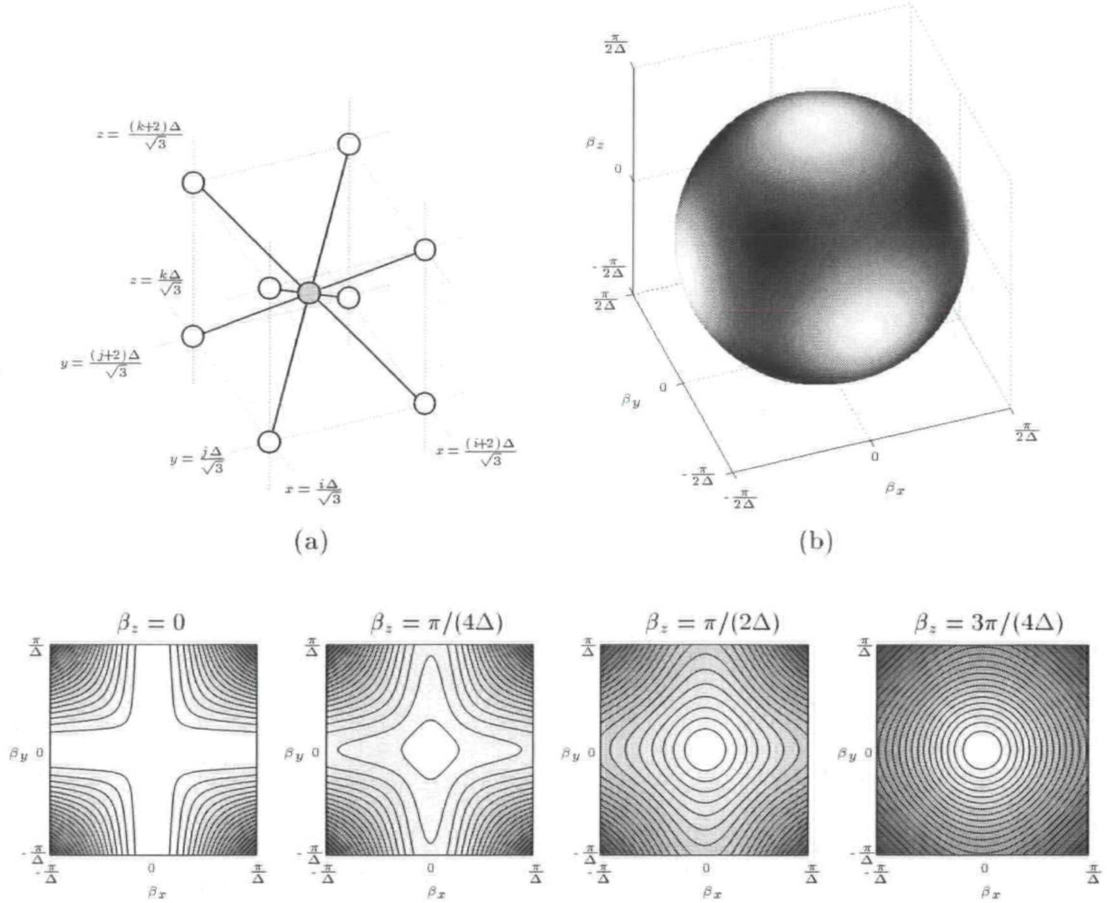

(a)

(b)

(c)

Figure A.9: *The octahedral scheme* (A.29)— (a) *numerical grid and connections, where grey/white coloring of points indicates a division into mutually exclusive subschemes at the stability bound;* (b) $v_{\boldsymbol{\beta},phase}/\gamma$ *for the scheme at the stability bound* $\lambda = 1/\sqrt{3}$, *for a spherical surface with* $\|\boldsymbol{\beta}\|_2 = \pi/(2\Delta)$*—the shading is normalized over the surface so that white corresponds to no dispersion error, and black to the maximum error over the surface (which is 5 per cent in this case).* (c) *Contour plots of the* $v_{\boldsymbol{\beta},phase}/\gamma$ *for various cross-sections of the space of spatial frequencies* $\boldsymbol{\beta}$*; contours indicate successive deviations of 2 per cent from the ideal value of 1 which is obtained at spatial DC.*

### A.3.3 The (3+1)D Interpolated Rectilinear Scheme

In the interest of achieving a more uniform numerical dispersion profile in (3+1)D, it is of course possible to define an interpolated scheme [155, 158], in the same way as was done in (2+1)D in §A.2.2. We will again have a two-step scheme, and updating at a given grid point is performed with reference to, at the previous time step, the grid point at the same location, as well as the 26 nearest neighbors: the six points a distance $\Delta$ away, twelve points at a distance of $\sqrt{2}\Delta$, and eight points that are $\sqrt{3}\Delta$ away—see Figure A.11(a). We present here a complete analysis of the relevant stability conditions, as well as the conditions under which a waveguide mesh implementation exists. We also look at a means of minimizing directional dependence of the numerical dispersion.

Like the cubic rectilinear and octahedral schemes, this scheme will be defined over a rectilinear grid indexed by $i$, $j$ and $k$ and will have the general form

$$\begin{aligned}
U_{i,j,k}(n+1)+U_{i,j,k}(n-1) = \; & \lambda^2 a\Big(U_{i+1,j,k}(n)+U_{i-1,j,k}(n)+U_{i,j+1,k}(n)+U_{i,j-1,k}(n)\\
& \quad +U_{i,j,k+1}(n)+U_{i,j,k-1}(n)\Big)\\
& +\lambda^2 b\Big(U_{i+1,j+1,k}(n)+U_{i+1,j-1,k}(n)+U_{i-1,j+1,k}(n)+U_{i-1,j-1,k}(n)\\
& \quad +U_{i+1,j,k+1}(n)+U_{i-1,j,k+1}(n)+U_{i,j+1,k+1}(n)+U_{i,j-1,k+1}(n)\\
& \quad +U_{i+1,j,k-1}(n)+U_{i-1,j,k-1}(n)+U_{i,j+1,k-1}(n)+U_{i,j-1,k-1}(n)\Big)\\
& +\lambda^2 c\Big(U_{i+1,j+1,k+1}(n)+U_{i+1,j+1,k-1}(n)+U_{i-1,j-1,k+1}(n)\\
& \quad +U_{i-1,j-1,k-1}(n)+U_{i+1,j-1,k+1}(n)+U_{i+1,j-1,k-1}(n)\\
& \quad +U_{i-1,j+1,k+1}(n)+U_{i-1,j+1,k-1}(n)\Big)\\
& +\lambda^2 d U_{i,j}(n)
\end{aligned} \tag{A.30}$$

In order for scheme (A.30) to satisfy the wave equation, we require the constants $a$, $b$, $c$ and $d$ to satisfy the constraints

$$c=\frac{1-a-4b}{4} \qquad\qquad d=\frac{2}{\lambda^2}-4a-4b-2 \tag{A.31}$$

and a family of difference schemes parametrized by $a$, $b$ and $\lambda$ results.

The stability analysis of this scheme proceeds along the same lines as that of the (2+1)D scheme, though as we shall see, the stability condition on the parameters $a$ and $b$ is considerably more complex. As before, we have an amplification polynomial of the form of (A.5), now with

$$\begin{aligned}
F_{\beta} = \; & a\big(\cos(\beta_x\Delta)+\cos(\beta_y\Delta)+\cos(\beta_z\Delta)\big)\\
& +2b\big(\cos(\beta_x\Delta)\cos(\beta_y\Delta)+\cos(\beta_x\Delta)\cos(\beta_z\Delta)+\cos(\beta_y\Delta)\cos(\beta_z\Delta)\big)\\
& +(1-a-4b)\cos(\beta_x\Delta)\cos(\beta_y\Delta)\cos(\beta_z\Delta)-2a-2b-1
\end{aligned}$$

where as before, $B_{\beta} = -2\lambda^2 F_{\beta} - 2$. Because $F_{\beta}$ is again multilinear in the three cosines, its extrema can only occur at the eight corners of the cubic region defined by $|\cos(\beta_x\Delta)| \leq 1$, $|\cos(\beta_y\Delta)| \leq 1$ and $|\cos(\beta_z\Delta)| \leq 1$. These extrema are

$$\begin{aligned} F_{\beta^T=[0,0,0]} &= 0 \\ F_{\beta^T=[\pi/\Delta,0,0]} = F_{\beta^T=[0,\pi/\Delta,0]} = F_{\beta^T=[0,0,\pi/\Delta]} &= -2 \\ F_{\beta^T=[\pi/\Delta,\pi/\Delta,0]} = F_{\beta^T=[\pi/\Delta,0,\pi/\Delta]} = F_{\beta^T=[\pi/\Delta,\pi/\Delta,0]} &= -4a - 8b \\ F_{\beta^T=[\pi/\Delta,\pi/\Delta,\pi/\Delta]} &= -4a + 8b - 2 \end{aligned}$$

The non-positivity requirement on $F_{\beta}$ then amounts to requiring that these extreme values be non-positive. The resulting stability region in the $(a, b)$ plane is shown in grey in Figure A.10(a).

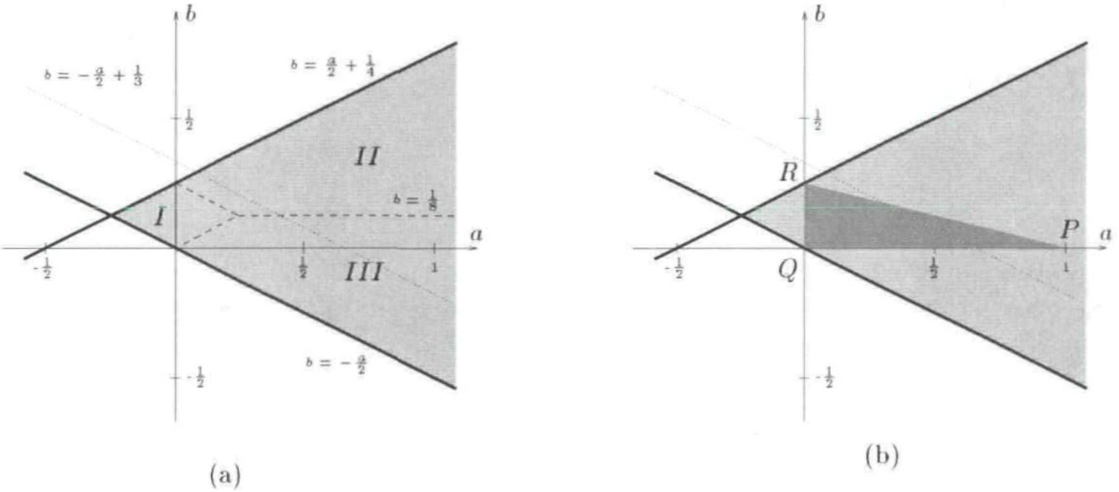

Figure A.10: (a) *Stability region, in grey, for the interpolated rectilinear scheme, plotted in the* $(a, b)$ *plane. This region can be divided into three sub-regions, labeled I, II, and III separated by dashed lines, over which different stability conditions on* $\lambda$ *apply. In region I, we must have* $\lambda \leq 1$, *in region II* $\lambda \leq 1/\sqrt{2a+4b}$, *and in region III* $\lambda \leq 1/\sqrt{2a-4b+1}$. *The dotted line indicates choices of a and b for which numerical dispersion is optimally direction-independent.* (b) *The subset of stable schemes for which a passive waveguide mesh implementation exists is shown in dark grey. Over this region, we require* $\lambda \leq 1/\sqrt{2a+2b+1}$. *This bound is more strict than the stability conditions mentioned above in the same region. We also remark that this interpolated scheme reduces to other simpler schemes under particular choices of a and b. At point P, we have the cubic rectilinear scheme (see §A.3.1), at point Q we have the octahedral scheme (see §A.3.2), and at point R we have what might be called a "dodecahedral" scheme. Notice in particular that none of these schemes is optimally direction-independent (i.e., P, Q and R do not lie on the dotted line).*

Assuming that $a$ and $b$ fall in this region, we must now find the values of $\lambda$ which satisfy (A.9). The minimum value of $F_{\beta}$ depends on $a$ and $b$ in a non-trivial way; referring to Figure A.10(a), the stability domain can be divided into three regions, and in each there is a different closed form expression for the upper bound on $\lambda$. These bounds are given explicitly in the caption to Figure

A.10(a).

In order to examine the directional dependence of the dispersion error, we may expand $F_{\boldsymbol{\beta}}$ in a Taylor series about $\boldsymbol{\beta}=\mathbf{0}$, as was done in the (2+1)D case. We have

$$F_{\boldsymbol{\beta}} = -\Delta^2\|\boldsymbol{\beta}\|_2^2 + \Delta^4\Big(\frac{1}{4!}\left(\beta_x^4+\beta_y^4+\beta_z^4\right) + \frac{1-a-2b}{4}\left(\beta_x^2\beta_y^2+\beta_x^2\beta_z^2+\beta_y^2\beta_z^2\right)\Big) + O(\Delta^6)$$

which implies that

$$F_{\boldsymbol{\beta}} = -\Delta^2\|\boldsymbol{\beta}\|_2^2 + \Delta^4\frac{1}{4!}\|\boldsymbol{\beta}\|_2^4 + O(\Delta^6) \qquad\qquad \text{for}\quad b=-a/2+1/3$$

and the dispersion error is directionally-independent to fourth order. This special choice of the parameters $a$ and $b$ is plotted as a dotted line in Figure A.10(a). It is well worth comparing this optimization method with the computer-based techniques applied to the same problem in [158].

The computational and add densities for the scheme will be

$$\rho_{3Dinterp} = \frac{v_0}{\Delta^4} \qquad\qquad \sigma_{3Dinterp} = \frac{27v_0}{\Delta^4}$$

Considerable computational savings are possible if any of $a$, $b$, $c$ or $d$ is zero.

Finally, we remark that the (3+1)D interpolated scheme can be realized as a waveguide mesh, where, at any given junction, we will have four types of waveguide connections: those of admittances $Y_a$, $Y_b$ and $Y_c$ are connected to the neighboring junctions located at gridpoints at distances $\Delta$, $\sqrt{2}\Delta$ and $\sqrt{3}\Delta$ away respectively, and a self-loop of admittance $Y_d$ is also connected to every junction. We end up with exactly difference scheme (A.30), with

$$\lambda^2a=\frac{2Y_a}{Y_J} \qquad \lambda^2b=\frac{2Y_b}{Y_J} \qquad \lambda^2c=\frac{2Y_c}{Y_J} \qquad \lambda^2d=\frac{2Y_d}{Y_J} \qquad\qquad Y_J=6Y_a+12Y_b+8Y_c+Y_d$$

The passivity condition is then a positivity condition on these admittances, and thus on the parameters $a$, $b$, $c$ and $d$. Recalling the expression for $c$ in terms of $a$ and $b$ from (A.31), we must have

$$a\geq 0 \quad b\geq 0 \quad b\leq\frac{1-a}{4}$$

This region is shown, in dark grey, in Figure A.10(b). The positivity condition on $d$ (expressed in terms of $a$, $b$ and $\lambda$ as per (A.31)) gives the bound on $\lambda$, which is

$$\lambda\leq\sqrt{\frac{1}{2a+2b+1}} \qquad\qquad \text{(for passivity)}$$

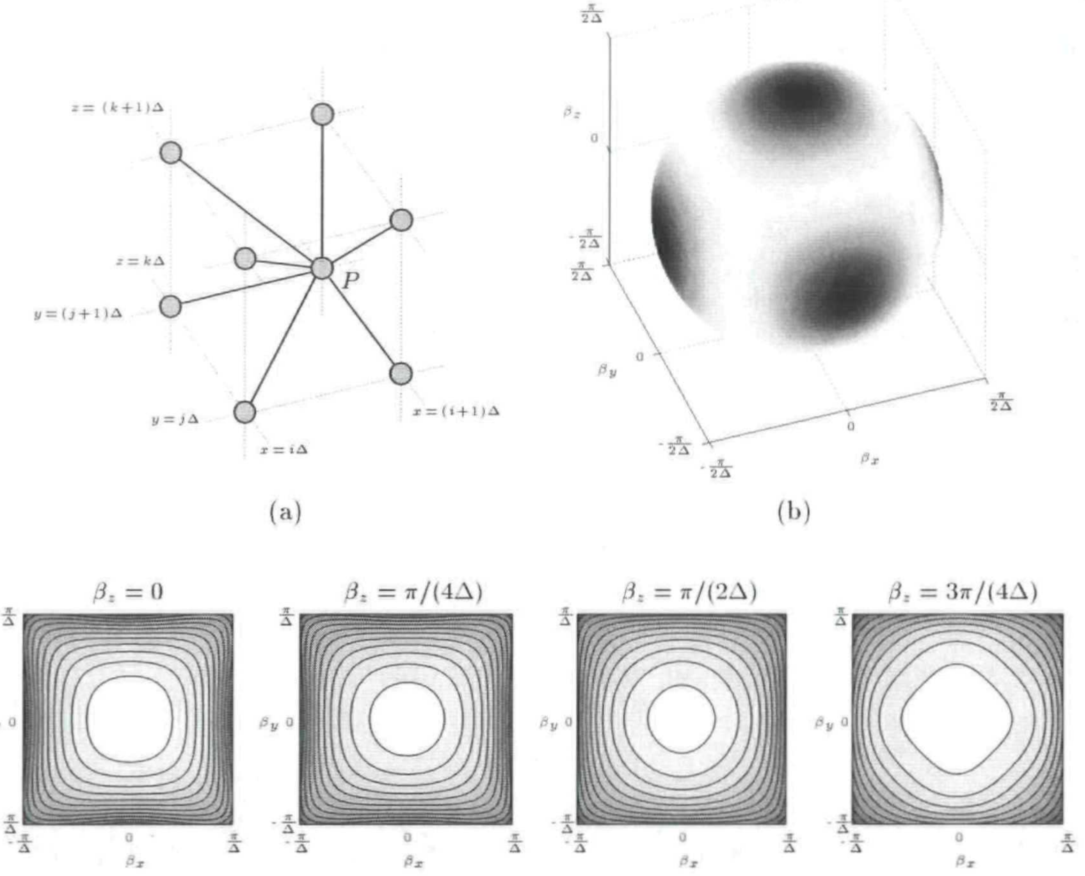

(a) (b)

(c)

Figure A.11: *The (3+1)D interpolated rectilinear scheme* (A.30)— (a) *numerical grid and connections, from a central grid point (labeled P) to its neighbors in one octant.* (b) $v_{\boldsymbol{\beta},phase}/\gamma$ *for the scheme with* $a=0.42$ *and* $b=0.1233$ *at the stability bound* $\lambda=0.8617$, *for a spherical surface with* $\|\boldsymbol{\beta}\|_2=\pi/(2\Delta)$*—the shading is normalized over the surface so that white and black refer to minimal and maximal dispersion error, respectively. Here, unlike for the cubic rectilinear and octahedral schemes, there are no dispersionless directions. The variation in the numerical phase velocity is, however, quite small, ranging from 96.81 to 97.32 per cent of the correct wave speed.* (c) *Contour plots of* $v_{\boldsymbol{\beta},phase}/\gamma$ *for various cross-sections of the space of spatial frequencies* $\boldsymbol{\beta}$; *contours indicate successive deviations of 2 per cent from the ideal value of 1 which is obtained at spatial DC.*

### A.3.4 The Tetrahedral Scheme

The tetrahedral scheme in (3+1)D [200] is somewhat similar to the hexagonal scheme in (2+1)D, in that the grid is divided evenly into two sets of points, at which updating is performed using "mirror-image" stencils. It is different, however, because grid points can easily be indexed with reference to a regular cubic lattice; the hexagonal scheme operates on a rectangular grid in stretched or transformed coordinates. In fact, a tetrahedral scheme can be obtained directly from an octahedral scheme simply by removing half of the grid points it employs; as such, any given grid point in the tetrahedral scheme has four nearest neighbors. As usual, we assume the nearest-neighbor grid spacing to be $\Delta$. See Figure A.12(a) for a representation of the numerical grid.

As per the hexagonal scheme, we will view this as a vectorized scheme operating on two distinct sub grids, labeled 1 and 2 in Figure A.12(a). The two grid functions $U_{1,i,j,k}(n)$ and $U_{2,i+1,j+1,k+1}(n)$ are defined for integers $i$, $j$ and $k$ all even such that $(i+j+k)/2$ is also even. $U_{1,i,j,k}$ will be used to approximate a continuous function $u_1$ at the point with coordinates $x = i\Delta/\sqrt{3}$, $y = j\Delta/\sqrt{3}$ and $z = k\Delta/\sqrt{3}$, and $U_{2,i+1,j+1,k+1}$ approximates $u_2$ at coordinates $x = (i+1)\Delta/\sqrt{3}$, $y = (j+1)\Delta/\sqrt{3}$ and $z = (k+1)\Delta/\sqrt{3}$. The numerical scheme can then be written as

$$\begin{aligned}
U_{1,i,j,k}(n+1) + U_{1,i,j,k}(n-1) &= \frac{3}{2}\lambda^2\Big(U_{2,i+1,j+1,k+1}(n) + U_{2,i+1,j-1,k-1}(n) \\
&\qquad + U_{2,i-1,j-1,k+1}(n) + U_{2,i-1,j+1,k-1}(n)\Big) \\
&\quad + 2\left(1-3\lambda^2\right)U_{1,i,j,k}(n) \qquad \text{(A.32a)} \\
U_{2,i+1,j+1,k+1}(n+1) + U_{2,i+1,j+1,k+1}(n-1) &= \frac{3}{2}\lambda^2\Big(U_{1,i,j,k}(n) + U_{1,i,j+2,k+2}(n) \\
&\qquad + U_{1,i+2,j+2,k}(n) + U_{1,i+2,j,k+2}(n)\Big) \\
&\quad + 2\left(1-3\lambda^2\right)U_{2,i+1,j+1,k+1}(n) \qquad \text{(A.32b)}
\end{aligned}$$

As for the hexagonal scheme, we may check consistency of this system with the wave equation by treating the grid functions as samples of continuous functions $u_1$ and $u_2$ and expanding (A.32) in terms of partial derivatives; both grid functions updated according to this scheme will approximate the solution to the wave equation on their respective grids.

Determining the stability condition proceeds as in the hexagonal scheme; taking spatial Fourier transforms of (A.32) gives a vector spectral update equation of the form (A.10), with $\mathbf{B}_{\boldsymbol{\beta}}$ given by

$$\mathbf{B}_{\boldsymbol{\beta}} = \begin{bmatrix} -2(1-3\lambda^2) & -\frac{3}{2}\lambda^2\psi_{\boldsymbol{\beta}} \\ -\frac{3}{2}\lambda^2\psi_{\boldsymbol{\beta}}^* & -2(1-3\lambda^2) \end{bmatrix}$$

with

$$\psi_{\boldsymbol{\beta}} = 2\Big(e^{j\Delta\beta_x/\sqrt{3}}\cos(\Delta(\beta_y+\beta_z)/\sqrt{3}) + e^{-j\Delta\beta_x/\sqrt{3}}\cos(\Delta(\beta_y-\beta_z)/\sqrt{3})\Big)$$

$\mathbf{B}_{\beta}$ is again Hermitian, and has eigenvalues

$$\begin{aligned}\Lambda_{\beta,1} &= -2\left(1-3\lambda^2\right)+\frac{3}{2}\lambda^2|\psi_{\beta}|\\ \Lambda_{\beta,2} &= -2\left(1-3\lambda^2\right)-\frac{3}{2}\lambda^2|\psi_{\beta}|\end{aligned}$$

The stability condition can thus be written as

$$\left|-2\left(1-3\lambda^2\right)\pm\frac{3}{2}\lambda^2|\psi_{\beta}|\right|\leq 2 \tag{A.33}$$

$\psi_{\beta}$ can be shown to take on a maximum of 4, and a minimum of 0, and it then follows that (A.33) will be satisfied if and only if $\lambda\leq 1/\sqrt{3}$, the same bound as obtained for the cubic rectilinear and octahedral schemes. The bound is the same as the bound for passivity of a tetrahedral mesh, as discussed in §4.7. We note that as for these other schemes, the grid permits a subdivision into mutually exclusive subschemes at this stability limit—see Figure A.12(a). By a simple comparison with the hexagonal scheme, we can obtain the four spectral amplification factors by

$$G_{\beta,1,\pm}=\frac{1}{2}\left(-\Lambda_{\beta,1}\pm\sqrt{\Lambda_{\beta,1}^2-4}\right)\qquad G_{\beta,2,\pm}=\frac{1}{2}\left(-\Lambda_{\beta,2}\pm\sqrt{\Lambda_{\beta,2}^2-4}\right)$$

it is easy to see that parasitic modes (characterized by the amplification factors $G_{\beta,1,\pm}$) will be present in the tetrahedral scheme, due to the non-uniformity of updating on the numerical grid. The numerical dispersion characteristics of the dominant modes with amplification factors $G_{\beta,2,\pm}$ are shown in planar and spherical cross-sections in Figure A.12(b) and (c).

The computational and add densities of this scheme, in general, are

$$\rho_{tetr}=\frac{3\sqrt{3}v_0}{8\Delta^4}\qquad \sigma_{tetr}=\frac{15\sqrt{3}v_0}{8\Delta^4}$$

for $v_0>\sqrt{3}\gamma$, and

$$\rho_{tetr}^{s}=\frac{9\gamma}{16\Delta^4}\qquad \sigma_{tetr}^{s}=\frac{9\gamma}{4\Delta^4}$$

at the stability limit $v_0=\sqrt{3}\gamma$.

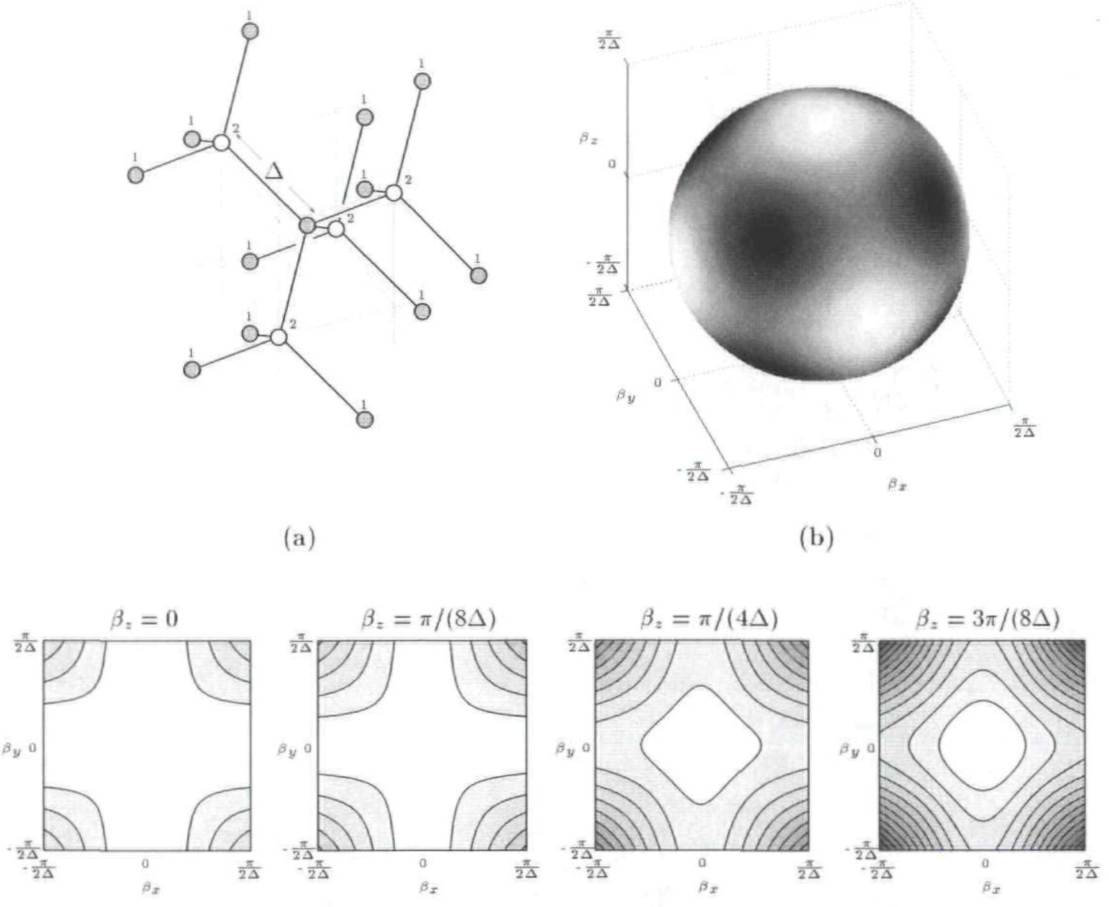

(a) (b)

(c)

Figure A.12: *The tetrahedral scheme* (A.32)— (a) *numerical grid and connections, where grey/white coloring of points indicates a division into mutually exclusive subschemes at the stability bound. The scheme can be indexed similarly to the octahedral scheme (see Figure A.9). The two sub grids with mutually inverse orientations are labeled 1 and 2.* (b) $v_{\boldsymbol{\beta},phase}/\gamma$ *for the scheme at the stability bound* $\lambda = 1/\sqrt{3}$, *for a spherical surface with* $\|\boldsymbol{\beta}\|_2 = \pi/(2\Delta)$*—the shading is normalized over the surface so that white corresponds to no dispersion error, and black to the maximum error over the surface (which is 6 per cent in this case).* (c) *Contour plots of* $v_{\boldsymbol{\beta},phase}/\gamma$ *for various cross-sections of the space of spatial frequencies* $\boldsymbol{\beta}$*; contours indicate successive deviations of 2 per cent from the ideal value of 1 which is obtained at spatial DC. Here we have only plotted spatial frequencies to* $|\beta_x|$, $|\beta_y|$, *and* $|\beta_z|$ *all less than* $\pi/(2\Delta)$.

# Appendix B

# Applications in Fluid Dynamics

One of the most interesting developments in the wave digital numerical integration field has been applications to highly nonlinear problems in fluid mechanics [16, 49, 70]. These systems, also described by hyperbolic systems of PDEs, have MD circuit representations, and as such, it is possible to develop numerical methods in the same way as outlined in Chapter 3; the procedure is, however, complicated by the necessarily nonlinear nature of the requisite circuit elements. The purpose of this brief appendix is to expand upon the very concise descriptions of the technique in the literature, and to add a few comments regarding alternative network formulations and fluid dynamical DWNs and a possible reformulation of the problem in terms of entropy variables [181, 183].

## B.1 Nonlinear Circuit Elements

It should be clear that in order to build circuit models for nonlinear systems of PDEs, we will need nonlinear distributed circuit elements. Nonlinear resistances are simple to model; a voltage-current relation of the form

$$v = iR$$

will correspond to a passive resistor as long as $R$ is positive, regardless of its dependence on $v$, $i$, or the independent variables of the problem. The definitions of transformers and gyrators also remain unchanged in the nonlinear case; the turns ratio or gyration coefficient may have any dependence without affecting losslessness.

Nonlinear reactances require only a slightly more involved treatment. Recall the generalized definition of the inductor as given in (3.42):

$$v = \sqrt{L}\frac{\partial}{\partial t_j}\left(\sqrt{L}i\right) = \frac{1}{2}\left(L\frac{\partial i}{\partial t_j} + \frac{\partial Li}{\partial t_j}\right) \tag{B.1}$$

Here again, $t_j$ is some coordinate defined by a transformation such as (3.15) or (3.21). The instantaneous absorbed power density will be

$$w_{inst} = vi = \sqrt{L}i\frac{\partial\sqrt{L}i}{\partial t_j} = \frac{1}{2}\frac{\partial Li^2}{\partial t_j}$$

and the element can be considered to be lossless as per the definition of (3.28) provided the stored energy flux **E** is defined to be

$$\mathbf{E} = \frac{1}{2}Li^2\mathbf{e}_j$$

where $\mathbf{e_j}$ is a unit vector in the direction $t_j$. This is the same as the definition in the linear case, from (3.35). Here, $L$ is constrained to positive, but may be be a function (smooth) of any of the dependent or independent variables in the problem. This losslessness is reflected in the MDWD one-port; if the port resistance is chosen to be $R = 2L/T_j$, for some step-size $T_j$ in direction $t_j$, then in terms of power-normalized waves $\underline{a}$ and $\underline{b}$ (see §2.3.2), the one-port is defined, at a grid point with coordinates $\mathbf{t}$, by

$$\underline{b}(\mathbf{t}) = -\underline{a}(\mathbf{t} - \mathbf{T}_j) \tag{B.2}$$

for a vector shift $\mathbf{T}_j = T_j\mathbf{e}_j$, just as in the linear case. It is important to mention that for a nonlinear problem, it is essential to use power-normalized waves, because passivity is not guaranteed otherwise [16]. (The reason for this should be clear from the discussion in §3.5.1; we cannot obtain a wave relation such as (B.2) in terms of voltage wave variables because the differential operator does not necessarily commute with the inductance.)

A nonlinear capacitor can be similarly defined, by

$$i = \sqrt{C}\frac{\partial}{\partial t_j}\left(\sqrt{C}i\right) = \frac{1}{2}\left(C\frac{\partial i}{\partial t_j} + \frac{\partial Ci}{\partial t_j}\right) \tag{B.3}$$

for some capacitance $C$, which again may have arbitrary smooth functional dependence; if $C$ is always positive, then the capacitance is lossless.

Notice that for all practical purposes, the nonlinear character of any one of these elements is essentially transferred to the port resistances of the adaptor to which it is connected; the wave digital elements themselves are identical to their linear counterparts. As long as the circuit element values remain positive, then so do the port resistances, and an adaptor scattering matrix will be forced to be orthogonal (see §2.3.5), and can be interpreted in terms of rotations and reflections. The problem, then, is in determining the scattering matrix, which, though orthogonal, may be dependent on the input waves; a system of nonlinear algebraic equations results. This problem is usually solved in practice using iterative methods, but existence and uniqueness of such a solution are matters which have not been broached in any detail (and should be). These systems of equations are usually small, however, and can be solved separately at a any given grid point.

## B.2 Burger's Equation

A simple nonlinear PDE which is often used as a model problem for fluid dynamical systems is given by the *inviscid Burger's equation* [82]:

$$\frac{\partial u}{\partial t} + u\frac{\partial u}{\partial x} = 0 \tag{B.4}$$

It is similar in form to the *advection equation* mentioned in §3.6, and as we will see, its circuit representation is identical. The problem is assumed to be defined for $x \in \mathbb{R}$, $t \geq 0$. $u$ can be considered to be a current, as before, through a single loop, and Kirchoff's Voltage Law around the loop will give (B.4). The question however, is of the type of circuit elements to be included in this loop; clearly they must be nonlinear, and certainly reactive as well. We note that the viscous form of Burger's equation was approached in this way in [202].

Using coordinate transformation (3.18), (B.4) can be rewritten as

$$\left(\frac{v_0 + u}{\sqrt{2}}\right)\frac{\partial u}{\partial t_1} + \left(\frac{v_0 - u}{\sqrt{2}}\right)\frac{\partial u}{\partial t_2} = 0$$

Assuming that the solution is differentiable[†], this can be rewritten as

$$\underbrace{\frac{1}{2}\left(L_1\frac{\partial u}{\partial t_1} + \frac{\partial L_1 u}{\partial t_1}\right)}_{v_1} + \underbrace{\frac{1}{2}\left(L_2\frac{\partial u}{\partial t_2} + \frac{\partial L_2 u}{\partial t_2}\right)}_{v_2} = 0 \tag{B.5}$$

where

$$L_1 = \frac{1}{\sqrt{2}}\left(v_0 + \frac{2}{3}u\right) \qquad L_2 = \frac{1}{\sqrt{2}}\left(v_0 - \frac{2}{3}u\right) \tag{B.6}$$

---

[†] This is an assumption made by Fettweis et al. in all of their fluid dynamics work, and is not entirely justified, especially if discontinuities (shocks) are to be modeled. Even in the simple model of Burger's equation, these shocks can develop [82]. Over regions of continuity in the problem, these numerical methods will give the correct solution, but shock velocities, should they develop, may not be correct for this reason.

Thus Burger's equation, in the form of (B.5), can be interpreted as a series combination of two nonlinear inductances, as shown in Figure B.1(a). The resultant MDWD network, with port resistances

$$R_1 = \frac{2L_1}{T_1} \qquad\qquad R_2 = \frac{2L_2}{T_2} \tag{B.7}$$

appears in Figure B.1(b). We emphasize that this network is passive only if power-normalized wave variables are employed. The positivity condition on these inductances now depends on the solution

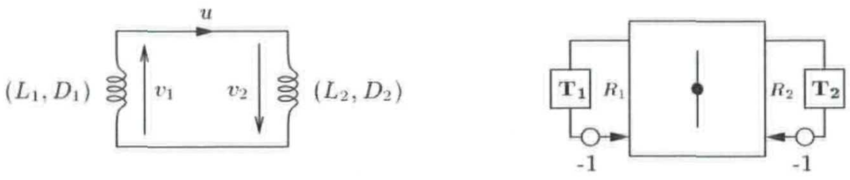

(a) (b)

Figure B.1: *The (1+1)D inviscid Burger's equation*— (a) *MDKC and* (b) *MDWD network.*

itself, $u$, and we must have

$$v_0 \geq \frac{2}{3} \max_{x\in\mathbb{R},t\geq 0} |u|$$

An *a priori* estimate of $\max_{x\in\mathbb{R},t\geq 0} |u|$ must be available; this is a consistent feature of all the circuit-based methods (and, it would seem, any explicit method) for the fluids systems that we will examine presently.

Let us now examine the scattering operation. First choose $T_1 = T_2 = \sqrt{2}\Delta$, so that the current grid function for the current at location $x = i\Delta$ and $t = nT$ can be written as $u_i(n)$. The two power-normalized input wave variables entering the adaptor at the same location and time step are $\underline{a}_{1,i}(n)$ $\underline{a}_{2,i}(n)$, and we have

$$u_i(n) = \frac{2}{R_{1,i}(n) + R_{2,i}(n)} \left(\sqrt{R_{1,i}(n)}\underline{a}_{1,i}(n) + \sqrt{R_{2,i}(n)}\underline{a}_{2,i}(n)\right)$$

which, from (B.6) and (B.7), and using $T_1 = T_2 = \sqrt{2}\Delta$ and $v_0 = \Delta/T$ can be rewritten as

$$u_i(n) = \frac{\sqrt{\Delta}}{v_0} \left(\sqrt{v_0 + \frac{2}{3}u_i(n)}\underline{a}_{1,i}(n) + \sqrt{v_0 - \frac{2}{3}u_i(n)}\underline{a}_{2,i}(n)\right) \tag{B.8}$$

This is precisely the nonlinear algebraic equation which is to be solved (in $u_i(n)$); once $u_i(n)$ is determined, then so are the port resistances, and the output wave variables $\underline{b}_{1,i}(n)$ and $\underline{b}_{2,i}(n)$ can be obtained through scattering as per (2.33). As mentioned before, it is not at all clear from the form of (B.8) whether a solution exists and is unique. We note, however, that we (and others [16, 70]) have successfully programmed simulations for the gas dynamics equations (see next section), using simple iterative methods to solve the nonlinear algebraic systems; the results would appear to be in accord with published simulation results using differencing methods [171].

## B.3 The Gas Dynamics Equations

The behavior of a lossless one-dimensional fluid is described by the following set of conservation equations, also known as *Euler's Equations:*

$$\frac{\partial \rho}{\partial t}+\frac{\partial(\rho v)}{\partial x}=0 \qquad \text{Conservation of mass} \tag{B.9a}$$

$$\frac{\partial(\rho v)}{\partial t}+\frac{\partial(\rho v^2+p)}{\partial x}=0 \qquad \text{Conservation of momentum} \tag{B.9b}$$

$$\frac{\partial(\rho e)}{\partial t}+\frac{\partial(\rho ve+pv)}{\partial x}=0 \qquad \text{Conservation of energy} \tag{B.9c}$$

where $\rho(x,t)$ is density, $v(x,t)$ is volume velocity, $p(x,t)$ is absolute pressure, and $e(x,t)$ is total energy, internal plus kinetic. The three equations are not complete without a constitutive relation among the four dependent variables. The WDF people, in their treatment of *hydrodynamics* [16] often leave out the energy equation and make an assumption of the type $p=G(\rho)$, which essentially reduces system (B.9) to a two-variable system (in $\rho$ and $v$). For gas dynamics, we assume polytropic gas behavior [181]:

$$e=\frac{v^2}{2}+\frac{p}{\rho(\gamma-1)} \tag{B.10}$$

where $\gamma>1$ is a constant which follows directly from thermodynamics (it is equal to the ratio of specific heats [203]).

Before proceeding any further, we mention the *scaling* of the dependent variables [16, 49]; this is done, as in the linear problems discussed in Chapters 3 and 5, in order to optimize the stability condition on the resulting network. The variables are scaled as

$$\hat{v}=\frac{v}{v_0} \qquad \hat{p}=\frac{p}{p_0} \qquad \hat{\rho}=\frac{\rho v_0^2}{p_0} \tag{B.11}$$

The parameters $v_0$ and $p_0$ have dimensions of velocity and pressure, respectively, and nondimensionalize the system. $v_0$ will again become the space-step/time-step ratio in the numerical simulation routine, and $p_0$ plays a role similar to that of $r_0$ in the (1+1)D transmission line problem as discussed in §3.7 and follows directly from physical considerations.

Using the energy density definition (B.10), system (B.9) can be written in *non-conservative* [203] form (after some tedious algebraic manipulations) as

$$\begin{bmatrix}1 & 0 & 0\\ 0 & \hat{\rho} & 0\\ 0 & 0 & 1\end{bmatrix}\frac{\partial}{\partial t'}\begin{bmatrix}\hat{\rho}\\ \hat{v}\\ \hat{p}\end{bmatrix}+\begin{bmatrix}\hat{v} & \hat{\rho} & 0\\ 0 & \hat{\rho}\hat{v} & 1\\ 0 & \gamma\hat{p} & \hat{v}\end{bmatrix}\frac{\partial}{\partial x}\begin{bmatrix}\hat{\rho}\\ \hat{v}\\ \hat{p}\end{bmatrix}=\mathbf{0}$$

The problem here is that this system is not, in its present form, suitable for a circuit representation involving reciprocal elements[†]. Although it is not explicitly stated anywhere in the literature, the solution of Fettweis et al. has been to scale system (B.9) by left multiplication by the matrix $\mathrm{diag}(1/\hat{\rho}, 1, 1/(\gamma\hat{p}))$ (though as previously mentioned, they work with the two-variable hydrodynamics system, or its analogues in higher dimensions). The scaled system takes the form:

$$\begin{bmatrix}\frac{1}{\hat{\rho}} & 0 & 0\\ 0 & \hat{\rho} & 0\\ 0 & 0 & \frac{1}{\gamma\hat{p}}\end{bmatrix}\frac{\partial}{\partial t'}\begin{bmatrix}\hat{\rho}\\ \hat{v}\\ \hat{p}\end{bmatrix}+\begin{bmatrix}\frac{\hat{v}}{\hat{\rho}} & 1 & 0\\ 0 & \hat{\rho}\hat{v} & 1\\ 0 & 1 & \frac{\hat{v}}{\gamma\hat{p}}\end{bmatrix}\frac{\partial}{\partial x}\begin{bmatrix}\hat{\rho}\\ \hat{v}\\ \hat{p}\end{bmatrix}=\mathbf{0} \tag{B.12}$$

While this scaling does not change smooth solutions to system (B.9), problems may occur if shocks are anticipated [181]. Such so-called *weak solutions* [181] to system (B.9) (solutions involving discontinuities which must be described using the integral formulation of (B.9)) are not necessarily preserved under such a scaling. Entropy variables, to be briefly mentioned in §B.3.3, allow a potential means of avoiding these difficulties.

Finally, by employing the conservation of mass equation to simplify the other equations, the scaled system (B.12) can be written in *skew-selfadjoint form* [181] as:

$$\mathbf{P}\frac{\partial\mathbf{w}}{\partial t'}+\frac{\partial\mathbf{P}\mathbf{w}}{\partial t'}+\mathbf{A}\frac{\partial\mathbf{w}}{\partial x}+\frac{\partial\mathbf{A}\mathbf{w}}{\partial x}=\mathbf{0} \tag{B.13}$$

where the symmetric matrices $\mathbf{P}$ and $\mathbf{A}$ are defined by

$$\mathbf{P}=\begin{bmatrix}\frac{1}{\hat{\rho}} & 0 & 0\\ 0 & \hat{\rho} & 0\\ 0 & 0 & \frac{1}{\alpha\hat{p}}\end{bmatrix}\qquad \mathbf{A}=\begin{bmatrix}\frac{\hat{v}}{\hat{\rho}} & 0 & 0\\ 0 & \hat{\rho}\hat{v} & 1\\ 0 & 1 & \frac{\hat{v}}{\alpha\hat{p}}\end{bmatrix}$$

and $\mathbf{w}$ is the state, $[\hat{\rho}, \hat{v}, \hat{p}]^T$, and $\alpha = \frac{2\gamma}{\gamma-1} > 0$. $\mathbf{P}$, in addition, will be positive definite if the density and pressure are positive everywhere. The significance of this skew-selfadjoint form can be seen by taking the inner product of (B.13) with $\mathbf{w}$, in which case we get

---

[†] We note, however, that Fries [70] has obtained an MDKC directly from these conservation laws, though certain extra parameters must be introduced in order to control stability.

$$\frac{1}{2}\frac{\partial \mathbf{w}^T\mathbf{P}\mathbf{w}}{\partial t'} + \frac{1}{2}\frac{\partial \mathbf{w}^T\mathbf{A}\mathbf{w}}{\partial x} = 0 \tag{B.14}$$

For the Cauchy problem (i.e., the problem is defined over the entire $x$ axis, so boundary conditions are effectively ignored), we may integrate over the domain to get

$$\frac{d}{dt'}\int_{-\infty}^{+\infty}\frac{1}{2}\mathbf{w}^T\mathbf{P}\mathbf{w}dx = 0 \tag{B.15}$$

and thus $\int_{-\infty}^{+\infty}\frac{1}{2}\mathbf{w}^T\mathbf{P}\mathbf{w}dx$ is the global conserved quantity. It can be seen, by comparison between (B.14) and (B.15) with (3.3) and (3.5) (in the lossless case), that this skew-selfadjointness property is the natural extension of symmetric hyperbolicity to the nonlinear case. It is interesting that the generalized definitions of the inductor and capacitor, as per (B.1) and (B.3), are completely commensurate; we will see this in the next section. The theory of skew-selfadjoint forms has recently seen quite a bit of activity, in particular with regard to so-called *entropy variables* [68, 84, 95, 180, 181, 182, 183], which we will look at briefly in §B.3.3.

### B.3.1 MDKC and MDWDF for the Gas Dynamics Equations

It is particularly easy to see the form of the MDKC for the gas dynamics equations in the scaled form of (B.13). Applying the usual coordinate transformation (3.18), (B.13) becomes

$$\frac{1}{2}\left(\mathbf{L}D_1\mathbf{w} + D_1\mathbf{L}\mathbf{w}\right) + \frac{1}{2}\left(\mathbf{M}D_2\mathbf{w} + D_2\mathbf{M}\mathbf{w}\right) + \mathbf{N}\mathbf{w} = \mathbf{0} \tag{B.16}$$

with

$$\mathbf{L} = \begin{bmatrix} \frac{1+\hat{v}}{\hat{\rho}} & 0 & 0 \\ 0 & \hat{\rho}(1+\hat{v})-1 & 0 \\ 0 & 0 & \frac{1+\hat{v}}{\alpha\hat{\rho}}-1 \end{bmatrix} \qquad \mathbf{M} = \begin{bmatrix} \frac{1-\hat{v}}{\hat{\rho}} & 0 & 0 \\ 0 & \hat{\rho}(1-\hat{v})-1 & 0 \\ 0 & 0 & \frac{1-\hat{v}}{\alpha\hat{\rho}}-1 \end{bmatrix}$$

and

$$\mathbf{N} = \begin{bmatrix} 0 & 0 & 0 \\ 0 & D_1+D_2 & D_1-D_2 \\ 0 & D_1-D_2 & D_1+D_2 \end{bmatrix}$$

The MDKC is shown in Figure B.2(a), where the inductances can be read directly from the entries of $\mathbf{L}$, $\mathbf{M}$ and $\mathbf{N}$. $\mathbf{L}$ and $\mathbf{M}$ represent the inductances in the three loops in directions $t_1$ and $t_2$ respectively, and $\mathbf{N}$ gives the coupling between the second and third loops (notice that it can be realized as a simple linear and shift-invariant Jaumann two-port, just as in the linear systems of Chapter 3). The first loop, with current $\hat{\rho}$ is decoupled from the other two, although the inductances in this loop are dependent on $\hat{v}$.

The MDWD network follows immediately, and is shown in Figure B.2(b). It should be kept in mind that the port resistances at the adaptors are now functions of the dependent variables (the currents in the MDKC), and thus of the wave variables themselves. In a given updating cycle, the current values of the port resistances must be determined from the incoming waves. Due to the fact that power normalized variables are used, this leads to a system of coupled nonlinear algebraic equations (three, one for each adaptor) to be solved at every grid point, and at every time step. Passivity is contingent upon the positivity of all the inductances in the network; this is essentially a

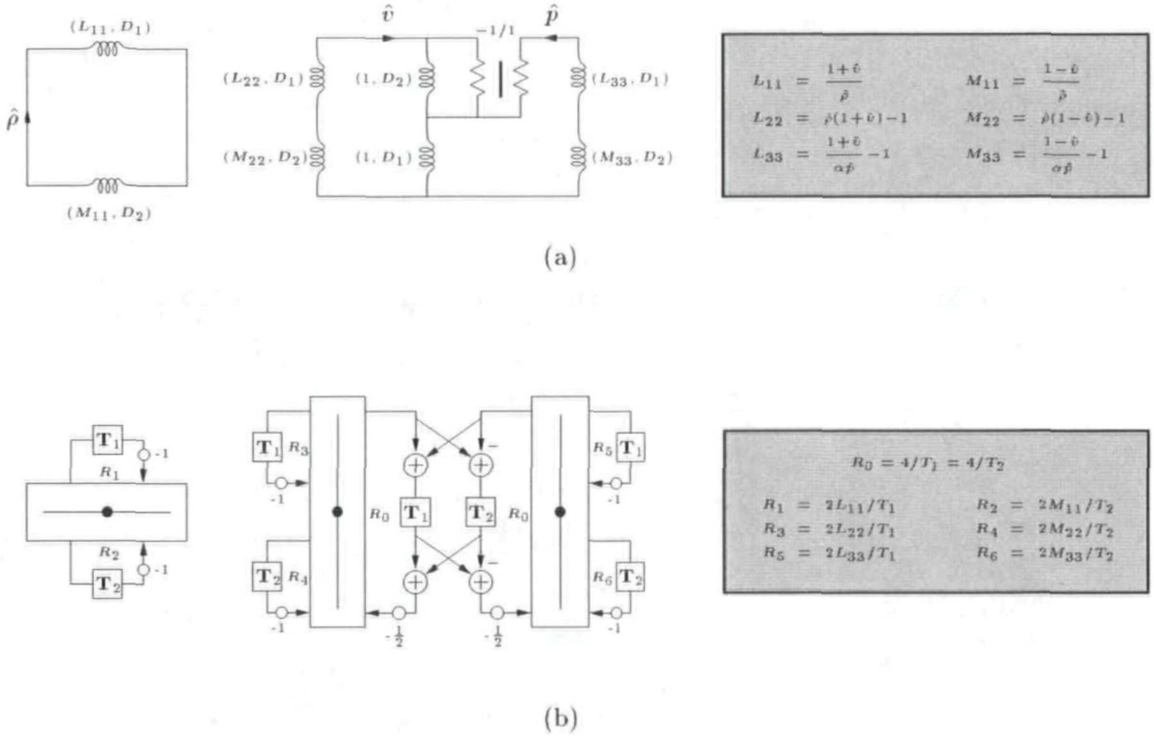
$(L_{11}, D_1)$
$\hat{\rho}$
$(M_{11}, D_2)$
$\hat{v}$
$-1/1$
$\hat{p}$
$(L_{22}, D_1)$
$(1, D_2)$
$(L_{33}, D_1)$
$(M_{22}, D_2)$
$(1, D_1)$
$(M_{33}, D_2)$
$L_{11} = \frac{1+\hat{v}}{\hat{\rho}}$
$M_{11} = \frac{1-\hat{v}}{\hat{\rho}}$
$L_{22} = \hat{\rho}(1+\hat{v})-1$
$M_{22} = \hat{\rho}(1-\hat{v})-1$
$L_{33} = \frac{1+\hat{v}}{\alpha\hat{p}}-1$
$M_{33} = \frac{1-\hat{v}}{\alpha\hat{p}}-1$
(a)
$\mathbf{T}_1$
$R_1$
-1
$R_2$
$\mathbf{T}_2$
-1
$\mathbf{T}_1$ $R_3$
-1
$\mathbf{T}_2$ $R_4$
-1
$R_0$
$\mathbf{T}_1$
$\mathbf{T}_2$
$R_0$
$-\frac{1}{2}$
$-\frac{1}{2}$
$R_5$ $\mathbf{T}_1$
-1
$R_6$ $\mathbf{T}_2$
-1
$R_0 = 4/T_1 = 4/T_2$
$R_1 = 2L_{11}/T_1$
$R_2 = 2M_{11}/T_2$
$R_3 = 2L_{22}/T_1$
$R_4 = 2M_{22}/T_2$
$R_5 = 2L_{33}/T_1$
$R_6 = 2M_{33}/T_2$
(b)

Figure B.2: *The (1+1)D gas dynamics system*— (a) *MDKC and* (b) *MDWD-network.*

condition on the positivity of the diagonal matrices **L** and **M**. Proceeding down the diagonals, this requirement on the first elements leads to the natural condition

$$1 \pm \hat{v} \geq 0 \qquad \Rightarrow \qquad v_0 \geq |v|_{max}$$

where $|v|_{max}$ is the maximum value that $|v|$ will take over the problem domain, and during the simulation period. We have also assumed that $\rho$ remains positive, and used the definition of the scaled quantity $\hat{v}$ from (B.11). The conditions on the other elements of **L** and **M** are more strict. We get

$$\hat{\rho}(1\pm\hat{v})-1\geq 0 \qquad \Rightarrow \quad 1\pm\hat{v}\geq\frac{1}{\hat{\rho}} \qquad \Rightarrow \quad v_0\geq\frac{p_0}{\rho_{min}v_0}+|v|_{max} \tag{B.17a}$$

$$\frac{1\pm\hat{v}}{\alpha\hat{p}}-1\geq 0 \qquad \Rightarrow \quad 1\pm\hat{v}\geq\alpha p \qquad \Rightarrow \quad v_0\geq\frac{\alpha p_{max}v_0}{p_0}+|v|_{max} \tag{B.17b}$$

where $\rho_{min}$ and $p_{max}$ are, respectively, the minimal value of $\rho$ and the maximum value of $p$ that will be encountered in the problem space. These quantities, as well as $|v|_{max}$ must be estimated *a priori*. It is also worth mentioning that for the above reasoning to be valid, it has been assumed that $\rho$ and $p$ will remain positive, and that $\rho$ is bounded from below. Although this has not been mentioned in the literature, there does not appear to be any assurance that these assumptions will remain valid during the course of a simulation.

We still have one degree of freedom left, namely the value of the parameter $p_0$. An optimal setting is easily shown to be

$$p_0=v_0\sqrt{\alpha p_{max}\rho_{min}}$$

in which case the two bounds on $v_0$ from (B.17) coalesce, giving

$$v_0\geq|v|_{max}+\sqrt{\frac{\alpha p_{max}}{\rho_{min}}}$$

### B.3.2 An Alternate MDKC and Scattering Network

The use of network manipulations and alternate spectral mappings in order to derive digital waveguide networks from an MDKC has been discussed in detail in §4.10, and we have seen the idea applied again in Chapter 5 to beam and plate systems. This same idea can be employed in the present case as well. Consider the network of Figure B.3(a), which is equivalent to that of Figure B.2(a); the right-hand pair of inductors in series in the "pressure" loop has been replaced by a gyrator closed on a parallel combination of capacitors; notice that although we are now transforming nonlinear operators, the network transformation techniques are no different from the linear case. We thus have a powerful means of developing stable numerical methods at our disposal.

The element values $L_{11}$, $L_{22}$, $M_{11}$ and $M_{22}$ are the same as before, except scaled by a factor $\Delta$, and the capacitance value will be

$$C_{33}=L_{33}\Delta/2 \qquad\qquad F_{33}=M_{33}\Delta/2$$

where $L_{33}$ and $M_{33}$ are as defined in Figure B.2. (Notice that we have scaled the entire system by $\Delta$, as in §4.10.)

The resulting MD digital network is shown in Figure B.3(b). As before, the two-port $AABB'$ transforms to a pair of bidirectional delay lines under the application of the spectral mappings defined by (4.107). The other circuit elements, namely the nonlinear inductors and capacitors, must be discretized using the trapezoid rule, and so we are left with a network which is neither an MDWDF nor a DWN, but which contains elements of both. The port resistance are determined in the usual way; for an inductance $L$ and direction $t_j$, by $R = 2L/T_j$ and for a capacitance $C$ of direction $t_j$ by $R = T_j/(2C)$. The port resistances of the paired multidimensional unit elements will be $R_0 = 1/\sqrt{2}$.

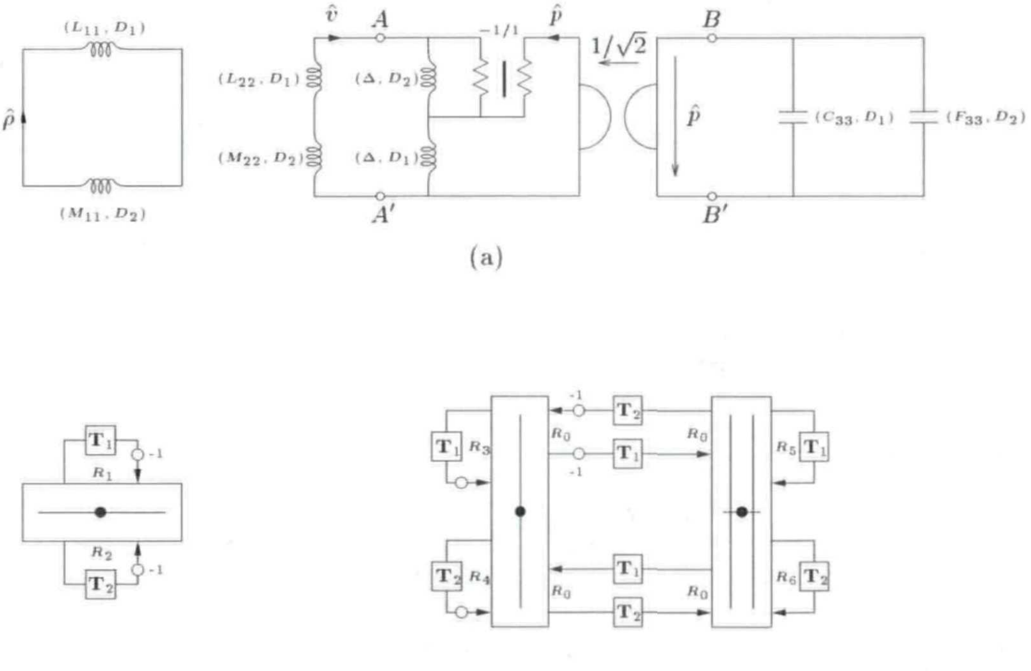

(a)

(b)

Figure B.3: *Alternative networks for the (1+1)D gas dynamics system*— (a) *MDKC and* (b) *scattering network.*

It would be possible to choose the directional shift lengths in the one-port inductances and capacitances differently from those in the unit elements such that the network could conceivably operate in an interleaved (offset) configuration; parallel junctions which calculate $p$ alternate with series junctions calculating $v$. A potential problem here is that the port resistances at the parallel junctions (say) depend on $v$, but $v$ are not calculated at these grid locations; some approximation is thus necessary, but we do not pursue the matter further here.

### B.3.3 Entropy Variables

In §B.3, we showed how Fettweis et al. have effectively employed a skew-selfadjoint form of the gas dynamics system in order to generate a circuit model. Such forms have been the subject of a great deal of research, especially in the last few years [181]. One particular form, which makes use of so-called *entropy variables* would appear to be of fundamental importance, because it arises from a change of variables (and not a simple scaling of the system, as was the case for the system arrived at in §B.3). We recap the results from [181] here.

Consider a system of conservation laws,

$$\frac{\partial \mathbf{u}}{\partial t} + \frac{\partial \mathbf{f}(\mathbf{u})}{\partial x} = \mathbf{0} \tag{B.18}$$

where the $\mathbf{f}(\mathbf{u})$ are smooth, possibly nonlinear mappings. The gas dynamics system (B.9), with $\mathbf{u} = [\rho, \rho v, \rho e]^T$ and $\mathbf{f}(\mathbf{u}) = [\rho v, \rho v^2 + p, \rho v e + p v]^T$, again complemented by the constitutive relation (B.10) is of this form. It is noted in [68, 116, 182] that (B.18) implies a further conservation law,

$$\frac{\partial \mathcal{U}}{\partial t} + \frac{\partial \mathcal{F}}{\partial x} = 0 \tag{B.19}$$

for some smooth convex scalar function $\mathcal{U}(\mathbf{u})$, and a scalar flux $\mathcal{F}(\mathbf{u})$, over any time interval over which solutions to (B.18) remain smooth. If discontinuities (shocks) develop, then (B.19) becomes an inequality ($\leq$). $\mathcal{U}$ and $\mathcal{F}$ are related by

$$\left(\frac{d\mathcal{U}}{d\mathbf{u}}\right)^T \frac{d\mathbf{f}}{d\mathbf{u}} = \left(\frac{d\mathcal{F}}{d\mathbf{u}}\right)^T$$

It was shown in [183] that system (B.18) is symmetrized through left-multiplication by the Hessian $\mathbf{P}_{\mathcal{U}}$ of $\mathcal{U}$,

$$\mathbf{P}_{\mathcal{U}} = \frac{d^2\mathcal{U}}{d\mathbf{u}^2}$$

so that we have

$$\mathbf{P}_{\mathcal{U}} \frac{\partial \mathbf{u}}{\partial t} + \mathbf{A}_{\mathcal{U}} \frac{\partial \mathbf{u}}{\partial x} = \mathbf{0} \tag{B.20}$$

where $\mathbf{A}_{\mathcal{U}}$ and $\mathbf{P}_{\mathcal{U}}$ are symmetric, and in addition $\mathbf{P}_{\mathcal{U}}$ is positive definite (a result of the convexity requirement on $\mathcal{U}$). This nonlinear system is of the same form as the (linear) symmetric hyperbolic system (3.1) discussed in §3.2, and possesses many similar properties; this form, however, can not be easily approached through MD circuit methods. Furthermore, *weak solutions* (i.e. solutions involving discontinuities) will not be preserved under such a scaling [181]. This is the same defect as that of Fettweis's MDKC for the Euler system, as discussed in §B.3.

It was later shown that (B.18) can also symmetrized with respect to a new variable $\mathbf{z}$, defined by

$$\mathbf{z} = \frac{d\mathcal{U}}{d\mathbf{u}}$$

In this case, symmetrization is carried out through a variable change and not a scaling, so weak solutions are indeed preserved. If, furthermore, the flux $\mathbf{f}$ is homogeneous [181], it can be shown that there is also a skew-selfadjoint form of (B.18). The gas dynamics system (B.9) can be written in skew-selfadjoint form as

$$\mathbf{P}_{\mathcal{U}}\frac{\partial \mathbf{z}}{\partial t} + \frac{\partial \mathbf{P}_{\mathcal{U}}\mathbf{z}}{\partial t} + \mathbf{A}_{\mathcal{U}}\frac{\partial \mathbf{z}}{\partial x} + \frac{\partial \mathbf{A}_{\mathcal{U}}\mathbf{z}}{\partial x} = \mathbf{0} \tag{B.21}$$

if $\mathcal{U}$ is chosen as

$$\mathcal{U} = -(p\rho^{\alpha})^{1/\alpha+\gamma} \qquad\qquad \alpha > 0$$

which is closely related to the physical entropy of the system [181]. The new variables $\mathbf{z}$ are referred to as *entropy variables.*

### An open problem

System (B.21) is of the same form as (B.13) (though note that we have neglected to perform the variable scalings), but it is written in terms of entropy variables $\mathbf{z}$ as opposed to non-conservative variables $\mathbf{w}$. Applying coordinate transformation (3.18), we can get the system into the form

$$\frac{1}{2}\left(\mathbf{L}_{\mathcal{U}}D_1\mathbf{z} + D_1\mathbf{L}_{\mathcal{U}}\mathbf{z}\right) + \frac{1}{2}\left(\mathbf{M}_{\mathcal{U}}D_2\mathbf{z} + D_2\mathbf{M}_{\mathcal{U}}\mathbf{z}\right) = \mathbf{0} \tag{B.22}$$

where

$$\mathbf{L}_{\mathcal{U}} = v_0\mathbf{P}_{\mathcal{U}} + \mathbf{A}_{\mathcal{U}} \qquad\qquad \mathbf{M}_{\mathcal{U}} = v_0\mathbf{P}_{\mathcal{U}} - \mathbf{A}_{\mathcal{U}}$$

Both $\mathbf{L}_{\mathcal{U}}$ and $\mathbf{M}_{\mathcal{U}}$ will be positive definite if $v_0$ is chosen sufficiently large. Though system (B.22) would appear to be in the correct form for an MDKC representation, there are certain difficulties.

First, the matrices $\mathbf{L}_{\mathcal{U}}$ and $\mathbf{M}_{\mathcal{U}}$, unlike $\mathbf{L}$ and $\mathbf{M}$ from (B.16), are not diagonal. Fettweis was able to take advantage of the fact that in terms of the variables $\mathbf{w}$, all inter-loop couplings are linear and shift-invariant (the coupling matrix $\mathbf{N}$ is a constant), so nonlinearities can be well-isolated. This is no longer the case here. It is of course possible to write down an MDKC corresponding to (B.22)—the entries of $\mathbf{L}_{\mathcal{U}}$ and $\mathbf{M}_{\mathcal{U}}$ become inductances directly. But positive definiteness of $\mathbf{L}_{\mathcal{U}}$ and $\mathbf{M}_{\mathcal{U}}$ does not imply that the off-diagonal entries will be positive, so our MDKC will not necessarily be a concretely passive representation.

We might attempt to avoid this by treating (B.22) as a simple series combination of two vector inductors, of inductances $\mathbf{L}_{\mathcal{U}}$ and $\mathbf{M}_{\mathcal{U}}$. In analogy with definitions of the coupled inductances in §2.3.7, it is certainly possible to define lossless nonlinear coupled inductances by

$$\begin{aligned}\mathbf{v}_1 &= \frac{1}{2}\left(\mathbf{L}_{\mathcal{U}}D_1\mathbf{z}+D_1\mathbf{L}_{\mathcal{U}}\mathbf{z}\right)\\ \mathbf{v}_2 &= \frac{1}{2}\left(\mathbf{M}_{\mathcal{U}}D_2\mathbf{z}+D_2\mathbf{M}_{\mathcal{U}}\mathbf{z}\right)\end{aligned}$$

and the resulting MDKC is essentially identical to that of Figure 3.6, for the simple linear advection equation, except that the current is now $\mathbf{z}$. It is difficult to introduce wave variables, however, because power-normalization is not straightforward in the nonlinear vector case; for an inductor of vector inductance $\mathbf{L} > \mathbf{0}$, the relationship analogous to (3.42) does not hold, i.e.,

$$\mathbf{v} = \frac{1}{2}\left(\mathbf{L}D_j\mathbf{i}+D_j(\mathbf{L}\mathbf{i})\right) \neq \mathbf{L}^{T/2}D_j\left(\mathbf{L}^{1/2}\mathbf{i}\right) \tag{B.23}$$

The second form of the inductor (which is distinct, and also lossless) on the right of (B.23), involving some left square root $\mathbf{L}^{T/2}$ of $\mathbf{L}$, is that which would be essential for power-normalization, because then we would be able to write

$$\mathbf{L}^{-T/2}\mathbf{v} = D_j(\mathbf{L}^{1/2}\mathbf{i})$$

and then define power-normalized vector wave variables by

$$\begin{aligned}\underline{\mathbf{a}} &= \frac{1}{2}\left(\mathbf{R}^{-T/2}\mathbf{v}+\mathbf{R}^{1/2}\mathbf{i}\right)\\ \underline{\mathbf{b}} &= \frac{1}{2}\left(\mathbf{R}^{-T/2}\mathbf{v}-\mathbf{R}^{1/2}\mathbf{i}\right)\end{aligned}$$

where $\mathbf{R}^{T/2}$ is the left square root of some positive definite matrix port resistance $\mathbf{R}$. Making the usual choice of $\mathbf{R} = 2\mathbf{L}/T_j$ (or rather $\mathbf{R}^{T/2} = \sqrt{2/T_j}\mathbf{L}^{T/2}$), we would then arrive at the familiar wave relationship of (3.38) in terms of the vector waves $\underline{\mathbf{b}}$ and $\underline{\mathbf{a}}$. The two inductor definitions of (B.23) do, however, coincide if the nonlinearity is confined to the diagonal elements of $\mathbf{L}$. This is precisely what Fettweis has taken advantage of in his formulation.

It would be of fundamental interest to know whether a passive MDKC for general nonlinear systems of the form of (B.22) (and its analogues in higher dimensions), amenable to wave digital discretization in fact exists. In such an MDKC or MDWD network, the global conserved quantity would have the interpretation of an entropy, which can be thought of as a generalized form of energy [68]. We also note that the numerical methods examined here can also be applied to fluid dynamic systems in (2+1)D [16] and (3+1)D [49]. The nonlinear algebraic systems to be solved become larger, but are still localized. Also, we mention that these numerical methods do not seem to reduce to conventional finite difference schemes along the lines of Godunov's method and its offspring [171].

# Bibliography

[1] S. Abarbanel and D. Gottlieb. A mathematical analysis of the PML method. *J. Computational Physics*, 134(2):357–63, 1 July 1997.

[2] S. Abarbanel and D. Gottlieb. On the construction and analysis of absorbing layers in CEM. *Applied Numerical Mathematics*, 27(4):331–40, Aug. 1998.

[3] R. Abraham. *Linear and Multilinear Algebra.* W. A. Benjamin, Inc., New York, 1966.

[4] S. Akhtarzad and P. B. Johns. Solution of Maxwell's equations in three space dimensions and time by the T.L.M. method of numerical analysis. *Proc. IEE*, 122(12):1344–8, Dec. 1975.

[5] K. Balemarthy and S. Bass. General, linear boundary conditions in MD wave digital simulations. In *Proc. 1995 IEEE Int. Symp. on Circuits and Systems*, volume 1, pages 73–76, Seattle, Washington, 28 Apr.–3 May 1995.

[6] M. Banerjee. On the vibration of skew plates of variable thickness. *J. Sound Vibration*, 63(3):377–83, 8 Apr. 1979.

[7] S. Bass. Sampling grid properties in wave digital PDE simulations. Technical Report CSE-TR-26-94, University of Notre Dame, 1994.

[8] S. Basu and A. Fettweis. On the factorization of scattering transfer matrices for multidimensional lossless two-ports. *IEEE Trans. Circuits and Systems*, CAS-32(9):925–34, Sept. 1985.

[9] S. Basu and A. Fettweis. On synthesizable multidimensional lossless two-ports. *IEEE Trans. Circuits and Systems*, 35(12):1478–86, Dec. 1988.

[10] S. Basu and A. Zerzghi. Multidimensional digital filter approach for numerical solution of a class of PDEs of the propagating wave type. In *Proc. 1998 IEEE Int. Symp. on Circuits and Systems*, volume 5, pages 74–77, Monterey, California, 31 May–3 June 1998. IEEE Press.

[11] V. Belevitch. Summary of the history of circuit theory. *Proc. IRE*, 50:848–55, May 1962.

[12] V. Belevitch. *Classical Network Theory.* Holden Day, San Francisco, 1968.

[13] J.-P. Berenger. A perfectly matched layer for the absorption of electromagnetic waves. *J. Computational Physics*, 114(2):185–200, Oct. 1994.

[14] J.-P. Berenger. Three-dimensional perfectly matched layer for the absorption of electromagnetic waves. *J. Computational Physics*, 127(2):363–379, Sept. 1996.

[15] D. P. Berners. *Acoustics and Signal Processing Techniques for Physical Modelling of Brass Instruments.* PhD thesis, Department of Electrical Engineering, Stanford University, 1999.

[16] R. Bernhardt and D. Dahlhaus. Numerical integration of the Euler equations by means of wave digital filters. In *Proc. IEEE Int. Conf. Acoust., Speech, and Sig. Proc.*, volume 6, pages 1–4, Adelaide, Australia, 19–22 Apr. 1994. IEEE Press.

[17] D. Beskos, editor. *Boundary Element Analysis of Plates and Shells.* Springer-Verlag, New York, 1991.

[18] S. Bilbao. Digital waveguide networks as multidimensional wave digital filters. In *Proc. COST G-6 Conference on Digital Audio Effects*, pages 49–54, Verona, Italy, 7–9 Dec. 2000.

[19] S. Bilbao. Digital waveguide networks in inhomogeneous media. In *Proc. COST G-6 Conference on Digital Audio Effects*, pages 249–253, Verona, Italy, 7–9 Dec. 2000.

[20] N. K. Bose. *Applied Multidimensional Systems Theory.* Van Nostrand Reinhold, New York, 1982.

[21] A. Bossavit and L. Kettunen. Yee-like schemes on a tetrahedral mesh, with diagonal lumping. *Int. J. of Numerical Modelling*, 12:129–42, Jan.–Apr. 1999.

[22] A. Bruckstein and T. Kailath. An inverse scattering framework for several problems in signal processing. *IEEE ASSP Magazine*, 4(1):6–20, Jan. 1987.

[23] K. P. Bube and R. Burridge. The one-dimensional inverse problem of reflection seismology. *SIAM Review*, 25(4):497–559, 1983.

[24] R. Cacoveanu, P. Saguet, and F. Ndagijimana. TLM method: A new approach for the central node in polar meshes. *Electronics Letters*, 31(4):297–8, 16 Feb. 1995.

[25] A. Chaigne and A. Askenfelt. Numerical simulations of struck strings. I. A physical model for a struck string using finite difference methods. *J. Acoust. Soc. Amer.*, 95(2):1112–8, Feb. 1994.

[26] D. Chandrasekharaiah. Thermoelasticity with second sound: A review. *Appl. Mech. Review*, 39(3):355–376, Mar. 1986.

[27] Z. Chen, M. M. Ney, and W. J. R. Hoefer. A new finite difference time-domain formulation and its equivalence with the TLM symmetrical condensed node. *IEEE Trans. Microwave Theory Tech.*, MTT-39(12), Dec. 1991.

[28] D. Cheng. *Field and Wave Electromagnetics*, page 438. Addison-Wesley, second edition, 1990.

[29] C. Christopoulos. *The Transmission-Line Modelling Method.* IEEE Press, New York, 1995.

[30] P. R. Cook. *Identification of Control Parameters in an Articulatory Vocal Tract Model with Applications to the Synthesis of Singing.* PhD thesis, Department of Electrical Engineering, Stanford University, 1990.

[31] R. Cooper and M. Naghdi. Propagation of non-axially symmetric waves in elastic cylindrical shells. *J. Acoust. Soc. Amer.*, 29(12):1365–73, Dec. 1957.

[32] G. Dahlquist. A special stability problem for linear multistep methods. *BIT*, 3:27–43, 1963.

[33] D. de Cogan. *Transmission Line Matrix (TLM) Techniques for Diffusion Applications.* Gordon and Breach Science Publishers, Amsterdam, 1998.

[34] C. de Vaal and R. Nouta. Suppression of parasitic oscillations in floating point wave digital filters. In *Proc. 1978 IEEE Int. Symp. on Circuits and Systems*, pages 1018–22, New York, New York, 17–19 May 1978.

[35] W. Elmore and M. Heald. *Physics of Waves.* McGraw-Hill, New York, 1969.

[36] M. Erbar and E.-H. Horneber. Models for transmission lines with connecting transistors based on wave digital filters. *Int. J. of Circ. Theory and Applications*, 23:395–412, July–Aug. 1995.

[37] K. Erickson and A. N. Michel. Stability analysis of fixed-point digital filters using computer generated Lyapunov functions—part ii: Wave digital filters and lattice digital filters. *IEEE Trans. Circuits and Systems*, CAS–32(2):132–142, Feb. 1985.

[38] C. Eswarappa and W. J. R. Hoefer. Bridging the gap between TLM and FDTD. *IEEE Microwave and Guided Wave Letters*, 43(8):4–6, Aug. 1995.

[39] T. Felderhoff. Simulation of nonlinear circuits with period-doubling and chaotic behavior by wave digital filter principles. *IEEE Trans. Circuits and Systems*, 41(7):485–9, July 1994.

[40] T. Felderhoff. Jacobi's method for massive parallel wave digital filter algorithm. In *Proc. 1996 IEEE Int. Symp. on Circuits and Systems*, volume 2, pages 1621–4, Atlanta, Georgia, 12–15 May 1996.

[41] A. Fettweis. Digital filters related to classical structures. *AEU: Archive für Elektronik und Übertragungstechnik*, 25:79–89, Feb. 1971. (See also U.S. Patent 3,967,099, 1976, now expired.).

[42] A. Fettweis. Pseudopassivity, sensitivity, and stability of wave digital filters. *IEEE Trans. Circuit Theory*, 19(6):668–673, Nov. 1972.

[43] A. Fettweis. On sensitivity and roundoff noise in wave digital filters. *IEEE Trans. on Acoust., Speech, and Signal Proc.*, ASSP–22(5):383–4, Oct. 1974.

[44] A. Fettweis. Digital signal processing. In J. K. Aggarwal, editor, *Principles of Multidimensional Wave Digital Filtering*, pages 261–82. Western Periodicals, North Hollywood, California, 1978.

[45] A. Fettweis. Multidimensional circuit and systems theory. In *Proc. 1984 IEEE Int. Symp. on Circuits and Systems*, pages 951–957, Montreal, Canada, 7–10 May 1984. IEEE Press.

[46] A. Fettweis. Wave digital filters: Theory and practice. *Proc. IEEE*, 74(2):270–327, Feb. 1986.

[47] A. Fettweis. The role of passivity and losslessness in multidimensional digital signal processing–new challenges. In *Proc. 1991 IEEE Int. Symp. on Circuits and Systems*, volume 1, pages 112–115, Singapore, 11–14 June 1991. IEEE Press.

[48] A. Fettweis. Discrete passive modelling of physical systems described by PDEs. In *SIGNAL PROCESSING VI: Theory and Applications. Proceedings of EUSIPCO-92, Sixth European Signal Processing Conference*, volume 1, pages 55–62, Brussels, Belgium, 24–27 Aug. 1992. Elsevier Science Publishers.

[49] A. Fettweis. Discrete passive modelling of viscous fluids. In *Proc. 1992 IEEE Int. Symp. on Circuits and Systems*, pages 1640–1643, San Diego, California, 10–13 May 1992. IEEE Press.

[50] A. Fettweis. Multidimensional wave digital filters for discrete-time modelling of Maxwell's equations. *Int. J. of Numerical Modelling*, 5:183–201, Aug. 1992.

[51] A. Fettweis. Multidimensional wave digital principles: From filtering to numerical integration. In *Proc. IEEE Int. Conf. Acoust., Speech, and Sig. Proc.*, volume 6, pages 173–181, Adelaide, Australia, 19–22 Apr. 1994. IEEE Press.

[52] A. Fettweis and S. Basu. On improved representation theorems for multidimensional lossless bounded matrices. *Int. J. of Circ. Theory and Applications*, 19(5):453–57, Sept.–Oct. 1991.

[53] A. Fettweis and T. Leickel. On floating-point implementations of modified wave digital filters. In *Proc. 1992 IEEE Int. Symp. on Circuits and Systems*, volume 4, pages 1812–5, San Diego, California, 10–13 May 1992.

[54] A. Fettweis, T. Leickel, M. Bolle, and U. Sauvagerd. Realization of filter banks by means of wave digital filters. In *Proc. 1990 IEEE Int. Symp. on Circuits and Systems*, volume 3, pages 2013–16, New Orleans, Louisiana, 1–3 May 1990.

[55] A. Fettweis, H. Levin, and A. Sedlmeyer. Wave digital lattice filters. *Int. J. of Circ. Theory and Applications*, 2(2):203–11, June 1974.

[56] A. Fettweis and K. Meerkötter. Suppression of parasitic oscillations in wave digital filters. *IEEE Trans. Circuits and Systems*, CAS-22(3):239–46, Mar. 1974.

[57] A. Fettweis and K. Meerkötter. On adaptors for wave digital filters. *IEEE Trans. on Acoust., Speech, and Signal Proc.*, ASSP-23(6):516–25, Dec. 1975.

[58] A. Fettweis and K. Meerkötter. On parasitic oscillations in digital filters under looped conditions. *IEEE Trans. Circuits and Systems*, CAS-24(9):475–81, Sept. 1975.

[59] A. Fettweis and G. Nitsche. Numerical integration of partial differential equations by means of multidimensional wave digital filters. In *Proc. 1990 IEEE Int. Symp. on Circuits and Systems*, volume 2, pages 954–7, New Orleans, Louisiana, 1–3 May 1990.

[60] A. Fettweis and G. Nitsche. Massively parallel algorithms for numerical integration of partial differential equations. In *Algorithms and Parallel VLSI Architectures. Lectures and Tutorials Presented at the International Workshop*, volume B, pages 475–484. Elsevier, 1991.

[61] A. Fettweis and G. Nitsche. Numerical integration of partial differential equations using principles of multidimensional wave digital filters. *J. of VLSI Sig. Proc.*, 3(1–2):7–24, June 1991.

[62] A. Fettweis and G. Nitsche. Transformation approach to numerically integrating PDEs by means of WDF principles. *Multidimensional Systems Sig. Proc.*, 2(2):127–159, May 1991.

[63] A. Fettweis and G. A. Seraji. New results in numerically integrating PDEs by the wave digital approach. In *Proc. 1999 IEEE Int. Symp. on Circuits and Systems*, volume 5, pages 17–20, Orlando, Florida, 30 May–2 June 1999.

[64] A. Fiedler and H. Grotstollen. Simulation of power electronic circuits with principles used in wave digital filters. *IEEE Trans. Industry Applications*, 33(1):49–57, Jan./Feb. 1997.

[65] H. D. Fischer. Wave digital filters for numerical integration. *ntz-Archiv*, 6:37–40, Feb. 1984.

[66] N. Fletcher and T. Rossing. *The Physics of Musical Instruments.* Springer-Verlag, New York, 1991.

[67] F. Fontana and D. Rocchesso. Physical modelling of membranes for percussive instruments. *Acustica United with Acta Acustica*, 84:529–542, May/June 1998.

[68] K. Friedrichs and P. Lax. Systems of conservation equations with a convex extension. In *Proceedings of the National Academy of Sciences of the U.S.A.*, pages 1686–1688. New York University, 1971.

[69] M. Fries. Multidimensional reactive elements on curvilinear coordinate systems and their MDWDF discretization. In *Proc. IEEE Int. Conf. Acoust., Speech, and Sig. Proc.*, volume 6, pages 9–12, Adelaide, Australia, 19–22 Apr. 1994. IEEE Press.

[70] M. Fries. Simulation of one-dimensional Euler flow by means of multidimensional wave digital filters. In *Proc. 1994 IEEE Int. Symp. on Circuits and Systems*, volume 6, pages 9–12, London, UK, 30 May–2 June 1994. IEEE Press.

[71] M. Fries and A. Schrick. MDWDF-Verfahren und TLM-Methode zur Integration der 2D Maxwell-Gleichungen. In *Tagungsband ITG-Diskussionssitzung Neue Anwendungen theoretischer Konzepte in der Elektrotechnik*, pages 137–144, Berlin, Germany, 1995. In German.

[72] M. Fusco. FDTD algorithm in curvilinear coordinates. *IEEE Trans. Antennas and Propagation*, 38(1):76–89, Jan. 1990.

[73] M. Fusco, M. Smith, and L. Gordon. A three-dimensional FDTD algorithm in curvilinear coordinates. *IEEE Trans. Antennas and Propagation*, 39(10):1463–6, Oct. 1991.

[74] P. Garabedian. *Partial Differential Equations.* Chelsea Publishing Company, New York, second edition, 1986.

[75] Y. Genin. An algebraic approach to A-stable linear multistep-multiderivative integration formulas. *BIT*, 14(4):382–406, 1974.

[76] C. Giguere and P. Woodland. A computational model of the auditory periphery for speech and hearing. *J. Acoust. Soc. Amer.*, 95(1):331–49, Jan. 1994.

[77] K. Graff. *Wave Motion in Elastic Solids.* Dover, New York, 1975.

[78] A. H. Gray, Jr. Passive cascaded lattice digital filters. *IEEE Trans. Circuits and Systems*, CAS-27(5):337–44, May 1980.

[79] A. H. Gray, Jr. and J. D. Markel. Digital lattice and ladder filter synthesis. *IEEE Trans. Audio and Electroacoustics*, AU-21:491–500, Dec. 1973.

[80] A. H. Gray, Jr. and J. D. Markel. A normalized digital filter structure. *IEEE Trans. on Acoust., Speech, and Signal Proc.*, ASSP-23:268–77, June 1975.

[81] J. Greenspon. Vibrations of a thick-walled cylindrical shell—comparison of the exact theory with approximate theories. *J. Acoust. Soc. Amer.*, 32(5):571–8, May 1960.

[82] B. Gustaffson, H.-O. Kreiss, and J. Oliger. *Time Dependent Problems and Difference Methods.* John Wiley and Sons, New York, 1995.

[83] C. Harris and C. Crede, editors. *Shock and Vibration Handbook.* McGraw-Hill, 1976.

[84] A. Harten. On the symmetric form of systems of conservation laws. *J. Computational Physics*, 49:151–164, Jan. 1983.

[85] G. Hemetsberger. Stability verification of multidimensional Kirchoff circuits by suitable energy functions. In *Proc. IEEE Int. Conf. Acoust., Speech, and Sig. Proc.*, volume 6, pages 13–16, Adelaide, Australia, 19–22 Apr. 1994. IEEE Press.

[86] G. Hemetsberger and R. Hellfajer. Approach to simulating acoustics in supersonic flow by means of multidimensional vector-WDFs. In *Proc. 1994 IEEE Int. Symp. on Circuits and Systems*, pages 73–76, London, UK, 30 May–2 June 1994. IEEE Press.

[87] J. L. Herring and C. Christolopoulos. Solving electromagnetic field problems using a multiple grid transmission-line modelling method. *IEEE Trans. Antennas and Propagation*, 42(12):1654–1658, Dec. 1994.

[88] J. L. Herring and C. Christopoulos. Multigrid transmission-line modelling method for solving electromagnetic field problems. *Electronics Letters*, 27(20):1794–5, 26 Sept. 1991.

[89] C. Hirsch. *Numerical Computation of Internal and External Flows*. Wiley, Chichester, England, 1988.

[90] W. J. R. Hoefer. *The Electromagnetic Wave Simulator*. Chichester, New York, 1991.

[91] R. Holland. Finite-difference solution of Maxwell's equations in generalized non-orthogonal coordinates. *IEEE Trans. Nuclear Science*, NS-30(6):4589–91, Dec. 1983.

[92] R. Horn and C. Johnson. *Matrix Analysis*. Cambridge University Press, Cambridge, England, 1985.

[93] F. Hu. On absorbing boundary conditions for linearized Euler equations by a perfectly matched layer. *J. Computational Physics*, 129(1):201–19, Nov. 1996.

[94] H. Huang. *Static and Dynamic Analyses of Plates and Shells*. Springer-Verlag, London, U.K., 1989.

[95] T. Hughes, L. Franca, F. Chalot, and Z. Johan. Stabilized finite element methods in fluid mechanics. Course reader for Mechanical Engineering 234, Stanford University, 1996-7.

[96] D. Jaffe and J. O. Smith. Extensions of the Karplus-Strong plucked string algorithm. *Computer Music J.*, 7(2):56–68, Summer 1983.

[97] P. B. Johns. The solution of inhomogeneous waveguide problems using a transmission-line matrix. *IEEE Trans. Microwave Theory Tech.*, MTT-22:209–215, Mar. 1974.

[98] P. B. Johns. On the relationship between TLM and finite-difference methods for Maxwell's equations. *IEEE Trans. Microwave Theory Tech.*, MTT-35(1), Jan. 1987.

[99] P. B. Johns. A symmetrical condensed node for the TLM method. *IEEE Trans. Microwave Theory Tech.*, MTT-35(4):370–7, Apr. 1987.

[100] P. B. Johns and R. L. Beurle. Numerical solution of 2-dimensional scattering problems using a transmission-line matrix. *Proc. IEE*, 118:1203–1208, Sept. 1971.

[101] S. Kaliski and L. Solarz. *Vibrations and Waves*. Elsevier, New York, 1992.

[102] M. Karjalainen and J. O. Smith. Body modelling techniques for string instrument synthesis. In *Proc. Int. Computer Music Conf.*, Hong Kong, 18–21 Aug. 1996.

[103] K. Karplus and A. Strong. Digital synthesis of plucked-string and drum timbres. *Computer Music J.*, 7(2):43–55, Summer 1983.

[104] J. L. Kelly and C. C. Lochbaum. Speech synthesis. In *Proc. Fourth Int. Congress on Acoustics*, pages 1–4, Copenhagen, Denmark, 1962. Paper G42.

[105] T. Koga. Synthesis of finite passive $n$-ports with prescribed two-variable reacance matrices. *IEEE Trans. Circuit Theory*, CT-13:31–52, Mar. 1966.

[106] H. Krauss. Wave digital simulation of transmission lines with arbitrary initial potential and current distributions. In *1996 IEEE Digital Signal Processing Workshop Proceedings*, pages 195–198, Loen, Norway, 1–4 Sept. 1996. IEEE Press.

[107] H. Krauss and R. Rabenstein. Application of multidimensional wave digital filters to boundary value problems. *IEEE Signal Processing Letters*, 2(7):183–201, July 1995.

[108] H. Krauss, R. Rabenstein, and M. Gerken. Simulation of wave propagation by multidimensional wave digital filters. *Simulation Practice and Theory*, 4:361–382, Nov. 1996.

[109] G. Kron. Equivalent circuit of the field equations of Maxwell. *Proc. IRE*, 32(5):284–299, May 1944.

[110] M. Krumpholz, C. Huber, and P. Russer. A field-theoretical comparison of FDTD and TLM. *IEEE Trans. Microwave Theory Tech.*, 43(8):1935–1950, Aug. 1995.

[111] W. Ku and S. Ming. Floating-point coefficient sensitivity and roundoff noise of recursive digital filters realized in ladder structures. *IEEE Trans. Circuits and Systems*, CAS–22(12):927–36, Dec. 1975.

[112] P. Kundu. *Fluid Mechanics*. Academic Press, San Diego, California, 1990.

[113] J. Kuttler and V. Sigillito. Vibrational frequencies of clamped plates of variable thickness. *J. Sound Vibration*, 86(2):181–9, 22 Jan. 1983.

[114] T. Laakso, V. Välimäki, M. Karjalainen, and U. Laine. Splitting the unit delay—tools for fractional delay filter design. *IEEE Signal Processing Magazine*, 13(1):30–60, Jan. 1996.

[115] S. Lawson, 2000. private communication.

[116] P. Lax. *Shock Waves and Entropy*, in *Contributions to Nonlinear Functional Analysis*, E. Zarantonello, Ed. Academic Press, New York, 1971.

[117] T. Leickel and A. Fettweis. Efficient digital-signal-processor realization of multirate filter banks using wave digital filters. In *Proc. 1992 IEEE Int. Symp. on Circuits and Systems*, volume 4, pages 1812–15, San Diego, California, 10–13 May 1992.

[118] P. Lennarz and W. Drews. Design of circularly symmetric 2-D wave digital filters. In *Proc. 2nd Eur. Signal Processing Conf.*, pages 199–202, Erlangen, Germany, Sept. 1983.

[119] P. Lennarz and L. Hofmann. Computer realization of two-dimensional wave digital filters. In *Proc. 1978 Eur. Conf. on Circuit Theory and Design*, pages 360–4, Lausanne, Switzerland, Sept. 1978.

[120] K. Liew, C. Wang, Y. Xiang, and S. Kitipornchai. *Vibration of Mindlin plates: Programming the p-version Ritz Method.* Elsevier, Amsterdam, The Netherlands, first edition, 1998.

[121] X. Liu and L. Bruton. A new three-port adaptor suitable for floating-point arithmetic and/or DSP implementations. In *Proc. IEEE Int. Conf. Acoust., Speech, and Sig. Proc.*, volume 6, pages 17–20, Adelaide, Australia, 19–22 Apr. 1994.

[122] X. Liu and A. Fettweis. Multidimensional digital filtering by using parallel algorithms based on diagonal processing. *Multidimensional Systems Sig. Proc.*, 1(1):51–66, Mar. 1990.

[123] R. H. MacNeal. An asymmetrical finite difference network. *Quarterly of App. Math.*, 9(3):295–310, Oct. 1953.

[124] J. D. Markel and A. H. Gray, Jr. *Linear Prediction of Speech Signals.* Springer-Verlag, New York, 1976.

[125] K. Meerkötter. Incremental pseudopassivity of wave digital filters. In *Signal Processing: Theories and Applications. Proceedings EUSIPCO-80, First European Signal Processing Conference*, pages 27–31, Lausanne, Switzerland, 1980.

[126] K. Meerkötter and T. Felderhoff. Simulation of nonlinear transmission lines by wave digital filter principles. In *Proc. 1992 IEEE Int. Symp. on Circuits and Systems*, volume 2, pages 875–8, San Diego, 10–13 May 1992.

[127] B. G. Mertzios and F. N. Koumboulis. Analysis and numerical integration of nonlinear systems using MD-passive circuits. In *Proc. 1999 IEEE Int. Symp. on Circuits and Systems*, volume 5, pages 25–28, Orlando, Florida, 30 May–2 June 1999.

[128] M. Naghdi and R. Cooper. Propagation of elastic waves in cylindrical shells, including the effects of transverse shear and rotatory inertia. *J. Acoust. Soc. Amer.*, 28(1):56–63, Jan. 1956.

[129] Y. Naka, H. Ikuno, M. Nishimoto, and A. Yata. FD-TD method with PMLs ABC based on the principles of multidimensional wave digital filters for discrete-time modelling of Maxwell's equations. *Trans. of the Inst. of Electronics, Information and Communication Engineers: Electronics*, 81(2):305–314, Feb. 1998.

[130] G. Nitsche. private communication.

[131] G. Nitsche. *Numerische Lösung partieller Differentialgleichungen mit Hilfe von Wellendigitalfiltern.* PhD thesis, Ruhr-Universität Bochum, 1993. In German.

[132] R. Nouta. The Jaumann structure in wave-digital filters. *Int. J. of Circ. Theory and Applications*, 2(2):163–74, June 1974.

[133] A. V. Oppenheim and R. Schafer. *Digital Signal Processing.* Prentice-Hall, Englewood Cliffs, New Jersey, 1975.

[134] A. V. Oppenheim and R. Schafer. *Discrete-time Signal Processing.* Prentice-Hall, Englewood Cliffs, New Jersey, 1989.

[135] H. Ozaki and T. Kasami. Positive real functions of several variables and their application to variable networks. *IRE. Trans. Circuit Theory*, CT-7:251–60, Sept. 1960.

[136] P. Penfield. *Tellegen's Theorem and Electrical Networks.* MIT Press, Cambridge, Massachusetts, 1970.

[137] J. Peng and C. Balanis. A generalized reflection-free domain-truncation method: Transparent absorbing boundary. *IEEE Trans. Antennas and Propagation*, 46(7), July 1998.

[138] P. Petropoulos, L. Zhao, and A. Cangellaris. A reflectionless sponge layer absorbing boundary condition for the solution of Maxwell's equations with high-order staggered finite difference schemes. *J. Computational Physics*, 139(1):184–208, 1 Jan. 1998.

[139] J. Proakis. *Digital Signal Processing.* Prentice-Hall, Englewood Cliffs, New Jersey, third edition, 1996.

[140] T. Pulliam. Course Notes, Aeronautics and Astronautics 214A, Autumn 1998-99, Stanford University.

[141] R. Rabenstein. A signal processing approach to the digital simulation of multidimensional continuous systems. In *Signal Processing III: Theories and Applications. Proceedings EUSIPCO-86, Third European Signal Processing Conference*, volume 2, pages 665–668, The Hague, The Netherlands, 2–5 Sept. 1986.

[142] R. Rabenstein, 2000. private communication.

[143] R. Rabenstein and L. Trautmann. Solution of vector partial differential equations by transfer function models. In *Proc. 1999 IEEE Int. Symp. on Circuits and Systems*, volume 5, pages 21–24, Orlando, Florida, 30 May–2 June 1999.

[144] R. Rabenstein and L. Trautmann. Solution of vector partial differential equations by transfer function models. In *Proc. 2000 IEEE Int. Symp. on Circuits and Systems*, volume 1, pages 407–10, Geneva, Switzerland, 28–31 May 2000.

[145] L. Rabiner and R. Schafer. *Digital Processing of Speech Signals.* Prentice-Hall, Englewood Cliffs, New Jersey, 1978.

[146] S. S. Rao. *Mechanical Vibrations, 2nd Ed.* Addison-Wesley, 1990.

[147] P. Regalia. The digital all-pass filter: A versatile signal-processing building block. *Proc. IEEE*, CAS-34(1):19–37, Jan. 1987.

[148] D. J. Riley and C. D. Turner. Interfacing unstructured tetrahedron grids to structured-grid FDTD. *IEEE Microwave and Guided Wave Letters*, 5(9):284–6, Sept. 1995.

[149] D. Rocchesso. Maximally diffusive yet efficent feedback delay networks for artificial reverberation. *IEEE Signal Processing Letters*, 4(9):252–255, Sept. 1997.

[150] D. Rocchesso and J. O. Smith. Circulant and elliptic feedback delay networks for artificial reverberation. *IEEE Trans. Speech and Audio Proc.*, 5(1):51–63, Jan. 1997.

[151] M. Roitman and P. S. R. Diniz. Simulation of non-linear and switching elements for transient analysis based on wave digital filters. *IEEE Trans. Power Delivery*, 11(4):2042–8, Oct. 1996.

[152] M. Roseau. *Vibrations in Mechanical Systems.* Springer-Verlag, Berlin, West Germany, 1984.

[153] Z. Sacks, D. Kingsland, R. Lee, and J. Lee. A perfectly matched absorber for use as an absorbing boundary condition. *IEEE Trans. Antennas and Propagation*, 43(12), Dec. 1995.

[154] A. Sarti and G. DePoli. Generalized adaptors with memory for nonlinear wave digital structures. In *Proceedings EUSIPCO-96, VII European Signal Processing Conference*, volume 3, pages 191–4, Trieste, Italy, 1996.

[155] L. Savioja. Improving the three-dimensional digital waveguide mesh by interpolation. In *Proc. Nordic Acoustical Meeting (NAM'98)*, pages 265–268, Stockholm, Sweden, 7-9 Sept. 1998.

[156] L. Savioja, T. Rinne, and T. Takala. Simulation of room acoustics with a 3-D finite-difference mesh. In *Proc. Int. Computer Music Conf.*, pages 463–466, Århus, Denmark, Sept. 1994.

[157] L. Savioja and V. Välimäki. Reducing the dispersion error in the digital waveguide mesh using interpolation and frequency-warping techniques. *IEEE Trans. Speech and Audio Proc.*, 8(2):184–194, Mar. 2000.

[158] L. Savioja and V. Välimäki. Interpolated 3-D digital waveguide mesh with frequency warping. In *Proc. IEEE Int. Conf. Acoust., Speech, and Sig. Proc.*, 7–11 May 2001. To appear.

[159] R. Scaramuzza and A. J. Lowery. Hybrid symmetrical condensed node for the TLM method. *Electronics Letters*, 26(23):1947–9, 1990.

[160] G. P. Scavone. *An Acoustic Analysis of Single-Reed Woodwind Instruments with an Emphasis on Design and Performance Issues and Digital Waveguide Techniques.* PhD thesis, Stanford University, 1997.

[161] J. O. Smith. A physical derivation of wave digital filters. In Lecture Notes for Music 421, Stanford University, Spring 1999–2000.

[162] J. O. Smith. *Techniques for Digital Filter Design and System Identification with Application to the Violin.* PhD thesis, Stanford University, 1983.

[163] J. O. Smith. A new approach to digital reverberation using closed waveguide networks. In *Proc. Int. Computer Music Conf.*, Vancouver, Canada, 1985. Appears in Technical Report STAN-M-39, pp. 1–7, Center for Computer Research in Music and Acoustics (CCRMA), Department of Music, Stanford University.

[164] J. O. Smith. Efficient simulation of the reed-bore and bow-string mechanisms. In *Music Applications of Digital Waveguides*, pages 29–34. 1987. Technical Report STAN-M-39, Center for Computer Research in Music and Acoustics (CCRMA), Department of Music, Stanford University.

[165] J. O. Smith. Elimination of limit cycles and overflow oscillations in time-varying lattice and ladder digital filters. In *Music Applications of Digital Waveguides*, pages 47–78. 1987. Technical Report STAN-M-39, Center for Computer Research in Music and Acoustics (CCRMA), Department of Music, Stanford University.

[166] J. O. Smith. Music applications of digital waveguides. Technical Report STAN-M-39, Center for Computer Research in Music and Acoustics (CCRMA), Department of Music, Stanford University, 1987.

[167] J. O. Smith. Waveguide digital filters. In *Music Applications of Digital Waveguides*, pages 108–181. 1987. Technical Report STAN-M-39, Center for Computer Research in Music and Acoustics (CCRMA), Department of Music, Stanford University.

[168] J. O. Smith, Spring 1999-2000. Course notes for Music 421, Stanford University.

[169] J. O. Smith and D. Rocchesso. Aspects of digital waveguide modelling for acoustic modelling applications. Submitted for publication.

[170] P. P. M. So, C. Eswarappa, and W. J. R. Hoefer. Parallel and distributed TLM computation with signal processing for electromagnetic field modeling. *Int. J. of Numerical Modelling*, 8(3–4):169–185, May–Aug. 1995.

[171] G. Sod. A survey of several finite difference methods for systems of nonlinear hyperbolic conservation laws. *J. Computational Physics*, 27(1):1–31, Apr. 1978.

[172] I. Sokolnikoff. *Tensor Analysis Theory and Applications to Geometry and Mechanics of Continua*. Wiley, New York, second edition, 1964.

[173] C. Steele, 2000. Department of Mechanical Engineering, Stanford University. Private communication.

[174] J. Stewart. *Calculus: Early Transcendentals*. Brooks/Cole, Pacific Grove, California, second edition, 1991.

[175] S. Stoffels. Full mesh warping techniques. In *Proc. COST G-6 Conference on Digital Audio Effects*, Verona, Italy, Dec. 7–9 2000.

[176] J. Strikwerda. *Finite Difference Schemes and Partial Differential Equations*. Wadsworth and Brooks/Cole Advanced Books and Software, Pacific Grove, Calif., 1989.

[177] H. Strube. Time-varying wave digital filters and vocal-tract models. In *Proc. IEEE Int. Conf. Acoust., Speech, and Sig. Proc.*, volume 2, pages 923–6, Paris, France, 3–5 May 1982.

[178] H. Strube. Time-varying wave digital filters for modelling analog systems. *IEEE Trans. on Acoust., Speech, and Signal Proc.*, ASSP-30(6):864–8, Dec. 1982.

[179] S. Summerfeld, T. Wicks, and S. Lawson. Wave digital filters using short signed digit coefficients. *Proc. IEE*, 143(5):259–66, Oct. 1996.

[180] L. Franca T. J. R. Hughes and M. Mallet. A new finite element formulation for computational fluid dynamics: I. Symmetric forms of the Euler and Navier-Stokes equations and the second law of thermodynamics. *Computer Methods in Applied Mechanics and Engineering*, 54:223–234, 1986.

[181] E. Tadmor. Skew-selfadjoint form for systems of conservation laws. *J. of Mathematical Analysis and Applications*, 103:428–442, 1984.

[182] E. Tadmor. A minimum entropy principle in the gas dynamics equations. *Applied Numerical Mathematics*, 2:151–164, Oct. 1986.

[183] E. Tadmor. Entropy functions for symmetric systems of conservation laws. *J. of Mathematical Analysis and Applications*, 122:355–359, Mar. 1987.

[184] A. Taflove. *Computational Electrodynamics*. Artech House, Boston, Massachusetts, 1995.

[185] A. Taflove. *Advances in Computational Electrodynamics*. Artech House, Boston, Massachusetts, 1998.

[186] L. Taxen. Polyphase filter banks using wave digital filters. *IEEE Trans. on Acoust., Speech, and Signal Proc.*, 29(3):423–8, June 1981.

[187] W. Thomson. *Theory of Vibrations with Applications*. Prentice-Hall, Upper Saddle River, New Jersey, fourth edition, 1993.

[188] B. Tongue. *Principles of Vibration*. Oxford University Press, New York, 1996.

[189] E. Turkel and A. Yefet. Absorbing PML boundary layers for wave-like equations. *Applied Numerical Mathematics*, 27(4):533–57, Aug. 1998.

[190] L. Tyler. Course notes for EE241, Stanford University, fall 1994-95.

[191] T. Utsunomiya and A. Fettweis. Discrete modelling of plasma equations with ion motion using technique of wave digital filters. In *Proc. IEEE Int. Conf. Acoust., Speech, and Sig. Proc.*, volume 6, pages 21–24, Adelaide, Australia, 19–22 Apr. 1994.

[192] P. P. Vaidyanathan. A unified approach to orthogonal digital filters and wave digital filters, based on LBR two-pair extraction. *IEEE Trans. Circuits and Systems*, CAS–32(7), July 1985.

[193] P. P. Vaidyanathan. *Multirate Systems and Filter Banks*, page 288. Prentice-Hall, Englewood Cliffs, New Jersey, 1993.

[194] V. Välimäki. *Discrete-Time Modeling of Acoustic Tubes Using Fractional Delay Filters*. PhD thesis, Helsinki University of Technology, Faculty of Electrical Engineering, Laboratory of Acoustics and Audio Signal Processing, Espoo, Finland, 1995.

[195] V. Välimäki and M. Karjalainen. Implementation of fractional delay waveguide models using allpass filters. In *Proc. IEEE Int. Conf. Acoust., Speech, and Sig. Proc.*, pages 8–12, Detroit, Michigan, May 1995.

[196] V. Välimäki, M. Karjalainen, and T. Laakso. Modeling of woodwind bores with finger holes. In *Proc. Int. Computer Music Conf.*, pages 32–9, Tokyo, Japan, 1993.

[197] S. A. VanDuyne, J. R. Pierce, and J. O. Smith. Travelling wave implementation of a lossless mode-coupling filter and the wave digital hammer. In *Proc. Int. Computer Music Conf.*, pages 411–418, Århus, Denmark, Sept. 1994.

[198] S. A. VanDuyne and J. O. Smith. Physical modelling with the 2D digital waveguide mesh. In *Proc. Int. Computer Music Conf.*, pages 40–47, Tokyo, Japan, 1993.

[199] S. A. VanDuyne and J. O. Smith. A simplified approach to modelling dispersion caused by stiffness in strings and plates. In *Proc. Int. Computer Music Conf.*, Århus, Denmark, Sept. 1994.

[200] S. A. VanDuyne and J. O. Smith. The 3D tetrahedral digital waveguide mesh with musical applications. In *Proc. Int. Computer Music Conf.*, pages 9–16, Hong Kong, 18–21 Aug. 1996.

[201] G. Verkroost and H. Butterweck. Suppression of parasitic oscillations in wave digital filters and related structures by means of controlled rounding. In *Proc. 1976 IEEE Int. Symp. on Circuits and Systems*, pages 628–9, Munich, West Germany, 27–29 Apr. 1976.

[202] X. Wang and S. Bass. The wave digital method and its use in a PIM chip array. Technical Report TR-97-11, University of Notre Dame, 1997.

[203] R. Warming, R. Beam, and B. Hyett. Diagonalization and simultaneous symmetrization of the gas-dynamic matrices. *Mathematics of Computation*, 29(132):1037–1045, Oct. 1975.

[204] W. Wegener. Design of wave digital filters with very short coefficient word lengths. In *Proc. 1976 IEEE Int. Symp. on Circuits and Systems*, pages 473–6, Munich, West Germany, 27–29 Apr. 1976.

[205] J. Wegner and J. Haddow. Linear thermoelasticity, second sound and the entropy inequality. *Wave Motion*, 18(1):67–77, Oct. 1993.

[206] L. Weinberg. *Network Analysis and Synthesis.* McGraw-Hill, New York, 1962.

[207] J. Wlodarczyk. New multigrid interface for the TLM method. *Electronics Letters*, 32(12):1111–1112, June 1996.

[208] M. R. Wohlers. *Lumped and Distributed Passive Networks; A Generalized and Advanced Viewpoint.* Academic Press, New York, 1969.

[209] F. Xiao and H. Yabe. Numerical dispersion relation for FDTD method in general curvilinear coordinates. *IEEE Microwave and Guided Wave Letters*, 7(2):48–50, Feb. 1997.

[210] C. Q. Xu. Accommodating lumped linear boundary conditions in the wave digital simulations of PDE systems. Master's thesis, University of Notre Dame, 1996. Available as Technical Report CSE-TR-26-94.

[211] C. Q. Xu, S. Bass, and X. Wang. Accommodating linear and nonlinear boundary conditions in wave digital simulations of PDE systems. *J. of Circuits Systems and Computers*, 7(6):563–597, Dec. 1997.

[212] C. Q. Xu, S. Bass, and X. Wang. Accomodating boundary conditions in the wave digital simulations of PDE systems. In *Proc. of the 40th Midwest Symp. on Circuits and Systems*, volume 2, pages 694–697. IEEE Press, 1997.

[213] A. E. Yagle. Fast algorithms for estimation and signal processing: An inverse scattering formulation. *IEEE Trans. on Acoust., Speech, and Signal Proc.*, 37(6):957–9, 1989.

[214] K. S. Yee. Numerical solution of initial boundary value problems involving Maxwell's equations in isotropic media. *IEEE Trans. Antennas and Propagation*, 14:302–7, 1966.

[215] B. Yegnanarayana. Design of recursive group delay filters by autoregressive modeling. *IEEE Trans. on Acoust., Speech, and Signal Proc.*, ASSP-30:632–7, Aug. 1982.

[216] L. Zhao and C. Cangellaris. A general approach for the development of unsplit-field time domain implementations of perfectly matched layers for FDTD grid truncation. *IEEE Microwave and Guided Wave Letters*, 6(5):209–11, May 1996.

[217] R. Ziolkowski. Time-derivative Lorentz material model-based absorbing boundary condition. *IEEE Trans. Antennas and Propagation*, 45(10), Oct. 1997.